

Brainstem Tumors

Diagnosis and Management

George I. Jallo

Mohammad Hassan A. Noureldine

Nir Shimony

Editors

 Springer

Brainstem Tumors

George I. Jallo
Mohammad Hassan A. Noureldine • Nir Shimony
Editors

Brainstem Tumors

Diagnosis and Management

 Springer

Editors

George I. Jallo
Department of Neurosurgery
Institute for Brain Protection Sciences
Johns Hopkins University School of Medicine
Johns Hopkins All Children's Hospital
Saint Petersburg, FL
USA

Mohammad Hassan A. Noureldine
Department of Neurosurgery
Institute for Brain Protection Sciences
Johns Hopkins University School of Medicine
Johns Hopkins All Children's Hospital
Saint Petersburg, FL
USA

Nir Shimony
Institute of Neuroscience
Geisinger Medical Center
Geisinger Commonwealth
School of Medicine
Danville, PA
USA

ISBN 978-3-030-38773-0 ISBN 978-3-030-38774-7 (eBook)
<https://doi.org/10.1007/978-3-030-38774-7>

© Springer Nature Switzerland AG 2020

This work is subject to copyright. All rights are reserved by the Publisher, whether the whole or part of the material is concerned, specifically the rights of translation, reprinting, reuse of illustrations, recitation, broadcasting, reproduction on microfilms or in any other physical way, and transmission or information storage and retrieval, electronic adaptation, computer software, or by similar or dissimilar methodology now known or hereafter developed.

The use of general descriptive names, registered names, trademarks, service marks, etc. in this publication does not imply, even in the absence of a specific statement, that such names are exempt from the relevant protective laws and regulations and therefore free for general use.

The publisher, the authors, and the editors are safe to assume that the advice and information in this book are believed to be true and accurate at the date of publication. Neither the publisher nor the authors or the editors give a warranty, expressed or implied, with respect to the material contained herein or for any errors or omissions that may have been made. The publisher remains neutral with regard to jurisdictional claims in published maps and institutional affiliations.

This Springer imprint is published by the registered company Springer Nature Switzerland AG
The registered company address is: Gewerbestrasse 11, 6330 Cham, Switzerland

I dedicate this book to my children, Maxwell, Nicky, and Lexi, for their unconditional love, understanding, and support.

George I. Jallo

To my parents – Ahmad and Fatima

To my siblings – Nour Al Zahraa, Mariam, Hussein, Wared, and Ali

To all patients and families of patients with brainstem tumors and lesions

Mohammad Hassan A. Noureldine

To my parents; my dear wife, Hila; and my kids, Liya, Darya, and Yahav, who remind me each and every day all about love and give me the strength to keep on going. To my patients who give me each and every time the motivation to never stop exploring for better solutions for their health and happiness

Nir Shimony



In memory of James T. Goodrich, MD, PhD (1946–2020)

Foreword 1

On March 25, 2015, Amador, my second 12-year-old son returned from his karate lessons and began to complain that his right arm and right leg hurt. He said that he was having difficulty moving his right limbs. We assumed it was an effect of his work in karate. Two days later, Amador could no longer hold a plate with his right hand. I also noticed that he spoke fast and skipped some words. The next day, Amador walked making the leg to the side, as if it was a neuropathy. He started to eat and write with the left hand, since it was impossible to do it with his right hand. By Sunday, March 29, Amador no longer moved his right arm in its entirety. We took him immediately to the Children's Hospital, and they informed us that it was a neurological issue, and we had to perform a magnetic resonance imaging (MRI).

That evening, he underwent MRI, and it turned out that he had a tumor in the brainstem. It was not possible to get a biopsy because of the sensitivity of the very delicate location in the medulla. As parents, this was the most painful news that we had ever received in our entire lives. We understood what a brain tumor meant, but we never guessed how delicate and perhaps fatal a brainstem glioma could be.

In our desperation, we looked for the best possible solution locally as well as internationally. We were terrified to hear the words "brain surgery," so we tried to avoid any possibility of an operation.

In the next few days, Amador was better after receiving high-dose steroids; he began to talk in a habitual way. He also recovered some movements. On April 6, Amador underwent gamma knife radiosurgery. It seemed to be successful, as his neurological function continued to improve. He was transferred to a rehabilitation center, where he received intense physiotherapy. He had some improvement, but 6 weeks later, his neurological function began to deteriorate. On Sunday, May 17, Amador had irregular respiratory efforts, and he required emergent admission to the intensive care unit (ICU).

The doctors informed us that he had a severe pneumonia. The following day, he had a respiratory arrest, which required resuscitation. The tumor had not grown but developed cystic components instead, which further compressed the important neural structures. He entered the operating room, and, because part of the inflated cyst was outside of the brainstem, they were able to take a biopsy sample. After 7 days

of ICU care, Amador started to recover, and he was extubated. He was a very intelligent child. He knew about his condition, and his worst fear was not being able to return to home. He suffered from stress when he was separated from his parents, since medical protocols in Mexico do not allow parents to stay close to their children in the pediatric ICU. Three days passed, and, again, he suffered from another respiratory arrest. We decided with the doctors that the best chance was to perform a tracheostomy. There was no time to tell Amador, so he was very angry and upset when he woke up without being able to speak or breath.

A few days passed, and the wound began to become infected. In turn, the biopsy indicated that it was a Grade 2 tumor, and, in other sections, it was a Grade 1 astrocytoma. However, there was a study that marked it as Grade 3. The oncology team started chemotherapy, but he developed several complications. Obviously, chemotherapy lowered his immune defenses, and he developed a wound infection. Amador had two ventricular drains to cleanse the infection in the cerebrospinal fluid (CSF). After 2 months of being in the ICU, the infection was treated, but the tumor continued to grow. The strangest thing about brainstem gliomas is that Amador was conscious in every minute and every second of this process. We read books, sang, and talked to him, and he understood everything; Amador never lost consciousness until the last minute.

We were transferred to another specialized unit where the team stabilized him in preparation for another surgery. Amador had already turned 13 years old. His condition was very complicated, but we all had that illusion. On August 13, I had to accompany him to the operating room, and he entered surgery at 10 am. At 1:00 pm, the surgeons came out to let us know that the surgery had been successful; the tumor was still a Grade 1 and was not malignant. Unfortunately, the infection was still present in the CSF and in the cyst fluid. The organism was a resistant bacterium.

The day after the surgery, Amador began to move his limbs. It made him happy. He laughed, a gesture that he could not do since months before. He moved his lips with greater emphasis and could move his toes. The infectious disease specialists had the difficult task of treating the *Escherichia coli* in Amador's head, since it was extremely disseminated throughout his brain. Although he was on the strongest antibiotics, we began to see a decline in his mood and neurological function. On the morning of August 21, an MRI demonstrated no solid tumor or cyst but inflammation in his brainstem and spinal cord. Two hours later, Amador went into a coma and cardiopulmonary arrest. The ICU and cardiology teams tried to revive his heart while we decided if we would connect him to the extracorporeal membrane oxygenation (ECMO) machine or not. However, I said, "Enough has been done." We had discussed the effects and damages after several minutes of cardiopulmonary resuscitation (CPR). My husband tried to extend what was inevitable, but we finally decided to let Amador's soul fly.

The soul of Amador flew at the hospital in front of 50 doctors who did everything possible to save his life. When did the brainstem tumor start to grow in Amador's head? Why do brainstem gliomas develop in children's brains? Did Amador have this tumor when he was born? Could we have detected the tumor in time? So many questions arise, and we still do not know the answers. The truth is that some of us

have to live this experience that makes us suffer, feel pain, grow, transform, and meet people who struggle daily to find these possible answers. Without a doubt, I will always fight as Amador's mother for being part of a world with better answers to our endless questions.

Mexico City, Mexico

Veronica Martinez Senties

Foreword 2

Help crack the code...

“I think we found something...I think we found something.” These are the words that will live forever in my mind, my heart, and my soul. These words that, for the last 12 years, have been the nemesis of my wife, my family, our community, and myself, and which we have chosen to make our fight to conquer and overcome.

One cannot imagine what happens when someone walks into a room and tells you that they think they found something. Your head starts spinning, and your mind goes all over the place, not knowing where you should turn, what does this mean, what should you think, and what should you do. As a parent, there is nothing on Earth worse than something happening to any child and, God forbid, your own child.

When faced with the unthinkable, a diagnosis of an inoperable brain tumor in the brainstem of our son, we decided not to be bystanders but rather to stand up and fight to see the change that we needed to happen, the answer – a cure. We went to and spoke with so many doctors and hospitals looking for answers, looking for that “special key” that might unlock the door to something, to anything. What we learned was that the key does not exist, yet! When we asked why, and where we were at it in research, the answer was always the same – “not very far along at all.” When I questioned the reason, I was always assured it was not from a lack of brain power but rather because of a lack of research funds.

Hence, the Ians Friends Foundation, a pediatric brain tumor research foundation, was born. What started as grassroots organization has now grown tremendously and has been able to fund pediatric brain tumor research around the country. While advancements have been made, with some projects having been successful, and/or having led to clinical trials, the unfortunate truth is that we still do not have a cure.

Is it the location that is the biggest issue? Who knows? You always hear in real estate: “location, location, location!” Well, I can tell you that this location sucks! Is it the lack of federal funding that is the major issue? Probably one of the major issues for sure. With less than 4% of all federal funds going to all of kids’ cancers and less than 0.5% going to the number one cause of health-related childhood deaths in children under the age of 20, we need more funding to get closer to a cure.

What I can say is that the doctors, many of whom have collaborated in writing this book, including Dr. George I. Jallo, are incredible people who happily would put themselves out of business. These doctors are desperately trying to find what will give a parent the greatest gift they could ever receive, the gift of a cure for their child. Again, to date, a cure still does not exist, but with hope, love, and hard work, God willing one will be available and hopefully soon.

Through this collaboration of brilliant minds, for the first time, there is now a resource, in essence a 360-degree blueprint of brainstem tumors. However, as I stated previously, there is still no cure. So, help find one. Yoda said, “Do or not do, there is no try!” As someone reading this book, you have now been given the blueprint to help and join those who are living by the mantra: “TRY just does not work.” So, read this book and see if you can help be the one who cracks the code. Unlocking the answer to a cure will truly be life-changing. If you are that person or can help in any way, I promise you that helping change the life of just one person will help save many generations to come.

As the chairman of a pediatric brain tumor research foundation, I thank you for reading this book and devoting your time and thought to help solve an issue that so many families need a solution for. As a parent of a son with a pediatric brainstem tumor, I beg you to help find a cure, to help crack the code!

I sincerely hope this book will give you the insight that you need to be the one to help the many. In advance, I thank you for your time and your efforts, and as the mantra of Ian’s Friends Foundation goes, “Until there is a cure!”

Atlanta, GA, USA

Phil Yagoda

Preface

Over the last 50 years, our understanding of the different lesions affecting the brainstem underwent exponential growth, triggering rapid paradigm shifts in the management strategies for these lesions. Similar to any other central nervous system structure, a wide spectrum of pathologies can affect the brainstem, including but not limited to tumors (benign or malignant, diffuse or focal, intrinsic or exophytic, solid, cystic, or mixed), vascular lesions (hemorrhage, aneurysm, arteriovenous or cavernous malformation), infectious lesions (abscess, encephalitis), and inflammatory/demyelinating lesions (multiple sclerosis, neuromyelitis optica spectrum disorder, connective tissue diseases). Previously categorized as inoperable, brainstem tumors and vascular lesions are more often managed by a multidisciplinary team of neurosurgeons, neuro-oncologists, and/or endovascular surgeons today than ever before. The ultimate goal of the contemporary management strategies for such lesions is to provide a complete cure with minimum invasiveness.

Brainstem pathologies remain the most challenging to manage surgically due to the high eloquence and the deep and hidden location of the brainstem, turning surgical treatment of brainstem pathologies into one of the most complex and demanding fields in neurosurgery. In recent years, however, technological advancements have allowed us to stretch the once rigid borders and limitations in the treatment of brainstem pathologies. Textbooks focusing on brainstem surgery are scarce. Therefore, we decided that the inception of this book will involve international leading figures in the field of brainstem surgery. Our intention was to cover every aspect of the management of brainstem pathologies. It is our sincere hope that this first edition will give the reader a thorough and full perspective of brainstem surgery as well as the diagnosis and management of related pathologies.

In this first edition, we attempt to guide the reader on this very complex anatomical territory, in which any pathology will lead to grave consequences. The book will take the reader through the depth of understanding the complex architecture of the brainstem in the clinical context, emphasizing the current treatment of different brainstem pathologies and reviewing what the future holds for the management of these pathologies. The book presents a review of the current state-of-the-art preoperative assessment modalities and surgical techniques, with extensive details

elaborated by respected experts for every topic, and covers brainstem-related pathologies from infancy to adulthood. Altogether, there are 15 chapters in this edition, focusing on current literature with guidance and pearls from current masters in the field.

The book starts with reviewing the history of diagnosing and managing brainstem pathologies. The rest of the book is organized in a way that Chaps. 2, 3, and 4 are focused on describing the complex anatomy, the clinical presentation, and the facts and pearls of brainstem imaging, respectively. Chapter 5 thoroughly discusses intraoperative neuromonitoring, a crucial tool for any surgical intervention in the brainstem. Chapters 6, 7, 8, 9, and 10 deal with a variety of brainstem pathologies and their current treatment paradigms. Chapters 11, 12, and 13 offer a comprehensive description of the different surgical approaches to the midbrain, pons, and medulla oblongata, respectively. The book is then wrapped up with two chapters describing the current and future adjuvant therapies. The thorough text is enriched with diagnostic and surgical images that cover almost all types of brainstem lesions reported in the literature. The book is written in a way that neurosurgery specialists and fellows will feel comfortable navigating throughout its contents, and the enthusiastic neurosurgery residents will find this book as a very valuable guide for understanding the complex management of brainstem tumors. Thanks to the broad list of specialists writing the different chapters, we also believe that this textbook is a useful reference book, even for experienced subspecialists dealing with brainstem treatment and surgery. Since we have emphasized the breakdown of complexity to simple steps and solutions, we believe that this book can also serve as a reference book for anyone who is involved in the treatment of patients suffering from brainstem pathologies, which may include the medical team, adult and pediatric neurosurgeons, neurologists, neuro-oncologists, residents and fellows, clinical neuropsychologists, electrophysiologists, neuroradiologists, and medical students who have a passion to learn about the assessment and surgical management of patients with brainstem diseases.

The contributing authors of this book's chapters are field experts from around the globe and are currently practicing in different countries in Asia, Europe, and North America. They represent a wide range of disciplines and experiences. The authors were given considerable flexibility and independence in writing the chapters so that they can share their own experience and knowledge with the reader without any limitation. We are honored to assemble and edit this vast body of work focusing on such a complex field in neurosurgery. We are grateful to our contributors for making this happen in a relatively short time!

Saint Petersburg, FL, USA
Saint Petersburg, FL, USA
Danville, PA, USA

George I. Jallo
Mohammad Hassan A. Noureldine
Nir Shimony

Acknowledgments

We would like to thank our colleagues, neuro-oncologists, neurologists, and neuro-physiologists, who are a crucial part of the multidisciplinary team, taking care of patients suffering from these complex pathologies. We would also like to deeply acknowledge our mentors, Fred Epstein, Rick Abbott, Shlomi Constantini, and Zvi Ram, who have seeded the enthusiasm to explore and study this complex field in neurosurgery. We also thank our fellows, residents, and medical students for their continuous stimulation and insight. Most of all, we are honored to care for our adult patients who trust us to carry their treatment decisions and for our children patients and their parents who entrust us with their most precious treasure.

We are grateful to Springer editorial and production team members. Their professionalism, expert assistance, and guidance enabled us to complete this book.

Contents

1	History of Brainstem Glioma Surgery	1
	Andrew J. Kobets and James T. Goodrich	
2	Anatomy of the Brainstem	41
	Jaafar Basma, Dom E. Mahoney, Andrei Tudose, Douglas Taylor, Kaan Yağmurlu, and Jeffrey Sorenson	
3	Imaging of Brainstem Lesions	61
	Miguel A. Flores, Ari M. Blitz, Sachin K. Gujar, and Thierry A. G. M. Huisman	
4	Clinical Presentation and Assessment for Brainstem Tumors	95
	Bahattin Tanrikulu and M. Memet Özek	
5	Intraoperative Neurophysiological Monitoring During Brainstem Surgery	109
	Francesco Sala and Alberto D’Amico	
6	Low-Grade Pediatric Brainstem Gliomas	131
	Jonathan Roth, Danil A. Kozyrev, and Shlomi Constantini	
7	High-Grade Tumors of the Brainstem (Except DIPG)	145
	Soma Sengupta, Daniel Pomeranz Krummel, Brent D. Weinberg, and Tobey J. MacDonald	
8	Diffuse Midline Glioma – Diffuse Intrinsic Pontine Glioma	159
	Mohammad Hassan A. Nouredine, Nir Shimony, and George I. Jallo	
9	Surgery for Vascular Lesions of the Brainstem	195
	Michael J. Lang and Michael T. Lawton	
10	Inflammatory and Infectious Lesions of the Brainstem	217
	Rechdi Ahdab, Fateme Salehi, and Raghid Kikano	

11 Surgical Approaches to Mesencephalic (Midbrain) Tumors 247
Nir Shimony, David S. Hersh, and Frederick A. Boop

12 Surgical Approaches to Pontine Tumors 265
Mohammad Hassan A. Noureldine, Nir Shimony,
and George I. Jallo

13 Surgical Approaches to Medullary Tumors 295
Helmut Bertalanffy, Souvik Kar, and Christian Hartmann

14 Radiation and Chemotherapy for Brainstem Tumors 321
Katherine E. Warren

15 Future Therapies for Malignant Brainstem Tumors 347
Zhiping Zhou and Mark M. Souweidane

Index 393

Contributors

Rechdi Ahdab, MD, PhD Department of Internal Medicine, Lebanese American University Medical Center, Rizk Hospital, Beirut, Lebanon

Jaafar Basma, MD Department of Neurosurgery, University of Tennessee Health Science Center, Memphis, TN, USA

Helmut Bertalanffy, MD, PhD Vascular Neurosurgery, International Neuroscience Institute, Hannover, Germany

Ari M. Blitz, MD Division Chief, Neuroradiology, University Hospitals, Case Western Reserve University, Cleveland, OH, USA

Frederick A. Boop, MD St. Jude Endowed Chair of Pediatric Neurosurgery, University of Tennessee Health Sciences Center, Memphis, TN, USA

Le Bonheur Neurosciences Institute, Memphis, TN, USA

Semmes Murphey Clinic, Memphis, TN, USA

Shlomi Constantini, MD, MSc Department of Pediatric Neurosurgery, Dana Children's Hospital, Tel-Aviv Medical Center, Tel-Aviv, Israel

Alberto D'Amico, MD Section of Neurosurgery, Department of Neurosciences, Biomedicine and Movement Sciences, University Hospital, Verona, Italy

Miguel A. Flores, MD Division of Neuroradiology, Russell H. Morgan Department of Radiology and Radiological Science, Johns Hopkins Hospital, Baltimore, MD, USA

James T. Goodrich, MD, PhD Division of Pediatric Neurosurgery, Leo M. Davidoff Department of Neurological Surgery, Montefiore Medical Center, Albert Einstein College of Medicine, Bronx, NY, USA

Sachin K. Gujar, MBBS Division of Neuroradiology, Russell H. Morgan Department of Radiology and Radiological Science, Johns Hopkins Hospital, Baltimore, MD, USA

Christian Hartmann, MD, PhD Department of Neuropathology, Institute of Pathology, Hannover Medical School – MHH, Hannover, Germany

David S. Hersh, MD Pediatric Neurosurgery, Department of Neurosurgery, Le Bonheur Children's Hospital, Memphis, TN, USA

Thierry A. G. M. Huisman, MD, PD, EDiNR, EDIPNR Radiologist-in-Chief and Edward B. Singleton Chair of Radiology, Department of Radiology, Texas Children's Hospital and Baylor College of Medicine, Houston, TX, USA

George I. Jallo, MD Department of Neurosurgery, Institute for Brain Protection Sciences, Johns Hopkins University School of Medicine, Johns Hopkins All Children's Hospital, Saint Petersburg, FL, USA

Souvik Kar, PhD International Neuroscience Institute, Hannover, Germany

Raghid Kikano, MD Radiology Department, Lebanese American University Medical Center, Rizk Hospital, Beirut, Lebanon

Andrew J. Kobets, MD, MHS Division of Pediatric Neurosurgery, Leo M. Davidoff Department of Neurological Surgery, Montefiore Medical Center, Albert Einstein College of Medicine, Bronx, NY, USA

Danil A. Kozyrev, MD Department of Pediatric Neurosurgery, Dana Children's Hospital, Tel-Aviv Medical Center, Tel-Aviv, Israel

Daniel Pomeranz Krummel, PhD University of Cincinnati Medical Center, Cincinnati, OH, USA

Michael J. Lang, MD Department of Neurosurgery, Barrow Neurological Institute, Phoenix, AZ, USA

Michael T. Lawton, MD Department of Neurosurgery, Barrow Neurological Institute, Phoenix, AZ, USA

Tobey J. MacDonald, MD Department of Pediatrics, Emory University School of Medicine, Aflac Cancer & Blood Disorders Center, and Children's Healthcare of Atlanta, Atlanta, GA, USA

Dom E. Mahoney, BSc Faculty of Health Sciences, University of Bristol, Bristol, UK

Mohammad Hassan A. Noureldine, MD, MSc Department of Neurosurgery, Institute for Brain Protection Sciences, Johns Hopkins University School of Medicine, Johns Hopkins All Children's Hospital, Saint Petersburg, FL, USA

M. Memet Özek, MD Division of Pediatric Neurosurgery, Department of Neurosurgery, Acibadem University School of Medicine, Istanbul, Turkey

Jonathan Roth, MD Department of Pediatric Neurosurgery, Dana Children's Hospital, Tel-Aviv Medical Center, Tel-Aviv, Israel

Francesco Sala, MD Section of Neurosurgery, Department of Neurosciences, Biomedicine and Movement Sciences, University Hospital, Verona, Italy

Fateme Salehi, MD, MSc, FRCPC Department of Neuroradiology, Toronto Western Hospital, Toronto, ON, Canada

Soma Sengupta, MD, PhD University of Cincinnati Brain Tumor Center, Cincinnati, OH, USA

Nir Shimony, MD Johns Hopkins University, School of Medicine, Department of Neurosurgery, Baltimore, MD, USA

Geisinger Commonwealth School of Medicine, Department of Neurosurgery, Danville, PA, USA

Institute of Neuroscience, Geisinger Medical Center, Geisinger Commonwealth School of Medicine, Danville, PA, USA

Jeffrey Sorenson, MD Department of Neurosurgery, University of Tennessee Health Science Center, Memphis, TN, USA

Semmes Murphey Brain and Spine Institute, Memphis, TN, USA

Mark M. Souweidane, MD, FACS, FAAP Department of Neurological Surgery, Weill Medical College of Cornell University, New York, NY, USA

Department of Pediatrics, Weill Medical College of Cornell University, New York, NY, USA

Department of Neurosurgery, Memorial Sloan Kettering Cancer Center, New York, NY, USA

Bahattin Tanrikulu, MD Division of Pediatric Neurosurgery, Department of Neurosurgery, Acibadem University School of Medicine, Istanbul, Turkey

Douglas Taylor, MD Department of Neurosurgery, University of Tennessee Health Science Center, Memphis, TN, USA

Andrei Tudose, MD Department of Neurosurgery, North Bristol Trust, Bristol, UK

Katherine E. Warren, MD Pediatric Neuro-Oncology, Dana Farber Cancer Institute, Boston, MA, USA

Brent D. Weinberg, MD, PhD Department of Radiology and Imaging Sciences, Emory University School of Medicine, Atlanta, GA, USA

Kaan Yağmurlu, MD Department of Neurosurgery, University of Virginia, Charlottesville, VA, USA

Zhiping Zhou, MD, PhD Department of Pediatrics, Memorial Sloan Kettering Cancer Center, New York, NY, USA

Chapter 1

History of Brainstem Glioma Surgery



Andrew J. Kobets and James T. Goodrich

Abbreviations

BG	Brain stem glioma
CP	Cerebellopontine
EGFR	Epidermal growth factor receptor
ICU	Intensive care unit
MRI	Magnetic resonance imaging

1.1 Introduction

Our understanding of brainstem gliomas (BGs) has matured immensely over the last two centuries, but on the scale of our greater understanding of neurological surgery, or even posterior fossa surgery, it remains a recent advancement. The incremental unraveling of anatomic relationships and surgical approaches by pioneering individuals in the context of improving antisepsis and neurological localization has allowed for the progressive comprehension of treatment strategies for BGs, but it has not been until the modern era that any meaningful therapeutic advancements have been made. Longstanding beliefs held by early surgeons considered the brainstem an extremely sensitive region to manipulation in which the patient's respiration, circulation, and wakefulness could rapidly be compromised resulting in significant morbidity and even death. Surgeons avoided surgery on this area or lacked the neurophysiological awareness to approach lesions in this region outright. The neuroanatomy began to be carved out of early renaissance dissections by artistic masters who paved the way for generations of anatomists, scientists, and surgeons to follow with further descriptions of the brainstem and cranial nerve anatomy as well as post-mortem and early intraoperative reports. With the development of posterior fossa approaches, the first pioneers

A. J. Kobets (✉) · J. T. Goodrich
Division of Pediatric Neurosurgery, Leo M. Davidoff Department of Neurological Surgery,
Montefiore Medical Center, Albert Einstein College of Medicine, Bronx, NY, USA
e-mail: Akobets@Montefiore.org

attempted resection with very little success, and it was not until the much later delineation and characterization of the heterogeneous nature of these lesions in the twentieth century that it was demonstrated that long-term survival was possible in a subset of patients. Finally, modern treatment paradigms were developed to optimize survival in the latter half of the twentieth century, utilizing major advances in imaging and stereotactic localization. As we trace the history of BGs, it is apparent that the few meaningful successes have unfortunately been riddled by the countless poor outcomes in which patients succumbed to their disease. Much remains to be written and discovered about our developing history of BGs, and we are very far from the end of the story. This chapter will review the evolution of surgical techniques and management of BGs from the first inferences of brainstem function and anatomy, to the first surgical reports by the early pioneers, to the modern era, with a focus on the individuals whose genius propelled our understanding of the brainstem and BGs forward.

1.2 Classical Era

For thousands of years in antiquity, little had been understood about the brain, and whatever physiology or anatomy had been known had been riddled with lore and myth, and the overwhelming majority of the study of neuroscience had been in the context of cranial trauma management. Galen of Pergamon (c. 129 AD – c. 210 AD), the well-known surgeon of the gladiators, was the first prominent figure to codify treatment strategies for cranial trauma and establish rudimentary anatomic relationships, which whether correct or incorrect, would become dogma for the next millennium and a half [1, 2]. In regard to investigations into the structure and function of the brainstem, Galen was the first to study the brainstem in a scientific manner on live monkeys and ungulates. He demonstrated that surgery in this region could result in cessation of respiratory function, plegia, anesthesia, voice changes, as well as death. He voiced the importance of a firm grasp of the anatomy in this region, although the methodology was flawed as he attempted to translate much of his knowledge from animal to human anatomy unsuccessfully. Nevertheless, his descriptions of the importance of this structure in maintaining the vital functions of the organism were extremely important as a basis for the next advances in our understanding of the brainstem, even though these next steps would not be undertaken for centuries to come due the warnings Galen would document of the dangers of study of this region in humans.

1.3 Fifteenth Through Seventeenth Centuries

As stated, it took nearly a millennium and a half for the dogma of antiquity to be rebuked by physicians who began to challenge the teachings of the past, which were often in conflict with their own bedside observations during anatomical dissections. While many barber-surgeons were still hindered by the adherence to the dogmas of

the past, which had been deeply engrained in their apprenticeships, few received any formal education, and the physicians who did, failed to develop a new perspective on anatomic studies as they were still taught the teachings of Galen in a dogmatic manner. It was first the great artists who in fact questioned the growing number of discrepancies arising between Greco-Roman teachings and the anatomic dissections that flourished during the renaissance. Michaelangelo di Lodovico Buonarroti Simoni (1475–1564), Leonardo da Vinci (1452–1519), and Tiziano Vecelli (Titian, c. 1488–1576) lead the way for Berengario da Carpi (1470–1550), Johannes Dryander (1500–1560), Andreas Vesalius (1514–1564), and others who spearheaded a new movement to correct the centuries-old inaccuracies of antiquity by using clinical observation to formulate anatomic knowledge of the posterior fossa and brainstem [3, 4] (Fig. 1.1). While neither a surgeon nor a physician, Leonardo was a key early figure in the observation and depiction of the structures in the posterior fossa, in a manner that was based on clinical observation, which had never been completed before [5–7]. In his lifetime, he created nearly 750 anatomical drawings, depictions of both surface and deep anatomy, in order to further his artistic work as well as engage his curiosity of the body. William Hunter (1728–1793), upon rediscovery of these works by Leonardo after nearly two centuries of being lost, stated, ‘*Leonardo had been a gen-*

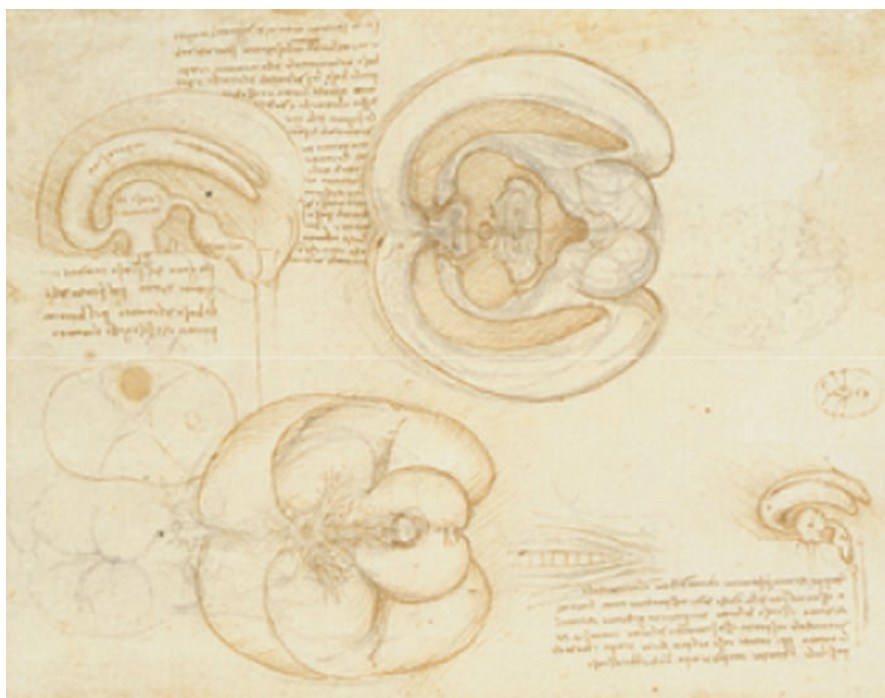


Fig. 1.1 Early depiction of the ventricular system by Leonardo da Vinci, with the first demonstration of the third and fourth ventricles with rudimentary brainstem in the right lower corner. From the senior author's personal collection

eral and a deep student. When I consider what pains he has taken upon every part of the body, the superiority of his universal genius...and the attention with which such a man would examine and see objects which he was to draw, I am fully persuaded that Leonardo was the best Anatomist, at that time, in the world.' [8]. This paradigm shift led by Leonardo inspired many other surgeons to work toward further unraveling the intricacies of the brain based on observation and direct study and not by the centuries-old work that few considered to question.

Johannes Dryander (1500–1560), developed his own anatomically accurate depictions of the posterior fossa anatomy in his 1537 monograph, detailing the earliest known demonstration of the tentorium, an early numbering of the cranial nerves, and early depictions of the anatomical relationship of the cerebellum and the brainstem [9, 10] (Fig. 1.2). Andreas Vesalius (1514–1564) was another major figure of the sixteenth century who created impressive anatomical plates that are still considered today as one of the best anatomic works of his era [11]. He depicted early relationships of posterior fossa structures in an unprecedented manner based on his strong belief that the anatomist must perform his own dissections. Vesalius published *De Humani Corporis Fabrica* in 1543, in which he included some of the most detailed images of the brainstem to date, demonstrating the brainstem by itself, rotated out of the skull base and with the exiting cranial nerves (Figs. 1.3, 1.4, and 1.5). The detail depicted by Vesalius

Fig. 1.2 Dryander provides the earliest illustration of the posterior fossa, cerebellum, and brainstem. From the senior author's personal collection

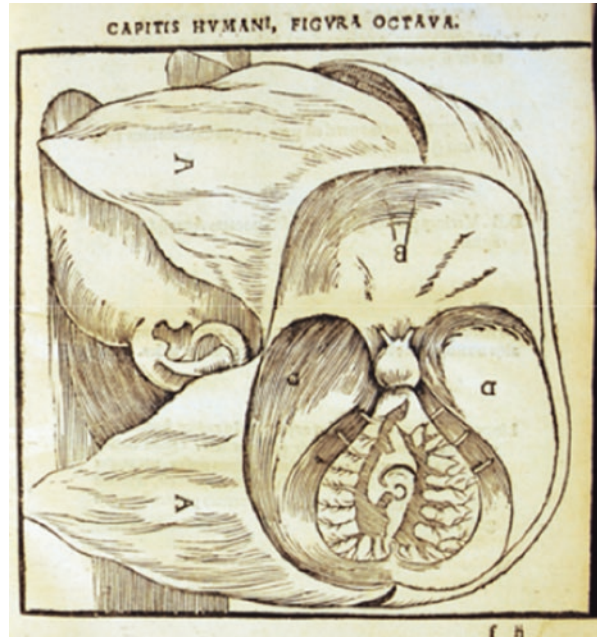
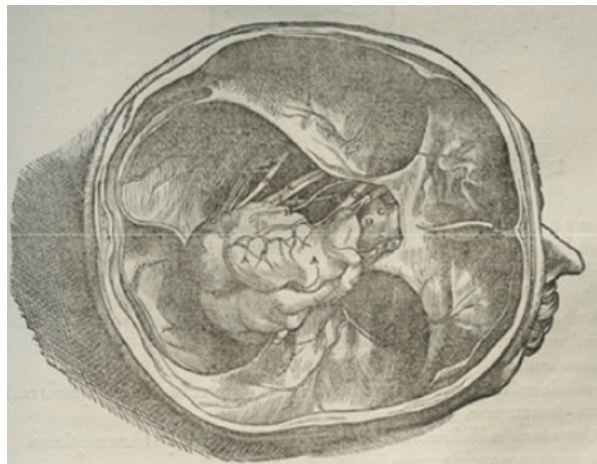


Fig. 1.3 Vesalius's depiction of the cerebellum and brainstem from his masterpiece *De Humani Corporis Fabrica*. From the senior author's personal collection



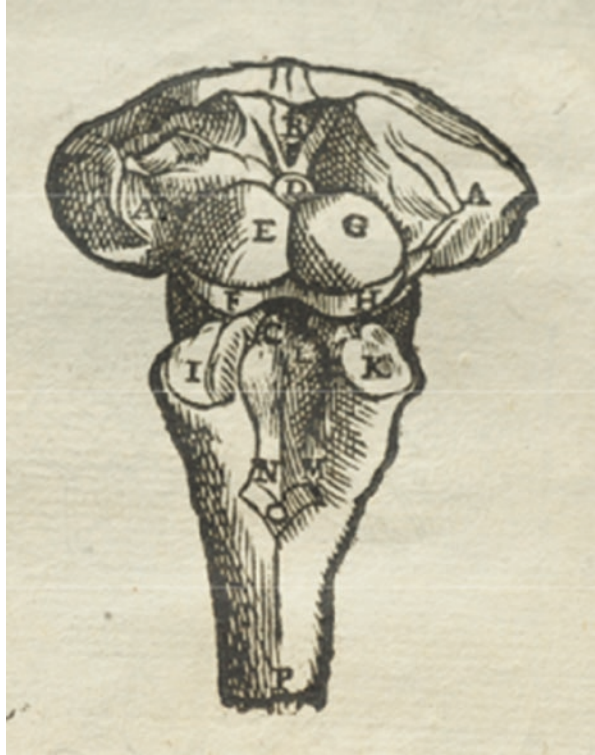
Fig. 1.4 Drawing of the brainstem and cranial nerves with the cerebellum and cerebrum removed, which is thought to be prepared by Vesalius. From the senior author's personal collection



was unprecedented and provided anatomical descriptions for surgeons of the time unlike what they have ever seen previously.

During the seventeenth century, the anatomic illustrations of the brain became far more detailed and refined, namely with the work of Thomas Willis (1621–1675) in *Cerebri Anatome*, where, with the assistance of Christopher Wren (1632–1723), illustrations of the brain surface anatomy as well as the brainstem and cranial nerves, were depicted with unprecedented realism [12] (Figs. 1.6, 1.7, and 1.8). Humphrey

Fig. 1.5 Vesalius' drawing of the brainstem viewed from dorsally, with the colliculi and fourth ventricle centered in the image. An advanced and anatomically detailed image for the time. From the senior author's personal collection



Ridley (1653–1708) defined an even more comprehensive review of pineal and posterior fossa anatomy than that of Willis and was the first to demonstrate the correct course of the third cranial nerve between the superior cerebellar artery and the posterior cerebral artery. The origins of the cranial nerves were clearly outlined, and the anatomy of the brainstem was further defined by Ridley's more accurate depictions.

The fifteenth through seventeenth centuries heralded in a new era for the description of brain anatomy that questioned the dogmas of the past and reconciled inaccuracies with clinical observation of cerebral anatomy. While the work of Galen stood for so long as the reference for cranial anatomy, this period of the early renaissance was a period of refinement, correction, and addition to the works of antiquity, which would form the new foundation for our understanding of the brainstem anatomy and pathophysiology into the modern era. Neuroanatomy was starting to be tied to the physiology of the brain, and scientific societies were beginning to be formed in this era to disseminate these medical advancements as had never been done before. Surgeons were still rudimentary in their techniques during this period but this great advancement in our understanding of brainstem anatomy would set the stage for the first surgical explorations and pathophysiological descriptions of lesions in the coming centuries.

Fig. 1.6 Drawing of Thomas Willis at the time of writing *Cerebri Anatome*. From the senior author's personal collection



1.4 Eighteenth Century

The eighteenth century heralded the advancement of education and surgical skills amongst surgeons, as they attained higher education and put a greater emphasis on bedside evaluation during their studies. For the most part, neurosurgical intervention revolved around trauma and true intraparenchymal surgery was quite rare. The identification of tumors was still in its infancy as they were thought to be a type of “fungus” or an unexplained growth of the brain. Further advancement of our understanding of tumors and other brain lesions would not be refined until the nineteenth century. Francois-Sauveur Morand (1697–1773) in 1768 first published a case of a large abscess removed successfully from the skull base and posterior fossa in a monk who presented with otitis media and mastoiditis, and who was successfully drained and survived the procedure [13]. Giovanni Battista Morgagni (1682–1771), a student of Valsalva, published his groundbreaking work *De sedibus, et causis*

Fig. 1.7 Title page from the first edition of *Cerebri Anatome* printed in London in 1664. From the senior author's personal collection

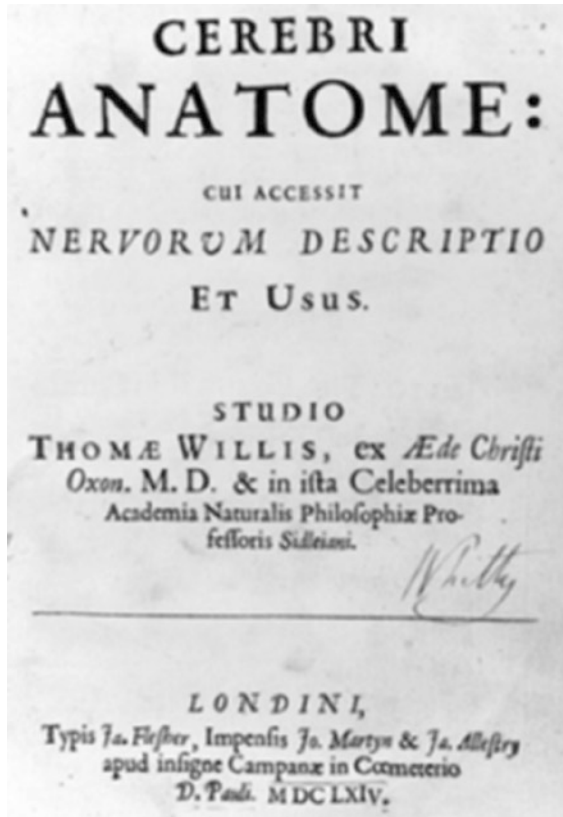


Fig. 1.8 Illustration of the eponymous "circle," which demonstrates the structure of the posterior fossa, and greater detail of the cranial nerve, pontine, brainstem, and cerebellar anatomy than had been previously described. From the senior author's personal collection

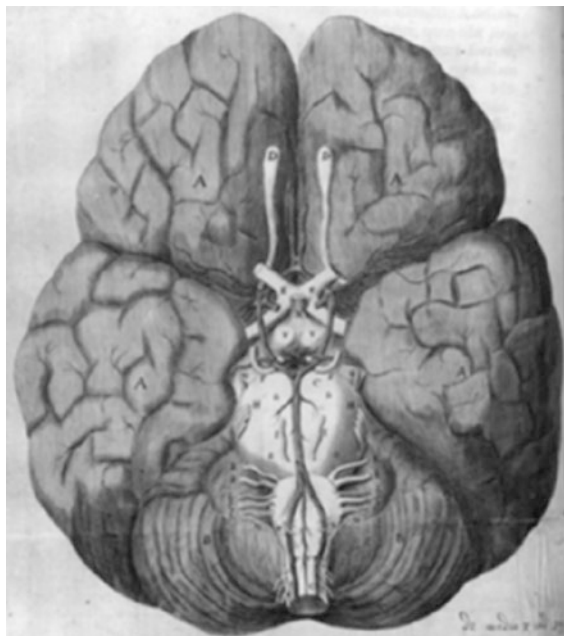


Fig. 1.9 Portrait of Morgagni. From the senior author's personal collection



morborum per anatomen in 1761, in which he discussed for the first time the categorization of lesions by pathological diagnosis and began to separate tumors from other commonly confused entities that were the result of infectious or inflammatory causes [14, 15] (Figs. 1.9 and 1.10). Describing his series of over 700 autopsies, he offered an explanation of treatments that were based on the diagnosis and the pathological basis of the disease.

In 1778, Samuel Thomas von Soemmering (1755–1830) was the first to demonstrate all 12 cranial nerve in history in his book *De basi encephali et originibus nervorum cranio egredientium*, refining the first reports of nine cranial nerves by Galen [16] (Figs. 1.11 and 1.12). Félix Vicq D’Azyr (1748–1794), for the first time in his *Traité d’anatomie et de physiologie*, demonstrated hand-colored plates of the brain prepared by Alexandre Briceau, a prominent engraver in Paris [17]. The detailed, colored sections were the most intricate and advanced of their time, demonstrating cerebellar and brainstem anatomy as it had never been accomplished before (Figs. 1.13, 1.14, and 1.15). Jacques Fabian Gautier D’Agoty (1717–1785)

Fig. 1.10 Title page from the first English translation of Morgagni's work *The Seats and Causes of Diseases*. From the senior author's personal collection

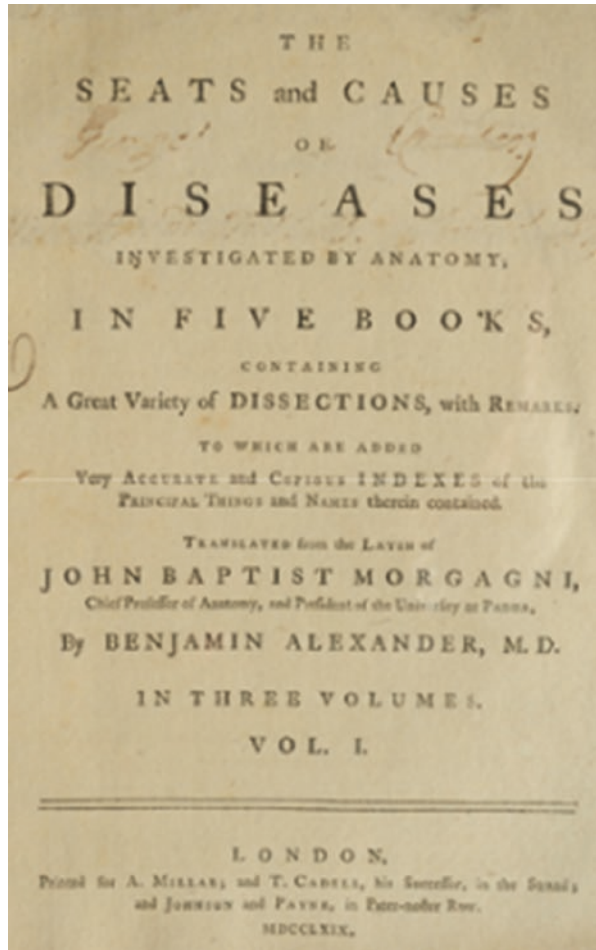


Fig. 1.11 Soemmering's detailed overview of the 12 cranial nerves. From the senior author's personal collection

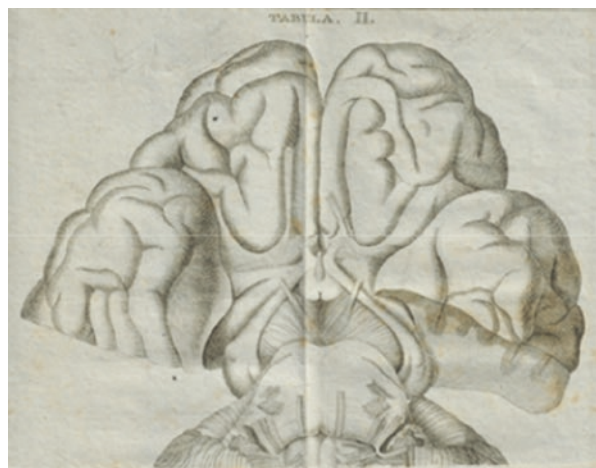


Fig. 1.12 Soemmering's depiction of the base of the brain, the pons, and the emanating cranial nerves. From the senior author's personal collection



Fig. 1.13 Title page of *Traité d'anatomie et de physiologie* by Vicq D'Azyr. From the senior author's personal collection

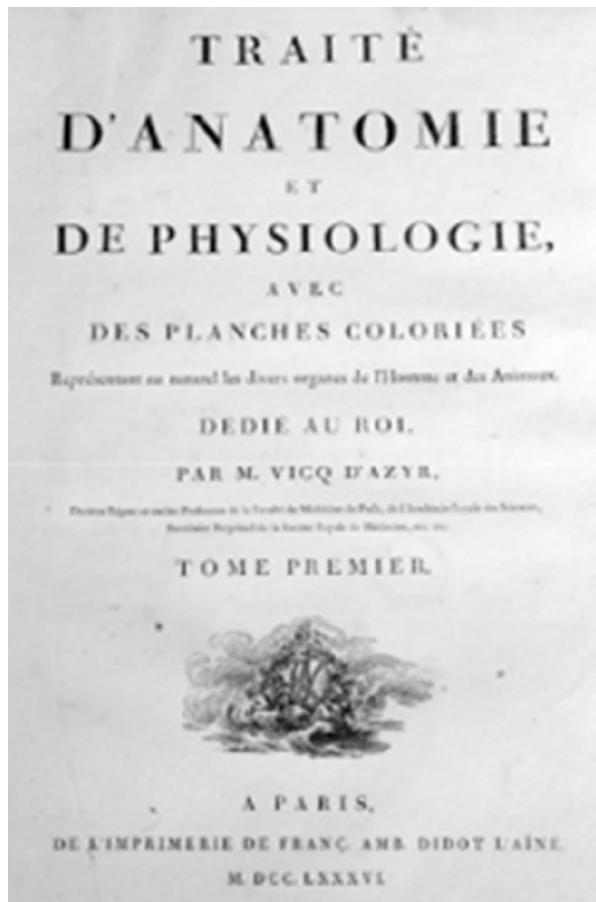


Fig. 1.14 Illustration by Vicq D'Azyr, with detailed anatomy of the pons and brainstem. From the senior author's personal collection

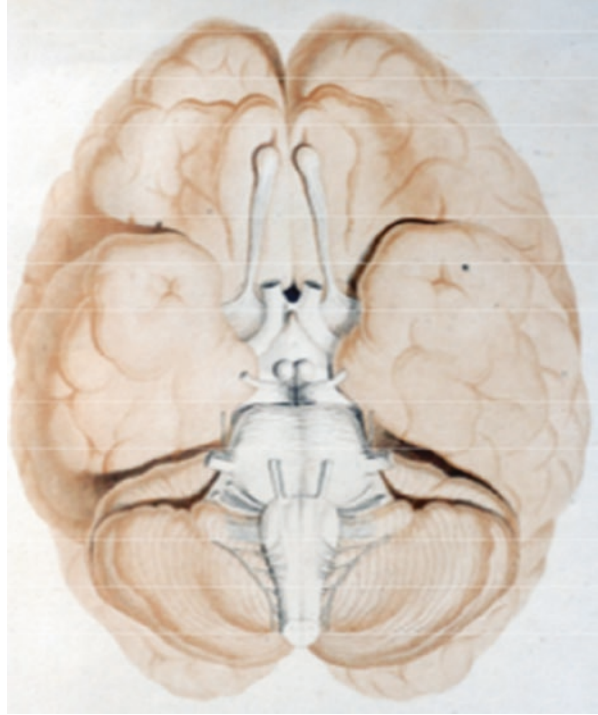


Fig. 1.15 Vicq D'Azyr's cross-section of the cerebellum showing the folia patterns and details of the brainstem. From the senior author's personal collection



Fig. 1.16 Title page from Gautier D'Agoty's seminal work on brain anatomy. From the senior author's personal collection



produced a similarly astounding work and used his background as a print maker and a pioneer in color printing to create life-sized colored plates that further made neuroanatomic studies palatable to the common surgeon of the era [18] (Figs. 1.16, 1.17, 1.18, and 1.19).

1.5 Nineteenth Century

The concept of different pathologies of the brain, coupled with even more realistic anatomically-accurate depictions of the brainstem and posterior fossa as well as higher education for surgeons at the time, resulted in incremental

Fig. 1.17 Detailed coronal section of the brainstem and cerebellum by Gautier D'Agoty. From the senior author's personal collection

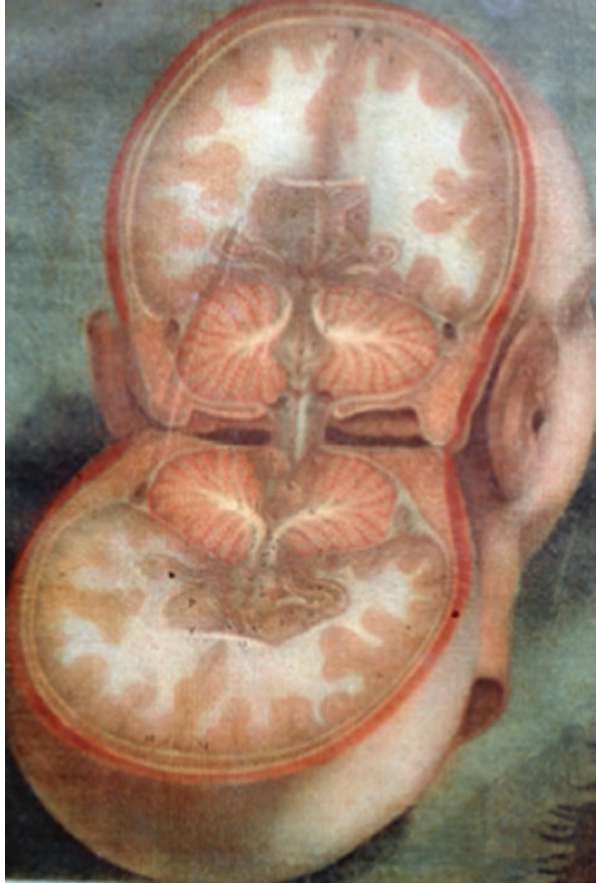


Fig. 1.18 Superbly detailed and colored view of the brain and brainstem lifted off the skull base in Gautier D'Agoty's work. From the senior author's personal collection

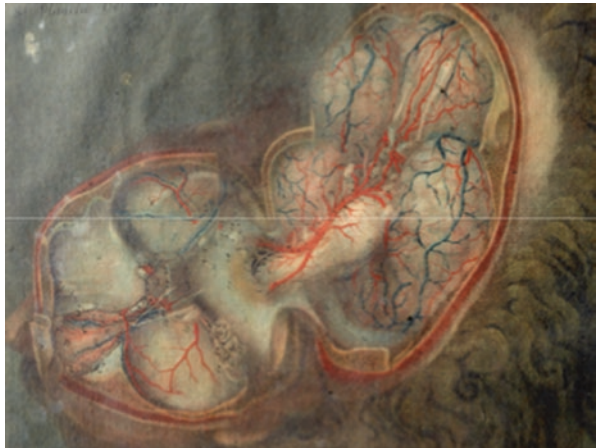


Fig. 1.19 Gautier D'Agoty details the venous sinuses and cerebellar hemispheres along with the cervical spine and nerve roots in this close-up image, with the skull and dura removed. From the senior author's personal collection



advancements of our understanding of brainstem anatomy in the eighteenth century, which would herald the first reports of brainstem tumors in the nineteenth century, as well as the first surgical explorations of the region that were possible largely due to developing antisepsis, anesthesia, and improved neurological localization [19].

These three key advances allowed for brain surgery to become a routine endeavor in a way that had never been possible prior to the nineteenth century. Antisepsis allowed for entry of the intracranial cavity without subjecting the patient to the 95% mortality risk of the past, largely due to infection. It was Oliver Wendell Holmes (1808–1894) and Ignác Fülöp Semmelweis (1818–1865) who noticed that obstetricians who had not washed their hands before procedures, compared to midwives who entered with clean hands and gowns, had much higher rates of infections in their patients [20, 21]. Whatever resistance they met from their contemporaries slowly faded with the discoveries of Louis Pasteur (1822–1895), Robert Koch (1843–1910), and Joseph Lister (1827–1912) who concreted the principle of antisepsis in the field of surgery [22–24] (Figs. 1.20 and 1.21). Mortality rates plummeted, and these principles took hold of surgical practice, supplementing the new use of steam sterilization, sterile gowns and gloves, and the use of metal surgical instruments. Improved neurological localization allowed surgeons to look for lesions in suspected anatomic regions that could potentially produce the patient's clinical syndrome. Sir Charles Bell (1774–1842), a Scottish surgeon and anatomist, composed an extremely detailed rendering of the brainstem in his time and described the differentiation between motor and sensory components of the cranial nerves [25, 26] (Fig. 1.22). In addition to his work on localization of function within the central nervous system, Bell also described the first posterior fossa tumor at the cerebellopontine (CP) angle (Fig. 1.23). In the 1860s, the so-called “decade of the brain,” G. T. Fritsch (1838–1927), E. Hitzig (1838–1907), and Paul Broca (1824–1880) substantially advanced the localization of function in the brain and started a revolution that would allow neurologists and neurosurgeons to localize the pathology based on

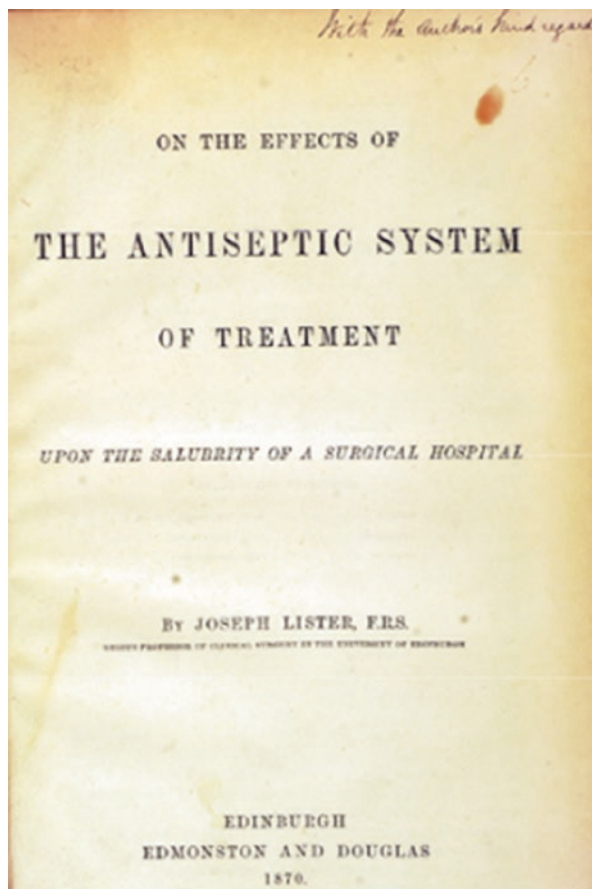
Fig. 1.20 Depiction of Sir Joseph Lister. From the senior author's personal collection



neurological deficits, nearly a century before the imaging revolution of the twentieth century [27, 28]. David Ferrier (1843–1928) removed brain regions in dogs in order to localize neurological function, similar to the work performed by Roberts Bartholow (1831–1904), in which he directly stimulated the brain and induced general seizures followed by contralateral weakness in patients in which he had been studying tumor localization as it related to clinical symptomatology [29–31]. Finally, anesthesia allowed the surgeon to take time with the procedure and work on an asleep patient without the threat that the patient would awaken and compromise the surgery. In the 1840s, nitrous oxide, ether, and chloroform were used for the first time. These discoveries were required to become routine for surgery of the brain and, in particular, for surgeons to endeavor upon surgery of the posterior fossa and brainstem.

Jean Cruveilhier (1791–1874) requires special praise for his work describing and illustrating posterior fossa pathology and studying the extensive pathological mate-

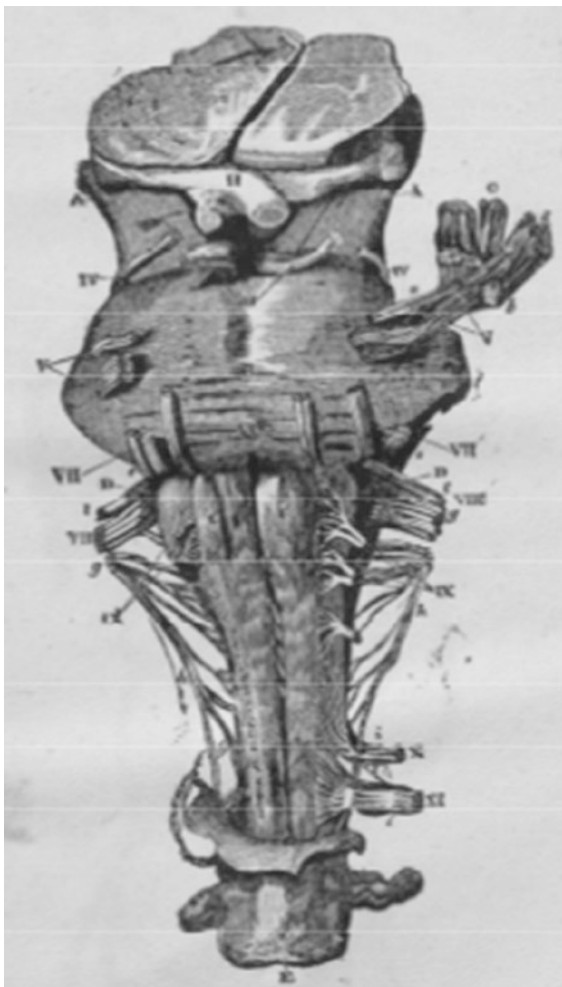
Fig. 1.21 Title page of Lister's monograph dealing with antiseptic surgery principles. From the senior author's personal collection



rial available for him during his post as the first chairman of pathology at the University of Paris. He described a CP angle tumor as well as an epidermoid lesion of the cerebellum and brainstem with stunningly realistic images in his work *Anatomie Pathologique de Corpus Humain* [32, 33] (Figs. 1.24, 1.25, 1.26, 1.27, 1.28, and 1.29). As a credit to his accurate and beautiful work, Harvey W. Cushing (1869–1939) recognized Cruveilhier and used some of his drawings in his own work [34, 35].

Another exceptional early work from the nineteenth century was composed by the pathologist Richard Bright (1789–1858), who in the second volume of his work *Reports of Medical Cases, Selected with a View of Illustrating the Symptoms and Cure of Diseases*, demonstrated the detailed anatomical relationships of structures of the posterior fossa, which would later help define surgical approaches to the brainstem [36] (Fig. 1.30). In his first volume, Bright was best known for his work on the kidney and was the first to describe glomerulonephri-

Fig. 1.22 Bell's superbly detailed description of the brainstem and cranial nerves. From the senior author's personal collection



tis (after which the eponymous Bright's disease was named), in addition to the relationship between edema, albuminuria and kidney disease, as well as nephrotic disease, through his astute clinicopathological descriptions. In the second volume of his book, published in two parts in 1831, Bright meticulously documented over 200 cases, coupled with 25 elegantly drawn plates, which would be credited as some of the most exquisite demonstrations of posterior fossa anatomy of the time. Bright provided detailed clinical notes on his patients and followed up with their pathological findings upon autopsy. Bright was the first in this series to describe a pediatric patient with a BG on post-mortem analysis, termed as *tumour of the Pons Varolii*. The beautifully detailed plates were the first to demonstrate a large expansile lesion in the pons from surface anatomy and sagittal sections (Figs. 1.31 and 1.32). This groundbreaking work appeared to be the first description of a BG in 1831. Bright's work, among his

Fig. 1.25 Cruveilhier's depiction of one of the first reported infiltrating tumors of the pons drawn in his work *Anatomie Pathologique de Corpus Humain*. From the senior author's personal collection

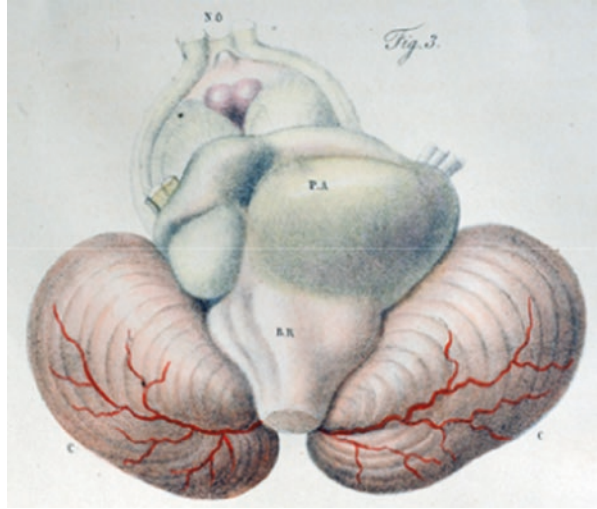


Fig. 1.26 Similar infiltrating tumor of the brainstem as depicted by Cruveilhier with punctate hemorrhages noted within the brainstem. From the senior author's personal collection



Fig. 1.27 Cruveilhier's depiction of an exophytic brainstem lesion arising from the pontomedullary junction. From the senior author's personal collection



Fig. 1.28 Sagittal section of the brainstem with a large epidermoid tumor arising from the midbrain from *Anatomie Pathologique de Corpus Humain*. From the senior author's personal collection



Fig. 1.29 Large epidermoid tumor of the skull base enveloping the brainstem, cranial nerves, and basilar artery. From the senior author's personal collection



contemporaries and those who preceded him, paved the way for the first true brain surgeries that were performed in the last quarter of the nineteenth century.

William Macewen (1848–1924) was one of the most successful early surgeons of the era, who – at the age of 40 – presented to the British Medical Association his first 21 brain surgeries, after which 18 patients survived for a long term [37, 38]. This address was the culmination of the cerebral localization and antiseptic techniques. He operated on four patients with posterior fossa lesions, only one of which perished perioperatively; this was an enormous advancement in reducing operative mortality for posterior fossa approaches. Macewen also innovated the use of endotracheal intubation over tracheostomy, the use of carbolic acid spray, and the donning of a sterilized operating room gown. Based on Macewen's experience,

Fig. 1.30 Bright's seminal work on the description of diseases of the brain and spinal cord. From the senior author's personal collection

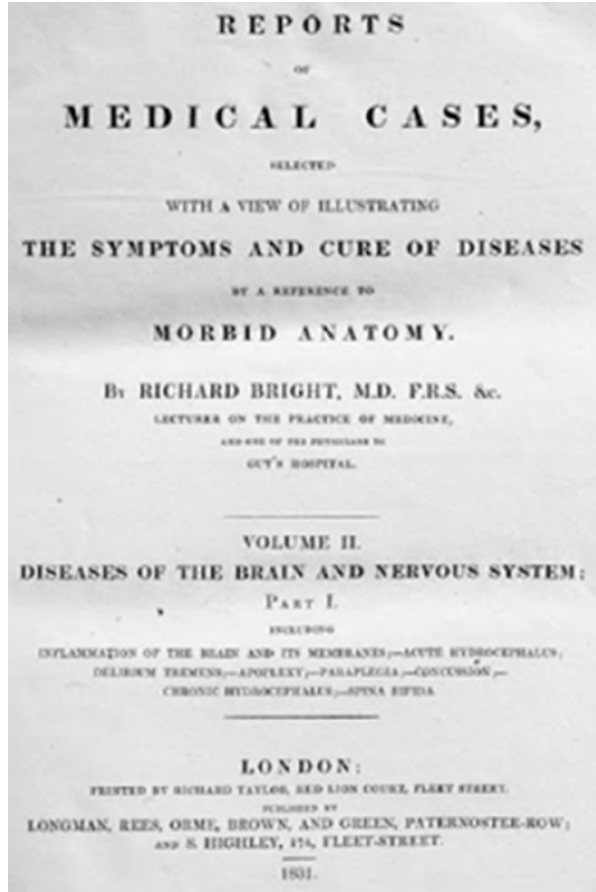


Fig. 1.31 A case of a pontine glioma demonstrated from a surface view in Bright's work. From the senior author's personal collection



Fig. 1.32 Sectional anatomy of the same pontine lesion in Bright's *Diseases of the Brain and Nervous System*. From the senior author's personal collection



autopsies, and other's surgical reports, the great New York neurologist M. Allen Starr (1854–1932) recognized and demonstrated that there was a propensity of tumors to rest within different cerebral tissues in different patients, for which he stated: *'It is evident . . . that all parts of the brain may be invaded by tumor, but that certain parts are invaded with special frequency both in childhood and in adult life. These parts are the cerebral axis and the cerebellum in children and the cortex in adults.'* [39]. This classification and further refinement of the clinical and neuroanatomical characteristics of brain tumors further ushered in a new era of brain surgery.

In 1881, Charles Mills (1845–1930) reported a brainstem lesion in a 32-year-old man with intranuclear ophthalmoplegia, defective articulation, and hemiparesis that progressed rapidly to diffuse plegia, left facial and right body numbness, torticollis, and dysconjugate movements of the eyes, which were associated with a quarter inch lesion in the cephalic portion of the pons. The patient was treated medically but succumbed to his tumor soon after [40]. Post-mortem analysis demonstrated a diffuse pontine lesion with cranial and caudal extension, which at the time was thought to be something more familiar, a syphilitic gumma (Figs. 1.33 and 1.34). Mills excellently correlated symptomatology and anatomic localization of these lesions with the surrounding nuclei and cranial nerves in meticulous detail, demonstrating the broad symptomatic profile that these lesions could present with. Such keen neuroanatomic localization represented an enormous evolution in our understanding of brainstem anatomy, vastly advanced from even 100 years prior. He reported on several more of these lesions and those adjacent to the brainstem, labeling them as "fibromas" in his texts. His description of these lesions with a thorough review of

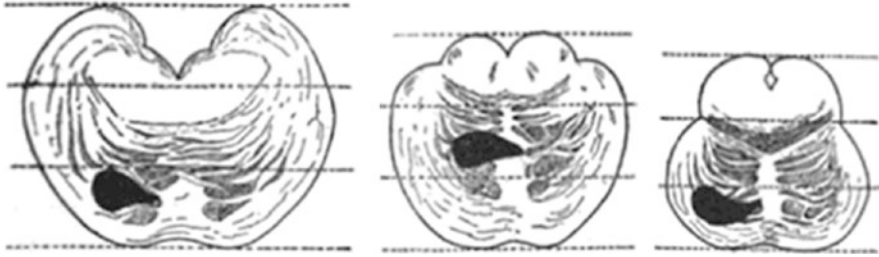


Fig. 1.33 A lesion of the pons described in a case by Mills. From the senior author's personal collection

Fig. 1.34 Gross anatomical specimen of the pontine lesion described by Mills. From the senior author's personal collection

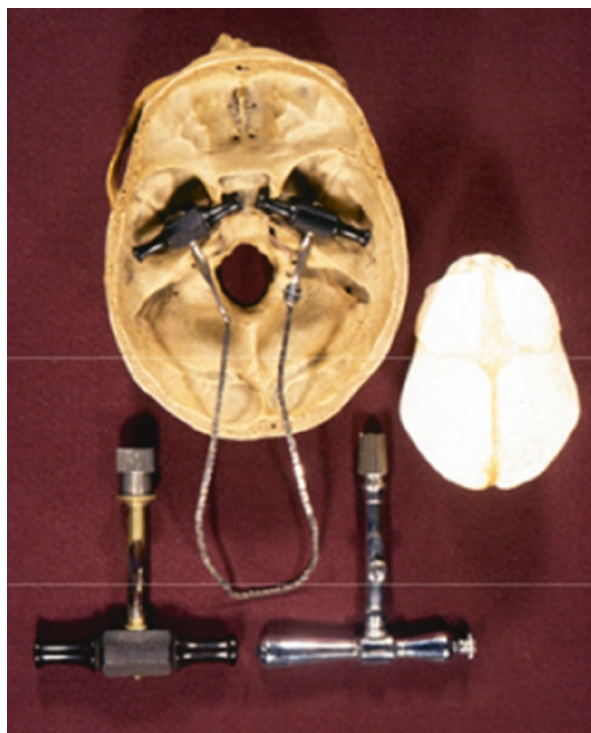


adjacent brainstem anatomy became a reference for surgeons in the future who would refer to Mills' work in preparation for the first attempted resections of these brainstem lesions.

In 1898, Leonardo Gigli (1863–1908) published his first series with his new Gigli saw, which was able to protect the dura during a craniotomy and elevated a bone flap, especially in the posterior fossa, in a much safer manner than the techniques available previously, including the 'hammer and chisel' craniectomy that some contemporaries were still clung to [41] (Fig. 1.35).

Reports at the turn of the century by James Collier (1870–1935), Theodore Diller (1863–1943), and Mary Putnam Jacobi (1842–1906) further demonstrated additional infiltrative brainstem lesions, yet they were still incompletely understood in regard to their anatomical relationships, and their natural course and heterogeneity was only beginning to be defined [42–44]. James Collier was noted to first describe tonsillar herniation, as well as early descriptions of uncus herniation, which would link rapid neurological decline to these syndromes. Pathological analyses were limited to post-mortem dissection in these cases. Ventricular tapping was the limitation

Fig. 1.35 Gigli saw, a hand-driven ebony-handled trephine in the lower left, and a steel trephine in the lower right. From the senior author's personal collection



of intervention available for a majority of these cases, with a report of prolonged survival first described by Diller in 1892 as the symptoms of hydrocephalus were abated [43].

1.6 Early Twentieth Century

At the turn of the century, neurological localization and operative techniques continued to incrementally improve with the growth in the number of completed brain surgeries, as reported by the early pioneers. Sir Victor Alexander Haden Horsley (1857–1916) was an innovator and advocate for the use of posterior fossa decompression for cerebellar tumors and the development of the first stereotactic frame [45, 46]. He reported a number of posterior fossa surgeries in 1906 [47]. From these reports, Horsley advocated for the internal decompression of posterior fossa tumors without a plan for gross total resection, in order to minimize morbidity for the patients. Antony Maxine Nicholas Chipault (1866–1920), inspired by the growing number of neurosurgical procedures being performed, formed the first dedicated neurosurgical journal, *Travaux de Neurologie Chirurgicale*, as well as a review of all the brain tumor cases that had been performed in the world up to that point in

time with outcomes listed [48, 49]. He also published a historical perspective of brain tumor surgery dating back to ancient times [50]. These surgical pioneers and the academics who studied and analyzed their cases truly demonstrated that brain surgery was maturing and growing out of its infancy. Additional important figures developed incremental gains in our understanding of neurological and surgical anatomy by building on the works of the early pioneers and utilizing the developing technology of the time.

Between 1909–1912, Fedor Krause (1857–1937) published a three-volume atlas, *Surgery of the Brain and Spinal Cord*, in which he built upon the work by Horsley, Macewen, Mills and Bright by building on the anatomical understanding of the Bright's era and by imbuing contemporary surgical techniques by Horsley and Macewen in the context of neurological localization that was outlined by Mills, Starr, and others [51]. Krause, known to be a rather aggressive surgeon, described his surgical approach in the context of a procedure to explore progressive hearing loss, right-sided paresis, diplopia, and left facial and tongue weakness in a 17-year-old girl. Localization was made to the left side of the pons and the CP angle, and surgical exploration was attempted. Krause described a generous dural flap, after which a '*considerable quantity of liquor was drained away*' (Fig. 1.36). The cerebellum fell into the surgical field given the sitting position of the patient, and the vermis was thoroughly inspected without the lesion being identified. The tentorium was traverse, and the petrous bone was inspected to no avail. He continued:

No pathologic condition could be recognized. The index finger gliding along the upper border of the petrous portion of the temporal bone for a distance of 6 cm, discovered neither hardness nor fluctuation. I was able to palpate the pons immediately beneath the brachia conjunctiva; its consistency did not differ from that of the normal cerebellar substance. The pons was finally punctured with a long cannula passed through the brachium conjunctivum, and 1/2 cm³, sero-sanguineous fluid aspirated.

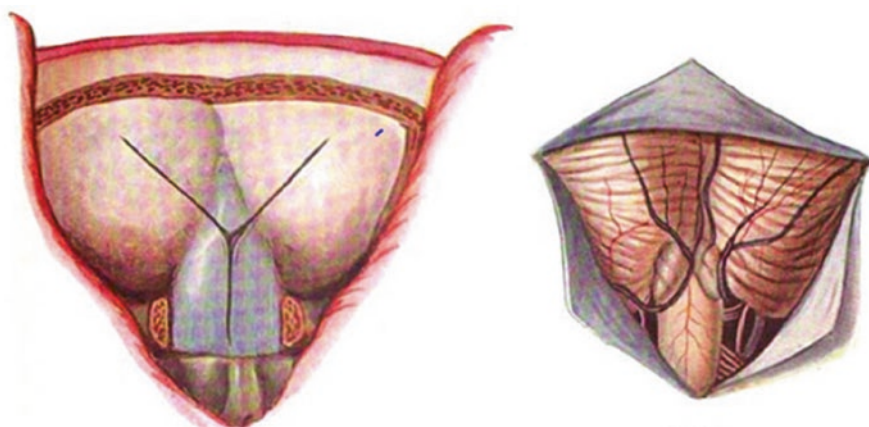


Fig. 1.36 Diagrams on surgical access and durotomy in Krause's work on surgical approaches to the posterior fossa. From the senior author's personal collection

He reported that the patient did well postoperatively and survived the procedure well, yet the contralateral paresis progressed. This early pioneering work, built on the advancements of the past, appears to be the first surgical attempt at entering the pons and attempting surgical decompression. This cutting-edge work was further elaborated upon in the coming years in his beautifully illustrated cases (Figs. 1.37 and 1.38). Finally, Krause was known for his advocacy of preoperative ventricular drainage in order to optimize outcomes and decrease intracranial pressure prior to posterior fossa surgery [52]. His work, while appearing aggressive by today's standards, may have been necessary to advance the field in treating a pathology that surgeons were once instructed to avoid due to fears of surgical outcomes.

In 1909, Theodore Weisenburg (1876–1934) described another attempt at surgical resection in a 46-year-old patient with progressive headache, ataxia, ptosis, and hearing loss, for which only a cerebellar decompression was performed [53]. No identifiable lesion was shown, and normal surface anatomy was demonstrated, sig-

Fig. 1.37 Title page from Krause's neurosurgical monograph *Surgery of the Brain and Spinal Cord*. From the senior author's personal collection

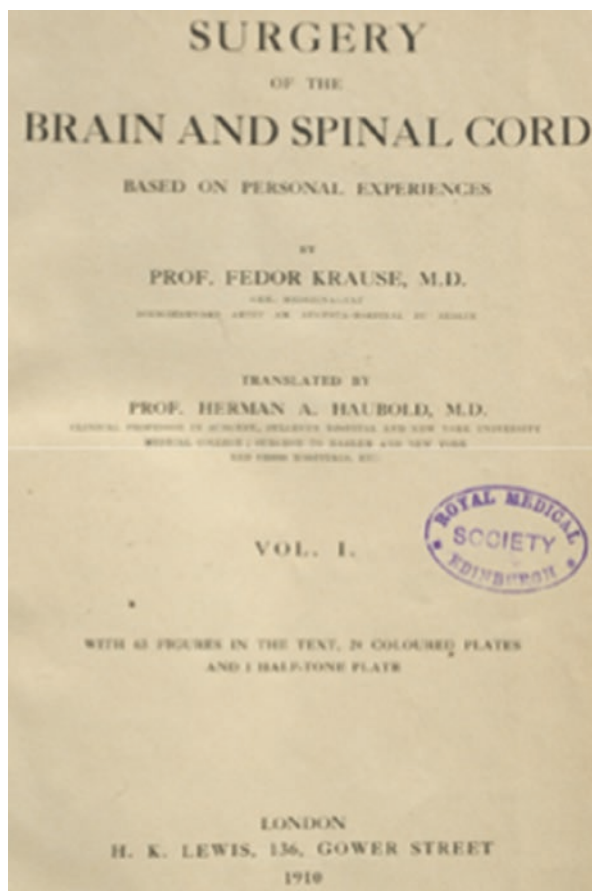
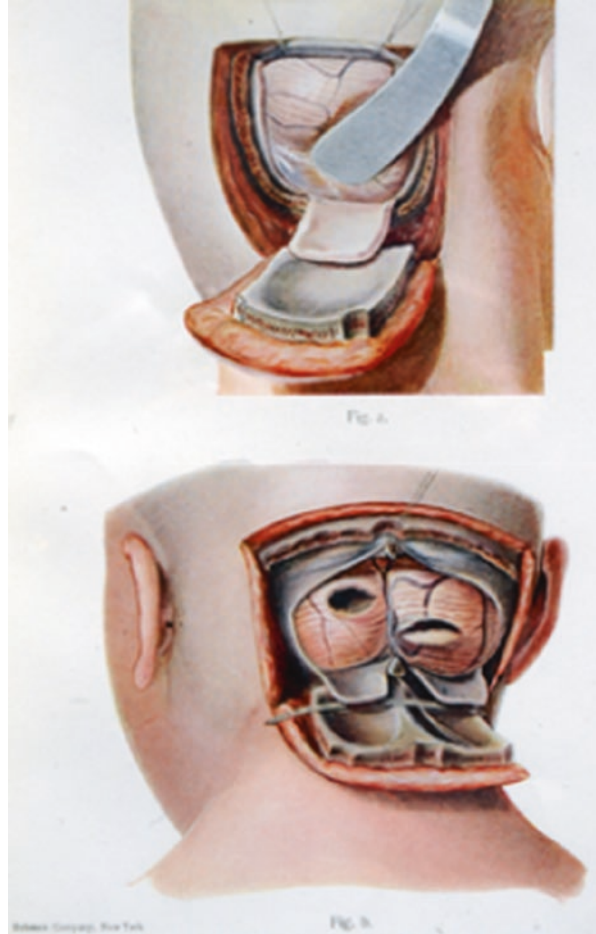


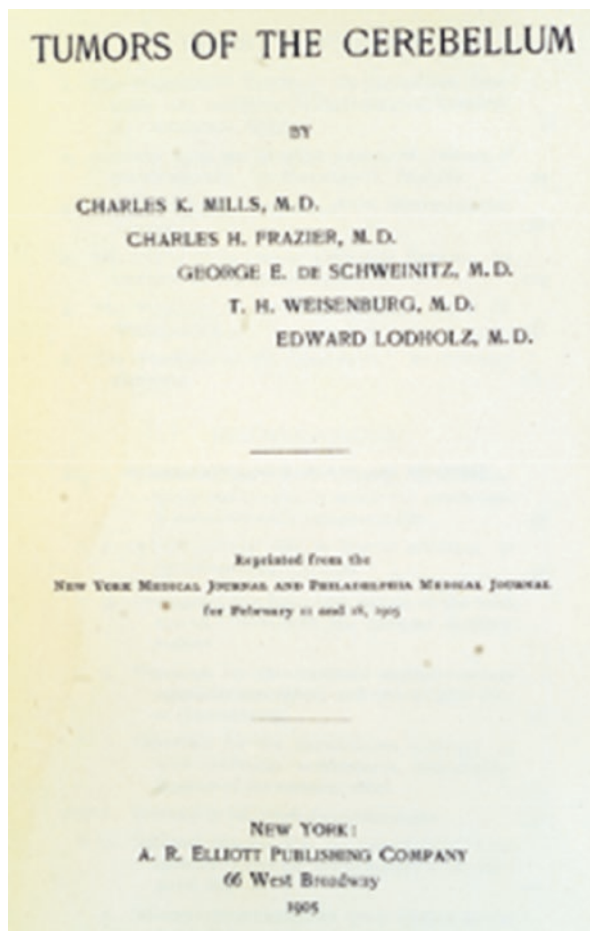
Fig. 1.38 Krause's technique for unilateral and bilateral osteoplastic craniotomies. From the senior author's personal collection



nifying that unlike Krause, some surgeons who attempted BG resection were still rightfully unwilling to enter and explore the brainstem, knowing the consequences that would result for the patient. As a result of this conservative approach, the patient's symptoms did improve mildly, and post-operative care was uneventful. The patient survived an additional 6 months, but then succumbed to his tumor. On post-mortem analysis, the tumor was demonstrated throughout the medulla, pons, cerebellar peduncles, and the cerebellum.

In 1910, Philip Zenner (1852–1956) performed a surgical exploration on a pediatric patient with a BG [54]. His approach was much more aggressive in terms of a more detailed exploration of the brainstem. While a pioneer in his approach, given the surgical limitations and restricted localization of the time, it was not surprising that the patient died quickly after surgery. At best, neurological localization of these lesions was gross and unable to determine invasiveness into surrounding brainstem tissue, nor to give detailed information regarding anatomical relations to

Fig. 1.39 Monograph by Charles Mills, Charles Frazier, George Schweinitz, Theodore Weisenburg, and Edward Lodholz detailing their experience with tumors of the cerebellum, in which both clinical evaluation and surgical considerations are discussed. From the senior author's personal collection

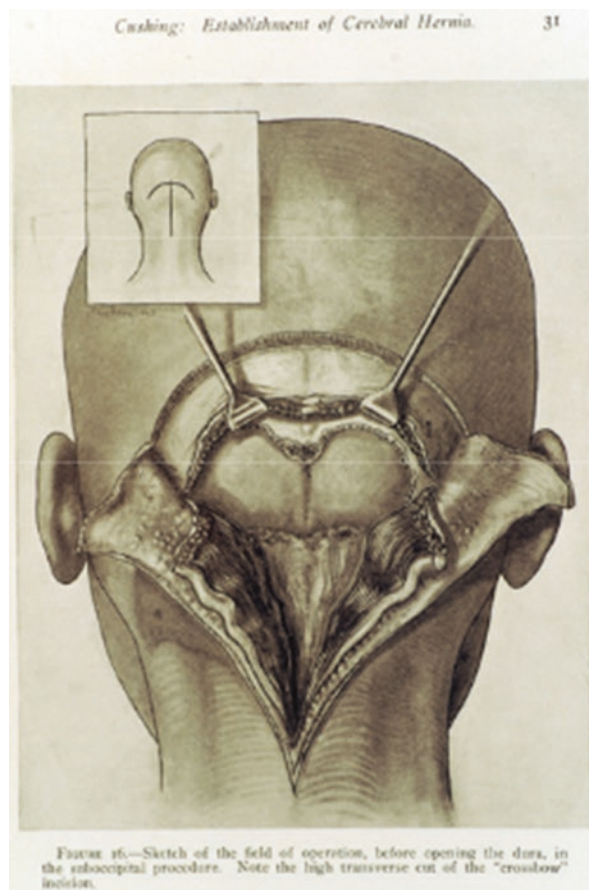


other structures. As a result, surgical procedures were largely of an exploratory nature and were nearly uniformly fatal when the brainstem was operated on.

Another noteworthy surgeon was Charles Frazier (1870–1936), who trained with Virchow and later became professor of surgery at the University of Pennsylvania. Frazier made several important contributions to the field that would further facilitate operative approaches to brainstem lesions. He advocated for the prone patient position and refined his ‘bloodless’ midline incision and exposure to the posterior fossa [55, 56]. He reported his series of posterior fossa surgeries in 1905 with Charles Mills and Theodore Weisenburg, among others in which his experience with a 42% mortality rate was documented (Fig. 1.39). As noted, for the time and type of exposure Frazier performed, this remained an improvement over contemporary mortality rates for posterior fossa surgery.

Harvey Cushing (1869–1939) is considered the father of American Neurosurgery and was a pioneer in posterior fossa surgery. While training at Johns Hopkins with

Fig. 1.40 Cushing's "crossbow" incision for tumor resection in the posterior fossa and for management of elevated intracranial pressure. From the senior author's personal collection



William H. Halsted (1752–1922), it was his travels abroad and work with Theodor Kocher (1841–1917) where he gained insight into surgery of the posterior fossa [57]. Maintaining his meticulous approach to problem solving and in an effort to reverse the widespread belief that surgery of the posterior fossa could not be performed with reliable safety, Cushing worked out several techniques to manage tumors in this region and published seminal works on tumors of the cerebellum and brainstem [58, 59]. He was an advocate for the "crossbow" incision, which did not gain popularity but allowed for adequate cerebellar decompression, retraction, as well as for an occipital burr hole to manage hydrocephalus [60] (Fig. 1.40). Similar to Horsley, Cushing advocated for tumor debulking, tissue diagnosis, and management of hydrocephalus. He published on medulloblastoma and astrocytoma resection of the cerebellum with an operative mortality rate of only 15% [61]. He first reported a case of a pediatric BG in January 1910, for which he performed a suboccipital exploration [62, 63]. During his time at Johns Hopkins Hospital until 1912, only a single pediatric BG case was reported. The patient was a 15-year-old girl

with a 5-month history of cognitive slowing, right-sided ptosis, and right cheek numbness that progressed to right ear deafness, vomiting, dizziness, imbalance, positional headache and paresthesia in the left hand and foot at 1 week prior to presentation. On examination, she was found to have right-sided anesthesia, paralysis, and nystagmus in all directions. She was bedbound for 10 days later and severely dysarthric, for which she was initially treated with potassium iodide. She returned home with moderate improvement in neurological function until a rapid deterioration returned her to her previous state. Cushing performed a wide suboccipital exploration to both mastoid processes and caudally to the foramen magnum. The dura was exposed down to the arch of C1 and upon opening, the cerebellum began to herniate uncontrollably. The decision was then made to open the dura widely through which the cerebellum continued to herniate, but no tumor was identified. Exploration of the cerebellum was performed to no avail, and the operation was aborted. The dura was left open as the muscles and skin were closed in layers. Cushing concluded: *“It is probable that the tumor actually is a pontial tumor, cerebellar symptoms due to involvement of the superior cerebellar peduncles. This accounted for the unusual state of sensory disturbances and for the right conjugate paralysis of the ocular movements.”* Despite a reportedly uncomplicated surgical decompression, the patient’s temperature rose to 105.7 °F within hours, and her pulse was found to be weak. She became comatose on the following day and died the day afterwards, likely from a profound septic response. An autopsy confirmed a *“soft gelatinous mass occupying the cerebellopontine region on the right, extending from the mid-line and including the triangle, measuring 5 cm in antero-posterior diameters. There is a cyst at the outer angle. The cranial nerves from the third to the eighth inclusive are definitely involved in the growth. The tumor itself is a most variegated affair. In many places, it contains gelatinous cysts, in others bright red patches of haemorrhage, many thrombosed vessels, yellowish areas of tissue degeneration, and a dry surrounding zone of grayish, opaque tissue evidently growing edge, which has the appearance of a section of unripe fruit”* (Fig. 1.41). A diagnosis of infiltrating glioma of the pons was made. The reason for Cushing’s limited exploration was not discussed, yet he may have considered the fatal consequences of extensive brainstem exploration. His report further documented the importance of detailed neurological examination for the diagnosis of these lesions, explaining the possible close relationship of various nuclei in the brainstem, even though there was still, rightfully so, a significant degree of reticence approaching the brainstem. Because of this work and his further refinement of operative approaches to infratentorial pediatric tumors that further developed the field over the following decades, his operative mortality rates fell from 20% to 4% for these approaches by 1928; these low rates were never seen before in neurological surgery history [62].

Following the work of Cushing was his former student Walter E. Dandy (1886–1946). Dandy was known to have a more aggressive surgical style and would often disagree with his former instructor. In addition to his work on developing ventriculography, a postoperative care unit and meticulous postoperative airway and electrolyte management, Dandy advocated for gross total resection of tumors in the CP angle. Yet understandably, his aggressive surgical nature did not translate to

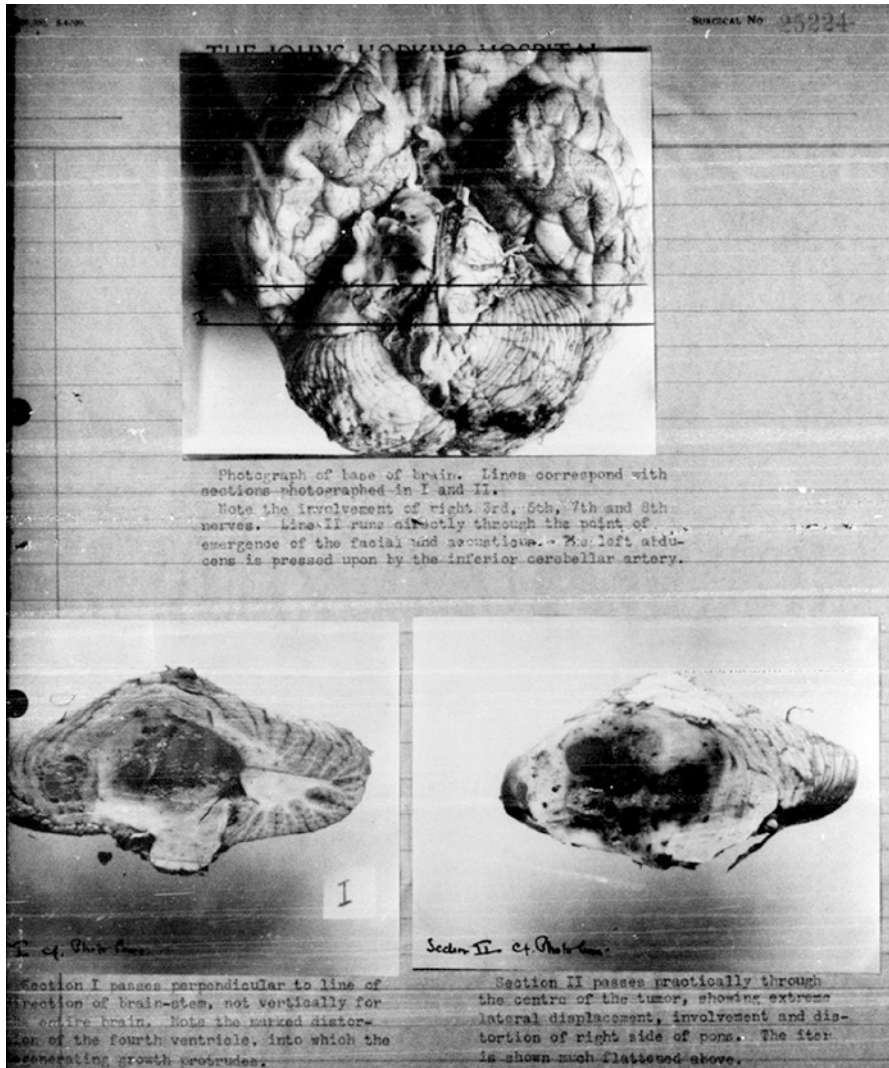


Fig. 1.41 Photographs of Cushing's gross specimen from his pediatric patient with a brainstem glioma. Courtesy of The Alan Mason Chesney Archives of The Johns Hopkins Medical Institutions

brainstem lesions, where such an approach would not be advocated for at this or any time by even the more aggressive surgeon [64–66]. When he passed away in 1946, Dandy had performed over 200 operations in the posterior fossa.

These early surgical pioneers demonstrated the frontiers of the operative capability at the start of the twentieth century, the limitations of a clinical diagnosis in understanding the complexity of the anatomical nuances of these lesions, and the uniformly fatal course that the patients undertook upon invasive surgical exploration of their lesions. As described, many cases concluded without tumor identification, and the patients

were only offered palliative decompression. Donald Matson (1913–1969) stated even decades later: “*regardless of specific histology, brainstem gliomas must be classified as malignant tumors since their location in itself renders them inoperable*” [67].

1.7 Mid-to-Late Twentieth Century

At earlier times, with so little known about BGs, they were all considered to be a single entity that is distinct from surrounding cystic, infectious, and inflammatory collections of the CP angle and otherwise surrounding the brainstem. Little was known of the true heterogeneous nature of these lesions, and only over the early twentieth century was it discovered that as many as 10% of all pediatric tumors were BGs, and that these lesions were a heterogeneous group of entities within the midbrain, pons, and medulla, which portended several very different prognostic outcomes [68–72]. Over the next 50 years, since these early surgeons attempted to resect these formidable lesions, little had advanced in regard to the improvement of perioperative care. Epidemiological evidence began to arise as more and more cases were being reported, neurological localization incrementally improved, imaging techniques allowed for subtype classification and localization in an unprecedented way, and the utilization of microsurgical techniques slowly moved our management of these lesions forward. Additionally, patients of likely focal lesions were delineated as having good outcomes, tempting the surgeons to attempt resection where they would otherwise defer treatment.

In 1968, J. Lawrence Pool (1906–2004) was one of the first to describe a series of resections of brainstem lesions after which the patients survived between 10 to 25 years [73]. The first case of this series likely represented an ependymoma of the fourth ventricle that abutted the brainstem but was not intrinsically associated with it. The patient only experienced papilledema, headaches, and mild nystagmus, which resolved postoperatively. X-rays were the only available modality for imaging at the time, and while this was a positive outcome to present, it is unclear as to whether this lesion could truly be described as a BG. The second case was that of an 8-and-half-year-old girl who presented with mild ataxia and headaches that progressed to multidirectional nystagmus, facial weakness, profound ataxia, and adiadochokinesis. A suboccipital craniectomy was performed in 1947, and discoloration of the floor of the fourth ventricle was noted and explored. A pontine cyst was aspirated for 30 cc of fluid; while some portion of what appeared to be a mural nodule was removed, a substantial amount of tumor was still noted invading the medulla and pons. A decision was made to not explore further. The patient did very well postoperatively with a resolution of her ataxia, nystagmus, and sensory disturbances, which were stable at 13-year follow-up. The final case was performed in 1957 and represented a 13-year-old boy with papilledema, diplopia, and mild ataxia. A ventricular catheter was placed preoperatively, and the surgery was performed with a suboccipital approach. A graying tumor was identified in the midbrain and at the roof of the sylvian aqueduct and was estimated to be 8 mm in diameter. A biopsy

was attempted but resulted in bleeding, which prevented further exploration. A soft rubber catheter was placed into the third ventricle and anchored to the subarachnoid space of the cisterna magna. The dura was closed in a watertight fashion in an uncomplicated manner, and the pathological diagnosis was astrocytoma. The patient's papilledema and ataxia improved, and he did well at 10-year follow-up. While it was assuring to other surgeons that survival after operative intervention for BG was possible, it is clear that these represented small, focal or cystic lesions, in which true and full operative resection was not attempted. It was prudent that Pool did not attempt more aggressive resection for better outcomes in his patients, given that they survived so long after surgery. However, it did not appear that these were aggressive diffuse lesions that others had struggled with; these may have been hand-selected cases but were somewhat misleading in the conclusions reached in this report by Pool. He states, "*appropriate treatment of a brainstem glioma can lead to long-term useful survival.*" He also credited "X-ray therapy," which was no more than a few intraoperative X-rays, as "*obviously prevent[ing] growth of the tumors.*" Despite his description of these cases' intraoperative details and patient presentations, he reassured surgeons that resection of all BGs could afford long-term survival, with somewhat inaccurate conclusions. However, in his discussion, he notes that these lesions were far from homogeneous lesions, which were seemingly benign but significantly heterogeneous in their anatomic localization within the brainstem and around the fourth ventricle. From this understanding, the true heterogeneous nature of these lesions was starting to be defined, and that all BGs were not made equally, nor should be treated as such.

Additional reports began to surface over the next three decades of these prognostically favorable outcomes, and it became accepted that this tumor was in fact not one, but a spectrum of lesions that have variable management strategies and outcomes dependent upon the surgical intervention undertaken. Undoubtedly, poor outcomes in larger lesions were underreported, yet more knowledge was obtained from magnetic resonance imaging (MRI) technology, which exponentially advanced our understanding of these lesions.

Over this period, diffuse gliomas were identified as the most common type of brainstem tumors, comprising 58–75% of all lesions, by their indistinct margins and expansion rather than compression of the brainstem [68, 74]. Clinical correlation was then possible between the 80% of children who presented with symptoms of less than 2 months, and those with significantly more indolent courses, to the imaging characteristics that would later identify less aggressive lesions with better prognostic profiles from more aggressive subtypes. Several radiographic classification systems also emerged, characterizing tumors as being diffuse or focal, exophytic or parenchymal, and by their enhancement patterns. Dorsally exophytic lesions were identified as arising from the subependymal glial tissue in the fourth ventricle, and as clinicians gained experience with their radiographic appearance, they began delineating them from choroid plexus papillomas or ependymomas. Focal lesions and those arising from either the midbrain or the cervicomedullary junction allowed for an understanding that these were usually low-grade, benign lesions that do not infiltrate. The differentiation of these tumors from diffuse lesions allowed clinicians

to understand why significant long-term survival could be obtained for some patients with surgical resection. Historically, surface discoloration or abnormalities in shape or quality of the brainstem were solely used as indicators for safe entry during exploratory surgery but were then starting to be replaced by a thorough analysis of preoperative imaging studies.

Epidemiological factors also were further defined in the 1990s, such as more indolent tumors documented in patients with neurofibromatosis type I, and longitudinal analyses of patients with serial MRIs were first being performed to further shift our thinking toward monitoring certain patients until the risks of surgery could be outweighed by the risks of not operating [75].

The first trials investigating the addition of chemotherapy to radiation therapy for children with these diffuse lesions began in the late 1970s in concert with advancements in imaging. Vincristine was added to irradiation, yet no differences in long-term outcomes were noted, despite a 20% overall survival. Additional trials were performed in the 1980s and 1990s including the use of agents such as cyclophosphamide, cisplatin, ifosfamide, and carboplatin prior to an intensive radiation therapy regimen; no significant improvement in survival was noted. A trial of etoposide with irradiation and vincristine similarly produced no survival benefit in the late 1990s [76]. Marrow-ablating chemotherapy also provided no survival benefit.

Although once thought to be so rare that multicenter clinical trials would not be possible for BGs, radiation oncologists from 13 institutions in 1983 participated for the first time in a questionnaire evaluating their success with radiation for BGs over the previous decades. Sixty-two patients were identified with a 3-year survival of only 23%. Failure of local control meant the ineffectiveness of this trial, with whole brain radiation showing no survival benefit. From this first collaborative effort, clinicians soon realized that more of these cooperations would be needed in order to make substantial advancements in treatment. Phase I/II trials began investigating various radiation schedules and combinations with chemotherapeutics. Trials to understand maximal radiation doses from 64.8 to 78 Gy demonstrated no improved survival, yet complications of corticosteroid dependency, vascular events, white matter changes, hearing loss, and seizures were encountered frequently. Median survival was 8–13 months for most trials [71, 72, 76]. Therefore, it was surmised from this work that lower radiation doses may be required and would suffice to manage lesions perioperatively or as a stand-alone treatment. Limitations of chemotherapeutic penetration, the risks of radiation exposure, and the indolent nature of some of these slower growing lesions were cited as some of the reasons that these trials were not more successful.

Today, the Children's Oncology Group and the Pediatric Brain Tumor Consortium are conducting trials with novel therapeutics including epidermal growth factor receptor (EGFR) inhibitors, antiangiogenesis agents, farnesyl transferase inhibitors, radiation sensitizers, histone deacetylase inhibitors, as well as agents that were proven successful in treating other high-grade gliomas such as temozolomide [71, 72, 76]. The hope still exists that meaningful tumor control may be achieved with these therapeutics, resulting in meaningful long-term survival for patients.

Even more, modern technological advances have also allowed for incremental advancement and evolution of surgical management of these lesions [77]. The use of advanced MRI techniques has allowed for better delineation of hemorrhage, cysts, and enhancing portions of these lesions in unprecedented ways, which lead to optimization of surgical entry locations; this may lead to as little transgression of normal surface tissue as possible. Neuronavigation and intraoperative imaging has allowed for resection of as much tumor tissue as possible in a guided manner, which no longer relies on the exploratory nature that early surgery was dependent upon. Stereotactic biopsies have allowed for the attainment of tumor tissue and a tissue diagnosis by planning the safest, least destructive path to the lesions in a manner that would have seemed to be science fiction for most of our history of understanding BGs. Intraoperative monitoring, including cranial nerve evoked potentials, brainstem auditory evoked potentials, motor and sensory evoked potentials, brainstem mapping, nerve conduction studies, and electromyography, optimizes the surgeon's awareness of his/her anatomical localization to maximize safe resection. Suprafacial and infrafacial entry zones have demonstrated safer areas to enter the brainstem, and neurophysiological monitoring has become invaluable in the real-time assessment of these entry points and the resection limits. Diffusion tensor imaging, demonstrating the distortion of vital neural tracts displaced by tumor tissue, has allowed for safer resection than ever possible. Intraoperative imaging can further be used in real-time to evaluate the amount of tumor resected, and by loading it into a neuronavigational hardware, it can further guide the rest of the resection of these lesions. Improvements in postoperative intensive care unit (ICU) management, oxygenation monitoring, airway protection, and careful swallowing assessments keep patients safer perioperatively and improve outcomes. A greater emphasis on physical and occupational therapies further optimizes outcomes postoperatively for patients with BGs in the modern era.

Even after nearly 200 years of identification and management of these lesions, outcomes remain poor for the majority of brainstem lesions, with only marginal improvement in long-term survival for diffuse and aggressive lesions. Adjuvant chemotherapy and radiotherapy have allowed for minimal survival benefits, yet patient selection and proper classification of lesions has the best implications for long-term survival, with or without surgical intervention. With improved outcomes, re-resection has also become an option for certain patients, which had not been possible historically [78]. A greater understanding of the genetic profiles of these lesions in order to identify targets for therapeutics must be accomplished for the next generation of treatments to have a meaningful impact on patients' survival. Substantial blood brain barrier disruption may also be required to facilitate entry of novel therapeutics, and direct delivery systems may also allow for better tumor control and fewer systemic side effects. Despite a long and troubling history of our understanding and management of BGs, diffuse lesions are still arguably not treated any more effectively than they have been over a century ago and still portend substantial mortality risk in an overwhelming majority of patients within 2 years. Major advances, however, have occurred in our classification of lesions by location and imaging

characteristics, which help identify tumors that can be cured by surgical resection. With our ever-expanding understanding of the molecular mechanisms of these lesions and the acceleration of our technological development, it is possible that single pathways, proteins, or interventions may be identified in our lifetime that may herald a novel class of effective therapeutics and a new age of treatment that will propel our current care forward, far beyond the care delivered in the time of Mills, Krause, and Cushing. It is our hope that these lesions will once again be categorized prognostically in a homogeneous manner, in regard to substantial long-term survival achievable for all patients. Having traced the exponentially advancing lineage of our understanding of BGs, it is astounding how much has changed over the past 30, 100, 200 and 2000 years in regard to our diagnosis and treatment of these lesions. Modern surgeons find themselves in a time of technological advancement that was never seen before throughout all our history, and the once asymptomatic point of cure for BGs may in fact not be far into the future [79].

1.8 Conclusion

On the larger scale of our scientific development, our understanding of BGs is only in its infancy. For much of our history, the posterior fossa was a region for surgeons to avoid, with transgression into the brainstem resulting in uniform death for patients. Only in the last half-century of advanced imaging and a shorter period of stereotactic localization, have we scratched the surface of humanity's potential to treat these unrelenting masses of the most precious region of the nervous system. It is unclear if surgical resection in such a valuable territory would be the answer for curing BGs in the future, but certainly targeted and highly selective therapeutic delivery will be required. More than with any other tumor of the body, preservation of neurological structure and function of the brainstem is paramount and remains the greatest challenge to BG treatment – a warning of non-disruption that has echoed throughout our history and resounds again as we look forward to the next therapeutic advancement just beyond the horizon.

References

1. Viale G. The surgical approach to the posterior cranial fossa according to Galen. *Neurosurgery*. 2007;61:ON5399–404.
2. Galen of Pergamon (1576–1577) *Omnia quae extant opera in Latinum sermonem conversa*. (Quinta ed) Apud Juntas, Venice.
3. Garrison FG, Streeter EC. Sculpture and painting as modes of anatomical illustrations. In: Choulant's history and bibliography of anatomical illustrations, translated by Mortimer Frank. Chicago: University of Chicago Press; 1920.
4. Goodrich JT. Sixteenth century renaissance art and anatomy: Andreas Vesalius and his great book – a new view. *Medical Heritage*. 1985;1:280–8.

5. Leonardo da Vinci. (1911–1916) *Quaderni d'anatomia*. Jacob Dybwad, Christiania. In six volumes. See also Hopstock, H. Leonardo as an anatomist. In: Singer C, editor. *Studies in the history of medicine*. Oxford, UK: Clarendon Press; 1921. p. 153–91.
6. Leonardo da Vinci. In: Keele KD, Pedretti C, editors. *Corpus of the anatomical studies in the collection of her majesty the queen at Windsor Castle*. New York: Harcourt Brace Jovanovich; 1979.
7. Todd EM. *The Neuroanatomy of Leonardo da Vinci*. Park Ridge, IL: American Association of Neurological Surgeons; 1991.
8. Hunter W. Two Introductory Lectures, delivered by Dr. William Hunter, to his last course of Anatomical Lectures, at his Theatre in Windmill Street. . . . London, Printed by the Order of the Trustees for J. Johnson, 1784. See page 39 for Leonardo quote.
9. Dryander J. *Anatomiae Apud Eucharium Ceruicornum*. Marburg, 1537.
10. Hanigan WC, Ragen W, Foster R. Dryander of Marburg and the first textbook of neuroanatomy. *Neurosurgery*. 1990;26:489–98.
11. Vesalius A. *De Humani Corporis Fabrica Libri septum*. Ex officina Joannis Oporini. Basel, 1543.
12. Willis T. *Cerebri anatome: cui accessit nervorum descriptio et usus*. London: J. Flesher; 1664.
13. Morand F-S. (1768–1772) *Opuscules de Chirurgie*. Paris, Guillaume Desprez, see pages 161–68).
14. Morgagni GB. *De sedibus, et causis morborum per anatomen indagatis libri quinque*. Venetiis, Italy: Typog Remondiniana; 1761.
15. Morgagni GB. *The seats and cause of diseases investigated by anatomy . . . Translated from the Latin by Benjamin Alexander*. London: Millar; 1769.
16. Soemmering ST. *Dissertatio inauguralis anatomica de basi encephali et originibus nervorum cranio egredientium libri quinque*. Gottingae, Germany apud A. Vanderboech vid.; 1778.
17. Vicq d'Azyr F. *Traité d'anatomie et de physiologie avec des planches coloriées représentant le naturel les divers organes de l'homme et des animaux*. Paris, France, A. Didot l'aîné, 1786.
18. Gautier D'Agoty JF. *Anatomie de la tête*. Paris: France. Chez le sieur Gautier, M. Duverney, Quillau; 1748.
19. Dandy WE. *Surgery of the brain*. In: *Lewis practice of surgery*. Hagerstown, MD: W.F. Prior Co.; 1945. p. 6–7.
20. Holmes OW. The contagiousness of puerperal fever. *New England Quart J*. 1843;1:503–30.
21. Semmelweis IF. *Die Aetiologie, der Begriff und die Prophylaxis des Kindbettfiebers*. Vienna, and Leipzig: C.A. Hartleben's Verlags-Expedition, Pest; 1861.
22. Lister J. *Collected papers*. Oxford, UK: Clarendon Press; 1909.
23. Lister J. On the principles of antiseptic surgery. *Inter Beiträge Wissen Med*. 1891;3:1–12. A paper in which Lister summarizes his work on antiseptics, presented in a festschrift to Rudolf Virchow on his 70th birthday.
24. Lister J. On the effects of the antiseptic system of treatment upon the salubrity of a surgical hospital. *Edmonston & Douglas*: Edinburgh; 1870.
25. Bell C. *The nervous system of the human body embracing the papers delivered to the Royal Society on the subject of nerves*. London, UK: Longman, Rees, Orme, Brown, and Green; 1830. See pp clxix, plate IV for brain stem illustration.
26. Bell C. *Illustrations of the great operations of surgery, trepan, hernia, amputation, aneurism, and lithotomy*. London: Longman, Hurst, Rees, Orme, and Brown; 1821.
27. Broca P. *Remarques sur le Siège de la faculté du langage articulé suivie d'une observation d'aphémie (perte de la parole)*. *Bull Soc Anat Paris*. 1861;36:330–6.
28. Broca P. *Perte de la parole; ramollissement chronique et destruction partielle du lobe antérieur gauche du cerveau*. *Bull Soc Anthropol Paris*. 1861;2:235–41.
29. Ferrier D. *The functions of the brain*. London, UK: Smith, Elder and Co.; 1876.
30. Bartholow R. *Tumours of the brain; clinical history and comments*. *Am J Med Sci*. 1868;110ns:339–59.

31. Bartholow R. Experimental investigations into the functions of the human brain. *Am J Med Sci.* 1874;67:305–13.
32. Cruveilhier J. *Anatomie pathologique du corps humain.* Paris: J.-B. Baillière; 1829–1842.
33. Flamm ES. The neurology of Jean Cruveilhier. *Med Hist.* 1973;17:343–53.
34. Cushing H. *Tumors of the nervus acousticus and the syndrome of the cerebellopontile angle.* Philadelphia: WB Saunders; 1917.
35. Cushing H, Eisenhardt L. *Meningiomas. Their classification, regional behaviour, life history, and surgical end results.* Charles C Thomas: Springfield; 1938.
36. Bright R. *Reports of Medical Cases, selected with a View of illustrating the symptoms and cure of Diseases by a Reference to Morbid Anatomy.* London: Richard Taylor for Longman et al.: 1827–1831.
37. Macewen W. An address on the surgery of the brain and spinal cord. *BMJ.* 1888;2:302–9.
38. Macewen W. *Pyogenic infective diseases of the brain and spinal cord.* J. Macle hose & Sons: Glasgow; 1893.
39. Starr A. *Brain surgery.* New York: William Wood & Company; 1893.
40. Mills CK. Tumor of the pons Varolii, with conjugate deviation of the eyes and rotation of the head. *J Nerv Ment Dis.* 1881;8:470–81.
41. Gigli L. Zur technik der temporären Schädelresektion mit meiner Drahtsäge. *Centrabl für Chir* 1989;25:425–8. For an English translation of this article see Wilkins RH. *Neurosurgical classics.* New York: Johnson Reprint Company; 1965: 380–82.
42. Collier J. The false localizing signs of intracranial tumour. *Brain.* 1904;27:490–508.
43. Diller T. A case of tumor of the pons in which tapping of the lateral ventricles was done for the relief of intra-cranial pressure. *Am J Med Sci.* 1892;104:509–14.
44. Jacobi MP. Case of probable tumor of the pons. *J Nerv Ment Dis.* 1889;14:115–29.
45. Gotch F, Horsley VAH. On the mammalian nervous system, its functions, and their localisation determined by an electrical method. *Phil Trans Royal Society B.* 1891;182:267–526.
46. Horsley VAH, Clarke RH. The structure and functions of the cerebellum examined by a new method. *Brain.* 1908;31:45–124.
47. Horsley V. On the techniques of surgeries of the central nervous system. *BMJ.* 1906; 2:411–23.
48. Chipault A, editor. *Travaux de Neurologie Chirurgicale.* Paris, France, 1896–1901.
49. Chipault A. *Chirurgie Opératoire du Système Nerveus.* Paris, France; Rueff Et. C. Editeurs ; 1894–95. For the pediatric cerebellar tumor cases listed by Chipault see case 23 and 24 on pp. 333–34; case 79 on p 354; case 88 on p 357; case 118 on p 369.
50. Chipault A. *Etudes de Chirurgie Médullaire (Historique, chirurgie opératoire, traitement).* Felix Alcan: Paris; 1894.
51. Krause F. *Surgery of the brain and spinal cord based on personal experiences.* Translated by H. Haubold and M. Thorek. New York: Rebman Co.; 1909–1912. Issued in three volumes.
52. Krause F. Operative freilegung der Vierhüget nebst beobachtungen über hirndruck und decompression. *Zentrabl Chir.* 1926;53:2812–9.
53. Weisenburg TH. Extensive gliomatous tumor involving the cerebellum and the posterior portions of the medulla, pons and cerebral peduncle and the posterior limb of one internal capsule. *J Am Med Assoc.* 1909;LIII:2086–91.
54. Zenner P. Two cases of tumor of the pons. *J Nerv Ment Dis.* 1910;37:27–36.
55. Frazier CH. Remarks on the surgical aspects of tumors of the cerebellum. *New York State J Med.* 1905;18:272–80. 332–7
56. Frazier CH. The midline bloodless approach to the posterior fossa. *Trans Am SA.* 1926;44:229–47.
57. Cushing H. The intracranial tumors of preadolescence. Report of a clinic for a combined meeting for the Pediatric Section of the New York Academy of Medicine, Philadelphia Pediatric Society, the New England Pediatric Society, held at the Peter Bent Brigham Hospital, Boston, October 16, 1926. *Am J Dis Child.* 1927;33:551–84.
58. Cushing H. Experiences with cerebellar astrocytomas. *Surg Gynecol Obstet.* 1931;52:129–204.

59. Cushing H. Experiences with cerebellar medulloblastomas. *Acta Path Microbiol Scand.* 1930;7:1–86.
60. Cushing H. The establishment of the cerebral hernia as a decompressive measure for inaccessible brain tumors, with the description of the intermuscular making of the bone defects in the temporal and occipital regions. *Surg Gynecol Obstet.* 1905;1:297–314.
61. Cushing H. Intracranial tumors. Notes on a series of two thousand verified cases with surgical mortality percentages pertaining thereto. Springfield: Charles C Thomas; 1932.
62. Sedora-Román NI, Pendleton C, Mohyeldin A, Quiñones-Hinojosa A. Harvey Cushing's early experience with pediatric gliomas. *Childs Nerv Syst.* 2011;27(5):819–24. <https://doi.org/10.1007/s00381-011-1392-2>. Epub 2011 Feb 2.
63. Dmetrichuk JM, Pendleton C, Jallo GI, Quiñones-Hinojosa A. Father of neurosurgery: Harvey Cushing's early experience with a pediatric brainstem glioma at the Johns Hopkins Hospital. *J Neurosurg Pediatr.* 2011;8(4):337–41. <https://doi.org/10.3171/2011.7.PEDS11101>.
64. Dandy WE. Ventriculography following the injection of air into the cerebral ventricles. *Ann Surg.* 1918;68:5–11.
65. Dandy WE. Röntgenography of the brain after the injection of air into the spinal canal. *Ann Surg.* 1919;70:397–403.
66. Dandy WE. Localization or elimination of cerebral tumors by ventriculography. *Surg Gynecol Obstet.* 1920;30:329–42.
67. Matson D. Tumors of the posterior fossa. In: *Neurosurgery of infancy and childhood.* 2nd ed. Springfield: Charles C Thomas; 1969. p. 469–77.
68. Jallo GI, Biser-Rohrbaugh A, Freed D. Brainstem gliomas. *Childs Nerv Syst.* 2004;20(3):143–53. Epub 2003 Dec 11. Review.
69. Littman P, Jarrett P, Bilaniuk LT, Rorke LB, Zimmerman RA, Bruce DA, et al. Pediatric brain stem gliomas. *Cancer.* 1980;45:2787–92.
70. Berger MS, Edwards MS, LaMasters D, Davis RL, Wilson CB. Pediatric brain stem tumors: radiographic, pathological, and clinical correlations. *Neurosurgery.* 1983;12:298–302.
71. Donaldson SS, Laningham F, Fisher PG. Advances toward an understanding of brainstem gliomas. *J Clin Oncol.* 2006;24(8):1266–72. Review.
72. Recinos PF, Sciubba DM, Jallo GI. Brainstem tumors: where are we today? *Pediatr Neurosurg.* 2007;43(3):192–201. Review.
73. Pool JL. Gliomas in the region of the brain stem. *J Neurosurg.* 1968;29:164–7.
74. Epstein F, Wisoff JH. Intrinsic brainstem tumors in childhood: surgical indications. *J Neuro-Oncol.* 1988;6:309–17.
75. Pollack IF, Schultz B, Mulvihill JJ. The management of brainstem gliomas in patients with neurofibromatosis 1. *Neurology.* 1996;46:1652–60.
76. Finlay JL, Zacharoulis S. The treatment of high grade gliomas and diffuse intrinsic pontine tumors of childhood and adolescence: a historical – and futuristic – perspective. *J Neuro-Oncol.* 2005;75(3):253–66.
77. Sabbagh AJ, Alaqeel AM. Focal brainstem gliomas. *Advances in intra-operative management. Neurosciences (Riyadh).* 2015;20(2):98–106.
78. Bowers DC, Krause TP, Aronson LJ, Barzi A, Burger PC, Carson BS, et al. Second surgery for recurrent pilocytic astrocytoma in children. *Pediatr Neurosurg.* 2001;34:229–34.
79. Goodrich JT. History of posterior Fossa tumor surgery. *Surgery of the posterior Fossa.* Springer Italia: Milan; 2011.

Chapter 2

Anatomy of the Brainstem



**Jaafar Basma, Dom E. Mahoney, Andrei Tudose, Douglas Taylor,
Kaan Yağmurlu, and Jeffrey Sorenson**

Abbreviations

AICA	Anterior inferior cerebellar artery
CN	Cranial nerve
CSF	Cerebrospinal fluid
IAC	Internal auditory canal
PCA	Posterior cerebral artery
PICA	Posterior inferior cerebellar artery
SCA	Superior cerebellar artery
VA	Vertebral artery

J. Basma (✉) · D. Taylor
Department of Neurosurgery, University of Tennessee Health Science Center,
Memphis, TN, USA
e-mail: jbasma@uthsc.edu

D. E. Mahoney
Faculty of Health Sciences, University of Bristol, Bristol, UK

A. Tudose
Department of Neurosurgery, North Bristol Trust, Bristol, UK

K. Yağmurlu
Department of Neurosurgery, University of Virginia, Charlottesville, VA, USA

J. Sorenson
Department of Neurosurgery, University of Tennessee Health Science Center,
Memphis, TN, USA

Semmes Murphey Brain and Spine Institute, Memphis, TN, USA

2.1 Introduction

Nestled between the clivus and the cerebellum, the brainstem is a relatively small, yet highly interconnected structure. Except for olfaction and vision, all sensory and motor pathways flow through the brainstem, making it a primary gateway between the mind and body. The complexity of the brainstem, combined with its concentration of vital structures and deep location, creates daunting surgical challenges. Its dense network of ascending and descending pathways, and nuclei that are essential for vital neurological function, accounts for only a part of its complexity. The surgeon must also understand its intricate relationships with surrounding neural, ventricular, cisternal, arterial, venous and bony structures. This knowledge will help the surgeon to predict what kind of neurological deficits might occur with various surgical trajectories into the brainstem. Of course, the location of the lesion and its proximity to the surface are very important factors when planning surgery. The safe entry zones for removal of a deeply located lesion have been described, while the two-point method has also been described for lesions reaching the pial-ependymal layer; one point is placed at the center of the lesion and the second point is placed on the part of the lesion closest to the pial-ependymal surface to obtain the surgical trajectory [1]. The amalgamation of these two methods, along with the knowledge of microsurgical anatomy and neuroimaging techniques, is crucial for maximizing surgical accuracy and safety.

2.2 Developmental Anatomy: Phylogeny and Ontogeny

An understanding of how the brainstem develops can help one grasp its basic schematic organization. It is speculated that the brainstem evolved as a hyper-specialized portion of the spinal cord to help the vertebrates adapt to the need for special senses and primitive coordination of movements [2]. Sensations related to the immediate environment (tactile, taste) might have been an early addition and are localized to the hindbrain. Distant sensations (vision, olfaction) emerged later; hence, they are located in the midbrain and forebrain. On the other hand, orientation in space (labyrinth) originated early along with motor coordination. Hearing later branched as an adaptation of the vestibular system and vibratory perception. Associative and correlative functions began to unfold in the midbrain (e.g., optic tectum), followed by the emergence of higher diencephalic centers [2]. Hence, the thalamus anatomically constitutes a rostral continuation of the midbrain with no sulcal separation between the two.

Following its formation at approximately 3 weeks of gestation, the neural tube tissue undergoes rudimentary differentiation into alar (dorsal) and basal (ventral) regions. These two parts are delineated by the sulcus limitans – bilateral grooves within the lumen of this tube. The alar and basal mantle form the sensory and motor grey matter of the spinal cord, respectively. This pattern is initially preserved during the development of the brainstem but is later disrupted by the emergence of more complex nuclei and by the transit of cortical, spinal and cerebellar projection fibers. Within 4 weeks of gestation, the neural tube starts to undergo a pattern of folding and dilation, forming the prosencephalon (forebrain), mesencephalon (midbrain) and rhombencephalon

(hindbrain). The latter two go on to form the brainstem structures, with the rhombencephalon later differentiating into the metencephalon and myelencephalon [3].

At approximately 3 months of gestation, the neural tube of the brainstem changes shape, opening dorsally and expanding the dorsal roof plate over this part of the lumen. In most parts of the brainstem, the roof plate is reduced to a thin ependymal layer, through which small overlying blood vessels form the choroid plexus [3]. This expansion leads to the repositioning of the sulcus limitans in the brainstem. In the spinal cord, the sulcus lies in the lateral walls of the lumen, dividing motor and sensory regions into ventral and dorsal locations, respectively. Where the tube has expanded to form the brainstem, the sulcus limitans is located anteriorly in the ventricle, appearing as a groove running down the posterior surface of the brainstem on either side, separating the motor and sensory nuclei medially and laterally, respectively. In the midbrain, however, the alar plate remains in the posterior position to form the tectum (*Latin: roof*). The quadrigeminal – or tectal – plate forms the roof of the sylvian aqueduct and is involved in associative auditory and visual circuitry. Below this level, the roof of the fourth ventricle is formed, along with the cerebellar peduncles, by the *velum*, which is a neural membrane whose inferior part has a vestigial neurological function.

The tegmentum (*Latin: covering*) is derived from the basal plate and forms the floor of the brainstem's ventricular system. The tegmental gray matter gives rise to the cranial nerve (CN) nuclei, secretory nuclei, and reticular formation. However, the most anterior part of the brainstem is not formed by the tegmentum, but mainly by the corticospinal and the corticobulbar fibers within the cerebral peduncles and pyramids. The pons is a specialization of the medulla that is prominent only in mammals due to the development of the cortico-ponto-cerebellar tracts, corticospinal tracts, and pontine nuclei. The corticospinal fibers are separated from the more posterior tegmentum by recognizable landmarks (e.g., lateral medullary sulcus, peritrigeminal area, inferior olivary body), which have been described in previous anatomical reports in relation to potential safe entry zones to subpial brainstem lesions. Sensory fibers such as the medial lemniscus and spinothalamic tract, on the other hand, penetrate the brainstem more posteriorly through the tegmentum.

2.3 Anatomical Features of the Brainstem

It is important to know the external features of the brainstem and how they relate to the underlying structures. The surgeon should be familiar with the anatomy surrounding the brainstem at each level. In every direction, except for the middle cerebellar peduncle and fourth ventricle, there is a subarachnoid cerebrospinal fluid (CSF) cistern immediately adjacent to the brainstem. Each of these typically contains vessels and one or more CNs (Fig. 2.1).

2.3.1 *Mesencephalon (Midbrain)*

The midbrain extends from the thalamus to the pontomesencephalic sulcus. Anteriorly, from lateral to medial, the *cerebral peduncles* are formed by the ipsilateral array of occipito-parieto-temporopontine, corticospinal, corticobulbar and

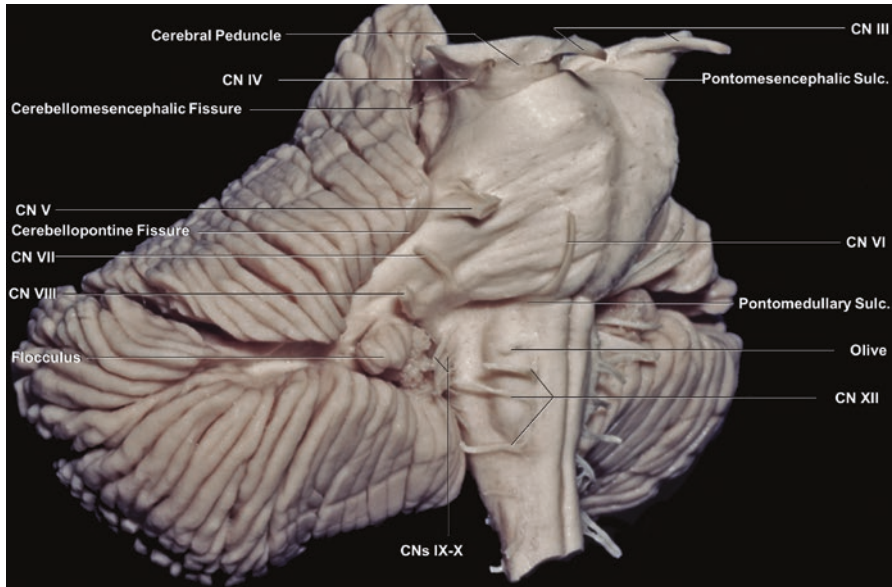


Fig. 2.1 Brainstem seen from the anterolateral perspective. Abbreviations: Sulc., sulcus; CN, cranial nerve

frontopontine fibers descending from the internal capsule. Between the two peduncles is a gap, called the *interpeduncular fossa*, which contains a cistern of the same name and is bounded posteriorly by the posterior perforated substance, which accepts perforators arising from the posterior cerebral artery (PCA) near the basilar apex. The oculomotor nerve has its origin at the medial aspect of the cerebral peduncle and is contained by the cistern that surrounds the remainder of the peduncle – the crural cistern. Beyond the peduncle and lateral mesencephalic sulcus, the posterolateral portion of the mesencephalon is enclosed by the ambient cistern. An incision in the lateral mesencephalic sulcus directed anteriorly leads to the medial lemniscus, which carries contralateral touch and position sense to the thalamus. The *substantia nigra*, which is part of the extrapyramidal system, separates the descending fibers of the peduncle anteriorly and ascending tracts posteriorly (medial lemniscus, ventral spinothalamic, ventral trigemino-thalamic and dentato-rubro-thalamic tracts). The *red nucleus* is located medial to the ascending tracts and is crossed by fibers of the third nerve. Fibers of the superior cerebellar peduncle course medial and posterior to the medial lemniscus to reach the red nucleus and thalamus.

Moving posteriorly in the midline, the sylvian aqueduct communicates the third ventricle with the fourth. The periaqueductal tegmentum holds a dense collection of nuclei including the periaqueductal gray, reticular formation, raphe nuclei, and nuclei of the third and fourth CNs. Fibers of the latter curve postero-medially around the periaqueductal gray matter and cross the midline to emerge from the posterior surface of the brainstem. More laterally, and in the most inferior sections of the midbrain, another series of ascending tracts can be found, including the lateral lemniscus, carrying auditory afferents, and the dorsal spinothalamic tract, contributing

to temperature and pain sensation. Posterior to the aqueduct is the quadrigeminal plate, containing the superior and inferior colliculi, which are concerned with visual and auditory reflexes, respectively. The quadrigeminal cistern separates the quadrigeminal plate from the *lingula* of the cerebellum posteriorly [4].

2.3.2 Pons (Bridge)

The pons is a convex structure extending from the pontomesencephalic sulcus superiorly to the pontomedullary sulcus inferiorly. The descending fibers (corticospinal and corticobulbar tracts) located in its anterior half are mixed with transverse fibers arising from pontine nuclei and flowing into the contralateral middle cerebellar peduncle. Intertwined between these cranio-caudal and latero-lateral systems of fibers, the pontine nuclei integrate a wide variety of inputs to the cortico-ponto-cerebellar circuit, which are thought to provide error correction for motor learning. At the midlevel of the pons convexity, fibers originating in the sensory nucleus of the trigeminal nerve converge to form the sensory root of CN V, anterior to the emergence of the middle cerebellar peduncle. The motor rootlets arise superior to the sensory root before merging with it. Most of the ascending tracts (e.g., medial and lateral lemniscus, ventral and dorsal spinothalamic tracts) are located posterior to the transverse pontine fibers and anterior to the reticular formation.

The posterior aspect of the pons can be considered as the superior half of the floor of the fourth ventricle, which approximates the shape of a rhombus with CSF flowing through openings at each of its vertices: lateral recesses (Luschka) on either side draining into the cerebellopontine cistern, obex (Magendie) inferiorly draining into the cisterna magna and ependymal canal, and the sylvian aqueduct superiorly. Between these vertices, the rhombus is outlined by the cerebellar peduncles. The floor of the fourth ventricle is divided vertically by the median sulcus, paramedian sulcus and sulcus limitans; and horizontally by an imaginary line between the two lateral recesses that divides it into superior (pontine) and inferior (medullary) halves. The *medullary striae* follow this line to the lateral recesses, entering the acoustic area. There are several CN nuclei near the floor of the fourth ventricle, divided by the sulcus limitans into medial motor and lateral sensory areas. In the superior half, the most prominent structure is the facial colliculus. Located in the medial eminence, this structure overlies both the abducens nucleus and facial nerve fibers that course around it after originating in the facial nucleus more anteriorly near the pontomedullary sulcus [4].

2.3.3 Medulla Oblongata

The medulla oblongata is the most inferior segment of the brainstem. Its anterior surface is dominated by the pyramids, which contain the corticospinal and corticobulbar tracts. In the most inferior (closed) portion of the medulla, the corticospinal tract decussates, with 85% of its fibers crossing the midline before flowing into

the contralateral spinal cord. Lateral to the pyramids, the olivary eminence – or body – is limited by the pre-olivary sulcus anteriorly, where the hypoglossal rootlets emerge. Posterior to the olive, the retro-olivary sulcus holds the origins of CNs IX, X and XI [5, 6]. Continuing posteriorly, the lateral eminence features the trigeminal tubercle (*tuberculum cinereum*), which is the prominence containing the spinal trigeminal nucleus and tract; then, more posteriorly are the cuneate and gracile tubercles that contain the continuation of the dorsal column fibers and their respective nuclei, where they synapse before decussating as internal arcuate fibers. This “sensory decussation” is more superior than the pyramidal decussation, continuing superiorly as the medial lemniscus, which travels posterior to the pyramids near the midline in the upper medulla.

The superior (open) part of the medulla faces the fourth ventricle posteriorly. Visible landmarks here include the hypoglossal nucleus medially, which is flanked by the dorsal nucleus of the vagus nerve and the vestibular nuclei laterally. Deep to the vestibular area are the solitary tract and nucleus. Within the medulla, the hypoglossal fibers leave their nucleus and course anteriorly between the pyramid and the inferior olivary nucleus. Posterior to the olive and anterior to the floor of the fourth ventricle and its nuclei lies the reticular formation of the medulla, which contains neurons projecting to several areas of the brain and spinal cord, and through which the vestibulospinal tracts pass. Laterally in the reticular formation, the fibers of the nucleus ambiguus join the motor fibers of the dorsal vagus nucleus, and then exit the medulla as the rootlets of the vagus nerve [4].

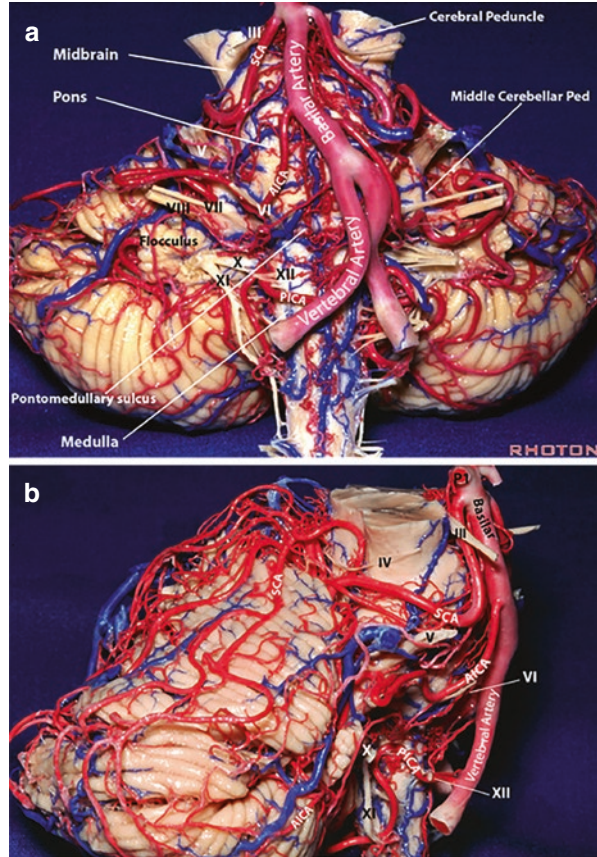
2.4 Vascular Anatomy of the Brainstem

2.4.1 Arterial Supply [7, 8]

2.4.1.1 Midbrain

Most of the mesencephalon is vascularized by perforator branches from the PCA, but branches of the anterior choroidal artery often contribute blood supply to the cerebral peduncle and substantia nigra, and posterior communicating branches may penetrate the posterior perforated substance. Another exception is the inferior quadrigeminal plate that is irrigated by the superior cerebellar artery (SCA). The anteromedial segments of the midbrain are perfused by paramedian perforators originating from the basilar bifurcation and P1 arteries that enter the posterior perforated substance in the interpeduncular fossa. Structures in this region include the red nucleus, medial longitudinal fasciculus, and oculomotor and Edinger-Westphal nuclei. Anterolateral structures of the midbrain, including parts of the cerebral peduncle and medial lemniscus, gain blood supply from small branches of the quadrigeminal and medial posterior choroidal arteries. There has been some variation reported in the origin of the quadrigeminal artery, including from the P1, proximal P2 or distal P2. The quadrigeminal plate is supplied by the quadrigeminal

Fig. 2.3 Neurovascular relationships of the brainstem. **(a)** Anterior view. **(b)** Lateral view. Abbreviations: III, oculomotor nerve; IV, trochlear nerve; V, trigeminal nerve; VII, facial nerve; VIII, vestibulocochlear nerve; IX, glossopharyngeal nerve; X, vagus nerve; XI, spinal accessory nerve; XII, hypoglossal nerve; AICA, anterior inferior cerebellar artery; PICA, posterior inferior cerebellar artery; SCA, superior cerebellar artery



of the pons is irrigated by the short circumferential branches of the basilar artery. The posterolateral pons is perfused by long circumferential arteries. The long circumferential blood supply is augmented by the SCA rostrally and posteriorly, and by the anterior inferior cerebellar artery (AICA) caudally and anteriorly. The middle cerebellar peduncle is perfused by the SCA superiorly and AICA inferiorly (see Figs. 2.2 and 2.3).

2.4.1.3 Medulla

The paramedian perforators from the caudal basilar artery also supply the medial rostral medulla; this is augmented by small branches from the vertebral arteries (VAs). Structures falling within this region include the medial longitudinal fasciculus, tectospinal tract, medial lemniscus and corticospinal tracts. More caudally, these structures and the hypoglossal nucleus are perfused by the anterior spinal artery. The VA gives rise to the anterior spinal artery, which fuses with its contralat-

eral artery to descend along the anterior median fissure on the surface of the medulla and spinal cord, contributing to the lower medulla's irrigation. Similar to the pons, the medial structures of the medulla form one distinct vascular territory, with the lateral regions forming multiple territories perfused by different vessels. In the medulla, the lateral region is supplied by the VA anteriorly and posterior inferior cerebellar artery (PICA) posteriorly. The vascular territories of the caudal medulla mirror those of the spinal cord: the posterior spinal arteries supply all of the posterior structures, and the anterior spinal artery, coursing over the ventral median sulcus, intermittently gives off perforators that become sulcocommissural arteries (see Figs. 2.2 and 2.3).

2.4.2 Venous Anatomy [9]

Venous drainage of the brainstem is highly variable. There is usually a network of horizontal and vertical veins. Many of these veins course in anatomical sulci and fissures and, hence, take their names (see Fig. 2.3).

2.4.2.1 Midbrain

The midbrain is encircled by a network of veins. Anteriorly, in the interpeduncular fossa, resides the medial anterior pontomesencephalic vein. In some cases, this vein may be duplicated, with two veins coursing upwards between the oculomotor nerves, joined by a commissural vein. The medial anterior pontomesencephalic veins drain into the peduncular vein, which in turn converges with the basal vein of Rosenthal. The lateral midbrain is drained by the lateral mesencephalic veins, which in turn also drain into the peduncular veins. These lateral mesencephalic veins form anastomoses with the vein of the pontomesencephalic sulcus, which itself courses anteriorly, joining the pontomesencephalic vein.

2.4.2.2 Pons

As in the midbrain, the pontomesencephalic vein courses along the anterior surface of the pons. There is some normal variation in its anatomy, and it may be duplicated. Various transverse tributaries deliver venous blood from more lateral portions of the pons to the anterior pontomesencephalic vein. Veins of the middle cerebellar peduncle take a vertical course more laterally on the pons and converge with the veins of the cerebellar fissures and transverse pontine veins to form the superior petrosal vein (Dandy's vein). Various bridging veins are emitted from the anastomotic venous network over the brainstem, draining into the dural sinuses.

2.4.2.3 Medulla

The medulla is drained by a network of vertical vessels, intermittently forming anastomoses with one another via transverse medullary veins. The medial anterior medullary vein is the most anterior of these, with the pre-olivary and retro-olivary veins lying more posteriorly. Although the medullary veins partially drain into the pontine venous network, they also emit bridging veins draining into the marginal sinus of the foramen magnum and the veins of the hypoglossal canal.

2.4.3 Vascular Relationships and the Rule of Three [8]

Dr. Albert Rhoton Jr. divided the posterior fossa into three groups of structures, each organized around a major posterior fossa artery. Branches of the vertebrobasilar system supply the brainstem and cerebellum. The VAs pierce the posterior fossa dura medial to the occipital condyles and pass anterior to the lower CNs before converging at the vertebrobasilar junction, near the pontomedullary junction. The basilar artery sends short and long circumflex arteries to the pons before it ultimately bifurcates into the PCAs at the level of the midbrain. Three pairs of cerebellar arteries arise from the vertebrobasilar system and have specific neural relationships during their course. While learning posterior fossa anatomy, it is helpful to relate the major posterior fossa arteries to the cisterns, brainstem and cerebellar surfaces, and CNs (see Figs. 2.2 and 2.3).

The *upper neurovascular complex* follows the SCA and includes the midbrain and upper pons, trigeminal nerve, trochlear nerve, superior petrosal vein and its tributaries, and the superior surface of the cerebellum. After arising near the basilar apex, the SCA travels immediately inferior to the oculomotor nerve before curving around the brainstem close to the pontomesencephalic junction. It often bifurcates into rostral and caudal branches. Laterally, these branches enter the cerebellomesencephalic fissure, where they travel with the trochlear nerve. Before entering this fissure, one of its branches may loop inferiorly to contact the trigeminal nerve, possibly causing trigeminal neuralgia. After coursing posteriorly around the superior cerebellar peduncle, then emerging from the cerebellomesencephalic fissure, the branches supply the superior surface of the vermis and cerebellar hemispheres. Perforating branches enter the superior cerebellar peduncle and supply deeper structures such as the dentate nucleus.

The *middle neurovascular complex* follows the AICA and includes the lower pons, middle cerebellar peduncle, cerebellopontine angle, and facial and vestibulocochlear nerves. The AICA usually originates from the lower half of the basilar artery. As it courses around the brainstem, it may pass near any of the CNs emerging from the pontomedullary fissure – the abducens, facial, cochlear and vestibular nerves. Impingement of the root entry zone of the facial nerve may cause hemifacial spasm. AICA enters the cerebellopontine angle to supply the middle cerebellar peduncle and the portion of the cerebellum facing the petrous temporal bone. Often, a loop of AICA extends into the internal auditory canal (IAC) and may impinge

upon the nervus intermedius to cause geniculate neuralgia. The AICA may also pass between the nerves of the VII/VIII complex before they enter the IAC.

The *lower neurovascular complex* follows the PICA and includes the medulla, lower CNs and inferior cerebellum. The PICA typically arises from the distal VA but can arise from any part of the VA, including its extradural portion, or from the proximal basilar artery. The PICA courses posteriorly from the anterior medulla either above or below the hypoglossal nerve rootlets. As it reaches the lateral medulla, it turns inferiorly before reaching the cerebellar tonsil and then passes anterior or posterior to the glossopharyngeal, vagus and spinal-accessory nerves in a variable manner. After forming its caudal loop, the PICA ascends along the inferior cerebellar peduncle, deep to the cerebellar tonsil, before bifurcating into branches supplying the inferior vermis and inferior hemisphere. Prior to this bifurcation, there are also branches supplying the choroid plexus of the fourth ventricle via the tela choroidea.

2.5 Special Microsurgical Regions and Surgical Safe Entry Zones

Given the high concentration of eloquent structures in the brainstem, lesions are usually resected through their exophytic portion, if present. When the lesion does not present itself to the pial surface, anatomical entry zones [10–14] can be exploited to access it with the least possible risk of neural injury. Below is a list of the described zones, which are also summarized in Table 2.1.

2.5.1 *Interpeduncular Fossa and Cerebral Peduncles* [15, 16]

The interpeduncular fossa is typically exposed to treat basilar apex aneurysms or tumors extending inferiorly from the parasellar and perichiasmatic areas. It is accessed through the optic-carotid and the carotid-oculomotor windows by opening Lilliequist's membrane, which has a variable configuration [15]. This exposure can be expanded by mobilizing the carotid artery and the optic or oculomotor nerves. Performing an anterior clinoidectomy and dissecting the posterior cavernous sinus and posterior clinoid process widens these windows and permits access through the oculomotor-tentorial corridor, lateral to the third nerve [17]. Alternatively, the interpeduncular fossa can be approached endoscopically by transposing the pituitary gland and drilling the dorsum sellae. For lesions in the anterior midbrain, the *perioculomotor entry zone* has been proposed (Fig. 2.4a). This zone lies between the pyramidal tract and the oculomotor nerve's emergence. A vertical incision here usually interrupts the frontopontine fibers and should be limited to less than one-fourth of the cerebral peduncle in width. The interpeduncular fossa approach directed between the mammillary bodies and the tip of the basilar artery and through the interpeduncular fossa can be alternatively used for lesions located in the ventromedian midbrain [18] (see Fig. 2.4a).

Table 2.1 Safe entry zones to the brainstem

Region	Safe Entry Zone(s)	Limits	Surgical Approach(s)
<i>Midbrain</i>			
Ventral	Periocolomotor zone	Pyramidal tract and exit of CN III	Pterional/ FOZ-Transcavernous
Antero-lateral	Lateral mesencephalic sulcus	Cerebral peduncle and tectal area	Subtemporal Lateral infratentorial
Posterior	Supracollicular zone	Transverse line above the superior colliculi	SCIT Occipital trans-tentorial
	Infracollicular zone	Transverse line below the inferior colliculi	
	Intercollicular zone	Vertical line between colliculi	
<i>Pons</i>			
Antero-lateral	Peritrigeminal zone	Vertical line on the medial aspect of CNs V and VII entry points, lateral to pyramidal tract	Retrosigmoid Transpetrosal approaches
	Area lateral to CNs V-VII; MCP	Lateral to entry points of CNs V and VII	
Dorsal	Median sulcus	Midline between bilateral MLFs	Transcerebellomedullary fissure telovelar Transvermian
	Suprafacial collicular zone	Above facial colliculus	
	Infracollicular zone	Facial colliculus and hypoglossal trigone	
<i>Medulla</i>			
Antero-lateral	Pre-olivary sulcus	Olive and pyramidal tract	Far lateral
	Retro-olivary sulcus	Olive and ICP/CNs IX and X	
Dorsal	Posterior median sulcus	Bilateral gracile tubercles	Suboccipital
	Posterior intermediate sulcus	Gracile and cuneate tubercles	
	Posterior lateral sulcus	Lateral to cuneate tubercle	

Abbreviations: *CN* cranial nerve, *FOZ* fronto-orbito-zygomatic, *ICP* inferior cerebellar peduncle, *MCP* middle cerebellar peduncle, *MLF* medial longitudinal fasciculus, *SCIT* supracerebellar-infratentorial

2.5.2 *Quadrigeminal and Ambient Cisterns*

The pineal region is the most rostral and posterior aspect of the brainstem and includes the pineal gland (part of the epithalamus) and quadrigeminal plate (posterior midbrain). It is enveloped by the quadrigeminal cistern and occupies a transition zone at the posterior incisura, interconnecting the infratentorial contents of the posterior fossa and the supratentorial forebrain. Therefore, it can be exposed through supra- or infra-tentorial approaches. The superior boundaries of this region are the thalamic pulvinar anterome-

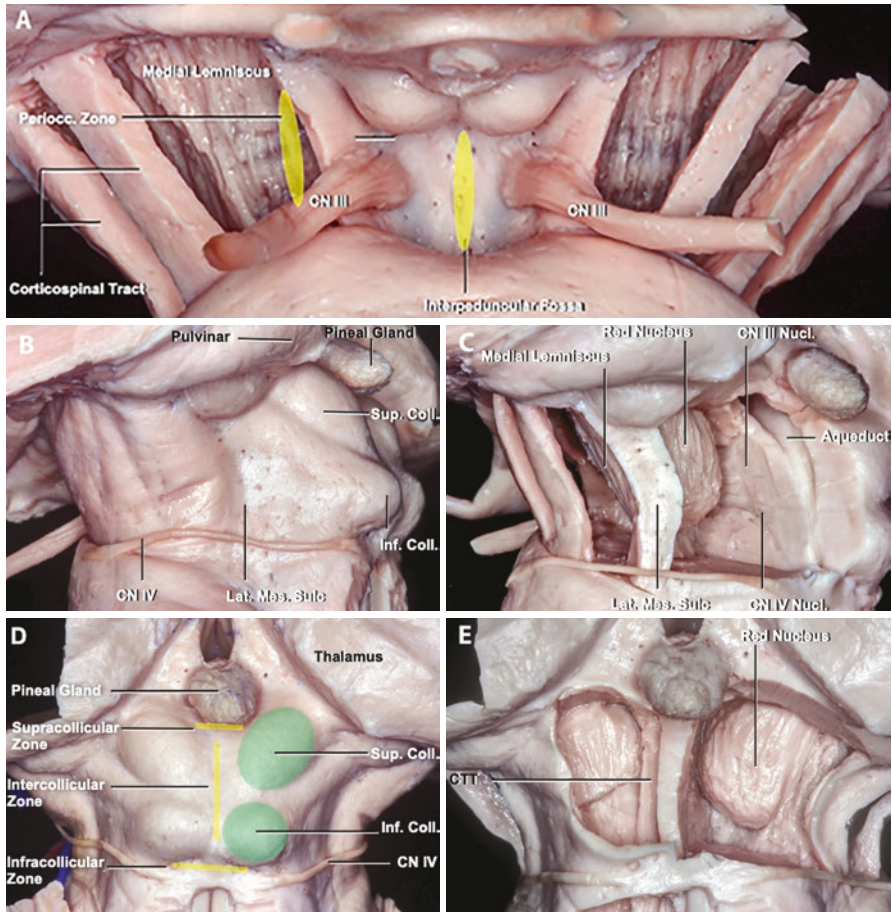


Fig. 2.4 Safe entry zones to the midbrain. (a) Anterior view of cerebral peduncles and interpeduncular fossa. (b) Left lateral view of midbrain. (c) Left lateral view of midbrain with dissection. (d) Posterior view of midbrain. (e) Posterior view of midbrain with dissection. Abbreviations: CN, cranial nerve; Coll., colliculus; CTT, central tegmental tract; Inf., inferior; Lat., lateral; Mes., mesencephalic; Nucl., nucleus; Periocc., perioloculomotor; Sulc., sulcus; Sup., superior

dially and the splenium of the corpus callosum centrally, which may be divided during supratentorial approaches [15]. The fornices are lateral, coursing superior to the pulvinar, but their commissure lies ventral to the corpus callosum in this area. Also, in the roof of this region, an arachnoid cloak inferior to the splenium joins anteriorly with the tela choroidea and velum interpositum to house a complex venous network. From anteromedially, the internal cerebral veins emerge from the velum interpositum to join with the laterally coursing basal vein of Rosenthal to drain into the vein of Galen posteromedially. It is here where tributary veins from both the supratentorial and infratentorial brain converge and form an estuary of venous outflow to the straight sinus.

The pillar of the pineal region is formed anteriorly. Rostral to the gland and medial to the habenular trigone is the suprapineal recess of the third ventricle. Inferior to the pineal gland, the posterior commissure lies above the superior colliculi, sending fibers dorsally around the periaqueductal gray. Inferomedial to the inferior colliculi, the trochlear nerve (CN IV) emerges. Caudally, at the level of the cerebellomesencephalic fissure is the superior medullary velum medially and the superior cerebellar peduncle. The lateral margins of the pineal region consist of the ambient cisterns and their contents. Inferior to the venous structures listed above, branches of the PCA and SCA emerge from the ambient cistern and help supply medial structures in the quadrigeminal cistern [15]. The medial posterior choroidal artery branch of the PCA follows this path and turns medially and anteriorly past the pineal body to supply the velum interpositum, which roofs the posterior third ventricle. Perforating branches of the PCA also supply the lateral brainstem above the groove between the superior and inferior colliculi. The SCA conversely supplies the brainstem below this intracollicular groove, before sending branches to the vermis and the cerebellar hemispheres.

Posterior approaches to midbrain lesions typically employ one of four entry zones. The *supracollicular area* is a transverse linear zone above the superior colliculi and is limited by the pineal body and habenula superiorly. Deep dissection should stop at the level of the aqueduct to avoid oculomotor nerve and medial longitudinal fasciculus injury. The area is usually covered by the precentral cerebellar veins draining into the vein of Galen, and care must be taken when dissecting them. The *infracollicular area* is a transverse linear zone below the inferior colliculi and above the trochlear nerve, and the *intercollicular* incision is oriented vertically in the midline of the quadrigeminal plate (see Fig. 2.4). Deep dissection here should also stop at the level of the aqueduct to prevent trespassing the trochlear nucleus, medial longitudinal fasciculus, and superior cerebellar decussating fibers. Finally, the *lateral mesencephalic sulcus* is near the boundary between the cerebral peduncle and the mesencephalic tegmentum. It can be accessed through a lateral infratentorial or subtemporal approach. It is limited by the cerebral peduncle medially and the tectal colliculi laterally, the pontomesencephalic sulcus inferiorly, and the medial geniculate body superiorly. The lateral mesencephalic vein overlies the sulcus and is a helpful landmark to identify it. An incision here can access the substantia nigra, medial lemniscus, and more posterior regions. The red nucleus and oculomotor and trochlear nerve nuclei are at risk as dissection proceeds deeper [10–14].

2.5.3 Floor of Fourth Ventricle [4, 19]

As described previously, the median sulcus divides the floor of the fourth ventricle vertically, while the sulcus limitans separates the motor and sensory areas (Fig. 2.5). Lateral to the median sulcus is the medial eminence, a prominent elevation in the superior half of the floor, which in turn is bounded laterally by the sulcus limitans. Lateral to the sulcus limitans in the upper fourth ventricle is the triangular superior fovea, which is bounded by the superior cerebellar peduncle above and the vestibular area below. At the superior end of the sulcus limitans, in the lateral part of the

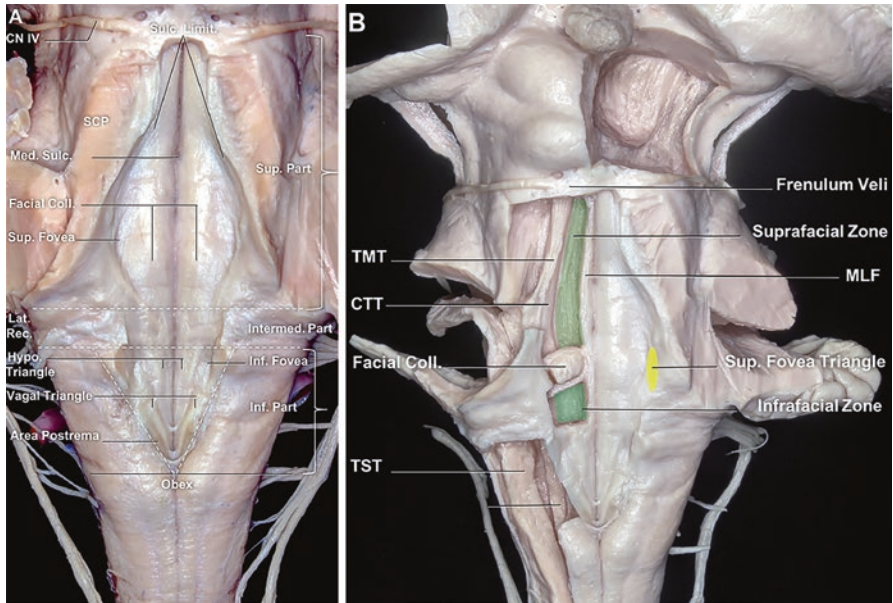


Fig. 2.5 Safe entry zones through the fourth ventricle. **(a)** Posterior view of brainstem and fourth ventricle. **(b)** Posterior view of brainstem and fourth ventricle with dissection. Abbreviations: CN, cranial nerve; Coll., colliculus; CTT, central tegmental tract; Hypo., hypoglossal; Inf., inferior; Interm., intermediate; Lat., lateral; Limit., limitans; Med., median; MLF, medial longitudinal fasciculus; Rec., recess; SCP, superior cerebellar peduncle; Sulc., sulcus; Sup., superior; TMT, trigeminal mesencephalic tract; TST, trigeminal spinal tract

floor, there is a bluish-gray area known as the *locus coeruleus*, which sends norepinephrine secreting fibers to many areas of the brain. The color is given by the underlying pigmented cells containing melanin. Lateral to this structure is the vestibular area. The medial eminence contains the facial colliculus – a prominence formed by the abducens nucleus and facial motor fibers wrapping around it. Below the medial eminence lie three triangular areas, which give the inferior part of the floor the shape of a pen nib, thus the name “calamus scriptorius.” The triangles are named according to the structures beneath them: the hypoglossal triangle containing the hypoglossal nucleus is the most medial structure, just lateral to the median sulcus. Lateral to hypoglossal triangle is the vagal triangle that contains the dorsal motor nucleus of the vagus nerve. The area postrema is lateral to the vagal triangle at the most inferior part of the fourth ventricle near the central canal.

Several safe entry zones to the brainstem through the fourth ventricle, typically accessed through a telovelar approach, have been described. The *median sulcus* may be opened to approach midline lesions above the facial colliculi, but this dorsal sulcus separates the two medial longitudinal fasciculi; therefore, this approach carries a high risk of causing internuclear ophthalmoplegia. The *suprafacial collicular zone* is located just above the facial colliculus. It is limited medially by the medial longitudinal fasciculus and laterally by the sulcus limitans, to avoid the locus coeruleus and the fibers deep to it, such as the trigeminal mesencephalic tract and

central tegmental tract. Superiorly, it is limited by the frenulum veli containing the trochlear nerve. The *infrafacial collicular zone* lies below the facial colliculus and above the hypoglossal trigone. A transverse incision could be made in the lateral recess of the fourth ventricle, just above the medullary striae. This area is also limited by the medial longitudinal fasciculus medially and the facial nucleus and nucleus ambiguus laterally. The superior fovea triangle approach, which is limited by the superior cerebellar peduncle superolaterally, vestibular area inferolaterally, and sulcus limitans medially, is used for dorsally located lesions at the level of the facial colliculus in the pons [20].

2.5.4 Cerebellopontine Angle and Related Cisterns

The cerebellopontine angle is a space situated between the superior and inferior parts of the cerebellopontine fissure, bordered by the petrosal surface of the cerebellum posteriorly, the middle cerebellar peduncle medially, and the petrous bone anterolaterally [5]. The 4-to-11th CNs are within or near the cerebellopontine angle, which must be considered when planning an incision into the brainstem. The prepontine and premedullary cisterns face the clivus. The premedullary cistern harbors the hypoglossal nerve, which originates between the pyramid and inferior olive, as well as the VA as it enters the cranial cavity and gives rise to the anterior spinal artery [15]. The cerebello-medullary cistern is limited by the cerebellar tonsil medially, and foramen magnum, occipital condyle and jugular tubercle laterally. Its contents include the VA, CNs IX-XII, and the origin of PICA. It is separated from the premedullary cistern by arachnoid trabeculae anterior to CN IX-XI at the dorsal aspect of the inferior olive (retro-olivary sulcus) [21]. The cerebello-medullary fissure is formed by the tonsillo-medullary and the uvulo-tonsillar spaces, which together form its L-shaped structure. While it communicates medially with the cisterna magna, it extends laterally towards the cerebello-medullary and cerebello-pontine cisterns. Antero-superiorly, the fissure is limited by the inferior and middle cerebellar peduncles. Dissection of the uvulo-tonsillar and tonsillo-medullary fissures are key steps to mobilize the cerebellar tonsil and expose the lateral recess during a telovelar approach [21].

Approaches to the brainstem should account for the anatomy related to the CNs. The trochlear nerve is the most superior and travels near the level of the incisura before reaching the cavernous sinus. After exiting the lateral pons anterior to the middle cerebellar peduncle, the trigeminal nerve travels anteriorly and superiorly towards the petrous apex, then below the superior petrosal sinus before entering Meckel's cave in the middle cranial fossa. The 6th, 7th and 8th CNs emerge from the pontomedullary sulcus. The more medial 6th CN travels upwards, pierces the dura and enters Dorello's canal to enter the paraclival venous confluence and cavernous sinus. The more lateral 7th and 8th CNs travel together laterally towards the IAC. The 9th, 10th and 11th CNs arise posterior to the olive and course laterally to enter the jugular foramen, whereas the 12th

CN has multiple rootlets exiting the pre-olivary sulcus, which exit the posterior fossa through the hypoglossal canal, just below the jugular foramen [5].

Entry zones through these areas include the *peritrigeminal zone*, described as a vertical zone in the medial aspect of the space between the exits of CNs V and VII, lateral to the pyramidal tract (Fig. 2.6) [11]. Dissection deep to this zone crosses the

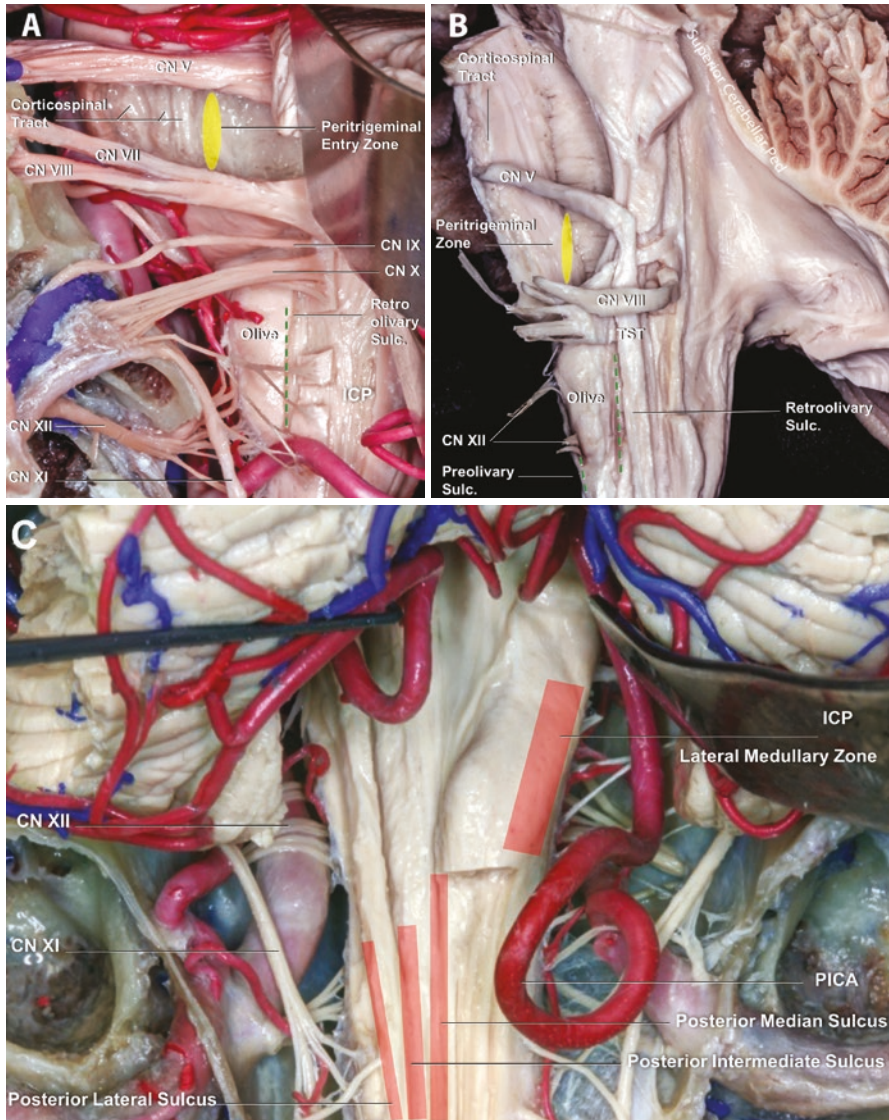


Fig. 2.6 Safe entry zones to the ventral and dorsal parts of the pons and medulla. (a) Left lateral view of pons and medulla with entry zones. (b) Lateral view of brainstem with dissection. (c) Posterior view of medulla with dissection and entry zones. Abbreviations: CN, cranial nerves; ICP, inferior cerebellar peduncle; Ped, peduncle; PICA, posterior inferior cerebellar artery; Sulc., sulcus; TST, trigeminal spinal tract

transverse pontine fibers and eventually leads to the pontine nuclei. The trigeminal motor nucleus is located about 1 cm dorsomedial to the junction of the trigeminal nerve with the pons. The nucleus of the facial nerve is encountered caudal to the emergence of the facial nerve. More laterally, the *middle cerebellar peduncle* may be incised. The petrosal fissure of the cerebellum is opened to minimize the need for cerebellar retraction [22]. The middle cerebellar peduncle carries pontocerebellar afferent fibers traveling from the pontine nuclei to the cerebellar hemisphere, and lesions here may cause ataxia and dysmetria with hypotonia during voluntary movement of the ipsilateral extremity. The pial incision should be carried out parallel to the pontocerebellar tract to minimize the number of disrupted fibers. Stereotactic navigation can be used to direct the dissection towards the deeper parts of the pons.

In the medulla, the *pre-olivary (anterolateral) sulcus* is a small zone anterior to the medullary olive and posterolateral to the pyramidal tract (see Fig. 2.6). It is located between the hypoglossal nerve and C1 rootlets. The pyramidal tract lies immediately medial to it and is at risk of injury. The *retro-olivary sulcus* is an entry zone located posterior to the olive and anterior to the inferior cerebellar peduncle and rootlets of the glossopharyngeal and vagus nerves [10–14]. The nucleus ambiguus within the reticular formation is at risk deep in this zone. For more dorsally located lesions, the lateral medullary zone over the inferior cerebellar peduncle is incised [23]. The *dorsal medullary zone*, in the caudal dorsal part of the medulla, contains multiple sulci that can be identified below the obex of the fourth ventricle and represent natural extensions of spinal cord sulci. The *posterior median sulcus* separates the two gracile tubercles. The *posterior intermediate sulcus* is located between the gracile and cuneate tubercles, while the *posterior lateral sulcus* is lateral to the cuneate tubercle. The spinal trigeminal tract could be inadvertently entered, as it lies deep and lateral to the cuneate fasciculus (see Fig. 2.6) [10–14].

2.6 Conclusion

Although not an exhaustive treatise on brainstem anatomy, we have presented an overview of surgically relevant external anatomical landmarks and related neurological structures. There are no completely “safe” entry zones to the brainstem, but knowledge of brainstem anatomy and how it relates to a particular lesion will help guide the surgeon to the best approach.

When planning an operation on the brainstem, an approach that minimizes morbidity should be selected. When a lesion reaches the surface, adjacent critical structures have already been displaced away from the surgical trajectory, so the risks are generally lower. Deeper lesions entail greater risks as healthy neural tissue must be injured to some degree to gain access. This requires an understanding of the relationship between external brainstem landmarks and underlying critical structures, such as CN nuclei or fiber tracts, which may be injured during surgical exposure. Because of the high density of important structures, no approach into the brainstem is without risk. Nonetheless, experience with a variety of “safe entry zones” that are

guided by anatomical principles described in this chapter has been growing. Perhaps nowhere else in the brain is knowledge of anatomy is as important for surgical planning.

Acknowledgments All figures are courtesy of the Rhoton Collection (<http://rhoton.ineurodb.org>). Dissections were carried out by Hiroshi Abe, Antonio Mussi, Hung Wen, and Kaan Yağmurlu.

References

1. Kalani MY, Yagmurlu K, Martirosyan NL, Cavalcanti DD, Spetzler RF. Approach selection for intrinsic brainstem pathologies. *J Neurosurg.* 2016;125(6):1596–607.
2. Sarnat HB, Netsky MG. *Evolution of the nervous system.* Oxford, UK: Oxford University Press; 1974.
3. Molnar Z. Development of the nervous system. In: Standring S, editor. *Gray's anatomy: the anatomical basis of clinical practice.* 41st ed. London: Elsevier; 2016.
4. Rhoton AL Jr. Cerebellum and fourth ventricle. *Neurosurgery.* 2000;47(3 Suppl):S7–27.
5. Rhoton AL Jr. The cerebellopontine angle and posterior fossa cranial nerves by the retrosigmoid approach. *Neurosurgery.* 2000;47(3 Suppl):S93–129.
6. Matsushima T, Inoue T, Inamura T, Natori Y, Ikezaki K, Fukui M. Transcerebellomedullary fissure approach with special reference to methods of dissecting the fissure. *J Neurosurg.* 2001;94(2):257–64.
7. Rhoton AL Jr. The cerebellar arteries. *Neurosurgery.* 2000;47(3 Suppl):S29–68.
8. Rhoton AL Jr. The three neurovascular complexes in the posterior fossa and vascular compression syndromes (honored guest lecture). *Clin Neurosurg.* 1994;41:112–49.
9. Rhoton AL Jr. The posterior fossa veins. *Neurosurgery.* 2000;47(3 Suppl):S69–92.
10. Cavalcanti DD, Preul MC, Kalani MY, Spetzler RF. Microsurgical anatomy of safe entry zones to the brainstem. *J Neurosurg.* 2016;124(5):1359–76.
11. Recalde RJ, Figueiredo EG, de Oliveira E. Microsurgical anatomy of the safe entry zones on the anterolateral brainstem related to surgical approaches to cavernous malformations. *Neurosurgery.* 2008;62(3 Suppl 1):9–15; discussion -7.
12. Yagmurlu K, Rhoton AL Jr, Tanriover N, Bennett JA. Three-dimensional microsurgical anatomy and the safe entry zones of the brainstem. *Neurosurgery.* 2014;10(Suppl 4):602–19; discussion 19–20.
13. Bricolo A. Surgical management of intrinsic brain stem gliomas. *Op Tech Neurosurg.* 2000;3(2):137–54.
14. Giliberto G, Lanzino DJ, Diehn FE, Factor D, Flemming KD, Lanzino G. Brainstem cavernous malformations: anatomical, clinical, and surgical considerations. *Neurosurg Focus.* 2010;29(3):E9.
15. Rhoton AL Jr. The posterior fossa cisterns. *Neurosurgery.* 2000;47(3 Suppl):S287–97.
16. Hebb MO, Spetzler RF. Lateral transpeduncular approach to intrinsic lesions of the rostral pons. *Neurosurgery.* 2010;66(3 Suppl Operative):26–9; discussion 9.
17. Basma J, Ryttefjors M, Latini F, Pravdenkova S, Krisht A. Mobilization of the transcavernous oculomotor nerve during basilar aneurysm surgery: biomechanical bases for better outcome. *Neurosurgery.* 2014;10(Suppl 1):106–14; discussion 14–5.
18. Kalani MYS, Yagmurlu K, Spetzler RF. The interpeduncular fossa approach for resection of ventromedial midbrain lesions. *J Neurosurg.* 2018;128(3):834–9.
19. Mussi AC, Rhoton AL Jr. Telovelar approach to the fourth ventricle: microsurgical anatomy. *J Neurosurg.* 2000;92(5):812–23.
20. Yagmurlu K, Kalani MYS, Preul MC, Spetzler RF. The superior fovea triangle approach: a novel safe entry zone to the brainstem. *J Neurosurg.* 2017;127(5):1134–8.

21. Matsushima T, Fukui M, Inoue T, Natori Y, Baba T, Fujii K. Microsurgical and magnetic resonance imaging anatomy of the cerebello-medullary fissure and its application during fourth ventricle surgery. *Neurosurgery*. 1992;30(3):325–30.
22. Kalani MY, Yagmurlu K, Martirosyan NL, Spetzler RF. The Retrosigmoid petrosal fissure Transpeduncular approach to central pontine lesions. *World Neurosurg*. 2016;87:235–41.
23. Bozkurt B, Kalani MYS, Yagmurlu K, Belykh E, Preul MC, Nakaji P, et al. Low Retrosigmoid Infratonsillar approach to lateral medullary lesions. *World Neurosurg*. 2018;111:311–6.

Chapter 3

Imaging of Brainstem Lesions



Miguel A. Flores, Ari M. Blitz, Sachin K. Gujar,
and Thierry A. G. M. Huisman

Abbreviations

¹⁸ F-FDG PET	¹⁸ F-2-fluoro-2-deoxy-D-glucose positron emission tomography
¹⁸ F-FET PET	¹⁸ F-fluoro-ethyl-tyrosine positron emission tomography
¹ H-MRS	¹ H-MR-spectroscopy
¹ H-MRSI	¹ H-Magnetic resonance spectroscopic imaging
3D	Three-dimensional
ADC	Apparent diffusion coefficient
ADEM	Acute disseminated encephalomyelitis
ASL	Arterial spin labeling
AVM	Arterio-venous malformation
BBB	Blood brain barrier
BSCMs	Brainstem cavernous malformations
BSGs	Brainstem Gliomas
b-SSFP	Balanced steady-state free precession
CBF	Cerebral blood flow
CBV	Cerebral blood volume
Cho	Choline
CISS	Constructive interference in steady state CN: cranial nerve
CNS	Central nervous system
CPA	Cerebellopontine angle cistern
Cr	Creatine

M. A. Flores · S. K. Gujar
Division of Neuroradiology, Russell H. Morgan Department of Radiology and Radiological
Science, Johns Hopkins Hospital, Baltimore, MD, USA

A. M. Blitz
Division Chief, Neuroradiology, University Hospitals, Case Western Reserve University,
Cleveland, OH, USA

T. A. G. M. Huisman (✉)
Radiologist-in-Chief and Edward B. Singleton Chair of Radiology, Department of Radiology,
Texas Children's Hospital and Baylor College of Medicine, Houston, TX, USA
e-mail: huisman@texaschildrens.org

CSF	Cerebral spinal fluid
CT	Computed tomography
DCE	Dynamic contrast enhancement
DIPG	Diffuse intrinsic pontine glioma
DRO	Dentate-rubro-olivary
DSC	Dynamic susceptibility contrast
DTI	Diffusion tensor imaging
DTT	Diffusion tensor tractography
DVA	Developmental venous anomaly
DWI	Diffusion weighted imaging
DWI/DTI	Diffusion weighted or tensor imaging
ED	Emergency department
EV71	Enterovirus 71
FA	Fractional anisotropy
FIESTA	Fast imaging employing steady-state acquisition
FLAIR	Fluid-attenuated inversion recovery
HOD	Hypertrophic olivary degeneration
HSV1	Herpes simplex virus 1
HU	Hounsfield units
IAC	Internal auditory canal
ICH	Intracranial hemorrhage
ION	Inferior olivary nucleus
IV	Intravenous
MRI	Magnetic resonance imaging
MS	Multiple sclerosis
MTT	Mean transit time
NAA	N-acetylaspartate
ODS	Osmotic demyelination syndrome
PCNSL	Primary central nervous system lymphoma
PET	Positron emission tomography
PPH	Primary pontine hemorrhage
PWI	Perfusion weighted imaging
rCBV	Relative cerebral blood volume
RE	Rhombencephalitis
SWI	Susceptibility-weighted imaging
TB	Tuberculosis
TTP	Time-to-peak
WHO	World Health Organization

3.1 Introduction

Brainstem lesions are defined as those centered within the midbrain, pons, or medulla oblongata. The brainstem serves to facilitate and control vital functions necessary for sustaining life, with many anatomic components located within a

compact space. In addition to facilitating/transmitting information between the cerebrum, cerebellum and spinal cord, the brainstem also contributes to regulation of consciousness, muscle tone/posture, and respiration [1]. Also, there are multiple cranial nerve (CN) nuclei that are centered within the brainstem and extend to the brainstem surface. Due to the high density of structures within the brainstem, even small intra-axial or extra-axial lesion(s), with associated mass-effect, may result in profound deficits [1]. Furthermore, lesions located within the brainstem may result in obstructive hydrocephalus secondary to compression of the cerebral aqueduct or fourth ventricle.

Lesions arising from the adjacent cerebellar peduncles, while not considered of primary brainstem origin [2], may extend into or exert mass-effect on the brainstem. Similarly, extra-axial lesions arising from adjacent structures may also result in significant mass-effect on the brainstem, most commonly arising from the cerebellopontine angle (CPA) cistern. Extra-axial lesions may also arise from the pineal gland region, clivus or cavernous sinus, or extend from the suprasellar region dorsally.

Neuroimaging of brainstem lesions may include magnetic resonance imaging (MRI), computed tomography (CT), and/or positron emission tomography (PET) imaging. Ultrasound imaging may be utilized to evaluate the posterior fossa of newborns.

3.2 Imaging Techniques

3.2.1 Magnetic Resonance Imaging (MRI)

MR imaging is the modality of choice for the evaluation of lesions involving the brainstem. MRI offers superior tissue contrast compared with the other common imaging modalities and allows for detailed evaluation of signal characteristics, lesion location, intrinsic features, and overall extent [3]. Furthermore, advanced MRI sequences, including diffusion-weighted or tensor imaging (DWI/DTI), perfusion-weighted imaging (PWI), susceptibility-weighted imaging (SWI) and ¹H-MR-spectroscopy (¹H-MRS) generate complementary information that allows for additional characterization of a lesion. Image acquisition, however, may consume a considerable amount of time, is sensitive to motion, and typically requires the patient to place their head within a “head coil” while in the scanner. Patient compliance may be especially limiting in pediatric patients, as well as in adult patients with behavioral issues.

Standard MR imaging sequences allow for structural characterization of brainstem lesions, such as primary location, overall size, contrast enhancement pattern, and differentiation between cystic and solid components. T1-weighted images allow for anatomical evaluation and for detection of contrast enhancement, secondary to blood brain barrier (BBB) breakdown, following intravenous (IV) gadolinium administration. Isotropic, or near-isotropic three-dimensional (3D),

T1-weighted images can be acquired within a reasonable amount of time [4]. This allows for better evaluation of brainstem anatomy and increased conspicuity of sub-centimetric lesions. 3D datasets allow for multi-planar reconstructions. Common lesions that are hyperintense on T1-weighted imaging include fat, lipids, proteinaceous content, and subacute blood products. Evaluation of any lesion with pre-contrast T1-weighted imaging is essential before reviewing post-contrast T1-weighted imaging, as a lesion may demonstrate intrinsic T1 shortening (T1 hyperintense signal not related to contrast enhancement), suggesting an associated fat content or hemorrhage.

T2-weighted MR imaging allows for further evaluation of the anatomy and offers superior contrast at the junctions between brainstem parenchyma, or lesion, and cerebral spinal fluid (CSF), either within the ventricles or subarachnoid space. Additionally, review of T2-weighted images is essential when evaluating a highly vascular lesion considering that vessels result in highly conspicuous “flow-related signal voids” and appear hypointense on T2-weighted imaging relative to the adjacent parenchyma and CSF. Common lesions/findings that are hyperintense on T2-weighted imaging include water/fluid content and chronic blood products (e.g., hemosiderin).

T2 fluid-attenuated inversion recovery (FLAIR) images suppress simple fluid, including CSF. T2-FLAIR images allow for increased conspicuity of parenchymal edema (vasogenic or cytotoxic) and/or intrinsically T2 hyperintense lesions that may otherwise be difficult to detect, especially if they are in close proximity to the ventricular system.

High-resolution 3D balanced steady-state free precession (b-SSFP) gradient-echo MR imaging accentuates CSF-soft tissue contrast and provides high spatial resolution. Examples of 3D b-SSFP sequences include constructive interference in steady state (CISS, Siemens) and fast imaging employing steady-state acquisition (FIESTA, GE). These sequences are well-suited for the evaluation of cranial nerves extending from the brainstem [5, 6]. Sagittal, high-resolution images obtained at midline may be used to evaluate the patency of the cerebral aqueduct in the setting of a mass-effect secondary to a brainstem lesion. The major disadvantage of b-SSFP MR imaging stems from its intrinsic lack of soft tissue contrast, which limits the evaluation of parenchymal lesions.

Susceptibility-weighted imaging (SWI) provides enhanced detection of blood products and calcifications [4]. SWI is more sensitive in the detection of blood and calcium relative to T2* gradient recalled echo (GRE) MR imaging, though images take longer to acquire. Diffusion-weighted imaging (DWI) allows for the detection of abnormal diffusion characteristics. Reduced, or restricted, diffusion [DWI hyperintense signal with matching low values on the apparent diffusion coefficient (ADC) map] is most commonly seen in the setting of ischemia or tumor hypercellularity. Caution is advised when interpreting DWI/ADC information in the setting of hemorrhage or calcification as their presence will result in a perceived signal abnormality. Facilitated, or enhanced, diffusion is typically seen secondary to vasogenic edema surrounding a tumor or focus of infection. Facilitated diffusion is typically hyperintense on DWI with matching elevated (bright) ADC values.

Diffusion tensor imaging (DTI) is created by measuring the full tensor of the diffusion, thus allowing for the study of the 3D shape, magnitude, and principal direction of diffusion [3]. Fractional anisotropy (FA) maps can be derived from DTI, with lower values correlating with higher-grade tumors [3, 7, 8]. Data generated by the FA maps can be post-processed to generate images depicting different tracts within the brain and brainstem, known as diffusion tensor tractography (DTT). Fiber tractography may be especially beneficial in the evaluation of brainstem lesions as it allows for detection of fiber tract deviation, infiltration, or disruption by an adjacent lesion [3]. The presurgical utilization of DTI/DTT for the purposes of surgical planning of brainstem lesions has been extensively described in the literature [9–14].

Perfusion-weighted imaging (PWI) involves the rapid and repeated acquisition of images through the brain following IV gadolinium administration. Imaging may be performed using dynamic susceptibility contrast (DSC) or dynamic contrast enhancement (DCE), with DSC representing the most commonly employed technique. The collected data is then post-processed to generate various perfusion maps, including cerebral blood flow (CBF), cerebral blood volume (CBV), time-to-peak (TTP), and mean transit time (MTT). Relative cerebral blood volume (rCBV) is also generated, with increased rCBV correlating with neovascularity in a brain lesion [2]. rCBV may also be utilized to evaluate tumor progression, such as progression from a grade I/II glioma to a grade III/IV, and to help differentiate between tumor progression and post-treatment changes [2, 15]. Arterial spin labeling (ASL) is an alternative non-contrast enhanced technique utilized to generate a single CBF perfusion map. Perfusion imaging at the level of the brainstem may be limited secondary to susceptibility artifacts from the skull base [2]. Also, as previously noted with DWI/ADC, caution is advised in the setting of hemorrhage and/or calcifications, as the presence of either may render the perfusion imaging non-diagnostic.

¹H-Magnetic resonance spectroscopic imaging (¹H-MRSI) allows for noninvasive evaluation of metabolic indices within a given voxel involving normal brain parenchyma and/or a brainstem lesion [16]. Acquisition of MR spectral data can be achieved using a single or multivoxel technique. ¹H-Magnetic resonance spectroscopy (¹H-MRS) is used to evaluate specific metabolites, including choline (Cho), N-acetylaspartate (NAA), lactate, lipids, and creatine (Cr) [15]. Concentrations of these metabolites may be used to evaluate for malignancy or tumor progression. For example, an increased ratio of Cho/NAA has been shown to represent underlying malignancy [15]. ¹H-MRS of posterior fossa lesions is technically more difficult compared to supratentorial lesions, because of the small brainstem size, adjacent skull base [2] and paranasal sinuses. As a result, imaging may be degraded by susceptibility artifacts from adjacent bone, fat, and air surfaces [16].

Pediatric imaging with MRI offers exquisite detail of posterior fossa structures. 3D T1-/T2-weighted sequences, T2-FLAIR, DWI/ADC, and SWI should be obtained; slice thickness should not exceed 4 mm. DWI, with a corresponding ADC map, are invaluable in the detection of acute cytotoxic/vasogenic edema resulting from inflammation, infection, or ischemia within the posterior fossa. SWI provides

increased sensitivity for the detection of posterior fossa hemorrhage. In the setting of infection or inflammation, 0.2 mL/kg of IV gadolinium chelate may be administered [17].

3.2.2 Computed Tomography (CT)

CT is especially valuable in the acute neuroradiological work-up. Advantages of CT include faster image acquisition, greater accessibility, and reduced cost relative to MRI. Disadvantages include radiation exposure and limited tissue contrast. Furthermore, lesions involving the brainstem may be particularly challenging to visualize on CT imaging secondary to beam-hardening artifact produced by the dense temporal bones of the skull base (Fig. 3.1) [18].

Primary indications for CT imaging include acute head trauma, suspected ischemic stroke or hemorrhage, suspected hydrocephalus and/or brain herniation, and postoperative intracranial assessment [19]. Patients with posterior fossa lesions, including the brainstem, often present with symptoms of nausea, vomiting, and ataxia. These patients will benefit from initial CT imaging for the reasons mentioned above.

3.2.3 Positron Emission Tomography (PET)

^{18}F -2-fluoro-2-deoxy-D-glucose positron emission tomography (^{18}F -FDG PET) may be used to evaluate brainstem lesions for hypermetabolic activity secondary to increased glucose consumption. Uptake may be seen with neoplastic and non-

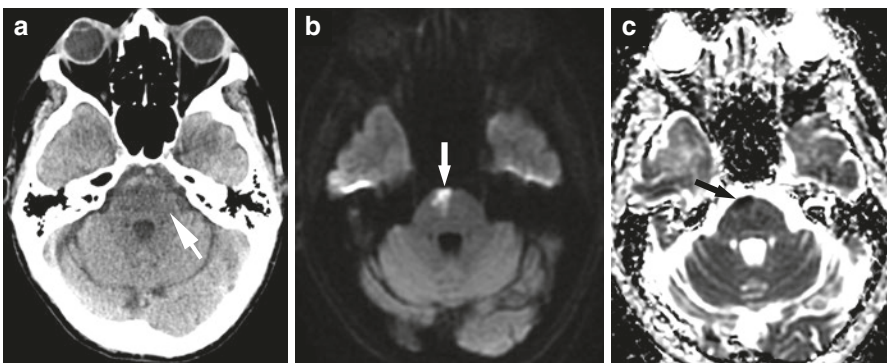


Fig. 3.1 CT skull base artifact limits evaluation through the brainstem (pons). (a) CT axial image at the level of the pons demonstrates linear horizontal bands of hypoattenuation (white arrow) produced by beam-hardening skull base artifact. MR imaging at the same level reveals a right paramedian pontine infarct evidenced by restricted diffusion with hyperintense signal on DWI (b) and matching low values on ADC map (c)

neoplastic lesions. In the setting of a brainstem glioma, hypermetabolic activity is associated with prognosis [2]. However, there is high background ^{18}F -FDG activity within the brain, particularly in the cortex and basal ganglia, resulting in degradation of signal-to-noise ratio [20].

^{18}F -fluoro-ethyl-tyrosine positron emission tomography (^{18}F -FET PET) may also be performed for brainstem lesions and provides complimentary metabolic information, with neoplastic lesions demonstrating significantly higher ^{18}F -FET PET uptake when compared with non-neoplastic lesions [2]. Unlike ^{18}F -FDG PET, ^{18}F -FET PET is an amino acid tracer, resulting in lower brain background activity [20].

3.2.4 *Ultrasound*

In the prenatal/perinatal patient population, ultrasound allows for the evaluation of a posterior fossa congenital abnormality or lesion without the required radiation by CT or prolonged acquisition time by MRI [4]. Use of ultrasound is limited to the first few months of life secondary to subsequent closure of the acoustic windows (e.g., cranial fontanelles) [17]. A study on preterm infants has noted superior detection of cerebellar hemorrhages using the mastoid fontanelle rather than the anterior fontanelle [17]. However, the limited deep spatial resolution and the single image contrast limits the use of ultrasound to a primarily screening technique for fetuses/neonates that present with macrocephaly secondary to hydrocephalus. Further evaluation of a detected abnormality should be performed utilizing pre- and/or post-natal MRI.

3.3 Intra-Axial Lesions: Neoplastic

3.3.1 *Brainstem Glioma*

Brainstem gliomas (BSGs) are the most common primary tumor arising from the brainstem, both in children and adults, with a bimodal age distribution [2].

Pediatric BSGs most commonly arise during the first decade of life and account for approximately 10–20% of all pediatric central nervous system (CNS) tumors [2, 21, 22]. Generally speaking, BSGs can be separated into 2 major subtypes: focal or diffuse brainstem gliomas, the former of which is typically low-grade and the latter of which is typically of higher grade [21, 23]. Focal gliomas account for 20% to 35% of BSGs and are more common in the midbrain and medulla. Focal subtypes include focal midbrain, dorsal exophytic from the pons, and cervicomedullary [21]. Diffuse gliomas most commonly arise within the pons and, unfortunately, account for 75% to 85% of BSGs in the pediatric population [21].

Adult BSGs most commonly arise during the 4th decade of life, accounting for 1–2% of all CNS tumors [2]. Imaging characteristics and location are important for

prognosis and classification, consisting of 4 subgroups: (a) diffuse intrinsic low-grade gliomas, (b) enhancing malignant gliomas, (c) focal tectal gliomas, and (d) exophytic gliomas/other subtypes [2, 21]. The most common subtype in adults is the diffuse, low-grade type. Approximately 60% of these gliomas are centered within the medulla and 30% within the pons [2].

3.3.1.1 Imaging

MRI characteristics of BSGs will vary depending on the underlying tumor grade, its location, and the patient's age.

Low-Grade Gliomas Pediatric BSGs are focal in appearance and demonstrate well-circumscribed margins. Gliomas will demonstrate hypointense to isointense signal on T1- and hyperintense signal on T2-weighted imaging relative to adjacent brain parenchyma. Lesions will demonstrate intrinsic T2-FLAIR signal, though lacking adjacent vasogenic edema [2, 21]. Tectal gliomas are focal gliomas that are centered within the tectum of the brainstem (Fig. 3.2). Focal midbrain gliomas may demonstrate minimal post-contrast enhancement and typically exert mass-effect on the cerebral aqueduct, possibly resulting in hydrocephalus. Dorsal exophytic lower brainstem gliomas may show mild post-contrast enhancement, predominantly involving the exophytic component [21].

Adult low-grade gliomas can have a focal or diffusely infiltrative appearance on MR imaging. Focal gliomas demonstrate hypointense and hyperintense signal on T1-weighted and T2-weighted/T2-FLAIR imaging, respectively, and may demonstrate associated post-contrast enhancement. Focal gliomas in the adult population may also have an exophytic component as seen in children (Fig. 3.3). Diffuse intrinsic low-grade gliomas will demonstrate similar T1/T2 signal to that seen with focal gliomas, but are not associated with post-contrast enhancement, areas of restricted diffusion on DWI/ADC, or internal necrosis [2].

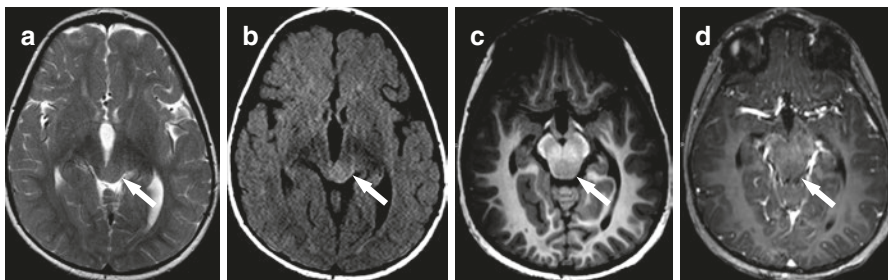


Fig. 3.2 Tectal glioma. Axial MR images demonstrate a focal mass centered within the left tectum of the midbrain. This mass is associated with hyperintense signal on T2-weighted and T2-FLAIR images, (a) and (b) respectively. Pre-contrast T1-weighted imaging (c) shows mild hypointense signal abnormality with no associated enhancement following administration of IV contrast (d)

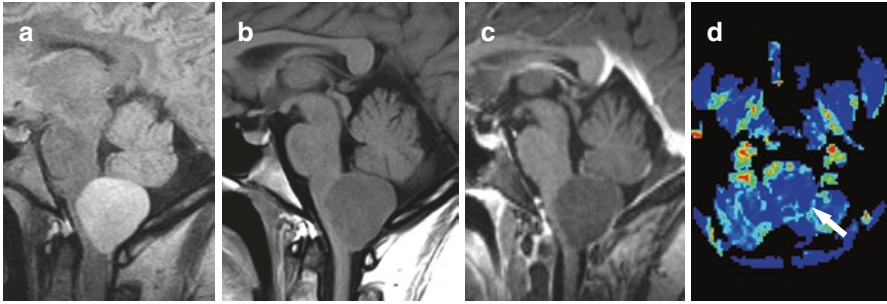


Fig. 3.3 Focal low-grade glioma (Adult). Sagittal T2-FLAIR (a) imaging demonstrates an intrinsically hyperintense exophytic mass within the dorsal aspect of the medulla. This mass is diffusely hypointense on pre-contrast T1-weighted imaging (b) with no associated enhancement (c). Perfusion imaging (d) demonstrates no elevation of cerebral blood volume

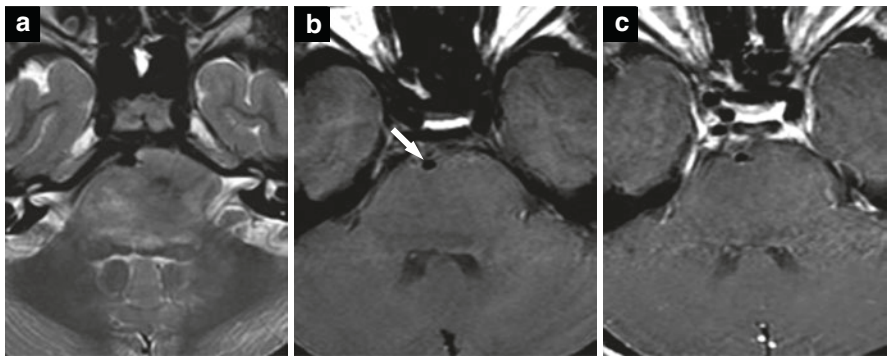


Fig. 3.4 Diffuse midline glioma (pediatrics). Axial T2-weighted (a), pre-contrast T1-weighted (b), and post-contrast T1-weighted (c) images demonstrate characteristic, diffuse expansion of the pons. The mass has ill-defined margins on both T1-weighted and T2-weighted images with associated hyperintense signal on T2-weighted images (a). Note the characteristic ventral displacement and encasement of the basilar artery (b, arrow). (Case and images courtesy of Dr. Thierry A.G.M. Huisman)

DTI/DTT in pediatric and adult low-grade gliomas can help visualize displacement of traversing fiber tracts within the brainstem, providing invaluable preoperative information to the neurosurgeon regarding altered anatomy [2].

High-Grade Gliomas Pediatric diffuse midline gliomas, formerly known as diffuse intrinsic pontine glioma (DIPG), represent a new distinct entity under the 2016 World Health Organization (WHO) classification [24]. According to the 2016 WHO classification, an associated mutation at position K27 in the gene for histone H3 automatically classifies the glioma as a grade IV, regardless of morphologic features [24]. The new name also recognizes the fact that these high-grade gliomas may occur throughout the midline extending from the thalamus to the spinal cord. Typical imaging characteristics include a diffusely expansile mass centered within the pons (Figs. 3.4 and 3.5). When centered within the pons, it is not uncommon to

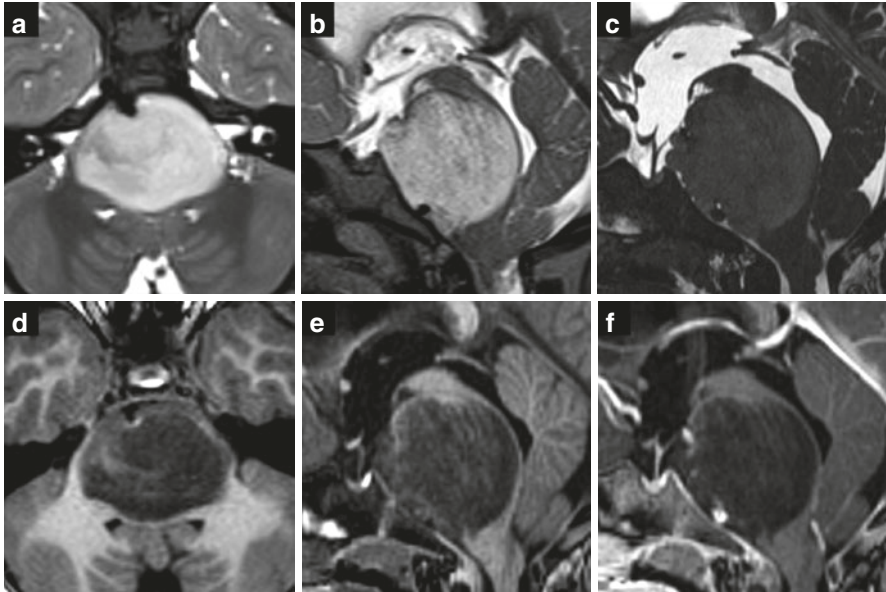


Fig. 3.5 Diffuse midline glioma (pediatrics). Classic expansion of the pons with hyperintense signal on T2-weighted imaging (**a, b, c**) and hypointense signal on pre-contrast T1-weighted imaging (**d, e**). No associated enhancement detected on post-contrast T1-weighted imaging (**f**). (Case courtesy of Dr. Daniel Bess)

have ventral neoplastic expansion with resultant encasement of the basilar artery [24]. These gliomas will demonstrate hypointense signal on T1- and hyperintense signal on T2-weighted imaging. Post-contrast enhancement typically involves less than 25% of the tumor volume, and the enhancement pattern is non-characteristic [24]. Leptomeningeal dissemination has been observed in approximately one-third of patients at the time of presentation [21].

^1H -MRS in diffuse midline gliomas has been shown to have a significant prognostic value. One study demonstrated that patients with an elevated ratio of Cho/NAA >4.5 had 100% mortality at 63 weeks. Patients with a Cho/NAA ratio <4.5 had a 50% chance of survival at 63 weeks [21].

Adult high-grade gliomas (grade III/IV) will have hypointense signal on T1- and hyperintense signal on T2-weighted imaging. Diffuse midline gliomas (grade IV) are also seen in adults. High-grade gliomas will demonstrate ill-defined post-contrast enhancement and may contain areas of necrosis and/or post-contrast enhancement (Fig. 3.6). Perfusion imaging may show elevated rCBV within the original tumor and helps in evaluating for treatment response. Perfusion imaging can also help in distinguishing neoplastic progression from post-treatment changes [2].

Non-necrotic, high-grade components of the lesion will demonstrate restricted diffusion on DWI/ADC. DTI/DTT can be used to identify neoplastic infiltration of the traversing fiber tracts within the brainstem [2].

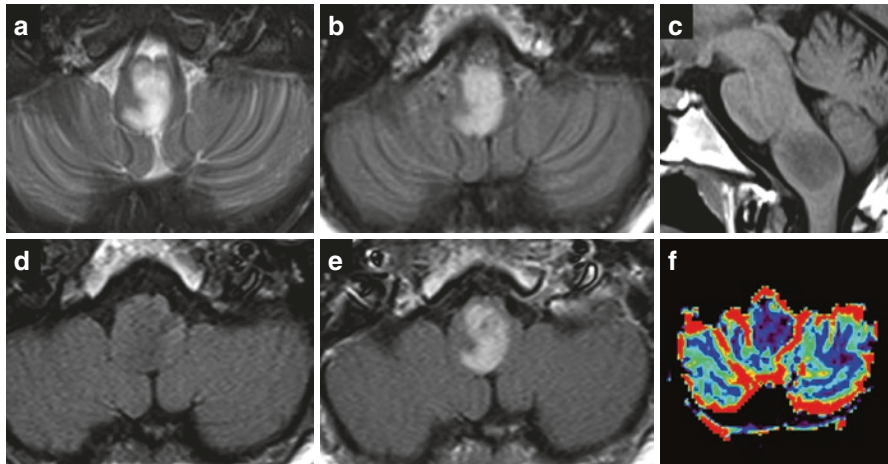


Fig. 3.6 Diffuse midline glioma, H3 K27 M-mutant (Adult). The mass is centered within the medulla and demonstrates hyperintense signal on axial MR T2-weighted (a) and T2-FLAIR (b) images. Sagittal and axial T1-weighted image (c, d) demonstrates associated expansion of the medulla, ill-defined margins, and hypointense T1 signal. There is associated enhancement on axial post-contrast T1-weighted image (e) without evidence for hyperperfusion on corrected CBV map (f)

^1H -MRS can be utilized for baseline evaluation of metabolites. Elevated Cho/NAA ratio at baseline has been associated with shorter survival. Follow-up evaluation can help monitor for treatment response versus tumor progression, with neoplastic progression demonstrating progressive elevation of Cho/NAA [15]. Malignant BSGs will also have a characteristic lipid-lactate peak suggestive of necrosis [2].

^{18}F -FET PET will provide information regarding the biologic activity of BSGs. It has been shown that gliomas of increasing tumor grade demonstrate increased propensity for ^{18}F -FET PET uptake, with 100% of grade IV gliomas demonstrating hypermetabolic activity [2]. Metabolic assessment may also prove valuable in the post-treatment setting, or in the evaluation of tumor grade progression [2].

3.3.2 Lymphoma

Primary CNS lymphoma (PCNSL) more commonly affects immunocompromised, rather than immunocompetent, individuals and accounts for less than 2% of primary brain neoplasms. PCNSL primarily centered within the brainstem is rare and occurs in 3% of patients with PCNSL [25–27]. The majority of primary lymphomas involving the brainstem are of T-cell origin [28]. PCNSL of the brainstem typically affects older individuals within their 7th and 8th decades of life [29]. PCNSL is exquisitely rare in the pediatric population.

3.3.2.1 Imaging

PCNSL involvement of the brainstem does not demonstrate a propensity for a specific location [25]. Of note, the use of corticosteroids may alter the enhancement pattern of the brain lesion(s) and can initiate apoptosis/necrosis within the lesion(s) [30]. Alternately, complete remission/disappearance of PCNSL has also been reported following corticosteroid therapy, for which PCNSL is sometimes referred to as “the ghost tumor” [31].

Magnetic Resonance Imaging (MRI) MR imaging appearance is variable and will vary based on the immune status. Immunocompetent individuals will present with a homogeneously enhancing mass in the majority of cases (Fig. 3.7). Immunocompromised individuals are more likely to have a ring-enhancing mass

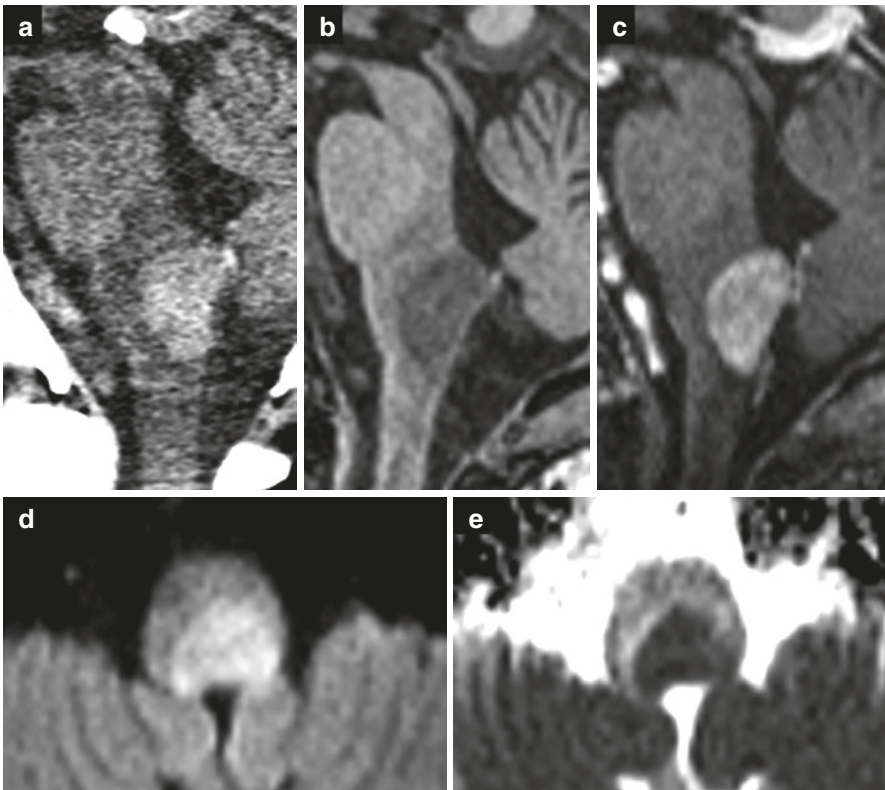


Fig. 3.7 Lymphoma. CT imaging through the posterior fossa is typically limited secondary to artifacts (a). However, the hypercellular composition of lymphoma will typically result in a well-defined, hyperattenuating mass (a) seen on the sagittal reformatted CT images. MR imaging demonstrates a focal medullary mass with intrinsic hypointense signal on T1-weighted imaging (b) and associated homogeneous enhancement (c). Additional MR images demonstrate restricted diffusion with hyperintense signal on DWI (d) and matching low values on ADC map (e)

revealed on post-contrast T1-weighted imaging with internal regions of necrosis [30]. This pattern of ring-enhancement will be seen in 75% of patients [30]. Lesions may be associated with a variable degree of adjacent vasogenic edema.

PCNSL is a hypercellular neoplasm and demonstrates restricted diffusion on DWI/ADC, often demonstrating markedly low values on ADC. Multiple studies have compared the quantitative ADC values of lymphoma versus glioblastoma and reported lower ADC values with lymphoma [30]. Furthermore, ADC values have been shown to have a prognostic significance. One study demonstrated that areas of tumor enhancement, which corresponded with low ADC values, correlated with shorter progression-free survival and overall survival [32].

Supratentorial PCNSL may demonstrate elevated rCBV compared with the normal contralateral cerebral hemisphere [33]. Specific perfusion imaging of brainstem PCNSL has not been performed to the best of our knowledge. rCBV of brainstem PCNSL may be less revealing considering the limitations at the level of the skull base.

Computed Tomography (CT) CT imaging may demonstrate a nonspecific isodense-to-hyperdense lesion within the brainstem with associated mass-effect [34]. Hyperattenuation on CT imaging, in the absence of hemorrhage, is secondary to hypercellularity.

3.3.3 *Metastatic Disease*

Intracranial metastatic disease may involve the supratentorial brain, infratentorial brain, or dura. Metastatic disease is the most common intracranial neoplasm in the adult population, with an incidence of approximately 8.3–11 per 100,000 [35]. Intracranial metastatic disease of tumors remote to the CNS is uncommon in the pediatric population, with an incidence of 2–6% [3], and more commonly secondary to neuroblastoma with a propensity for metastases to the skull and dura. Intracranial metastatic dissemination in pediatric patients typically results from primary brain tumors, which most frequently include high-grade/anaplastic gliomas, ependymomas, and medulloblastomas.

3.3.3.1 **Imaging**

Imaging findings for metastatic disease are nonspecific, though the probability increases in the setting of a known primary malignancy. Intracranial metastatic disease will usually present with multiple lesions. Parenchymal involvement favors the supratentorial brain and cerebellar hemispheres, though lesions can also involve the brainstem.

Magnetic Resonance Imaging (MRI) MR imaging is preferred, with higher field strength magnets improving detection of metastatic lesions [20]. Volumetric 3D

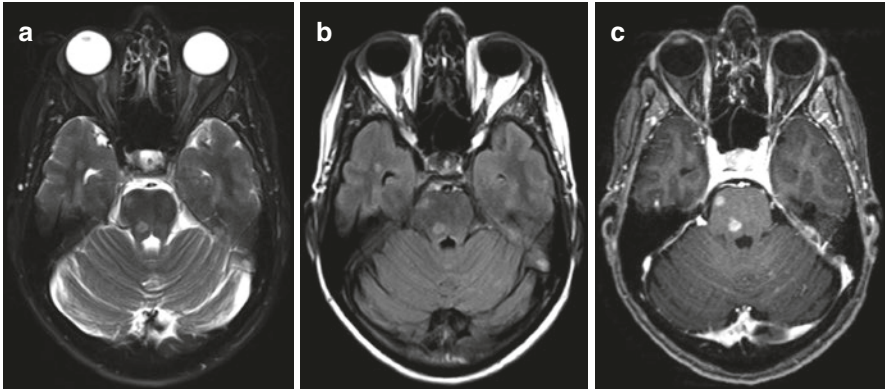


Fig. 3.8 Metastatic disease. Axial T2-weighted (a), T2-FLAIR (b), and post-contrast T1-weighted (c) images demonstrate metastatic lesions within the right pons

T1-weighted imaging can be acquired to improve visualization of smaller metastases. Lesions will typically demonstrate hypointense signal on pre-contrast T1-weighted imaging with subsequent enhancement on post-contrast T1-weighted imaging (Fig. 3.8). Time-delayed post-contrast acquisition (15–20 minutes) has been shown to increase the detection of metastatic lesions, specifically in those less than 10 mm [20]. Time-delayed post-contrast imaging may offer particular benefit when imaging metastatic disease within the posterior fossa [20]. T2-FLAIR imaging will demonstrate hyperintense signal associated with the lesion(s) and reveal any associated vasogenic edema as confluent, perilesional T2-FLAIR hyperintense signal abnormality. Metastatic lesions are often associated with reduced/restricted diffusion on DWI/ADC, an imaging finding that may facilitate the detection of metastatic lesions.

Lesions with subacute hemorrhage will contain foci of hyperintense signal on T1-weighted imaging. Chronic blood products will contain hemosiderin and demonstrate marked hypointense signal on T2-weighted imaging. Intrinsic foci of T1 hyperintense signal may also be seen in lesions containing melanin, though these are uncommon. SWI offers increased sensitivity for the detection of small hemorrhagic metastatic lesions [20].

Computed Tomography (CT) CT imaging serves as a screening tool in patients with acute neurological deficits and known intracranial metastatic disease. Nonenhanced CT imaging may demonstrate the development/progression of mass-effect, hydrocephalus, and hemorrhage [20]. Detection of parenchymal metastatic lesions may be associated with focal hypoattenuation secondary to vasogenic edema. Sensitivity for small lesions is limited, though administration of IV contrast improves detection [20].

Positron Emission Tomography (PET) ^{18}F -FET PET, an amino acid tracer, is currently being investigated for use in imaging/evaluation of brain metastatic disease [20].

3.4 Intra-Axial Lesions: Non-Neoplastic

3.4.1 *Cavernous Malformation*

Cavernomas, or brainstem cavernous malformations (BSCMs), are one of four major cerebral vascular malformations, the remaining three of which consist of capillary telangiectasia, developmental venous anomaly (DVA), and arterio-venous malformation (AVM) [36]. BSCMs are low-flow venous vascular malformations that consist of dilated, malformed capillaries [37] and are commonly associated with an adjacent DVA. BSCMs are less common than their supratentorial counterparts and account for approximately 20% of all intracranial cavernous malformations. The prevalence of spontaneously occurring intracranial cavernous malformations is estimated at 0.16% to 0.5% [38]. The most common location for a BSCM is within the pons, followed by the midbrain and medulla, respectively. Differences in lesion size based on brainstem location has been described, with medullary lesions typically on the smaller end of the spectrum and lesions at the pontomesencephalic junction on the larger end of the spectrum [39]. BSCMs measuring larger than 15 mm in diameter have been associated with a less favorable postsurgical outcome in a retrospective review consisting of a Latin American patient population [37]. BSCM may occur spontaneously, as part of a hereditary/familial etiology, or secondary to remote radiation treatment. If multiple cavernomas are identified without a history of radiation treatment, MR examination of direct relatives should be considered to rule out a familial etiology.

3.4.1.1 Imaging

Imaging plays an important role in the identification and evaluation of BSCMs, as detailed by the Angioma Alliance in the Synopsis of Guidelines for the Clinical Management of Cerebral Cavernous Malformations. MRI is considered the preferred imaging modality [38, 40]. Evaluation within 2 weeks of symptom onset is preferred, adding increased sensitivity and specificity in the detection of cavernous malformations [38].

Magnetic Resonance Imaging (MRI) Cavernous malformations demonstrate intrinsic signal associated with evolving blood products on T1- and T2-weighted MR imaging. The combination of evolving blood products produce a characteristic appearance on T1-weighted images commonly described as a “popcorn” appearance [41]. Hyperintense signal on T1-weighted imaging suggests subacute blood products between 2 to 3 days and 2 months. Hypointense signal on T1- and T2-weighted imaging suggests chronic blood products. A peripheral rim of T2 hypointense signal may be present secondary to chronic hemosiderin deposition and is considered characteristic (Fig. 3.9) [41]. T2-FLAIR images may demonstrate adjacent hyperintense signal secondary to vasogenic edema in the setting of recent hemorrhage.

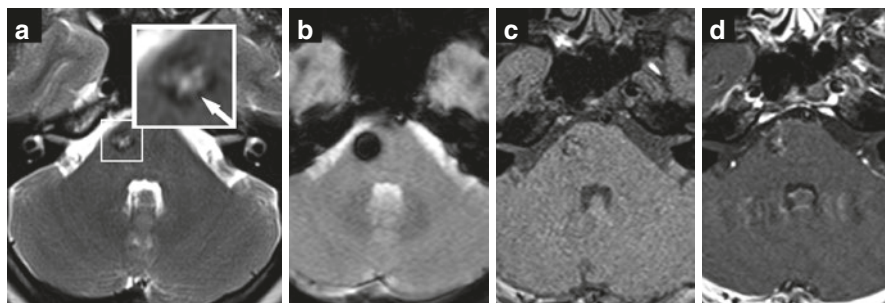


Fig. 3.9 Cavernous malformation. The lesion is centered within the right ventrolateral pons with a characteristic hypointense peripheral rim on T2-weighted image (a, arrow). Axial SWI image (b) demonstrates marked susceptibility artifact secondary to the paramagnetic effects of the associated blood products. Pre-contrast T1-weighted image demonstrates stippled intrinsic hyperintense foci (c); there is minimal associated enhancement on post-contrast T1-weighted image (d)

Evolving hemoglobin breakdown and subsequent hemosiderin deposition result in susceptibility, or “blooming,” artifact on T2-weighted GRE and SWI [40]. This artifact is exploited in the detection of cavernous malformations and provides increased sensitivity compared with conventional T1- and T2-weighted sequences. Furthermore, SWI provides greater sensitivity in the detection of cavernous malformations compared with GRE imaging [40, 42, 43]. Post-contrast T1-weighted imaging may serve to identify associated DVAs, a finding that should be reported, particularly in the preoperative setting. SWI may also serve to identify associated DVAs. Lesions are expansile and may enlarge over time secondary to intralesional hemorrhage; no intralesional white or gray matter should be present.

In the surgical candidate, preoperative DTI/DTT may provide invaluable information regarding spatial location of the BSCM relative to the densely packed eloquent areas/fibers within the brainstem [40, 44]. Furthermore, DTI/DTT may be beneficial during the planning of intervention to help decide on the surgical approach [9, 40, 45, 46].

Computed Tomography (CT) CT imaging may demonstrate an amorphous hyperdense appearance or punctate foci of mineralization. However, published guidelines discourage the use of CT beyond 1 week of symptom onset [38]. CT imaging may be utilized in the acute setting to evaluate for hemorrhage or ventricular obstruction secondary to mass-effect on or within the brainstem.

3.4.2 Capillary Telangiectasia

Capillary telangiectasia is a type of cerebral vascular malformation that represents a collection of thin-walled, ectatic vessels on a background of normal neuropil [36, 47]. These lesions are typically found incidentally on MRI. One study evaluating 6399 contrast-enhanced MRIs demonstrated a prevalence of 0.67% [47]. An increased incidence has been reported in Sturge-Weber-Dimitri syndrome as well as

in Rendu-Osler-Weber syndrome. Capillary telangiectasias most commonly occur within the pons, though a small percentage can have an extrapontine location [36].

3.4.2.1 Imaging

MR imaging is the preferred modality for the visualization of these lesions as they are occult on conventional angiography and not visualized on CT imaging.

Magnetic Resonance Imaging (MRI) Capillary telangiectasias are most commonly isointense to the adjacent parenchyma on conventional T1- and T2-weighted images. Approximately 39% of lesions may demonstrate subtle signal alteration on T1-weighted, T2-weighted, or T2-FLAIR images (Fig. 3.10) [47]. Characteristically, T2-FLAIR signal will be strikingly normal, or near normal, in contrast to findings on other imaging sequences. Signal alteration on T1-weighted imaging will show hypointense signal relative to the adjacent parenchyma; T2-weighted imaging will show hyperintense signal relative to the adjacent parenchyma. Nearly all lesions will demonstrate faint, homogeneous enhancement on post-contrast MRI, which may appear web-like, possibly reflecting underlying ectatic vessels [47].

Evaluation with SWI is useful, considering that all lesions should demonstrate associated signal loss. One study has suggested that signal loss on SWI with associated post-contrast enhancement in the setting of unremarkable signal alteration on T1-/T2-weighted imaging is highly specific for a brainstem capillary telangiectasia [47].

3.4.3 Hemorrhage/Hematoma

Acute hemorrhage within the brainstem may occur secondary to an underlying lesion, such as an AVM or BSCM, or may occur spontaneously. In general, the incidence of intracranial hemorrhage (ICH) is 13.9 (men) and 12.3 (women) per 100,000

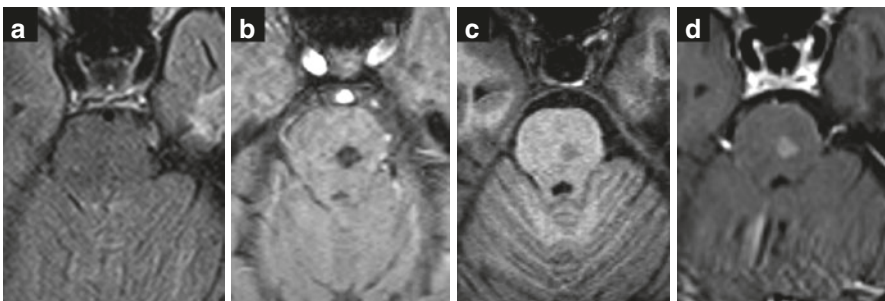


Fig. 3.10 Capillary telangiectasia. A subtle lesion is centered within the left paramedian pons with no significant mass-effect (a–d). Axial T2-FLAIR image (a) demonstrates isointense signal to adjacent parenchyma and no vasogenic edema. The lesion demonstrates mild hypointense signal on pre-contrast T1-weighted image (c) with faint, homogenous enhancement on post-contrast T1-weighted image (d). There is mild susceptibility artifact on SWI image (b)

per year, according to one prospective study [48]. Spontaneous brainstem hemorrhage more commonly involves the pons, with primary pontine hemorrhage (PPH) accounting for up to 10% of all intracranial hemorrhages [49, 50]. Two studies specifically evaluating PPH included patients in their 30s–90s; neither study contained pediatric patients [49, 50]. The leading cause for PPH is arterial hypertension, accounting for 90%, with additional etiologies including anticoagulation and underlying amyloid angiopathy [50]. Brainstem hemorrhage secondary to anticoagulation is typically larger and portend a poorer prognosis [51]. Generally speaking, poor prognostic indicators include comatose presentation, intraventricular extension of blood products, and acute hydrocephalus [50].

3.4.3.1 Imaging

Patients presenting acutely to the emergency department (ED) will first undergo CT imaging. This initial imaging will identify critical findings possibly requiring urgent intervention. MRI may be performed once the patient is stabilized in order to evaluate for an underlying vascular anomaly or neoplasm.

Magnetic Resonance Imaging (MRI) In the setting of parenchymal hemorrhage, conventional T1- and T2-weighted sequences provide invaluable information regarding the age of the blood products. For example, T1-weighted imaging can help distinguish between hyperacute/acute and early/late subacute blood products, with the former demonstrating hypo-to-isointense signal and the latter demonstrating hyperintense signal. Effectively, identification of hyperintense signal on T1-weighted imaging suggests subacute hemorrhage (Fig. 3.11). Furthermore, T2-weighted imaging can be used to distinguish between early subacute and late subacute blood products, with the former demonstrating hypointense signal and the latter demonstrating hyperintense signal [52]. T2-weighted and T2-FLAIR images will demonstrate associated vasogenic edema adjacent to the hematoma.

SWI will demonstrate associated hypointense signal with blood products that are no longer considered hyperacute (>12 hours). This occurs secondary to the evolution of blood from oxy-hemoglobin into deoxy-hemoglobin and the resultant paramagnetic effects of deoxy-hemoglobin [52].

Post-contrast T1-weighted imaging may be obtained to evaluate for an underlying etiology, though evolving subacute hematoma may demonstrate associated enhancement. Associated enhancement, however, may be difficult to detect within a subacute timeframe considering the degree of hyperintense signal on T1-weighted imaging. Furthermore, the acute hemorrhage may compress and limit the identification of the underlying culprit lesion, such as a vascular anomaly or neoplasm.

Time-resolved contrast-enhanced MR angiography can also be used for further evaluation of a vascular anomaly and may be considered in the diagnostic work-up of an acute/subacute focal hemorrhage [53].

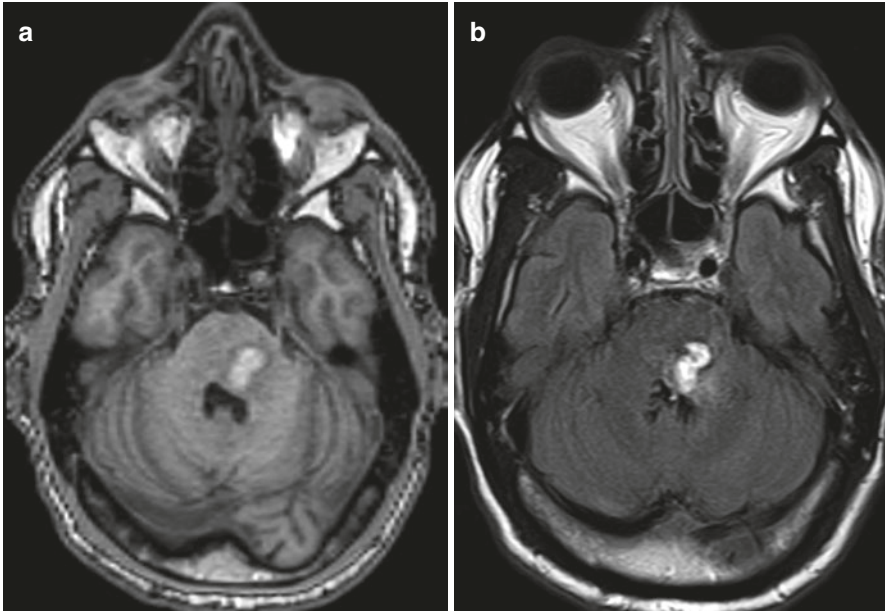


Fig. 3.11 Primary pontine hemorrhage. Focal signal abnormality centered within the left dorsal pons with associated mass-effect (**a, b**) and subtle vasogenic edema on the left dorsolateral margin (**b**). There is associated hyperintense signal on T1-weighted (**a**) and FLAIR (**b**) images consistent with late subacute blood products

Computed Tomography (CT) As previously noted, patients presenting to the ED with brainstem hemorrhage will invariably undergo CT imaging. Prompt imaging will identify hyperacute/acute hemorrhage, as well as associated complications, such as acute hydrocephalus secondary to mass-effect. Hyperacute hemorrhage will appear isodense to adjacent brain parenchyma, with increased attenuation of the hematoma developing within hours of hemorrhage [52]. Continued evolution of the hematoma will result in decreased attenuation, with resultant isoattenuation to the adjacent parenchyma during the subacute timeframe. Subacute hematomas may be difficult to visualize considering the isodense attenuation on non-contrast CT imaging, but may demonstrate peripheral contrast enhancement secondary to breakdown of the blood brain barrier [52, 54].

3.4.4 Infarction

Acute ischemic stroke is considered a leading cause of serious physical and cognitive long-term disability in adults [55]. One study examining acute ischemic stroke in a United States population noted an incidence of 3.29 per 1000 [55], with 1/3 involving the vertebrobasilar system [51]. When acute ischemic stroke involves the vertebrobasilar circulation, ischemic injury within the pons is the most common

location [56]. Pediatric brainstem ischemia is rare. However, it may occur in children with systemic hematologic disorders such as sickle cell disease or leukemia. Ischemia may also occur secondary to focal radiation treatment.

3.4.4.1 Imaging

Patients presenting to the ED with symptoms of acute stroke will initially undergo CT imaging. However, as previously discussed, CT evaluation through the level of the brainstem is significantly limited secondary to artifacts. If acute ischemic stroke involving the brainstem is clinically suspected, MRI is the preferred modality for further evaluation.

Magnetic Resonance Imaging (MRI) Ischemic injury involving the supratentorial or infratentorial brain will demonstrate associated signal abnormality secondary to the restricted diffusion of water molecules, visualized as hyperintense signal on DWI with matching low values on ADC map (Figs. 3.12 and 3.13). DWI/ADC evaluation of the supratentorial brain, perfused by the anterior circulation, is highly sensitive and specific, with a false-negative rate of 2% [51]. However, parenchymal evaluation within the posterior circulation may yield a false-negative in up to 31% of cases [51]. Impaired detection of posterior circulation infarction with DWI/ADC occurs secondary to limited resolution and magnetic susceptibility artifacts typically experienced at the level of the skull base [51]. DWI/ADC may also help in the detection of thrombus within a vessel, demonstrating DWI hyperintense signal.

Infarcts involving the pons and medulla may demonstrate a characteristic imaging appearance with sharp margins and a paramedian location, best visualized on T2-weighted imaging. Infarcts will also demonstrate orientation along the axis of the supplying pontine perforating artery [51]. In the setting of basilar occlusion, infarction may involve the majority of the bilateral pons. MR imaging in acute isch-

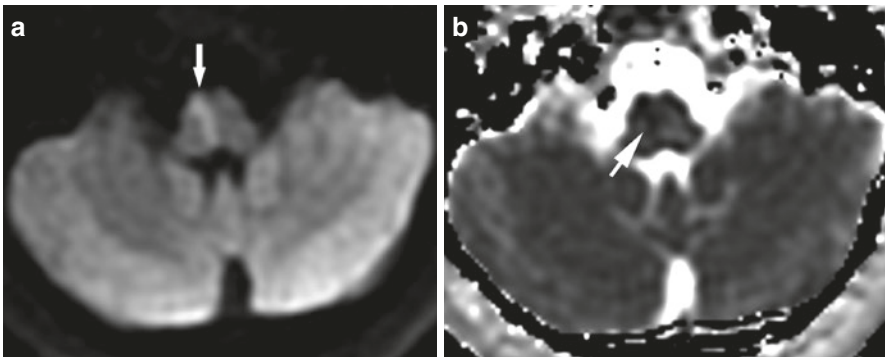


Fig. 3.12 Right medial medullary infarction. MRI demonstrates restriction of diffusion involving the right medial medulla. There is hyperintense signal on DWI (a) with matching low values on ADC map (b)

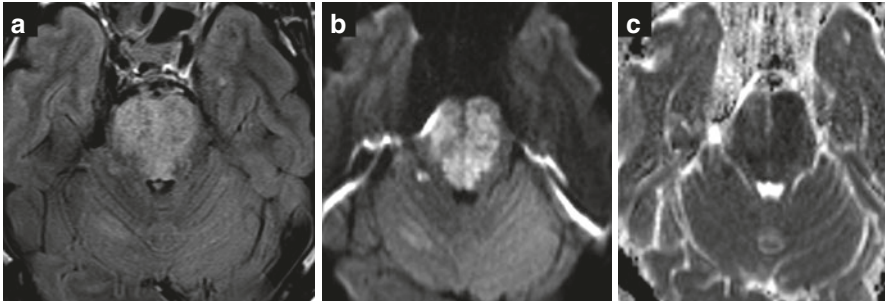


Fig. 3.13 Diffuse pontine infarction. The pons demonstrate abnormal T2-FLAIR hyperintense signal with resultant expansion (a), consistent with edema. There is diffuse restriction of diffusion with hyperintense signal on DWI (b) and matching low values on ADC map (c). Additional focus of restricted diffusion is noted involving the ventral right cerebellar hemisphere

emic stroke will demonstrate associated restricted diffusion and hyperintense signal on T2-weighted imaging reflecting cytotoxic edema.

Computed Tomography (CT) The role of CT imaging in acute brainstem infarction is limited, as noted above. However, CT may provide information regarding hemorrhagic transformation or reveal a hyperdense vessel (basilar artery) suggesting thrombosis [51]. Hyperdense vessels, particularly within the posterior fossa, must be interpreted with caution, as the hyperattenuation may be artifactual.

3.4.5 Hypertrophic Olivary Degeneration

Hypertrophic olivary degeneration (HOD) refers to the transsynaptic (or transneuronal) degeneration of the inferior olivary nucleus (ION) that results from disruption of the dentate-rubro-olivary (DRO) pathway, also known as Guillain-Mollaret triangle [57–59]. Disruption of the DRO pathway may occur secondary to infarction/hemorrhage, a brainstem lesion (neoplastic/non-neoplastic), surgery, or trauma [57–59]. However, the majority of cases reported in the literature are secondary to a cavernous malformation, tumor, or hematoma [57]. Histopathological analysis has demonstrated that macroscopic hypertrophy occurs secondary to neuronal cytoplasmic vacuolization, hypertrophy of astrocytes, and increased gliosis and demyelination of the ION [58, 60]. Palatal myoclonus is a classic clinical manifestation associated with HOD, occurring at 10–11 months subsequent to the anatomic insult [57–59].

3.4.5.1 Imaging

HOD is typically diagnosed in patients undergoing routine MRI surveillance for a primary lesion and are generally asymptomatic at diagnosis [57]. Familiarity with this entity is important to avoid confusion with alternative

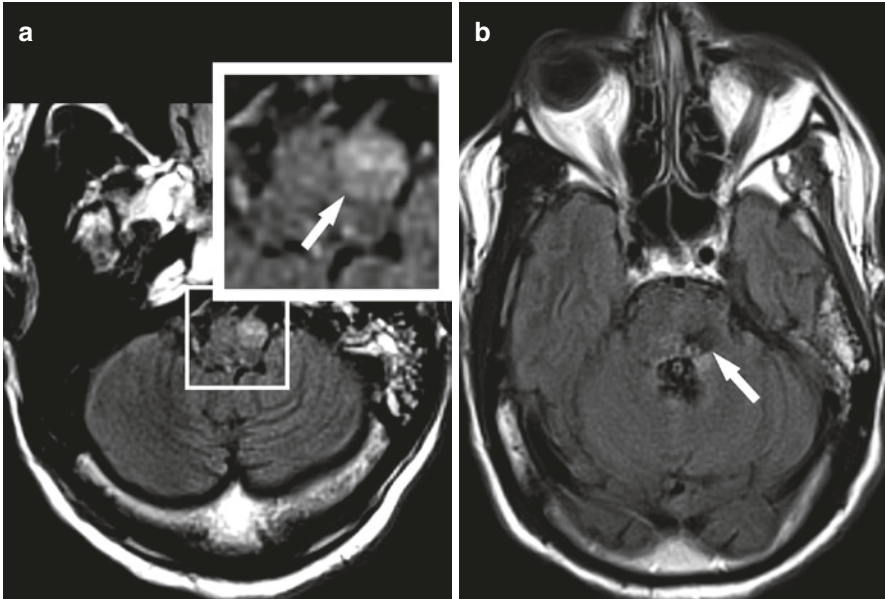


Fig. 3.14 Hypertrophic olivary degeneration. An axial T2-FLAIR image through the medulla demonstrates focal hyperintense signal and mild enlargement of the left inferior olivary nucleus (**a**, arrow). Evaluation through the pons reveals a site of prior hemorrhage that most likely resulted in disruption of the Guillain-Mollaret triangle (**b**, arrow)

pathologies, and identification of a primary lesion that results in disruption of the DRO pathway is essential for diagnosis [58].

Magnetic Resonance Imaging (MRI) Once there is disruption of the afferent fibers extending to the ION, hyperintense signal on T2-weighted imaging will develop within 1–2 months [58, 59]. The ION will subsequently undergo hypertrophic changes detectable on MRI as early as 6 months following the anatomic insult, with hypertrophy of the ION persisting for up to 3–4 years (Fig. 3.14). Eventually, the hypertrophic changes will evolve, and the ION will undergo atrophy, though its hyperintense signal on T2-weighted imaging may resolve or persist indefinitely [57–59].

HOD is not associated with post-contrast gadolinium enhancement [57, 58]. Detection of enhancement should prompt consideration of underlying tumor or infection/inflammation [58].

DTI may demonstrate decreased axial/radial diffusivity during initial hypertrophy of the ION with subsequent increase in axial/radial diffusivity on follow-up imaging, possibly secondary to astrocytic proliferation and gliosis [61]. Preoperative DTI/DTT may be utilized to evaluate for involvement of the DRO pathway due to a brainstem lesion, as well as its anatomical relationship. This information can be used to assess the postoperative risk of developing HOD. It has been suggested that the integration of DTT into stereo-navigational systems, along with T1-weighted

anatomical images, may reduce the risk of surgical DRO pathway injury resulting in the development of HOD [61].

Computed Tomography (CT) Conventional CT imaging is limited in the evaluation of HOD. However, ^{18}F -FDG PET/CT may demonstrate hypermetabolic activity localizing to the affected ION [57, 62].

3.4.6 Demyelination

Brainstem demyelination may occur secondary to multiple etiologies, including inflammation or acquired/inborn metabolic disorders [63, 64]. Multiple sclerosis (MS) and acute disseminated encephalomyelitis (ADEM) are examples of inflammatory demyelination that may involve the brainstem. Early-onset MS, affecting patients younger than 18 years of age, accounts for 2–10% of all MS cases [17]. Osmotic demyelination syndrome (ODS) occurs secondary to a metabolic etiology, characteristically following the rapid correction of hyponatremia [65]. Although brainstem demyelination may demonstrate overlapping imaging features, correlation of the imaging findings with the clinical presentation can help identify the underlying pathology. For example, symptomatology secondary to ADEM may be seen following a viral infection or immunization [66]. Patients with ODS will have a history of hyponatremia with subsequent rapid overcorrection. Classic clinical symptoms include spastic quadriparesis and pseudobulbar palsy [65, 67].

3.4.6.1 Imaging

MR imaging findings of inflammatory versus metabolic demyelination may share overlapping features. In addition to the clinical context, evaluation of the brainstem lesion location and identification of characteristic imaging findings will be helpful. Evaluation of the supratentorial brain can also provide invaluable information. In children, inborn errors of metabolism may result in focal brainstem lesions with associated post-contrast enhancement on T1-weighted MR imaging, possibly mimicking a primary malignancy. An example of brainstem involvement can be seen in Alexander disease (Fig. 3.15) [63, 64].

Magnetic Resonance Imaging (MRI)

- **Inflammatory Demyelination:** Differences in lesion location and signal characteristics have been described in the setting of MS or ADEM. Lesions visualized in patients with MS favor the pons, are more likely asymmetrical/unilateral, and more commonly demonstrate well-circumscribed margins on T2-weighted imaging (Fig. 3.16). Conversely, lesions in a patient with ADEM are more likely to have poorly-defined margins on T2-weighted imaging and favor a symmetric/bilateral distribution within the brainstem (Fig. 3.17) [66]. Evaluation of the

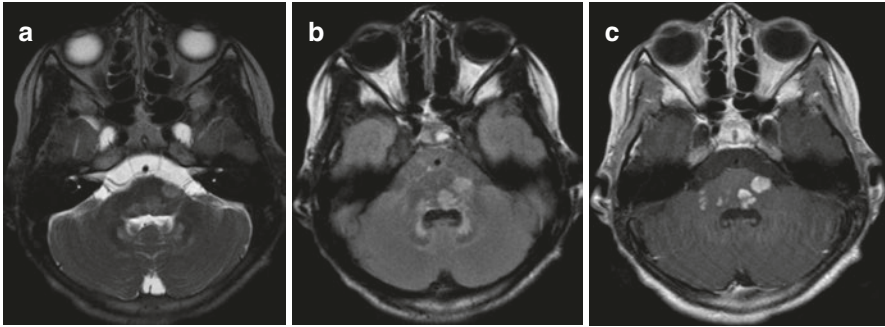


Fig. 3.15 Alexander disease (pediatrics). Axial T2-weighted (a) and T2-FLAIR (b) images demonstrate multiple hyperintense lesions within the lower pons; there is associated enhancement on post-contrast T1-weighted imaging (c). (Case and images courtesy of Dr. Thierry A.G.M. Huisman)

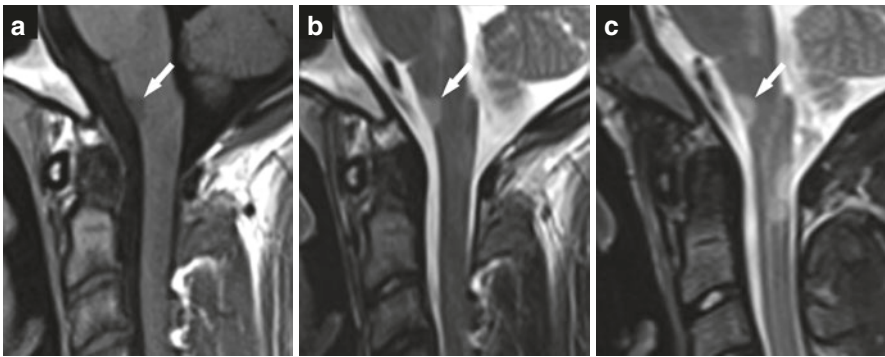


Fig. 3.16 Multiple sclerosis. Sagittal T1-weighted (a, arrow) and T2-weighted (b, c, arrows) images demonstrate a well-circumscribed medullary lesion that is hypointense on T1-weighted and hyperintense on T2-weighted imaging. Note the additional lesions within the pons and upper dorsal cervical spinal cord

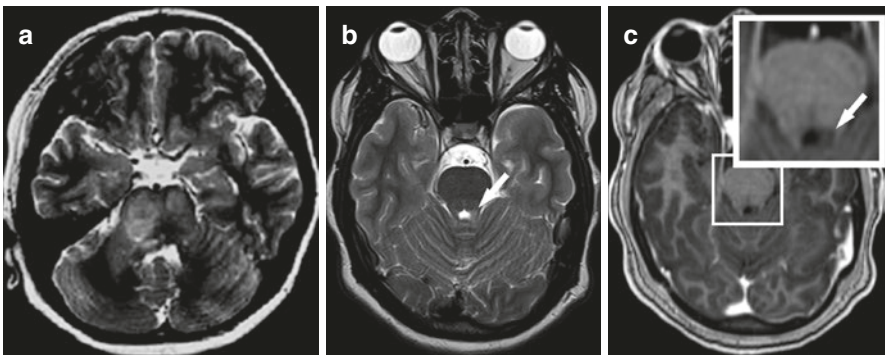


Fig. 3.17 Acute demyelinating encephalomyelitis versus multiple sclerosis (pediatrics). An axial T2-weighted image in a patient with ADEM demonstrates diffuse hyperintense signal within the pons with associated ill-defined margins (a). In contrast, imaging of a patient with pediatric onset MS revealed a single, well-circumscribed lesion within the left dorsal pons, with extension into the left superior cerebellar peduncle (b, c). (Image [a] courtesy of Dr. Thierry A.G.M. Huisman)

supratentorial brain in patients with suspected MS may help in the differentiation or confirmation of diagnosis. MS lesions are the manifestations of perivenular inflammation (Fig. 3.18) [65]. Lesions, therefore, are best identified as hyperintense lesions on T2-weighted and T2-FLAIR images in a perivenular distribution, characteristically appearing orthogonal to the plane of the lateral ventricles.

- **Metabolic Demyelination:** Osmotic demyelination most commonly involves the central pons and results in a symmetric hyperintense signal on T2-weighted and T2-FLAIR images (Fig. 3.19). Characteristic central pontine signal abnormality on T2-weighted/T2-FLAIR images may resemble a “trident-shape,” which

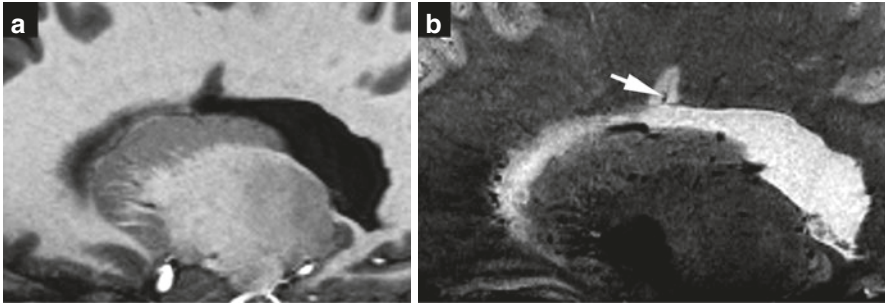


Fig. 3.18 Multiple sclerosis. Sagittal T1- and T2-weighted (a, b) MR imaging at 7 T demonstrates a supratentorial, periventricular lesion within a perivenular distribution (b, arrow)

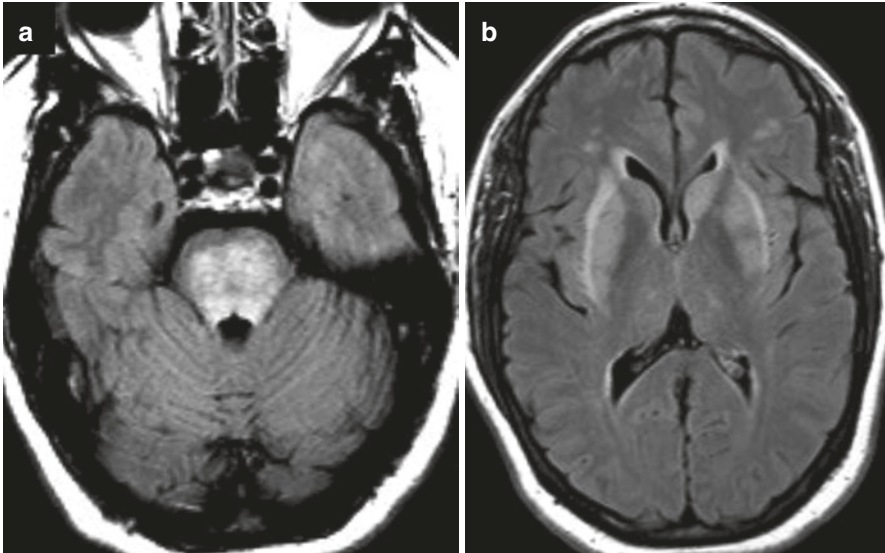


Fig. 3.19 Osmotic demyelination syndrome. Axial T2-FLAIR image through the pons (a) demonstrates diffuse abnormal hyperintense signal with relative sparing of the right, greater than the left, ventrolateral pons. Evaluation of the supratentorial brain in the same patient revealed abnormal T2-FLAIR signal symmetrically within the external capsules and basal ganglia (b)

results from sparing of the ventrolateral pons and corticospinal tracts [65]. Early MRI findings may include restricted diffusion on DWI/ADC within the central pons [65]. Evaluation of the supratentorial brain may demonstrate hyperintense signal abnormality on T2-weighted imaging involving the external and extreme capsules, basal ganglia, thalami, and lateral geniculate nuclei [65, 67, 68].

Computed Tomography (CT) Considering the lack of mass-effect and hemorrhage, lesions are readily undetectable on CT imaging. Nonspecific hypoattenuation may be visualized within the pons in patients with ODS, though conspicuity will be severely hampered secondary to skull base artifacts [67].

3.4.7 Infection

The rhombencephalon, known as the “hindbrain,” consists of the pons, medulla oblongata, and cerebellum. Despite exclusion of the mesencephalon, the midbrain, the term rhombencephalitis (RE) has been used interchangeably with “brainstem encephalitis” [17, 69, 70]; it will be used to denote brainstem encephalitis, including the midbrain, within this section. RE may occur secondary to an infectious, autoimmune, or paraneoplastic etiology [69]. The most common infectious culprits affecting adults and children, in order of decreasing incidence, are *Listeria*, enterovirus 71 (EV71), and herpes viruses [17, 69, 70]. *Listeria* is a gram-positive, facultative anaerobic, intracellular rod and is the leading pathogen resulting in RE, affecting patients aged 14–79 [69].

3.4.7.1 Imaging

MRI is the modality of choice for evaluation of infectious RE, though findings may be nonspecific [70]. MR imaging allows for superior contrast resolution and ability to image through the posterior fossa without the artifacts and radiation encountered with CT imaging. Additionally, it has been reported that in patients with infectious RE, MR imaging will be abnormal in greater than 70% of cases [17]. In patients with RE secondary to *Listeria*, MR imaging will be abnormal in 100% of cases [69].

Magnetic Resonance Imaging (MRI) MR imaging in patients with RE typically demonstrates hyperintense signal on T2-weighted and T2-FLAIR images involving the pons, medulla, upper cervical cord, cerebellum, and midbrain [17, 69]. *Listeria* will demonstrate nonspecific signal abnormality involving the brainstem. However, unlike the aforementioned viral etiologies, *Listeria* may progress into parenchymal ring-enhancing lesions on post-contrast T1-weighted imaging secondary to abscess formation [69]. Bacterial abscesses are typically associated with central restricted diffusion on DWI/ADC map and hyperintense signal on T2-weighted images. In contrast, brainstem tuberculomas secondary to tuberculo-

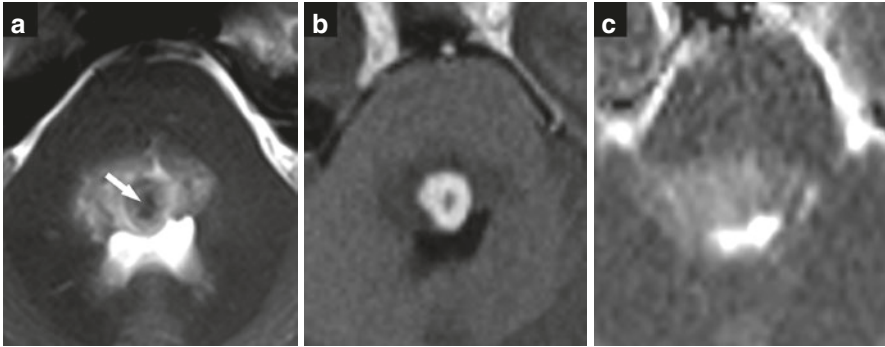


Fig. 3.20 Tuberculoma. Axial images demonstrate a round lesion centered within the region of the right facial colliculus. T2-weighted image reveals a central region of hypointense signal (**a**, arrow) and associated peripheral enhancement (**b**). ADC map does not demonstrate associated low values to suggest restriction of diffusion (**c**)

sis (TB) will demonstrate characteristic central hypointense signal on T1- and T2-weighted images [70, 71], without associated diffusion restriction on DWI/ADC map (Fig. 3.20) [71].

RE secondary to EV71 may result in characteristic hypointense and hyperintense signal on T1- and T2-weighted images, respectively, along the dorsal aspect of the brainstem at the pontomedullary junction. This signal abnormality may appear unilateral or bilateral [17].

Herpes simplex viruses will demonstrate hyperintense signal abnormality on T2-weighted and T2-FLAIR images, preferentially involving the medulla and upper cervical cord [69]. Herpes simplex virus 1 (HSV1) has been noted to have an affinity for the cerebellar peduncles [17].

¹H-MRS may demonstrate elevated Cho/Cr and decreased NAA/Cr ratios. Identification of peaks including succinate or acetate have been strongly associated with infection [17].

3.5 Extra-Axial Lesions

Extra-axial lesions can arise from various locations adjacent to the brainstem and exert significant mass-effect. As noted at the beginning of the chapter, origins for extra-axial lesions include the CPA, the pineal gland region, the clivus or cavernous sinus, or the suprasellar region. Associated mass-effect may result in parenchymal edema or, at times, even mimic an intra-axial mass (Fig. 3.21). Lesions arising from the CPA are the most common and account for 5–10% of all intracranial masses in adults [72]. The most common lesions encountered in the CPA include schwannomas, meningiomas, and epidermoid cysts, in order of decreasing frequency [72].

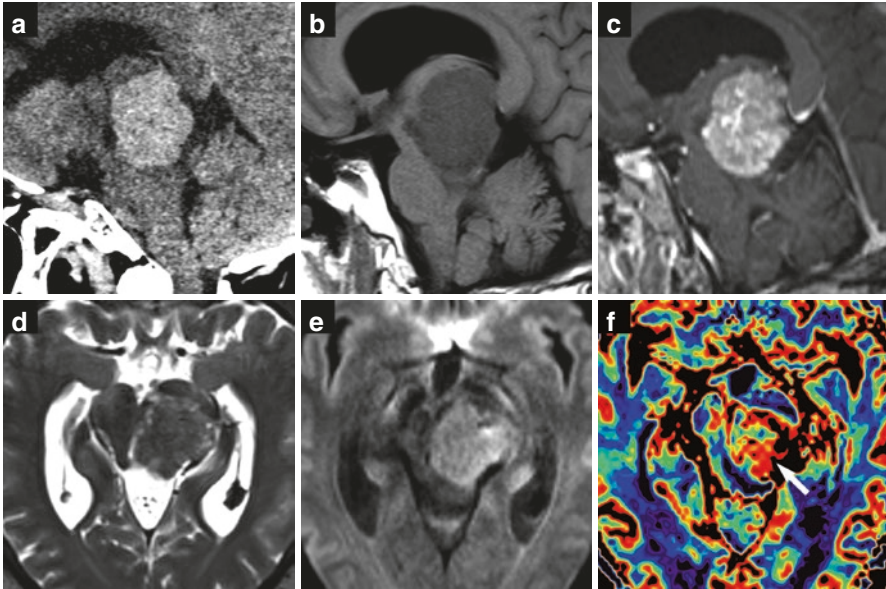


Fig. 3.21 Germinoma (pineal region mass mimicking intra-axial origin [a–e]). Sagittal reformat CT image (a) demonstrates a mass centered within the pineal gland region with intrinsic hyperattenuation, reflecting hypercellularity. Pre- (b) and post-contrast (c) MR T1-weighted images demonstrate enhancement and associated mass-effect on the midbrain. There is elevated cerebral blood volume on perfusion imaging (f). (Case courtesy of Dr. Gary Gong)

3.5.1 Schwannoma

3.5.1.1 Imaging

Magnetic Resonance Imaging (MRI) MR imaging of a schwannoma typically demonstrates hypo/isointense and hyperintense signal on T1- and T2-weighted images, respectively. Post-contrast T1-weighted imaging typically demonstrates homogeneous enhancement centered within the internal auditory canal (IAC). As they enlarge, schwannomas are characteristically associated with bony expansion of the IAC and extension into the CPA, resulting in an “ice cream cone” appearance (Fig. 3.22). Cisternal component of the schwannoma may demonstrate cystic changes on T2-weighted imaging [72]. High-resolution 3D heavily T2-weighted imaging may facilitate identification of the compressed/displaced adjacent cranial nerves.

Computed Tomography (CT) CT imaging is preferred for evaluation of bony remodeling involving the IAC.



Fig. 3.22 Schwannoma. Axial high-resolution CISS (a) and post-contrast T1-weighted (b) images demonstrate a solid and cystic mass centered within the left IAC, which extends into the CPA. Left IAC mass results in mild expansion of the porus acusticus (a, arrow) relative to the right. Post-contrast T1-weighted image (c) demonstrates bilateral masses arising from the IACs and extending into the CPAs in a patient with neurofibromatosis type 2. Bilateral IAC masses (c) exert mass-effect on the pons and cerebellum on the right greater than the left side

3.5.2 Meningioma

3.5.2.1 Imaging

Magnetic Resonance Imaging (MRI) MR imaging of a meningioma typically demonstrates hypo/isointense on T1-weighted imaging and, unlike schwannomas, remain hypo/isointense on T2-weighted imaging. Meningiomas will show marked enhancement on post-contrast T1-weighted imaging and may have associated dural enhancement, reflecting a “dural tail” (Fig. 3.23). Dural enhancement may reflect infiltration or reactive changes. The epicenter of a meningioma is located along the CPA, and not within the IAC. Therefore, ipsilateral expansion of the IAC is not compatible with a meningioma. However, meningiomas will typically develop hyperostosis involving the underlying bone [72].

Computed Tomography (CT) CT imaging is preferred for the evaluation of hyperostosis involving bony structures subjacent to the meningioma.

3.5.3 Epidermoid Cyst

3.5.3.1 Imaging

Magnetic Resonance Imaging (MRI) MR imaging of an epidermoid cyst is pathognomonic. These lesions will have a predominant hypointense signal on T1- and hyperintense signal on T2-weighted imaging, typically with incomplete sup-

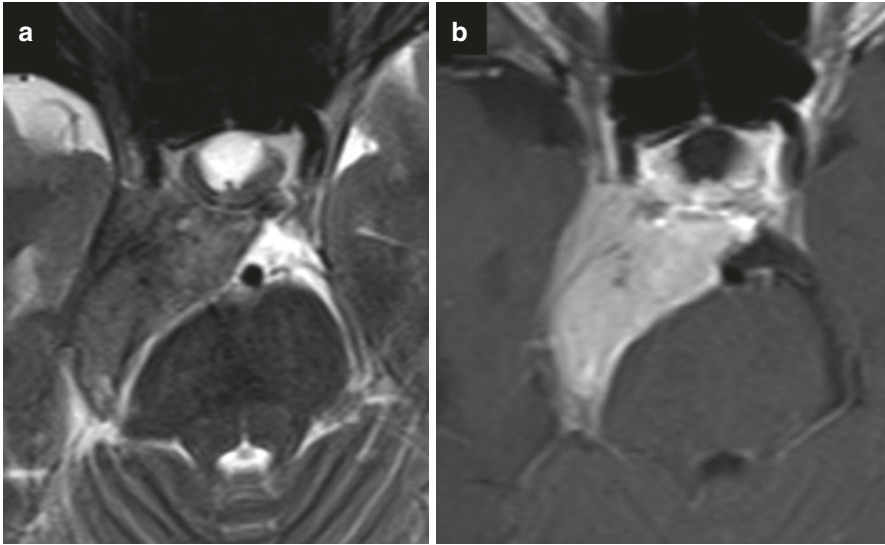


Fig. 3.23 Meningioma. Axial T2-weighted (a) and post-contrast T1-weighted (b) images demonstrate a T2 hypointense mass arising from the right cavernous sinus and extending posteriorly into the preponine cistern. The mass demonstrates homogenous enhancement (b) and exerts mass-effect on the right ventrolateral pons

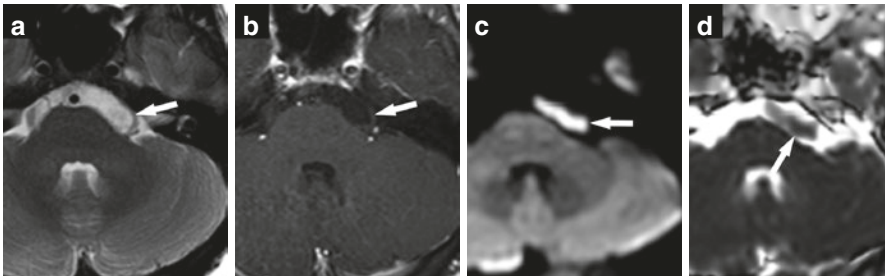


Fig. 3.24 Epidermoid cyst. Axial T2-weighted image (a) demonstrates a cystic lesion within the left preponine cistern that extends into the left CPA cistern. The cystic lesion is isointense to CSF on T2-weighted imaging (a) and not associated with post-contrast enhancement (b). However, there is associated restriction of diffusion with hyperintense signal on DWI (c) and matching low values on ADC map (d). (Case and images courtesy of Dr. Thierry A.G.M. Huisman)

pression on T2-FLAIR images. MR images may demonstrate a lamellated (onion-skin) appearance secondary to accumulation of desquamated material. DWI/ADC will demonstrate reduced/restricted diffusion secondary to internal proteinaceous and/or lipid content (Fig. 3.24) [72]. The resultant hyperintense signal on DWI significantly enhances the lesion conspicuity, given the juxtaposition of DWI-hypointense CSF within the basal cisterns. The degree of mass effect on the adjacent brainstem is well depicted by MRI.

Computed Tomography (CT) CT imaging may contain foci of low attenuation reflecting internal lipid content at approximately 10-to-20 Hounsfield units (HU). Evaluation of the adjacent bone may demonstrate scalloping, depending on the location.

3.6 Conclusion

Brainstem lesions represent a wide spectrum of pathologies. A parenchymal mass may be secondary to a primary neoplasm (benign or malignant), metastatic disease, congenital vascular malformation, infection, infarction, or inflammation. In addition, pseudolesions may also be identified within the brainstem, as previously seen with HOD. Evaluation of the supratentorial brain should also be performed to identify associated findings that may help in the diagnosis, such as periventricular lesions within a perivenular distribution in patients with MS. Although different imaging modalities may be utilized, MRI remains the preferred modality for the evaluation of brainstem lesions. Lesion-specific imaging appearance can provide invaluable pre-treatment information to aid in the diagnosis, assess impact on adjacent structures, assist in treatment planning, and evaluate for treatment response.

References

1. Querol-Pascual M. Clinical approach to brainstem lesions. *Semin Ultrasound CT MR*. 2010;31(3):220–9.
2. Purohit B, Kamli AA, Kollias SS. Imaging of adult brainstem gliomas. *Eur J Radiol*. 2015;84(4):709–20.
3. Poretti A, Meoded A, Huisman TAGM. Neuroimaging of pediatric posterior fossa tumors including review of the literature. *J Magn Reson Imaging*. 2012;35(1):32–47.
4. Bosemani T, Orman G, Boltshauser E, Tekes A, Huisman TAGM, Poretti A. Congenital abnormalities of the posterior fossa. *Radiographics*. 2015;35(1):200–20.
5. Blitz AM, Macedo LL, Chonka ZD, Ilica AT, Choudhri AF, Gallia GL, et al. High-resolution CISS MR imaging with and without contrast for evaluation of the upper cranial nerves. *Neuroimaging Clin*. 2014;24(1):17–34.
6. Blitz AM, Choudhri AF, Chonka ZD, Ilica AT, Macedo LL, Chhabra A, et al. Anatomic considerations, nomenclature, and advanced cross-sectional imaging techniques for visualization of the cranial nerve segments by MR imaging. *Neuroimaging Clin*. 2014;24(1):1–15.
7. Inoue T, Ogasawara K, Beppu T, Ogawa A, Kabasawa H. Diffusion tensor imaging for preoperative evaluation of tumor grade in gliomas. *Clin Neurol Neurosurg*. 2005;107(3):174–80.
8. Price SJ, Burnet NG, Donovan T, Green HL, Peña A, Antoun NM, et al. Diffusion tensor imaging of brain tumours at 3T: a potential tool for assessing white matter tract invasion? *Clin Radiol*. 2003;58(6):455–62.
9. Li D, Jiao YM, Wang L, Lin FX, Wu J, Tong XZ, et al. Surgical outcome of motor deficits and neurological status in brainstem cavernous malformations based on preoperative diffusion tensor imaging: a prospective randomized clinical trial. *J Neurosurg*. 2018;130(1):286–301.

10. Cao Z, Lv J, Wei X, Quan W. Appliance of preoperative diffusion tensor imaging and fiber tractography in patients with brainstem lesions. *Neurol India*. 2010;58(6):886–90.
11. Chen X, Weigel D, Ganslandt O, Buchfelder M, Nimsky C. Diffusion tensor imaging and white matter tractography in patients with brainstem lesions. *Acta Neurochir*. 2007;149(11):1131; discussion 1131.
12. Chen X, Weigel D, Ganslandt O, Fahlbusch R, Buchfelder M, Nimsky C. Diffusion tensor-based fiber tracking and intraoperative neuronavigation for the resection of a brainstem cavernous angioma. *Surg Neurol*. 2007;68(3):291; discussion 291.
13. Wu J, Zhou L, Tang W, Mao Y, Hu J, Song Y, et al. Clinical evaluation and follow-up outcome of diffusion tensor imaging-based functional neuronavigation: a prospective, controlled study in patients with gliomas involving pyramidal tracts. *Neurosurgery*. 2007;61(5):949.
14. Yao Y, Ulrich NH, Guggenberger R, Alzarhani YA, Bertalanffy H, Kollias SS. Quantification of corticospinal tracts with diffusion tensor imaging in brainstem surgery: prognostic value in 14 consecutive cases at 3T magnetic resonance imaging. *World Neurosurg*. 2015;83(6):1006–14.
15. Hipp SJ, Steffen-Smith E, Hammoud D, Shih JH, Bent R, Warren KE. Predicting outcome of children with diffuse intrinsic pontine gliomas using multiparametric imaging. *Neuro-Oncology*. 2011;13(8):904–9.
16. Laprie A, Pirzkall A, Haas-Kogan DA, Cha S, Banerjee A, Le TP, et al. Longitudinal multi-voxel MR spectroscopy study of pediatric diffuse brainstem gliomas treated with radiotherapy. *Int J Radiat Oncol Biol Phys*. 2005;62(1):20–31.
17. Rossi A, Martinetti C, Morana G, Severino M, Tortora D. Neuroimaging of infectious and inflammatory diseases of the pediatric cerebellum and brainstem. *Neuroimaging Clin N Am*. 2016;26(3):471–87.
18. Bahrami S, Yim CM. Quality initiatives: blind spots at brain imaging. *Radiographics*. 2009;29(7):1877–96.
19. Vogl T, Harth M. Chapter 3: neuro imaging of the posterior Fossa. 2011; Available at: <https://pdfs.semanticscholar.org/5f8d/0abf76715d2dfadca3fc943da1beba32acb1.pdf>.
20. Pope WB. Brain metastases: neuroimaging. *Handb Clin Neurol*. 2018;149:89–112.
21. Lin TF, Prados M. Brainstem Gliomas. In: Gupta N, Banerjee A, Haas-Kogan DA, editors. *Pediatric CNS tumors*. Cham: Springer International Publishing; 2017. p. 51–67.
22. Jallo G. Brainstem gliomas. *Childs Nerv Syst*. 2006;22(1):1–2.
23. Rossi AL, Kieran MW. Pediatric brainstem gliomas: new understanding leads to potential new treatments for two very different tumors. *Curr Oncol Rep*. 2015;17(3):436.
24. Johnson DR, Guerin JB, Giannini C, Morris JM, Eckel LJ, Kaufmann TJ. 2016 updates to the WHO brain tumor classification system: what the radiologist needs to know. *Radiographics*. 2017;37(7):2164–80.
25. Guzmán-De-Villoria JA, Ferreiro-Argüelles C, Fernández-García P. Differential diagnosis of T2 hyperintense brainstem lesions: Part 2. Diffuse lesions. *Semin Ultrasound CT MR*. 2010;31(3):260–74.
26. O'Neill BP, Illig JJ. Primary central nervous system lymphoma. *Mayo Clin Proc*. 1989;64(8):1005–20.
27. Murray K, Kun L, Cox J. Primary malignant lymphoma of the central nervous system. Results of treatment of 11 cases and review of the literature. *J Neurosurg*. 1986;65(5):600–7.
28. Shams PN, Waldman A, Plant GT. B cell lymphoma of the brain stem masquerading as myasthenia. *J Neurol Neurosurg Psychiatry*. 2002;72(2):271–3.
29. Carlson BA. Rapidly progressive dementia caused by nonenhancing primary lymphoma of the central nervous system. *AJNR Am J Neuroradiol*. 1996;17(9):1695–7.
30. Nabavizadeh SA, Vossough A, Hajmomenian M, Assadsangabi R, Mohan S. Neuroimaging in central nervous system lymphoma. *Hematol Oncol Clin North Am*. 2016;30(4):799–821.
31. Vaquero J, Martínez R, Rossi E, López R. Primary cerebral lymphoma: the “ghost tumor”. Case report. *J Neurosurg*. 1984;60(1):174–6.

32. Barajas RF, Rubenstein JL, Chang JS, Hwang J, Cha S. Diffusion-weighted MR imaging derived apparent diffusion coefficient is predictive of clinical outcome in primary central nervous system lymphoma. *AJNR Am J Neuroradiol.* 2010;31(1):60–6.
33. Blasel S, Vorwerk R, Kiyose M, Mittelbronn M, Brunnberg U, Ackermann H, et al. New MR perfusion features in primary central nervous system lymphomas: pattern and prognostic impact. *J Neurol.* 2018;265(3):647–58.
34. Haldorsen IS, Kråkenes J, Krossnes BK, Mella O, Espeland A. CT and MR imaging features of primary central nervous system lymphoma in Norway, 1989–2003. *AJNR Am J Neuroradiol.* 2009;30(4):744–51.
35. Barnholtz-Sloan JS, Sloan AE, Davis FG, Vigneaun FD, Lai P, Sawaya RE. Incidence proportions of brain metastases in patients diagnosed (1973 to 2001) in the Metropolitan Detroit Cancer Surveillance System. *J Clin Oncol.* 2004;22(14):2865–72.
36. Lee RR, Becher MW, Benson ML, Rigamonti D. Brain capillary telangiectasia: MR imaging appearance and clinicohistopathologic findings. *Radiology.* 1997;205(3):797–805.
37. Nathal E, Patiño-Rodríguez HM, Arauz A, Imam SS, Acosta E, Evins AI, et al. Risk factors for unfavorable outcomes in surgically treated brainstem cavernous malformations. *World Neurosurg.* 2018;111:e484.
38. Akers A, Al-Shahi Salman R, Awad I, Dahlem K, Flemming K, Hart B, et al. Synopsis of guidelines for the clinical Management of Cerebral Cavernous Malformations: consensus recommendations based on systematic literature review by the Angioma Alliance Scientific Advisory Board Clinical Experts Panel. *Neurosurgery.* 2017;80(5):665–80.
39. Abla AA, Lekovic GP, Turner JD, de Oliveira JG, Porter R, Spetzler RF. Advances in the treatment and outcome of brainstem cavernous malformation surgery: a single-center case series of 300 surgically treated patients. *Neurosurgery.* 2011;68(2):5.
40. Mokin M, Agazzi S, Dawson L, Primiani CT. Neuroimaging of cavernous malformations. *Curr Pain Headache Rep.* 2017;21(12):47.
41. Rivera PP, Willinsky RA, Porter PJ. Intracranial cavernous malformations. *Neuroimaging Clin N Am.* 2003;13(1):27–40.
42. de Souza JM, Domingues RC, Cruz LCH, Domingues FS, Iasbeck T, Gasparetto EL. Susceptibility-weighted imaging for the evaluation of patients with familial cerebral cavernous malformations: a comparison with t2-weighted fast spin-echo and gradient-echo sequences. *AJNR Am J Neuroradiol.* 2008;29(1):154–8.
43. Bulut HT, Sarica MA, Baykan AH. The value of susceptibility weighted magnetic resonance imaging in evaluation of patients with familial cerebral cavernous angioma. *Int J Clin Exp Med.* 2014;7(12):5296.
44. Flores BC, Whittemore AR, Samson DS, Barnett SL. The utility of preoperative diffusion tensor imaging in the surgical management of brainstem cavernous malformations. *J Neurosurg.* 2015;122(3):653–62.
45. Faraji AH, Abhinav K, Jarbo K, Yeh F, Shin SS, Pathak S, et al. Longitudinal evaluation of corticospinal tract in patients with resected brainstem cavernous malformations using high-definition fiber tractography and diffusion connectometry analysis: preliminary experience. *J Neurosurg.* 2015;123(5):1133–44.
46. Kovanlikaya I, Firat Z, Kovanlikaya A, Uluğ AM, Cihangiroglu MM, John M, et al. Assessment of the corticospinal tract alterations before and after resection of brainstem lesions using Diffusion Tensor Imaging (DTI) and tractography at 3T. *Eur J Radiol.* 2011;77(3):383–91.
47. El-Koussy M, Schroth G, Gralla J, Brekenfeld C, Andres RH, Jung S, et al. Susceptibility-weighted MR imaging for diagnosis of capillary telangiectasia of the brain. *Am J Neuroradiol.* 2012;33(4):715–20.
48. Giroud M, Gras P, Chadan N, Beuriat P, Milan C, Arveux P, et al. Cerebral haemorrhage in a French prospective population study. *J Neurol Neurosurg Psychiatry.* 1991;54(7):595–8.
49. Murata Y, Yamaguchi S, Kajikawa H, Yamamura K, Sumioka S, Nakamura S. Relationship between the clinical manifestations, computed tomographic findings and the outcome in 80 patients with primary pontine hemorrhage. *J Neurol Sci.* 1999;167(2):107–11.

50. Wessels T, Möller-Hartmann W, Noth J, Klötzsch C. CT findings and clinical features as markers for patient outcome in primary pontine hemorrhage. *Am J Neuroradiol.* 2004;25(2):257–60.
51. Ortiz de Mendivil A, Alcalá-Galiano A, Ochoa M, Salvador E, Millán JM. Brainstem stroke: anatomy, clinical and radiological findings. *Semin Ultrasound CT MR.* 2013;34(2):131–41.
52. Parizel PM, Makkat S, Van Miert E, Van Goethem JW, van den Hauwe L, De Schepper AM. Intracranial hemorrhage: principles of CT and MRI interpretation. *Eur Radiol.* 2001;11(9):1770–83.
53. Higgins LJ, Koshy J, Mitchell SE, Weiss CR, Carson KA, Huisman TAGM, et al. Time-resolved contrast-enhanced MRA (TWIST) with gadofosveset trisodium in the classification of soft-tissue vascular anomalies in the head and neck in children following updated 2014 ISSVA classification: first report on systematic evaluation of MRI and TWIST in a cohort of 47 children. *Clin Radiol.* 2016;71(1):32–9.
54. Huisman TAGM. Intracranial hemorrhage: ultrasound, CT and MRI findings. *Eur Radiol.* 2005;15(3):434–40.
55. Koton S, Schneider ALC, Rosamond WD, Shahar E, Sang Y, Gottesman RF, et al. Stroke incidence and mortality trends in US communities, 1987 to 2011. *JAMA.* 2014;312(3):259–68.
56. Burger KM, Tuhirim S, Naidich TP. Brainstem vascular stroke anatomy. *Neuroimaging Clin N Am.* 2005;15(2):324, x.
57. Onen MR, Moore K, Cikla U, Ucer M, Schmidt B, Field AS, et al. Hypertrophic Olivary degeneration: neurosurgical perspective and literature review. *World Neurosurg.* 2018;112:e771.
58. Gatlin JL, Wineman R, Schlakman B, Buciu R, Khan M. Hypertrophic Olivary degeneration after resection of a pontine cavernous malformation: a case report. *J Radiol Case Rep.* 2011;5(3):24–9.
59. Goyal M, Versnick E, Tuite P, Cyr JS, Kucharczyk W, Montanera W, et al. Hypertrophic olivary degeneration: metaanalysis of the temporal evolution of MR findings. *AJNR Am J Neuroradiol.* 2000;21(6):1073–7.
60. Kitajima M, Korogi Y, Shimomura O, Sakamoto Y, Hirai T, Miyayama H, et al. Hypertrophic olivary degeneration: MR imaging and pathologic findings. *Radiology.* 1994;192(2):539–43.
61. Orman G, Bosemani T, Jallo GI, Huisman TAGM, Poretti A. Hypertrophic olivary degeneration in a child following midbrain tumor resection: longitudinal diffusion tensor imaging studies. *J Neurosurg Pediatr.* 2014;13(4):408–13.
62. Dubinsky RM, Hallett M, Di Chiro G, Fulham M, Schwankhaus J. Increased glucose metabolism in the medulla of patients with palatal myoclonus. *Neurology.* 1991;41(4):557–62.
63. Huisman TAGM. Tumor-like lesions of the brain. *Cancer Imaging.* 2009;9(Special issue A):S13.
64. Tavasoli A, Armangue T, Ho C, Whitehead M, Bornhorst M, Rhee J, et al. Alexander disease. *J Child Neurol.* 2017;32(2):184–7.
65. Ruzek KA, Campeau NG, Miller GM. Early diagnosis of central pontine myelinolysis with diffusion-weighted imaging. *AJNR Am J Neuroradiol.* 2004;25(2):210–3.
66. Lu Z, Zhang B, Qiu W, Kang Z, Shen L, Long Y, et al. Comparative brain stem lesions on MRI of acute disseminated encephalomyelitis, neuromyelitis optica, and multiple sclerosis. *PLoS One.* 2011;6(8):e22766.
67. Miller GM, Baker HL, Okazaki H, Whisnant JP. Central pontine myelinolysis and its imitators: MR findings. *Radiology.* 1988;168(3):795–802.
68. Alleman AM. Osmotic demyelination syndrome: central pontine myelinolysis and extrapontine myelinolysis. *Semin Ultrasound CT MR.* 2014;35(2):153–9.
69. Jubelt B, Mihai C, Li TM, Veerapaneni P. Rhombencephalitis/brainstem encephalitis. *Curr Neurol Neurosci Rep.* 2011;11(6):543–52.
70. Quattrocchi CC, Errante Y, Rossi Espagnet MC, Galassi S, Della Sala SW, Bernardi B, et al. Magnetic resonance imaging differential diagnosis of brainstem lesions in children. *World J Radiol.* 2016;8(1):1–20.
71. Lyons JL, Neagu MR, Norton IH, Klein JP. Diffusion tensor imaging in brainstem tuberculoma. *J Clin Neurosci.* 2013;20(11):1598–9.
72. Smirniotopoulos JG, Yue NC, Rushing EJ. Cerebellopontine angle masses: radiologic-pathologic correlation. *Radiographics.* 1993;13(5):1131–47.

Chapter 4

Clinical Presentation and Assessment for Brainstem Tumors



Bahattin Tanrıkulu and M. Memet Özek

Abbreviations

LCN Lower cranial nerves
MLF Medial longitudinal fasciculus

4.1 Introduction

Brainstem tumors comprise 10–20% of all central nervous system tumors in the pediatric age group [1]. Brainstem tumors includes tumors that arise from the midbrain, pons, medulla oblongata, and upper cervical cord [2]. Their peak incidence is between 7 and 9 years of age. They do not show sex predilection [3]. These tumors may grow as focal or diffuse lesions [4]. According to their location and growth pattern, they are classified as diffuse, focal, dorsal exophytic, and cervico-medullary tumors [4, 5]. Nearly 75% of brainstem tumors are diffuse gliomas with dismal prognosis, whereas focal ones are amenable to surgical excision with favorable prognosis [5, 6].

4.2 Patient History

Patients with brainstem gliomas present with variable patient history and neurological deficits depending on the tumors' growth pattern and location within the brainstem. Patients with a history of more acute onset with signs of involvement of several brainstem nuclei most probably have diffuse brainstem tumors with poor prognosis. On the other hand, patients with focal brainstem lesions generally have history of symptoms with longer durations [7–9]. Patient history may reveal subtle

B. Tanrıkulu · M. M. Özek (✉)

Division of Pediatric Neurosurgery, Department of Neurosurgery, Acibadem University
School of Medicine, Istanbul, Turkey

symptoms of brainstem tumors such as failure to thrive because of profuse vomiting, head tilt, low school performance because of double vision, dysphonia, altered facial expressions, and coughing secondary to swallowing problems due to cranial nerve nuclei involvement [2, 10].

4.3 Neurological Examination

Neurological examination findings of patients with brainstem gliomas may be classified under different categories, such as cranial nerve palsies, pyramidal tract signs, truncal ataxia, and fundoscopic changes [11]. Selvapandian et al. reported that the most common clinical sign in pediatric patients with brainstem gliomas are pyramidal weakness (83.1%) and facial palsy (80.3%), followed by cerebellar signs (76.1%) and palatal palsy (69%). They also reported that the most common clinical signs in adult patients with brainstem glioma are facial palsy (86.7%) and pyramidal weakness (83.3%), followed by palatal palsy (80%) and cerebellar signs (76.7%). Papilledema was also encountered in 21.1% of pediatric and 40% of adult patients with brainstem gliomas [12].

4.3.1 Cranial Nerve Palsies

4.3.1.1 Trochlear Nerve Palsy

The trochlear nerve nucleus is placed inferior to the oculomotor nucleus, posterior to the medial longitudinal fasciculus (MLF), and anterolateral to the cerebral aqueduct at the level of the inferior colliculus [13, 14]. Motor fibers emerge from the trochlear nerve nucleus, pass around the cerebral aqueduct and decussate at the superior medullary velum [15]. Then, the trochlear nerve emerges from the lower midbrain, just caudal to the inferior colliculus. Trochlear nerve fibers exit the brainstem on the contralateral side of their nucleus [16]. The trochlear nerve is the thinnest cranial nerve with a long intracranial course. It is also the only cranial nerve that exits the brainstem from the posterior side [15]. It supplies motor impulses to the superior oblique muscle. The major function of the trochlear nerve is intorsion of the eyeball. Other functions are depression and abduction of the eyeball [13]. Lesions involving the midbrain or superior medullary velum may cause trochlear nerve palsies [17]. Since one of the functions of the superior oblique muscle is to depress the eyeball, palsy of the superior oblique muscle results in upward deviation of the eyeball. These patients suffer from vertical diplopia, especially during downward gaze and while looking towards the contralateral side of the affected superior oblique muscle [13]. Many patients tend to tilt their heads to the contralateral side of the effected eye to avoid the double vision (Fig. 4.1).

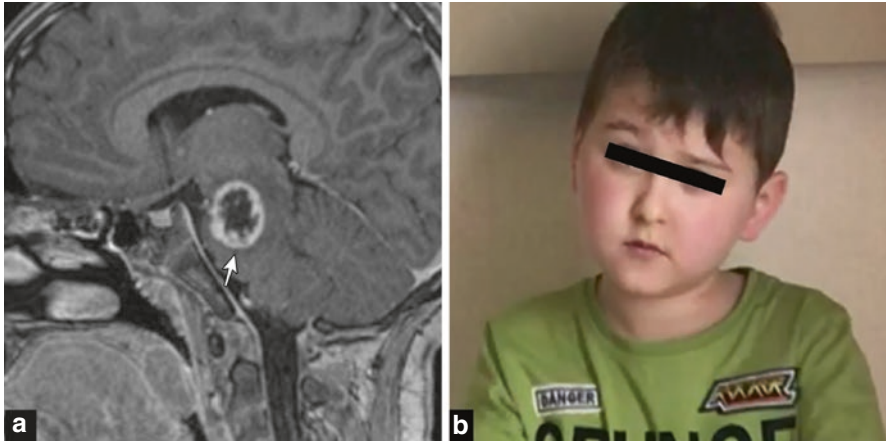


Fig. 4.1 (a) A patient with a brainstem tumor (arrow) has paralysis of his right superior oblique muscle secondary to involvement of the left trochlear nerve nucleus. (b) The patient tends to tilt his head to the left side to compensate for the extorsion of the right eyeball and to correct the double vision

4.3.1.2 Trigeminal Nerve Palsy

The trigeminal nerve has sensory and motor fibers. It has a main sensory nucleus, a spinal nucleus, a mesencephalic nucleus, and a motor nucleus [18, 19]. The main sensory nucleus is located at the posterior part of pons, just lateral to the trigeminal motor nucleus [20, 21]. Facial sensations of pressure and touch are carried by afferent nerve fibers that terminate at the trigeminal main sensory nucleus [22, 23].

The spinal nucleus continues superiorly as the main sensory nucleus of the trigeminal nerve within the pons and passes through the whole medulla oblongata inferiorly until the C2 level of the spinal cord [20, 24, 25]. Sensations of facial pain and temperature are transferred to the spinal nucleus of the trigeminal nerve. The inferior part of the spinal nucleus receives sensory fibers from the ophthalmic division of the trigeminal nerve. The middle part of the spinal nucleus receives fibers from the maxillary division of trigeminal nerve, and the superior part of the trigeminal nucleus receives fibers from the mandibular division of the trigeminal nerve [20, 26]. The mesencephalic nucleus of the trigeminal nerve is located within the mesencephalon and elongates until the level of the main sensory nucleus within the pons [24]. It receives proprioceptive impulses from the muscles of mastication, facial muscles, and extraocular muscles [20, 27]. The motor nucleus of the trigeminal nerve is located at the level of the pons, medial to the main sensory nucleus of the trigeminal nerve. It innervates the anterior belly of the digastric muscle, the mylohyoid muscle, the tensor tympani, the tensor veli palatini, and the muscles of mastication [27].

When the trigeminal nerve is affected by a brainstem tumor, the patient will most probably experience unilateral loss of corneal sensation and reflex, weakness in the muscles of mastication, and hemifacial hypoesthesia with contralateral hypoesthesia of the body [11] (Fig. 4.2).

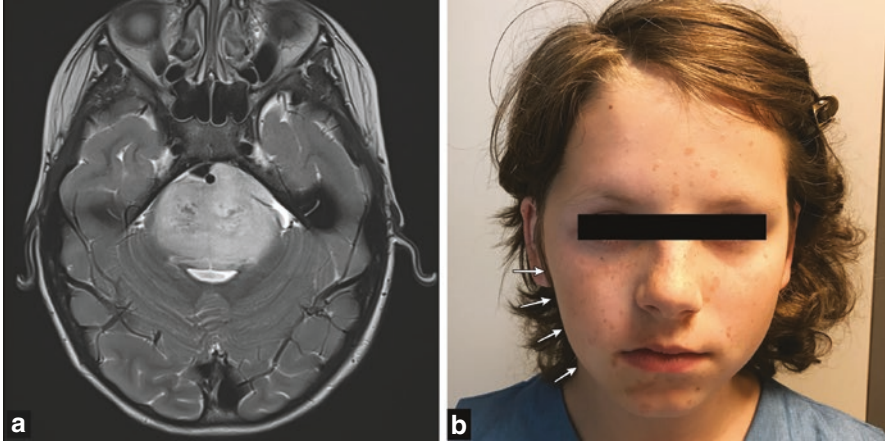


Fig. 4.2 (a) A 12-year-old patient with facial asymmetry had a diagnosis of diffuse midline glioma. (b) She has multiple cranial nerve palsies including marked right-sided atrophy of the masseter muscle (arrows) secondary to trigeminal nerve motor nucleus involvement

4.3.1.3 Abducens Nerve Palsy

The abducens nucleus is located in the lower part of the pons and abducts the ipsilateral eyeball [28]. It is in close contact with the MLF, which is responsible for conjugate eye movements [24, 29, 30]. The MLF is the main pathway that connects the vestibular and cochlear nerve nuclei with the oculomotor, trochlear and abducens nerve nuclei; it is located in the floor of the fourth ventricle, just posterior to the abducens nuclei [20, 21, 25].

The abducens nerve is the most commonly involved cranial nerve in brainstem gliomas. Unilateral or bilateral involvement may be observed. Patients have strabismus and double vision during horizontal gaze. The affected eye looks medially because of the unbalanced tonus of the ipsilateral orbital muscles that are innervated by the third nerve [11, 31]. Abducens nuclei injuries such as those sustained by brainstem tumors impair ipsilateral conjugate gaze of both eyes; this is because of the interneurons that make connections with the contralateral third nerve nucleus via the MLF [32]. For this reason, patients with brainstem lesions have a horizontal conjugate gaze palsy toward the side of the lesion. These patients may also have signs of ipsilateral or bilateral facial nerve involvement [33] (Fig. 4.3).

4.3.1.4 Facial Nerve Palsy

The facial nerve has both motor and sensory fibers. It has one motor nucleus called the facial motor nucleus, one parasympathetic nucleus called the superior salivatory nucleus, and a sensory nucleus called the solitary nucleus. Motor fibers of the facial

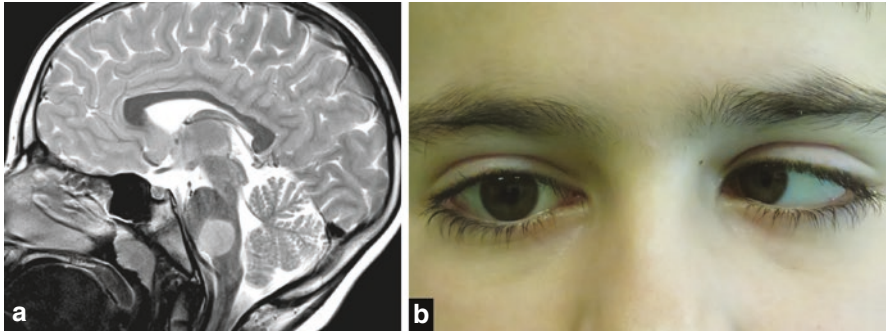


Fig. 4.3 A 6-year-old boy with a histone-mutant diffuse midline glioma (a) who presented with left-sided abducens paralysis (b)

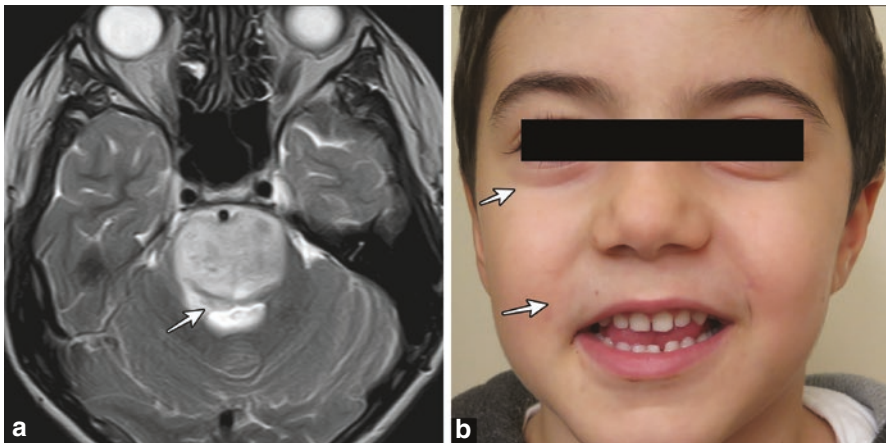


Fig. 4.4 (a) A 9-year-old boy, who had a diffuse midline glioma that also invaded the facial colliculus (arrow), presented with right sided peripheral facial paralysis (b). Please note the effacement of the right nasolabial and infrapalpebral sulci (arrows)

nerve originate from the facial nucleus in front of the abducens nucleus [21, 34]. They run posteromedially, pass around the abducens nucleus underneath the facial colliculus in the floor of the fourth ventricle, and then turn anteriorly to exit the brainstem through the pontomedullary sulcus [20, 25, 31].

It is the second most commonly affected cranial nerve by brainstem gliomas after the abducens nerve. The facial nerve motor nuclei lie very close to the floor of the fourth ventricle. For this reason, facial nerve motor nuclei can easily be affected by any pathology involving the floor of the fourth ventricle, such as brainstem tumors [11]. Affected patients will experience weakness in the muscles of facial expression. These patients will have effacement of the infrapalpebral and nasolabial sulci [35] (Fig. 4.4). Severely affected patients will have a difficulty in eye closure, which may lead to development of keratitis as the disease becomes chronic (Fig. 4.5).



Fig. 4.5 A 12-year-old boy with a brainstem pilocytic astrocytoma. The right abducens nucleus and right facial motor nucleus were involved. Since the disease had a slowly progressive course, the patient suffered from keratitis and conjunctivitis in the right eye secondary to a long-standing difficulty in right eye closure and subsequent chronic corneal irritation

4.3.1.5 Lower Cranial Nerves Palsy

The term lower cranial nerves (LCN) designates the paired glossopharyngeal, vagus, accessory and hypoglossal nerves. Motor nuclei of all these nerves are located within the medulla oblongata [21].

These nerves are responsible for the functional gag reflex, coordination of swallowing, function of vocal cords, and movement of tongue and neck muscles. Brainstem tumors involving the medulla oblongata may result in functional loss of the muscles innervated by these nerves [11].

Affected patients may have dysphagia, dysarthria, dysphonia, diminished gag reflex, hypoglossal weakness, and atrophy of the tongue. Patients may also have hiccup attacks and, rarely, palatal myoclonus [36] (Figs. 4.6, 4.7, and 4.8).

4.3.2 Pyramidal Tract Signs

Corticospinal tracts are the axons of the pyramidal cells within the cerebral cortex. Thirty percent of fibers originate from the primary motor cortex, another 30% originate from the pre-motor cortex and supplementary motor areas, and the remaining 40% originate from the somatosensory area, parietal lobe, and cingulate gyrus [37, 38]. While descending, they converge to give rise to the corona radiata, then pass through the internal capsule and crus cerebri, to finally arrive in the pons. After passing through the pons, the corticospinal tract fibers arrive in the medulla oblongata, and at the upper part of the anterior medulla oblongata, they form two swellings called the pyramids. At the junction of the medulla oblongata and the spinal cord, more than 80% of pyramidal fibers cross the midline to the contralateral side. This anatomical structure is called the decussation of pyramids. Decussated corticospinal fibers continue as the lateral corticospinal tracts on the lateral sides of the spinal cord. The remaining non-decussated fibers continue as the anterior corticospinal tracts in front of the spinal cord [20, 39].

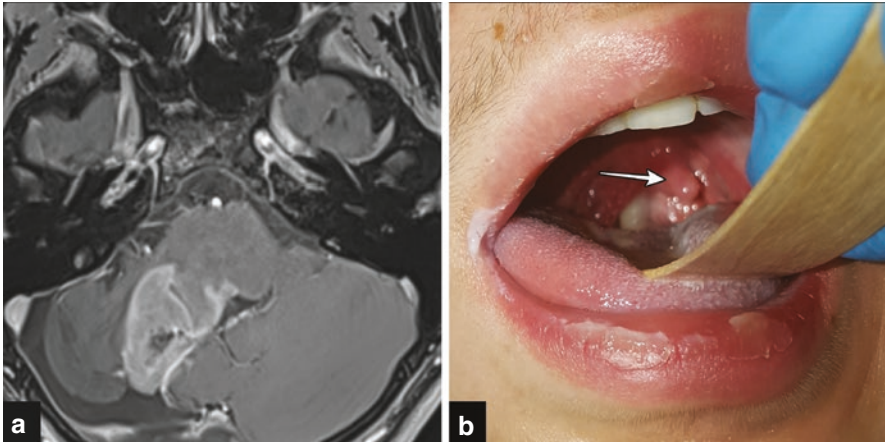


Fig. 4.6 (a) A 16-year-old boy with a histone-mutant exophytic brainstem tumor who had ataxia and difficulty in swallowing. (b) His neurological examination revealed left-sided deviation of the uvula (arrow) secondary to paralysis of the right-sided lower cranial nerves (mainly the vagus nerve)

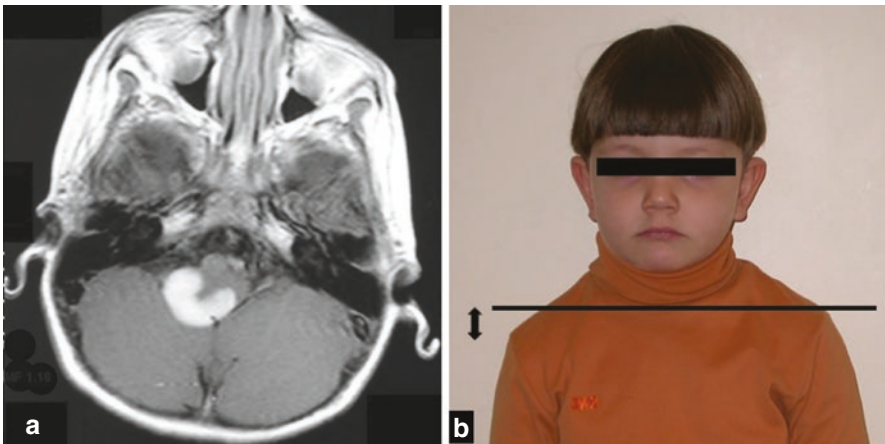


Fig. 4.7 (a) A 4-year-old boy with a right-sided brainstem tumor involving the lower cranial nerves. (b) There is a right-sided shoulder drop secondary to involvement of the right accessory nerve

Patients with brainstem tumors that disrupt the corticospinal tracts will have hyperactive reflexes, most markedly in the lower extremities. Unilateral or bilateral Babinski sign or clonus affecting lower extremities are common. Diminished superficial abdominal reflexes and positive Hoffmann's sign may be seen. These patients may experience motor paralysis in the form of hemiplegia, diplegia, or quadriplegia [11]. If hemiplegia occurs, it is generally on the contralateral side of any unilateral motor nuclear paralysis [11]. Even when motor paralysis is unilateral, there is generally



Fig. 4.8 (a) Partial paralysis of the hypoglossal nerve secondary to a medulla oblongata tumor results in deviation of the tongue to the affected side. The picture shows deviation of the tongue towards the left secondary to involvement of the left hypoglossal nerve nucleus. (b) More chronic and pronounced paralysis of the hypoglossal nerve in another patient with a medullary tumor. The picture shows overt atrophy of the tongue muscles on the left side

bilateral hyperactive deep tendon reflexes. As the disease progresses, unilateral paralysis may evolve to bilateral paralysis [8, 11]. In a patient with spastic diplegia and normal bladder function, with no level of sensory loss and with accompanying upper motor neuron and cranial nerve signs, a brainstem tumor must be ruled out [40].

4.3.3 *Truncal Ataxia*

Gait disturbance is one of the major signs among patients with brainstem tumors. This is hypothesized to occur due to disruption of the pontocerebellar tracts and infiltration of the vestibular nucleus by tumor cells [33]. Affected patients walk with a wide-based gait as well as a pelvis tilted forward and a trunk tilted backward. These patients are more prone to fall backward during walking. Extremity ataxia may be minimal [11]. These patients typically do not have hypotonia, which is one of the other cerebellar signs. Thus, the presence of truncal ataxia without hypotonia is in favor of a brainstem tumor. Nystagmus and other cerebellar signs are less commonly seen [11].

4.3.4 *Fundoscopy Changes*

This is the major sign that differentiates a brainstem glioma from the majority of other posterior fossa tumors. Papilledema is generally absent in patients with intrinsic brainstem tumors. When papilledema is found in a patient with symp-

toms of a posterior fossa tumor, the most probable diagnosis is cerebellar or fourth ventricular tumor obstructing the fourth ventricle instead of a brainstem glioma, most probably because hydrocephalus due to compression of the aqueduct and related papilledema are late signs of intrinsic brainstem tumors [2, 11]. Including diffuse midline gliomas affecting the brainstem, the overall risk of developing hydrocephalus is less than 10% in patients with intrinsic brainstem tumors [40].

4.3.5 Nystagmus

Nystagmus is the involuntary movement of eyes in any direction. When the eyes move in a sinusoidal direction like a pendulum with no fast phase, this instability of gaze is called pendular nystagmus, which is generally seen in patients with visual problems [33]. If the nystagmus is rapid and the amplitude of movements is not equal, it is called jerk nystagmus. Vestibular system abnormalities cause gaze-evoked jerk nystagmus, whereas vertical nystagmus may point to a brainstem tumor [41]. Downbeat nystagmus may be seen in patients with medullary compression around the foramen magnum. Chiari malformations, tumors of the medulla oblongata, and vascular and demyelinating diseases may cause downbeat nystagmus [33]. Upbeat nystagmus generally indicates the presence of a gray matter lesion around the pontomesencephalic and pontomedullary junctions or tumoral lesions of the vermis [42, 43]. Seesaw nystagmus is characterized by involuntary eye movements in which one eye moves up and other one moves down. In addition to the contradictory vertical movements of the eyes, there is also a rotational component [44]. This kind of nystagmus is generally seen in midline diencephalic and hypothalamic tumors. Childhood optic gliomas may also present with rotational nystagmus [33]. Periodic alternating nystagmus is a jerky nystagmus seen on horizontal gaze but periodically shifting its direction from right to left and left to right [45]; it may designate diffuse bilateral brainstem pathology [33].

4.4 Brainstem Syndromes Associated with Tumors

4.4.1 Midbrain Syndromes

Midbrain tumors may result in intranuclear ophthalmoplegia and Parinaud syndrome [33]. Intranuclear ophthalmoplegia is manifested as paralysis of the adducting eye and horizontal nystagmus that is more marked in the abducting eye during horizontal gaze. There may be additional deficits such as ptosis and paralysis of vertical gaze. Convergence, however, is preserved in both eyes. The combination of these palsies with vertical nystagmus generally points to brainstem lesions [46].

Parinaud syndrome manifests mainly as a vertical upward gaze palsy with or without a pupillary palsy. It is generally secondary to aqueductal compression due to a pineal or tectal plate tumor, which results in obstructive hydrocephalus with increased intracranial pressure. If the tumor grows into the tegmentum, an additional third and/or fourth nerve palsy may accompany this syndrome [11].

4.4.2 Pontine Syndromes

Tumoral lesions involving the pons may result in spastic paralysis of the extremities due to disruption of the corticospinal tracts, facial and abducens nerve paralysis, ataxia due to damage to pontocerebellar tracts, and conjugate eye movement defects due to damage to the MLF and pontine gaze centers [33]. The dorsolateral pontine syndrome is characterized by ipsilateral gaze palsy and contralateral hemiplegia; this syndrome points to a lesion in the tegmentum of the pons [47]. Another pontine syndrome associated with tumoral or vascular lesions of the pons is the ventral pontine syndrome; which is characterized by unilateral abducens and facial nerve palsy and contralateral hemiplegia [48].

4.4.3 Medullary Syndromes

Medullary syndromes are mainly due to decreased blood flow to the medulla, which results in medullary ischemia and infarction. Less frequently, medullary tumors and/or their post-surgical complications may also cause medullary syndromes [49]. Medial medullary (Dejerine) and lateral medullary (Wallenberg) are the most frequently encountered syndromes. There are also rare medullary syndromes such as Babinski-Nageotte syndrome (ipsilateral sensory deficit of face, Horner's syndrome, cerebellar ataxia, and contralateral hemiparesis and sensory loss), Cestan-Chenais syndrome (ipsilateral hemiasynergia and lateropulsion, paralysis of larynx and soft palate, Horner's syndrome, and contralateral hemiplegia and hemianesthesia), and Reinhold syndrome (ipsilateral palate and vocal cord paralysis, nystagmus, upper limb ataxia, and contralateral anesthesia and flaccid hemiplegia), all of which have overlapping clinical signs of both lateral and medial medullary syndromes with variable degrees [50–53].

The medial medullary (Dejerine) syndrome is manifested by ipsilateral hypoglossal nerve palsy, and contralateral hemiparesis and loss of proprioception and vibration senses. These clinical presentations are due to involvement of the corticospinal tracts and medial lemniscus above the decussation of pyramids in close proximity to the hypoglossal nerve nucleus [54–56].

The lateral medullary (Wallenberg) syndrome is mainly caused by infarction involving the posterior inferior cerebellar artery territory within the lateral medulla. Rarely, brainstem tumors or their post-surgical complications may also mimic signs

and symptoms of the lateral medullary syndrome. Patients suffer from vertigo, nystagmus, nausea and vomiting due to inferior vestibular nucleus involvement; difficulty in swallowing, hoarseness and ipsilateral loss of gag reflex due to involvement of ninth and tenth cranial nerves; Horner syndrome due to involvement of sympathetic fibers; ataxia due to involvement of inferior cerebellar peduncle, spinocerebellar fibers and inferior part of cerebellum; ipsilateral loss of pain and temperature sensations in the face due to involvement of ipsilateral descending trigeminal tract; and contralateral loss of pain and temperature sensations in extremities due to ipsilateral spinothalamic tract involvement [57–59].

4.5 Conclusion

Brainstem tumors are quite concerning in terms of their anatomical locations and growth patterns, and are usually associated with distinctive clinical presentations and physical examination findings. The patient's clinical history and neurological examination can give some clues about the growth pattern of the tumor. If the patient's symptoms started recently, and the neurological examination reveals involvement of multiple cranial nerve nuclei, one must suspect a diffuse pathology. On the other hand, symptoms with insidious onset and single cranial nerve involvement point to focal brainstem tumors. After obtaining a thorough neurological examination, physicians generally have an idea about the tumor location according to the involved cranial nerves, with or without concomitant neurological syndromes. During neurological examination, trochlear nerve involvement with a Parinaud syndrome points to mesencephalic lesions, abducent and/or facial nerve involvement with MLF syndrome designates pontine lesions, whereas LCN involvement with signs of lateral medullary syndrome designates tumors of the medulla oblongata. Thorough medical history with detailed neurological examination is the cornerstone of the diagnostic approach for brainstem tumors.

References

1. Walker DA, Punt JA, Sokal M. Clinical management of brain stem glioma. *Arch Dis Child*. 1999;80(6):558–64.
2. Recinos PF, Sciubba DM, Jallo GI. Brainstem tumors: where are we today? *Pediatr Neurosurg*. 2007;43(3):192–201.
3. Berger MS, Edwards MS, LaMasters D, Davis RL, Wilson CB. Pediatric brain stem tumors: radiographic, pathological, and clinical correlations. *Neurosurgery*. 1983;12(3):298–302.
4. Epstein F. A staging system for brain stem gliomas. *Cancer*. 1985;56(7 Suppl):1804–6.
5. Choux M, Lena G, Do L. Brainstem tumors. In: Choux M, Di Rocco C, Hockley A, editors. *Pediatric neurosurgery*. New York: Churchill Livingstone; 2000. p. 471–91.
6. Mauffrey C. Paediatric brainstem gliomas: prognostic factors and management. *J Clin Neurosci*. 2006;13(4):431–7.

7. Albright AL, Guthkelch AN, Packer RJ, Price RA, Rourke LB. Prognostic factors in pediatric brain-stem gliomas. *J Neurosurg.* 1986;65(6):751–5.
8. Epstein F, Wisoff JH. Intrinsic brainstem tumors in childhood: surgical indications. *J Neuro-Oncol.* 1988;6(4):309–17.
9. Rosenthal MA, Ashley DM, Drummond KJ, Dally M, Murphy M, Cher L, et al. Brain stem gliomas: patterns of care in Victoria from 1998–2000. *J Clin Neurosci.* 2008;15(3):237–40.
10. Barkovich AJ, Krischer J, Kun LE, Packer R, Zimmerman RA, Freeman CR, et al. Brain stem gliomas: a classification system based on magnetic resonance imaging. *Pediatr Neurosurg.* 1990;16(2):73–83.
11. Needham CW. Posterior Fossa syndromes. *Neurological syndromes of the brain.* Illinois: Charles C Thomas; 1973. p. 276–346.
12. Selvapandian S, Rajshekhar V, Chandy MJ. Brainstem glioma: comparative study of clinico-radiological presentation, pathology and outcome in children and adults. *Acta Neurochir.* 1999;141(7):721–6; discussion 6–7.
13. Brazis PW. Palsies of the trochlear nerve: diagnosis and localization—recent concepts. *Mayo Clin Proc.* 1993;68(5):501–9.
14. Gentry LR, Mehta RC, Appen RE, Weinstein JM. MR imaging of primary trochlear nerve neoplasms. *AJNR Am J Neuroradiol.* 1991;12(4):707–13.
15. Keane JR. Fourth nerve palsy: historical review and study of 215 inpatients. *Neurology.* 1993;43(12):2439–43.
16. Buttner-Ennever JA, Horn AK, Graf W, Ugolini G. Modern concepts of brainstem anatomy: from extraocular motoneurons to proprioceptive pathways. *Ann N Y Acad Sci.* 2002; 956:75–84.
17. Richards BW, Jones FR Jr, Younge BR. Causes and prognosis in 4,278 cases of paralysis of the oculomotor, trochlear, and abducens cranial nerves. *Am J Ophthalmol.* 1992;113(5):489–96.
18. Menetrey D, Basbaum AI. Spinal and trigeminal projections to the nucleus of the solitary tract: a possible substrate for somatovisceral and viscerovisceral reflex activation. *J Comp Neurol.* 1987;255(3):439–50.
19. Bathla G, Hegde AN. The trigeminal nerve: an illustrated review of its imaging anatomy and pathology. *Clin Radiol.* 2013;68(2):203–13.
20. Snell RS. The brainstem. In: Snell RS, editor. *Clinical neuroanatomy.* 7th ed. Baltimore: Lippincott Williams & Wilkins; 2007. p. 186–229.
21. Naidich TP, Duvernoy HM, Delman BN, Sorensen AG, Kollias SS, Haacke EM. Internal architecture of the brain stem with key axial section. *Duvernoy’s atlas of the human brain stem and cerebellum.* Wien: Springer; 2009. p. 53–93.
22. Darian-Smith I, Phillips G, Ryan RD. Functional organization in the trigeminal main sensory and rostral spinal nuclei of the cat. *J Physiol.* 1963;168:129–46.
23. Joo W, Yoshioka F, Funaki T, Mizokami K, Rhoton AL Jr. Microsurgical anatomy of the trigeminal nerve. *Clin Anat.* 2014;27(1):61–88.
24. Nieuwenhuys R, Voogd J, Huijzen CV. *Brain slices. The human central nervous system.* Heidelberg: Steinkopff-Verlag; 2008. p. 137–73.
25. Cavalheiro S, Yagmurlu K, da Costa MD, Nicacio JM, Rodrigues TP, Chaddad-Neto F, et al. Surgical approaches for brainstem tumors in pediatric patients. *Childs Nerv Syst.* 2015;31(10):1815–40.
26. Kruger L, Siminoff R, Witkovsky P. Single neuron analysis of dorsal column nuclei and spinal nucleus of trigeminal in cat. *J Neurophysiol.* 1961;24:333–49.
27. Jerge CR. The function of the nucleus supratrigeminalis. *J Neurophysiol.* 1963;26(3):393–402.
28. Morota N, Deletis V, Epstein FJ, Kofler M, Abbott R, Lee M, et al. Brain stem mapping: neurophysiological localization of motor nuclei on the floor of the fourth ventricle. *Neurosurgery.* 1995;37(5):922–9; discussion 9–30.
29. Frohman TC, Galetta S, Fox R, Solomon D, Straumann D, Filippi M, et al. Pearls & Oy-sters: the medial longitudinal fasciculus in ocular motor physiology. *Neurology.* 2008;70(17):e57–67.

30. King WM, Lisberger SG, Fuchs AF. Responses of fibers in medial longitudinal fasciculus (MLF) of alert monkeys during horizontal and vertical conjugate eye movements evoked by vestibular or visual stimuli. *J Neurophysiol.* 1976;39(6):1135–49.
31. Strauss C, Romstock J, Nimsky C, Fahlbusch R. Intraoperative identification of motor areas of the rhomboid fossa using direct stimulation. *J Neurosurg.* 1993;79(3):393–9.
32. Kyoshima K, Sakai K, Goto T, Tanabe A, Sato A, Nagashima H, et al. Gross total surgical removal of malignant glioma from the medulla oblongata: report of two adult cases with reference to surgical anatomy. *J Clin Neurosci.* 2004;11(1):75–80.
33. Işık U. Clinical Presentation ÖMM. Neusologic evaluation in posterior Fossa tumors in children. In: Özek MM, Cinalli G, Maixner W, Sainte-Rose C, editors. *Posterior Fossa tumors in children.* Switzerland: Springer; 2015. p. 119–27.
34. Spetzler RF, M. Yashar S, Kalani, Nakaji P, Yagmurlu K. Anatomy. In: Spetzler RF, M. Yashar S, Kalani, Nakaji P, Yagmurlu K, editors. *Color atlas of brainstem surgery.* New York: Thieme Medical Publisher; 2017. p. 50–1.
35. Masterson L, Vallis M, Quinlivan R, Prinsley P. Assessment and management of facial nerve palsy. *BMJ.* 2015;351:h3725.
36. Finsterer J, Grisold W. Disorders of the lower cranial nerves. *J Neurosci Rural Pract.* 2015;6(3):377–91.
37. Rathelot JA, Dum RP, Strick PL. Posterior parietal cortex contains a command apparatus for hand movements. *Proc Natl Acad Sci U S A.* 2017;114(16):4255–60.
38. Welniarz Q, Dusart I, Roze E. The corticospinal tract: evolution, development, and human disorders. *Dev Neurobiol.* 2017;77(7):810–29.
39. Ugawa Y, Rothwell JC, Day BL, Thompson PD, Marsden CD. Percutaneous electrical stimulation of corticospinal pathways at the level of the pyramidal decussation in humans. *Ann Neurol.* 1991;29(4):418–27.
40. Freeman CR, Farmer JP. Pediatric brain stem gliomas: a review. *Int J Radiat Oncol Biol Phys.* 1998;40(2):265–71.
41. Rett D. Gaze-evoked nystagmus: a case report and literature review. *Optometry.* 2007;78(9):460–4.
42. Gilman N, Baloh RW, Tomiyasu U. Primary position upbeat nystagmus. A clinicopathologic study. *Neurology.* 1977;27(3):294–8.
43. Fisher A, Gresty M, Chambers B, Rudge P. Primary position upbeat nystagmus. A variety of central positional nystagmus. *Brain.* 1983;106(Pt 4):949–64.
44. Druckman R, Ellis P, Kleinfeld J, Waldman M. Seesaw nystagmus. *Arch Ophthalmol.* 1966;76(5):668–75.
45. Togliola JU. Periodic alternating nystagmus. *Arch Otolaryngol.* 1968;88(2):148–51.
46. Stroud MH, Newman NM, Keltner JL, Gay AJ. Abducting nystagmus in the medial longitudinal fasciculus (MLF) syndrome (internuclear ophthalmoplegia (INO)). *Adv Otorhinolaryngol.* 1973;19:367–76.
47. Silverman IE, Liu GT, Volpe NJ, Galetta SL. The crossed paralyses. The original brainstem syndromes of Millard-Gubler, Foville, Weber, and Raymond-Cestan. *Arch Neurol.* 1995;52(6):635–8.
48. Krasnianski M, Neudecker S, Zierz S. Classical crossed pontine syndromes. *Fortschr Neurol Psychiatr.* 2004;72(8):460–8.
49. Hanyu H, Yoneda Y, Katsunuma H, Miki T, Miwa T. Wallenberg’s syndrome caused by a brain tumor—a case report and literature review. *Rinsho Shinkeigaku.* 1990;30(3):324–6.
50. Balucani C, Barlinn K. Medullary infarcts and hemorrhages. *Front Neurol Neurosci.* 2012;30:166–70.
51. Fukuoka T, Takeda H, Dembo T, Nagoya H, Kato Y, Deguchi I, et al. Clinical review of 37 patients with medullary infarction. *J Stroke Cerebrovasc Dis.* 2012;21(7):594–9.
52. Krasnianski M, Neudecker S, Schluter A, Zierz S. Babinski-Nageotte’s syndrome and Hemimedullary (Reinhold’s) syndrome are clinically and morphologically distinct conditions. *J Neurol.* 2003;250(8):938–42.

53. Krasnianski M, Muller T, Stock K, Zierz S. Between Wallenberg syndrome and hemimedullary lesion: Cestan-Chenais and Babinski-Nageotte syndromes in medullary infarctions. *J Neurol*. 2006;253(11):1442–6.
54. Caplan LR, Zarins CK, Hemmati M. Spontaneous dissection of the extracranial vertebral arteries. *Stroke*. 1985;16(6):1030–8.
55. Mizutani T, Lewis RA, Gonatas NK. Medial medullary syndrome in a drug abuser. *Arch Neurol*. 1980;37(7):425–8.
56. Gan R, Noronha A. The medullary vascular syndromes revisited. *J Neurol*. 1995;242(4):195–202.
57. Ferbert A, Bruckmann H, Drummen R. Clinical features of proven basilar artery occlusion. *Stroke*. 1990;21(8):1135–42.
58. Schneider JI, Olshaker JS. Vertigo, vertebrobasilar disease, and posterior circulation ischemic stroke. *Emerg Med Clin North Am*. 2012;30(3):681–93.
59. Hosoya T, Watanabe N, Yamaguchi K, Kubota H, Onodera Y. Intracranial vertebral artery dissection in Wallenberg syndrome. *AJNR Am J Neuroradiol*. 1994;15(6):1161–5.

Chapter 5

Intraoperative Neurophysiological Monitoring During Brainstem Surgery



Francesco Sala and Alberto D'Amico

Abbreviations

APB	Abductor pollicis brevis
BAEPs	Brainstem auditory evoked potentials
CMAP	Compound muscle action potential
CSF	Cerebrospinal fluid
CSTs	Corticospinal tracts
DTI	Diffusor tensor imaging
EMG	Electromyography
ION	Intraoperative neurophysiology
MEPs	Motor evoked potentials
mMEP	Muscle motor evoked potential
SSEPs	Somatosensory evoked potentials
TA	Tibialis anterior
TES	Transcranial electrical stimulation

5.1 Introduction

Brainstem surgery is still considered among the most challenging neurosurgical procedures due to the significant risk of neurological morbidity. The high concentration of essential neural structures such as cranial nerve nuclei, sensorimotor and auditory pathways, as well as the reticular formation makes the brainstem a real minefield. Therefore, even a small injury to the brainstem can hinder the functional integrity of one or more of these neural pathways and result in neurological deficits. In fact, brainstem surgical morbidity is significantly higher than that of other areas of the central nervous system due to the lack of structural redundancy and plasticity.

F. Sala (✉) · A. D'Amico
Section of Neurosurgery, Department of Neurosciences, Biomedicine and Movement Sciences, University Hospital, Verona, Italy
e-mail: francesco.sala@univr.it

Aggressive surgical treatment of tumors in the medulla oblongata increases the risk of compromising the respiratory function and threatens the patient's ability to swallow or protect the airways; this may ultimately result in the need for gastrostomy and tracheostomy. An overall risk of 15% of permanent lower cranial nerve injury has been reported in children who underwent surgery for medullary tumors [1]. Rostrally, surgery in the pons and midbrain can result in diplopia – due to internuclear ophthalmoplegia – as well as sixth and seventh nerve palsy [2–4].

During the 90s, a number of authors discussed the functional anatomy of the brainstem, particularly with regards to the floor of the fourth ventricle, as most of the surgical approaches were through this posterior route. If the tumor is exophytic outside the brainstem surface, its removal begins at such outgrowth. In these cases, the tumor itself creates the entry path into the brainstem. However, when the tumor is truly intrinsic, i.e., lacking a surface component, a deep knowledge of the underlying local functional anatomy is required.

On the basis of a detailed map of the most dangerous surgical approaches to the brainstem, some relatively safe entry zones – mainly to the posterior brainstem – have been identified based on anatomical landmarks [5–7]. However, these landmarks turned out to often be unreliable due to the distortion of normal anatomy secondary to the tumor mass effect. For example, when approaching pontine tumors, the facial colliculus and/or striae medullaris were rarely recognizable at the beginning of the surgery and could not assist the surgeon in selecting the best entry zone [8].

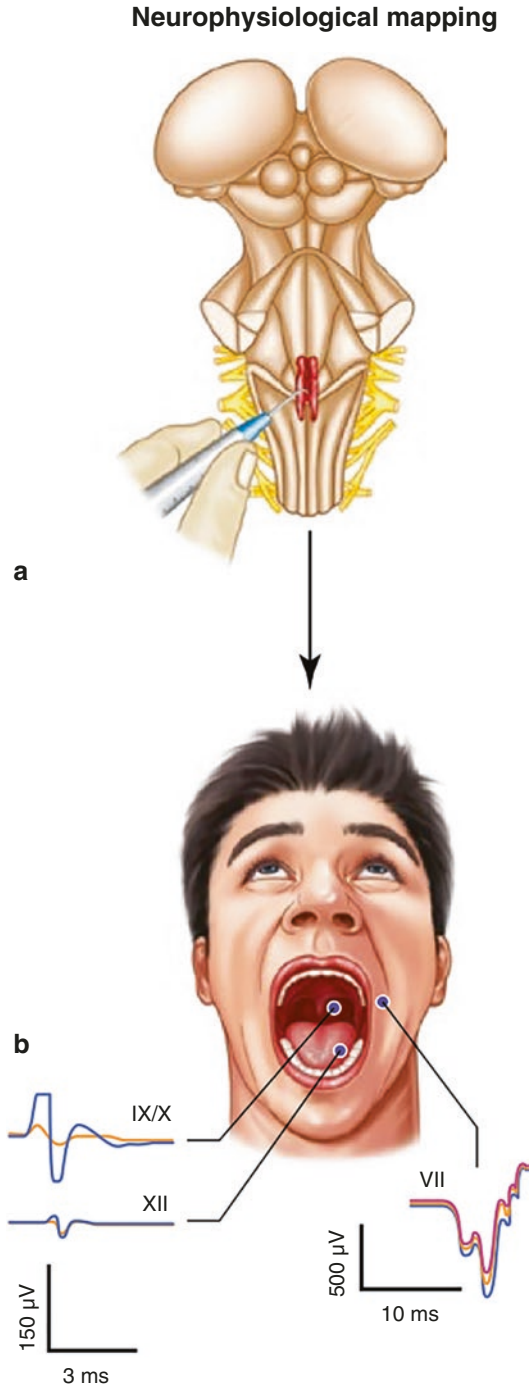
Injury to brainstem neural structures can occur either during the attempt to approach an intrinsic lesion by selecting the wrong entry zone and/or during the removal of the lesion due to excessive manipulation of the brainstem, including traction, misplacement of retractors, and inadvertent coagulation of perforating vessels.

Intraoperative neurophysiology (ION) has emerged over the past two decades as a discipline aimed not merely to predict but also to prevent neurological injury, thanks to the tailored intraoperative use of standard clinical neurophysiological techniques such as electromyography (EMG), and somatosensory (SSEPs), brainstem auditory (BAEPs) and motor evoked potentials (MEPs). Monitoring these potentials allows to prevent an injury to the long pathways within the brainstem. In addition, the so-called mapping techniques provide a functional identification of critical anatomical landmarks – such as the facial colliculus, the cerebral peduncle or the lower motor cranial nerve nuclei – to avoid an injury to these structures when selecting the safest entry route to the brainstem [8–10] (Figs. 5.1 and 5.2).

Since the mid-90s, a number of ION monitoring and mapping techniques have been developed to assist neurosurgeons during brainstem surgery. Some of these techniques are nowadays considered standard and have well passed the test of time. Others are less popular and/or are considered less reliable because of the risk of false positive and false negative results.

In this chapter we will critically review, for each anatomical location – midbrain, pons, and medulla oblongata, the various ION mapping and monitoring techniques that can be used during surgery for brainstem lesions.

Fig. 5.1 Schematic classification of intraoperative neurophysiology mapping techniques in the posterior fossa. These techniques allow for the identification of functional landmarks such as the nuclei of motor cranial nerves on the floor of the fourth ventricle. **(a)** A handheld monopolar (or bipolar concentric) probe is used to electrically stimulate the rhomboid fossa. **(b)** Compound muscle action potentials (CMAPs) are recorded from the muscles innervated by motor cranial nerves (see text for details). VII: CMAP recorded from the orbicularis oris for the facial nerve. IX/X: CMAP recorded from the posterior wall of the pharynx for the glossopharyngeal/vagus complex. XII: CMAP recorded from the tongue muscles for the hypoglossal nerve. (Reprinted with permission from Sala et al. [56])



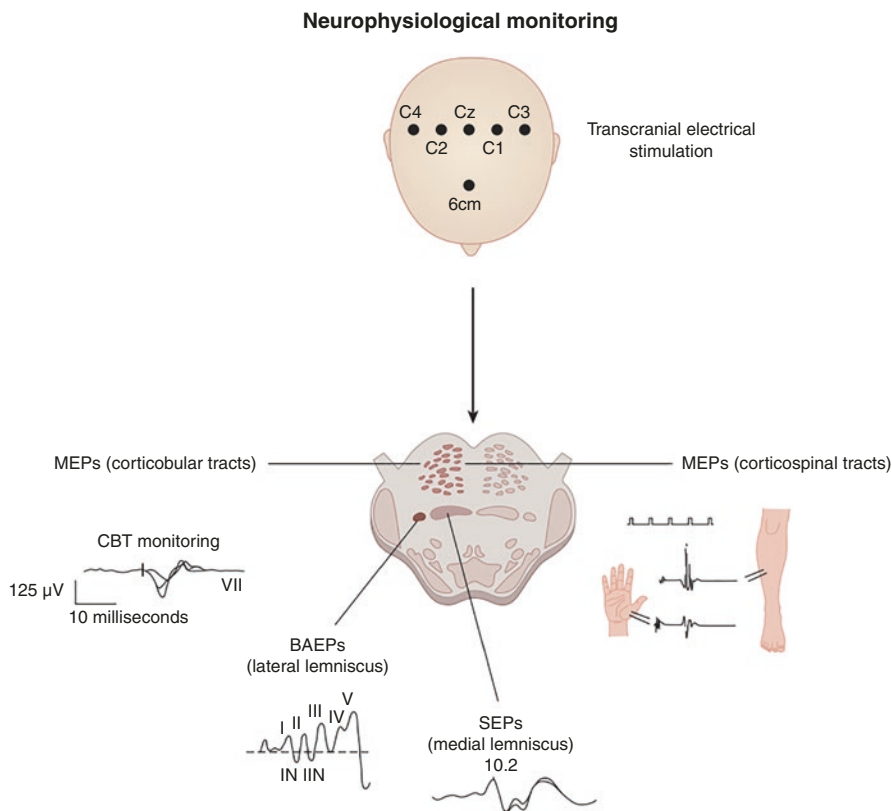


Fig. 5.2 Schematic classification of neurophysiological monitoring techniques. These allow to monitor the functional integrity of neural pathways (motor, sensory, auditory) within the brain-stem on-line, throughout the surgery. See the text for further details on each monitoring technique. Abbreviations: MEPs, motor evoked potentials; SEPs, somatosensory evoked potentials; BAEPs, brainstem auditory evoked responses; CBT, corticobulbar tract. (Modified with permission from Sala et al. [56])

5.2 Surgery of the Midbrain

5.2.1 Mapping

5.2.1.1 Identification of the Oculomotor Nerve Nuclei at the Level of the Tectal Plate

The midbrain occupies the notch of the tentorium and consists of a dorsal part (i.e., tectal plate), a large ventral portion (i.e., tegmentum), and the cerebral peduncles. Dorsal approaches, through either the supracerebellar infratentorial route or the occipital transtentorial route, can be used to approach intrinsic mid-brain lesions.

Avoiding injury to the oculomotor nerve nuclei and their intramedullary tracts is important to avoid oculomotor deficits, such as Parinaud syndrome, which can compromise the quality of life of the patients. Midbrain tumors are quite common in the pediatric age group; while most of these lesions may have an indolent course with little tendency to grow and no surgical indication, surgery is indicated for growing lesions.

Direct neurophysiological mapping of the tectal plate can be used to identify safe entry zones to approach intrinsic midbrain lesions. Vice versa, the need for intraoperative mapping of peripheral oculomotor nerves is anecdotal in brainstem surgery, but it may be used for tumors involving the cisternal, cavernous or intraorbital segment of these nerves.

For direct identification of the peripheral cranial nerves III, IV, and VI, either a handheld monopolar probe or a bipolar concentric probe can be used. Rectangular pulses of 0.2 ms duration at 1–3 Hz and intensity up to 0.5–3 mA can be used. In general, the advantage of using a bipolar concentric probe is the higher focality of the stimulation and limited spreading of the current. For direct stimulation of the brainstem, the current is usually kept very low, starting at 0.05 mA and not exceeding 1–1.5 mA.

Recordings are obtained by placing tiny wire Teflon-coated electrodes in muscles innervated by the respective cranial nerves. Typically, responses are recorded from the external (lateral) rectus for cranial nerve VI, superior rectus for cranial nerve III, and superior oblique for cranial nerve IV. When placing the recording electrodes in extrinsic ocular muscles, care should be taken to avoid misplacement of the electrodes, which may cause an injury to the ocular bulb.

Muscle responses from extraocular muscles are usually of low amplitude because the muscle units have a small number of fibers innervated by a single axon. The latency of the response depends on the point of stimulation along the peripheral nerve or within the midbrain, ranging anywhere between 2 and 5 ms [11, 12].

We have repeatedly attempted direct identification of the superior colliculi through brain mapping. However, this has been mostly unsuccessful. One of the reasons could be related to the fact that the superficial layers of the colliculus connect to the visual system by projection to the thalamus and the lateral geniculate nuclei. Additionally, the nuclei of the oculomotor nerves are embedded in the periaqueductal grey matter, too deep to be activated by superficial stimulation (Fig. 5.3). Although reports on direct stimulation of the colliculi are anecdotal [12–14], similar limitations have been reported by Ishihara et al., who found that direct mapping is of little help to decide on the site of the incision [14].

5.2.1.2 Identification of the Corticospinal Tract at the Level of the Cerebral Peduncle

When dealing with lesions close to the cerebral peduncle or the ventral part of the medulla, injury to the corticospinal tracts (CSTs) is of concern. Mapping of the CST at the level of the cerebral peduncle is valuable to prevent injury.

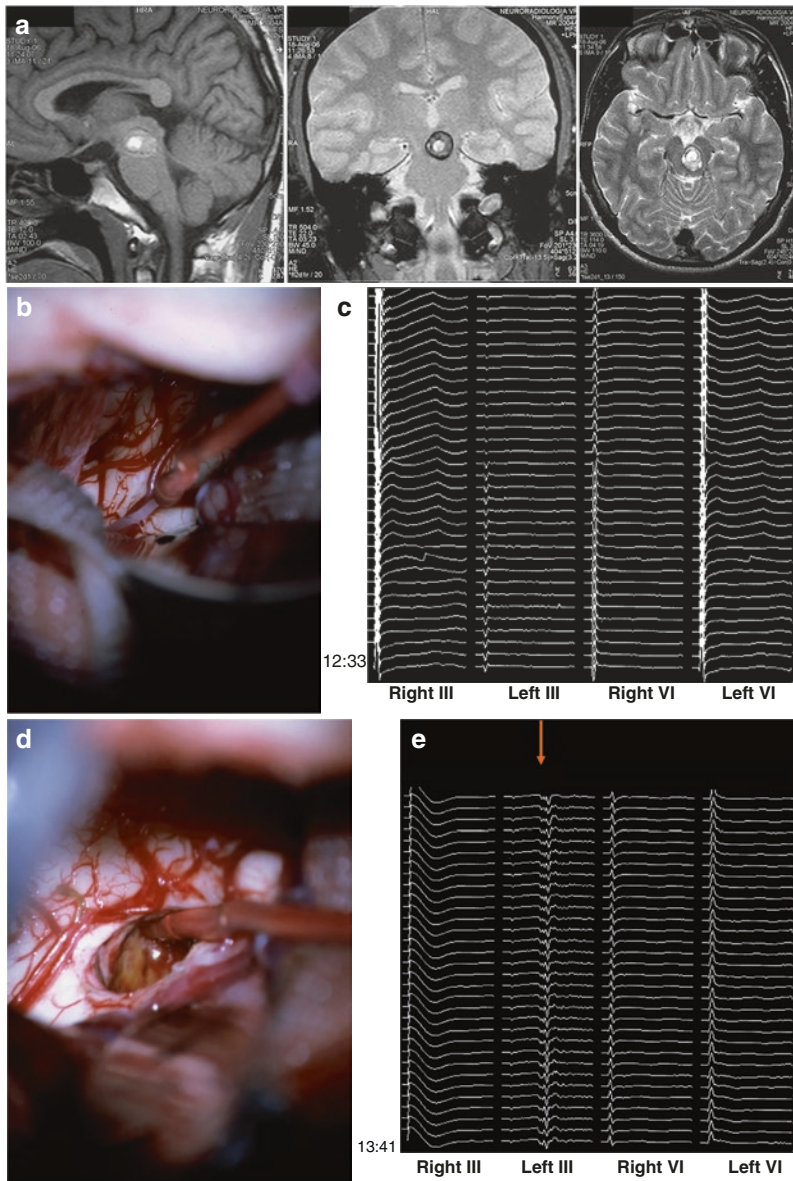


Fig. 5.3 Identification of the oculomotor nerve nuclei at the level of the tectal plate. (a) Sagittal (left), coronal (middle), and axial (right) magnetic resonance images of a left paramedian midbrain cavernoma. (b) Upon exposure of the superior colliculi, initial (time 12:33) direct stimulation of the left colliculus does not elicit any response from the oculomotor muscles innervated by the III and VI cranial nerves (c). (d) Later on (time 13:41), stimulation from inside the surgical cavity, during removal of the cavernoma, elicits a consistent response (red arrow) from the left upper rectus muscles (Left III), indicating stimulation of the nearby nuclei (e). Abbreviations: Right III, right upper rectus muscle; Left III, left upper rectus muscle; Right VI, right lateral rectus muscle; Left VI, left lateral rectus muscle. (Modified with permission from Sala et al. [36])

Nowadays, diffusor tensor imaging (DTI) plays an important role in the pre-surgical planning of surgery for brain gliomas to determine subcortical functional boundaries. The role of DTI in brainstem and spinal cord tumor surgery is more controversial; only few studies have specifically addressed the role of DTI in brainstem surgery [15, 16], but it is expected that DTI may guide neurophysiological mapping techniques, which remain the gold standard to localize the CST intraoperatively.

To identify the CST, we used for many years a handheld monopolar stimulator (tip diameter 0.75 mm) as cathode, with a needle electrode inserted in nearby muscles as anode (Fig. 5.4). More recently, we have switched to the use of a bipolar concentric electrode. The response is recorded as a compound muscle action potential (CMAP) from the contralateral limb, following a train of five stimuli of 0.5 ms duration at 1–2 Hz. Stimulation intensity is progressively increased up to 2 mA, starting from 0.5 mA, until a motor response is recorded. At this point, the probe is

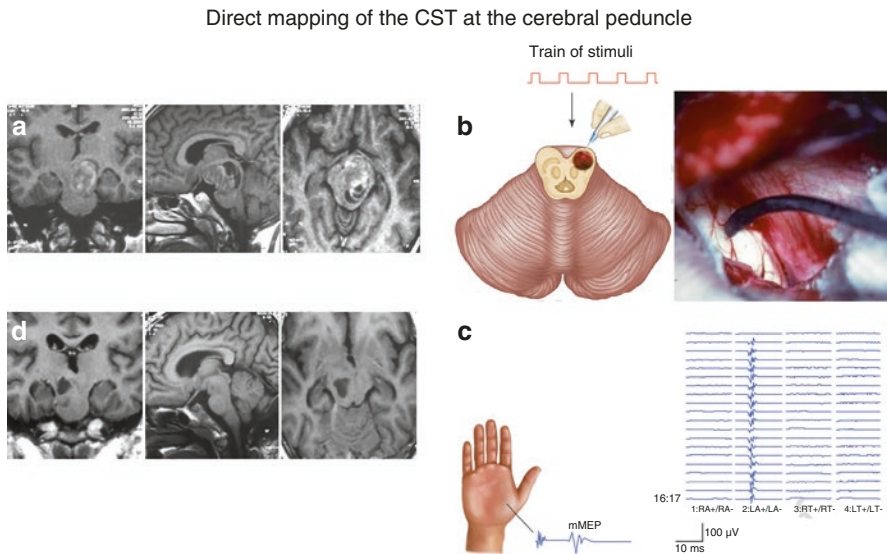


Fig. 5.4 Identification of the corticospinal tract at the level of the cerebral peduncle. (a) Enhanced T1-weighted images of a pilocytic astrocytoma of the left cerebral peduncle; coronal (left), sagittal (middle), and axial (right) view. (b) Schematic illustration of direct stimulation of the corticospinal tract at the level of the cerebral peduncle using a monopolar handheld probe (reference needle in the paraspinal muscles) with a short train of stimuli (each stimulus has a 0.5 ms duration) at 1 Hz and current up to 2 mA (left panel). Intraoperative view of stimulation of the left cerebral peduncle in the patient depicted in (a). The tumor was approached through a left lateral supracerebellar infratentorial route (right panel). (c) Muscle motor evoked potential (mMEP) recorded from the left abductor pollicis brevis (LA), while no responses were recorded in the left tibialis anterior muscle (LT) and right-sided muscles (RA and RT). (d) The tumor was then removed by entering the lateral midbrain posterior to the zone where the motor response was elicited. Postoperative gadolinium-enhanced T1-weighted images documented complete removal of the lesion. The patient presented with no additional motor deficits. (Modified with permission from Sala et al. [36])

moved in small increments of 1 mm in order to find the lowest threshold to elicit that response. The lowest threshold corresponds to the closest point to the CST. In the case of a cystic lesion, mapping is sometimes negative at the beginning of the procedure, but CMAPs can be recorded during mapping from within the cystic cavity towards the CST.

In principle, mapping of the CST along the brainstem is equivalent to subcortical CST mapping during brain tumor surgery. The technique is straightforward and well established. In supratentorial surgery, it is assumed that a roughly linear correlation exists between the threshold intensity in mA – to elicit a CMAP – and the distance from the CST in mm [17, 18]. This has not been investigated at the level of the brainstem, but one may expect a similar correlation.

5.2.2 *Monitoring*

5.2.2.1 **Monitoring of Motor Evoked Potentials**

Muscle motor evoked potential (mMEP) monitoring is a standard technique to assess the functional integrity of the CST.

During brainstem surgery, mMEP monitoring is likely more relevant for lesions involving or adjacent to the cerebral peduncle as well as during surgery in the medulla oblongata. Pontine tumors are mainly approached through the floor of the fourth ventricle, whereas the CSTs run ventrally, thus an injury to these pathways is quite unlikely.

To elicit mMEPs, the primary motor cortex is activated by a short train of stimuli delivered through transcranial electrical stimulation (TES). The short train of stimuli overcomes the blocking effects of anesthetic agents at the level of the alpha motoneuron and allows to record a muscle response [19–21]. TES is performed using scalp corkscrew-like electrodes placed at C1-C2 scalp sites for the upper extremities, while a Cz-C6 cm montage is usually preferred for the lower extremities, where Cz is placed at 1 cm behind the typical Cz point (see Fig. 5.2). A stimulus duration of 0.5 ms and an interstimulus interval of 4 ms is applied, at a repetition rate of 1–2 Hz. TES is usually safe [22], although a tongue bite block should always be inserted to avoid tongue injury by strong jaw muscle twitches that may occur during high intensity stimulation.

Muscle responses are recorded via pairs of needle electrodes inserted into the upper and lower extremity muscles. We usually monitor the abductor pollicis brevis (APB) for the upper extremity and the tibialis anterior (TA) or the abductor hallucis for the lower extremity. Since the CST fibers are concentrated in a very small ventral area in the brainstem, a selective injury to either upper extremity or lower extremity CST fibers is very unlikely to occur and, per se, monitoring the APB may suffice.

Warning criteria for mMEP monitoring during brainstem surgery are not well defined. Neuloh et al. [23] observed that stable or only transiently deteriorated MEPs warranted unchanged motor outcomes, while both irreversible deterioration

(namely, >50% drop in the amplitude) or a reversible loss were predictive of transient motor deficits in 37% of the cases; irreversible MEP loss was predictive of long-term, severe paresis. They concluded that, in comparison to supratentorial surgery, new deficits in brainstem surgery could occur only after more pronounced mMEP changes, but the “all or none” criterion – commonly used in spinal cord tumor surgery – was too little sensitive, potentially leading to false negative results.

Kodama et al. reported that SSEP and/or MEP decrements were observed during brainstem surgery at higher rates (47.5%) than in any other location within the posterior fossa [24]. In the same study, more than 50% of patients with SSEP and/or MEP decline during surgery had a hemiparesis at the time of hospital discharge, suggesting that MEP changes are indicative of at least short-term motor deficit.

In a surgical series focusing only on brainstem cavernomas, Shibani et al. observed an MEP sensitivity and specificity of 33% and 88%, respectively [25]. In general, low specificity may increase the risk of unjustified termination of surgery, potentially leading to incomplete tumor removal. Another observation by these authors was the fact that most of the MEP changes were rapid rather than progressive, with limited chances to alert the surgeon in time to take corrective measures. Overall, acute MEP deterioration is quite unusual and, when it occurs, is mainly due to a vascular injury that is related to arterial perforators during brainstem surgery. However, the main limitation of this study was the fact that because of MEP changes that occurred during non-critical stages of the operation, the surgeons never terminated the surgery prematurely despite ION alerts. Therefore, ION did not influence the surgical course.

In conclusion, during mMEP monitoring in brainstem surgery, the same limitations of MEP monitoring in supratentorial surgery apply, and quantitative warning criteria based on amplitude drop or increased threshold are still not ideal. Yet, in most studies, preservation of mMEPs remains a reliable predictor of good motor outcome.

5.2.2.2 Monitoring of Brainstem Auditory Evoked Potentials

Brainstem auditory evoked potentials (BAEPs) represent responses of the auditory nerve, the brainstem, and probably higher subcortical structures to acoustic stimuli. BAEPs are represented by seven different waves with different latencies [26] (Fig. 5.5).

The first wave (I) is the first negative near-field potential recorded near the ipsilateral stimulated ear and arises from the distal auditory nerve action potentials. The second wave (II) probably originates from both the proximal portion of the auditory nerve and the presynaptic activity of the auditory nerve ending at the cochlear nucleus. Wave III is thought to originate in the lower pons, at the level of the superior olivary complex. It is important to point out that ascending projections from the cochlear nucleus are bilateral, so wave III may receive contributions from brainstem auditory structures both ipsilateral and contralateral to the stimulated ear. The fourth and fifth waves usually join to form an IV-V complex, with anatomical generators

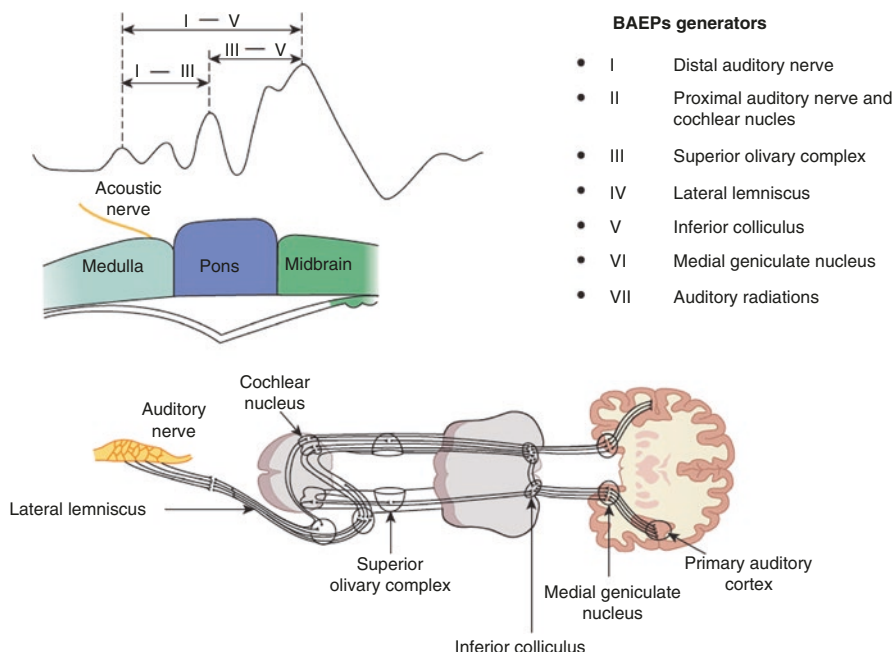


Fig. 5.5 Schematic illustration of brainstem auditory evoked potentials (BAEPs). Waves I to V and their generators are indicated (see text for details). (Republished with permission of McGraw-Hill Education, from *Intraoperative Neuromonitoring*, Christopher M. Loftus, José Biller, Eli M. Baron, 1st ed., 2014; permission conveyed through Copyright Clearance Center, Inc.)

that are in close proximity. Wave IV is thought to be generated in the high pons or lower midbrain at the level of the lateral lemniscus, and wave V is generated at the level of the inferior colliculus. During brainstem surgery, these two waves are commonly together either affected or unaffected, with some exceptions. Finally, waves VI and VII are supposed to arise at the level of the medial geniculate nucleus and auditory radiations, respectively, but these two waves are highly variable and not used in clinical practice.

BAEPs are elicited by transient acoustic 90–100 dB click stimuli (trains of 100-microsecond duration, electrical square pulses) delivered to the involved ear. White noise masking at 60–70 dB is simultaneously delivered to the contralateral ear. Alternating click polarities are often utilized during intraoperative BAEPs monitoring to minimize stimulus artefacts. Recording of BAEPs is performed with cork-screw/monopolar electrodes positioned at Cz (according to 10–20 International System) and monopolar needle at the earlobes (A1-generally left/A2-generally right, or Ai-ipsilateral/Ac-contralateral) or the mastoid process (Mi-ipsilateral/Mc-contralateral).

The recommended system bandpass for BAEPs is 100–150 Hz to 3000 Hz; BAEPs usually require 1000 or more acquisitions, with an adequate signal-to-noise ratio.

Standard criteria to interpret BAEP changes are based on amplitude and/or latency changes of waves I, III, and V. Changes in amplitude are more common than changes in latency. A 50% decrease in the amplitude and/or a 1-millisecond prolongation in the absolute latency of wave V or the I-V interpeak interval are considered warning criteria. A more sensitive criterion for changes in latency is a delay of more than 10% of the baseline peak V latency [27].

A number of surgical maneuvers can induce dysfunction or injury to the auditory pathways during posterior fossa surgery, including vascular derangements at the level of the cochlea, the auditory nerve, or the brainstem. Within the brainstem, the use of ultrasonic aspiration can also induce mechanical injury to the auditory pathways. An abrupt drop in the BAEP amplitude is more indicative of a vascular injury, but the majority of BAEP changes occur in a stepwise, reversible fashion. Therefore, if feedback to the neurosurgeon is promptly provided, there is enough time to take corrective measures and reverse an impending injury to the brainstem.

Some BAEP changes are more indicative of brainstem injury and retain some localizing value within the brainstem. For example, damage to the lower pons – near the area of the cochlear nucleus or the superior olivary complex – will induce a wave III and V delay or loss. Damage to the brainstem rostral to the lower pons, but below the level of the mesencephalon will affect wave V, but not waves I or III. Loss of wave V is not necessarily predictive of hearing loss, as it may just reflect temporal dispersion without a true, irreversible conduction block.

On the other hand, it should be pointed out that BAEPs assess only a very restricted area of the brainstem. At the level of the pons, likely no more than 20% of the brainstem area is covered by simultaneous SSEP and BAEP monitoring, suggesting that significant brainstem injury could occur in the absence of BAEP changes [28].

In our experience, while BAEP monitoring can offer an overview on the general “well-being” of the brainstem, it has rather been anecdotal to change the intraoperative surgical strategy exclusively on the basis of BAEP changes. BAEPs are therefore better interpreted in the context of a multimodal monitoring approach, where this information is integrated with that from SSEPs and mMEP monitoring.

5.3 Surgery of the Pons

5.3.1 Mapping

5.3.1.1 Mapping of the Facial Colliculus on the Floor of the Fourth Ventricle

Entering the floor of the fourth ventricle carries a significant risk of neurological injury due to the high concentration of eloquent neural structures in a very small area. At the level of the pons, the facial colliculus represents a highly dangerous brainstem “entry zone” through the rhomboid fossa [6]. Damage to this area causes

facial (VII) and abducens (VI) nerve paralysis as well as lateral gaze disturbances due to an injury to the paramedian pontine reticular formation. A midline injury involving the medial longitudinal fasciculus bilaterally may result in internuclear ophthalmoplegia.

Although the facial colliculus represents a classic anatomical landmark, its identification can be challenging when anatomy is significantly distorted by the tumor, and neurophysiological mapping could be the only way to functionally identify the nuclei or the intramedullary roots of the VI and VII cranial nerves.

A handheld bipolar concentric electrode could be used. A single stimulus of 0.2 ms duration is delivered at a frequency of 1–2 Hz. In general, two different mapping strategies can be used to identify the facial colliculus. In the first case, the surgeon looks for each site at the lowest threshold intensity, which allows to record a CMAP from the orbicularis oculi and/or the orbicularis oris muscles. By moving the stimulator 1 mm apart, it is possible to explore the floor of the fourth ventricle and identify the area closer to either the nucleus or the intramedullary root of the nerve. The other method is to work with a fixed intensity of approximately 0.5–1 mA and determine the amplitude of the muscle response for each point. The point corresponding to the highest amplitude indicates proximity to the mapped nucleus, while small amplitudes or no response at all suggest a safe distance from the nucleus or tracts.

There are yet two main limitations in the reliability of the mapping of the facial colliculus. The first is related to the fact that it cannot detect an injury to the supranuclear tracts originating in the motor cortex and ending on the cranial nerve motor nuclei. Therefore, preservation of the lower motoneuron per se may not exclude a postoperative facial palsy if the corticobulbar pathway has been injured proximal to the nucleus. The second limitation is that the possibility of stimulating the intramedullary root of the facial nerve, rather than the nuclei itself, exists. Therefore, this could result in a peripheral response that will still be recorded despite an injury to the motor nuclei [8] and, consequently, a postoperative facial palsy.

Even with these limitations, facial mapping remains a standard, very valuable ION technique, which undoubtedly facilitates the identification of the facial nerves/nuclei whenever the anatomy is ambiguous.

5.3.2 *Monitoring*

5.3.2.1 **Monitoring of the Facial Nerve**

Free-Running Electromyography While mapping techniques allow to identify the facial colliculus to select the safest entry zone through the floor of the fourth ventricle, only monitoring techniques can continuously assess the functional integrity of the facial nerve during surgery. Free-running EMG has been for many years the gold standard for facial nerve monitoring and is still widely used [11, 29, 30]. The spontaneous activity of the facial nerve is recorded through needle electrodes

placed in the muscles innervated by the facial nerve. Therefore, this is not an evoked potential. Different criteria have been proposed to interpret EMG activity, but convincing data regarding the correlation between EMG patterns and clinical outcome are still lacking [11, 30]. Paradoxically, the lack of spontaneous activity usually indicates no injury, but it could also be observed after a complete sectioning of the peripheral nerve. On the other hand, neurotonic discharges could reflect injury activity but sometimes occur following simple irrigation of the surgical field with cold saline. So, the real specificity and sensitivity of free-running EMG remains disputable. A higher degree of reliability has been documented for a specific pattern of high frequency, sustained neurotonic discharges, called A-trains. The occurrence and duration of A-trains has proved to be highly predictive of postoperative facial palsy. However, the A-train analysis is performed offline, and the predictive value of this specific pattern of EMG activity has been described only with regards to the surgery for vestibular schwannomas [31, 32], not in brainstem surgery.

Facial Motor Evoked Potentials A second method to monitor the functional integrity of the facial nerve is represented by corticobulbar MEPs (see Fig. 5.2). Essentially, the same principle of MEP monitoring for limb muscles is herein extended to the muscles innervated by motor cranial nerves. Facial MEPs are elicited through TES using a train of 4 stimuli, 0.5 ms each at a rate of 1–2 Hz and intensity ranging between 60 and 120 mA. The electrode montage is usually C3/Cz for right-sided muscles and C4/Cz for left-sided muscles. For recording, the same electrodes used during mapping of the facial nerve are used, and muscle responses can be recorded by both the orbicularis oris and oculi or any other muscle innervated by branches of the facial nerve. Facial MEPs are true evoked potentials, which assess the integrity of the corticobulbar pathway from the motor cortex to the muscles. Although there are no standard warning criteria for facial MEP interpretation, irreversible MEP loss is a poor prognostic sign, correlating with severe and long-lasting facial palsy [33]. The preservation of MEPs usually predicts no deficits or only minor and transient facial palsy, while significant amplitude drops – in our experience, in the range of 50% to 80% of baseline values – are indicative of at least a transient deficit.

One of the limitations of facial MEP monitoring is that the use of a lateral montage, with C3 or C4 as an anodal stimulating electrode, increases the risk that a strong TES may activate the corticobulbar pathways deep in the brain or at the level of the brainstem and foramen magnum [34]. This would increase the risk of a direct activation of the peripheral facial nerve. If this occurs, an injury to the corticobulbar pathway rostral to the point of activation of the facial nerve will not be recognized, and the patient will wake up from surgery with a facial palsy in spite of the preservation of facial MEPs. To minimize the risk of these false-negative results, it is always recommended to keep the stimulation intensity as low as possible. However, the only possibility to predict the threshold for peripheral activation is to repeat the same stimulation while keeping the same parameters (stimulus duration, intensity,

and frequency), except for the number of stimuli, which is decreased from 4 to 1. A single pulse TES should not elicit muscle MEPs during general anesthesia because neural transmission through a polysynaptic pathway would be blocked by the anesthetics; if a muscle response is still present, this response should be interpreted as a direct activation of the cranial nerve and is, therefore, not reliable for monitoring. Alternatively, a muscle response that is present with a train of stimuli and absent following a single stimulus is likely generated by a true corticobulbar activation and can be used for monitoring [35, 36]. Due to the physiological variation of this threshold during surgery, secondary to anesthesia, room temperature or other factors, it is important to re-check the threshold for peripheral activation several times during surgery. For example, if surgery is performed in a semi-sitting position, a significant cerebrospinal fluid (CSF) leak occurs after opening the dura and may produce pneumocephalus; the presence of air between the cortex and the skull will increase the threshold for TES and, therefore, new corticobulbar MEP baselines should be taken after the dura is opened.

Acioly et al. [37] have recently reviewed the literature on facial nerve monitoring in skull base and cerebellopontine angle surgery, concluding that: "Although there is a general agreement on the satisfactory functional prediction of different electrophysiological criteria, the lack of standardization in electrode montage and stimulation parameters precludes a definite conclusion regarding the best method." These considerations can certainly be extended to facial nerve monitoring in brainstem surgery.

5.4 Surgery of the Medulla Oblongata

Surgery of the medulla carries a significant risk of neurological morbidity because an injury to the lower cranial nerves or the cardiorespiratory centers can be life-threatening. Here, within the small concavity of the calamus scriptorius, between the obex and the striae medullaris, lie the hypoglossal and vagal triangles. Immediately below the two medial triangles lie the hypoglossal nuclei, which control the muscles of the tongue. Severe tongue paralysis and atrophy secondary to hypoglossal injury represents one of the most devastating cranial nerve deficits, and even a minor injury in this area must be avoided. Lateral to the hypoglossal triangles are the vagal triangles and under these triangles lie the dorsal nuclei of the vagus nerves. These provide motor fibers to the bronchi, heart, and stomach. Slightly deeper and lateral lies the nucleus ambiguus, which provides fibers to the glosso-pharyngeal (IX), vagus (X), and accessory (XI) nerves. These fibers ultimately innervate the musculature of the palate, pharynx, and larynx. Therefore, even a small injury to this area can cause dysphonia and may impair the swallowing and coughing reflexes, exposing the patient to the risk of aspiration pneumonia and/or inability to eat or drink [38, 39].

5.4.1 Mapping

5.4.1.1 Mapping the IX/X, XI and XII Cranial Nerve Nuclei

Neurophysiological mapping of the lower motor cranial nerves is performed similarly to mapping of the facial colliculus. The stimulating parameters are the same, with emphasis that at the level of the medulla – due to the close proximity of the cardiovascular centers – no intensity higher than 2 mA should be used as it may induce severe bradycardia and even cardiac arrest [40]. A bipolar concentric electrode is preferred for more focal stimulation. CMAPs are recorded from wire electrodes inserted in the muscles innervated by the lower cranial nerves. It should be pointed out that the glossopharyngeal nerve provides motor fibers only to the stylopharyngeus muscle, which elevates the pharynx during swallowing and speech. However, selective placement of recording electrodes in the stylopharyngeus muscle only is not possible, and it is expected that most of the muscle activity recorded from the pharyngeal muscles or soft palate likely reflects a mixed activation of both the IX and X cranial nerves. Another limitation of mapping of the glossopharyngeal nuclei is that stimulation on the floor of the fourth ventricle assesses only the functional integrity of the efferent arc of the swallowing reflex, while no information on the integrity of afferent pathways and afferent/efferent connections within the brainstem is obtained [41].

To record CMAPs for the IX/X and XII cranial nerves, we generally prefer to use tiny wire electrodes inserted in the posterior wall of the pharynx (inserted lateral to the endotracheal tube, bilaterally) and the tongue muscles, respectively. Other techniques to place recording electrodes either directly on the endotracheal tube or transcutaneously in other vocalis muscles can be used [42–44]. For the accessory nerve, regular needle recording electrodes are inserted in the trapezius muscle.

Morota et al. [8, 45] suggested that medullary tumors tend to displace the motor cranial nerve nuclei ventrally. So, whether the tumor is intra-axial or a fourth ventricular tumor – such as a medulloblastoma or an ependymoma – infiltrating the floor, neurophysiological mapping can be used to select the entry zone in the first case and to determine when to stop resection in both cases (Figs. 5.6 and 5.7). It should be considered that a positive mapping response with a low threshold intensity, lower than 0.5 mA, suggests a close proximity to the nuclei, which lie just a few millimeters below the ependyma. In this case, we recommend abandoning tumor resection as the risk of injuring the nuclei and/or the intramedullary roots is high, and this will expose the patient to life-threatening conditions. While a subtotal removal may be undesirable for medulloblastomas and ependymomas, most of the intra-axial medullary tumors, especially in children, are low-grade gliomas, and even if a tiny sole of the tumor is left on the floor of the fourth ventricle, close neuroradiological follow-up may suffice with no need to start adjuvant therapies upfront [46].

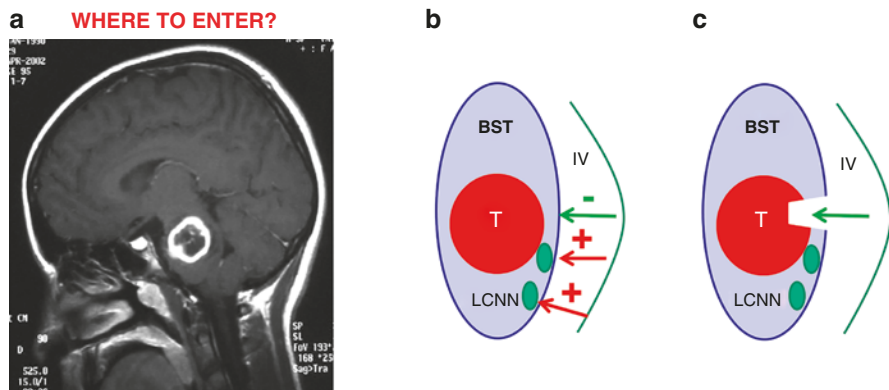


Fig. 5.6 Schematic illustration of the role of neurophysiological mapping on the floor of the fourth ventricle, for fully intra-axial brainstem tumors (a). Direct stimulation of the floor of the fourth ventricle is performed with either a monopolar or bipolar concentric stimulator (arrows). A positive mapping result (red arrow) indicates proximity to either cranial nerve nuclei or their intra-axial roots. Therefore, this is not a safe entry zone (b). Alternatively, negative stimulation (green arrow) or a stimulation requiring much higher intensity, indicates safe distance from the nuclei and their intra-axial roots, and can be used as an entry zone to the brainstem and the tumor (c)

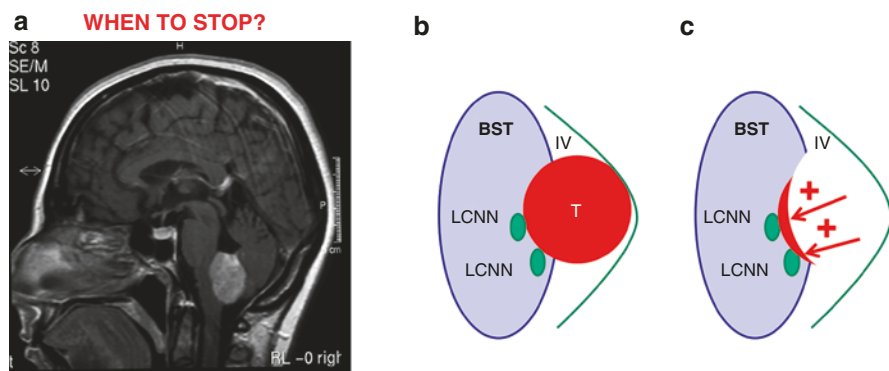


Fig. 5.7 Schematic illustration of the role of neurophysiological mapping on the floor of the fourth ventricle, for dorsally exophytic brainstem tumors or for fourth ventricular tumors infiltrating the floor (a). In these cases, neurophysiological mapping is often negative at the beginning of the case because the nuclei are displaced ventral to the tumor, especially at the level of the medulla (b). However, when stimulation of the last sole of tumor elicits a positive mapping response at low intensity (c), this is the time to stop resection in order not to violate and injure the lower cranial nerve nuclei or their intra-axial roots, which are only few millimeters underneath

5.4.2 Monitoring

5.4.2.1 Lower Cranial Nerve Monitoring

Free-Running Electromyography Despite the fact that recording of free-running EMG for the facial nerve in vestibular schwannoma surgery has proved to be reliable [31, 32, 47], the overall reliability of free-running EMG for other motor cranial

nerves remains controversial [11, 30]. In particular, Schlake et al. [48] observed rather high rates of false positive and, of most concern, false negative results, concluding that the predictive value of free-running EMG is limited.

Corticobulbar Motor Evoked Potentials As an alternative to free-running EMG, some authors [36, 49, 50] in the past 20 years have extended the use of facial nerve corticobulbar MEPs to the lower cranial nerves. The same parameters of stimulation and the same criteria (namely, a single stimulus versus a train of stimuli) to differentiate a real corticobulbar response from a peripheral activation of lower cranial nerves apply. Recordings are obtained from the same wire electrodes used for neurophysiological mapping. In our experience, MEPs from the hypoglossal nerve, recorded from the tongue, are very stable with little spontaneous activity and can be well monitored throughout the surgical procedure. Alternatively, MEPs for the IX/X nerves are unstable, and their interpretation is sometimes complicated by a more frequent spontaneous activity as compared to cranial nerve XII.

Finally, it should be considered that at the current state-of-the-art ION techniques, only efferent pathways are monitorable for the lower cranial nerve-mediated reflexes such as swallowing and coughing. Therefore, an injury to the afferent arch of these reflexes will not be recognized by current monitoring and mapping techniques [41]. This explains why discrepancies between ION data and postoperative neurological outcomes can occur. Very recently, Sinclair et al. [51] documented the possibility to monitor the laryngeal abductor reflex during thyroid surgery. Since this reflex is mediated at the level of the lower brainstem, it can indirectly provide information on the functional integrity of the involved area. Although this is still a very preliminary report on a small number of patients, it has certainly shed new light on the ION monitoring of the lower brainstem [52]. Hopefully, monitoring of brainstem-mediated reflexes, such as the laryngeal abductor reflex or the blink reflex, will improve the reliability of ION monitoring in surgeries of the pons and medulla oblongata.

5.5 Other Monitoring Techniques in the Brainstem

Some other methodologies related to the monitoring of trigeminal SSEPs (T-SSEPs) and brainstem reflexes have emerged over the past few years. A reliable methodology for eliciting T-SSEPs under general anesthesia was described by Malcharek et al. [53]. They recorded long-latency T-SSEPs from the scalp after simultaneously stimulating V2 and V3 branches of the trigeminal nerve. Although this method was tested in patients undergoing carotid endarterectomy, it may be important to assess the functional integrity of sensory fibers of the trigeminal nerve during brainstem surgery.

The blink reflex has also been monitored under general anesthesia [54]. This reflex is mediated by an afferent pathway – the nasociliary branch of the ophthalmic branch (V1) of the trigeminal nerve, and an efferent pathway – the temporal and zygomatic branches of the facial nerve. Deletis et al. were able to elicit the R1 com-

ponent in 86% of 27 patients aged 1 to 78 years. They applied one to seven rectangular constant-current stimuli with an interstimulus interval of 2 ms, an intensity of 20–40 mA, and a train repetition rate of 0.4 Hz over the supraorbital nerve. Recording was done from the ipsilateral orbicularis oculi muscle [54]. The integrity of this reflex reflects the functional integrity of the neural structures involved at the level of the pons.

Finally, the masseter reflex, also known as the jaw jerk reflex, can be monitored intraoperatively by inserting percutaneous hook-wire electrodes just under the zygomatic arch, approximately 5 mm lateral to the temporomandibular joint. Single stimuli with a duration of 0.2–0.5 ms and progressively increasing intensity are applied. The insertion depth of the stimulating wire electrode is determined when the stimulation elicits a response in the masseter and temporalis muscles. Recordings are obtained by inserting subdermal needle electrodes into the ipsilateral masseter and temporalis muscles [55].

5.6 Conclusion

Surgery of brainstem lesions remains challenging despite all the remarkable advancements in the field of neuroanesthesia, postoperative intensive care, and pre-surgical planning, including tractography. This small region of the central nervous system represents a minefield even for the experienced neurosurgeon.

To date, ION remains essential to improve the safety of brainstem surgery. With the only exception of the localization of oculomotor nerve nuclei following stimulation of the superior colliculi, mapping techniques are reliable and very useful in determining the safest entry route for intrinsic, focal brainstem lesions. Additionally, these techniques help to decide when to stop the removal of fourth ventricular tumors infiltrating the floor, in order to avoid an injury to the VII, IX/X and XII cranial nerve nuclei.

ION monitoring can nowadays support the surgeon in two ways: (1) by providing functional information aimed to identify ambiguous neural structures – this may assist in identifying the safest entry zone to intra-axial lesions and/or determine the proximity of cranial nerve nuclei to stop the resection of brainstem exophytic tumors or fourth ventricular tumors infiltrating the ependyma; and (2) by on-line monitoring of the functional integrity of somatosensory, motor and auditory pathways to minimize the risk of a permanent injury.

SSEPs and BAERs are well established techniques since many years but only cover a small area of the brainstem, and focal injury may occur despite their preservation. Therefore, a multimodal neuromonitoring approach, including corticospinal and corticobulbar MEPs, should be used instead. MEPs, in general, are good predictors of motor outcome, though warning criteria in the brainstem are not well set, especially for corticobulbar MEPs of the lower cranial nerves, where only few studies are reported in the literature. Nevertheless,

corticobulbar MEPs, for the VII and especially for the IX/X and XII cranial nerves, are a valid alternative to free-running EMG, which often lacks specificity and sensitivity.

The lack of ION techniques to reliably monitor afferent pathways of the lower brainstem mediated reflexes, such as swallowing and coughing, remains problematic. Recently, however, novel techniques have been proposed to monitor brainstem reflexes at the level of the pons and medulla oblongata, and these developments are opening new perspectives to further enhance the reliability of brainstem monitoring in neurosurgery.

References

1. Jallo GI, Shiminski-Maher T, Velazquez L, Abbott R, Wisoff J, Epstein F. Recovery of lower cranial nerve function after surgery for medullary brainstem tumors. *Neurosurgery*. 2005;56(1):74–7; discussion 78.
2. Abbott R. Brainstem gliomas. In: Mc Lone DG, editor. *Pediatric neurosurgery: surgery of developing nervous system*. Philadelphia: WB Saunders; 1996. p. 859–67.
3. Bricolo A. Surgical management of intrinsic brain stem gliomas. *Oper Tech Neurosurg*. 2000;3:137–54.
4. Jallo GI, Biser-Rohrbaugh A, Freed D. Brainstem gliomas. *Childs Nerv Syst*. 2004;3(Mar;20):143–53.
5. Kyoshima K, Kobayashi S, Gibo H, Kuroyanagi T. A study of safe entry zones via the floor of the fourth ventricle for brain-stem lesions. *J Neurosurg*. 2009;78:987–93.
6. Lang J, Ohmachi N, Sen JL. Anatomical landmarks of the rhomboid fossa (floor of the 4th ventricle), its length and its width. *Acta Neurochir*. 1991;113(1–2):84–90.
7. Strauss C, Lütjen-Drecoll E, Fahlbusch R. Pericollicular surgical approaches to the rhomboid fossa. Part I Anatomical basis. *J Neurosurg*. 2009;87(6):893–9.
8. Morota N, Deletis V, Epstein FJ, Kofler M, Abbott R, Lee M, et al. Brain stem mapping: neurophysiological localization of motor nuclei on the floor of the fourth ventricle. *Neurosurgery*. 1995;37(5):922–9; discussion 929–30.
9. Abbott R. The use of physiological mapping and monitoring during surgery for ependymomas. *Childs Nerv Syst*. 2009;25(10):1241–7.
10. Strauss C, Romstöck J, Fahlbusch R. Pericollicular approaches to the rhomboid fossa. Part II. Neurophysiological basis. *J Neurosurg*. 1999;91(5):768–75.
11. Schlake HP, Goldbrunner R, Siebert M, Behr R, Roosen K. Intra-operative electromyographic monitoring of extra-ocular motor nerves (Nn. III, VI) in skull base surgery. *Acta Neurochir*. 2001;143(3):251–61.
12. Sekiya T, Hatayama T, Shimamura N, Neurosurgery SS. Intraoperative electrophysiological monitoring of oculomotor nuclei and their intramedullary tracts during midbrain tumor surgery. *Neurosurgery*. 2000;47(5):1170–6; discussion 1176–7.
13. Duffau H, Sichez JP. Intraoperative direct electrical stimulation of the lamina quadrigemina in a case of a deep tectal cavernoma. *Acta Neurochir*. 1998;140(12):1309–12.
14. Ishihara H, Bjeljac M, Straumann D, Kaku Y, Roth P, Yonekawa Y. The role of intraoperative monitoring of oculomotor and trochlear nuclei – safe entry zone to tegmental lesions. *Minimal Invasive Neurosurg*. 2006;49(3):168–72.
15. Li Z, Wang M, Zhang L, Fan X, Tao X, Qi L, et al. Neuronavigation-guided corticospinal tract mapping in brainstem tumor surgery: better preservation of motor function. *World Neurosurg*. 2018;116:e291–7.

16. Czernicki T, Maj E, Podgórska A, Kunert P, Prokopienko M, Nowak A, et al. Diffusion tensor tractography of pyramidal tracts in patients with brainstem and intramedullary spinal cord tumors: relationship with motor deficits and intraoperative MEP changes. *J Magn Reson Imaging*. 2017;46(3):715–23.
17. Nossek E, Korn A, Shahar T, Kanner AA, Yaffe H, Marcovici D, et al. Intraoperative mapping and monitoring of the corticospinal tracts with neurophysiological assessment and 3-dimensional ultrasonography-based navigation. *J Neurosurg*. 2010;114:738–46.
18. Ohue S, Kohno S, Inoue A, Yamashita D, Harada H, Kumon Y, et al. Accuracy of diffusion tensor magnetic resonance imaging-based tractography for surgery of gliomas near the pyramidal tract: a significant correlation between subcortical electrical stimulation and postoperative tractography. *Neurosurgery*. 2012;70:283–94.
19. Jones SJ, Harrison R, Koh KF, Mendoza N, Crockard HA. Motor evoked potential monitoring during spinal surgery: responses of distal limb muscles to transcranial cortical stimulation with pulse trains. *Electroencephalogr Clin Neurophysiol – Evoked Potentials*. 1996;100(5):375–83.
20. Pechstein U, Cedzich C, Nadstawek J, Schramm J. Transcranial high-frequency repetitive electrical stimulation for recording myogenic motor evoked potentials with the patient under general anesthesia. *Neurosurgery*. 1996;3982:335–43; discussion 343–4.
21. Taniguchi M, Cedzich C, Taniguchi M, Cedzich C, Schramm J. Modification of cortical stimulation for motor evoked potentials under general anesthesia: technical description. *Neurosurgery*. 1993;32(2):219–26.
22. MacDonald DB. Safety of intraoperative transcranial electrical stimulation motor evoked potential monitoring. *J Clin Neurophysiol*. 2002;19(5):416–29.
23. Neuloh G, Bogucki J, Schramm J. Intraoperative preservation of corticospinal function in the brainstem. *J Neurol Neurosurg Psychiatry*. 2009;80(4):417–22.
24. Kodama K, Javadi M, Seifert V, Széleányi A. Conjoint SEP and MEP monitoring in resection of infratentorial lesions: lessons learned in a cohort of 210 patients. *J Neurosurg*. 2014;121:1453–61.
25. Shiban E, Zerr M, Huber T, Boeck-Behrends T, Wostrack M, Ringel F, et al. Poor diagnostic accuracy of transcranial motor and somatosensory evoked potential monitoring during brainstem cavernoma resection. *Acta Neurochir*. 2015;157811:1963–9.
26. Legatt AD, Arezzo JC, Vaughan HG Jr. The anatomic and physiologic bases of brain stem auditory evoked potentials. *Neurol Clin*. 1988;6(4):681–704.
27. Legatt AD. Brainstem Auditory Evoked Potentials: methodology, interpretation, and clinical application. In: Aminoff MJ, editor. *Electrodiagnosis in clinical Neurology*. New York: Churchill Livingstone; 2005. p. 489–523.
28. Fahlbusch R, Strauss C. Surgical significance of brainstem cavernous hemangiomas. *Zentralbl Neurochir*. 1991;52:25–32.
29. Eisner W, Schmid UD, Reulen HJ, Oeckler R, Olteanu-Nerbe V, Gall C, et al. The mapping and continuous monitoring of the intrinsic motor nuclei during brain stem surgery. *Neurosurgery*. 1995;37:255–65.
30. Grabb PA, Albright AL, Sclabassi RJ, Pollack IF. Continuous intraoperative electromyographic monitoring of cranial nerves during resection of fourth ventricular tumors in children. *J Neurosurg*. 1997;86:1–4.
31. Prell J, Rapp S, Romstöck J, Fahlbusch R, Strauss C. Train time as a quantitative electromyographic parameter for facial nerve function in patients undergoing surgery for vestibular schwannoma. *J Neurosurg*. 2007;106(5):826–32.
32. Romstöck J, Strauss C, Fahlbusch R. Continuous electromyography monitoring of motor cranial nerves during cerebellopontine angle surgery. *J Neurosurg*. 2009;93:586–93.
33. Dong CCJ, MacDonald DB, Akagami R, Westerberg B, AlKhani A, Kanaan I, et al. Intraoperative facial motor evoked potential monitoring with transcranial electrical stimulation during skull base surgery. *Clin Neurophysiol*. 2005;116:588–96.

34. Rothwell J, Burke D, Hicks R, Stephen J, Woodforth I, Crawford M. Transcranial electrical stimulation of the motor cortex in man: further evidence for the site of activation. *J Physiol.* 1994;481(Pt 19):243–50.
35. Téllez MJ, Ulkatan S, Urriza J, Arranz-Arranz B, Deletis V. Neurophysiological mechanism of possibly confounding peripheral activation of the facial nerve during corticobulbar tract monitoring. *Clin Neurophysiol.* 2016;127:1710–6.
36. Sala F, Lanteri P, Bricolo A. Intraoperative neurophysiological monitoring of motor evoked potentials during brain stem and spinal cord surgery. *Adv Tech Stand Neurosurg.* 2004;29:133–69.
37. Acioly MA, Liebsch M, De Aguiar PHP, Tatagiba M. Facial nerve monitoring during cerebellopontine angle and skull base tumor surgery: a systematic review from description to current success on function prediction. *World Neurosurg.* 2013 Dec;80(6):e271–300.
38. Blessing W. The lower brainstem and bodily homeostasis. New York: Oxford University Press; 1997.
39. Procaccio F, Gambin R, Gottin L, Bricolo A. Complications of brain stem surgery: prevention and treatment. *Oper Tech Neurosurg.* 2000;3(2):155–7.
40. Suzuki K, Matsumoto M, Ohta M, Sasaki T, Kodama N. Experimental study for identification of the facial colliculus using electromyography and antidromic evoked potentials. *Neurosurgery.* 1997;41:1130–6.
41. Sala F, Manganotti P, Tramontano V, Bricolo A, Gerosa M. Monitoring of motor pathways during brain stem surgery: what we have achieved and what we still miss? *Neurophysiol Clin.* 2007;37:399–406.
42. Deletis V, Fernandez-Conejero I, Ulkatan S, Costantino P. Methodology for intraoperatively eliciting motor evoked potentials in the vocal muscles by electrical stimulation of the corticobulbar tract. *Clin Neurophysiol.* 2009;120(2):336–41.
43. Husain AM, Wright DR, Stolp BW, Friedman AH, Keifer JC. Neurophysiological intraoperative monitoring of the glossopharyngeal nerve: technical case report. *Neurosurgery.* 2008;63(4 Suppl 2):277–8; discussion 278.
44. Skinner SA. Neurophysiologic monitoring of the spinal accessory nerve, hypoglossal nerve, and the spinomedullary region. *J Clin Neurophysiol.* 2011;28(6):587–98.
45. Morota N, Deletis V, Lee M, Epstein FJ. Functional anatomic relationship between brain stem tumors and cranial motor nuclei. *Neurosurgery.* 1996;39:787–94.
46. Abbott R, Shimimki-Mether T, Epstein FJ. Intrinsic tumors of the medulla: predicting outcome after surgery. *Pediatr Neurosurg.* 1996;25:41–4.
47. Prell J, Rachinger J, Scheller C, Alfieri A, Strauss C, Rampp S. A real-time monitoring system for the facial nerve. *Neurosurgery.* 2010;66(6):1064–73; discussion 1073.
48. Schlake HP, Goldbrunner RH, Milewski C, Krauss J, Trautner H, Behr R, et al. Intra-operative electromyographic monitoring of the lower cranial motor nerves (LCN IX–XII) in skull base surgery. *Clin Neurol Neurosurg.* 2001;103(2):72–82.
49. Ito E, Ichikawa M, Itakura T, Ando H, Matsumoto Y, Oda K, et al. Motor evoked potential monitoring of the vagus nerve with transcranial electrical stimulation during skull base surgeries. *J Neurosurg.* 2013;118(1):195–201.
50. Fukuda M, Oishi M, Hiraishi T, Saito A, Fujii Y. Pharyngeal motor evoked potentials elicited by transcranial electrical stimulation for intraoperative monitoring during skull base surgery. *J J Neurosurg.* 2012;116(3):605–10.
51. Sinclair CF, Téllez MJ, Tapia OR, Ulkatan S, Deletis V. A novel methodology for assessing laryngeal and vagus nerve integrity in patients under general anesthesia. *Clin Neurophysiol.* 2017;128(7):1399–405.
52. Sala F. A spotlight on intraoperative neurophysiological monitoring of the lower brainstem. *Clin Neurophysiol.* 2017;128(7):1369–71.

53. Malcharek MJ, Landgraf J, Hennig G, Sorge O, Aschermann J, Sablotzki A. Recordings of long-latency trigeminal somatosensory-evoked potentials in patients under general anaesthesia. *Clin Neurophysiol.* 2011;122(5):1048–54.
54. Deletis V, Urriza J, Ulkatan S, Fernandez-Conejero I, Lesser J, Misita D. The feasibility of recording blink reflexes under general anesthesia. *Muscle Nerve.* 2009;39(5):642–6.
55. Ulkatan S, Jaramillo AM, Téllez MJ, Goodman RR, Deletis V. Feasibility of eliciting the H reflex in the masseter muscle in patients under general anesthesia. *Clin Neurophysiol.* 2017;128(1):123–7.
56. Sala F, Gallo P, Tramontano V. Intraoperative neurophysiological monitoring in posterior fossa surgery. In: Ozek M, Cinalli G, Maixner WJ, Sainte-Rose C, editors. *Posterior Fossa Tumors in Children.* Springer: 2015, p. 239–62.

Chapter 6

Low-Grade Pediatric Brainstem Gliomas



Jonathan Roth, Danil A. Kozyrev, and Shlomi Constantini

Abbreviations

¹⁸ F-FET	O-(2- ¹⁸ F-fluoroethyl)-L-tyrosine
BSG	Brainstem gliomas
CN	Cranial nerve
CNS	Central nervous system
DIPG	Diffuse intrinsic pontine gliomas
DPG	Diffuse pontine gliomas
DTI	Diffusion tensor imaging
DWI	Diffusion-weighted imaging
EMG	Electromyographic
ETV	Endoscopic third ventriculostomy
FLAIR	Fluid-attenuated inversion recovery
GTR	Gross total resection
ICP	Intracranial pressure
IDH	Isocitrate dehydrogenase
IOM	Intraoperative monitoring
LGBSG	Low-grade brainstem gliomas
LGG	Low-grade gliomas
MRI	Magnetic resonance imaging
MRS	Magnetic resonance spectroscopy
NF	Neurofibromatosis
OS	Overall survival
PET	Positron emission tomography
PFS	Progression free survival

J. Roth (✉) · D. A. Kozyrev · S. Constantini
Department of Pediatric Neurosurgery, Dana Children's Hospital, Tel-Aviv Medical Center,
Tel-Aviv, Israel

PNET	Primitive neuroectodermal tumors
TIVA	Total intravenous anesthesia
WHO	World Health Organization

6.1 Introduction

Low-grade (a.k.a. benign) brainstem gliomas (LGBSG) in children include a diverse group of tumors with different presenting symptoms and tumor configurations that lead to a plethora of biological behaviors and variable prognoses. Brainstem gliomas (BSG) represent 10–20% of all pediatric brain tumors and about 20–30% of infratentorial tumors. About 60–70% of all pediatric brainstem tumors are diffuse pontine gliomas (DPG), and most others include a spectrum of low-grade gliomas (LGG).

BSG are diagnosed at all ages. However, they are rarely diagnosed before the age of 5 years, and their occurrence peaks at around the age of 10 years. Males and females are more-or-less equally affected.

As opposed to cerebellar and many supratentorial tumors, LGBSG involve supereloquent neural tissue, and thus were previously considered inoperable. However, as has been showed by Epstein and others, in selected subgroups of tumors and with the integration of intraoperative mapping and monitoring, resection is feasible with reasonable neurological and oncological outcomes [1–3]. With the addition of gentle-chemotherapy and modern radiation techniques, decision-making on the combination of treatment options has become more complex. Currently, there is no unified management approach for LGBSG. The treatment is dictated by tumor location, configuration, and biological behavior. In this chapter, we review the various LGBSG tumors and propose a schematic treatment paradigm.

6.2 Classification

With improvements in neuroimaging, the diagnosis and classification of BSG has been refined, depending mainly on the location, texture and tumor configuration (e.g., whether the tumor is focal, cystic, or diffuse), as follows:

- A. **Configuration:** Generally speaking, **focal** and **cystic** tumors tend to be low-grade and behave in a more indolent manner, while **diffuse** tumors tend to be high-grade and behave aggressively. This concept is true for all brainstem locations.
- B. **Location:** BSG may be located in the midbrain, pons, or medulla, with some overlap depending on the extent of the tumor.
 - (a) **Midbrain** tumors include:
 - (i) Tectal tumors (with or without exophytic components) (Fig. 6.1)
 - (ii) Aqueductal tumors (Fig. 6.2)
 - (iii) Tegmental tumors

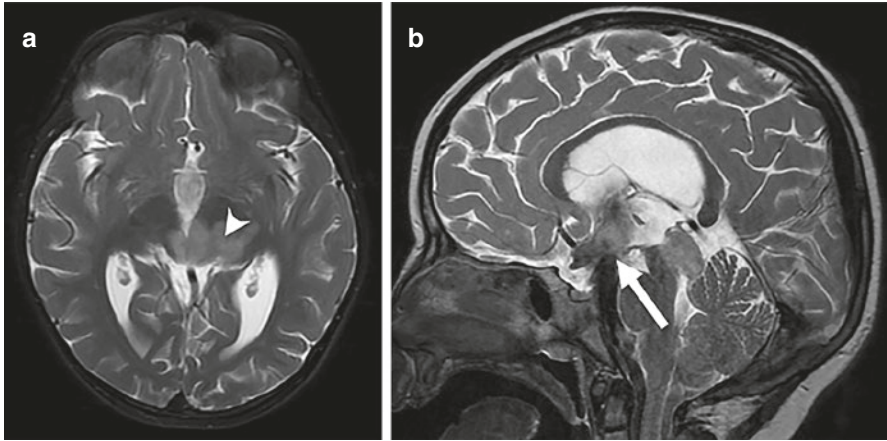


Fig. 6.1 Axial (a) and sagittal (b) T2-weighted MRI showing a tectal glioma. Note the flow artifact on the sagittal view (arrow, following an endoscopic third ventriculostomy), and the extension to the left thalamus/pulvinar (arrowhead)

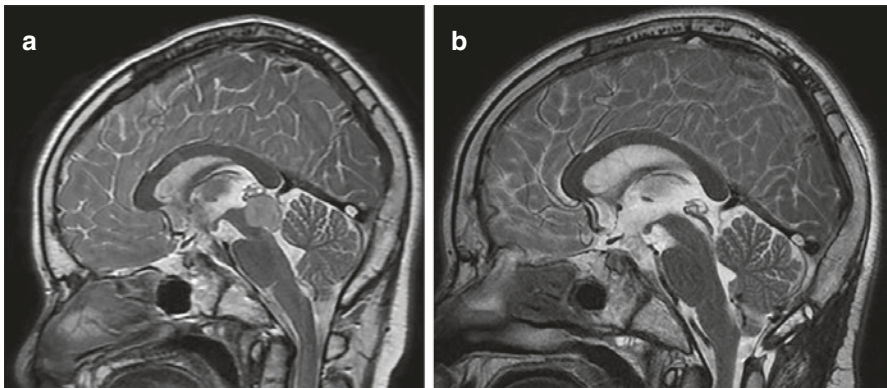


Fig. 6.2 Aqueductal tumor – ependymoma. Preoperative (a) and postoperative (b) T2-weighted images. The tumor was resected through a trans-fourth ventricular approach

(b) **Pontine** tumors include:

- (i) Focal (isolated) pontine tumors, or pontine tumors with extension to the brachium pontis (middle cerebellar peduncle)
- (ii) Diffuse (intrinsic) pontine gliomas (DPG, DIPG)

(c) **Medullary** tumors include:

- (i) Dorsal exophytic tumors (Figs. 6.3 and 6.4)
- (ii) Cervico-medullary tumors
- (iii) Focal intrinsic medullary tumors
- (iv) Diffuse medullary tumors

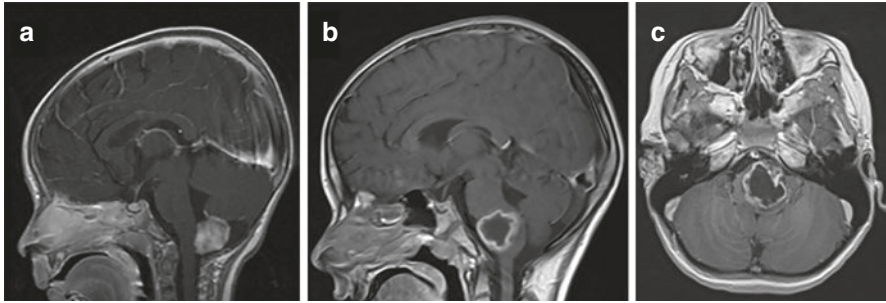


Fig. 6.3 (a) Exophytic and (b, c) focal medullary gliomas. Both pathologies were pilocytic astrocytomas

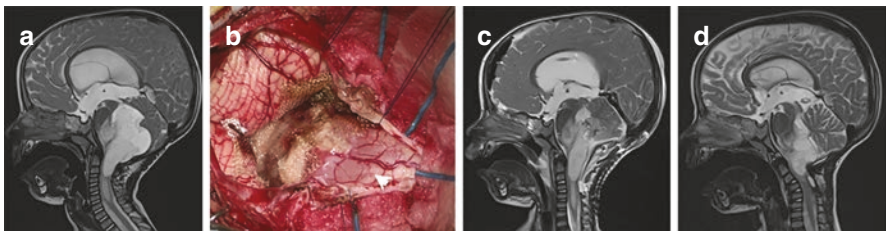


Fig. 6.4 (a) Exophytic medullary pilocytic astrocytoma. (b) Intraoperative picture after partial tumor resection. The tumor's infiltrative part was left intact; the arrowhead shows the border between the tumor and the medulla. Preoperative (a) and postoperative (c) T2-weighted images showing the tumor before and after resection. (d) A T2-weighted image at 10 months after surgery. In spite of several cycles of chemotherapy (vincristine, carboplatin, cyclophosphamide, cisplatin), tumor progression is observed

6.3 Symptoms

BSG may produce several types of symptoms [4]:

- A. **Elevated intracranial pressure (ICP):** BSG may cause hydrocephalus by obstructing the aqueduct, fourth ventricle, or fourth ventricular outlet. Hydrocephalus may develop gradually or acutely, leading to headache, vomiting, and drowsiness.
- B. **Cranial nerve (CN) deficits:** These may occur in any location and are related to CN nuclei involvement by the tumors, or from injuries to the CN themselves.

Upper brainstem tumors may cause pseudobulbar palsy.

Midbrain region tumors may cause Parinaud syndrome (secondary to pressure on the upper tectal region and hydrocephalus) and third or fourth CN palsies. Oculomotor nerve palsy may include pupil dilation if the Edinger-Westphal nucleus is involved.

Pontine tumors may cause facial or abducens nerve palsy. Cochlear and trigeminal nerve symptoms are rare.

Medullary tumors may cause lower cranial nerve deficits, manifesting with hoarseness and difficulty in swallowing as well as recurrent aspirations. Failure to thrive may occur in infants.

Torticollis is a common finding in cervico-medullary tumors, which cause impaction of the foramen magnum and compression of the spinal accessory nerve.

- C. **Long-tract symptoms:** These include general weakness and pyramidal signs. Sensory symptoms are relatively rare, most probably as they are less overt.
- D. **Cerebellar symptoms:** These are more common in pontine tumors, especially those involving the brachium pontis.
- E. **Other symptoms,** such as respiratory decline and abnormal respiratory patterns. These occur secondary to involvement of the medullary and lower pontine respiratory centers, and secondary to generalized decreased respiratory muscle innervation. Vomiting is a common symptom of tumors involving the obex and may be the sole presenting symptom. Thus, brain magnetic resonance imaging (MRI) should be part of the evaluation of children with recurrent vomiting, even in the absence of other symptoms or signs.

Symptoms may evolve slowly, over the course of a few months, or in an accelerated fashion, within days to weeks. Fast symptom eruption is associated with high-grade tumors, such as DPG, and are less common in LGBSG [5].

6.4 Diagnosis and Imaging

The diagnostic gold standard is brain MRI, including T1-weighted with and without contrast, T2-weighted, and fluid-attenuated inversion recovery (FLAIR) images. These images will accurately outline the location of the tumor, relationship of the tumor to neighboring structures such as the aqueduct, fourth ventricle and blood vessels, enhancing components, ventricular size and orientation, and leptomeningeal spread. Most LGBSG are hypointense on T1, hyperintense on T2 and FLAIR, and may have an enhancing component. Importantly, enhancing tumors are not necessarily high-grade; World Health Organization (WHO) grade I lesions often have an enhancing component.

T1-T2 overlap is an important sign of focal BSG. When the T1 hypointensity overlaps with the T2 hyperintense signal, this suggests a non-infiltrative or low-grade tumor. However, DPG typically presents with a diffuse T1 hypointensity of the pons, which overlaps with the T2 hyperintensity. Thus, the T1-T2 overlap must be assessed in the wider context of other radiological and clinical findings. DPG typically shows a generalized swelling of the pons, with engulfment of the basilar artery anteriorly, as well as a progressive clinical course.

Diffusion-weighted imaging (DWI) is important when assessing pontine tumors, as primitive neuroectodermal tumors (PNET) may mimic DPG [6], and are associated with a restricted signal on DWI.

Tectal tumors have a typical radiological appearance. They are epicentered in the tectum (posterior to the aqueduct), though they may extend to the medial aspect of the pulvinar (see Fig. 6.1). They are hypo-isointense on T1, hyperintense on T2, and usually do not enhance. Tectal tumors typically compress the aqueduct, leading to obstructive hydrocephalus. Enhancing tectal tumors tend to have a more aggressive behavior, as they tend to grow.

Aqueductal tumors are distinct from tectal or other pineal-region tumors, as they are epicentered within the aqueduct, and the tectum is placed posterior to the tumor [7]. Radiologically, sagittal T2 and non-contrast sagittal T1 sequences assist to differentiate between aqueductal and tectal tumors, although an overlap exists.

Magnetic resonance spectroscopy (MRS) has been proposed as part of the evaluation of BSG to distinguish between low- and high-grade tumors. However, there is currently no consensus regarding the role of MRS. Note that some BSG (such as DPG) may have a low-grade histological and MRS appearance, but have an aggressive biological behavior similar to high-grade tumors. Thus, MRS may be part of the diagnostic workup, but only as a complementary tool.

O-(2-¹⁸F-fluoroethyl)-L-tyrosine (¹⁸F-FET) positron emission tomography (PET) has been used to differentiate between supratentorial low- and high-grade gliomas. A recent study suggested its use to evaluate brainstem tumors too, especially when MRI is equivocal [8].

Although BSG rarely metastasize, it is a good policy to perform spinal MRI as part of the primary screening, especially if there are symptoms suggesting spinal seeding, or in the presence of brain leptomeningeal spread.

6.5 Pathology

BSG include all WHO grades I-IV astrocytomas. Grade I tumors (pilocytic astrocytomas) usually present as discrete lesions, often with a cystic component; however, they may present as dorsally exophytic tectal or medullary (and cervico-medullary) tumors. They usually enhance following gadolinium injection and may be associated with significant edema (for instance, in the cervical spine). Often, the tumor includes non-enhancing components too. Another group of grade I tumors are the gangliogliomas. These are rare tumors, which tend to enhance, and are usually located at the cervico-medullary region.

WHO grade II tumors (diffuse low-grade astrocytomas) may present in any location along the brainstem [9]. Their biological behavior is very diverse. Tectal and exophytic tumors usually have a very indolent course. On the other hand, DPG may have the histological appearance of WHO grade II tumors but behave aggressively [9]. WHO grade II astrocytomas usually do not enhance and are hypointense on T1 and hyperintense on T2 and FLAIR.

Other glial pathologies may rarely arise in the brainstem, including oligodendrogliomas [10], gangliogliomas, and pilomyxoid astrocytomas [4].

6.6 Differential Diagnosis

Other types of lesions that may mimic BSG include:

1. Inflammatory changes (such as multiple sclerosis, acute disseminated encephalomyelitis)
2. Other oncological pathologies (such as brainstem PNET)
3. Non-specific benign findings (such as neurofibromatosis (NF) hamartomas-NF spots)
4. Vascular lesions (such as cavernomas, vasculitis)

Thus, the diagnosis depends on the specific clinical and radiological aspects.

6.7 Treatment Rationale

Depending on the clinical status, mass effect, location, and radiological suspicion of a high-grade lesion, LGBSG may be followed and treated once they change their radiological appearance or cause symptoms. Thus, small “benign” appearing lesions do not necessitate any active treatment, be it surgical, chemotherapeutic, or radiation [11].

The rationale for treatment is for lesions suspicious of being high-grade (or other unknown pathology as discussed below), for lesions causing mass effect-related symptoms or hydrocephalus, or for growing lesions.

6.8 Biopsy Considerations

Both tectal tumors and DPG are usually diagnosed radiologically, with no need for a biopsy. The biopsy considerations in DPG are beyond the scope of this chapter, and are discussed elsewhere in this book; however, most agree that typical radiological appearance is sufficient for diagnosis, and that biopsy should only be performed in atypical lesions (e.g., eccentric pontine lesions, or lesions that are restricted on DWI) or as part of trial protocols.

Aqueductal tumors may be of various pathologies, including low- and high-grade astrocytomas or ependymomas, and thus we recommend performing an endoscopic biopsy as part of the surgery to treat the related hydrocephalus with an endoscopic third ventriculostomy (ETV) [7] (see Sect. 6.9.1 for technical considerations).

Focal intrinsic or exophytic tumors are usually low-grade; however, high-grade lesions may have a similar radiological pattern, and thus a biopsy may be recommended [5]. Stereotactic biopsies of brainstem tumors are associated with a permanent morbidity of about 1.7% and mortality of about 1% [12], and are associated with a high accuracy rate.

6.9 Surgical Treatment

The surgical treatment for BSG must address two aspects: alleviating secondary hydrocephalus and treating the tumor.

6.9.1 Treatment of Hydrocephalus

Since the hydrocephalus is obstructive, an ETV is often the preferred treatment. Tectal gliomas are an example of BSG that typically favor ETV, and, as explained previously, there is no need to perform a biopsy of the lesion. Long-term success rates are about 80–95% [13].

As opposed to typical tectal gliomas, aqueductal tumors are rare and may include other pathologies such as high-grade gliomas and ependymomas. Therefore, we recommend performing an endoscopic biopsy as part of the ETV procedure [7]. Various techniques may be used to combine an ETV with an endoscopic biopsy, such as using a rigid endoscope for the ETV and a flexible endoscope for the biopsy. The advantage of this approach is that the entry point planned for the ETV can be used for the biopsy too. Another option is to perform two entry holes, one for the ETV, and another one, more anteriorly, for the biopsy. The disadvantage of such an approach is the need for two openings and two trajectories through the tissue. A third option is to create a *compromise* opening midway between the ideal entry point for the ETV and the ideal entry point for the biopsy. The downside of this approach is the fact that this approach is not optimal for either procedure; the surgeon is actually compromising on the ideal trajectories for both tasks. As recently published, a combination of rigid and flexible endoscopy may be a valid technical option to perform an ETV concurrently with a biopsy of a lesion at the posterior region of the third ventricle [14].

With secondary hydrocephalus caused by other BSG, such as midbrain or pontine tumors, the tumors may severely distort the anatomy, pushing the basilar artery anteriorly and diminishing the brainstem-clival distance. Despite these limitations, an ETV may be performed addressing the anatomical nuances with a low related risk [15]. However, for DPG-associated hydrocephalus, due to a significant distortion of the basilar artery, a shunt is preferred.

6.9.2 Tumor Resection

Before discussing the technical aspects of BSG surgery, it is important to stress the multimodality approach necessary for such tumors. Over the recent years, radiation and chemotherapy have proven to be efficient treatments for focal and low-grade tumors [16]. Thus, careful decision-making regarding the role of maximally-safe surgery as well as additional treatments is paramount.

Tectal gliomas and diffuse brainstem tumors are not amenable to resection. The role of resection is for treatment of focal tumors, especially for tumors exhibiting an exophytic component. It is generally accepted that, similar to low-grade astrocytomas located elsewhere in the central nervous system (CNS), aggressive resection of focal BSG (which are often low-grade) may increase the progression free survival (PFS) and overall survival (OS). When possible, removal of a focal tumor (which often is the enhancing part of the lesion) or the exophytic component of the tumor is considered the surgical goal [17, 18]. Often, gross total resection (GTR) may not be performed safely, and thus, an extensive resection (even if subtotal) is done [9]. Most focal tumors are exophytic medullary or cervico-medullary tumors; however, they may be located in any part of the brainstem.

Successful BSG resection heavily relies on intraoperative monitoring (IOM) and mapping [1–3]. These include long-tract monitoring (such as motor evoked potentials and somatosensory evoked potentials) as well as electromyographic (EMG) monitoring of cranial nerves (including CN V, VII, IX, X, XI, and XII). Mapping includes direct monopolar or bipolar stimulation of brainstem regions to identify the CN nuclei locations and continuity of the CNs. The surgical approaches to the brainstem are vast, depending on the exact lesion location, as well as IOM-defined “safe zones” [19].

Diffusion tensor imaging (DTI) is important when operating on tegmental lesions (in the midbrain or pons). DTI outlines the location of the pyramidal tracts and assists in surgical planning [20]. DTI should not replace IOM, as the accuracy of the DTI is limited.

Anesthesia protocols must enable optimal electrophysiological monitoring, and thus mainly include total intravenous anesthesia (TIVA) with propofol and remifentanyl. Volatile anesthesia may negatively affect the accuracy of the monitoring.

Surgical approaches include midline suboccipital telovelar approaches (for paraventricular pontine and medullary tumors, cervico-medullary tumors, and tumors located in the lower part of the aqueduct). Paramedian approaches are useful for laterally located exophytic medullary BSG. Transtemporal approaches are used for focal laterally extending midbrain tumors. Supracerebellar-infratentorial, occipital-transtentorial, or interparietal-transsplenic approaches are used for dorsal exophytic tectal gliomas. For cervico-medullary tumors, upper cervical laminectomies or laminotomies are performed.

Regardless of the surgical approach, careful and judicious resection should be performed, focusing only on clearly pathological tissue [18]. The cavitron aspirator is a recommended tool for resection of BSG.

6.9.3 Postoperative Complications

Resection of BSG may lead to specific neurological complications, including cranial neuropathy, sensory deficits (deep, superficial, and pain), and motor deficits.

Other complications, depending on the surgical region, may include a decline in consciousness (upper brainstem), respiratory insufficiency (lower brainstem), and vomiting (obex).

Thus, extubation should only be performed once the patient is awake and able to demonstrate a positive gag reflex and cough. Over the first few hours and days following the surgery, the patient should be monitored with focus on the presence of gag reflex, cough, aspiration, and apnea.

6.10 Adjuvant Oncological Treatments

As stated above, treatment of LGBSG is multimodal, with an aim to perform a radical resection when possible; however, given the surgical-related morbidity in this highly functional region, a limited resection or a biopsy are often performed. This is not to state that a LGBSG should be actively treated, as spontaneous involution has been described, and many tumor residuals remain stable. However, for growing or symptomatic residual tumors, adjuvant treatment with chemotherapy or radiation should be considered [16, 18].

Different chemotherapeutic regimens have been described, which are similar to supratentorial and chiasmatic-hypothalamic low-grade tumors (such as vincristine-carboplatin) [21]. Over the recent years, newer drugs, aimed at the BRAF and MEK pathways have been implemented as secondary treatment lines, depending on the molecular profile of the tumor [22].

Radiotherapy has been applied in treating LGBSG too [18]. Generally, radiation is precluded for the younger ages due to secondary brain injury and the potential to induce secondary tumors. Thus, in children under 10 years of age, chemotherapy will usually be the primary adjuvant treatment. Various radiation technologies exist such as radiosurgery, proton beam therapy, among others [23]. The discussion on these technologies is beyond the scope of this chapter.

6.11 Outcome and Prognostic Factors

In a recent long-term follow-up study of pediatric LGBSG, the median OS was nearly 15 years, with a 1-, 5-, and 10-year OS of 85%, 67%, and 59%, respectively [9]. GTR was associated with improved OS compared to biopsy. Improved OS was also linked to tumor grade. Location of the tumor was associated with OS and PFS, especially for focal intrinsic and cervico-medullary tumors. Other studies have

found even higher OS and PFS rates reaching 100% and 70% over 10 years, respectively [16, 18].

Molecular markers, such as BRAF V600E mutations, have been shown to be a risk factor for ganglioglioma grade I recurrence [24]. Similar mutations have been shown to be a risk factor for the malignant transformation of LGG, including those in the posterior fossa [25].

6.12 Follow-Up Modalities

The standard follow-up method is by conventional MRI. However, in recent years, more accurate techniques such as volumetrics have been applied to measure the tumor size. This enables a better understanding of the true growth rate and may aid in decision-making regarding treatment timing.

In addition to the radiological follow-up, recent studies underlined the need for functional and cognitive follow-up in patients with a history of pediatric LGBSG [4, 26]. According to these studies, a significant proportion of these patients suffer from various cognitive deficits and neurological decline, often associated with a lower baseline function at diagnosis [4]. Thus, awareness among the general medical practitioners to the importance of early diagnosis and treatment of LGBSG may reduce the long-term morbidity.

6.13 Adult Low-Grade Brainstem Tumors

Most brainstem gliomas present in childhood and are low-grade, whereas adult brainstem tumors are rare [27]. LGBSG tend to occur in younger adults, present over a longer course, and are located in the pons with an exophytic component, compared to high-grade tumors [28]. Similar to children, some high-grade tumors in adults may resemble LGBSG and present as focal exophytic tumors too [29]. LGBSG in adults include a histopathological differential diagnosis similar to that in the pediatric group [27, 28, 30]. Generally speaking, presenting symptoms are similar to those in the pediatric tumors and are usually of subacute-to-chronic nature.

Non-invasive diagnosis is made using imaging, including MRS and PET, and is generally similar to the pediatric modalities. However, differential diagnosis in adults should also include ischemic changes, demyelinating diseases, and metabolic diseases (e.g., central pontine myelinolysis) [31]. Other pathologies, such as metastases, hemangioblastomas, and vascular lesions should be contemplated too.

Similar to the pediatric group, molecular profiling of adult BSG correlates with prognosis. H3 K27 M mutations define a subgroup of isocitrate dehydrogenase (IDH)-wild-type gliomas behaving like a grade IV glioma, despite a low-grade histopathological diagnosis [32, 33].

As opposed to children, chemotherapy is less effective for adult-related LGBSG, and radiation is commonly administered [34]. Other treatments, such as interstitial brachytherapy have been described [35]; however, they are not widely accepted.

6.14 Conclusion

Low-grade brainstem gliomas constitute a heterogeneous pathological entity. The main factors affecting tumor growth, treatment, and patient outcomes include tumor location, clinical course, presence of hydrocephalus, and radiological characteristics.

Treatment of LGBSG is multimodal. Some lesions are followed up conservatively. The role of surgery and oncological treatments (chemotherapy and radiation) have been discussed in this chapter.

References

1. Constantini S, Epstein F. Surgical indication and technical considerations in the management of benign brain stem gliomas. *J Neuro-Oncol.* 1996;28(2–3):193–205.
2. Epstein F, Constantini S. Practical decisions in the treatment of pediatric brain stem tumors. *Pediatr Neurosurg.* 1996;24(1):24–34.
3. Morota N, Deletis V, Lee M, Epstein FJ. Functional anatomic relationship between brain-stem tumors and cranial motor nuclei. *Neurosurgery.* 1996;39(4):787–93; discussion 93–4.
4. Sadighi ZS, Curtis E, Zabrowski J, Billups C, Gajjar A, Khan R, et al. Neurologic impairments from pediatric low-grade glioma by tumor location and timing of diagnosis. *Pediatr Blood Cancer.* 2018;65(8):e27063.
5. Klimo P Jr, Nesvick CL, Broniscer A, Orr BA, Choudhri AF. Malignant brainstem tumors in children, excluding diffuse intrinsic pontine gliomas. *J Neurosurg Pediatr.* 2016;17(1):57–65.
6. Zagzag D, Miller DC, Knopp E, Farmer JP, Lee M, Biria S, et al. Primitive neuroectodermal tumors of the brainstem: investigation of seven cases. *Pediatrics.* 2000;106(5):1045–53.
7. Roth J, Chaichana KL, Jallo G, Mirone G, Cinalli G, Constantini S. True aqueductal tumors: a unique entity. *Acta Neurochir.* 2015;157(2):169–77.
8. Tscherpel C, Dunkl V, Cecon G, Stoffels G, Judov N, Rapp M, et al. The use of O-(2-18F-fluoroethyl)-L-tyrosine PET in the diagnosis of gliomas located in the brainstem and spinal cord. *Neuro-Oncology.* 2017;19(5):710–8.
9. Ahmed KA, Laack NN, Eckel LJ, Orme NM, Wetjen NM. Histologically proven, low-grade brainstem gliomas in children: 30-year experience with long-term follow-up at Mayo Clinic. *Am J Clin Oncol.* 2014;37(1):51–6.
10. Fukuoka K, Yanagisawa T, Watanabe Y, Suzuki T, Shirahata M, Adachi J, et al. Brainstem oligodendroglial tumors in children: two case reports and review of literatures. *Childs Nerv Syst.* 2015;31(3):449–55.
11. Fried I, Hawkins C, Scheinemann K, Tsangaris E, Hesselson L, Bartels U, et al. Favorable outcome with conservative treatment for children with low grade brainstem tumors. *Pediatr Blood Cancer.* 2012;58(4):556–60.
12. Kickingereeder P, Willeit P, Simon T, Ruge MI. Diagnostic value and safety of stereotactic biopsy for brainstem tumors: a systematic review and meta-analysis of 1480 cases. *Neurosurgery.* 2013;72(6):873–81; discussion 82; quiz 82.

13. Li KW, Roonprapunt C, Lawson HC, Abbott IR, Wisoff J, Epstein F, et al. Endoscopic third ventriculostomy for hydrocephalus associated with tectal gliomas. *Neurosurg Focus*. 2005;18(6A):E2.
14. Roth J, Constantini S. Combined rigid and flexible endoscopy for tumors in the posterior third ventricle. *J Neurosurg*. 2015;122(6):1341–6.
15. Souweidane MM, Morgenstern PF, Kang S, Tsiouris AJ, Roth J. Endoscopic third ventriculostomy in patients with a diminished prepontine interval. *J Neurosurg Pediatr*. 2010;5(3):250–4.
16. Upadhyaya SA, Koschmann C, Muraszko K, Venneti S, Garton HJ, Hamstra DA, et al. Brainstem low-grade gliomas in children-excellent outcomes with multimodality therapy. *J Child Neurol*. 2017;32(2):194–203.
17. Teo C, Siu TL. Radical resection of focal brainstem gliomas: is it worth doing? *Childs Nerv Syst*. 2008;24(11):1307–14.
18. Klimo P Jr, Pai Panandiker AS, Thompson CJ, Boop FA, Qaddoumi I, Gajjar A, et al. Management and outcome of focal low-grade brainstem tumors in pediatric patients: the St. Jude experience. *J Neurosurg Pediatr*. 2013;11(3):274–81.
19. Cavalheiro S, Yagmurlu K, da Costa MD, Nicacio JM, Rodrigues TP, Chaddad-Neto F, et al. Surgical approaches for brainstem tumors in pediatric patients. *Childs Nerv Syst*. 2015;31(10):1815–40.
20. Phillips NS, Sanford RA, Helton KJ, Boop FA, Zou P, Tekautz T, et al. Diffusion tensor imaging of intraaxial tumors at the cervicomedullary and pontomedullary junctions. Report of two cases. *J Neurosurg*. 2005;103(6 Suppl):557–62.
21. Ronghe M, Hargrave D, Bartels U, Tabori U, Vaidya S, Chandler C, et al. Vincristine and carboplatin chemotherapy for unresectable and/or recurrent low-grade astrocytoma of the brainstem. *Pediatr Blood Cancer*. 2010;55(3):471–7.
22. Green AL, Kieran MW. Pediatric brainstem gliomas: new understanding leads to potential new treatments for two very different tumors. *Curr Oncol Rep*. 2015;17(3):436.
23. Liao CH, Pan DH, Yang HC, Wu HM, Ho DM, Wong TT, et al. Gamma knife radiosurgery as a treatment modality for low-grade pediatric brainstem gliomas: report of two cases. *Childs Nerv Syst*. 2012;28(1):175–8.
24. Chen X, Pan C, Zhang P, Xu C, Sun Y, Yu H, et al. BRAF V600E mutation is a significant prognosticator of the tumour regrowth rate in brainstem gangliogliomas. *J Clin Neurosci*. 2017;46:50–7.
25. Mistry M, Zhukova N, Merico D, Rakopoulos P, Krishnatry R, Shago M, et al. BRAF mutation and CDKN2A deletion define a clinically distinct subgroup of childhood secondary high-grade glioma. *J Clin Oncol*. 2015;33(9):1015–22.
26. Clark KN, Ashford JM, Pai Panandiker AS, Klimo P, Merchant TE, Billups CA, et al. Cognitive outcomes among survivors of focal low-grade brainstem tumors diagnosed in childhood. *J Neuro-Oncol*. 2016;129(2):311–7.
27. Salmaggi A, Fariselli L, Milanesi I, Lamperti E, Silvani A, Bizzi A, et al. Natural history and management of brainstem gliomas in adults. A retrospective Italian study. *J Neurol*. 2008;255(2):171–7.
28. Tasic G, Repac N, Nikolic I, Bogosavljevic V, Scepanovic V, Janicijevic A, et al. Adult brainstem gliomas: retrospective analysis of 51 patients. *Turk Neurosurg*. 2017;27(4):558–62.
29. Das KK, Bettaswamy GP, Mehrotra A, Jaiswal S, Jaiswal AK, Behari S. Dorsally exophytic glioblastoma arising from the medulla oblongata in an adult presenting as 4(th) ventricular mass. *Asian J Neurosurg*. 2017;12(2):224–7.
30. Lagares A, Gomez PA, Lobato RD, Ricoy JR, Ramos A, de la Lama A. Ganglioglioma of the brainstem: report of three cases and review of the literature. *Surg Neurol*. 2001;56(5):315–22; discussion 22–4.
31. Purohit B, Kamli AA, Kollias SS. Imaging of adult brainstem gliomas. *Eur J Radiol*. 2015;84(4):709–20.
32. Meyronet D, Esteban-Mader M, Bonnet C, Joly MO, Uro-Coste E, Amiel-Benouaich A, et al. Characteristics of H3 K27M-mutant gliomas in adults. *Neuro-Oncology*. 2017;19(8):1127–34.

33. Daoud EV, Rajaram V, Cai C, Oberle RJ, Martin GR, Raisanen JM, et al. Adult brainstem gliomas with H3K27M mutation: radiology, pathology, and prognosis. *J Neuropathol Exp Neurol*. 2018;77(4):302–11.
34. Hundsberger T, Tonder M, Hottinger A, Brugge D, Roelcke U, Putora PM, et al. Clinical management and outcome of histologically verified adult brainstem gliomas in Switzerland: a retrospective analysis of 21 patients. *J Neuro-Oncol*. 2014;118(2):321–8.
35. Lopez WO, Trippel M, Doostkam S, Reithmeier T. Interstitial brachytherapy with iodine-125 seeds for low grade brain stem gliomas in adults: diagnostic and therapeutic intervention in a one-step procedure. *Clin Neurol Neurosurg*. 2013;115(8):1451–6.

Chapter 7

High-Grade Tumors of the Brainstem (Except DIPG)



Soma Sengupta, Daniel Pomeranz Krummel, Brent D. Weinberg,
and Tobey J. MacDonald

Abbreviations

ATRT	Atypical teratoid rhabdoid tumor
CCNU	Lomustine
CNS-PNET	Central nervous system primitive neuroectodermal tumor
DIPG	Diffuse intrinsic pontine glioma
ETMR	Embryonal tumor with multilayered rosettes
FISH	Fluorescence in situ hybridization
GBM	Glioblastoma
HDC	High-dose chemotherapy
IDH1	Isocitrate dehydrogenase-1
IMRT	Intensity-modulated radiation therapy
MGMT	O ⁶ -methylguanine–DNA methyltransferase
MRI	Magnetic resonance imaging
OS	Overall survival
PCV	Vincristine
PFS	Progression-free survival
PTEN	Phosphatase and tensin homolog
WHO	World Health Organization

S. Sengupta (✉)
University of Cincinnati Brain Tumor Center, Cincinnati, OH, USA

D. P. Krummel
University of Cincinnati Medical Center, Cincinnati, OH, USA

B. D. Weinberg
Department of Radiology and Imaging Sciences, Emory University School of Medicine,
Atlanta, GA, USA

T. J. MacDonald
Department of Pediatrics, Emory University School of Medicine, Aflac Cancer & Blood
Disorders Center, and Children’s Healthcare of Atlanta, Atlanta, GA, USA

7.1 Adult Malignant Brainstem Tumors

7.1.1 Introduction

Hare and Wolf (1934) discussed intramedullary tumors of the brainstem, based on Cushing's clinical documentation of brainstem tumors [1]. White (1963) evaluated a series of 44 patients accumulated over 31 years at the Neurological Institute in New York, and the mean age of the patients was 42 years (range is 17–68 years); most of those who were studied pathologically had astrocytic tumors of various grades [2]. The clinical presentation and course of patients in this adult brainstem glioma series was comparable to the pediatric series studied earlier at the same institution [2]. Adult brainstem gliomas are rare tumors (~2%) and are slightly more common in males in their 30s [3]. Over 60% of adult brainstem tumors are found in the pons, about a quarter of them are found in the medulla oblongata, and the rest are encountered in the midbrain [4]. It is also important to note that brainstem lesions that are diffuse have a wide differential, including tumors such as gliomas and lymphomas, vasculitis, brainstem injury, infections, central pontine myelinolysis, amongst others [5].

7.1.2 Clinical Presentation

Brainstem gliomas in adults are subdivided based upon clinicopathological and radiographic characteristics: diffuse intrinsic, low-grade brainstem gliomas; focal, malignant brainstem gliomas; focal tectal gliomas; and exophytic growing tumors [4]. The focus of this section is not on the diffuse tumor type, but all other types of tumors, which are less frequent: focal malignant brainstem gliomas (~25%), tectal gliomas (~3–8%) and other brainstem tumors (~15%) [4]. The clinical signs correlate with the anatomy of the lesion, and these include cranial nerve dysfunction (87% of patients), gait disturbances (61% of patients), and long-tract signs (~58% of patients). Headaches and raised intracranial pressure symptoms are variable in this patient group [5]. Patients older than 40 with a higher pathological grade and a non-Caucasian ethnicity have been identified as unfavorable prognostic factors [6]. In a study conducted by Dellaretti and colleagues, the histological grade was a significant prognostic factor in terms of patient survival [7].

7.1.3 Imaging and Histopathological Diagnosis

7.1.3.1 Focal Malignant Brainstem Gliomas

These tend to be localized, discrete masses, and can occupy <50% of the greatest dimension of the brainstem [4]. These tumors occur in patients older than 40 and are characterized by the rapid onset and progression of brainstem dysfunction [8].

Radiographically, these tumors have been described to exhibit ring-like enhancement of contrast that is ill-defined (Fig. 7.1) [4]. Neuropathology of these tumors is often consistent with anaplastic astrocytomas (World Health Organization (WHO) Grade III) or glioblastomas (GBM) (WHO Grade IV tumors) [9, 10]. As suggested by the high grades of these tumors, the prognosis is poor and median survival is 12.5 months [8]. Molecular markers that should be checked for these tumors include: O⁶-methylguanine–DNA methyltransferase (MGMT), phosphatase and tensin

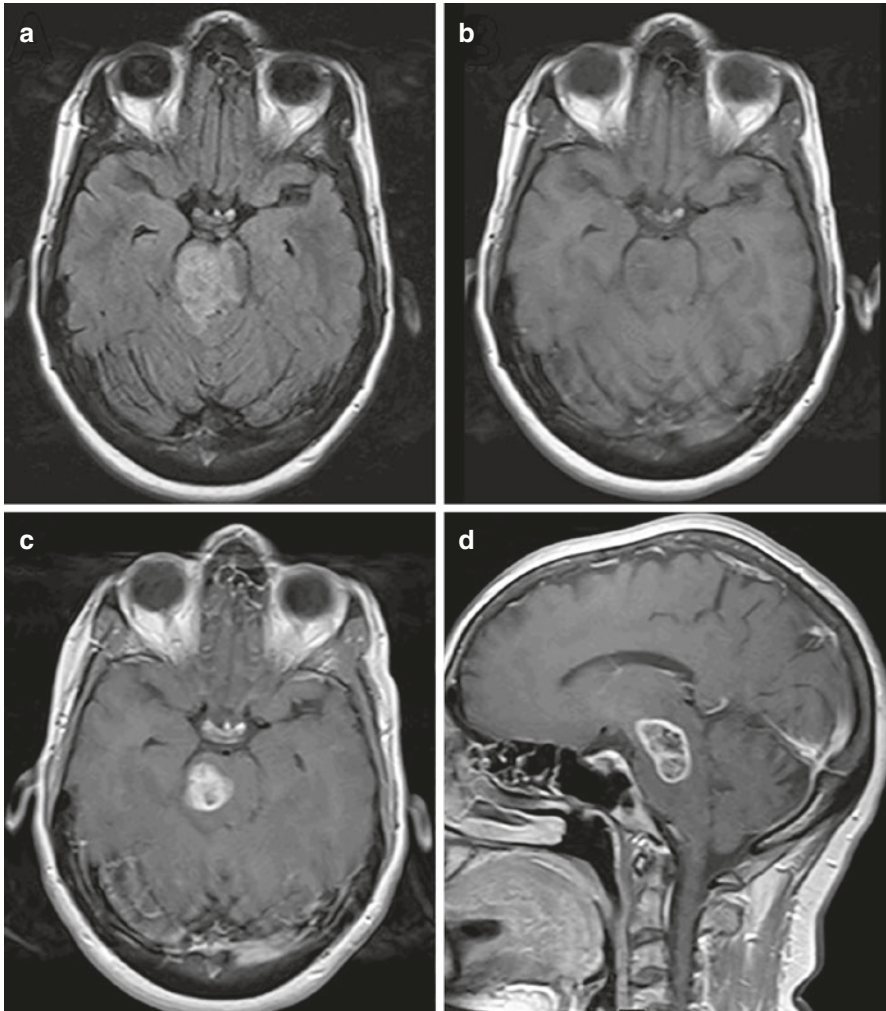


Fig. 7.1 Midbrain and pontine high-grade glioma. (a) Fluid-attenuated inversion recovery (FLAIR) demonstrates an expansile mass in the right anterior midbrain and pons. (b) Pre- and (c, d) post-contrast T1-weighted images show a mass with heterogenous and avid enhancement with central necrosis. This mass was treated as a high-grade glioma without biopsy

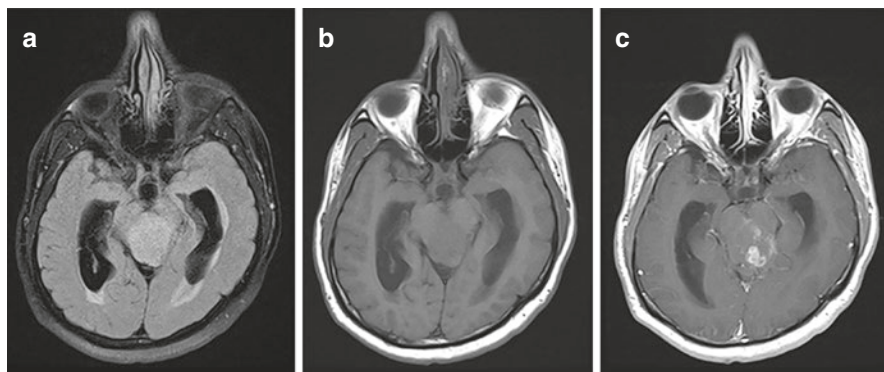


Fig. 7.2 Midbrain and tectal glioblastoma (biopsy-proven). (a) FLAIR demonstrates an expansile mass in the superior aspect of the midbrain and tectum. (b) Pre- and (c) post-contrast T1-weighted images show a mass with heterogenous and avid enhancement

homolog (PTEN) loss, R132H isocitrate dehydrogenase-1 (IDH1) mutation, epidermal growth factor receptor vIII variant, histone H3.3, and activating A receptor type 1 mutations [4].

7.1.3.2 Focal Tectal Gliomas

The presentation is often innocuous and can be incidentally identified. The most common presentation is headaches, and patients are found to have obstructive hydrocephalus. Due to their clinical presentation and radiologic appearance (Fig. 7.2), surgical biopsy is often deemed unnecessary. If biopsied, they tend to be WHO Grade II oligoastrocytomas, and higher grades are exceedingly rare [9]. These types of tumors are typically indolent and are associated with a more favorable prognosis. In a recent review, survival has been around 84 months irrespective of tumor treatment [4].

7.1.3.3 Other Brainstem Gliomas

These include dorsally exophytic brainstem gliomas, oligodendrogliomas, and glial tumors associated with Neurofibromatosis type 1. Note that in adults, these exophytic gliomas are usually contrast-enhancing and highly aggressive, thus surgical resection and pathologic evaluation is key, if possible [4].

7.1.4 Chemotherapy

Unfortunately, the role of chemotherapy in treating adults with brainstem gliomas is unclear. Salmaggi et al. described a retrospective analysis of 20 patients who received either temozolomide (18 patients received 75 mg/m² temozolomide during

radiation, followed by adjuvant temozolomide 200 mg/m², and the 2 other patients received combined procarbazine, lomustine (CCNU) and vincristine (PCV) (procarbazine 75 mg/m² days 8–21, CCNU 110 mg/m² on day 1, and vincristine 1 mg/m² on days 8–28) with radiation (48–54 Gy in 1.8 Gy fractions) [3]. Only 50% of these patients had disease stabilization by imaging, and the patients who received PCV had grade 3 and 4 myelotoxicity, in addition to 6 of the patients who received temozolomide who also had the same level of myelotoxicity. At the time of recurrence, the role of chemotherapy is even less clear, the use of PCV, carboplatin, cisplatin, salvage bevacizumab, etoposide and paclitaxel have been reported, and these options cause significant chemotoxicity in patients, who need to be carefully monitored [4].

7.1.5 Conclusion

Brainstem gliomas are just as heterogeneous in terms of genetic complexity as their supratentorial counterparts [11]. In adult brainstem gliomas, the most significant gene alterations are IDH1 and H3F3A(K27M). One hopes that more targeted therapies are an option in the future, as opposed to concomitant radiation and temozolomide, and during recurrent salvage radiotherapy. The rarity of IDH1 mutations in brainstem gliomas is also emphasized in an earlier work by Theeler et al. [12]. Interestingly, in 1998, Landolfi et al. mentioned that adults with brainstem gliomas fare better in terms of survival than children [13]. In addition, they recommended that patients with tectal or cervicomedullary tumors can be managed by observation alone, and very little has changed in terms of current management since these authors initially recommended this conservative strategy.

7.2 Pediatric Malignant Brainstem Tumors, Excluding Diffuse Intrinsic Pontine Gliomas (DIPG)

7.2.1 Introduction

Neoplasms that arise in the brainstem account for 10–15% of pediatric brain tumors [14, 15]. The majority of these tumors (80%) are DIPG, with the remainder being predominantly focal low-grade gliomas. Thus, non-DIPG pediatric malignant brainstem tumors are exceedingly rare. In one retrospective review from a single institution, non-DIPG malignant brainstem tumors constituted less than 5% of all pediatric brainstem tumors [16]. Non-DIPG malignant histologic types of the brainstem in children have been recognized as either: (1) high-grade glial neoplasms (~60%), including WHO Grade IV glioblastoma (GBM) or WHO Grade III anaplastic astrocytoma, oligodendroglioma and ganglioglioma, occurring within the midbrain,

medulla or eccentrically displaced within less than one-third of the pons (non-DIPG); or (2) embryonal tumors (~40%), including atypical teratoid rhabdoid tumor (ATRT), embryonal tumor with multilayered rosettes (ETMR), and what had previously been classified as central nervous system primitive neuroectodermal tumor (CNS-PNET) [14–16]. In 2016, the WHO classification for CNS tumors removed CNS-PNET as a unique histological entity based on evidence from molecular profiling studies showing that the majority of these tumors are actually a diverse group of other known histologic entities, including high-grade gliomas (HGG) [17, 18]. Furthermore, according to the 2016 revised WHO classification, midline gliomas that harbor H3K27M mutation are now considered a single histologic entity termed as diffuse midline glioma (WHO Grade IV), irrespective of location, further blurring what constitutes a DIPG from a non-DIPG. Thus, the precise histologic types of malignant non-DIPG brainstem tumors and their incidence are unclear. Individual case reports have also described the presence of astroblastoma and angiocentric glioma in the brainstem of children [19, 20]; however, this review will attempt to summarize the key features in the diagnosis and management of the most commonly encountered non-DIPG pediatric malignant brainstem tumors.

7.2.2 *Clinical Presentation*

The mean age of non-DIPG brainstem tumors in children has been reported to be approximately 7.5 years (peak age range is 5–10 years), with the majority (90%) occurring in those less than 18 years of age [14–16]. The tumor location is either the pons or pontocerebellar junction in over half of the cases, followed by the medulla or pontomedullary junction (~20%), and finally the midbrain (~15%) [14–16]. Nearly half of the cases will have an exophytic portion of the tumor on imaging [15]. The most common presenting signs and symptoms relate to tumor location within the brainstem, irrespective of histology, and include cranial nerve deficits, pyramidal tract signs, and ataxia [14–16, 21]. In general, patients typically present with progressive neurological symptoms of short duration.

7.2.3 *Imaging and Histopathological Diagnosis*

7.2.3.1 **High-Grade Gliomas (HGG)**

The majority of non-DIPG HGG of the brainstem will present in the middle cerebellar peduncle junction or pontomedullary junction (80–90%); however, it is unclear whether the HGG tumors in these locations that harbor the H3K27M mutation, a hallmark of DIPG, would now be considered eccentrically displaced “atypical-appearing DIPG” given the 2016 WHO re-classification of H3K27M-mutated diffuse midline gliomas as a single entity [17]. The remaining HGG (10–20%) occur in the midbrain.

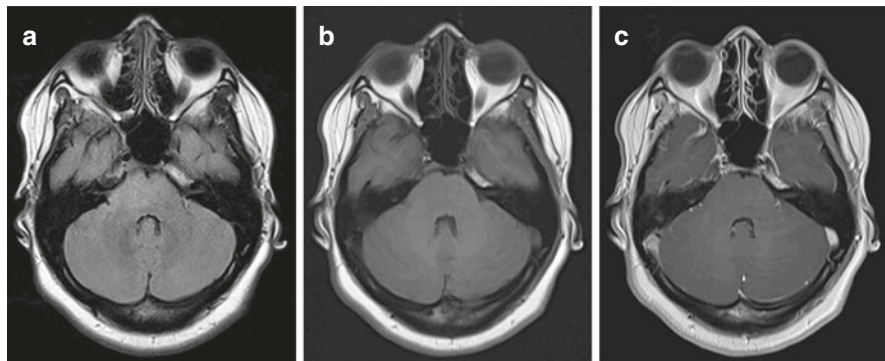


Fig. 7.3 Midline pontomedullary glioma, H3K27M-mutant. (a) FLAIR demonstrates an expansile mass in the right anterior and midline pons. (b) Pre- and (c) post-contrast T1-weighted images show a mass with no post-contrast enhancement. This lesion was biopsied and was found to be an H3K27M-mutated midline glioma

On magnetic resonance imaging (MRI), these tumors have the typical characteristics of HGG as in other locations (Fig. 7.3). The imaging features include heterogeneous signal intensities, prominent heterogeneous and ring-like enhancement with poorly defined margins, and multi-centricity or extra-axial metastases. Likewise, the histopathology of brainstem HGGs is identical to that of the corresponding Grade III and Grade IV HGGs in other locations. Histologic diagnostic features include infiltrative tumor cells with nuclear atypia, high mitotic activity, pseudopalisading necrosis, and florid microvascular proliferation.

7.2.3.2 Atypical Teratoid Rhabdoid Tumor (ATRT)

ATRT is a rare, highly malignant WHO Grade IV tumor that occurs in children and adults but has a predilection for infants, with 70% presenting in children <1 year old and 90% under the age of 3 years [22]. On MRI, ATRT is generally circumscribed, with heterogeneous contrast enhancement and signal intensity, usually secondary to areas of hemorrhage and necrosis (Fig. 7.4). Leptomeningeal spread is a common radiological finding, being present in approximately a quarter of cases at diagnosis [22].

Histological heterogeneity is characteristic of ATRT, with neuroectodermal, mesenchymal, and, rarely, epithelial differentiation being evident [22]. The neuroectodermal component can closely mimic medulloblastoma. Most ATRTs are composed of sheets of pleomorphic cells that typically have large nuclei with open, vesicular chromatin and prominent nucleoli, and a small-to-moderate amount of lightly eosinophilic cytoplasm. Many cases have at least focal rhabdoid morphology; however, the presence of rhabdoid morphology is not required for the diagnosis of ATRT [22].

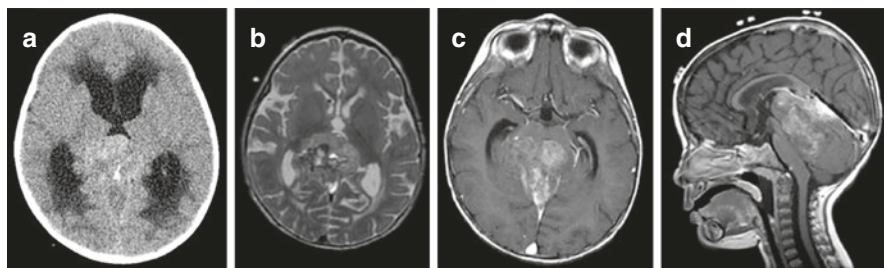
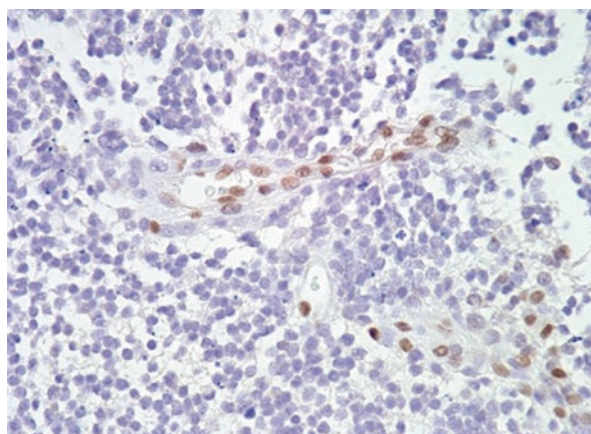


Fig. 7.4 Atypical teratoid rhabdoid tumor (ATRT). (a) Computed tomography (CT) image showing a hyperdense and partially calcified mass with obstructive hydrocephalus. (b) T2-weighted image demonstrates a markedly heterogenous mass. (c) Axial and (d) sagittal post-contrast T1-weighted images show a mass with heterogenous and avid enhancement involving the tectum and superior vermis with compression of the midbrain and pons

Fig. 7.5 Atypical teratoid rhabdoid tumor (ATRT). Immunohistochemistry demonstrates loss of INI1 expression in tumor cells, while native endothelial cells retain staining (brown) for INI1



Unlike other CNS neoplasms, ATRTs demonstrate remarkable uniformity in genetic alterations of the *SMARCB1* locus on chromosome 22q11.2 [23]. Reported alterations include homogenous and heterozygous deletions, loss of heterozygosity, and mutations of *SMARCB1*, especially in exons 5 or 9 [23]. Since loss of expression or function of INI1 is thought to be a key molecular event in the formation of ATRT, demonstration of its loss or mutation is a reliable way to diagnose ATRT in patients who present with an embryonal brain tumor (Fig. 7.5). Use of fluorescence in situ hybridization (FISH) along with genomic sequencing permits identification of more than 75% of ATRTs [24]. While there are embryonal brain tumors that exhibit histologies that are consistent with ATRT but positive immunohistochemical staining for the *SMARCB1* protein, INI1, these are considered even more rare and are thought to represent only 2% of all ATRTs [25]. ATRTs that retain wild-type *SMARCB1* and its protein product often have a mutation in *SMARCA4* and its related chromatin modeling protein, BRG1, which, along with *SMARCB1*, is an

important component of the SWI/SNF complex, which plays an important role in lineage specification and stem cell maintenance [26].

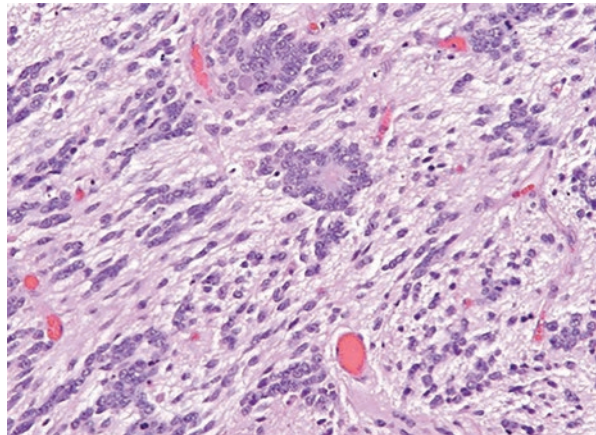
7.2.3.3 Embryonal Tumor with Multilayered Rosettes (ETMR) and Historical Central Nervous System Primitive Neuroectodermal Tumor (CNS-PNET)

Recent identification of focal amplification of a micro-RNA cluster on chromosome 19q13.42 (C19MC) has led to a new designation of ETMR (ETMR, C19MC-altered), which encompasses medulloepithelioma, ependyoblastoma, and the previously-described entity, embryonal tumor with abundant neuropil and true rosettes (ETANTR) [27, 28]. ETMR occurs in young children, with a mean age of about 2 years, reaching up to almost 5 years, with a female predominance of around 2:1 female-to-male ratio. The most common MRI appearance is a heterogeneously-enhancing, well-circumscribed, solid mass [29].

The histological appearance consists of islands of embryonal tumor cells in a sea of neuropil-like matrix, forming luminal or “ependyoblastic” rosettes (Fig. 7.6). The ependyoblastic rosettes appear in both the hypo- and hyper-cellular areas, and are formed of multi-layered, elongated tumor cells that are arranged radially around a well-defined, round to slit-like lumen. Similar to nodular medulloblastomas, ETANTR tumor cells show varying levels of differentiation, from embryonal within the areas of cellularity to neurocytic, and even occasionally ganglionic, within the hypocellular areas. Although the undifferentiated cells within the clusters generally fail to stain for neuronal or glial markers, NeuN, synaptophysin and neurofilament staining can be strong within the more differentiated cells of the neuropil-like areas.

CNS-PNETs, which account for 1% of pediatric brain tumors, are a heterogeneous group of undifferentiated, highly malignant tumors that are histologically

Fig. 7.6 Embryonal tumor with multilayered rosettes (ETMR). Although the hematoxylin and eosin stain demonstrates relatively low cellularity compared to other CNS malignancies, ETMR is a highly aggressive embryonal tumor



composed of neuroepithelial-like cells. MRI characteristics of CNS-PNETs include a focal intrinsic or exophytic non-enhancing brainstem tumor with low T1- and high T2-weighted signals [16]. Hydrocephalus and leptomeningeal dissemination are common presenting features. More recently, methylation profiling studies have found that CNS-PNETs do not cluster distinctly from other pediatric CNS tumors. Among the 323 analyzed CNS-PNETs, 61% were re-classified as another tumor type based on molecular profiling. Of the remaining CNS-PNETs, 11% clustered with known ETMRs, 15% formed small clusters that failed to associate with each other or with other known pediatric CNS tumors, and 24% formed four distinct, novel entities: CNS neuroblastoma with *FOXR2* activation (14%), CNS Ewing sarcoma family tumor with *CIC* alteration (4%), CNS high-grade neuroepithelial tumor with *MNI* alteration (3%), and CNS high-grade neuroepithelial tumor with *BCOR* alteration (3%) [18]. The 2016 WHO revised classification of CNS tumors thereby removed the term CNS-PNET; thus, the actual occurrence and distribution of these distinct entities within the brainstem is unknown.

7.2.4 Treatment and Outcome

It is estimated that the majority of children (>90%) with non-DIPG high-grade tumors of the brainstem can successfully undergo either surgical biopsy (open or stereotactic needle) or partial tumor resection as part of the initial management plan [14–16]. In the absence of non-surgical treatment, gross total resection of malignant brainstem tumors at the time of diagnosis is not feasible. The treatments administered, and the associated outcomes, are specific for the tumor type (as described below); however, survival in general is dismal for this group of patients as a whole, with at least one report describing a median overall survival (OS) of 6.4 months following the diagnosis, and only 31% of patients surviving more than 1 year [15].

7.2.4.1 Atypical Teratoid Rhabdoid Tumor (ATRT)

ATRT is an aggressive tumor that carries a poor overall prognosis. Published studies report a median survival from 8 to 17 months from diagnosis. Two factors that have repeatedly been associated with a poor outcome are age less than 3 years at diagnosis and the presence of metastatic disease [30]. Treatment considerations for ATRT of the brainstem would be the same as that for non-brainstem ATRT. The role of conventional versus high-dose chemotherapy (HDC) with autologous stem cell rescue remains controversial. At least two published studies reported a greater than 50% survival when patients with an ATRT were treated with a carboplatin-thiotepa-based HDC regimen [31]. The only prospective, front-line ATRT study using a modified rhabdomyosarcoma-type IRS-III regimen along with intrathecal chemotherapy and either focal or cranio-spinal irradiation reported a 2-year progression-

free survival (PFS) and OS of 53% and 70%, respectively [32]. Also controversial are the role and timing of radiotherapy; some clinicians consider radiotherapy as crucial to the treatment of ATRT, while others prefer to defer the use of irradiation due to its potentially devastating side-effects on cognition when used in young children [33]. Data from St. Jude Children's Hospital lend support to the early use of irradiation for ATRT [30]. Overall, newer treatment regimens have improved the prognosis for ATRT and led to a long-term cure in a minority of patients. Due to the paucity of cases, it is not yet known whether the outcome is significantly different in brainstem ATRT compared to ATRT in other locations.

7.2.4.2 Embryonal Tumor with Multilayered Rosettes (ETMR) and Historical Central Nervous System Primitive Neuroectodermal Tumor (CNS-PNET)

Due to historically poor outcomes, children with CNS-PNET have been treated according to the high-risk arm of treatment protocols for medulloblastoma. Yet, 5-year survival has remained around 50–60% in children [34]. The median survival in patients with ETMR is 13 months from diagnosis, although clinical outcome has been accurately documented in only 48 patients to date [35]. In six patients with subtotal surgical resection and aggressive adjuvant therapy with radiation and/or chemotherapy, only one patient was reported alive without disease at 34 months after diagnosis following multiple resections and HDC [36]. Of the 48 cases reported to date, 6 children have survived beyond 30 months. The longest reported survival is 42 months [35]. Similar to other histologic entities, due to the rarity of this tumor type overall, it is unclear whether the outcome is different for brainstem ETMRs compared to ETMRs in non-brainstem locations. There is a case report of a 17-month-old boy with an ETANTR of the brainstem, and despite chemotherapy, the child died 3 months after initial diagnosis [37].

In a retrospective report of 83 children with brainstem CNS-PNETs treated between 1973–2013, the median OS was reported as 53 months [38]. A survival advantage was observed for patients older than 4 years of age, those who received surgery, chemotherapy and radiation, and those with gross or subtotal tumor resection. Another report described the outcome for 6 children with histologically-proven brainstem CNS-PNET and 2 with brainstem ependyoblastoma who were treated according to the multimodal HIT protocol therapy [21]. All patients had postoperative residual disease, including one with metastasis. All tumors progressed, with one exception, within 2.5–10.4 months. After progression, patients succumbed early to their disease resulting in a 1-year OS rate of 25%. The only surviving patient had a partially resected tumor, received chemotherapy and was reported without progression at 14 months after diagnosis [21]. With the recent evidence that the majority of PNETs are actually other known histologies, the optimal treatment and outcomes for each histologic type observed in the brainstem remains to be determined.

7.2.4.3 High-Grade Gliomas (HGG)

Treatment for HGG of the brainstem is identical to that for DIPG, namely, local irradiation of the tumor to 54 Gy in 1.8-Gy fractions using intensity-modulated radiation therapy (IMRT); this is administered alone, as standard therapy, or in conjunction with an investigational therapy on a clinical trial. As of yet, there has been no clinical benefit observed with any therapy apart from radiation. Multiple case reports indicate that secondary GBM with distinct histological features can arise after treatment for childhood medulloblastoma [39]. Other reports indicate that secondary HGG may result from malignant transformation of low-grade glial neoplasms, especially those harboring the BRAFV600E mutation and CDKN2A deletion [40]. Indeed, the majority of gangliogliomas of the brainstem have the BRAFV600E mutation, and HGG with this mutation may be treated with BRAF inhibitors on clinical trials evaluating the efficacy of these new agents [41]. The precise portion of these secondary HGG that arise in the brainstem secondary to radiation and/or underlying BRAFV600E mutation/CDKN2A deletion is unclear. However, secondary HGG of the brainstem appear to have a particularly dismal prognosis, with one report demonstrating median OS of 124 days compared to 6 months for the presumed primary HGG of the brainstem [15]. OS for brainstem HGG also appears to be worse than the median OS of 9–12 months for pediatric DIPG and HGG in non-brainstem locations [15].

7.2.5 Conclusion

Non-DIPG pediatric high-grade tumors of the brainstem are uncommon, but tend to occur in younger aged patients, almost always present with at least cranial neuropathies of short duration, and typically have a very poor prognosis, with relatively rapid disease progression despite multi-modality therapy. Larger prospective studies are needed, especially for the group of tumors that had been classified as CNS-PNETs, given the new molecular information indicating that these are actually composed of a highly diverse group of different histologic tumors.

References

1. Hare CC, Wolf A. Intramedullary tumors of the brainstem. *Arch Neur Psych*. 1934;32(6):1230–52.
2. White HH. Brainstem tumors occurring in adults. *Neurology*. 1963;13:292–300.
3. Salmaggi A, Fariselli L, Milanese I, Lamperti E, Silvani A, Bizzi A, et al. Natural history and management of brainstem gliomas in adults. A retrospective Italian study. *J Neurol*. 2008;255(2):171–7.
4. Eisele SC, Reardon DA. Adult Brainstem Gliomas. *Cancer*. 2016;122:2799–809.

5. Guzmán-De-Villoria JA, Ferreiro-Argüelles C, Fernández-García P. Differential diagnosis of T2 hyperintense brainstem lesions: Part 2. Diffuse lesions. *Semin Ultrasound CT MR*. 2019;31(3):260–74.
6. Kesari S, Kim RS, Markos V, Drappatz J, Wen PY, Pruitt AA. Prognostic factors in adult brainstem gliomas: a multicenter, retrospective analysis of 101 cases. *J Neuro-Oncol*. 2008;88:175–83.
7. Dellaretti M, Reyns N, Touzet G, Doublet F, Gusmão S, Pereira JL, Blond S. Diffuse brainstem glioma: prognostic factors. *J Neurosurg*. 2012;117:810–4.
8. Babu R, Kranz PG, Karikari IO, Friedman AH, Adamson C. Clinical characteristics and treatment of brainstem gliomas in elderly patients. *J Clin Neurosci*. 2013;20:1382–6.
9. Guillamo JS, Monjour A, Taillandier L, Devaux B, Varlet P, Haie-Meder C, et al. Brainstem gliomas in adults: prognostic factors and classification. *Brain*. 2001;124:2528–39.
10. Stark AM, Maslehaty H, Hugo HH, Mahvash M, Mehdorn HM. Glioblastoma of the cerebellum and brainstem. *J Clin Neurosci*. 2010;17:1248–51.
11. Hu J, Western S, Kesari S. Brainstem gliomas in adults. *Front Oncol*. 2016;6:180.
12. Theeler BJ, Ellezam B, Melguizo-Gavilanes I, de Groot JF, Mahajan A, Aldape KD, et al. Adult brainstem gliomas: correlation of clinical and molecular features. *J Neurol Sci*. 2015;353(1–2):92–7.
13. Landolfi JC, Thaler HT, DeAngelis LM. Adult brainstem gliomas. *Neurology*. 1998;51(4):1136–9.
14. Xue Z, Kong L, Pan CC, Wu Z, Zhang JT, Zhang LW. Fluorescein-guided surgery for pediatric brainstem gliomas: preliminary study and technical notes. *J Neurol Surg B Skull Base*. 2018;79(Suppl 4):S340–6.
15. Klimo P Jr, Nesvick CL, Broniscer A, Orr BA, Choudhri AF. Malignant brainstem tumors in children, excluding diffuse intrinsic pontine gliomas. *J Neurosurg Pediatr*. 2016;17(1):57–65.
16. Zagzag D, Miller DC, Knopp E, Farmer JP, Lee M, Biria S, et al. Primitive neuroectodermal tumors of the brainstem: investigation of seven cases. *Pediatrics*. 2000;106(5):1045–53.
17. Fuller CE, Jones DTW, Kieran MW. New classification for central nervous system tumors: implications for diagnosis and therapy. *Am Soc Clin Oncol Educ Book*. 2017;37:753–63.
18. Sturm D, Orr BA, Toprak UH, Hovestadt V, Jones DTW, Capper D, et al. New brain tumor entities emerge from molecular classification of CNS-PNETs. *Cell*. 2016;164(5):1060–72.
19. Shin SA, Ahn B, Kim SK, Kang HJ, Nobusawa S, Komori T, et al. Brainstem astroblastoma with *MNI* translocation. *Neuropathology*. 2018;38:631–7.
20. Weaver KJ, Crawford LM, Bennett JA, Rivera-Zengotita ML, Pincus DW. Brainstem angiocentric glioma: report of 2 cases. *J Neurosurg Pediatr*. 2017;20(4):347–51.
21. Friedrich C, Warmuth-Metz M, von Bueren AO, Nowak J, Bison B, von Hoff K, et al. Primitive neuroectodermal tumors of the brainstem in children treated according to the HIT trials: clinical findings of a rare disease. *J Neurosurg Pediatr*. 2015;15(3):227–35.
22. Lau CS, Mahendraraj K, Chamberlain RS. Atypical teratoid rhabdoid tumors: a population-based clinical outcomes study involving 174 patients from the surveillance, epidemiology, and end results database (1973–2010). *Cancer Manag Res*. 2015;7:301–9.
23. Roberts CW, Biegel JA. The role of *SMARCB1/INI1* in development of rhabdoid tumor. *Cancer Biol Ther*. 2009;8:412–6.
24. Jalali GR, Vorstman JA, Errami A, Vijzelaar R, Biegel J, Shaikh T, et al. Detailed analysis of 22q11.2 with a high density MLPA probe set. *Hum Mutat*. 2008;29:433–40.
25. Fruhwald MC, Hasselblatt M, Wirth S, Köhler G, Schneppenheim R, Subero JI, et al. Non-linkage of familial rhabdoid tumors to *SMARCB1* implies a second locus for the rhabdoid tumor predisposition syndrome. *Pediatr Blood Cancer*. 2006;47:273–8.
26. Hasselblatt M, Nagel I, Oyen F, Bartelheim K, Russell RB, Schüller U, et al. *SMARCA4*-mutated atypical teratoid/rhabdoid tumors are associated with inherited germline alterations and poor prognosis. *Acta Neuropathol*. 2014;128:453–6.

27. Korshunov A, Remke M, Gessi M, Ryzhova M, Hielscher T, Witt H, et al. Focal genomic amplification at 19q13.42 comprises a powerful diagnostic marker for embryonal tumors with ependymoblastic rosettes. *Acta Neuropathol.* 2010;120:253–60.
28. Korshunov A, Sturm D, Ryzhova M, Hovestadt V, Gessi M, Jones DT, et al. Embryonal tumor with abundant neuropil and true rosettes (ETANTR), ependymoblastoma, and medulloepithelioma share molecular similarity and comprise a single clinicopathological entity. *Acta Neuropathol.* 2014;128:279–89.
29. Gessi M, Giangaspero F, Lauriola L, Gardiman M, Scheithauer BW, Halliday W, et al. Embryonal tumors with abundant neuropil and true rosettes: a distinctive CNS primitive neuroectodermal tumor. *Am J Surg Pathol.* 2009;33:211–7.
30. Tekautz TM, Fuller CE, Blaney S, Fouladi M, Broniscer A, Merchant TE, et al. Atypical teratoid/rhabdoid tumors (ATRT): improved survival in children 3 years of age and older with radiation therapy and high-dose alkylator-based chemotherapy. *J Clin Oncol.* 2005;23:1491–9.
31. Gardner SL, Asgharzadeh S, Green A, Horn B, McCowage G, Finlay J. Intensive induction chemotherapy followed by high dose chemotherapy with autologous hematopoietic progenitor cell rescue in young children newly diagnosed with central nervous system atypical teratoid rhabdoid tumors. *Pediatr Blood Cancer.* 2008;51:235–40.
32. Chi SN, Zimmerman MA, Yao X, Cohen KJ, Burger P, Biegel JA, et al. Intensive multimodality treatment for children with newly diagnosed CNS atypical teratoid rhabdoid tumor. *J Clin Oncol.* 2009;27:385–9.
33. Chen YW, Wong TT, Ho DM, Huang PI, Chang KP, Shiau CY, et al. Impact of radiotherapy for pediatric CNS atypical teratoid/rhabdoid tumor (single institute experience). *Int J Radiat Oncol Biol Phys.* 2006;64:1038–43.
34. Jakacki RI, Burger PC, Kocak M, Boyett JM, Goldwein J, Mehta M, et al. Outcome and prognostic factors for children with supratentorial primitive neuroectodermal tumors treated with carboplatin during radiotherapy: a report from the Children's Oncology Group. *Pediatr Blood Cancer.* 2015;62:776–83.
35. Mozes P, Hauser P, Hortobagyi T, Benyó G, Peták I, Garami M, et al. Evaluation of the good tumor response of embryonal tumor with abundant neuropil and true rosettes (ETANTR). *J Neuro-Oncol.* 2016;126:99–105.
36. La Spina M, Pizzolitto S, Skrap M, Nocerino A, Russo G, Di Cataldo A, et al. Embryonal tumor with abundant neuropil and true rosettes. A new entity or only variations of a parent neoplasms (PNETs)? This is the dilemma. *J Neuro-Oncol.* 2006;78:317–20.
37. Adamek D, Sofowora KD, Cwiklinska M, Herman-Sucharska I, Kwiatkowski S. Embryonal tumor with abundant neuropil and true rosettes: an autopsy case-based update and review of the literature. *Childs Nerv Syst.* 2013;29(5):849–54.
38. Chamdine O, Elhawary GAS, Alfaar AS, Qaddoumi I. The incidence of brainstem primitive neuroectodermal tumors of childhood based on SEER data. *Childs Nerv Syst.* 2018;34(3):431–9.
39. Wang Y, Song S, Su X, Wu J, Dai Z, Cui D, et al. Radiation-induced glioblastoma with rhabdoid characteristics following treatment for medulloblastoma: a case report and review of the literature. *Mol Clin Oncol.* 2018;9(4):415–8.
40. Mistry M, Zhukova N, Merico D, Rakopoulos P, Krishnatry R, Shago M, et al. BRAF mutation and CDKN2A deletion define a clinically distinct subgroup of childhood secondary high-grade glioma. *J Clin Oncol.* 2015;33(9):1015–22.
41. del Bufalo F, Carai A, Figà-Talamanca L, Pettorini B, Mallucci C, Giangaspero F, et al. Response of recurrent BRAFV600E mutated ganglioglioma to Vemurafenib as single agent. *J Transl Med.* 2014;12:356.

Chapter 8

Diffuse Midline Glioma – Diffuse Intrinsic Pontine Glioma



Mohammad Hassan A. Noureldine, Nir Shimony, and George I. Jallo

Abbreviations

ADC	Apparent diffusion coefficient
BBB	Blood-brain barrier
CD44	Cluster of differentiation 44
CED	Convection-enhanced delivery
Cho/Cr	Choline/creatine
CN	Cranial nerve
CNS	Central nervous system
CSF	Cerebrospinal fluid
CT	Computed tomography
DIPG	Diffuse intrinsic pontine glioma
DNA	Deoxyribonucleic acid
DTI	Diffusion tensor imaging
EGFR	Epidermal growth factor receptor
EMA	Epithelial membrane antigen
EZH2	Enhancer of Zeste homologue 2
FA	Fractional anisotropy
FLAIR	Fluid attenuated inversion recovery
GFAP	Glial fibrillary acidic protein
GFAP δ	Glial fibrillary acidic protein delta
HATs	Histone acetyltransferases
HDACs	Histone deacetylases

M. H. A. Noureldine · G. I. Jallo (✉)

Department of Neurosurgery, Institute for Brain Protection Sciences, Johns Hopkins University School of Medicine, Johns Hopkins All Children's Hospital, Saint Petersburg, FL, USA

e-mail: gjallo1@jhmi.edu

N. Shimony

Institute of Neuroscience, Geisinger Medical Center, Geisinger Commonwealth School of Medicine, Danville, PA, USA

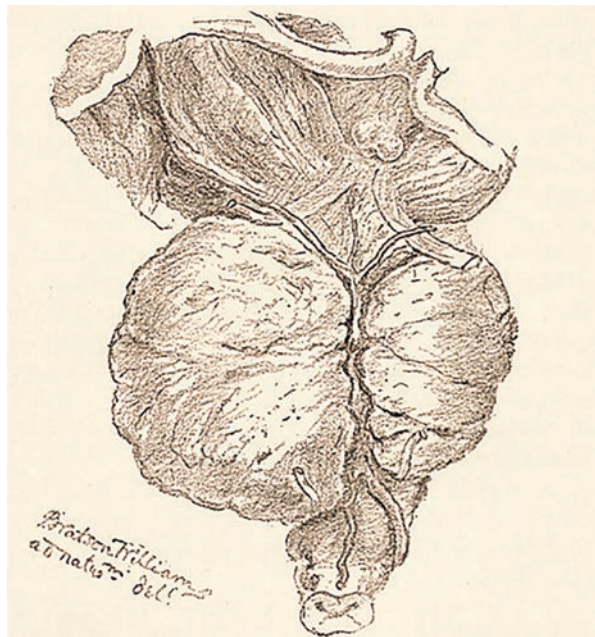
ICP	Intracranial pressure
LPS	Lansky play scale
MRI	Magnetic resonance imaging
MRS	Magnetic resonance spectroscopy
mTOR	Mammalian target of rapamycin
NAA	<i>N</i> -acetyl aspartate
Olig2	Oligodendrocyte transcription factor 2
PDGFR	Platelet-derived growth factor receptor
PET	Positron emission tomography
PNET	Primitive neuroectodermal tumor
PPCs	Precursor-like cells
PRC2	Polycomb repressive complex 2
RTK	Receptor tyrosine kinase
SAHA	Vorinostat
SPECT	Single photon emission computed tomography
SWI	Susceptibility-weighted imaging
TMZ	Temozolomide
T2*-GRE	T2*-weighted gradient echo
WHO	World Health Organization

8.1 Introduction

The first published case of potential diffuse intrinsic pontine glioma (DIPG), to our knowledge, was reported by Dr. Edward H. Hensch from Charité hospital, Berlin, in 1880. He described an 11 years old girl who suffered from ataxia, swallowing and speech problems, and cranial nerve (CN) VI palsy. Autopsy showed an isolated pontine mass with no sharp boundaries that seemed to extend diffusely into the substance of the pons from multiple small foci secondary to the principal mass [1]. Another potential case was presented in detail by Dr. Henry Hun to the American Neurological Association in 1887. It was referred to by Dr. Mary Putnam Jacobi in an article published in 1889, reporting a similar case in terms of clinical presentation and progression but without obtaining an autopsy [2]. The outstanding explanation of the clinical assessment and follow-up as well as the autopsy and microscopic examination of the pontine tumor tissue of Dr. Hun's 6-year-old female patient still stands out as accurate compared to today's description of DIPG. Quoting Dr. Jacobi on describing the autopsy result of Dr. Hun's patient, some of the interesting statements were, "*Dr. Hun ascribes the incoordination of movements to pressure upon the transverse fibres of the pons, and the origin of the crura cerebelli; the absence of the absolute paralysis to the fact that the nerve elements were compressed but not destroyed by the infiltration. He explains the absence of sensory disturbance by a greater resistance of sensory function, even when sensory fibres are submitted to the same pressure as motor fibres*" [2]. Subsequent reports of similar cases were even more in favor of DIPG. In 1891, Dr. P. Watson Williams reported a 6-year-old patient

presenting with a typical DIPG picture, which was supplemented by an autopsy described as, “*Externally this infiltrating growth was colourless and almost translucent on the surface. Internally it was red and very vascular. Microscopical examination showed that it consisted of small round and oval cells enclosed in a granular, finely fibrillated inter-cellular substance, a typical glioma.*” Fig. 8.1 shows the drawing of the pontine glioma by Dr. Williams [3]. In spite of the fact that brainstem lesions were reported as early as 1881 [4] and definitely confirmed only on autopsy, the first attempt at surgical treatment was performed as late as 1909 by Dr. Weisenburg [5]. Nevertheless, Dr. Philip Zenner [6] and Dr. Harvey Cushing [7] were the first neurosurgeons to operate on pediatric brainstem tumors in 1910 (Fig. 8.2). Prevalence studies of brainstem gliomas were documented in large series of brain tumors published in the 1930s [8–10]. When surgical treatment was deemed hopeless in patients with brainstem tumors, radiation therapy was attempted since the 1950s with the goals of offering temporary improvement and prolonged survival [11–13].

Fig. 8.1 Drawing and legend of the pontine glioma by Dr. Williams in one of the earliest reports about DIPG. (Reprinted from Williams [3])



Description of the Drawing.

The base of the brain from the optic chiasma to the medulla oblongata is represented. From above downwards are seen the optic tracts running over the crura cerebri to form the chiasma, below which the posterior perforated space and corpora albicantia appear. On either side are the crura cerebri, the right crus especially being considerably enlarged by the infiltrating growth, and lying on the crura are the 3rd nerves, both very much flattened, and coming forward between the posterior cerebral and superior cerebellar arteries. The 4th nerve on the right side is seen. The enormously swollen pons shows the greatest enlargement in the right half, and in the deep central groove lies the basilar artery, almost concealed by the overhanging lateral swellings. Coming forward from beneath the bulging posterior borders of the pons are the 6th nerves. Below the pons are seen the irregularly distributed vertebral arteries lying on the medulla. The amount of stretching and displacement of the parts may be estimated from the drawing.

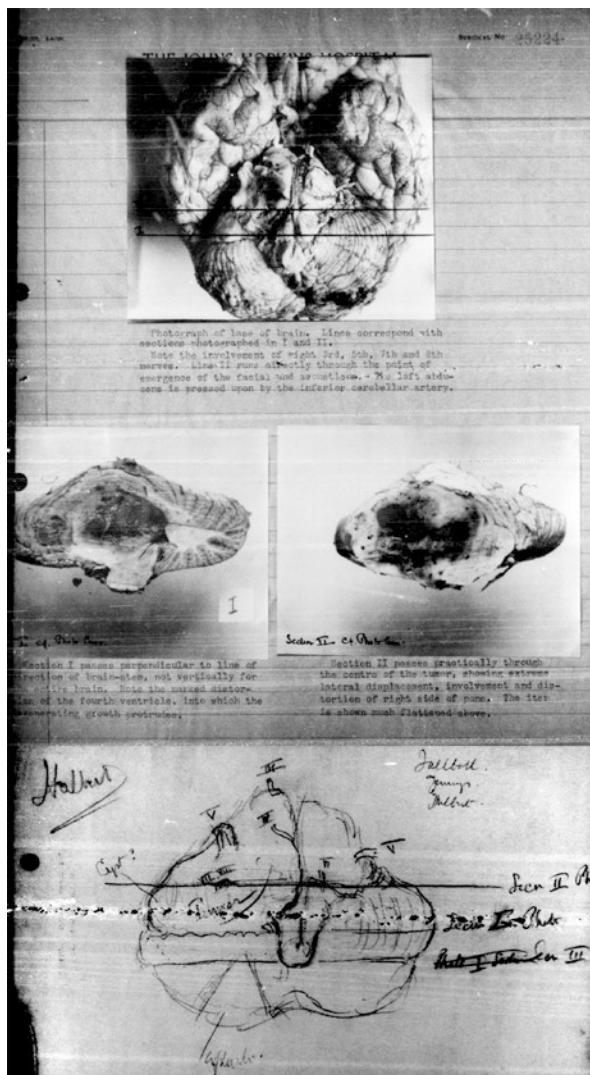


Fig. 8.2 Cushing's photographs of the specimen obtained for pathological investigation, with his accompanying captions. Upper: "Photograph of base of brain. Lines correspond with sections photographed in I and II. Note the involvement of right 3rd, 5th, 7th and 8th nerves. Line II runs directly through the point of emergence of the facial and acoustic. The left abducens is pressed upon by the inferior cerebellar artery." Lower left: "Section I passes perpendicular to line of [...] of brain stem [...] Note the marked distortions of the fourth ventricle into which the [...] growth protrudes." Lower right: "Section II passes practically through the centre of the tumor, showing extreme lateral displacement, involvement and distortion of right side of pons. The latter is shown much flattened above." Photographs were obtained from an archived microfilm of the handwritten records, courtesy of The Alan Mason Chesney Archives of The Johns Hopkins Medical Institutions

DIPG or *diffuse midline glioma, H3 K27M-mutant* (new World Health Organization [WHO] classification, 2016) is a highly malignant glial neoplasm primarily affecting school-aged children, almost equally distributed between males and females, with a peak incidence between 4 and 7 years of age at diagnosis [14]. DIPG represents 10–15% of all childhood brain tumors [15]. While 15–20% of brainstem gliomas are low-grade astrocytomas, around 75% of brainstem tumors are considered diffuse pontine tumors, which biologically tend to be aggressive tumors with poor outcome [16, 17]. Despite the extraordinary biomedical advances in the management of central nervous system (CNS) neoplasms over the last century, DIPG remains among the most challenging to treat with a very poor prognosis, where less than 10% of patients survive beyond 2 years from diagnosis [18]. The median time of tumor progression is 5–6 months, and the median overall survival ranges between 4 and 17 months. Different overall survival rates have been reported; in their review, Jansen and colleagues published overall survival rates at 1, 2 and 3 years that ranged from 14% to 70%, 0 to 25% and 0 to 10%, respectively [15]. Lately, others published median survival rate of 11.2 months and overall survival rates of 86.6% at 6 months, 66.1% at 9 months, and 45.3% at 1 year [19]. The typical presentation is that of a previously healthy child with rapid onset of signs/symptoms indicative of brainstem dysfunction and pathognomonic magnetic resonance imaging (MRI) findings. In adults, diffuse intrinsic brainstem gliomas resemble the pediatric DIPG in terms of clinical and radiological presentation but seem to have a more benign course that is associated with a much better prognosis and a median survival of up to 7.3 years. The adult malignant type, however, is predominantly found in older adults (sixth decade) and has a dismal prognosis with very short survival [20].

Given the infiltrative nature of DIPG in a highly delicate and surgically inaccessible anatomical structure – the pons, management strategies have been directed towards radiation therapy, medical interventions, or a combination of both. Nevertheless, little-to-no benefit have been reported in more than 200 clinical trials so far. The reintroduction of biopsies, which were previously considered dangerous and unnecessary in the context of an MRI diagnosis, and autopsies have made DIPG tissue available for molecular and genomic studies. The number of published studies on the molecular, genetic and epigenetic peculiarities of DIPG is undergoing an exponential growth, which will hopefully help us further understand the biology of the disease and adopt effective targeted therapies. In this chapter, we present an overview of the current standards as well as the most important recent and clinically-relevant advances in the diagnosis and management of DIPG.

8.2 Clinical Presentation

The clinical signs and symptoms of patients with DIPG are direct sequelae of the location of the neoplasm and extent of infiltration in the adjacent anatomical structures. Unlike the less common focal brainstem gliomas usually localized to the mid-

brain, medulla and cervicomedullary junction, which typically have a prolonged clinical course often reaching up to years, the symptomatic progression of DIPG is quite short, and symptoms typically progress within days-to-weeks. In general, the duration of symptomatic progression has a significant prognostic value in brainstem tumors; tumors with slowly progressing symptoms, roughly for over 6 months at the time of diagnosis, carry a much better prognosis compared to those with symptoms progressing over a shorter duration (less than 3 months) [21, 22], and should prompt searching for a diagnosis other than DIPG. In patients with DIPG, age ≤ 3 years was associated with good prognosis [22]; however, atypical presentations such as mood or behavioral changes or acquired torticollis may delay the diagnosis in younger patients [23, 24]. Unlike pediatric DIPG, the duration of symptoms in adult diffuse intrinsic brainstem glioma is often long, and unique clinical findings such as isolated facial paralysis or hemispasm may occur up to 5 years prior to tumor recognition. Nevertheless, the clinical presentation of the malignant adult type is very similar to that of the pediatric DIPG, where CN palsies and long tract signs have an acute onset and progress over a short period [20].

Bulbar signs and symptoms, particularly those related to CN nuclei situated at the level of the pons and CNs passing through the pontine tissue, are sensitive, although not very specific to this pathology. CNs VI and VII are mostly involved, and DIPG seems to have a predilection to originate close to the region of CN VI nuclei [25]. Such involvement may manifest as diplopia, limited or abnormal eye movements, and asymmetric smile. As the tumor grows superiorly towards the mid-brain and inferiorly towards the medulla, involvement of other CNs such as III, IV, IX and X is possible albeit less common, and appears in advanced stages after the tumor invades through the pontomesencephalic and pontomedullary junctions [26]. Diffuse expansion within the basis pontis also affects the pontocerebellar and long tract fibers manifesting as loss of balance, clumsiness, ataxia, difficulty walking, hemiparesis, spasticity, hyperreflexia, clonus, positive Babinski reflex, among others [27]. Sensory abnormalities are less common, probably because the sensory pathways are more resistant to infiltration by the neoplasm [21, 28].

In a retrospective study on 39 patients with DIPG (median age at diagnosis and duration of presenting symptoms were 6.8 years and 4 weeks, respectively), CN palsy was the most common presenting symptom (90%), followed by ataxia (72%) and long tract signs (54%) [29]. In another study on 86 patients (mean age of 14.2 years) with brainstem gliomas, headaches (29%) and motor deficits (24%) were the most common symptoms on disease onset, followed by visual complaints (20%) and ataxia (13%) [21]. Acute obstructive hydrocephalus is an uncommon presentation, although signs of elevated intracranial pressure (ICP) and active hydrocephalus can be found and were reported as high as 50% in some previous publications; this presentation, however, is more common in exophytic brainstem tumors rather than DIPG [30, 31]. DIPG tends to expand in different vectors. Usually, the tumor will expand anteriorly into the prepontine cistern and encase the basilar artery to some degree. Posterior expansion into the fourth ventricle is less common in early stages; the ventricular floor is rather strained craniocaudally and laterally, reducing the risk of developing obstructive hydrocephalus at the level of

the fourth ventricle. Upward expansion towards the midbrain can potentially lead to obstructive hydrocephalus from aqueductal stenosis secondary to mass effect. On rare occasions, disruption of the pontine micturition center by neoplastic infiltration may lead to urinary retention and voiding abnormalities [32].

8.3 Imaging Characteristics

MRI has emerged as the primary modality to establish the diagnosis and follow-up on any brainstem lesion, further subclassify these lesions into diverse categories, and predict the biological behavior of the tumor, for which different management strategies could be utilized. Lesion classification on MRI is also important for prognostication purposes (e.g., focal lesions of the midbrain, cervicomedullary region and medulla oblongata carry a better prognosis than DIPG) [33]. In the context of limited surgical and biopsy options, DIPG is a typical example, where the diagnosis is based on the history and clinical presentation, which are supplemented by an MRI revealing characteristic findings.

DIPG typically appears as a hypo- to iso-dense, non-enhancing or variably enhancing pontine mass on computed tomography (CT) scans, with or without extension into the adjacent anatomical structures and rarely harboring calcifications (Fig. 8.3). On structural MRI, DIPG is best described as a large, expansile, infiltrative and often asymmetric mass occupying more than 50% of the pons. The epicenter of DIPG lies within and expands the pons rather than displacing it; however, this tumor is often exophytic anteriorly (the path with least resistance) and may engulf the basilar artery (in up to 82% of cases [29]) (Fig. 8.4). Upon presentation, DIPG is generally more than 2 cm in size and appears hypo- (92%) to iso-intense on T1-weighted and homogeneously or heterogeneously hyper-intense on T2-weighted images [29] (Fig. 8.5). Fluid attenuated inversion recovery (FLAIR) images show a relatively homogeneous enhancement of the tumor and surrounding tissue (Fig. 8.6). Intra-tumoral petechial hemorrhages, but not hematomas, are common at diagnosis, and can be detected with better sensitivity on susceptibility-weighted imaging (SWI) compared to T2*-weighted gradient echo (T2*-GRE) imaging in more than 40% of cases [34]. Contrast enhancement may be present in up to 51% of cases [29], although typically weak and patchy around the time of diagnosis and does not have any prognostic significance [24, 35] (see Figs. 8.5 and 8.6). As the tumor grows, the absent-to-weak enhancement pattern frequently progresses to areas of focal necrosis with ring enhancement and subsequent diffuse enhancement and necrosis at later stages [36] (Fig. 8.7). It is important to note, however, that the evaluation of DIPG on serial MRIs is not always straightforward due to signal heterogeneity and inter-observer variability in the measurement of such lesions, which necessitates utilizing more objective endpoints in clinical trials [37].

Hargrave and colleagues [29] retrospectively reviewed baseline MRI scans of 39 DIPG patients (median age at diagnosis and duration of presenting symptoms were 6.8 years and 4 weeks, respectively) and reported local tumor extension in upper

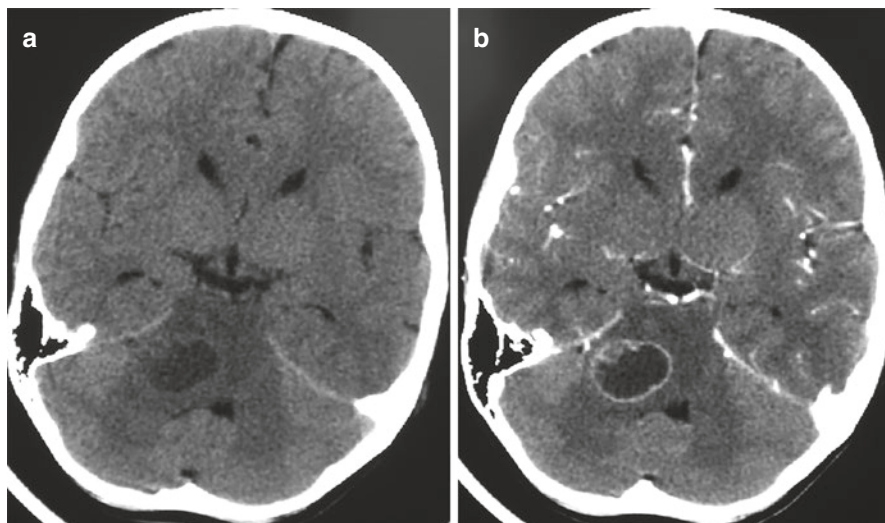
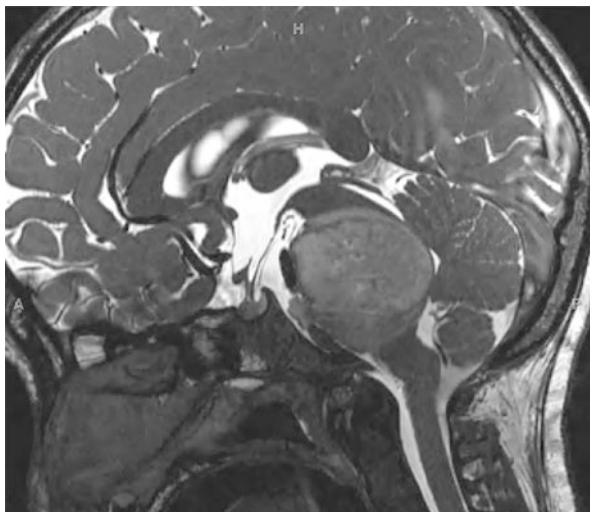


Fig. 8.3 Brain CT of a young patient with DIPG showing a hypodense lesion localizing to the right side of the pons (a) with ring enhancement and central necrosis post contrast injection (b). Case and images courtesy of George Jallo, MD

Fig. 8.4 MRI showing the anterior exophytic growth of DIPG, which is starting to engulf the basilar artery. Case and images courtesy of George Jallo, MD



medulla (74%), midbrain (62%), cerebellar peduncles (15.5%) and cervical spinal cord (2.5%), exophytic component (72%), necrosis (33%), intra-tumoral hemorrhage (26%), and hydrocephalus (23%). Leptomeningeal metastasis was found in 3% of cases on baseline MRI and increased to 16% on post-treatment MRI (performed at 4–12 weeks after first treatment course; usually radiotherapy). Tumor enhancement also increased from 51% to 72%, as well as T2 heterogeneity (28 to 64%), cystic necrosis (33% to 48%), and intra-tumoral hemorrhages (26% to 32%).

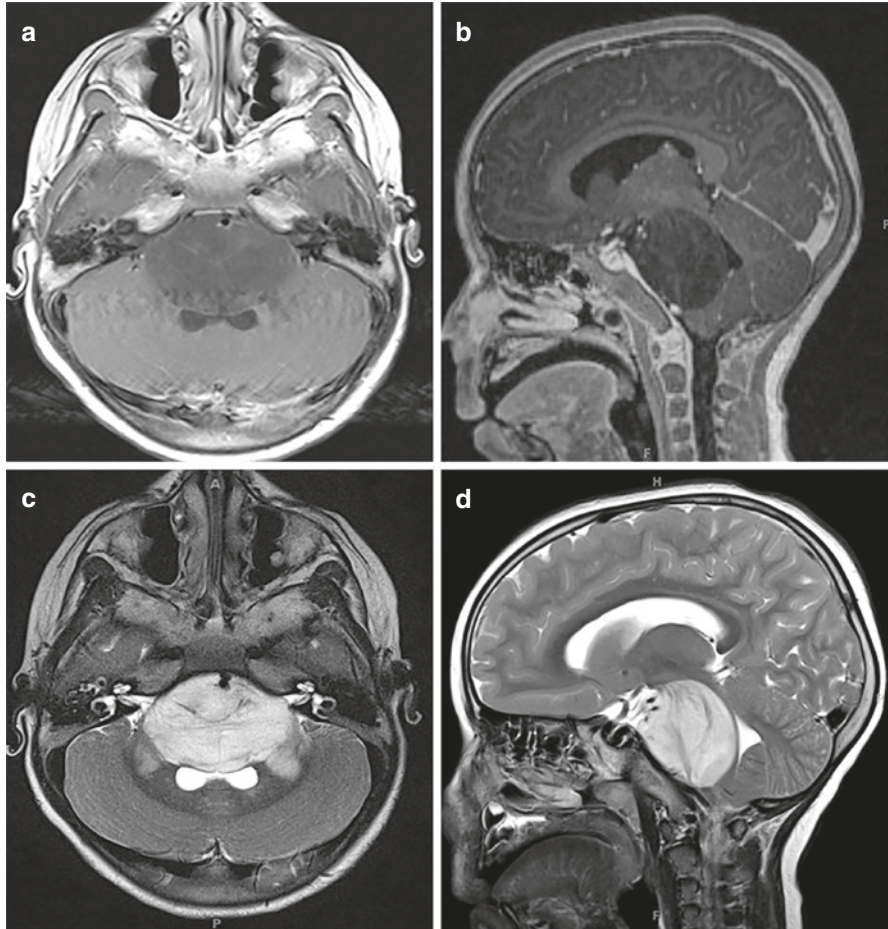


Fig. 8.5 MRI of DIPG with a histology pattern of anaplastic astrocytoma. (a) Axial and (b) sagittal T1-WI post contrast. (c) Axial and (d) sagittal T2-WI. Note the diffuse anterior growth that engulfs the basilar artery and the proximal portion of its superior branches. Case and images courtesy of George Jallo, MD

Positron emission tomography (PET) using ^{18}F -labeled fluorodeoxyglucose (^{18}F -FDG) fused with MRI was used to investigate the association between ^{18}F -FDG uptake and progression free survival, overall survival and MRI indices in patients with diffuse intrinsic brainstem gliomas. Poor survival was associated with ^{18}F -FDG uptake involving at least half compared to less than 50% of the tumor. Higher uptake was also associated with enhancement on MRI, and uniform uptake throughout the tumor was linked to increased tumor cellularity, as reflected by restricted MRI diffusion [38]. In a small case study, diffusion tensor imaging (DTI), using serial apparent diffusion coefficient (ADC) and fractional anisotropy (FA) values as well as tractography data, showed initial tumor infiltration of the corticospinal, transverse pontine and medial lemniscus tracts, transient improvement following

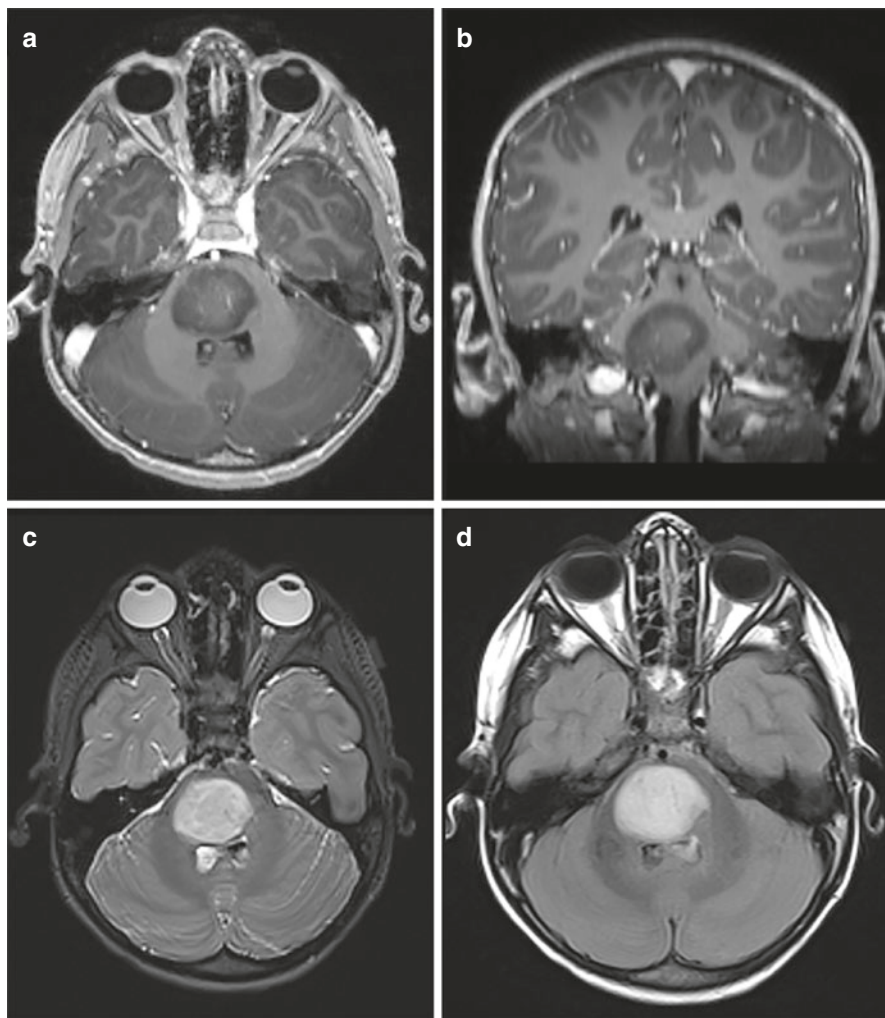


Fig. 8.6 MRI of DIPG with a histology pattern of anaplastic astrocytoma. (a) Axial and (b) coronal T1-WI post contrast. Axial (c) T2-WI and (d) FLAIR images. Case and images courtesy of George Jallo, MD

treatment, and subsequent loss of tract anisotropy during tumor progression [39]. In recent years, ADC maps have been shown to be a strong predictor of tumor cellularity and, hence, poor prognosis. Recent research suggests that sites of tumor enhancement correlate with sites of reduced diffusivity, lower ADC values, and, eventually, a more aggressive disease [40–42]. Volumetric ADC histogram metrics were found to be significantly correlated with survival, where lower diffusion and ADC values

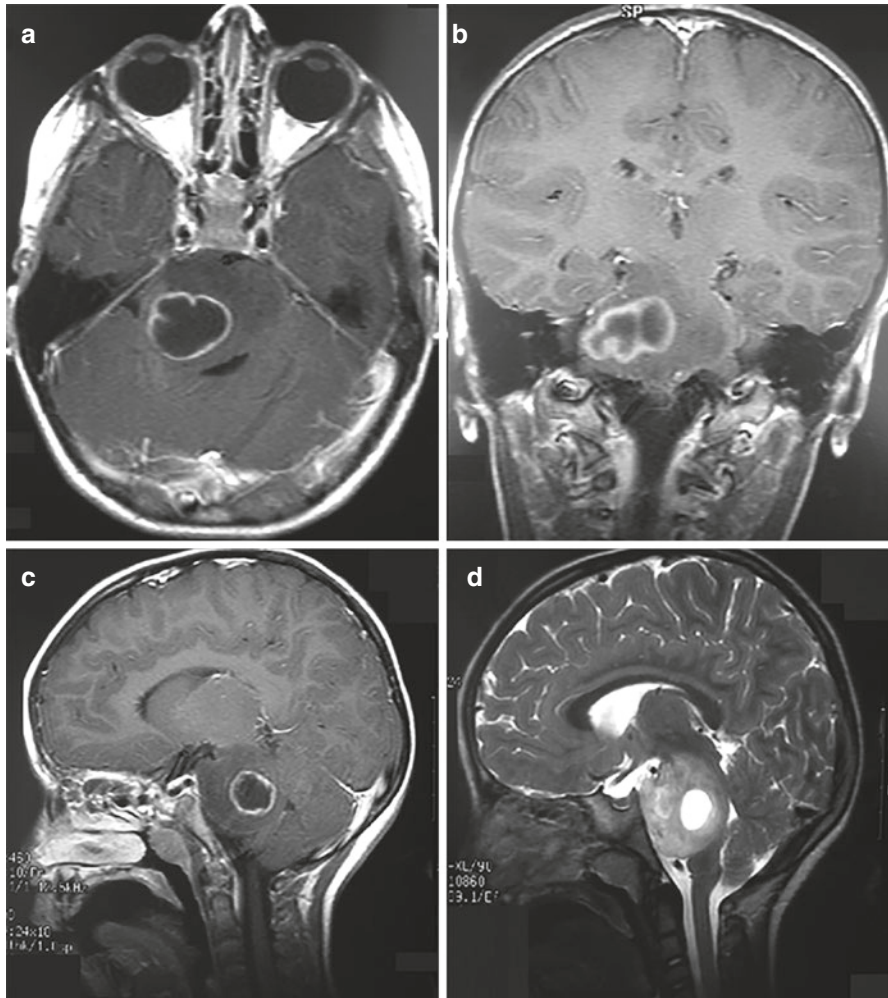


Fig. 8.7 MRI of DIPG with a histology pattern of glioblastoma. (a) Axial, (b) coronal and (c) sagittal T1-WI post contrast. (d) Sagittal T2-WI. Case and images courtesy of George Jallo, MD

were associated with poor prognosis and shorter survival [43]. Since none of the current tools can truly predict the nature of the disease, recent studies tried to integrate different modalities into an assessment tool. One of them showed that the combination of ^{18}F -FDG PET and ADC histogram metrics in pediatric DIPG demonstrates different characteristics, often with a negative correlation between PET and ADC pixel values. This means that a higher negative correlation is associated with a worse progression free survival, which may indicate high-grade elements within the tumor and, hence, overall poor prognosis [44].

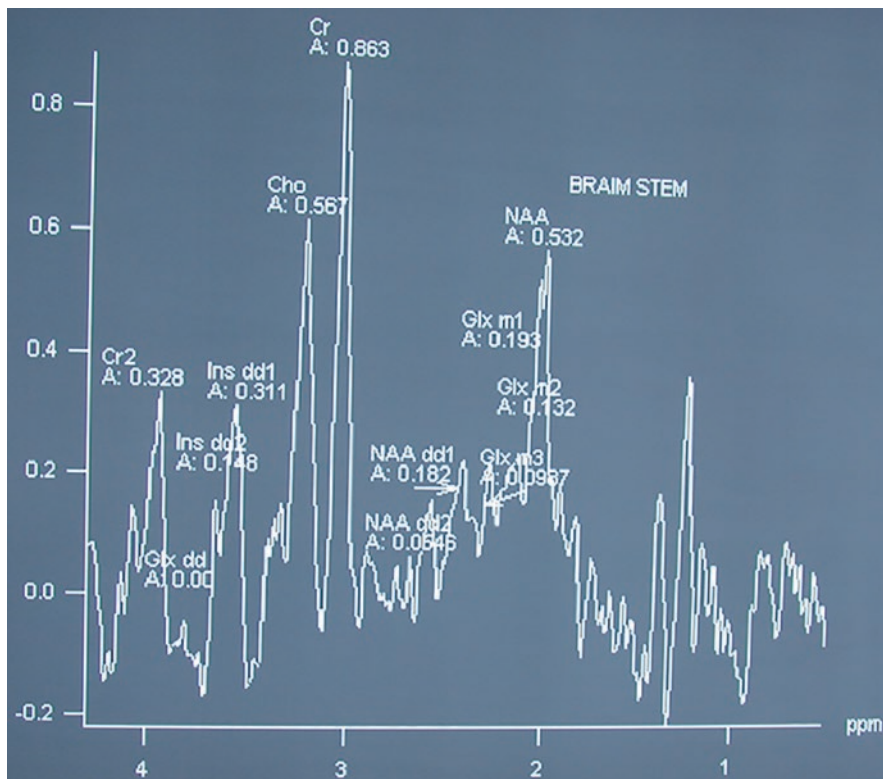


Fig. 8.8 MRI spectroscopy at the level of the pons. This tool has become widely utilized in the recent years, as it can give a better understanding in regard to changes in the brainstem parenchyma. Case and images courtesy of George Jallo, MD

Proton magnetic resonance spectroscopy (MRS) findings (Fig. 8.8) of elevated metabolic ratios of choline/creatine (Cho/Cr) and Cho/*N*-acetyl aspartate (NAA), along with lactate and lipids peaks, suggest poor prognosis. The inability of conventional MRI to differentiate radiation-induced contrast enhancement and necrosis from tumor progression or a combination of both processes with breakdown of the blood-brain barrier (BBB) renders MRS a valuable tool in the follow-up of DIPG. In patients treated with radiotherapy, increased Cho/Cr and Cho/NAA ratios in enhancing and non-enhancing regions indicate neoplastic progression and predict worse outcomes, while stable ratios provide evidence against radiation-induced metabolic alterations [45, 46]. On the other hand, a clinical response to radiotherapy may be inferred from a decreasing Cho/Cr ratio [47].

These advanced imaging modalities, in addition to other functional techniques such as tumor perfusion and blood volume characterization methods [46, 48] and thallium single photon emission computed tomography (SPECT) [49], may preclude the need for stereotactic biopsy in cases with uncertain diagnoses and hold promise in distinguishing recurrence from treatment-induced changes as well as predicting response to treatment and duration of survival.

8.4 Surgical Options

The infiltrative nature of DIPG in one of the most intricate anatomical structures – the pons – has long been a limitation to surgical interventions due to profound surgical toxicity. Radical surgical resection has been previously attempted in patients with diffuse brainstem tumors, the outcome of which was not satisfactory [50, 51]. Even biopsies, which were once utilized to obtain brainstem tumor tissue for diagnostic purposes and to plan further therapy [52], were abandoned and considered highly dangerous and unnecessary in the context of typical clinical and radiological features [53]. Until recently, this trend has been internationally accepted and utilized in the diagnostic and management approaches to DIPG, although some neurosurgical teams continued to biopsy brainstem lesions in cases with diagnostic uncertainty as well as for inclusion in therapeutic trials [54–57]. The trend is changing nowadays, however, with the advancement of stereotactic biopsy techniques, although still requiring significant training and expertise to safely perform the procedure [58].

8.4.1 To Biopsy or Not to Biopsy a Potential DIPG?

The safety of obtaining a brainstem biopsy have been tackled in newer studies and meta-analyses, the overall results of which were satisfactory. In two meta-analyses, the diagnostic yield ranged between 94.9% and 96%, whereas morbidity and mortality reached a maximum of 4.9% and 0.7%, respectively. Transient and permanent deficits occurred in up to 1% and 4% of patients, respectively [59, 60]. Subsequent studies reported a diagnostic yield range of 93–100%, and morbidity ranging between 2.8% and 25%, almost all of which were transient deficits. None reported any death related to the procedure [56–58, 61–63]. The latest large-scale study was conducted by Puget and colleagues [58], who prospectively analyzed 130 DIPG biopsied patients and reported a transient morbidity of 3.9% and no mortality. The diagnostic yield and morbidity rates were comparable to those reported for other brain locations, and increasing the number of specimens per trajectory was not a significant risk factor for morbidity. The authors concluded that, “*Stereotactic biopsy of DIPG can be considered as a safe procedure in well-trained neurosurgical teams and could be incorporated in protocols*” [58].

While patient safety remains a major concern, the reluctance to biopsy such lesions has impeded any substantial progress in understanding the biology of DIPG over the last 50 years. In 2013, a consensus statement was released concerning the surgical approaches to DIPG and recommended biopsy in the context of clinical trials to understand the behavior of tumor and enhance targeting of treatments [64]. Indeed, the reintroduction of biopsy in the last few years, in addition to the implementation of standardized autopsy protocols [65] and advancement of high-throughput sequencing technology, opened doors for important molecular, genetic

and epigenetic studies that distinguished different DIPG subtypes [14, 66–68], giving way for promising targeted therapeutic trials to commence in light of the consistently failing conventional management strategies.

8.4.2 Tenets for Obtaining a DIPG Biopsy

Brainstem biopsies may be obtained through a trans-frontal or suboccipital trans-cerebellar route (Fig. 8.9). With or without a frame and under general anesthesia, the patient is positioned supine for the trans-frontal approach or prone for the trans-cerebellar approach. While the trans-frontal route allows to obtain a biopsy from any brainstem segment, the trans-cerebellar route may be utilized to sample upper medullary and pontine lesions only. Preoperative planning of the needle trajectory using a software is recommended for both routes to decrease the risk of complications. The trans-frontal route has a longer and more eloquent trajectory; the bur hole is best placed 3 cm from the midline in the peri-coronal region, and the trajectory should remain within the neuroaxis, does not violate the ventral surface of the brainstem, and avoid the vascular structures, ventricles and tentorium cerebelli. The trans-cerebellar route is shorter and has a safer trajectory, crossing through the middle cerebellar peduncle. The frame should be rotated 180° and positioned as inferiorly as possible onto the skull, just above the base of the neck, allowing the target to fall within the stereotactic space. The bur hole incision is placed at mid-distance between the midline and the mastoid, and the dural opening is carefully performed below the transverse sinus. The optimal outcome from any of the two approaches is to sample both enhancing and non-enhancing tumor regions along one trajectory, while avoiding

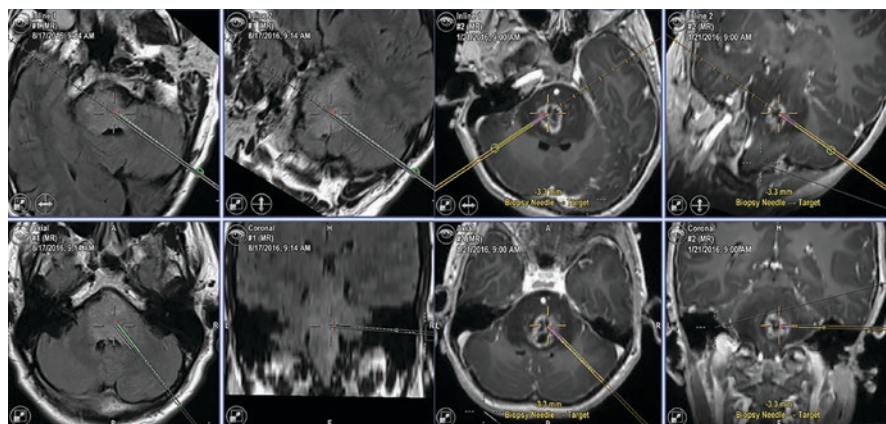


Fig. 8.9 Stereotactic biopsy of DIPG. There are two main approaches: trans-frontal and trans-cerebellar. In the trans-cerebellar approach, the entry point is paramedian aiming for the middle cerebellar peduncle (as shown in the figure). Enhancing regions, if present, are the most yielding targets of the biopsy needle. Case and images courtesy of George Jallo, MD

the pyramidal tracts, CN nuclei and anterior pons. If this outcome is not possible to achieve, the enhancing regions are the preferred target or, otherwise, the infiltrative region, which appears hyperintense on T2-weighted and FLAIR images. In the case of ring enhancing regions with central necrosis, the most yielding trajectory is the one crossing tangential to the enhancing edge of the ring so that more tumor tissue rather than necrotic fluid could be obtained. A side-cutting biopsy needle is used to obtain four quadrant biopsies from each region (enhancing and non-enhancing), if possible, by applying gentle aspiration; several biopsies should be obtained in different projections of the needle's tip. It is better to continue taking biopsies until frozen sections return positive for the presence of tumor tissue. The sampled tissue is fixed in formaldehyde, snap-frozen in the operating room and stored at -80° for molecular studies, and/or used as a xenograft and/or for cell culture. Neuroimaging, preferably T2-weighted axial images, is recommended after the procedure to confirm the trajectory and site of biopsy and document possible surgical complications [57, 58]. Dellaretti and colleagues [69] compared the two approaches, suboccipital trans-cerebellar versus trans-frontal, and reported no statistically significant differences in success and complication rates. The trans-cerebellar route may seem more appealing for DIPG biopsies in specific due to shorter trajectory to the target and possibility to avoid CN nuclei by sampling the interface between the pons and middle cerebellar peduncle; however, some authors are utilizing single-staged, robot-assisted stereotactic biopsy through the trans-frontal route with an optimal diagnostic yield and a favorable risk profile [70]. To conclude, neurosurgeons should be well experienced in performing both approaches, weighing the risks versus benefits, and choosing the most suitable route on a case-by-case basis.

8.5 Pathology and Molecular Signatures

High-grade gliomas were thought to arise from stem-like gliomagenic cells in the subventricular zone [71, 72]. This notion, however, has been challenged by subsequent studies suggesting that the origins of these tumors are distributed throughout the white matter and not exclusively limited to the subventricular zone [73]. Human pontine precursor-like cells (PPCs), residing in the ventral pons and temporally correlated to the incidence of DIPG, are potentially the cell of origin of this tumor. DIPG neurosphere cells are immunophenotypically similar to PPCs, i.e. nestin- and vimentin-positive, with a subset expressing the glial-restricted cell progenitor oligodendrocyte transcription factor 2 (Olig2) [74].

Classified under the newly defined entity, *diffuse midline glioma, H3 K27M-mutant* [75], DIPG is a WHO grade IV CNS tumor, with significant intra-tumoral heterogeneity in terms of histologic phenotype and malignancy grade, ranging from grade I to grade IV [76, 77]. Grade I areas are focal and present in up to 56% of specimens, some of which are pilocytic astrocytoma-like characterized by piloid tumor cell processes and presence of Rosenthal fibers, while others are paucicellular, subependymoma-like with marked clustering of tumor cells that may show dot-like

epithelial membrane antigen (EMA)-positivity or express Olig2 [77]. The relatively high prevalence of grade I-like regions may lead to false negative biopsy results in some DIPG cases, and their presence does not indicate better survival in these patients [78]. WHO grade II (diffuse astrocytoma; cytological atypia), grade III (anaplastic astrocytoma; anaplasia and increased mitotic activity) and grade IV (glioblastoma; microvascular proliferation and necrosis) features are dispersed throughout the tumor; higher grade features are mostly limited to the pons, whereas lower grade features are found in the pons as well as in the nearby infiltrated structures and metastatic lesions [77–79], implying spatial histological heterogeneity. The intra-tumoral heterogeneity is also evident on immunohistochemistry in terms of astrocytic differentiation and expression of stem cell markers, namely glial fibrillary acidic protein (GFAP) and its delta isoform (GFAP δ), nestin and cluster of differentiation 44 (CD44), that partially overlap with the degree of cellular atypia, as well as focal expression of neuronal markers such as synaptophysin and neurofilament [77].

Although there is potentially no significant difference in overall survival based on histology, the age of diagnosis increases with higher tumor grades [78]. Leptomeningeal and distant spread may be detected at higher rates on autopsy [78, 80] compared to neuroimaging studies [29]. Metastatic and/or infiltrative cells were found in the spinal cord, thalamus and frontal lobes, and patients with leptomeningeal spread had worse overall survival outcomes [78]. In few cases, primitive neuroectodermal tumor (PNET) features such as poorly differentiated cells with scant cytoplasm and round nuclei were reported on autopsy studies of patients with typical clinical presentation and MRI findings of DIPG [78, 81], again highlighting the importance of biopsy to arrive at the correct diagnosis and to tailor therapy accordingly.

In light of the recent large-scale molecular, genomic and epigenomic studies, tissue diagnosis of diffuse midline gliomas, including DIPG, is undergoing a paradigm shift. It is clear that our old understanding of the definition of DIPG, which mainly relied on radiographic appearance of a large tumor that invaded more than 50% of the pons, is now going through a major change. Current classification and sub-classifications of these tumors will most likely continue to have adjustments in light of the ongoing progress in our understanding in regard to molecular subtyping. The significant overlap in histological features between diffuse midline gliomas and other pediatric/adult glioma types may now be compensated for by detecting highly specific and recurrent hot-spot mutations in histone genes causing epigenetic dysregulation, the significance of which lead to establishing a new WHO CNS tumor classification termed as ‘diffuse midline glioma, H3 K27M-mutant’ [14]. It seems that the majority of pediatric midline and high-grade gliomas undergo recurrent somatic mutations in genes encoding for the replication-dependent histone H3 isoform, H3.1 (*HIST1H3B/C*), and the replication-independent H3.3 isoform (*H3F3A*), mostly resulting in lysine 27 to methionine substitution (H3.1 or H3.3 K27M) or glycine 34 to valine or arginine substitution (H3.3 G34V/R). Notably, more than 90% of DIPG and 50–60% of diffuse thalamic and spinal cord gliomas harbor H3 K27 mutations, whereas the G34V/R mutation is observed in up to 30% of pediatric hemispheric

gliomas [82–85]. While the histopathological characteristics of the H3.3 G34R-mutant tumors look similar, comprising of mostly small cells with some giant cells, perivascular invasion, perineuronal satellitosis and microcalcifications, the radiological patterns are quite variable in different patients. This finding raises the speculation that different pathogenic mechanisms may be found in tumors harboring the G34R mutation [86], the discussion of which is beyond the scope of this chapter.

By sequestering the histone methyltransferase enhancer of Zeste homologue 2 (EZH2), the K27M-mutant H3 protein inhibits the polycomb repressive complex 2 (PRC2), which ultimately causes a global decrease in H3 K27 trimethylation [87]. Although all H3 K27M-mutant tumors have been shown to lose H3 K27 trimethylation detected by immunohistochemistry, caution should be taken so as not to exclusively rely on this finding since H3 K27 wild-type tumors may also contain focal H3 K27 trimethylation-immunonegative areas, leading to a false positive diagnosis of H3 K27M-mutant glioma [77]. Additionally, almost all cases of H3 K27M-mutant tumors are characterized by *MGMT* overexpression due to lack of *MGMT* promoter methylation, which implies lower efficacy of temozolomide (TMZ)-based therapy [88, 89]. While H3.3 mutations have been detected in diffuse gliomas across different midline structures and mostly affect children aged 7–10 years, H3.1 mutations seem to occur exclusively in the pons, affect younger children aged 4–6 years, and are associated with a slightly better outcome compared to their H3.3 counterparts [90]. A recent study revealed that DIPG patients with the H3.1 mutation had significantly better survival after relapse. In the same study, other predictors of survival at relapse were Lansky play scale (LPS) above 50% and steroid-independence [91]. The deleterious effects of H3 mutations are reflected by the lack of clinical response to therapies, which may work very well in patients with H3 wild-type gliomas, as well as a more aggressive course and poor overall prognosis [83, 90, 92]. Optimizing the detection of H3 mutations in the deoxyribonucleic acid (DNA) of diffuse midline gliomas, including DIPG, by obtaining tissue biopsy or even less dangerous techniques such as cerebrospinal fluid (CSF) analysis [67], may be utilized as a diagnostic and prognostic marker and may help stratify patients to targeted therapies as well as monitor the clinical response to treatment.

Further recurrent mutations may occur concomitantly with those in the histone genes in up to 50% of diffuse midline gliomas. The p53 pathway is involved in around 70% of cases and includes mutations in the *ATM*, *TP53*, *CHEK2* or *PPM1D* genes. The receptor tyrosine kinase (RTK)/RAS/PI3K pathway may also be involved through mutations in the *PIK3CA*, *PIK3R*, *PDGFRA* or *PTEN* genes. These mutations may be associated with recurrent focal amplifications of the *CCND1-3*, *CDK4/6*, *EGFR*, *ID2*, *KDR*, *KIT*, *MET*, *MYC/MYCN*, *PARP1*, *PDGFRA*, and/or *TOP3A* genes, among others [66, 93–98]. Specifically, recurrent mutations in the *ACVR1* gene, occurring in almost one-third of DIPGs, were found to be associated with H3.1 K27M mutations [79, 90, 94].

The discovery of selective driver mutations, namely the histone H3 among several others, has consequently led to the implementation of therapeutic clinical trials targeting the associated unique molecular mechanisms, many of which are currently ongoing.

8.6 Management Strategies

The massive knowledge gained in the last decade about the genetic and molecular abnormalities in diffuse midline gliomas – including DIPG – has been paralleled by an equal excitement at the level of investigating novel effective therapies. Radiotherapy, chemotherapy and combination radio-chemotherapy studies (Table 8.1) have consistently failed to provide satisfactory survival outcomes, and the vast majority of patients live a poor quality of life that is prolonged to 1–3 years after diagnosis [15].

8.6.1 Radiotherapy and Chemotherapy

Fractionated, focal intensity-modulated, external beam radiotherapy of the tumor along with 1–2 cm margins remains the standard of care in the management of DIPG. The generally accepted total dose is 5400–6000 cGy, usually administered in fractions of 180–200 cGy per day and delivered over approximately 6 weeks (given once daily for 5 days per week). At these doses, clinical improvement and objective tumor response are observed in up to 70% and 60% of patients, respectively [15]. While hyperfractionation of the radiotherapy schedule to higher total doses of 7020 cGy and 7800 cGy did not show benefit over the conventional protocol and may be associated with neurotoxicity [104, 134], hypofractionation over 3–4 weeks may lead to nearly the same outcome of conventional radiotherapy with less treatment burden and risks [109, 119, 135]. Short-course radiation protocols for DIPG are being developed to attain treatment outcomes that are comparable to conventional radiation [128]. Radiosensitizers such as cisplatin [134], motexafin gadolinium [118] as well as other platinoids, nitosureas, etoposide and topotecan [18, 136–138] were investigated in hope to improve the efficacy of radiotherapy, but no additional benefit was reported, and the results were equally disappointing. Nevertheless, recent studies re-irradiated DIPG patients at first and second progression and reported an increase in survival outcomes of few additional months with acceptable tolerability [130, 131].

The role of conventional chemotherapeutic agents has been investigated at different stages of the management of DIPG (prior to, concurrent with and adjunctive to radiotherapy). Used alone, in multiple combinations and/or at variable dose intensities, these agents included, but were not limited to, 5-fluorouracil/lomustine, prednisone/lomustine/vincristine, cisplatin/cyclophosphamide, cisplatin/etoposide/vincristine/cyclophosphamide, TMZ, TMZ/*cis*-retinoic acid, vincristine/etoposide, TMZ/thalidomide, methotrexate, cisplatin/etoposide/vincristine/ifosfamide, gefitinib, tipifarnib, nimotuzumab, PEGylated interferon α -2b, bevacizumab, irinotecan/cetuximab, tamoxifen, and busulfan/thiotepa [89, 99, 100, 103, 106, 108, 110–112, 114, 129, 132, 139–145]. None of these agents/combinations, at different dose intensities with or without radiotherapy, were able to show better survival outcomes compared to radiotherapy alone (Table 8.1).

Table 8.1 Summary of the outcomes of radiotherapy, chemotherapy or combination radio-chemotherapy studies in patients with DIPG. Note that more than 200 studies have been conducted so far, and only examples of old and new studies are included in this table

References	Study Institution/ Group	Regimen/Agent(s)	Radiotherapy Dose Range in cGy (Mean/ Median)	Number/Gender/ Category of Patients	Median Age (Years)	Response/Survival Outcomes
Levin et al. [99]	Brain Tumor Research Center & Children's Cancer Group	5-fluorouracil + lomustine → RT + hydroxyurea + misomidazole (during RT)	5000–6306 (5527)	F 14; M 14	7.5	mEFS 32 wks; mOS 44 wks
Jenkin et al. [100]	Children's Cancer Study Group	RT → lomustine + VCR + prednisone vs RT alone	4200–6199	F 38; M 26 RT + CT 39; RT 35	NA	mPFS 7 (RT + CT) vs 8 (RT) mths; 5-y OS 23% (RT + CT) vs 17% (RT) [NS]
Hibi et al. [101]	Tokyo Metropolitan Toshima Hospital	RT	4000–7550	F 21; M 18	6	All BSG: PR 71.2%; RR at <4499, 4500–5499, 5500–6499 & >6500 cGy: 45.5%, 83.3%, 66.7% & 100%, respectively; 1-y OS 47.4%; 2-y OS 14%; mOS at <4499, 4500–5499, 5500–6499 & >6500 cGy: 9, 13, 11.5 & 10 mths [NS]; mOS for PR & No PR: 13.5 & 9 mths, respectively [S] ----- DIPG: PR 70% ----- mOS for LGG vs HGG: 14 vs 9 mths, respectively [NS]
Shrieve et al. [102]	University of California, San Francisco	RT	7200–7800	Children: F 19; M 22 Adults: F 13; M 6	9.3	Pontine/medullary gliomas: Children: mOS 53 wks; 2-y OS 16% Adults: mOS 190 wks; 2-y OS 57% ----- Diffuse gliomas: Children: mOS 53 wks; 2-y OS 5% Adults: mOS 190 wks; 2-y OS 50%
Kretschmar et al. [103]	Pediatric Oncology Group	Cisplatin + cyclophosphamide → RT	6600	F 20; M 12	6	PR 9%; mOS 9 mths
Packer et al. [104]	Children's Cancer Group	RT	7800	F 34; M 32	6.8	PR 12%; mPFS 8 mths; 1-y OS 35%; 2-y OS 22%; 3-y OS 11%

(continued)

Table 8.1 (continued)

References	Study Institution/ Group	Regimen/Agent(s)	Radiotherapy Dose Range in cGy (Mean/ Median)	Number/Gender/ Category of Patients	Median Age (Years)	Response/Survival Outcomes
Fleischhack et al. [105]	University of Bonn	RT + nimotuzumab → nimotuzumab	5400	41 pts	7	PR 9.8%; mPFS 5.5 mths; mOS 9.6 mths
Haas-Kogan et al. [106]	Pediatric Brain Tumor Consortium	RT + tipifarnib → tipifarnib	5580	F 25; M 15	5.5	PR 17.5%; mPFS 5.9 mths; 1-y PFS 7.5%; 1.5-y PFS 2.5%; mOS 8.9 mths; 1-y OS 35%; 1.5-y OS 10%
Kivivuori et al. [107]	Children's Hospital, University of Helsinki	RT + topotecan → thalidomide + celecoxib + etoposide vs RT alone	(4680 in 1 pt)-5400	RT + CT: 8 pts RT alone: 8 pts	RT + CT: 7.5 RT alone: 7.5	RT + CT: 1-y OS 63% mOS 12.5 (RT + CT) vs 8.5 (RT alone) mths [NS]; mTTP 11 (RT + CT) vs 6.8 (RT alone) mths [S]; mPTD 0.75 (RT + CT) vs 2 (RT alone) mths [S]
Massimino et al. [108]	Fondazione IRCCS Istituto Nazionale Tumori	RT + nimotuzumab → nimotuzumab	5400	F 21; M 16	7.5	mPFS 7 mths; mOS 11 mths
Negretti et al. [109]	Institut Gustave Roussy	hypo-RT	4500-(6000 in 1 pt)	F 10; M 12	5.9	mTTP 5.7 mths; mOS 7.6 mths; mPTD 3 mths
Pollack et al. [110]	Pediatric Brain Tumor Consortium	RT + gefitinib → gefitinib	5580	F 29; M 14	7	PR 14%; mPFS 7.4 mths; 1-y & 2-y PFS 20.9 & 9.3%, respectively; 1-y & 2-y OS 56.4% & 19.6%, respectively
Wolff et al. [111]	HIT-GBM-D Study – Floating Hospital for Children at Tufts Medical Center	Methotrexate → RT + CT (cisplatin, etoposide, vincristine, ifosfamide, lomustine, prednisone)	5400	F 11; M 19	10.8	PR 42%; EFS at 6, 12, 24, 36, 48 & 60 mths: 77%, 43%, 20%, 17%, 13% & 13%, respectively; OS at 6, 12, 24, 36, 48 & 60 mths: 97%, 77%, 40%, 28%, 17% & 13%, respectively ----- mEFS with (11 pts) vs without (15 pts) dexamethasone: 1.5 vs 3.1 y, respectively [S]

Chassot et al. [112]	Institute Gustave Roussy	RT + TMZ → TMZ	5400	21 pts	6.4	PR 52.6%; mTTP 7.5 mths; mOS 11.7 mths; mPTD 3.5 mths; 1-y PFS 33%; 1-y OS 50%
Fontamilla et al. [113]	MD Anderson Cancer Center	RT + CT (cisplatin, etoposide, vincristine, topotecan, vandetanib, TMZ, methotrexate, ifosfamide, alone or in different combinations) → CT (irinotecan, bevacizumab, alemtuzumab, nimotuzumab, vandetanib, TMZ, vincristine, lomustine, etoposide, valproic acid, in different combinations) → re-RT in different combinations, alone or + CT (bevacizumab, irinotecan, TMZ, cisplatin, etoposide, alone or in different combinations)	5400–5580 → 1800–2000	F 4; M 2	4	mTTP 4 mths; mPFS 5 mths; mOS 6 mths
Warren et al. [114]	National Cancer Institute	RT → INF- α -2b	5040–6720 (5470)	F 19; M 13	5.3	2-y OS 14.3%; mOS 351 d; mTTP 235 d
Wolff et al. [115]	MD Anderson Cancer Center	2nd- or >2nd-line treatment: CT (etoposide, bevacizumab, irinotecan, valproic acid, nimotuzumab, TMZ, cetuximab, rapamycin, cis-retinoic acid, labradimil, cisplatin, carboplatin, vincristine, lomustine, temsirolimus, notch inhibitor MK0752, cyclophosphamide, Ruxo 6, procarbazine, sorafenib, topotecan, vinorelbine, celecoxib, vitamin D, fenofibrate, alone or in different combinations) +/- re-RT	re-RT in 7 pts: 200–2000	F 18; M 13	6.1	PR 12%; mTTP 2 mths; mEFS 2.5 mths
Aguilera et al. [116]	Children's Healthcare of Atlanta	RT → TMZ + bevacizumab	5400	F 1; M 1	9	Pt-1: PFS 37 mths Pt-2: PFS 47 mths

(continued)

Table 8.1 (continued)

References	Study Institution/ Group	Regimen/Agent(s)	Radiotherapy Dose Range in cGy (Mean/ Median)	Number/Gender/ Category of Patients	Median Age (Years)	Response/Survival Outcomes
Bailey et al. [117]	Children's Cancer and Leukaemia Group (CCLG)-CNS Group	RT + TMZ → TMZ	5400	F 19; M 24	8	mOS 9.5 mths; 9-mths, 1-y & 2-y OS 56%, 35% & 17%, respectively
Bradley et al. [118]	Children's Oncology Group	RT + motexafin + gadolinium	5400	F 34; M 30	6.4	PR 30%; 1-y EFS 18%; 1-y OS 53%, mPFS 7.2 mths; mOS 11.4 mths
Janssens et al. [119]	Radboud University Nijmegen Medical Centre & Academic Medical Center Amsterdam; Erasmus Medical Centre in Rotterdam	hypo-RT (+ TMZ in 11 pts) vs conv-RT (+ CT in 9 pts: TMZ in 3, etoposide in 2, nimotuzumab in 1, thalidomide + etoposide + cyclophosphamide in 1, foterumstine in 1, tamoxifen in 1)	3900–5400	hypo-RT: F 15; M 12 conv-RT: F 10; M 17	hypo-RT: 7.5 conv-RT: 7.3	mOS 9 (hypo-RT) vs 9.4 (conv-RT) mths [NS]; mTTP 5 (hypo-RT) vs 7.6 (conv-RT) mths [NS] ----- Hypo-RT: OS at 6, 9 & 12 mths: 74%, 44% & 22%, respectively; PFS at 3, 6 & 9 mths: 77%, 43% & 21%, respectively
Kebudi et al. [120]	Cerrahpasa Medical Faculty & Oncology Institute, Istanbul University	Gp-1: RT (12 pts) Gp-2: RT + cis-platinum or VCR → lomustine + VCR (17 pts) Gp-3: RT + TMZ → TMZ (21 pts)	5400–6000	F 26; M 24	7	All pts: mOS 13 mths mOS, 1-y OS, 2-y OS & 3-y OS for Gp-1: 12 mths, 41.7%, 0% & 0% respectively; mOS, 1-y OS, 2-y OS & 3-y OS for Gp-2: 12 mths, 55.3%, 37% & 37%, respectively; mOS, 1-y OS, 2-y OS & 3-y OS for Gp-3: 15 mths, 47.5%, 27% & 20%, respectively; 1-y OS, 2-y OS & 3-y OS for Gp-2 + Gp-3: 61%, 32% & 28%, respectively OS: Gp-1 vs Gp-2 [S]; Gp-1 vs Gp-3 [S]; Gp-1 vs Gp-2 + Gp-3 [S]
Zaky et al. [121]	Children's Hospital of Los Angeles	CT (carboplatin + etoposide in 5 pts & TMZ in 1 pt) → irinotecan + TMZ + bevacizumab	5540–6000	F 4; M 2	6.6	PR 66.7%, mEFS 10.4 mths; mOS 14.6 mths

Massimino et al. [122]	Fondazione IRCCS Istituto Nazionale dei Tumori	Nimotuzumab + vinorelbine → RT +/- re-RT (11 pts) → nimotuzumab + vinorelbine	5400 → 1980	F 10; M 15	6.1	PR 8%; RR 96%; mPFS 8.5 mths; 1-y & 2-y PFS 30% & 12%, respectively; mOS 1.5 mths; 1-y & 2-y OS 76% & 27% ----- re-RT vs No re-RT: mPFS 8.3 (re-RT) vs 8.5 (No re-RT) mths, respectively [NS]; mOS 16 (re-RT) vs 13.3 (No re-RT) mths, respectively [NS] ----- Tumor shrinkage >20% vs <20%: 1-y OS 100% vs 67%, respectively [S]; 2-y OS 50% vs 17%, respectively [S] ----- Age <4 y vs >4 y: 2-y OS 75% vs 15%, respectively [S] ----- Shunting vs No shunting: 1y OS 60% vs 22%, respectively [S]
Muller et al. [123]	Gesellschaft für Pädiatrische Onkologie und Hämatologie (GPOH)-HIT-HGG Study Group	RT + metronomic TMZ (+ nimotuzumab in 1 pt)	3520–5400	F 5; M 1	8.3	mPFS 4 mths; mOS 7.6 mths
Zaghloul et al. [124]	Children's Cancer Hospital, Egypt	hypo-RT vs conv-RT	3900–5400	hypo-RT: F 16; M 19 II conv-RT: F 18; M 18	7.9	mOS (all pts) 8.9 mths; mOS 7.8 (hypo-RT) vs 9.5 (conv-RT) mths; 1-y OS 36.4% (hypo-RT) vs 26.2% (conv-RT); 1.5-y OS 10.9 (hypo-RT) vs 13.1% (conv-RT) [NS]; mPFS 6.3 (hypo-RT) vs 7.3 (conv-RT) mths; 1-y PFS 22.5% (hypo-RT) vs 17.9% (conv-RT); 1.5-y PFS 9.6% (hypo-RT) vs 10.8% (conv-RT) [NS] 7.3-mths PFS 85.7%; 9-mths OS 71.4%; 1-y OS 57.1%
Epelman et al. [125]	Santa Marcelina Hospital	Nimotuzumab + RT	5400	F 14; M 7	7.6	PR 66.6%; mPFS 7.15 mths; 1y PFS 20%; mOS 15.6 mths; 1y OS 60%
Rizzo et al. [126]	Catholic University of Rome	RT + TMZ → TMZ	4500–5940	F 9; M 6	9	

(continued)

Table 8.1 (continued)

References	Study Institution/ Group	Regimen/Agent(s)	Radiotherapy Dose Range in cGy (Mean/ Median)	Number/Gender/ Category of Patients	Median Age (Years)	Response/Survival Outcomes
Vanan et al. [127]	University of Manitoba	re-RT	2160–3600	F 6; M 4	6.5	mOS (post re-RT) 9 mths; mPTD 171 d (re-RT) vs 91.5 d (No re-RT; 46 pts from historic cohort) [S]
Hankinson et al. [128]	University of Colorado & Children's Hospital Colorado	RT	2500	F 3; M 4	4.5	mOS 6.6 mths; 6-, 9- & 12-mths OS 58%, 28% & 28%, respectively; mPFS 6.3 mths; 3-, 6- & 9-mths PFS 72%, 58% & 0%, respectively
Hummel et al. [129]	Cincinnati Children's Hospital Medical Center; Ann & Robert H Lurie Children's Hospital	RT + bevacizumab → bevacizumab + irinotecan + TMZ (TMZ for HGG but not DIPG pts)	5400–5940	DIPG 15: F 7; M 8 HGG 12: F 7; M 5	10	DIPG: mPFS 8.2 mths; mOS 10.4 mths ----- HGG: mPFS 15.2 mths; mOS 25.4 mths; 1-y PFS 92%; 1-y OS 92%; 3-y PFS 33%; 3-y OS 55%
Janssens et al. [130]	Societe' Internationale d'Oncologie Pediatrique- Europe-HGG/ DIPG Working Group	RT + re-RT vs RT + re-RT + ST vs RT + BSC vs RT + ST	1800–3000	re-RT: F 17; M 14 No re-RT: F 20; M 19	re-RT 6 No re-RT 7	mPFS 8.2 (re-RT) vs 7.7 (No re-RT) mths [NS]; mOS 13.7 (re-RT) vs 10.3 (No re-RT) mths [S]; OS (re-RT vs No re-RT) at 6, 9, 12 & 18 mths: 100% vs 95%, 87% vs 67%, 71% vs 33%, 23% vs 10%, respectively; mOS 6.1 (re-RT + ST) vs 5.4 (re-RT) [NS] ----- In re-RT subgroups of interval between end of RT & re-RT; mOS of re-RT vs No re-RT for 3–6 mths & 6–12 mths intervals: 4 vs 2.7 mths [S] & 6.4 vs 3.3 mths [S], respectively
La Madrid et al. [131]	Hospital Sant Joan de Deu	RT → re-RT	Pt-1: 5400 → 3060 → 2160 Pt-2: 3900 → 2000 → 2000	F 1; M 1	5.5	Pt-1: PFS 8 (post RT), then 4 (post re-RT) & 3 (post 2nd re-RT) mths Pt-2: PFS 11 (post RT), then 8 (post re-RT) & 12 (post 2nd re-RT) mths

<p>Macy et al. [132]</p>	<p>Pediatric Oncology Experimental Therapeutics Investigators' Consortium</p>	<p>Cetuximab + RT → cetuximab + irinotecan</p>	<p>5940</p>	<p>F 24; M 21 DIPG 25; HGG 20</p>	<p>8</p>	<p>DIPG: mPFS/TTP 7.12 mths; 1-y PFS 29.6%; mEFS 6.9 mths; mOS 12.1 mths HGA: mPFS/TTP 9.02 mths; 1-y PFS 18%; mEFS 8.9 mths; mOS 17.4 mths</p>
<p>Yoshida et al. [133]</p>	<p>Kobe University Graduate School of Medicine</p>	<p>RT +/- CT (TMZ, nimustine, IFN-β, nimustine+IFN-β, TMZ + IFN-β or nimustine+IFN-β + vincristine) ----- Only 76% of pts received RT + concurrent CT</p>	<p>5000–7000 (5600)</p>	<p>Children: F 9; M 5 Adults: F 6; M 10</p>	<p>Children 8; Adults 49</p>	<p>mOS 15 mths (Children: mOS 9.5 mths; Adults: mOS 39 mths); 1-y, 2-y & 3-y OS 53%, 43% & 27%, respectively; 1-y, 2-y & 3-y PFS 43%, 26% & 19%, respectively; Children/Adult 1-y, 2-y & 3-y OS 29%/75%, 14%/68% & 0%/53%, respectively [S]; Children/Adult 1-y, 2-y & 3-y PFS 14%/69%, 0%/49% & 0%/35%, respectively [S] ----- 2-y OS/PFS for Diffuse intrinsic vs Other (focal, exophytic): 39%/57% vs 26%/29%, respectively [NS]; 2-y OS/PFS for Pontine vs Non-pontine: 36%/80% vs 24%/40%, respectively [NS]; 2-y OS/PFS for pts with vs without pretreatment tumor enhancement: 50%/40% vs 21%/33%, respectively [NS]; 3-y OS/PFS for pts treated with vs without TMZ: 34%/50% vs 21%/31%, respectively [NS]</p>

Abbreviations: BSC best supportive care, BSG brainstem glioma, cGY centigray, conv-RT conventional radiotherapy, CT chemotherapy, d days, DIPG diffuse intrinsic pontine glioma, F female, Gp group, HGA high-grade astrocytoma, hypo-RT hypofractionated radiotherapy, IFN-β interferon-β, M male, mEFS median event-free survival, mOS median overall survival, mPFS median progression free survival, mPTD median time from progression to death, mths months, NA not available, OS overall survival, PR partial response [defined as the presence of either (1) a 50% or greater reduction in tumor bulk or at least 30% decrease in the sum of the longest diameter of target lesion as seen on computed tomography scan or magnetic resonance imaging or (2) the disappearance of at least one of the neurological signs (pyramidal tract sign, cranial nerve deficit, or cerebellar sign), or both], Pt(s) patient(s), re-RT re-irradiation, RR response rate, RT radiotherapy, ST systemic therapy, TMZ temozolomide, TTP median time to progression, VCR vincristine, vs versus, wks weeks, y year, [NS] not significant, & and, → followed by

8.6.2 Targeted Therapy

The management trend of DIPG is leaning towards therapies targeting specific tumoral molecular pathways for two reasons: (1) The conventional radio-chemotherapies are consistently failing to provide satisfactory outcomes, i.e., prolonging patients' lives for few months with very poor quality; and (2) the literature is being enriched with unique molecular, genetic and epigenetic characteristics of diffuse midline gliomas/DIPG, thus paving the road for such studies to commence.

Following the recent discovery of epigenetic alterations in histone genes, inhibition of histone deacetylases (HDACs) is being explored as a potential therapeutic strategy. Overexpression of HDACs is reported in many cancers [146], possibly contributing to the development of malignancy due to disruption of the balance between transcriptional activation and repression of gene expression for post-translational acetylation of histone tails, which are maintained by histone acetyltransferases (HATs) and HDACs, respectively [147]. Panobinostat (LBH589), an oral inhibitor of several HDACs that has been reported to decrease proliferation of H3 K27M-mutant diffuse midline gliomas and has a synergistic effect when combined with the histone demethylase inhibitor GSK-J4 in preclinical experiments [148], is currently under study in patients with DIPG ([ClinicalTrials.gov: NCT02717455](https://clinicaltrials.gov/ct2/show/study/NCT02717455)). For tumors that harbor the H3 K27M mutation (most of DIPG), there is loss of trimethylation that will potentially lead to abnormal cell-cycle control, inhibition of autophagy, and augmentation of tumor resistance to radiotherapy [149]. Panobinostat was shown to increase trimethylation and acetylation levels of H3 K27M-mutant tumors, hence augmenting the potential efficacy of radiation or other treatments. Panobinostat has been shown to have antitumor efficacy on H3 K27M-expressing cells *in vitro*, reducing both cell proliferation and viability, and potent activity in some *in vivo* models, but not in others [149]. Vorinostat (SAHA), another HDAC inhibitor, has been well tolerated in combination with TMZ in children with high-grade gliomas [150] and is currently being investigated in combination with radiotherapy in a phase II trial ([ClinicalTrials.gov: NCT01189266](https://clinicaltrials.gov/ct2/show/study/NCT01189266)) and with temsirolimus, a mammalian target of rapamycin (mTOR) pathway inhibitor, along with radiotherapy in a phase I trial ([ClinicalTrials.gov: NCT02420613](https://clinicaltrials.gov/ct2/show/study/NCT02420613)). In preclinical studies, other epigenetic drugs such as GSK-J4 [151], EZH2 inhibitors [152], and BET bromodomain inhibitors [153] have been effective in inhibiting the growth of H3 K27M-mutant diffuse midline gliomas; these drugs, however, are yet to be tested in human subjects.

Dasatinib and crenolanib are inhibitors of the platelet-derived growth factor receptor (PDGFR), one of the most frequently amplified molecules in pediatric high-grade gliomas/DIPG [98], and are being investigated in ongoing and completed clinical trials, the results of which are not published yet ([ClinicalTrials.gov: NCT02233049](https://clinicaltrials.gov/ct2/show/study/NCT02233049); [NCT01393912](https://clinicaltrials.gov/ct2/show/study/NCT01393912)). Another ongoing trial ([ClinicalTrials.gov: NCT01644773](https://clinicaltrials.gov/ct2/show/study/NCT01644773)) combines dasatinib with crizotinib, an ALK and c-MET inhibitor. Preliminary data showed anti-tumoral effects of dasatinib in DIPG cell lines, which also revealed a synergistic effect when combined with the c-MET inhibitor, cabozantinib [154].

Epidermal growth factor receptor (EGFR) inhibitor, erlotinib, was studied in combination with focal radiotherapy, but did not show improvement in outcomes of patients with newly diagnosed high-grade gliomas [155]. Ongoing trials, however, are investigating its efficacy in combination with bevacizumab, TMZ and radiotherapy ([ClinicalTrials.gov: NCT01182350](https://clinicaltrials.gov/ct2/show/study/NCT01182350)), as well as with everolimus and dasatinib ([ClinicalTrials.gov: NCT02233049](https://clinicaltrials.gov/ct2/show/study/NCT02233049)).

Convection-enhanced delivery (CED), a new technique that allows to bypass the BBB by direct delivery of drugs into the tumor, holds promise in increasing the efficacy of DIPG targeted therapy [156]. Carboplatin was successfully delivered into a DIPG using robot-guided CED [157]. CED of a radiolabeled antibody [¹²⁴I]-8H9 [158], panobinostat [159], as well as other agents such as irinotecan is being considered and/or currently under study in patients with malignant glioma, including DIPG ([ClinicalTrials.gov: NCT03086616](https://clinicaltrials.gov/ct2/show/study/NCT03086616)).

8.7 Conclusion

Diffuse midline glioma, H3 K27M-mutant or DIPG remains among the most challenging tumors to treat despite extensive efforts from field experts through hundreds of trials to find the “magical” management recipe. Nevertheless, the recent molecular discoveries offer hope for better outcomes through the implementation of many targeted therapeutic trials, the results of many of which are still pending and/or the dose, frequency and combination of the studied molecule(s) with other therapies require further optimization. Until then, radiotherapy remains the cornerstone in the management of this debilitating disease.

References

1. Hensch E. Fall VI. Sarcom des pons varoli. *Charité-Ann.* 1880;461–5.
2. Jacobi MP. Case of probable tumor of the pons. *J Nerv Ment Dis.* 1889;14(2):115–29.
3. Williams P. Case of tumour of the pons. *Bristol Med Chir J* (1883). 1891;9(33):163–7.
4. Mills CK. Tumor of the pons varolii, with conjugate deviation of the eyes and rotation of the head. *J Nerv Ment Dis.* 1881;8(3):470–81.
5. Weisenburg T. Extensive gliomatous tumor involving the cerebellum and the posterior portions of the medulla, pons and cerebral peduncle and the posterior limb of one internal capsule. *J Am Med Assoc.* 1909;53(25):2086–91.
6. Zenner P. Two cases of tumor of the pons. *J Nerv Ment Dis.* 1910;37(1):27–36.
7. Dmetrichuk J, Pendleton C, Jallo G, Quiñones-Hinojosa A. Father of neurosurgery: Harvey Cushing’s early experience with a pediatric brainstem glioma at the Johns Hopkins Hospital. *J Neurosurg Pediatr.* 2011;8(4):337–41.
8. Bailey P, Eisenhardt L. Spongioblastomas of the brain. *J Comp Neurol.* 1932;56(2):391–430.
9. Cushing H. The surgical mortality percentages pertaining to a series of two thousand verified intracranial tumors: standards of computation. *Arch Neurol Psychiatr.* 1932;27(6):1273–80.
10. Pilcher C. Spongioblastoma polare of the pons: clinicopathologic study of eleven cases. *Arch Neurol Psychiatr.* 1934;32(6):1210–29.
11. Bray PF, Carter S, Taveras JM. Brainstem tumors in children. *Neurology.* 1958;8(1):1–7.

12. Whyte T, Colby JM, Layton JD. Radiation therapy of brain-stem tumors. *Radiology*. 1969;93(2):413–6. *passim*.
13. Reigel D, Scarff T, Woodford J. Biopsy of pediatric brain stem tumors. *Childs Brain*. 1979;5(3):329–40.
14. Louis D, Ohgaki H, Wiestler O, Cavenee W. WHO classification of tumours of the central nervous system. Revised 4th ed. Geneva: WHO Press; 2016.
15. Jansen M, Van Vuurden D, Vandertop W, Kaspers G. Diffuse intrinsic pontine gliomas: a systematic update on clinical trials and biology. *Cancer Treat Rev*. 2012;38(1):27–35.
16. Walker D, Punt J, Sokal M. Brainstem tumors. In: Walker D, Perilongo G, Punt J, Taylor R, editors. *Brain and spinal tumors of childhood*. Oxford: Arnold Publisher; 2004. p. 291–313.
17. Ostrom QT, Gittleman H, Liao P, Vecchione-Koval T, Wolinsky Y, Kruchko C, et al. CBTRUS statistical report: primary brain and other central nervous system tumors diagnosed in the United States in 2010–2014. *Neuro-Oncology*. 2017;19(suppl_5):v1–v88.
18. Hargrave D, Bartels U, Bouffet E. Diffuse brainstem glioma in children: critical review of clinical trials. *Lancet Oncol*. 2006;7(3):241–8.
19. Cooney T, Lane A, Bartels U, Bouffet E, Goldman S, Leary SE, et al. Contemporary survival endpoints: an International Diffuse Intrinsic Pontine Glioma Registry Study. *Neuro-Oncology*. 2017;19(9):1279–80.
20. Guillamo J-S, Monjour A, Taillandier L, Devaux B, Varlet P, Haie-Meder C, et al. Brainstem gliomas in adults: prognostic factors and classification. *Brain*. 2001;124(12):2528–39.
21. Ueoka DI, Nogueira J, Campos JC, Maranhão Filho P, Ferman S, Lima MA. Brainstem gliomas—retrospective analysis of 86 patients. *J Neurol Sci*. 2009;281(1):20–3.
22. Jansen MH, Veldhuijzen van Zanten SE, Sanchez Aliaga E, Heymans MW, Warmuth-Metz M, Hargrave D, et al. Survival prediction model of children with diffuse intrinsic pontine glioma based on clinical and radiological criteria. *Neuro-Oncology*. 2015;17(1):160–6.
23. Guillamo J-S, Doz F, Delattre J-Y. Brain stem gliomas. *Curr Opin Neurol*. 2001;14(6):711–5.
24. Laigle-Donadey F, Doz F, Delattre J-Y. Brainstem gliomas in children and adults. *Curr Opin Oncol*. 2008;20(6):662–7.
25. Fisher PG, Breiter SN, Carson BS, Wharam MD, Williams JA, Weingart JD, et al. A clinicopathologic reappraisal of brain stem tumor classification. *Cancer*. 2000;89(7):1569–76.
26. Epstein FJ, Farmer J-P. Brain-stem glioma growth patterns. *J Neurosurg*. 1993;78(3):408–12.
27. Sandri A, Sardi N, Genitori L, Giordano F, Peretta P, Basso M, et al. Diffuse and focal brain stem tumors in childhood: prognostic factors and surgical outcome. *Childs Nerv Syst*. 2006;22(9):1127–35.
28. Patten J. The brain stem. In: Patten J, editor. *Neurological differential diagnosis*. 2nd ed. New York: Springer; 1996. p. 162–77.
29. Hargrave D, Chuang N, Bouffet E. Conventional MRI cannot predict survival in childhood diffuse intrinsic pontine glioma. *J Neuro-Oncol*. 2008;86(3):313–9.
30. Green A, Kieran M. Pediatric brainstem gliomas: new understanding leads to potential new treatments for two very different tumors. *Curr Oncol Rep*. 2015;17(3):436.
31. Garzón M, García-Fructuoso G, Guillén A, Suñol M, Mora J, Cruz O. Brain stem tumors in children and adolescents: single institutional experience. *Childs Nerv Syst*. 2013;29(8):1321–31.
32. Soler D, Borzyskowski M. Lower urinary tract dysfunction in children with central nervous system tumours. *Arch Dis Child*. 1998;79(4):344–7.
33. Barkovich A, Krischer J, Kun L, Packer R, Zimmerman R, Freeman C, et al. Brain stem gliomas: a classification system based on magnetic resonance imaging. *Pediatr Neurosurg*. 1990;16(2):73–83.
34. Löbel U, Sedlacik J, Sabin ND, Kocak M, Broniscer A, Hillenbrand CM, et al. Three-dimensional susceptibility-weighted imaging and two-dimensional T2*-weighted gradient-echo imaging of intratumoral hemorrhages in pediatric diffuse intrinsic pontine glioma. *Neuroradiology*. 2010;52(12):1167–77.
35. Frazier JL, Lee J, Thomale UW, Noggle JC, Cohen KJ, Jallo GI. Treatment of diffuse intrinsic brainstem gliomas: failed approaches and future strategies. A review. *J Neurosurg Pediatr*. 2009;3(4):259–69.

36. Ramos A, Hilario A, Lagares A, Salvador E, Perez-Nuñez A, Sepulveda J. Brainstem gliomas. *Semin Ultrasound CT MR*. 2013;34(2):104–12.
37. Hayward RM, Patronas N, Baker EH, Vézina G, Albert PS, Warren KE. Inter-observer variability in the measurement of diffuse intrinsic pontine gliomas. *J Neuro-Oncol*. 2008;90(1):57–61.
38. Zukotynski KA, Fahey FH, Kocak M, Alavi A, Wong TZ, Treves ST, et al. Evaluation of 18F-FDG PET and MRI associations in pediatric diffuse intrinsic brain stem glioma: a report from the Pediatric Brain Tumor Consortium. *J Nucl Med*. 2011;52(2):188–95.
39. Prabhu SP, Ng S, Vajapeyam S, Kieran MW, Pollack IF, Geyer R, et al. DTI assessment of the brainstem white matter tracts in pediatric BSG before and after therapy. *Childs Nerv Syst*. 2011;27(1):11–8.
40. Poussaint TY, Kocak M, Vajapeyam S, Packer RI, Robertson RL, Geyer R, et al. MRI as a central component of clinical trials analysis in brainstem glioma: a report from the Pediatric Brain Tumor Consortium (PBTC). *Neuro-Oncology*. 2011;13(4):417–27.
41. Löbel U, Sedlacik J, Reddick WE, Kocak M, Ji Q, Broniscer A, et al. Quantitative diffusion-weighted and dynamic susceptibility-weighted contrast-enhanced perfusion MR imaging analysis of T2 hypointense lesion components in pediatric diffuse intrinsic pontine glioma. *AJNR Am J Neuroradiol*. 2011;32(2):315–22.
42. Lober RM, Cho YJ, Tang Y, Barnes PD, Edwards MS, Vogel H, et al. Diffusion-weighted MRI derived apparent diffusion coefficient identifies prognostically distinct subgroups of pediatric diffuse intrinsic pontine glioma. *J Neuro-Oncol*. 2014;117(1):175–82.
43. Poussaint TY, Vajapeyam S, Ricci KI, Panigrahy A, Kocak M, Kun LE, et al. Apparent diffusion coefficient histogram metrics correlate with survival in diffuse intrinsic pontine glioma: a report from the Pediatric Brain Tumor Consortium. *Neuro-Oncology*. 2016;18(5):725–34.
44. Zukotynski KA, Vajapeyam S, Fahey FH, Kocak M, Brown D, Ricci KI, et al. Correlation of 18F-FDG PET and MRI apparent diffusion coefficient histogram metrics with survival in diffuse intrinsic pontine glioma: a report from the Pediatric Brain Tumor Consortium. *J Nucl Med*. 2017;58(8):1264–9.
45. Thakur S, Karimi S, Dunkel I, Koutcher J, Huang W. Longitudinal MR spectroscopic imaging of pediatric diffuse pontine tumors to assess tumor aggression and progression. *AJNR Am J Neuroradiol*. 2006;27(4):806–9.
46. Hipp SJ, Steffen-Smith E, Hammoud D, Shih JH, Bent R, Warren KE. Predicting outcome of children with diffuse intrinsic pontine gliomas using multiparametric imaging. *Neuro-Oncology*. 2011;13(8):904–9.
47. Laprie A, Pirzkall A, Haas-Kogan DA, Cha S, Banerjee A, Le TP, et al. Longitudinal multivoxel MR spectroscopy study of pediatric diffuse brainstem gliomas treated with radiotherapy. *Int J Radiat Oncol Biol Phys*. 2005;62(1):20–31.
48. Sugahara T, Korogi Y, Kochi M, Ushio Y, Takahashi M. Perfusion-sensitive MR imaging of gliomas: comparison between gradient-echo and spin-echo echo-planar imaging techniques. *AJNR Am J Neuroradiol*. 2001;22(7):1306–15.
49. Nadvi S, Ebrahim FS, Corr P. The value of 201 thallium-SPECT imaging in childhood brainstem gliomas. *Pediatr Radiol*. 1998;28(8):575–9.
50. Epstein F, Wisoff JH. Intrinsic brainstem tumors in childhood: surgical indications. *J Neuro-Oncol*. 1988;6(4):309–17.
51. Epstein F, McCleary EL. Intrinsic brain-stem tumors of childhood: surgical indications. *J Neurosurg*. 1986;64(1):11–5.
52. Gleason CA, Wise BL, Feinstein B. Stereotactic localization (with computerized tomographic scanning), biopsy, and radiofrequency treatment of deep brain lesions. *Neurosurgery*. 1978;2(3):217–22.
53. Albright AL, Packer RJ, Zimmerman R, Rorke LB, Boyett J, Hammond GD. Magnetic resonance scans should replace biopsies for the diagnosis of diffuse brain stem gliomas: a report from the Children’s Cancer Group. *Neurosurgery*. 1993;33(6):1026–30.
54. Roujeau T, Machado G, Garnett MR, Miquel C, Puget S, Georger B, et al. Stereotactic biopsy of diffuse pontine lesions in children. *J Neurosurg*. 2007;107(1 Suppl):1–4.

55. de León FC-P, Perezpena-Diazconti M, Castro-Sierra E, Guerrero-Jazo F, Gordillo-Dominguez L, Gutierrez-Guerra R, et al. Stereotactically-guided biopsies of brainstem tumors. *Childs Nerv Syst.* 2003;19(5-6):305–10.
56. Dellaretti M, Touzet G, Reynolds N, Dubois F, Gusmão S, Pereira JLB, et al. Correlation among magnetic resonance imaging findings, prognostic factors for survival, and histological diagnosis of intrinsic brainstem lesions in children. *J Neurosurg Pediatr.* 2011;8(6):539–43.
57. Rajshekhar V, Moorthy RK. Status of stereotactic biopsy in children with brain stem masses: insights from a series of 106 patients. *Stereotact Funct Neurosurg.* 2010;88(6):360–6.
58. Puget S, Beccaria K, Blauwblomme T, Roujeau T, James S, Grill J, et al. Biopsy in a series of 130 pediatric diffuse intrinsic pontine gliomas. *Childs Nerv Syst.* 2015;31(10):1773–80.
59. Samadani U, Judy KD. Stereotactic brainstem biopsy is indicated for the diagnosis of a vast array of brainstem pathology. *Stereotact Funct Neurosurg.* 2003;81(1-4):5–9.
60. Pincus DW, Richter EO, Yachnis AT, Bennett J, Bhatti MT, Smith A. Brainstem stereotactic biopsy sampling in children. *J Neurosurg Pediatr.* 2006;104(2):108–14.
61. Pirotte BJ, Lubansu A, Massager N, Wikler D, Goldman S, Levivier M. Results of positron emission tomography guidance and reassessment of the utility of and indications for stereotactic biopsy in children with infiltrative brainstem tumors. *J Neurosurg.* 2007;107(5 Suppl):392–9.
62. Phi JH, Chung H-T, Wang K-C, Ryu SK, Kim S-K. Transcerebellar biopsy of diffuse pontine gliomas in children: a technical note. *Childs Nerv Syst.* 2013;29(3):489–93.
63. Wang ZJ, Rao L, Bhambhani K, Miller K, Poulik J, Altinok D, et al. Diffuse intrinsic pontine glioma biopsy: a single institution experience. *Pediatr Blood Cancer.* 2015;62(1):163–5.
64. Walker DA, Liu J, Kieran M, Jabado N, Picton S, Packer R, et al. A multi-disciplinary consensus statement concerning surgical approaches to low-grade, high-grade astrocytomas and diffuse intrinsic pontine gliomas in childhood (CPN Paris 2011) using the Delphi method. *Neuro-Oncology.* 2013;15(4):462–8.
65. Kambhampati M, Perez JP, Yadavilli S, Saratsis AM, Hill AD, Ho C-Y, et al. A standardized autopsy procurement allows for the comprehensive study of DIPG biology. *Oncotarget.* 2015;6(14):12740–7.
66. Wu G, Diaz AK, Paugh BS, Rankin SL, Ju B, Li Y, et al. The genomic landscape of diffuse intrinsic pontine glioma and pediatric non-brainstem high-grade glioma. *Nat Genet.* 2014;46(5):444–50.
67. Huang TY, Piunti A, Lulla RR, Qi J, Horbinski CM, Tomita T, et al. Detection of Histone H3 mutations in cerebrospinal fluid-derived tumor DNA from children with diffuse midline glioma. *Acta Neuropathol Commun.* 2017;5(1):28.
68. Jones C, Baker SJ. Unique genetic and epigenetic mechanisms driving paediatric diffuse high-grade glioma. *Nat Rev Cancer.* 2014;14(10):651.
69. Dellaretti M, Reynolds N, Touzet G, Dubois F, Gusmão S, Pereira JLB, et al. Stereotactic biopsy for brainstem tumors: comparison of transcerebellar with transfrontal approach. *Stereotact Funct Neurosurg.* 2012;90(2):79–83.
70. Carai A, Mastronuzzi A, De AB, Messina R, Cacchione A, Miele E, et al. Robot-assisted stereotactic biopsy of diffuse intrinsic pontine glioma: a single-center experience. *World Neurosurg.* 2017;101:584–8.
71. Alcantara SL, Chen J, Kwon C, Jackson E, Li Y, Burns D, et al. Malignant astrocytomas originate from neural stem/progenitor cells in a somatic tumor suppressor mouse model. *Cancer Cell.* 2009;15(1):45–56.
72. Wang Y, Yang J, Zheng H, Tomasek G, Zhang P, McKeever P, et al. Expression of mutant p53 proteins implicates a lineage relationship between neural stem cells and malignant astrocytic glioma in a murine model. *Cancer Cell.* 2009;15(6):514–26.
73. Bohman L-E, Swanson KR, Moore JL, Rockne R, Mandigo C, Hankinson T, et al. Magnetic resonance imaging characteristics of glioblastoma multiforme: implications for understanding glioma ontogeny. *Neurosurgery.* 2010;67(5):1319–28.
74. Monje M, Mitra S, Freret M, Raveh T, Kim J, Masek M, et al. Hedgehog-responsive candidate cell of origin for diffuse intrinsic pontine glioma. *Proc Natl Acad Sci U S A.* 2011;108(11):4453–8.

75. Louis DN, Perry A, Reifenberger G, Von Deimling A, Figarella-Branger D, Cavenee WK, et al. The 2016 World Health Organization classification of tumors of the central nervous system: a summary. *Acta Neuropathol.* 2016;131(6):803–20.
76. Epstein F. A staging system for brain stem gliomas. *Cancer.* 1985;56(S7):1804–6.
77. Bugiani M, van Zanten SEV, Caretti V, Schellen P, Aronica E, Noske DP, et al. Deceptive morphologic and epigenetic heterogeneity in diffuse intrinsic pontine glioma. *Oncotarget.* 2017;8(36):60447.
78. Buczkowicz P, Bartels U, Bouffet E, Becher O, Hawkins C. Histopathological spectrum of paediatric diffuse intrinsic pontine glioma: diagnostic and therapeutic implications. *Acta Neuropathol.* 2014;128(4):573–81.
79. Hoffman L, DeWire M, Ryall S, Buczkowicz P, Leach J, Miles L, et al. Spatial genomic heterogeneity in diffuse intrinsic pontine and midline high-grade glioma: implications for diagnostic biopsy and targeted therapeutics. *Acta Neuropathol Commun.* 2016;4:1–8.
80. Yoshimura J, Onda K, Tanaka R, Takahashi H. Clinicopathological study of diffuse type brainstem gliomas: analysis of 40 autopsy cases. *Neurol Med Chir (Tokyo).* 2003;43(8):375–82.
81. Sufit A, Donson AM, Birks DK, Knipstein JA, Fenton LZ, Jedlicka P, et al. Diffuse intrinsic pontine tumors: a study of primitive neuroectodermal tumors versus the more common diffuse intrinsic pontine gliomas. *J Neurosurg Pediatr.* 2012;10(2):81–8.
82. Gielen GH, Gessi M, Hammes J, Kramm CM, Waha A, Pietsch T. H3F3A K27M mutation in pediatric CNS tumors: a marker for diffuse high-grade astrocytomas. *Am J Clin Pathol.* 2013;139(3):345–9.
83. Lulla R, Saratsis A, Hashizume R. Mutations in chromatin machinery and pediatric high-grade glioma. *Sci Adv.* 2016;2(3):e1501354.
84. Schwartzentruber J, Korshunov A, Liu X, Jones D, Pfaff E, Jacob K, et al. Driver mutations in histone H3. 3 and chromatin remodelling genes in paediatric glioblastoma. *Nature.* 2012;482(7384):226–31.
85. Wu G, Broniscer A, McEachron T, Lu C, Paugh B, Becksfort J, et al. Somatic histone H3 alterations in pediatric diffuse intrinsic pontine gliomas and non-brainstem glioblastomas. *Nat Genet.* 2012;44(3):251–3.
86. Puntonet J, Dangouloff-Ros V, Saffroy R, Pagès M, Andreiuolo F, Grill J, et al. Historadiological correlations in high-grade glioma with the histone 3.3 G34R mutation. *J Neuroradiol.* 2018;45(5):316–22.
87. Lewis P, Müller M, Koletsky M, Cordero F, Lin S, Banaszynski L, et al. Inhibition of PRC2 activity by a gain-of-function H3 mutation found in pediatric glioblastoma. *Science.* 2013;340(6134):857–61.
88. Korshunov A, Ryzhova M, Hovestadt V, Bender S, Sturm D, Capper D, et al. Integrated analysis of pediatric glioblastoma reveals a subset of biologically favorable tumors with associated molecular prognostic markers. *Acta Neuropathol.* 2015;129(5):669–78.
89. Cohen K, Pollack I, Zhou T, Buxton A, Holmes E, Burger P, et al. Temozolomide in the treatment of high-grade gliomas in children: a report from the Children’s Oncology Group. *Neuro-Oncology.* 2011;13(3):317–23.
90. Castel D, Philippe C, Calmon R, Le Dret L, Truffaux N, Boddaert N, et al. Histone H3F3A and HIST1H3B K27M mutations define two subgroups of diffuse intrinsic pontine gliomas with different prognosis and phenotypes. *Acta Neuropathol.* 2015;130(6):815–27.
91. Lobon-Iglesias M, Giraud G, Castel D, Philippe C, Debily M, Briandet C, et al. Diffuse intrinsic pontine gliomas (DIPG) at recurrence: is there a window to test new therapies in some patients? *J Neuro-Oncol.* 2018;137(1):111–8.
92. Khuong-Quang D, Buczkowicz P, Rakopoulos P, Liu X, Fontebasso A, Bouffet E, et al. K27M mutation in histone H3. 3 defines clinically and biologically distinct subgroups of pediatric diffuse intrinsic pontine gliomas. *Acta Neuropathol.* 2012;124(3):439–47.
93. Fontebasso A, Papillon-Cavanagh S, Schwartzentruber J, Nikbakht H, Gerges N, Fiset P, et al. Recurrent somatic mutations in ACVR1 in pediatric midline high-grade astrocytoma. *Nat Genet.* 2014;46(5):462–6.

94. Buczkowicz P, Hoeman C, Rakopoulos P, Pajovic S, Letourneau L, Dzamba M, et al. Genomic analysis of diffuse intrinsic pontine gliomas identifies three molecular subgroups and recurrent activating ACVR1 mutations. *Nat Genet.* 2014;46(5):451–6.
95. Taylor K, Mackay A, Truffaux N, Butterfield Y, Morozova O, Philippe C, et al. Recurrent activating ACVR1 mutations in diffuse intrinsic pontine glioma. *Nat Genet.* 2014;46(5):457–61.
96. Zarghooni M, Bartels U, Lee E, Buczkowicz P, Morrison A, Huang A, et al. Whole-genome profiling of pediatric diffuse intrinsic pontine gliomas highlights platelet-derived growth factor receptor alpha and poly (ADP-ribose) polymerase as potential therapeutic targets. *J Clin Oncol.* 2010;28(8):1337–44.
97. Gilbertson R, Hill D, Hernan R, Kocak M, Geyer R, Olson J, et al. ERBB1 is amplified and overexpressed in high-grade diffusely infiltrative pediatric brain stem glioma. *Clin Cancer Res.* 2003;9(10 Pt 1):3620–4.
98. Mackay A, Burford A, Carvalho D, Izquierdo E, Fazal-Salom J, Taylor KR, et al. Integrated molecular meta-analysis of 1,000 pediatric high-grade and diffuse intrinsic Pontine Glioma. *Cancer Cell.* 2017;32(4):520–37.
99. Levin V, Edwards M, Wara W, Allen J, Ortega J, Vestnys P. 5-Fluorouracil and 1-(2-chloroethyl)-3-cyclohexyl-1-nitrosourea (CCNU) followed by hydroxyurea, misonidazole, and irradiation for brain stem gliomas: a pilot study of the Brain Tumor Research Center and the Childrens Cancer Group. *Neurosurgery.* 1984;14(6):679-81.
100. Jenkin R, Boesel C, Ertel I, Evans A, Hittle R, Ortega J, et al. Brain-stem tumors in childhood: a prospective randomized trial of irradiation with and without adjuvant CCNU, VCR, and prednisone. A report of the Childrens Cancer Study Group. *J Neurosurg.* 1987;66(2):227–33.
101. Hibi T, Shitara N, Genka S, Fuchinoue T, Hayakawa I, Tsuchida T, et al. Radiotherapy for pediatric brain stem glioma: radiation dose, response, and survival. *Neurosurgery.* 1992;31(4):643–51.
102. Shrieve D, Wara W, Edwards M, Sneed P, Prados M, Cogen P, et al. Hyperfractionated radiation therapy for gliomas of the brainstem in children and in adults. *Int J Radiat Oncol Biol Phys.* 1992;24(4):599–610.
103. Kretschmar C, Tarbell N, Barnes P, Krischer J, Burger P, Kun L. Pre-irradiation chemotherapy and hyperfractionated radiation therapy 66 Gy for children with brain stem tumors. A phase II study of the Pediatric Oncology Group, Protocol 8833. *Cancer.* 1993;72(4):1404–13.
104. Packer R, Boyett J, Zimmerman R, Albright A, Kaplan A, Rorke L, et al. Outcome of children with brain stem gliomas after treatment with 7800 cGy of hyperfractionated radiotherapy. A Childrens Cancer Group Phase I/II Trial. *Cancer.* 1994;74(6):1827–34.
105. Fleischhack G, Siegler N, Zimmermann M, Warmuth-Metz M, Kortmann R, Massimino M, et al. Concomitant therapy of nimotuzumab and standard radiotherapy for the treatment of newly diagnosed diffuse intrinsic pontine gliomas in children and adolescents: Dipp. 05. *Neuro Oncol.* 2010;12(6):ii9.
106. Haas-Kogan D, Banerjee A, Poussaint T, Kocak M, Prados M, Geyer J, et al. Phase II trial of tipifarnib and radiation in children with newly diagnosed diffuse intrinsic pontine gliomas. *Neuro-Oncology.* 2011;13(3):298–306.
107. Kivivuori S, Riikonen P, Valanne L, Lönnqvist T, Saarinen-Pihkala U. Antiangiogenic combination therapy after local radiotherapy with topotecan radiosensitizer improved quality of life for children with inoperable brainstem gliomas. *Acta Paediatr.* 2011;100(1):134–8.
108. Massimino M, Bode U, Biassoni V, Fleischhack G. Nimotuzumab for pediatric diffuse intrinsic pontine gliomas. *Expert Opin Biol Ther.* 2011;11(2):247–56.
109. Negretti L, Bouchireb K, Levy-Piedbois C, Habrand J, Dhermain F, Kalifa C, et al. Hypofractionated radiotherapy in the treatment of diffuse intrinsic pontine glioma in children: a single institution's experience. *J Neuro-Oncol.* 2011;104(3):773–7.
110. Pollack I, Stewart C, Kocak M, Poussaint T, Broniscer A, Banerjee A, et al. A phase II study of gefitinib and irradiation in children with newly diagnosed brainstem gliomas: a report from the Pediatric Brain Tumor Consortium. *Neuro-Oncology.* 2011;13(3):290–7.

111. Wolff J, Kortmann R, Wolff B, Pietsch T, Peters O, Schmid H, et al. High dose methotrexate for pediatric high grade glioma: results of the HIT-GBM-D pilot study. *J Neuro-Oncol.* 2011;102(3):433–42.
112. Chassot A, Canale S, Varlet P, Puget S, Roujeau T, Negretti L, et al. Radiotherapy with concurrent and adjuvant temozolomide in children with newly diagnosed diffuse intrinsic pontine glioma. *J Neuro-Oncol.* 2012;106(2):399–407.
113. Fontanilla H, Pinnix C, Ketonen L, Woo S, Vats T, Rytting M, et al. Palliative reirradiation for progressive diffuse intrinsic pontine glioma. *Am J Clin Oncol.* 2012;35(1):51–7.
114. Warren K, Bent R, Wolters P, Prager A, Hanson R, Packer R, et al. A phase 2 study of pegylated interferon α -2b (PEG-Intron (®)) in children with diffuse intrinsic pontine glioma. *Cancer.* 2012;118(14):3607–13.
115. Wolff J, Rytting M, Vats T, Zage P, Ater J, Woo S, et al. Treatment of recurrent diffuse intrinsic pontine glioma: the MD Anderson Cancer Center experience. *J Neuro-Oncol.* 2012;106(2):391–7.
116. Aguilera D, Mazewski C, Hayes L, Jordan C, Esiashivilli N, Janns A, et al. Prolonged survival after treatment of diffuse intrinsic pontine glioma with radiation, temozolamide, and bevacizumab: report of 2 cases. *J Pediatr Hematol Oncol.* 2013;35(1):e42–6.
117. Bailey S, Howman A, Wheatley K, Wherton D, Boota N, Pizer B, et al. Diffuse intrinsic pontine glioma treated with prolonged temozolomide and radiotherapy—results of a United Kingdom phase II trial (CNS 2007 04). *Eur J Cancer.* 2013;49(18):3856–62.
118. Bradley K, Zhou T, McNall-Knapp R, Jakacki R, Levy A, Vezina G, et al. Motexafin-gadolinium and involved field radiation therapy for intrinsic pontine glioma of childhood: a children’s oncology group phase 2 study. *Int J Radiat Oncol Biol Phys.* 2013;85(1):e55–60.
119. Janssens G, Jansen M, Lauwers S, Nowak P, Oldenburger F, Bouffet E, et al. Hypofractionation vs conventional radiation therapy for newly diagnosed diffuse intrinsic pontine glioma: a matched-cohort analysis. *Int J Radiat Oncol Biol Phys.* 2013;85(2):315–20.
120. Kebudi R, Cakir F, Agaoglu F, Gorgun O, Ayan I, Darendeliler E. Pediatric diffuse intrinsic pontine glioma patients from a single center. *Childs Nerv Syst.* 2013;29(4):583–8.
121. Zaky W, Wellner M, Brown R, Blüml S, Finlay J, Dhall G. Treatment of children with diffuse intrinsic pontine gliomas with chemoradiotherapy followed by a combination of temozolomide, irinotecan, and bevacizumab. *Pediatr Hematol Oncol.* 2013;30(7):623–32.
122. Massimino M, Biassoni V, Miceli R, Schiavello E, Warmuth-Metz M, Modena P, et al. Results of nimotuzumab and vinorelbine, radiation and re-irradiation for diffuse pontine glioma in childhood. *J Neuro-Oncol.* 2014;118(2):305–12.
123. Müller K, Schlamann A, Guckenberger M, Warmuth-Metz M, Glück A, Pietschmann S, et al. Craniospinal irradiation with concurrent temozolomide for primary metastatic pediatric high-grade or diffuse intrinsic pontine gliomas. A first report from the GPOH-HIT-HGG Study Group. *Strahlenther Onkol.* 2014;190(4):377–81.
124. Zaghoul M, Eldebawy E, Ahmed S, Mousa A, Amin A, Refaat A, et al. Hypofractionated conformal radiotherapy for pediatric diffuse intrinsic pontine glioma (DIPG): a randomized controlled trial. *Radiol Oncol.* 2014;111(1):35–40.
125. Epelman S, Odone V, Gorender E, Medeiros RSS, Martins L. Phase II study of nimotuzumab and radiotherapy in children and adolescents with newly diagnosed diffuse intrinsic pontine gliomas (DIPG). *J Clin Oncol.* 2015;33(15_suppl):10061.
126. Rizzo D, Scalzone M, Ruggiero A, Maurizi P, Attinà G, Mastrangelo S, et al. Temozolomide in the treatment of newly diagnosed diffuse brainstem glioma in children: a broken promise? *J Chemother.* 2015;27(2):106–10.
127. Vanan M, Eisenstat D. DIPG in children-what can we learn from the past? *Front Oncol.* 2015;5:237.
128. Hankinson T, Patibandla M, Green A, Hemenway M, Foreman N, Handler M, et al. Hypofractionated radiotherapy for children with diffuse intrinsic pontine gliomas. *Pediatr Blood Cancer.* 2016;63(4):716–8.

129. Hummel T, Salloum R, Drissi R, Kumar S, Sobo M, Goldman S, et al. A pilot study of bevacizumab-based therapy in patients with newly diagnosed high-grade gliomas and diffuse intrinsic pontine gliomas. *J Neuro-Oncol.* 2016;127(1):53–61.
130. Janssens G, Gandola L, Bolle S, Mandeville H, Ramos-Albiac M, Benghiat H, et al. Survival benefit for patients with diffuse intrinsic pontine glioma (DIPG) undergoing re-irradiation at first progression: a matched-cohort analysis on behalf of the SIOP-E-HGG/DIPG working group. *Eur J Cancer.* 2017;73:38–47.
131. La Madrid AM, Santa-María V, Cruz OM, Mora J, Puerta PR, Guillen AQ, et al. Second re-irradiation for DIPG progression, re-considering “old strategies” with new approaches. *Childs Nerv Syst.* 2017;33(5):849–52.
132. Macy M, Kieran M, Chi S, Cohen K, MacDonald T, Smith A, et al. A pediatric trial of radiation/cetuximab followed by irinotecan/cetuximab in newly diagnosed diffuse pontine gliomas and high-grade astrocytomas: a Pediatric Oncology Experimental Therapeutics Investigators’ Consortium study. *Pediatr Blood Cancer.* 2017;64(11):e26621.
133. Yoshida K, Sulaiman NS, Miyawaki D, Ejima Y, Nishimura H, Ishihara T, et al. Radiotherapy for brainstem gliomas in children and adults: a single-institution experience and literature review. *Asia Pac J Clin Oncol.* 2017;13(2):e153–e60.
134. Mandell L, Kadota R, Freeman C, Douglass E, Fontanesi J, Cohen M, et al. There is no role for hyperfractionated radiotherapy in the management of children with newly diagnosed diffuse intrinsic brainstem tumors: results of a Pediatric Oncology Group phase III trial comparing conventional vs. hyperfractionated radiotherapy. *Int J Radiat Oncol Biol Phys.* 1999;43(5):959–64.
135. Janssens G, Gidding C, Van EL, Oldenburger F, Erasmus C, Schouten-Meeteren A, et al. The role of hypofractionation radiotherapy for diffuse intrinsic brainstem glioma in children: a pilot study. *Int J Radiat Oncol Biol Phys.* 2009;73(3):722–6.
136. Allen J, Siffert J, Donahue B, Nirenberg A, Jakacki R, Robertson P, et al. A phase I/II study of carboplatin combined with hyperfractionated radiotherapy for brainstem gliomas. *Cancer.* 1999;86(6):1064–9.
137. Freeman C, Kepner J, Kun L, Sanford R, Kadota R, Mandell L, et al. A detrimental effect of a combined chemotherapy-radiotherapy approach in children with diffuse intrinsic brain stem gliomas? *Int J Radiat Oncol Biol Phys.* 2000;47(3):561–4.
138. Bernier-Chastagner V, Grill J, Doz F, Bracard S, Gentet J, Marie-Cardine A, et al. Topotecan as a radiosensitizer in the treatment of children with malignant diffuse brainstem gliomas: results of a French Society of Paediatric Oncology Phase II Study. *Cancer.* 2005;104(12):2792–7.
139. Jennings M, Sposto R, Boyett J, Vezina L, Holmes E, Berger M, et al. Preradiation chemotherapy in primary high-risk brainstem tumors: phase II study CCG-9941 of the Children’s Cancer Group. *J Clin Oncol.* 2002;20(16):3431–7.
140. Jalali R, Raut N, Arora B, Gupta T, Dutta D, Munshi A, et al. Prospective evaluation of radiotherapy with concurrent and adjuvant temozolomide in children with newly diagnosed diffuse intrinsic pontine glioma. *Int J Radiat Oncol Biol Phys.* 2010;77(1):113–8.
141. Sirachainan N, Pakakasama S, Visudithbhan A, Chiamchanya S, Tuntiyatorn L, Dhanachai M, et al. Concurrent radiotherapy with temozolomide followed by adjuvant temozolomide and cis-retinoic acid in children with diffuse intrinsic pontine glioma. *Neuro-Oncology.* 2008;10(4):577–82.
142. Korones D, Fisher P, Kretschmar C, Zhou T, Chen Z, Kepner J, et al. Treatment of children with diffuse intrinsic brain stem glioma with radiotherapy, vincristine and oral VP-16: a Children’s Oncology Group phase II study. *Pediatr Blood Cancer.* 2008;50(2):227–30.
143. Kim C, Kim S, Phi J, Lee M, Kim I, Kim I, et al. A prospective study of temozolomide plus thalidomide during and after radiation therapy for pediatric diffuse pontine gliomas: preliminary results of the Korean Society for Pediatric Neuro-Oncology study. *J Neuro-Oncol.* 2010;100(2):193–8.
144. Michalski A, Bouffet E, Taylor R, Hargrave D, Walker D, Picton S, et al. The addition of high-dose tamoxifen to standard radiotherapy does not improve the survival of patients with diffuse intrinsic pontine glioma. *J Neuro-Oncol.* 2010;100(1):81–8.

145. Bouffet E, Raquin M, Doz F, Gentet J, Rodary C, Demeocq F, et al. Radiotherapy followed by high dose busulfan and thiotepa: a prospective assessment of high dose chemotherapy in children with diffuse pontine gliomas. *Cancer*. 2000;88(3):685–92.
146. Khan O, La NT. HDAC inhibitors in cancer biology: emerging mechanisms and clinical applications. *Immunol Cell Biol*. 2012;90(1):85–94.
147. Dawson M, Kouzarides T. Cancer epigenetics: from mechanism to therapy. *Cell*. 2012;150(1):12–27.
148. Grasso C, Tang Y, Truffaux N, Berlow N, Liu L, Debily M, et al. Functionally defined therapeutic targets in diffuse intrinsic pontine glioma. *Nat Med*. 2015;21(6):555–9.
149. Lapin DH, Tsoli M, Ziegler DS. Genomic insights into diffuse intrinsic pontine glioma. *Front Oncol*. 2017;7:57.
150. Hummel T, Wagner L, Ahern C, Fouladi M, Reid J, McGovern R, et al. A pediatric phase 1 trial of vorinostat and temozolomide in relapsed or refractory primary brain or spinal cord tumors: a Children’s Oncology Group phase 1 consortium study. *Pediatr Blood Cancer*. 2013;60(9):1452–7.
151. Hashizume R, Andor N, Ihara Y, Lerner R, Gan H, Chen X, et al. Pharmacologic inhibition of histone demethylation as a therapy for pediatric brainstem glioma. *Nat Med*. 2014;20(12):1394–6.
152. Mohammad F, Weissmann S, Leblanc B, Pandey D, Højfeldt J, Comet I, et al. EZH2 is a potential therapeutic target for H3K27M-mutant pediatric gliomas. *Nat Med*. 2017;23(4):483–92.
153. Piunti A, Hashizume R, Morgan M, Bartom E, Horbinski C, Marshall S, et al. Therapeutic targeting of polycomb and BET bromodomain proteins in diffuse intrinsic pontine gliomas. *Nat Med*. 2017;23(4):493–500.
154. Truffaux N, Philippe C, Paulsson J, Andreiuolo F, Guerrini-Rousseau L, Cornilleau G, et al. Preclinical evaluation of dasatinib alone and in combination with cabozantinib for the treatment of diffuse intrinsic pontine glioma. *Neuro-Oncology*. 2015;17(7):953–64.
155. Qaddoumi I, Kocak M, Pai AP, Armstrong G, Wetmore C, Crawford J, et al. Phase II trial of erlotinib during and after radiotherapy in children with newly diagnosed high-grade gliomas. *Front Oncol*. 2014;4:67.
156. Zhou Z, Singh R, Souweidane M. Convection-enhanced delivery for diffuse intrinsic pontine glioma treatment. *Curr Neuropharmacol*. 2017;15(1):116–28.
157. Barua N, Lewis S, Woolley M, O’Sullivan S, Harrison R, Gill S. Robot-guided convection-enhanced delivery of carboplatin for advanced brainstem glioma. *Acta Neurochir*. 2013;155(8):1459–65.
158. Souweidane MM, Kramer K, Pandit-Taskar N, Zhou Z, Haque S, Zanzonico P, et al. Convection-enhanced delivery for diffuse intrinsic pontine glioma: a single-centre, dose-escalation, phase I trial. *Lancet Oncol*. 2018;19(8):1040–50.
159. Singleton W, Collins A, Bienemann A, Killick-Cole C, Haynes H, Asby D, et al. Convection enhanced delivery of panobinostat (LBH589)-loaded pluronic nano-micelles prolongs survival in the F98 rat glioma model. *Int J Nanomedicine*. 2017;12:1385–99.

Chapter 9

Surgery for Vascular Lesions of the Brainstem



Michael J. Lang and Michael T. Lawton

Abbreviations

AICA	Anterior inferior cerebellar artery
AVM	Arteriovenous malformation(s)
BA	Basilar artery
BRAT	Barrow Ruptured Aneurysm Trial
BT	Basilar trunk
BVR	Basal vein of Rosenthal
CM	Cavernous malformation
CN	Cranial nerve
CSF	Cerebrospinal fluid
CST	Corticospinal tracts
CT	Computed tomography
CTA	Computed tomography angiography
DSA	Digital subtraction angiography
DTI	Diffusion tensor imaging
IA	Intracranial aneurysm
IAC	Internal auditory canal
ISAT	International Subarachnoid Aneurysm Trial
ISUIA	International Study of Unruptured Intracranial Aneurysms
MAPonMesV	Median anterior pontomesencephalic vein
MCP(s)	Middle cerebellar peduncle(s)
mOZ	Modified orbitozygomatic
MRA	MR angiography
MRI	Magnetic resonance imaging

M. J. Lang · M. T. Lawton (✉)

Department of Neurosurgery, Barrow Neurological Institute, Phoenix, AZ, USA

e-mail: neuropub@barrowneuro.org

OA-PICA EC-IC	Occipital artery-posterior inferior cerebellar artery external carotid-internal carotid
OZ	Orbitozygomatic
PCA	Posterior cerebral arteries
PCP	Posterior clinoid process
PICA	Posterior inferior cerebellar artery
SAH	Subarachnoid hemorrhage
SCA	Superior cerebellar artery
SCIT	Supracerebellar infratentorial
SPetrV	Superior petrosal vein
SPS	Superior petrosal sinus
SS-EPI	Single-shot echo planar imaging
T2*GRE	T2*-Gradient Recalled Echo
VA	Vertebral arteries
VBJ	Vertebrobasilar junction

9.1 Introduction

Vascular lesions of the brainstem are rare entities that pose significant challenges to surgical management. The dense eloquence of the brainstem significantly increases the risk of surgery compared to similar lesions in the supratentorial space. The intimate relationship of critical perforating arteries and the limited working corridors magnify these challenges. Preoperative evaluation requires consideration of multiple treatment modalities, including microsurgery, endovascular therapy, or radiotherapy, alone or in combination. The risks of intervention must be balanced against the natural history of these lesions, which, generally speaking, have higher rates of rupture than their supratentorial counterparts. Although increased rupture rates and the devastating sequelae of a brainstem hemorrhage often support an aggressive surgical posture, close observation of unruptured brainstem-associated vascular lesions is sometimes preferred. Decision-making for ruptured lesions is frequently much more straightforward, given the ruinous consequences of re-rupture.

Elegantly described by Rhoton, the posterior fossa can be considered in groups of threes. There are three segments of the brainstem: midbrain, pons, and medulla [1]. Each of these is associated with a respective segment of the large vessels of the posterior circulation (basilar artery [BA] apex, basilar trunk [BT], and vertebral arteries [VA]/vertebrobasilar junction [VBJ], respectively) and associated branch vessels (superior cerebellar artery [SCA], anterior inferior cerebellar artery [AICA], and posterior inferior cerebellar artery [PICA]). Likewise, the three neurovascular complexes are associated with a group of cranial nerves (CN) and their associated nuclei: CN III-V are related to the midbrain, CN VI-VIII with the pons, and CN IX-XII with the medulla. Using this organization, aneurysms, arteriovenous malformations (AVM) and cavernous malformations (CM) will be considered regionally. The following chapter outlines the general approach to the diagnosis and management of vascular lesions of the brainstem; a full technical description of the surgical nuances is beyond the scope of this chapter.

9.2 Natural History

The risk of symptomatic rupture has been described extensively for aneurysms, AVMs, and CMs, and, in general, the risks of rupture are known to be higher for brainstem locations. Posterior circulation aneurysms represent 15% of all intracranial aneurysms (IAs), and the increased risk of rupture relative to size-matched anterior circulation aneurysms has been described. In the International Study of Unruptured Intracranial Aneurysms (ISUIA) trial, small posterior circulation aneurysms (<7 mm) had a 5-year cumulative rupture rate of 2.5% (compared to 0% for anterior circulation aneurysms), and these rates ranged up to 50% for giant aneurysms [2]. Brainstem AVMs account for 2–6% of all intracranial AVMs. The majority of AVMs in this location present with ruptured status and have substantially higher annual rupture rates (15–17.5%/year) than generally quoted for supratentorial brain AVMs (1–4%/year) [3]. While brainstem AVMs may have an intrinsically higher rate of rupture, including an increased chance of harboring nidal aneurysms, it has been posited that the absence of cortical findings, such as seizures, decreases the likelihood of discovering brainstem AVMs prior to rupture [4]. Similarly, brainstem CMs have been shown to have a substantially higher rate of hemorrhage than supratentorial CMs. A recent meta-analysis by Taslimi et al. showed nearly a 10-fold higher annual rupture rate of brainstem CMs compared to non-brainstem CMs (0.3%/year vs. 2.8%/year) [5]. Patients presenting with ruptured brainstem CMs had an annual rupture risk of 32.3%/year compared to 6.3%/year for non-brainstem locations [5]. Given the chronic deposition of blood products (evidenced by prominent susceptibility artifact on T2*-gradient recalled echo [T2*GRE] magnetic resonance imaging [MRI]), it is likely that CMs undergo regular micro-rupture in addition to frank intralesional and intraparenchymal hemorrhagic events, accounting for the increased rate of symptomatic presentation. Furthermore, these estimates of rupture rate may significantly underestimate the true annual rate. Documented *de novo* formation for all three pathologies has been demonstrated, decreasing the denominator in event rate calculations. Overall, the high rates of hemorrhage and consequences thereof for brainstem vascular lesions argues for an aggressive surgical posture.

9.3 Presentation and Diagnosis

9.3.1 Clinical Presentation

Presentation varies by the type of vascular lesion and its location within the brainstem. Hemorrhagic brainstem vascular lesions generally result in a more critical clinical condition than those in the supratentorial space, regardless of the particular pathology [6–8]. This is largely due to the comparatively smaller volume of the posterior fossa, as well as the highly eloquent nature of the brainstem parenchyma. Furthermore, posterior fossa AVMs and aneurysms presenting with subarachnoid hemorrhage (SAH) are more likely to be complicated by hydrocephalus and have

been shown to require higher rates of permanent cerebrospinal fluid (CSF) diversion. Likewise, CMs of the brainstem tend to present with clinical deficits with a smaller volume of parenchymal hemorrhage, or with a purely intralesional hemorrhage.

Focal neurologic deficits, either from CN compression, parenchymal mass effect or vascular steal phenomenon, are dependent on the particular location within the brainstem. As stated earlier, cranial neuropathies can result from compression of the cisternal segment of the affected nerve and, thus, are always ipsilateral to the lesion. By comparison, cranial neuropathies resulting from parenchymal injury can be remote from the lesional site relative to the level of the brainstem associated with the cisternal segment of that nerve. An example of this is facial numbness occurring as a result of injury to the spinal trigeminal nucleus in the medulla (despite the association of CN V with the pontomesencephalic junction based on its surface anatomy). Similarly, deficits from parenchymal injury can be either ipsilateral or contralateral to the lesion, depending on the presence or absence of tract decussation. As such, the need for a thorough neurologic examination and localization cannot be overstated and is the cornerstone of preoperative and postoperative evaluation.

9.3.2 *Imaging*

Initial imaging workup also depends heavily on the presentation and suspected type of lesion. Imaging workup for patients presenting with SAH or symptoms concerning for brainstem hemorrhage should begin with non-contrast-enhanced computed tomography (CT) of the head as the initial modality of choice. The diagnosis may be suggested but is rarely confirmed by head CT alone. For patients with potentially life-threatening hemorrhages requiring emergent decompression, CT angiography (CTA) is considered the vascular imaging study of choice due to its rapid acquisition. In the senior author's practice, CTA is frequently sufficient to guide decision-making in aneurysms presenting either unruptured or with SAH (particularly to guide clip versus coiling allocation) and is particularly useful in understanding the relationship of a given aneurysm to the skull base bony anatomy. However, the gold standard remains cerebral digital subtraction angiography (DSA), particularly for those aneurysms with complex morphologies or those that may potentially necessitate revascularization as part of the treatment [9]. While the risk of major neurologic complications associated with DSA is extremely low, improvements in resolution of CTA on modern scanners may obviate the need for invasive imaging for more and more aneurysms. Conversely, given that endovascular treatment of cerebral aneurysms related to the brainstem is considered the first-line treatment at many centers, DSA still plays a major role in the evaluation and treatment of most brainstem-associated aneurysms.

By contrast, we recommend the use of DSA for all AVMs, except for those necessitating emergent surgery. While advances have been made in noninvasive imaging of AVMs, such as the so-called "4D imaging" techniques, DSA remains essential for several reasons [10]. First, the resolution of DSA has not been matched by non-

invasive imaging techniques and is essential for identifying anatomical landmarks associated with the malformation to help guide the resection. Likewise, AVM surfaces fed by small parenchymal feeding vessels (coined “little red devils” by Charles Wilson) are much more easily identified on DSA. The architecture of these vessels makes them much more challenging to coagulate and divide than larger feeding arteries and generates a diffuse nidus surface, the presence of which increases the risk of perioperative morbidity and mortality. As such, identification of this feature is essential and has been included into the Lawton-Young Supplementary AVM scale to aid preoperative decision making [11]. Secondly, AVMs are dynamic lesions by nature, and noninvasive imaging techniques have yet to replicate the ability to see the flow from arterial feeders, through nidus, and into draining veins as clearly as with DSA. The ability to translate radiographic features of both arterial and venous anatomy in one’s mind while developing a surgical plan is critical, and DSA aids substantially in differentiating these vessels within the teeming mass of the AVM. Finally, formal angiography allows for the use of preoperative embolization. Despite the evolution of endovascular embolization, such as transvenous or “pressure cooker” techniques, cure rates remain low with embolization alone [12]. However, preoperative embolization frequently improves the safety and efficiency of surgical resection whenever it can be performed without placing normal vessels at risk. One must pay careful attention, though, because normal perforating arteries may not be well visualized, and the consequences of inadvertent embolization can be devastating.

MRI has different applications for each of the three main types of vessel malformations. For aneurysms, MR angiography (MRA) can be useful as a screening tool and for long-term noninvasive follow-up imaging, but does not have sufficient resolution to guide operative decision-making alone in most cases [13]. However, in those patients with large or giant aneurysms with significant brainstem compression, such as dolichoectatic basilar aneurysms, MRI offers the best brain tissue contrast of any available imaging modality. Similarly, MRI is essential for delineating the parenchymal surface of a brainstem AVM. For AVMs that are purely pial, total resection may be a viable strategy, whereas those with a significant parenchymal component may benefit from *in situ* disconnection, radiosurgery, or observation [14]. For CMs, however, MRI plays much more of a fundamental role. Until its development in the 1980s, CMs were an under-recognized entity, with a variety of names applied to these “occult” lesions. Subsequent description of its MRI appearance (including four radiographic subtypes in the Zabramski classification) drove broader understanding of these lesions as a clinical entity and as a target for surgical intervention. The advent of diffusion tensor imaging (DTI)-based tractography has aided the identification of the associated fiber tracts and the displacement or disruption thereof [15]. Anatomical MRI and tractography should be interpreted cautiously, however. The superparamagnetic properties of deposited hemosiderin result in a substantial susceptibility artifact in T2-weighted scans. This biophysical property is utilized in T2*GRE imaging, producing “blooming” of susceptibility artifact in the region of hemosiderin due to use of magnetic gradient instead of radiofrequency refocusing pulses. Unfortunately, the single-shot echo planar imaging (SS-EPI) sequences on which DTI is based are also affected by the susceptibility

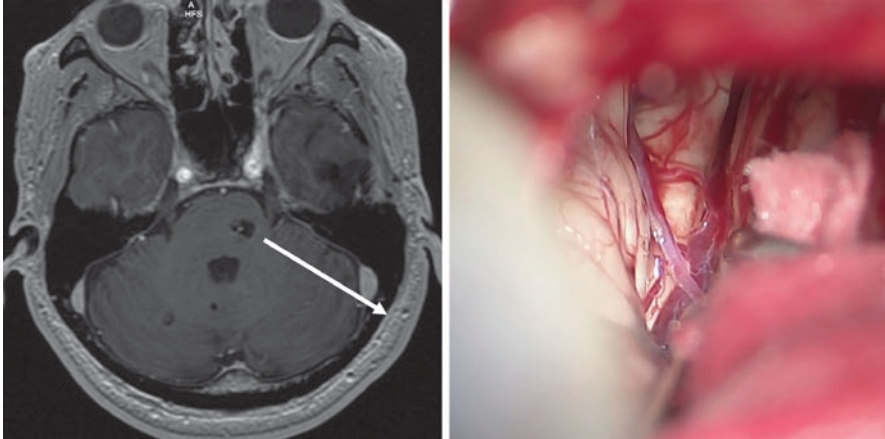


Fig. 9.1 Cavernous malformations residing in the lateral aspect of the pons are safely approached through the middle cerebellar peduncle (MRI left). Projecting this trajectory back onto the skull suggests that a retrosigmoid craniotomy is best suited for resecting this lesion. Opening the petrosal fissure of the cerebellum (right) establishes a more posterior entry point into the MCP, allowing for a more favorable trajectory into the brainstem. Used with permission from Barrow Neurological Institute

artifact, affecting the reliability of tractography around a CM with significant hemosiderin staining, an effect that scales with field-strength. We recommend careful evaluation of non-contrast-enhanced T1-weighted images prior to planning surgical intervention, as lesions that appear to reach the pial surface on T2-weighted sequences can often be up to several millimeters deep to the surface on T1-weighted images, changing the surgical approach or risk profile of the surgical intervention.

Finally, the optimal imaging evaluation for a brainstem vascular lesion should include consideration of neuronavigation. Aneurysms, including those of the posterior circulation, can often be approached using a standard array of workhorse approaches and anatomical dissection, rendering image guidance superfluous in many cases. Conversely, large and giant aneurysms of the posterior circulation, and all AVMs and CMs of the brainstem, benefit from the routine use of navigation. Complex skull base approaches may also benefit from the use of CT scans to guide the extent of bone drilling. With brainstem surgery, trajectory planning, pial entry and depth of surgical resection are all aided with the use of image guidance. Tackling pontine CMs through a trans-middle cerebellar peduncle (MCP) approach is a classic example in which image guidance aids in the identification of the ideal entry point in the MCP (Fig. 9.1).

9.4 Regional Management Strategies for Brainstem Vascular Lesions

Surgery for vascular pathology of the brainstem requires a working knowledge of an array of surgical approaches. We have considered only open transcranial approaches here, as opposed to endoscopic endonasal approaches. While some groups have

advocated endoscopic surgery for brainstem vascular lesions [16], we feel that the technology necessary for safe treatment of posterior circulation aneurysms or intraparenchymal dissection is currently unavailable. That said, technological advancements in endoscopes, instruments, and robotic assistance may make endonasal approaches more practicable in the future. It should also be noted that the ideal approach is often dictated by subtle anatomical variations, so thorough review of imaging should be performed before selecting an approach for a given patient.

9.4.1 *Midbrain*

9.4.1.1 *Aneurysms*

Aneurysms associated with the midbrain most frequently include those arising from the BA apex, SCA, and proximal posterior cerebral arteries (PCA), constituting 5–10% of all IAs and over 50% of posterior circulation aneurysms [17], and are closely associated with the cerebral peduncles. Aneurysms of the distal PCA or SCA (and their associated branches) are rare by comparison and necessitate approaches to the lateral or dorsal midbrain. Endovascular treatment of these aneurysms is considered first-line in many centers, due to its relative ease compared to clipping in this location [18]. The intimate relationship with the perforating arteries arising from the BA apex and P1 PCAs makes dissection of BA and proximal PCA aneurysms particularly challenging, and the consequences of including even a single perforator in a clip construct can be devastating. However, aneurysm recurrence after endovascular treatment and the need for revascularization often drive the demand for microsurgery for these aneurysms.

Until the pioneering work of Charles Drake at the University of Western Ontario, aneurysms of the BA apex were considered beyond the realm of treatment. Since then, surgery for these aneurysms has become a key part of the armamentarium of vascular microneurosurgeons. Drake advocated the use of a subtemporal approach with division of the tentorium posterior to the entry point of CN IV [19]. This approach has the advantage of permitting a clear view along the posterior wall of BA aneurysms, aiding perforator dissection, but is limited by the temporal lobe retraction necessary to reach the BA apex and the exposure of the contralateral PCA. Yaşargil, by contrast, made use of the pterional transsylvian approach, and the need for access to high-riding BA apex aneurysms led to the development of the orbitozygomatic (OZ) osteotomy and its many modifications [20]. While some have advocated that the modified OZ (mOZ) achieves nearly the same degree of upward exposure with less cosmetic deformity, we believe that there are several reasons to justify the use of a full OZ in most aneurysms in this location [21, 22]. Removal of the zygomatic arch allows for inferior mobilization of the temporalis muscle, broadening the angle of attack to the ventral midbrain. This maneuver also aids in posterolateral mobilization of the temporal lobe to achieve a pretemporal approach, which can be increased by division of the subtemporal veins and, when necessary, division of the anterior temporal and/or posterior communicating artery (Fig. 9.2). This in turn enables wide visualization of the BA apex and exposes the P2A PCA in the oculomotor-tentorial

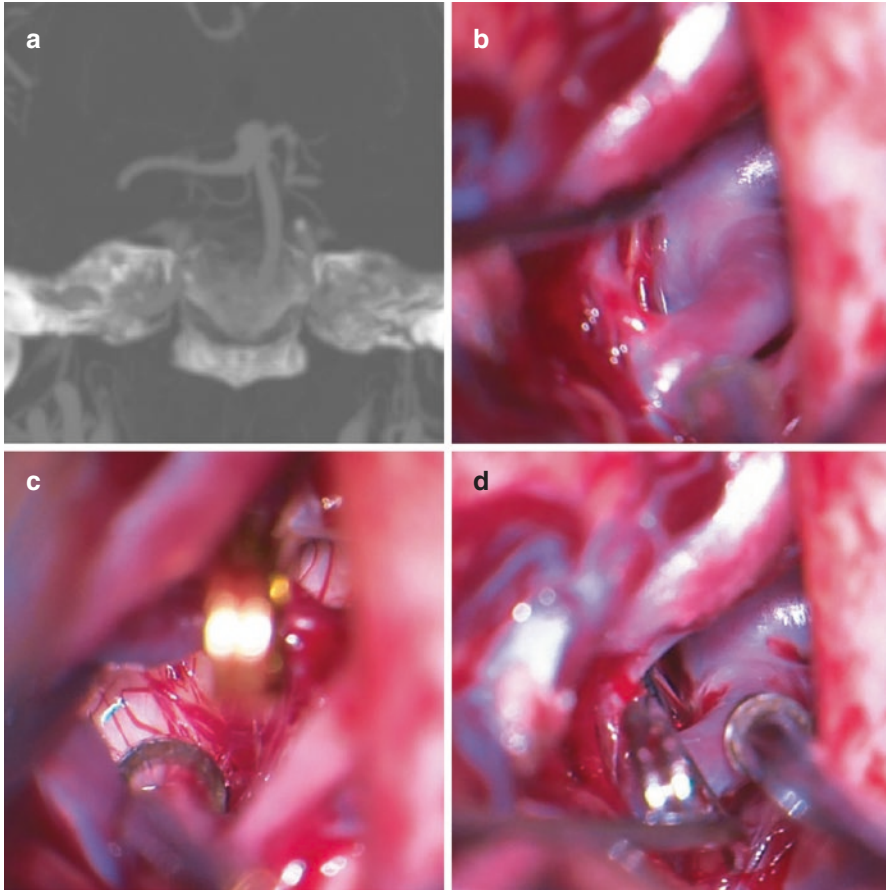


Fig. 9.2 An unruptured basilar apex aneurysm (a) was approached through a right-sided full orbi-zygomatic craniotomy. Mobilization of the temporal lobe is accomplished by division of the bridging veins and dissection along the course of the anterior choroidal artery, bringing the basilar apex into view (b). The pretemporal trajectory allows for a tangential view to the PIs and enables visualization of the basilar perforators arising posterior to the aneurysm dome (c). A single fenestrated clip encircles the PCA and completely closes the aneurysm (d). Used with permission from Barrow Neurological Institute

triangle in cases where revascularization is necessary. Establishing proximal control on the BA is often aided by drilling the posterior clinoid process (PCP), or the addition of transcavernous approaches (as advocated by Krisht and others) [23]. The Kawase anterior petrosectomy has also been used to approach low-lying basilar aneurysms down to the level of the internal auditory canal (IAC) [24]. Distal PCA and SCA aneurysms can be addressed through a variety of approaches, including subtemporal and variations of the supracerebellar infratentorial (SCIT) approaches.

Since the publication of the International Subarachnoid Aneurysm Trial (ISAT) in 2002, there has been a substantial shift in the treatment of aneurysms arising at the basilar terminus. This trial demonstrated an improvement in early outcomes

with coiling compared to clipping, with favorable outcomes achieved in 76.5% and 69.1% of coiling and clipping patients, respectively, at 1 year after treatment [25]. Unfortunately, ISAT only included 17 BA apex aneurysms out of 2143 patients, limiting its applicability. The Barrow Ruptured Aneurysm Trial (BRAT) included a much larger cohort of BA apex aneurysms (4.7% of enrolled patients), and also demonstrated improved clinical outcomes for posterior circulation aneurysms at 1-, 3- and 6-year time points, though the large proportion of PICA aneurysms in the clipping group may skew these results. For all aneurysms, clipping achieved a 96% complete occlusion rate compared to 48% for coiling at 6 years [6]. The majority of BA aneurysms are now treated by endovascular coiling in most of the developed world. In spite of this, the relatively few series published on clipping of basilar apex aneurysms after the publication of ISAT seem to suggest that favorable outcomes were achieved at higher rates than in older series (58–92%) and similar to contemporary series of coiled patients (78–95%), with lower occlusion rates in the coiling series [26]. Though, the overall data generally favor coil embolization for these aneurysms. However, patients with small aneurysm domes, severe allergy to nickel, poor vascular access, and PCA configurations that make branch vessel preservation difficult have clear indications for microsurgery, and younger patients may benefit from the higher long-term occlusion rates with clipping.

9.4.1.2 Arteriovenous Malformations (AVMs)

As with all brainstem AVMs, midbrain AVMs are located in an eloquent region and drain into the deep venous system. However, in the senior author's experience, up to 70% of brainstem AVMs are located on the brainstem surface, in a pial or epipial location, as opposed to intraparenchymal [4]. In the patients undergoing surgical resection in that series, one quarter of brainstem AVMs were located in the mesencephalon. AVMs of the midbrain can be divided into two main groups, anterior and posterior midbrain AVMs. Despite the relatively large surface area, AVMs located on the lateral surface of the midbrain were not encountered [27].

Anterior midbrain AVMs are defined as those located in the cerebral peduncles, on their surface, or in the interpeduncular space. They are fed by feeders arising from the P1 and P2A PCA (and their associated perforating arteries) and lie in close association with one or both third nerves. Drainage is into tributaries of the basal vein of Rosenthal (BVR), such as the median anterior pontomesencephalic (MAPonMesV) and peduncular veins. While the anterior surface of the midbrain can be seen with a standard pterional transsylvian approach, we recommend the use of a full OZ for these lesions to expand the Sylvian corridor. The primary working window is the oculomotor-carotid triangle, but additional access can be obtained medially through the optico-carotid triangle, superiorly through the supra-carotid triangle, or laterally through the oculomotor-tentorial triangle. Arterial dissection identifies nidus feeding vessels while preserving critical normal perforating arteries. Circumdissection is carried out and the aneurysm is either resected from its pial plane or occluded *in situ* without parenchymal dissection depending on its specific anatomy.

Posterior midbrain AVMs are located in the tectum and may sit in the quadrigeminal cistern in a primarily exophytic configuration. They are closely associated with the trochlear nerve. Feeding arteries arise from the circumflex perforators of the P1 and P2 PCA segments, as well as from the cerebellomesencephalic segment of the SCA. Venous drainage is into the vein of the cerebellomesencephalic flexure and tectal vein, which in turn drain into the vein of Galen. They are approached through a torcular craniotomy/SCIT approach, which exposes the dura across the bilateral transverse sinuses and distal superior sagittal sinus. The exposure of the sinuses allows a curvilinear dural flap to retract the transverse sinuses upward, expanding the operative corridor. We favor placing the patient in the sitting position when feasible, as gravity retraction greatly expands the operative corridor. While surgeon fatigue is a concern in this position, the added exposure is generally a worthwhile tradeoff. Patients with patent foramen ovale (confirmed by bubble test with echocardiogram), older patients at higher risk for dural tear and air embolism, or those with large AVMs requiring prolonged operative times may be better suited for prone positioning. Occlusion of the arterial inputs begins inferiorly and laterally, with circumdissection progressing toward the draining veins arising superiorly in the field. As with anteriorly located AVMs, the decision to resect the AVM versus *in situ* occlusion is made intra-operatively depending on the pial plane. In the senior author's experience, outcomes from surgical resection of posterior midbrain AVMs have not been favorable, with 50% of patients experiencing neurological decline or death [4].

9.4.1.3 Cavernous Malformations (CMs)

CMs of the midbrain may present with symptoms isolated to the structures in this region and may also extend cranially into the thalamus or caudally into the pons when they reach larger dimensions. Ventrally located lesions frequently present with weakness or diplopia due to involvement of the cerebral peduncles or fibers of the third nerve. Dorsally located lesions often present with dysconjugate gaze and cerebellar ataxia due to involvement of the superior colliculus and superior cerebellar peduncle, respectively. The dorsolateral location is accompanied by facial and body numbness from compression of the trigeminothalamic tract and medial lemniscus in the midbrain tegmentum.

Facility with a variety of surgical approaches is necessary to safely address mesencephalic CMs. For CMs centered in the cerebral peduncle or posterior to the interpeduncular cistern, the OZ approach (or its variants) are favored. Dorsolaterally situated lesions are best approached through a lateral/extreme-lateral SCIT approach, which can be used to reach as anteriorly as the lateral mesencephalic sulcus, whereas midline dorsal CMs are approached from a traditional midline SCIT approach [28] (Fig. 9.3). Given the reach achieved by these workhorse approaches, use of the more limited subtemporal approach (with or without anterior petrosectomy) to the lateral midbrain is rarely necessary. For the posterior fossa approaches to the midbrain, we favor use of the sitting position when it can be performed safely. While it can be challenging to operate in the sitting position for

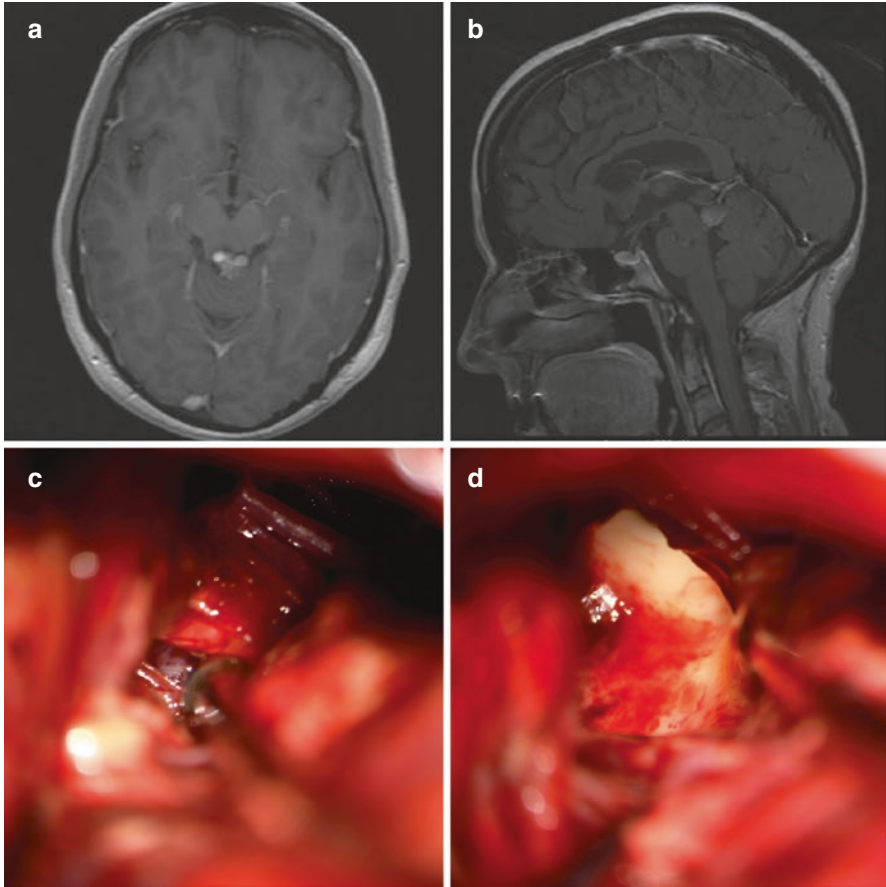


Fig. 9.3 A patient presenting with diplopia and paresthesia was found to have a dorsal midbrain CM with a classic “popcorn” appearance on axial (a) and sagittal (b) MRI sequences. A supracerebellar-infratentorial craniotomy was planned to approach this lesion. Even with the patient in the sitting position, to maximize gravity retraction of the cerebellum, the CM was not completely visible. Resection of a small area of the medial cerebellar hemisphere exposed the lesion in the cerebellomesencephalic flexure (c). This partially exophytic CM enabled resection without transgression of normal brainstem (d). Used with permission from Barrow Neurological Institute

prolonged cases, the wide corridor afforded by this approach provides excellent exposure of the midbrain surface along its craniocaudal extent. Conversely, SCIT craniotomies performed in the prone or lateral positions may necessitate resection of a small notch of the cerebellar hemisphere in order to reach down into the ponto-mesencephalic flexure.

Spetzler and colleagues have described a number of safe entry zones into the midbrain for lesions that do not approach the pial surface of the midbrain [29]. For ventrally located CMs, the interpeduncular and anterior mesencephalic sulcus safe entry zones have been described. These two entry zones are centered on either side

of CN III. When the anterior mesencephalic zone is used as an entry point, the pial incision is situated medially on the peduncle through the frontopontine fibers while sparing the corticospinal tracts (CST) occupying the middle 3/5th of the peduncle. The safe entry zone into the dorsolateral midbrain is entered in the lateral mesencephalic sulcus and is directed between the fibers of the medial lemniscus and the substantia nigra. For dorsally located lesions, vertically oriented intercollicular incisions and horizontally oriented supra- and infra-collicular approaches have been described [30].

9.4.2 Pons

9.4.2.1 Aneurysms

Aneurysms associated with the pons are among the most challenging cerebrovascular lesions. VBJ and BT aneurysms are situated ventrally along the brainstem, for which working corridors are frequently limited or necessitate increasingly morbid transpetrous approaches to increase anterior exposure. For smaller AICA aneurysms, the narrow corridor afforded by middle fossa Kawase anterior petrosotomy or the limited ventral exposure of the extended retrosigmoid approaches may be sufficient. The intimate association of these aneurysms with critical pontine perforating arteries demands meticulous dissection and limits the tolerance to temporary clipping or Hunterian ligation.

For the above reasons, there has been significant growth in the use of endovascular techniques for the treatment of these aneurysms. Successful treatments of these aneurysms have been reported with coiling, stent-assisted coiling, flow-diversion, or flow-diversion assisted coiling [31]. While avoiding invasive skull base approaches is appealing, endovascular techniques are faced with two major challenges for aneurysms associated with the pons. First, the presence of pontine perforating arteries can cause significant complications when flow diversion is employed. Perforating artery flow can be maintained when flow diverting stents are well-opposed to the parent vessel wall, but thrombosis can be devastating if not. For this reason, stent-assisted coiling may be preferable to flow diversion for ventrally projecting VBJ aneurysms [32]. Longer follow-up is necessary to understand the lifetime cumulative risk of perforator strokes in this situation. Second, these aneurysms frequently present with symptoms of pontine mass effect. Coiling procedures for large or giant aneurysms add significant mass effect, decreased compliance to the aneurysm dome, and are associated with high rates of recurrence. The up-front risks of open procedures may be well-justified to reduce brainstem compression. More limited approaches, such as the “macrovascular decompression” may achieve the desired goal of decompression in patients harboring unclippable aneurysms [33].

Dolichoectatic basilar aneurysms warrant particular consideration, and, despite widespread advances in open and endovascular techniques, remain the single most daunting cerebrovascular lesion [34]. Their size, fusiform morphology, brainstem compression, and presence of calcification and intraluminal thrombosis present significant challenges to any therapeutic technique. However, the dismal outcomes associated with both natural history and surgical interventions to date demand innovation for this disease. Evolution of the senior author's practice has resulted in preference for a strategy combining revascularization of the basilar apex (preferentially with 3rd or 4th generation intracranial-intracranial bypass techniques), thrombectomy and brainstem decompression, and proximal occlusion below the AICA origins (Fig. 9.4). The recent addition of rapid ventricular pacing to our practice enables controlled hypotension to aid aneurysm dissection.

9.4.2.2 Arteriovenous Malformations (AVMs)

Pontine AVMs are also divided into two groups, anterior and lateral. Malformations arising on the dorsal pons have not been encountered. Both groups are preferentially approached through the use of an extended retrosigmoid craniotomy, in which a limited mastoidectomy skeletonizes the sigmoid sinus and enables its anterior mobilization. This serves to widen the corridor by several millimeters and enables a more anterior trajectory onto the pons. In patients with supple necks, supine positioning with an ipsilateral shoulder bump is preferred in order to reduce obstruction of the shoulder on the surgeon's hand. For patients with constrained neck mobility, lateral or park bench positioning is used.

Anterior pontine AVMs are centered in the quadrangular space bordered by the basilar impression medially, trigeminal nerve root entry zone laterally, and the pontomesencephalic and pontomedullary fissures cranially and caudally, respectively. They are unilateral in location, and blood supply is from both the s1 SCA and a1 AICA segments. Additional feeders may arise from the BA or from the meningohypophyseal trunk branches tracing back along CN V. Drainage may be directed superiorly to BVR via the MAPonMesV, or laterally into the superior petrosal vein (SPetrV) and superior petrosal sinus (SPS). Arterial disconnection of the AICA feeders is performed in the infratrigeminal triangle, while the SCA feeders are visualized in the supratrigeminal triangle. Coverage of the lateral border by the trigeminal root limits its dissection. Limited exposure and dense eloquence of the ventral pons has resulted in overall poorer outcomes compared to laterally situated AVMs and favors a more conservative approach for these lesions [4].

Lateral pontine AVMs, by contrast, have much more favorable operative and clinical outcomes and represent 25% of all encountered brainstem AVMs. These lesions are centered on the transitional zone between the lateral pons and the MCP and are bounded medially by the CN V root entry zone. They can lie on the pial surface or intraparenchymally, though the brachium pontis is particularly tolerant of

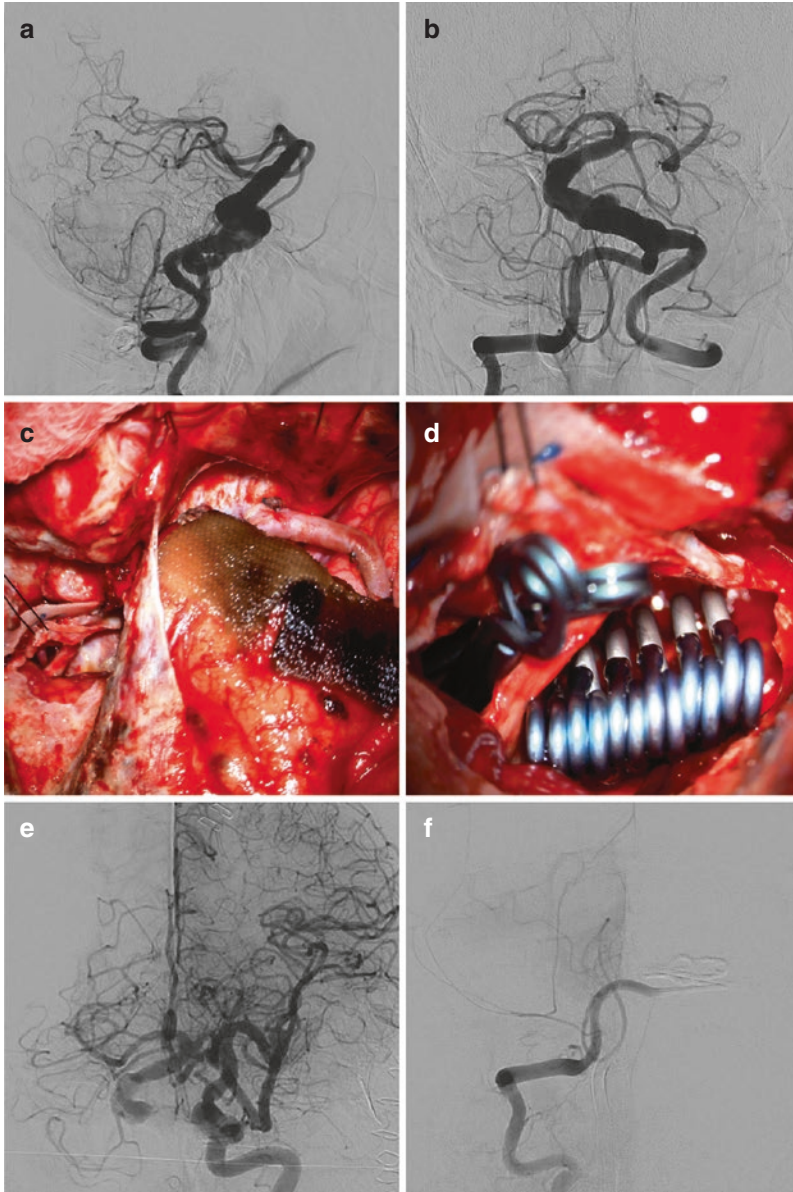


Fig. 9.4 A patient with symptoms of pontine compression was found to have a giant partially thrombosed dolichoectatic basilar trunk aneurysm on angiography (lateral and AP views; **a** and **b**). Given the wide diameter and basilar perforators/AICAs arising from the dolichoectatic segment, flow diversion or clip trapping were not feasible options. A combined skull base approach was utilized to enable high-flow revascularization of the basilar apex and trunk as well as aneurysmorrhaphy/thrombectomy and proximal occlusion. A full orbitozygomatic craniotomy allowed for M2-P2 intracranial-intracranial bypass with a radial artery interposition graft (**c**). A transcochlear craniotomy with facial nerve transposition was used for proximal occlusion at the VBJ. Multiple stacked clips closed the arteriotomy after thrombectomy (**d**). Postoperative angiography demonstrates patency of the bypass with spontaneous thrombosis of the aneurysm below the AICAs (**e**) and complete occlusion of inflow through the VAs proximally (**f**). Used with permission from Barrow Neurological Institute

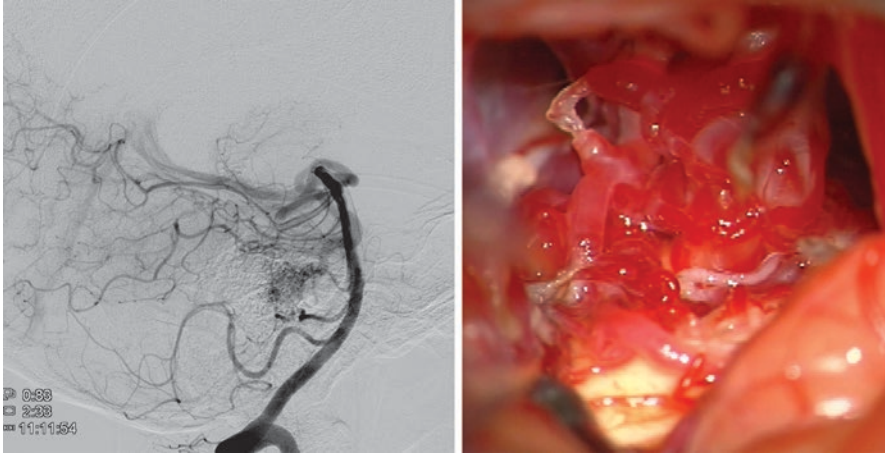


Fig. 9.5 An unruptured petrosal AVM was discovered incidentally and found to be fed by duplicated AICAs on cerebral angiography (left). A retrosigmoid craniotomy exposed the AVM, which was dissected by establishing the pial plane laterally at the pontine/MCP interface and then rolling the AVM away from the pontine surface (right), enabling gross total resection. Used with permission from Barrow Neurological Institute

parenchymal dissection. Unlike anterior pontine AVMs, laterally located lesions receive blood supply exclusively from the AICA, which is identified in the infratrigeminal triangle. Likewise, drainage into the SPetrV does not obstruct the operative field as with anterior AVMs. Furthermore, these AVMs are bounded by non-eloquent cerebellum, which frees dissection along these surfaces and improves control over the eloquent surfaces along the pons and MCP. All of these AVMs accommodate parenchymal dissection, and *in situ* occlusion is unnecessary (Fig. 9.5).

9.4.2.3 Cavernous Malformations (CMs)

CMs of the pons are found ventrally within the basis pontis from the pontomesencephalic fissure to the pontomedullary fissure. The majority of this region is formed by the MCPs, transverse pontine fibers, central pontine nuclei, and CST. Dorsally located lesions within the pontine tegmentum are defined in relation to the central tegmental tract, medial longitudinal fasciculus, medial lemniscus, and the nuclei and associated tracts of CN V-VIII. The superior part of the floor of the fourth ventricle overlies these structures, and the pontine part of the fourth ventricle is found from the opening of the cerebral aqueduct to the facial colliculus (with transitional and medullary zones found caudally).

The majority of ventral pontine CMs are approached through an extended retrosigmoid craniotomy. Lesions that reach the pial surface of the pons are easily identified and can be entered, decompressed, and circumferentially dissected. For deeper ventral lesions, however, entry through normal brainstem structures is necessary to reach the CM. The MCP is remarkably tolerant to transgression and permits safe

entry into the basilar pons as it continues into the transverse pontine fibers. Careful preoperative evaluation of imaging is essential for precise localization, particularly as extensive hemosiderin staining may obscure the true location of the CM on T2-weighted images. Dissection of the petrosal fissure extends the entry point into the MCP laterally, enabling a shallower approach into the peduncle and minimizing morbidity associated with cerebellar retraction or transgression of the CST. Peritrigeminal and supratrigeminal safe entry zones have been described and function as medial extensions of the trans-MCP approach [29]. Anterior petrosectomy or SCIT approaches can be used to treat cranially located transitional lesions, while a far-lateral trans-pontomedullary sulcus approach can access caudal pontine transitional CMs.

Dorsal pontine CMs are reached by means of a midline suboccipital craniotomy. While transvermian approaches have been described classically, we prefer transventricular approaches without transgression of the vermis whenever feasible. Opening the telovelar membrane allows access to the lateral recess of the fourth ventricle, and doing so bilaterally enables elevation of the vermis and wide exposure to the rhomboid fossa. Entry into the floor of the fourth ventricle for lesions that do not reach the ependymal surface has been described, via superior fovea, suprafacial-collicular, and median sulcus entry zones. However, we would recommend caution in patients whose CMs do not approach the ependymal surface, as the floor of the fourth ventricle tends to be exquisitely sensitive to manipulation. Overall, outcomes from CM resection in the pons have been favorable, with 80–90% of patients achieving stable-to-improved neurological status postoperatively [35].

9.4.3 Medulla

9.4.3.1 Aneurysms

Both PICA and V4 VA aneurysms arise in close proximity to the medulla. Patients presenting with ruptured aneurysms in these locations have significantly worse clinical outcomes than those in the anterior circulation or more distally in the posterior circulation. Their close association with the medulla and lower CNs has prompted growth in endovascular approaches, particularly for ruptured aneurysms. However, the complex morphology of these aneurysms can make definitive endovascular treatment challenging. This is particularly true for PICA aneurysms, in which the PICA frequently arises from the aneurysm dome, or the aneurysm arises more distally on the PICA. These anatomic variants favor the use of bypass techniques to enable definitive treatment and preservation of VA and PICA blood flow. A wide variety of bypass configurations have been applied to PICA aneurysms, including PICA-PICA side-to-side, PICA-VA reimplantation, excision-reanastomosis, and occipital artery-PICA external carotid-internal carotid (OA-PICA EC-IC) bypasses [22]. These revascularization techniques frequently simplify the clipping strategies or make an otherwise unclippable aneurysm curable [36] (Fig. 9.6). Endovascular treatment of PICA aneurysms is associated with relatively high rates of recurrence

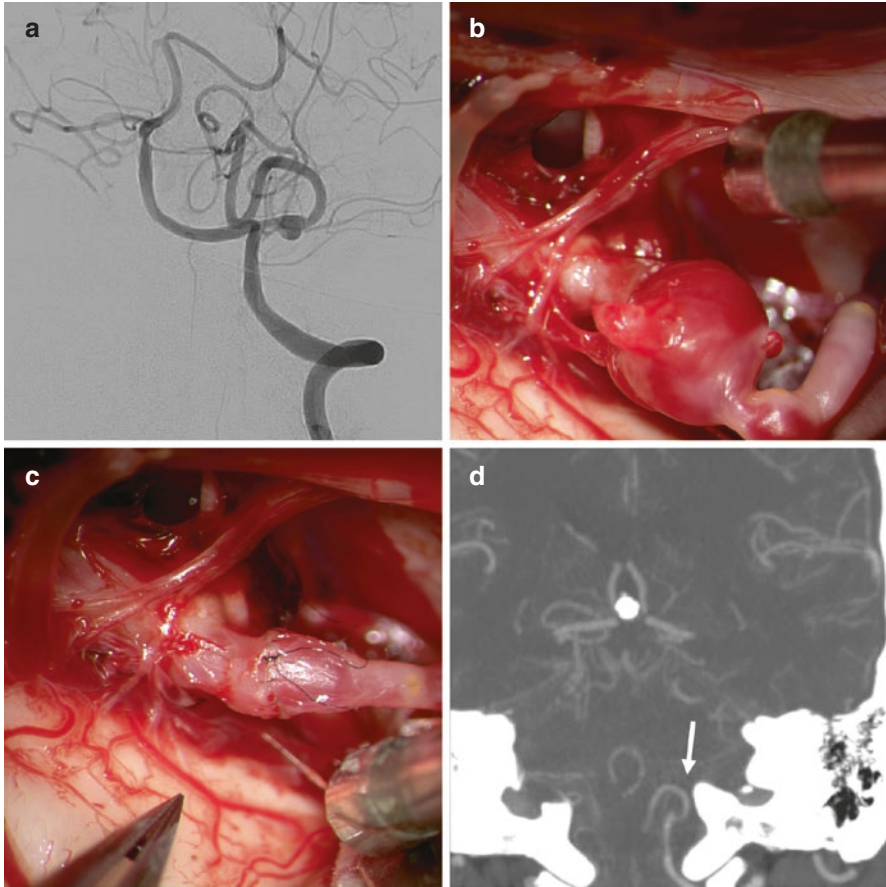


Fig. 9.6 A patient presenting with subarachnoid hemorrhage was found to have a fusiform aneurysm at the junction of the p1 and p2 segments of the left PICA (a). A far-lateral craniotomy exposed the aneurysm (b). An undiseased segment of PICA was identified proximal to the aneurysm without associated perforators, enabling aneurysm excision and end-to-end reanastomosis (c). Postoperative CTA demonstrated patency of the bypass and confirmed complete excision of the aneurysm (d, arrow). Used with permission from Barrow Neurological Institute

or PICA occlusion, and the value of partial treatment has not been definitively established (particularly for ruptured aneurysms).

On the other end of the spectrum, V4 aneurysms tend to be fusiform in nature, frequently as a result of intracranial dissection. When ruptured, these aneurysms frequently have friable domes that poorly accommodate primary clip occlusion and may necessitate parent vessel sacrifice, clip-wrap, or bypass techniques. While experience is limited compared to the many years of open approaches, there is certainly promise to the use of flow diversion for these aneurysms [37]. Deployment is generally straightforward in this segment of the VA. The major limitation tends to be enlargement of the VA at the V3/V4 junction beyond the maximal nominal diameter of the stent, resulting in poor wall apposition, foreshortening, and device migra-

tion. Experience with ruptured dissecting VA aneurysms is still relatively limited, and justifiable concerns exist about the risk of re-rupture after placement of a device that does not immediately occlude an aneurysm and demands dual antiplatelet therapy. Likewise, concerns about occlusion of a jailed PICA or VA perforators are valid, although published reports suggest that PICA occlusions tend to be asymptomatic in this situation [38]. Long-term follow-up is necessary to clearly define the ideal approach to these aneurysms.

9.4.3.2 Arteriovenous Malformations (AVMs)

As with the pons, AVMs of the medulla are divided into anterior and lateral groups (again, we have not encountered posterior medullary AVMs). Anterior medullary AVMs sit medial to the anterolateral medullary sulci and below the pontomedullary fissure, taking blood supply from perforating arteries arising at the VBJ and distal V4 VAs. There is no open approach that provides sufficient exposure to this surface of the medulla, and endoscopic transclival approaches do not afford sufficient bimanual dexterity or precise vascular control to make this a viable approach. In the senior author's operative series, only one patient was considered a viable operative candidate, presenting with a medullary hemorrhage that had dissected dorsally permitting a suboccipital posterior approach, but without such severe deficits that would negate the value of resection.

Conversely, lateral medullary AVMs permit a more aggressive surgical posture. They are located lateral to the anterolateral sulcus and rootlets of CN XII and are approached through a far-lateral craniotomy. Arterial inputs are from the V4 VA and from the p1 and p2 segments of the PICA. Venous drainage through the lateral medullary vein may be visualized early on, whereas the medial medullary vein may not be visible until significant dissection of the AVM has been performed. These AVMs tend to be small and respect the pia, allowing for complete resection in two-thirds of cases, while *in situ* disconnection was performed in the remaining cases. Good outcomes were achieved in 75% of patients in the senior author's experience [4] (Fig. 9.7).

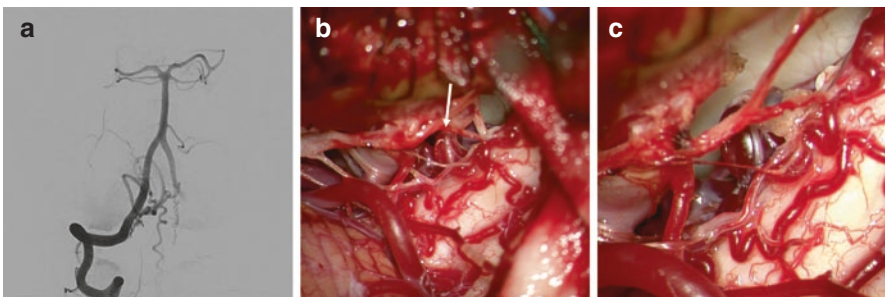


Fig. 9.7 A patient presenting with symptoms of cervical myelopathy was found to have a lateral medullary AVM. Digital subtraction angiography suggested that the malformation was fed predominantly from a single feeding artery (a), which was confirmed intraoperatively (b, arrow). *In situ* disconnection without pial resection (c) resulted in angiographic cure postoperatively. Used with permission from Barrow Neurological Institute

9.4.3.3 Cavernous Malformations (CMs)

CMs of the medulla are approached through either a far-lateral craniotomy for anterolaterally located lesions, or a midline suboccipital craniotomy for dorsally located CMs. Safe entry zones for deep-seated CMs are relatively limited in the medulla compared to the midbrain and pons. The trans-anterolateral sulcus approach has been described for ventrally located CMs, and identification of the CSTs with DTI is particularly useful for surgical planning for these lesions. For transitional lesions at the cervicomedullary junction, division of the median sulcus between the gracile fasciculi is also feasible, as well as through the posterior intermediate and posterolateral sulci [29]. Otherwise, we would recommend caution when considering intervention on smaller CMs that do not approach the pial surface. This is particularly true in the medullary fourth ventricular surface, where lower CN nuclei are intolerant to manipulation, which can result in significant morbidity. While resection of lesions in the medulla can be associated with high rates of tracheostomy, feeding tube placement, and/or ventilator dependence, surgical resection drastically reduces the risk of recurrent brainstem hemorrhage compared to the natural history of these lesions [39].

9.5 Conclusion

Vascular lesions of the brainstem are among the most technically demanding surgical pathologies in neurosurgery. Clinical decision-making in patients presenting with these lesions is predicated based on a thorough understanding of the natural history of various vascular lesions (particularly when located in the posterior fossa/brainstem). Successful treatment requires detailed knowledge of the anatomy, including vascular, surface and parenchymal structures. Furthermore, facility with an array of skull base approaches necessary to safely access the various regions and surfaces of the brainstem is essential. Likewise, surgeons should have a clear understanding of endovascular and radiosurgical techniques, used as alternative or combined treatment approaches, as well as a clear understanding of the surgical goals for a particular patient. Surgical intervention is associated with significant perioperative and long-term risks, but treatment results in drastic reduction of hemorrhage compared to the natural history of the disease in many patients. With dedication to developing surgical skills and decision-making, vascular lesions of the brainstem can be treated safely.

References

1. Rhoton ALJ. Microsurgical anatomy of the posterior fossa cranial nerves. *Clin Neurosurg.* 1979;26:398–462.
2. Wiebers DO, Whisnant JP, Huston J, Meissner I, Brown RDJ, Piepgras DG, et al. Unruptured intracranial aneurysms: natural history, clinical outcome, and risks of surgical and endovascular treatment. *Lancet.* 2003;362(9378):103–10.

3. Goldberg J, Raabe A, Bervini D. Natural history of brain arteriovenous malformations: systematic review. *J Neurosurg Sci.* 2018;62(4):437–43.
4. Han SJ, Englot DJ, Kim H, Lawton MT. Brainstem arteriovenous malformations: anatomical subtypes, assessment of “occlusion in situ” technique, and microsurgical results. *J Neurosurg.* 2017;58(4):107–17.
5. Taslimi S, Modabbernia A, Amin-Hanjani S, Barker FG II, Macdonald RL. Natural history of cavernous malformation. *Neurology.* 2016;86(21):1984–91.
6. Spetzler RF, McDougall CG, Zabramski JM, Albuquerque FC, Hills NK, Russin JJ, et al. The barrow ruptured aneurysm trial: 6-year results. *J Neurosurg.* 2015;123(3):609–17.
7. Torne R, Rodriguez-Hernandez A, Arikian F, Romero-Chala F, Cicuendez M, Vilalta J, et al. Posterior fossa arteriovenous malformations: significance of higher incidence of bleeding and hydrocephalus. *Clin Neurol Neurosurg.* 2015;134:37–43.
8. Ene C, Kaul A, Kim L. Natural history of cerebral cavernous malformations. *Handb Clin Neurol.* 2017;143:227–32.
9. Philipp LR, McCracken DJ, McCracken CE, Halani SH, Lovasik BP, Salehani AA, et al. Comparison between CTA and digital subtraction angiography in the diagnosis of ruptured aneurysms. *Neurosurgery.* 2017;80(5):769–77.
10. Chen KK, Guo WY, Yang HC, Lin CJ, Wu CHF, Gehrisch S, et al. Application of time-resolved 3D digital subtraction angiography to plan cerebral arteriovenous malformation radiosurgery. *AJNR Am J Neuroradiol.* 2017;38(4):740–6.
11. Lawton MT, Kim H, McCulloch CE, Mikhak B, Young WL. A supplementary grading scale for selecting patients with brain arteriovenous malformations for surgery. *Neurosurgery.* 2010;66(4):702–13. Discussion 713.
12. Mosimann PJ, Chapot R. Contemporary endovascular techniques for the curative treatment of cerebral arteriovenous malformations and review of neurointerventional outcomes. *J Neurosurg Sci.* 2018;62(4):505–13.
13. Rustemi O, Alaraj A, Shakur SF, Orning JL, Du X, Aletich VA, et al. Detection of unruptured intracranial aneurysms on noninvasive imaging. Is there still a role for digital subtraction angiography? *Surg Neurol Int.* 2015;6:175.
14. Walcott BP, Choudhri O, Lawton MT. Brainstem cavernous malformations: natural history versus surgical management. *J Clin Neurosci.* 2016;32:164–5.
15. Li D, Jiao Y-M, Wang L, Lin F-X, Wu J, Tong X-Z, et al. Surgical outcome of motor deficits and neurological status in brainstem cavernous malformations based on preoperative diffusion tensor imaging: a prospective randomized clinical trial. *J Neurosurg.* 2018;130(1):286–301.
16. Somanna S, Babu RA, Srinivas D, Narasinga Rao KVL, Vazhayil V. Extended endoscopic endonasal transclival clipping of posterior circulation aneurysms—an alternative to the transcranial approach. *Acta Neurochir.* 2015;157(12):2077–85.
17. Lawton MT. Basilar apex aneurysms: surgical results and perspectives from an initial experience. *Neurosurgery.* 2002;50(1):1–8. Discussion 8–10.
18. Bender MT, Wendt H, Monarch T, Lin L-M, Jiang B, Huang J, et al. Shifting treatment paradigms for ruptured aneurysms from open surgery to endovascular therapy over 25 years. *World Neurosurg.* 2017;106:919–24.
19. Drake CG, Peerless SJ, Hernesniemi J. *Surgery of vertebrobasilar aneurysms.* Vienna: Springer Science & Business Media; 2012. 1 p.
20. Yaşargil MG. *Microneurosurgery, volume I.* New York: Thieme; 1984. 1 p.
21. Seckin H, Avci E, Uluc K, Niemann D, Baskaya MK. The work horse of skull base surgery: orbitozygomatic approach. Technique, modifications, and applications. *Neurosurg Focus.* 2008;25(6):E4.
22. Lawton MT. *Seven aneurysms.* New York: Thieme; 2010. 1 p.
23. Krisht AF, Krayenbuhl N, Sercl D, Bikmaz K, Kadri PAS. Results of microsurgical clipping of 50 high complexity basilar apex aneurysms. *Neurosurgery.* 2007;60(2):242–50. Discussion 250–2.
24. Aziz KM, van Loveren HR, Tew JM Jr, Chicoine MR. The Kawase approach to retrosellar and upper clival basilar aneurysms. *Neurosurgery.* 1999;44(6):1225–34. Discussion 1234–6.

25. Molyneux A, Kerr R, Stratton I, Sandercock P, Clarke M, Shrimpton J, et al. International Subarachnoid Aneurysm Trial (ISAT) of neurosurgical clipping versus endovascular coiling in 2143 patients with ruptured intracranial aneurysms: a randomised trial. *Lancet*. 2002;360(9342):1267–74.
26. Tjahjadi M, Serrone J, Hernesniemi J. Should we still consider clips for basilar apex aneurysms? A critical appraisal of the literature. *Surg Neurol Int*. 2018;9(1):44.
27. Lawton MT. In: Lawton MT, editor. *Seven AVMs*. Stuttgart: Thieme; 2014. 1 p.
28. Vishteh AG, David CA, Marciano FF, Coscarella E, Spetzler RF. Extreme lateral supracerebellar infratentorial approach to the posterolateral mesencephalon: technique and clinical experience. *Neurosurgery*. 2000;46(2):384–8. Discussion 388–9.
29. Spetzler RF, Kalani MYS, Nakaji P. *Color atlas of brainstem surgery*. New York: Thieme; 2017. 1 p.
30. Yağmurlu K, Rhoton ALJ, Tanriover N, Bennett JA. Three-dimensional microsurgical anatomy and the safe entry zones of the brainstem. *Neurosurgery*. 2014;10(Suppl 4):602–19. Discussion 619–20.
31. Tan LA, Moftakhar R, Lopes DK. Treatment of a ruptured vertebrobasilar fusiform aneurysm using pipeline embolization device. *J Cerebrovasc Endovasc Neurosurg*. 2013;15(1):30–4.
32. Graziano F, Ganau M, Iacopino DG, Boccardi E. Vertebro-basilar junction aneurysms: a single centre experience and meta-analysis of endovascular treatments. *Neuroradiol J*. 2014;27(6):732–41.
33. Choudhri O, Connolly ID, Lawton MT. Macrovascular decompression of the brainstem and cranial nerves: evolution of an anteromedial vertebrobasilar artery transposition technique. *Neurosurgery*. 2017;81(2):367–76.
34. Lawton MT, Abla AA, Rutledge WC, Benet A, Zador Z, Rayz VL, et al. Bypass surgery for the treatment of dolichoectatic basilar trunk aneurysms: a work in progress. *Neurosurgery*. 2016;79(1):83–99.
35. Porter RW, Detwiler PW, Spetzler RF, Lawton MT, Baskin JJ, Derksen PT, et al. Cavernous malformations of the brainstem: experience with 100 patients. *J Neurosurg*. 1999;90(1):50–8.
36. Lawton MT. *Seven bypasses*. New York: Thieme; 2018. 1 p.
37. Corley JA, Zomorodi A, Gonzalez LF. Treatment of dissecting distal vertebral artery (V4) aneurysms with flow diverters. *Oper Neurosurg (Hagerstown)*. 2018;15(1):1–9.
38. Chalouhi N, Patel PD, Atallah E, Starke RM, Chitale A, Lang M, et al. Low yield of cerebral angiography in adequately occluded aneurysms after flow diversion. *Neurosurgery*. 2018;83(6):1294–7.
39. Abla AA, Lekovic GP, Turner JD, de Oliveira JG, Porter R, Spetzler RF. Advances in the treatment and outcome of brainstem cavernous malformation surgery: a single-center case series of 300 surgically treated patients. *Neurosurgery*. 2011;68(2):403–14. Discussion 414–5.

Chapter 10

Inflammatory and Infectious Lesions of the Brainstem



Rechdi Ahdab, Fateme Salehi, and Raghid Kikano

Abbreviations

ADEM	Acute disseminated encephalomyelitis
AQ4	Aquaporin 4
BBE	Bickerstaff's brainstem encephalitis
BS	Brainstem
CIS	Clinically isolated syndrome
CLIPPERS	Chronic lymphocytic inflammation with pontine perivascular enhancement responsive to steroids
CN	Cranial nerve
CNS	Central nervous system
CSF	Cerebrospinal fluid
CTDs	Connective tissue diseases
DIS	Dissemination in space
DIT	Dissemination in time
DWI	Diffusion-weighted imaging
ELISA	Enzyme-linked immunosorbent assay
EV	Enterovirus
FLAIR	Fluid-attenuated inversion recovery
HIV	Human Immunodeficiency virus
HSV	Herpes Simplex virus
Ig	Immunoglobulin
IIDB	Idiopathic inflammatory demyelinating diseases of the brain

R. Ahdab (✉)

Department of Internal Medicine, Lebanese American University Medical Center, Rizk Hospital, Beirut, Lebanon

e-mail: rechdi.ahdab@laumcrh.com

F. Salehi

Department of Neuroradiology, Toronto Western Hospital, Toronto, ON, Canada

R. Kikano

Radiology Department, Lebanese American University Medical Center, Rizk Hospital, Beirut, Lebanon

INO	Internuclear ophthalmoplegia
IVIg	Intravenous immunoglobulins
JC	John Cunningham
LETM	Longitudinally extensive transverse myelitis
MOG	Myelin oligodendrocyte glycoprotein
MRI	Magnetic resonance imaging
MS	Multiple sclerosis
NMO	Neuromyelitis optica
NMOSD	Neuromyelitis optica spectrum disorder
OCB	Oligoclonal bands
OMM	Oculomasticatory myorhythmia
OpM	Opsoclonus-myoclonus
PACNS	Primary angiitis of the central nervous system
PAN	Polyarteritis nodosa
PCR	Polymerase chain reaction
REM	Rapid eye movement
RRMS	Relapsing-remitting multiple sclerosis
SLE	Systemic lupus erythematosus
SN	Substantia nigra
SS	Sjögren's syndrome
T. pallidum	Treponema pallidum
TB	Tuberculosis
VZV	Varicella zoster virus
WD	Whipple's disease

10.1 Introduction

The brainstem (BS) is unique among other central nervous system (CNS) structures in that it holds in a very narrow space a number of critical neural elements such as the long tracts of the CNS, the cranial nerve (CN) nuclei and respective nerves, the reticular system, and various reflex centers, including the cardiorespiratory centers. Consequently, localizing a disease process to the brainstem is often an easy task given the abundance of objective physical findings. Conversely, determining the exact nature of the disease can prove very challenging. BS lesions span a wide range of pathologies including tumors, infections, and various inflammatory/autoimmune disorders. The main concern is often the distinction between an inflammatory/infectious disorder and a BS tumor in order to avoid unnecessary surgical intervention.

It is usually easy to exclude a BS tumor based on imaging findings, but this is not always the case. Many non-neoplastic diseases of the BS can present as a space-occupying lesion [1]. Conversely, diffuse BS tumors such as lymphomas are known to masquerade as inflammatory or infectious lesions [2]. In difficult cases, additional tests are often needed, including cerebrospinal fluid (CSF) analysis, serum testing, and advanced imaging techniques such as magnetic resonance (MR) spec-

troscopy and MR perfusion. Once a BS tumor is excluded with a reasonable degree of certainty, the next logical question becomes: is this an infectious process? The distinction between infectious and noninfectious etiologies is important in order to select the best initial therapy. BS abscesses need to be differentiated from tumefactive inflammatory lesions, and the origin of more diffuse encephalitic lesions should be rapidly determined. When faced with a case of BS encephalitis, the diagnostic approach is somewhat different from that of encephalitis in general. Unlike classical encephalitis, which is mostly infectious [3], BS encephalitis is typically an autoimmune disorder. The outcome of BS encephalitis is intimately linked to the underlying etiology. Generally speaking, the outcome is good with full or near full recovery in most patients. Nevertheless, some etiologies are potentially severe and life-threatening. As such, prompt identification of the most plausible etiology and early initiation of the most appropriate empiric treatment is often necessary.

This chapter will address the various infectious and inflammatory disorders of the brainstem with emphasis on their clinical presentation, key radiological and laboratory findings, and general principles of management. Our current understanding of many of these entities is based on case reports and small case series. Consequently, evidence-based guidelines for managing such entities are inexistent to date, as described in this chapter. In such cases, expert opinions and the limited evidence found in the literature will be provided for guidance.

10.2 Clinical Presentation

BS involvement in inflammatory and infectious disorders is often suspected on clinical grounds. Lesions of the BS may manifest as cerebellar, somatosensory, motor symptoms, as well as CN dysfunction. The clinical finding of ipsilateral CN dysfunction and contralateral hemiparesis and/or sensory loss (the so-called crossed symptoms) is the hallmark of BS injury. The involved CN(s) help(s) in determining the approximate rostro-caudal level of a lesion. A disease process affecting the mid-brain manifests clinically as diplopia, ptosis, and a dilated pupil (CN III, IV). Lesions lying in the pons present with facial weakness (CN VII), horizontal diplopia (CN VI), vertigo, nystagmus and hearing loss (CN VIII), jaw weakness (CN V), and facial anesthesia to light touch (principle sensory nucleus of the trigeminal nerve). Dysphonia, dysarthria, dysphagia, and facial anesthesia to pain and temperature are suggestive of a medullary lesion.

Broadly speaking, motor deficits (affecting the limbs, ocular muscles, and tongue), sensory loss to light touch, vibration and joint position (medial lemniscus), and internuclear ophthalmoplegia (INO) tend to occur with more medial lesions. INO occurs with lesions disrupting the median longitudinal fasciculus. In this condition, the affected eye fails to adduct, whereas the contralateral eye abducts with a nystagmus. Lateral lesions are more likely to cause loss of thermal and pain sensations (spinothalamic pathways and CN V), ataxia (spinocerebellar pathways), and a Horner sign (sympathetic pathways). Cerebellar signs and symptoms ipsilateral to

CN involvement are commonly encountered with pontine lesions causing injury to the cortico-ponto-cerebellar pathways. Horizontal gaze palsy is commonly seen with pontine lesions and vertical gaze palsy with midbrain lesions. Palatal tremor is indicative of a lesion affecting the Guillain-Mollaret triangle, which includes the red nucleus, the dentate nucleus and the inferior olive [4]. Choreoathetosis and tremor may be seen with midbrain lesions involving the red nucleus.

Although strongly suggestive of BS involvement, symptoms and signs are rarely disease-specific. Nevertheless, some disease states have a distinctive tropism to certain BS structures and tend to spare others. This concerns, for example, viral infections and paraneoplastic syndromes, which almost invariably cause ataxia and often spare the motor and sensory tracts [5]. On the other hand, some forms of vasculitis, such as Behçet disease, have a tendency to cause motor and sensory symptoms with minimal ataxia [5]. Altered level of consciousness is suggestive of an infectious etiology, especially when it is associated with fever and meningismus [5]. In some cases, symptoms and signs of BS dysfunction can be fairly characteristic of a disease process. Opsoclonus-myoclonus (OpM), for instance, is often indicative of an infectious or paraneoplastic origin [6]. OpM is the combination of involuntary, arrhythmic and multi-directional saccades with myoclonic jerks in the limbs [6]. It is commonly accompanied by ataxia, tremor, and encephalopathy. Similarly, oculomasticatory myorhythmia (OMM) is pathognomonic of Whipple's disease (WD) of the CNS. It consists of a continuous pendular convergent-divergent nystagmus with concurrent contractions of the masticatory muscles and occasional rhythmic movements of the limbs [7]. OMM is often associated with supranuclear vertical gaze palsy. Deficient upward gaze is a typical feature of anti-Ma2 paraneoplastic encephalitis [29], whereas bilateral and symmetrical ophthalmoplegia is typical of Bickerstaff's brainstem encephalitis (BBE) [8].

Some disease states will produce lesions outside the BS. The occurrence of such lesions and their clinical features often provide valuable guidance as to the underlying origin of the BS lesion. Other disorders produce symptoms outside the CNS. This concerns, for example, CTDs, vasculitis, and paraneoplastic syndromes. Such symptoms can be present at the time of diagnosis or may develop later, occasionally several years after presentation. Their occurrence is also very helpful in securing a specific diagnosis.

10.3 Diagnostic Approach

The diagnostic approach to BS encephalitis involves a detailed history, a thorough physical examination, and an array of ancillary tests such as brain imaging, and serum and CSF analysis. In more difficult cases where the etiology remains unknown, a BS biopsy may be indicated.

Epidemiological data often offer a first clue as to the underlying etiology. While viral infections and demyelinating diseases are more frequent in the young, paraneoplastic diseases tend to affect older age groups [5]. Autoimmune diseases are more likely to affect women, but some exceptions exist. The immune status is also a key element to consider, since immunodeficiency increases the likelihood of an

infectious disorder. The presence of an antecedent febrile illness in the preceding weeks is supportive of an autoimmune disorder.

Although the history and physical findings provide some insight as to the underlying etiology, a specific diagnosis is rarely secured at this stage and various ancillary tests are usually ordered. Magnetic resonance imaging (MRI) is often the single most useful test to advance in the diagnostic process. Imaging abnormalities involving the BS are found in most patients but are rarely disease-specific. On the other hand, when supratentorial or spinal cord lesions are present, their radiological features could be fairly characteristic of a disease process; this is particularly true in demyelinating diseases. The absence of MRI abnormalities reliably excludes some entities such as demyelinating disorders. In other conditions such as paraneoplastic syndromes and BBE, MRI is frequently unremarkable [5]. Rarely, MRI characteristics of BS lesions are virtually diagnostic; chronic lymphocytic inflammation with pontine perivascular enhancement responsive to steroids (CLIPPERS) is one such example [9].

Lumbar puncture is often recommended if not contraindicated by the presence of an intracranial mass effect. Most patients will have CSF abnormalities including pleocytosis, high protein levels, or low glucose. CSF analysis is pivotal when an infectious origin is suspected [5]. A white cell count exceeding 100 cells/ μ l is usually indicative of bacterial infection or certain forms of vasculitis such as Behçet disease [5]. Neutrophil predominance is often seen in Listeriosis and Behçet disease, whereas lymphocyte predominance is found in viral infections, tuberculosis (TB), and autoimmune diseases. Low glucose is usually indicative of an infectious etiology, such as Listeria and TB. The demonstration of intrathecal production of immunoglobulin G (IgG) and the presence of oligoclonal bands (OCB) are characteristic of demyelinating disorders and some CTDs.

Serum testing often adds little to the clinical, imaging, and CSF findings. However, in rare clinical settings, these can prove extremely helpful by detecting specific antibodies such as aquaporin 4 (AQ4), myelin oligodendrocyte glycoprotein (MOG), and GQ1b antibodies. When a specific diagnosis cannot be reached or a certain degree of uncertainty remains, stereotactic BS biopsy should be considered. When performed with appropriate MRI guidance and by experienced staff, this procedure is both safe and accurate [10]. However, obtaining tissue does not guarantee that a final diagnosis will be reached, because sampling errors and misinterpretation of histological findings can occur [11]. Despite all efforts, the etiology will remain unknown in up to 30% of cases [5]. Most cases of undefined BS encephalitis will eventually turn out to be immune-mediated, and it seems justifiable to offer such patients a trial of immunosuppressants under close clinical and radiological monitoring.

10.4 Etiologies

10.4.1 Brainstem Infections

Infectious lesions of the BS are collectively rare and include BS abscess and encephalitis. Infectious diseases can be further subdivided by etiology: bacterial, viral, fungal, and parasitic. Before these pathogens can infect the BS, they first need

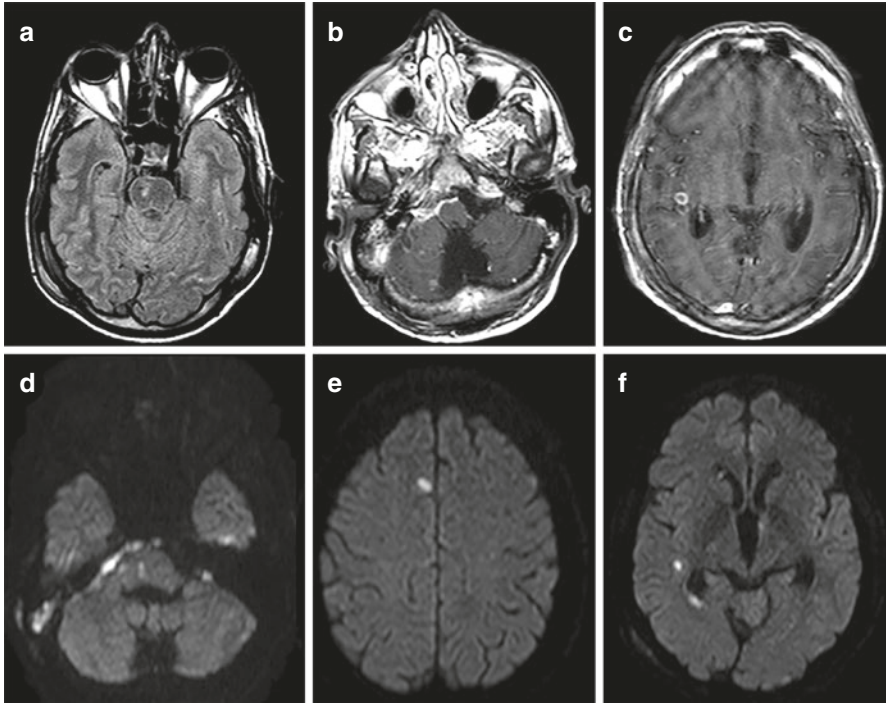


Fig. 10.1 Patient with right-sided mastoiditis and multiple brain micro-abscesses. (a) Axial FLAIR image showing a right paramedian pontine abscess. (b) Post-contrast axial T1-weighted image showing right-sided mastoiditis and leptomenigeal enhancement. (c) Postcontrast axial T1-weighted image showing a ring-enhancing lesion at the supratentorial level. (d) Empyema in the right prepontine cistern showing restricted diffusion. (e, f) DWI showing central restricted diffusion within the supratentorial lesions

to travel and gain access to the CNS. The most common portal of entry is the haematogenous route. Alternatively, some pathogens, such as bacteria, can also gain access to the brain by direct extension from a contiguous focus, such as sinusitis, otitis media, and mastoiditis (Fig. 10.1). Neurosurgical procedures and trauma, by breaching the integrity of the skull and meninges, also allow easy access to the CNS. The last portal of entry is nerves, whereby the pathogen travels along the peripheral nerve and bypasses the defense mechanisms of the CNS. One classical example is the varicella zoster virus (VZV). Regardless of the route, once the pathogen enters the brain, it sets off an inflammatory reaction; many of the manifestations and complications of CNS infections are attributed to the immune response mounted against the pathogen rather than its direct effect on brain tissue. Occasionally, infectious agents trigger an immune reaction directed against the CNS itself, a condition known as postinfectious encephalitis. In this condition, no evidence of direct invasion of the pathogen can be found. In rare cases, the infectious agent invades the brain's vasculature, a condition known as infectious vasculopathy.

10.4.1.1 Brainstem Abscess

Clinically, BS abscesses behave like a brainstem mass with focal neurological symptoms and signs, with or without signs of increased intracranial pressure. The onset is typically subacute. The most frequent presenting symptoms in decreasing order are headache, diplopia, hemiparesis, and nausea/vomiting [12, 13]. Although the presence of fever should alert to the infectious nature of the underlying lesion, it is present in fewer than a third of the cases [13]. In an afebrile patient, the clinical presentation is no different from other space-occupying lesions, and the distinction between an abscess and a tumor can be difficult. This is compounded by the fact that white blood cell count can be normal in roughly 50% of patients with BS abscesses [13]. Brain MRI plays a pivotal role in the diagnosis and management of BS abscesses; these are recognizable by their round shape, ring-enhancement, and varying amount of perilesional edema (see Fig. 10.1). MRI is usually able to distinguish abscesses from other ring-enhancing lesions such as tumors and tumefactive inflammatory lesions. Brain abscesses are characterized by central restricted diffusion indicating the presence of a fluid with high protein content (pus), lack of restricted diffusion of the enhancing part, and a T2-hypointense capsule [11]. MRI findings may differ depending on the patient's immune status [14]; this concerns contrast enhancement and the degree of edema, which seem to parallel the white cell count. With less severe immunosuppression, the host's defense system is able to mount an immune response and isolate the agent. This results in nodular or ring-enhancement of the lesion [14]. Lumbar puncture is not recommended and may even be contraindicated because of the risk of herniation [15].

Pyogenic Brain Abscess Pyogenic brain abscesses as a whole have become less frequent since the widespread use of antibiotics. They rarely localize to the brainstem (mostly the pons) and represent fewer than 1% of brain abscesses [12]. They reach the BS by direct spread from a contiguous site or by hematogenous seeding. Spread from a contiguous site generally causes a solitary lesion, whereas hematogenous spread typically causes multiple CNS abscesses. The most common underlying infectious agents are the *Streptococcus* species, *Staphylococcus* species, and TB [13]. Immunocompromised hosts can have a vast array of pathogens, from the usual organisms to other more unusual pathogens such as *Listeria* [16] and *Nocardia* [17].

The treatment options for a solitary BS abscess include stereotactic drainage, open microsurgical excision, or antimicrobial agents alone. Microsurgery and stereotactic aspiration help in establishing a diagnosis, identifying the causative agent, and relieving the mass effect. Stereotactic drainage has a favorable safety profile and has become the surgical option of choice in many centers [18]. Hydrocephalus is treated by insertion of a temporary or permanent CSF draining shunt. For patients with a small lesion and mild neurological deficits on presentation, medical treatment alone is a valid option, especially if the abscess is deep-seated and difficult to access surgically. If the patient fails to improve or deteriorates, then drainage and identification of the underlying organism becomes essential. The outcome is variable and is dependent on several factors including the severity of the neurological

deficit on admission and the treatment regimen (medical treatment alone versus surgery) [13]. The majority of patients will eventually recover with no or mild neurological sequelae [13].

Tuberculous Brain Abscess TB should be considered in endemic regions or immigrants originating from these regions. TB brain abscess is a rare form of CNS TB and may occur in the absence of signs of active systemic infection [19]. More commonly, CNS TB manifests as a single or multiple tuberculomas. Tuberculomas are caseating granulomas rather than true abscesses. Tuberculomas may affect the BS and present as a solitary mass, especially in children [20, 21]. MRI findings characteristically show an outer hyperintense rim (representing the cellular infiltrate), a hypointense inner region (representing the central necrotic components), and perilesional edema. Contrast enhancement is rather patchy, and the margins are ill-defined [22]. The diagnosis can be challenging since more than half of the cases have no evident systemic signs of TB [23]. This is compounded by the fact that tuberculomas can develop or paradoxically grow during anti-TB treatment [24]. Treatment is based on anti-tuberculous drugs. The addition of steroids often offers symptomatic relief. There is no consensus regarding the optimal duration of treatment, which is usually dictated by the clinical and radiological responses.

Parasitic Brain Abscess Parasitic infections should be considered in endemic regions or immigrants originating from these regions. Cysticercosis, a condition caused by the larvae of *Taenia solium*, classically presents with multiple supra- and infratentorial abscesses [25]. Although neurocysticercosis can cause almost any neurological symptom, late-onset epilepsy and intracranial hypertension are its most common manifestations [25]. BS cysticerci most often appear as small, well-defined, round enhancing lesions [25]. These primarily localize to the midbrain and tend to have a good prognosis if promptly treated with cysticidal drugs [26]. Rare cases of isolated BS abscesses have been described in the literature [26].

In immunocompromised patients, CNS toxoplasmosis is always a consideration. Toxoplasmosis is caused by the intracellular protozoan parasite *Toxoplasma gondii* [27]. The clinical disease usually results from the reactivation of a latent infection during immunosuppression. The clinical manifestations are protean and most often include headaches, confusion, and focal neurological findings including hemiparesis, ataxia and CN palsies [27]. Typical MRI findings include multiple ring-enhancing lesions involving the basal ganglia and cerebral/cerebellar hemispheres with perilesional edema [27]. Solitary lesions are not uncommon and occur in roughly 20% of cases [27–30]. BS lesions are rare and tend to affect the midbrain [30, 31], and solitary BS lesions are exceptional [30, 31]. Confirming the diagnosis of CNS toxoplasmosis can be challenging. High titers of IgG anti-toxoplasma antibodies are helpful; however, the results need to be interpreted with caution given the high seroprevalence in the general population and the possibility of false-negative results [27, 32]. Some studies suggested the utility of polymerase chain reaction (PCR) on the CSF samples [33]. Occasionally, the only simple means of confirming the diagnosis is a

therapeutic trial with anti-toxoplasma medications. Treatment should be initiated early and consists of pyrimethamine and a sulfonamide. The outcome is not always favorable, especially in severe cases, where up to 50% of patients are expected to have a poor outcome (severe residual disability or death) [34]. Bad prognostic factors include profound immunosuppression and impaired consciousness [34]. Other parasitic infections of the BS are rare and include Amoebiasis [35] and Schistosomiasis [36].

Fungal Brain Abscess Fungal infections can also disseminate to the CNS, usually by the hematogenous route [37, 38]. The most frequently identified agent is the *Aspergillus* species followed by the *Candida* species [37, 39]. Fungal CNS infections are mostly seen in immunosuppressed patients but have also been described in patients with no clear defect in the immune system. BS involvement is exceedingly rare.

10.4.1.2 Brainstem Encephalitis

There is a long list of pathogens that can cause BS encephalitis, including viral, bacterial, and fungal agents. The clinical manifestations are rarely disease-specific. On the other hand, epidemiological features often help in narrowing the broad differential diagnosis. Key elements include age at onset, immune status, season during which the disease was contracted, geographic location, travel and exposure history, contact with animals, similar cases in the family or neighbors, and known cases of encephalitis in the surrounding. The patient's occupation, hobbies, and vaccination history are other important factors to consider. Physical examination can provide some insight regarding the underlying pathogen. For instance, the presence of an exanthem or enanthem are supportive of some forms of viral encephalitis. The diagnosis is often supported by an elevated white blood cell count and protein levels in the CSF, and serology helps in pinpointing the underlying pathogenic agent. Because IgM antibodies do not readily diffuse across the blood-brain barrier, the finding of IgM antibodies by enzyme-linked immunosorbent assay (ELISA) is diagnostic of CNS disease, though false-negative results are not uncommon [40]. IgM antibodies by ELISA testing are available for several pathogens including the VZV and flaviviruses. PCR assays are useful in diagnosing herpes encephalitis and have a high sensitivity and specificity (95–99%), although false-positive and false-negative tests can occur [40]. Imaging findings are often nonspecific. The outcome is dependent on the underlying infectious agent. Although most viral infections are self-limited, some have a particularly poor outcome if the treatment is delayed; this concerns, for example, the herpes simplex virus (HSV) and the VZV BS encephalitis. Bacterial and parasitic BS infections are almost uniformly fatal if untreated. Patients with BS encephalitis often require supportive care to ensure oxygenation, airway protection, and circulatory support. Close monitoring for cerebral edema, increased intracranial pressure, epileptic seizures and acute hydrocephalus is recommended.

Viral Encephalitis Virtually any viral encephalitis can spread to the BS. Host factors affecting the susceptibility to a particular pathogen include the immune status, age, and various genetic factors. When viral encephalitis is suspected, diagnostic efforts should initially focus on differentiating HSV from the other causative agents. To this end, serological tests are pivotal. These include serological testing of CSF IgM, as well as PCR and reverse-transcriptase PCR assays of a CSF sample to identify DNA and RNA viruses, respectively. It is recommended to start empirical acyclovir therapy in all patients with suspected encephalitis [40] until the underlying pathogen is identified and/or HSV encephalitis is excluded. The addition of glucocorticoids is a common practice but is of uncertain benefit [41]. MRI findings in BS encephalitis are often non-specific with patchy areas of increased T2-weighted signal and variable mass effect [42–45]. Lesions are typically non-enhancing [44, 46] or display minimal patchy enhancement [45]. Locations outside the BS such as the cortex, basal ganglia, thalamus, and cerebellum are often affected [42, 44–46]. Spinal cord lesions centered on the ventral horns have been described in West Nile virus and enterovirus (EV) encephalitis [44, 47]. Hippocampal involvement is typical of HSV encephalitis [48] but has also been described in Japanese encephalitis [49].

HSV is the most common cause of viral encephalitis in general and accounts for 50–75% of the identified viral cases [41]. Infection is non-seasonal, affects both sexes equally, and can occur at any age. HSV characteristically involves the temporal/cingulate cortices but only rarely the infratentorial compartment [43, 50]. BS involvement in HSV is typically associated with evidence of supratentorial involvement [51], but restricted BS infection has also been reported [52]. Although HSV encephalitis is predominantly caused by HSV-1, it has also been described with HSV-2, usually as a complication of genital herpes [53]. BS involvement without any evidence of genital herpes infection has also been described [54].

EV71 is another cause of BS encephalitis [47, 55]. EV71 is largely restricted to infants and classically presents as hand-foot-mouth disease or herpangina [56]. EV71 can also cause epidemics of aseptic meningitis, BS encephalitis, encephalomyelitis, and acute flaccid paralysis. BS encephalitis is the most common neurological manifestation. Children usually present with ataxia, myoclonic jerks, nystagmus, CN dysfunction, and tremor [57]. MRI shows abnormal areas of T2-hyperintense signal in the BS in most patients. These findings characteristically involve the dorsal pons and medulla oblongata [58]. The outcome is generally good and most patient fully recover in a few days [57]. Severe cases are usually treated with intravenous immunoglobulins (IVIg) and corticosteroids despite the lack of evidence to support this approach [59]. EV68 is another EV linked to BS involvement. This virus has a distinctive tropism to the anterior horn cells and BS motor nuclei leading to flaccid paralysis and CN dysfunction [60]. Most children who develop neurological complications are left with some degree of motor weakness and CN dysfunction including permanent dysphagia [60].

Epidemics of BS encephalitis have been described with Japanese and St. Louis encephalitis viruses [61]. These infections preferentially affect the midbrain and more particularly the substantia nigra (SN), with parkinsonism as a classical sequela

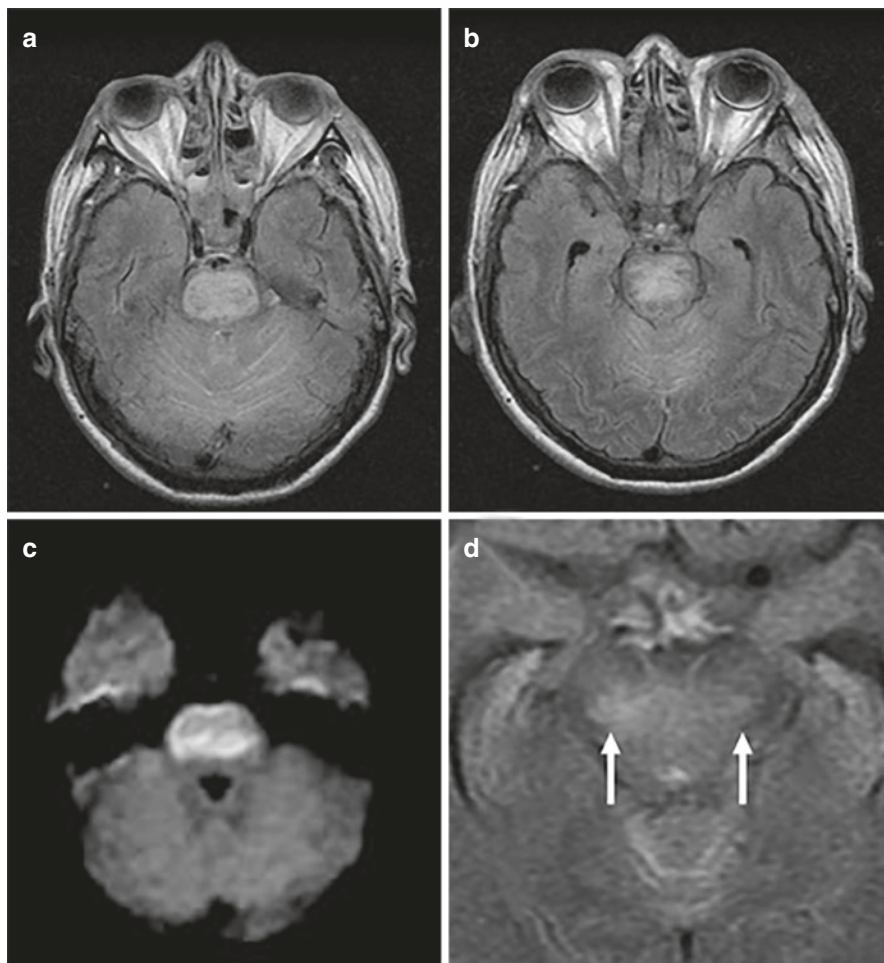


Fig. 10.2 Brainstem encephalitis caused by West Nile virus. (a, b) Axial FLAIR images of the brainstem, showing diffuse central spread at the midbrain-pons region. (c) Axial DWI, at the same level, demonstrating avid restricted diffusion. (d) Axial FLAIR image showing bilateral involvement of the substantia nigra, more pronounced on the right (arrows)

[62, 63]. Sporadic cases of SN involvement have been reported with Epstein-Barr virus (EBV) and West Nile virus infections [64, 65] (Fig. 10.2). BS encephalitis has been rarely reported with other viral infections such as adenovirus [45], Nipah virus [66], influenza A virus [67], and VZV [68].

As opposed to classical viral encephalitis, which has an acute onset and a rapid clinical course, some viral infections follow a slower clinical course. Progressive multifocal leukoencephalopathy (PML) is a subacute encephalitis caused by the John Cunningham (JC) polyomavirus, occurring almost exclusively in immunocompromised patients [69]. This includes patients with hematological malignancies, those

infected with the human immunodeficiency virus (HIV), or those treated with various immunosuppressant drugs such as natalizumab for multiple sclerosis (MS) [70]. Clinically, the disease manifests as cognitive decline with cortical symptoms and signs. MRI typically displays multiple subcortical areas of high signal on fluid-attenuated inversion recovery (FLAIR) images in both hemispheres. Isolated BS PML is very rare and poses a serious diagnostic challenge [69, 71]. The challenge is even greater when BS PML occurs in the setting of MS, where it can masquerade as an MS relapse [72]. Early marked T1 hypointensity, diffusion-weighted imaging (DWI) hyperintensity, and close MRI follow-up may distinguish new MS activity from PML [72]. Treatment is based on reversal of immunosuppression whenever possible and initiation of highly active antiretroviral therapy in HIV-infected patients. Prognosis is often poor.

Bacterial Brainstem Encephalitis Bacterial infections rarely localize to the BS with the exception of *Listeria monocytogenes*, which affects the BS in 9% of cases of CNS infections [73]. Predisposing factors for listeriosis are age >50 and immunosuppression. Neurological manifestations usually follow a prodrome of fever, headache, nausea, and vomiting. Signs and symptoms may also include single or multiple asymmetrical CN palsies, cerebellar signs, hemiparesis, hypoesthesia, and impairment of consciousness [74, 75]. MRI displays hyperintense, patchy lesions within the BS and/or multiple microabscesses [74]. CSF findings are often non-specific with lymphocytic pleocytosis and negative cultures in more than half of the cases [74]. Blood cultures are more likely to be positive in this setting [74]. Early empiric treatment with ampicillin is crucial in patients at risk. Prognosis is often poor with an overall mortality of 50% [74].

In rare cases, bacterial infections can follow a more subacute clinical course. WD is a systemic bacterial infection caused by *Tropheryma whippelii*. It classically manifests as gastrointestinal symptoms, weight loss, and arthropathy [76]. CNS manifestations occur in 10–50% of patients and can precede other manifestations of the disease [76, 77]. These include cognitive decline, cerebellar ataxia, myelopathy, hypothalamic-pituitary axis dysfunction, and various BS syndromes [77, 78]. The latter can present as the pathognomonic finding of OMM or oculofacial-skeletal myorhythmia, which generally occur in combination with supranuclear vertical gaze palsy [7]. Focal MRI abnormalities are observed in 50% of patients, ranging from focal lesions without mass effect to multiple enhancing lesions with mass effect [7] (Fig. 10.3). Neuro-WD can be diagnosed using PCR applied to a CSF sample. Neurological symptoms often respond dramatically to antibiotics; however, they may recur after discontinuation, prompting prolonged treatment periods that may extend up to 1 year [76].

10.4.1.3 Postinfectious Brainstem Encephalitis

BBE is a rare postinfectious disorder, where the inflammatory process is typically confined to the BS. BBE is clinically characterized by progressive impairment of consciousness along with ataxia and bilateral external ophthalmoplegia [8]. Some

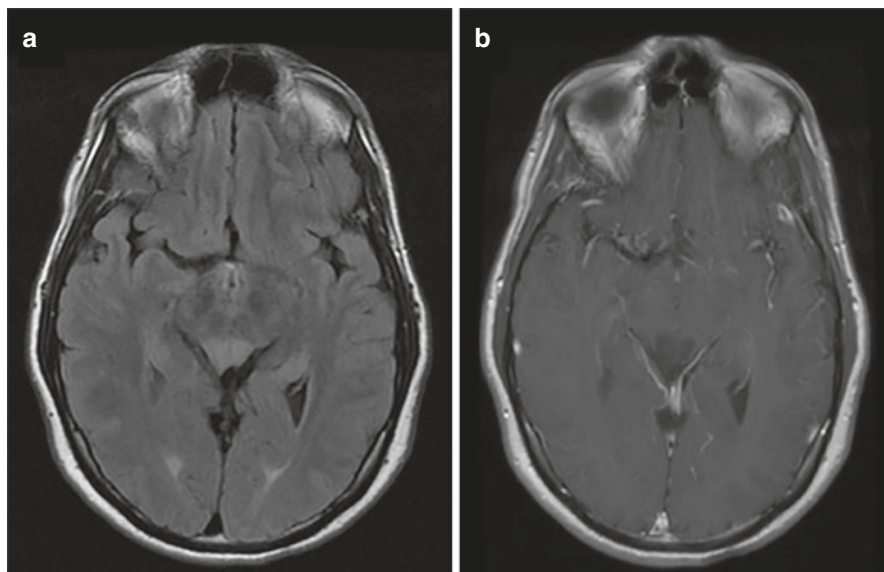


Fig. 10.3 Brainstem involvement in a patient with biopsy-proven Whipple's disease. (a) Tectal hyperintensity on FLAIR images. (b) Lack of enhancement on post-contrast T1-weighted images

additional features were occasionally described such as bilateral facial palsy, pupillary abnormalities, bulbar palsy, and generalized limb weakness [79]. The disease follows a monophasic course with a subacute onset and a favorable outcome in most cases. BBE is usually preceded by an infectious event, most often an upper respiratory tract infection [79]. CSF analysis shows pleocytosis in roughly half of the patients. Brain MRI is usually normal but may occasionally show T2-weighted BS anomalies [8]. IgG anti-GQ1b antibodies are highly specific for this disorder but can be absent in up to one-third of the cases [80]. These antibodies are also found in Miller-Fisher syndrome, a variant of Guillain-Barré syndrome characterized by ataxia, ophthalmoplegia and areflexia. Whether these two entities represent a spectrum of the same disorder remains unsettled. There are no evidence-based recommendations for the treatment of BBE. Patients are typically offered immunotherapy such as plasma exchange therapy, IVIg, or high-dose steroids [79]. The clinical outcome is usually good.

Acute disseminated encephalomyelitis (ADEM) is another disease state believed to be caused by an immune response mounted against an infectious agent. ADEM is preceded by a bacterial or viral infection in 50–75% of cases, most frequently a non-specific upper respiratory tract infection. A long list of viral infections has been associated with ADEM, including influenza, EV, hepatitis A, HSV, EBV, measles, mumps, rubella, VZV, and cytomegalovirus [81]. It may also develop after vaccination [82]. ADEM affects children more often than adults. Onset is acute with rapid clinical progression, often with fever and occasionally meningismus [1]. The inflammatory process is usually multifocal and primarily affects the white matter of

the brain and spinal cord. The clinical manifestations include altered mental status and multifocal neurological symptoms or signs. The infratentorial compartment is frequently affected in ADEM, especially in children who often present with signs and symptoms attributable to BS/cerebellar dysfunction (ataxia, oculomotor disturbance, and dysarthria) [83]. Typical MRI findings include patchy, asymmetrical, bilateral subcortical white matter confluences seen on the T2/FLAIR-weighted images, with ill-defined margins, limited mass effect, and variable contrast enhancement [1]. CSF findings include normal glucose, increased protein level, and lymphocytic pleocytosis. Serum testing is positive for MOG antibodies in up to 59% of cases [84]. The presence of these antibodies seems to portend a better clinical and radiological outcome. Currently, high-dose intravenous corticosteroids are the mainstay of treatment. Plasma exchange therapy and IVIg can be used in non-responders [1]. The disease usually follows a monophasic course and most patients achieve a good recovery with no or little residual disability [1].

10.4.1.4 Infectious Brainstem Vasculitis

Some infectious agents have a tropism for vessels. Among the various bacterial agents, *Treponema pallidum* (*T. pallidum*) and *Borrelia burgdorferi* are known to affect CNS vessels. *T. pallidum* vasculopathy (meningovascular syphilis) usually presents during the secondary stage of syphilis and manifests as encephalopathy, cognitive decline, focal neurological findings, and CN abnormalities [85]. The most frequently involved arteries are the middle cerebral artery and branches of the basilar artery [86]. BS infarcts are found in 14% of patients with neurosyphilis [85]. When the diagnosis is suspected on clinical grounds, serological testing helps in confirming the diagnosis. Treatment consists of intravenous penicillin G for 10–14 days.

Cerebral vasculitis is also a complication of Lyme neuroborreliosis, a multisystem infection caused by *Borrelia burgdorferi*. The disease tends to affect large and medium-sized vessels including the vertebral and basilar arteries and their branches [87]. This results in single or multiple areas of stenosis and dilatation, leading to ischemic stroke. There is a strong predilection towards the posterior cerebral circulation, especially in children [88]. Appropriate antibiotic treatment often results in a favorable clinical outcome.

Viral agents can also cause CNS vasculitis. VZV vasculopathy is a rare complication of chickenpox in children and herpes zoster in adults [89]. This condition leads to ischemic and hemorrhagic strokes that classically occur 7 weeks after herpes reactivation, but longer intervals have been described. Although VZV vasculopathy is classically a complication of herpes zoster ophthalmicus and involves the anterior circulation, it has been described in the posterior circulation following reactivation of VZV in the cervical region [90]. Treatment of VZV vasculopathy is with anti-viral agents.

10.4.2 Brainstem Inflammatory Lesions

Brainstem inflammatory lesions fall into one of two broad categories: (1) primary inflammatory diseases of the CNS and (2) systemic diseases, where CNS involvement is only one of many manifestations of the disease. In the latter case, CNS manifestations often occur in the setting of a known disorder, and the diagnosis is usually straightforward. Alternatively, neurological symptoms can precede other manifestations of the disease, and establishing the correct diagnosis becomes significantly more challenging. In this setting, the demonstration of subclinical symptoms/signs or specific biological markers can be valuable clues as to the underlying etiology.

10.4.2.1 Idiopathic Inflammatory Demyelinating Diseases of the Brainstem

This group represents a broad spectrum of disorders with variable severity, disease course, lesion distribution, and outcome. MS is the most representative form of idiopathic inflammatory demyelinating diseases of the brain (IIDB). Other entities include neuromyelitis optica (NMO), ADEM, and rare MS variants, such as Marburg disease, Balo concentric sclerosis, and Schilder disease [1]. Although the BS is a frequent target for demyelination, lesions in other parts of the CNS are usually present at the time of presentation. In such cases, the diagnosis of IIDB is relatively straightforward. Rarely, BS lesions occur in isolation, and establishing the correct diagnosis becomes much more challenging. In these cases, more advanced imaging techniques, serum testing, and, in more difficult cases, brain biopsy may be necessary.

Multiple Sclerosis MS is a chronic demyelinating CNS disease, characterized pathologically by areas of inflammation, demyelination, axonal loss, and gliosis scattered throughout the CNS [91]. The clinical course of MS can follow several patterns. A relapsing-remitting course (RRMS) accounts for 85% of cases and is characterized by recurrent clinical events that recover to a varying degree [92]. Evidence of dissemination in space (DIS) and dissemination in time (DIT) of the disease process is a prerequisite for diagnosis. Accordingly, the diagnosis of MS can be secured clinically by two clinical relapses occurring at least 30 days apart (i.e., DIT) and affecting separate sites within the CNS (i.e., DIS). A first clinical event consistent with demyelination is called a clinically isolated syndrome (CIS) [93]. Short of a second event, the diagnosis of MS cannot be secured on clinical grounds at this stage. In this case, MRI and CSF findings can replace some clinical criteria. MRI showing subclinical areas of demyelination that fulfill the criteria for DIS (≥ 1 lesion in ≥ 2 areas typical for MS) and DIT (simultaneous presence of enhancing and non-enhancing lesions) can substitute for a second clinical event [94]. For patients with CIS who meet the criteria of DIS, the presence of CSF-specific OCB can substitute for the demonstration of DIT by MRI [94].

Demyelinating lesions frequently involve the BS in MS. Relapses typically present sub-acutely, with progressive worsening over hours or days, a plateau lasting for days or weeks, followed by gradual improvement. Symptoms are those of nonspecific BS dysfunction, such as diplopia, facial sensory symptoms, and gait disturbance [95]. Other more characteristic symptoms include bilateral INO, continuous facial myokemias, and Uhthoff phenomenon (transient worsening of symptoms and signs when core body temperature increases, such as after exercise or a hot bath). The occurrence of trigeminal neuralgia in a young patient, especially when bilateral, is also suggestive of MS [96].

When a BS syndrome occurs in the setting of established MS, the diagnosis is usually straightforward. On the other hand, when BS dysfunction is the first manifestation of MS, further testing is usually needed to secure the diagnosis. MRI is the single most useful test in this setting by demonstrating that the BS lesion is consistent with a demyelinating event (Fig. 10.4). Of equal importance, MRI can confirm the diagnosis if it demonstrates the presence of subclinical lesions that meet the criteria for DIT and DIS. Supratentorial lesions have a predilection to localize to the periventricular white matter and tend to have an ovoid configuration, with the major axis perpendicular to the ventricular surface (see Fig. 10.4d). Cortical/juxtacortical and callosal lesions are also typically seen in MS. Acute lesions enhance with contrast administration. When no additional lesions outside the BS can be demonstrated, a yearly follow-up study is recommended. Occasional patients show no subsequent evidence of clinical activity and follow a monophasic course [95].

In the BS, MS lesions have the propensity to affect the peripheral aspect of the pons and the middle cerebellar peduncle while sparing the central white matter [97] (see Fig. 10.4). Compared to MS lesions in other locations, BS lesions tend to be less bright on T2-weighted images and more diffuse. MS can rarely present as a solitary, tumor-like mass. These so-called tumefactive MS lesions often display mass effect, perilesional edema, and/or ring-enhancement with gadolinium contrast and can be easily mistaken for a glioma or a cerebral abscess. MRI findings that favor a demyelinating lesion include open ring-enhancement directed towards the cortical surface, relatively little mass effect relative to size, ring-shaped diffusion restriction on DWI, and a T2-hypointense rim [1, 98]. The changes on DWI tend to evolve rapidly as opposed to tumors and abscesses [1]. Tumefactive MS lesions mostly occur in the supratentorial regions but involves the BS in up to 24% of cases [99]. Recognition of this MS variant is important to avoid unnecessary surgical intervention.

The importance of early diagnosis of MS cannot be overemphasized since early initiation of immunotherapy is an important determinant of long-term outcome [100]. Relapses are treated with high-dose intravenous steroids.

Neuromyelitis Optica Spectrum Disorder NMO is a more anatomically restricted form of IIDB characterized by severe unilateral or bilateral optic neuritis and longitudinally extensive transverse myelitis (LETM). The term NMO spectrum disorder (NMOSD) is currently favored to avoid the distinction between phenotypes not completely expressed at presentation (restricted forms of the disorder such as recurrent optic neuritis, relapsing transverse myelitis) and classical NMO. NMOSD also includes some BS and encephalitic presentations. The disease course is characterized

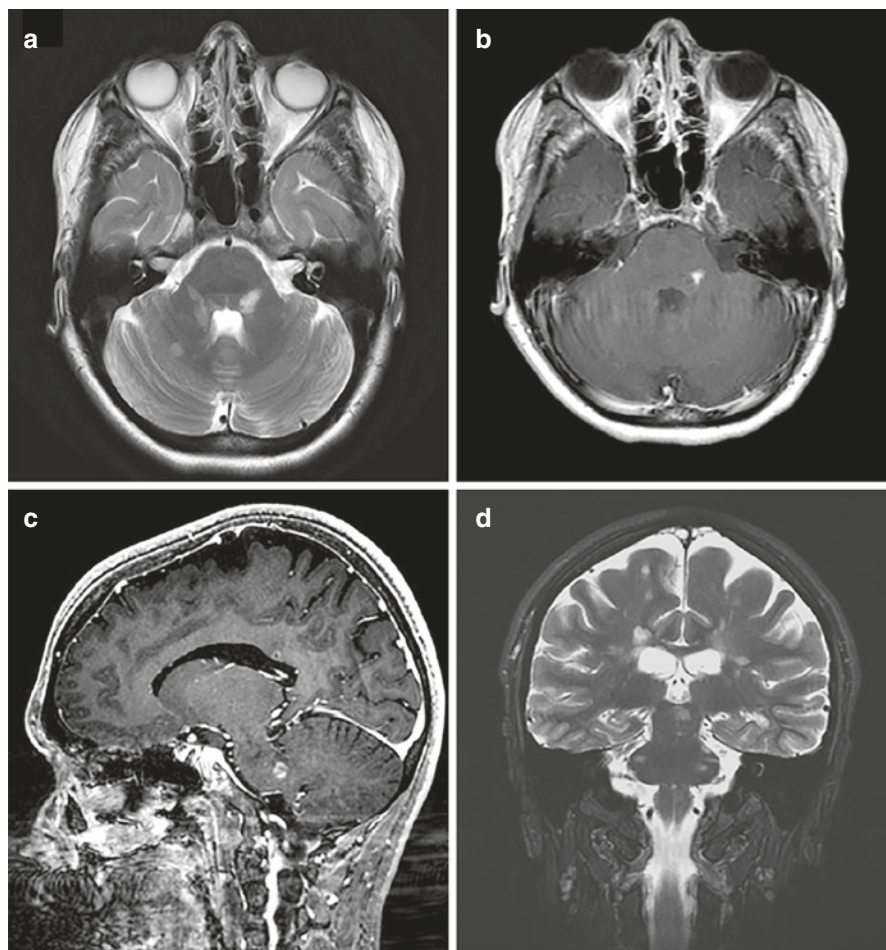


Fig. 10.4 Left brainstem lesion in a patient with multiple sclerosis. (a) Axial T2-weighted image. (b, c) Same lesion showing abnormal enhancement on post-contrast T1-weighted images, indicating an active lesion. (d) Multiple associated lesions with typical distribution in the subcortical, periventricular and ponto-medullary white matter on coronal T2-weighted images

by relapses of variable frequency. MRI characteristically shows LETM (involving more than 3 vertebral levels) and/or large areas of hyperintense signals of the optic nerve/chiasma. MRI changes outside of these disease-defining regions are common [101] (Fig. 10.5). These changes have the tendency to distribute near the ventricular system, an area rich in AQP4, which is the target antigen in NMO. Common locations include the thalamus, hypothalamus, and BS around the cerebral aqueduct [1]. CSF analysis shows high protein levels and pleocytosis. As opposed to MS, OCB are only seen in 30% of patients [102]. Serum is positive for AQP4 antibodies in 70–80% of cases [103]. AQP4 is a cell membrane water channel that is highly expressed on astrocytic foot processes. Up to one third of AQP4-seronegative NMOSD patients have MOG antibodies [104]. These patients have less acute

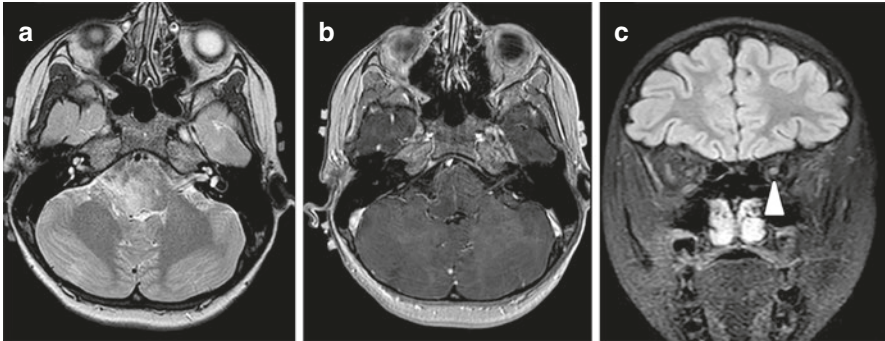


Fig. 10.5 Brainstem involvement in aquaporin 4-positive neuromyelitis optica. (a) Signal abnormality within the pons on axial FLAIR images. (b) Absence of enhancement on axial post-contrast T1-weighted images. (c) Left-sided optic neuritis on coronal T2-weighted images

attack-related disability and relatively less relapses than those who are AQP4-positive [1].

Symptoms related to BS involvement occur in around 40% of cases, especially in children who are AQP4-positive [105]. Common BS manifestations include diplopia, dysarthria, dysphagia, facial weakness, and ataxia [106]. NMOSD has a propensity to affect the area postrema leading to intractable hiccough, nausea and vomiting [107, 108]. These symptoms may herald the onset of NMO and pose a diagnostic challenge. Lesions involving the medullary respiratory center occasionally lead to a life-threatening respiratory compromise [109].

Management of relapses is with high-dose intravenous cortisone. Patients who fail to improve on steroids might benefit from plasma exchange. Given the high morbidity of relapses in NMOSD, early initiation of immunosuppressants is recommended as a preventive measure. These include azathioprine, methotrexate, mycophenolate mofetil, and rituximab. Disease-modifying treatments for MS seem to be poorly effective in NMOSD.

10.4.2.2 Connective Tissue Diseases (CTDs) and Vasculitis

Many CTDs have CNS manifestations, including BS dysfunction [110]. In most cases, however, there is no particular tropism for the BS. Sjögren's syndrome (SS) causes a broad spectrum of neurological manifestations, including focal BS lesions or BS encephalitis. Occasionally, these can be the first manifestation of the disease and precede the diagnosis of SS by up to 2 years [60, 111–113]. In this setting, the clinical and imaging features can mimic MS and cause significant diagnostic and therapeutic dilemmas. This is compounded by the fact that CSF often shows OCB in SS patients with MS-like lesions [114]. Systemic lupus erythematosus (SLE) can also manifest as focal or diffuse CNS lesions, including the BS [115–117]. Rarely, BS involvement can occur in isolation and precede other manifestations of the disease [117]. It is also important to mention that CTDs such as SLE and SS can coex-

ist with NMO [118]. This case scenario should be considered when LETM or optic neuritis occur in the setting of a known systemic inflammatory disease.

Similarly, most systemic vasculitis can involve the CNS, including Behçet disease, granulomatosis with polyangiitis (Wegener's granulomatosis), eosinophilic granulomatosis with polyangiitis (Churg–Strauss syndrome), and polyarteritis nodosa (PAN) [110]. These entities have no predilection for the BS, except for Behçet disease (Fig. 10.6). Behçet disease is recognizable by its hallmark clinical

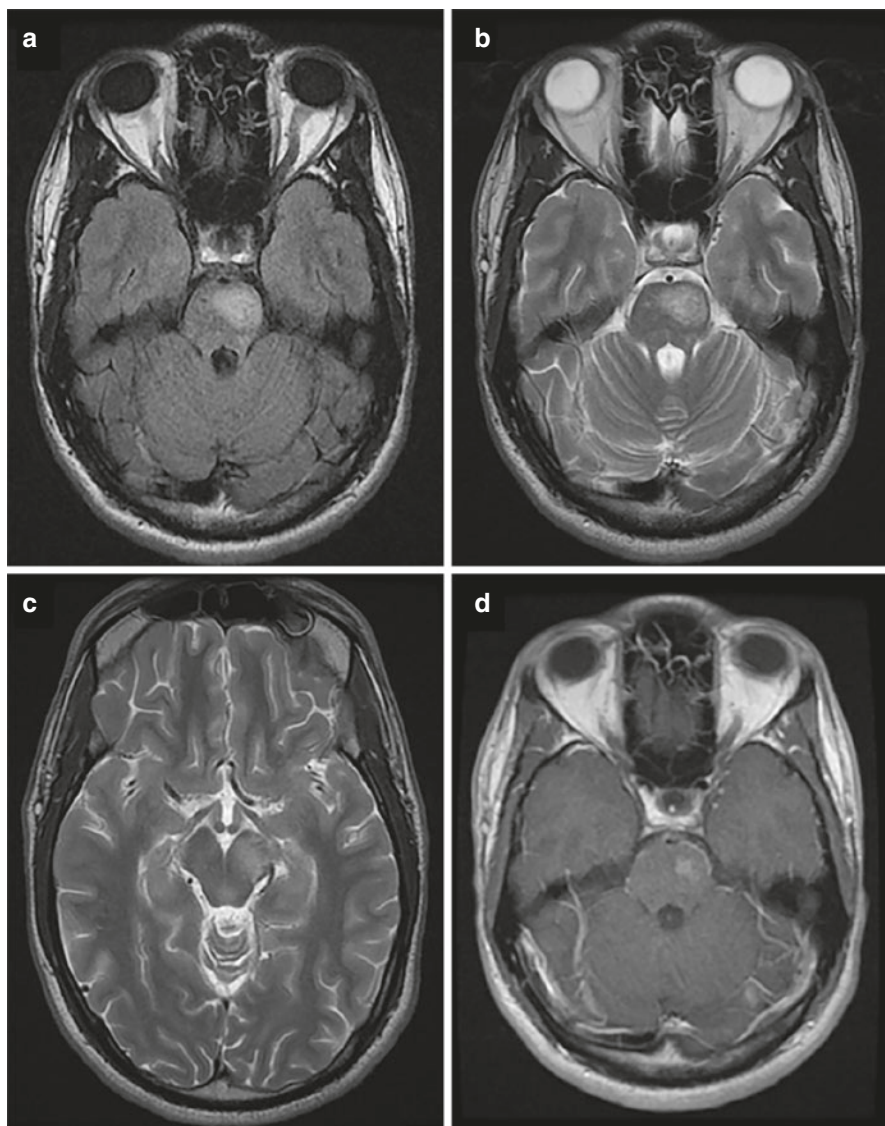


Fig. 10.6 Brainstem involvement in a patient with Behçet disease. (a, b) Axial FLAIR and T2-weighted images showing left pons involvement with surrounding edema. (c) Axial T2-weighted image showing spread of the disease to the left midbrain. (d) Central nodular enhancement of the lesion is seen on post-contrast axial T1-weighted images

signs that include uveitis, and oral-aphthous and genital ulcers. While this triad is virtually diagnostic, it is not always present at presentation. Behçet disease affects young adults, predominantly men, in their 3rd to 4th decade. Neurological complications occur in 5–14% of patients and usually occur a few years into the illness [119]. However, these may precede other manifestations of the disease in 6% of cases [120]. BS lesions most commonly affect the posterior aspect of the midbrain-diencephalic junction, characteristically sparing the red nucleus [121]. CSF typically shows slightly increased protein levels, no OCB, and mononuclear or polynuclear pleocytosis. Patients tend to respond favorably to steroids. Approximately 30–50% of patients with neuro-Behçet disease have a relapsing course [122]. Relapses or progressive disease are treated with immunosuppressant drugs.

Primary angiitis of the CNS (PACNS) is an organ-specific vasculitis affecting small-to-medium sized vessels of the brain and spinal cord [123]. In the absence of a specific serum marker of the disease, diagnosis is based on the demonstration of vasculitic findings either on angiography or on brain biopsy. Clinical manifestations depend on the involved CNS region. Headache is the most common symptom on presentation, followed by cognitive impairment and focal neurological deficits [123]. CSF findings are nonspecific and include mild pleocytosis and elevated proteins. MRI characteristically shows small cortical/subcortical infarcts, leptomeningeal enhancement, intracranial hemorrhage, and areas of T2-hyperintense signal. Less commonly, PACNS presents as BS lesions or as a solitary pseudo-tumoral mass [124, 125]. When the BS is the seat of such pseudo-tumoral lesions, accurate and timely diagnosis can be particularly challenging [124]. Prognosis is usually favorable with early immunotherapy [126].

As the name indicates, CLIPPERS is a chronic inflammatory disorder of the CNS responsive to steroids [9]. It is characterized by episodic BS symptoms, including cranial sensory abnormalities, diplopia, ataxia, and dysarthria [9]. The MRI signature of this condition is a punctate pattern of patchy gadolinium enhancement centered on the pons (Fig. 10.7). These lesions can also be seen in other parts of the BS, spinal cord, and cerebellum [9]. Although these findings are highly suggestive of the disease, they are not absolutely specific. Similar abnormalities have been described in other disorders such as BS lymphoma and gliomas [127, 128]. On the other hand, atypical cases presenting as a progressively expanding tumor-like lesion have been described [129]. BS biopsy shows prominent perivascular lymphocytic infiltrate. Most patients respond well to immunosuppressants; however, symptoms tend to recur with early tapering of steroids, and most patients require prolonged therapy [9].

10.4.2.3 Paraneoplastic Brainstem Encephalitis

Paraneoplastic diseases of the CNS are a group of immune-mediated disorders with a wide range of clinical manifestations. Although BS encephalitis is not a classical paraneoplastic syndrome, some antibodies have been clearly linked to BS dysfunc-

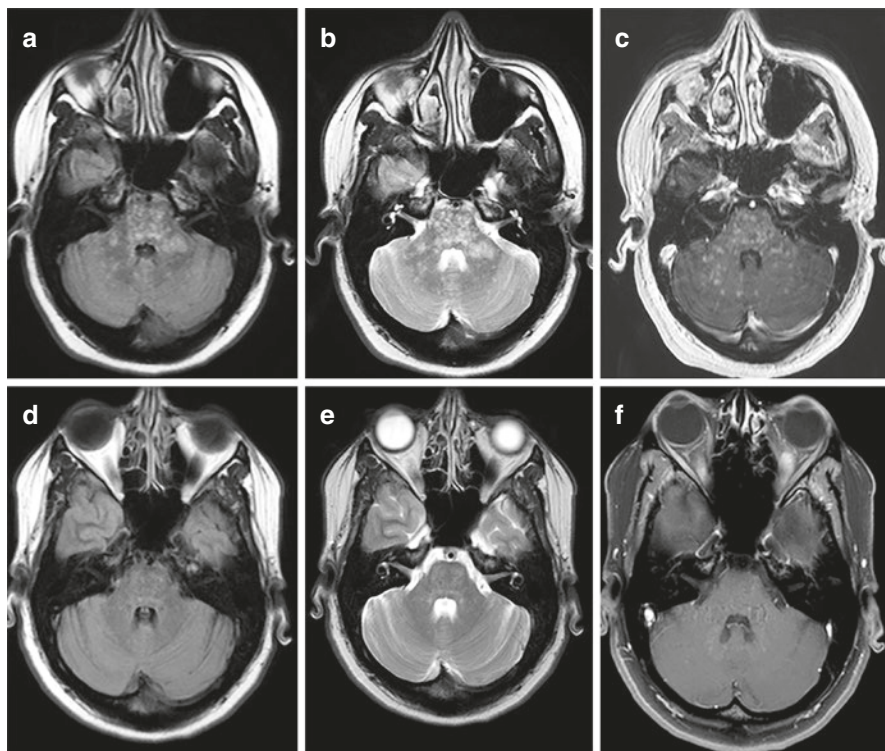


Fig. 10.7 Chronic lymphocytic inflammation with pontine perivascular enhancement responsive to steroids (CLIPPERS). Axial FLAIR (a), T2- (b) and post-contrast T1-weighted (c) images showing the typical multiple punctuate signal abnormalities, most prominent in the pons, but also involving the middle cerebellar peduncles and cerebellar hemispheres. After steroid administration, axial FLAIR (d), T2- (e) and post-contrast T1-weighted (f) images demonstrate marked resorption of the punctate signal abnormalities and enhancement pattern

tion. These include anti-Hu, anti-Ri, and anti-Ma2 antibodies, each resulting in a specific pattern of BS dysfunction. The onset is typically subacute, with rapid worsening and often devastating consequences.

Anti-Hu antibodies are classically associated with paraneoplastic encephalomyelitis, almost always in the setting of small cell lung carcinoma. The typical manifestation is extensive or multifocal encephalomyelitis. Early in the disease course, more focal syndromes can be seen, such as limbic encephalitis, cerebellar degeneration, or BS encephalitis [130, 131]. BS encephalitis is the predominant syndrome in 11% of cases [132]. This entity has a distinctive tropism for the medulla [131], and most patients present with dysphagia, dysarthria, and hypoventilation [131]. CN VI/VII palsy, vertical nystagmus, and ataxia are other possible manifestations [131]. MRI and CSF analysis are typically normal. The prognosis is usually poor despite immunotherapy and treatment of the underlying tumor.

Patients with anti-Ma2-associated BS encephalitis are clinically and radiologically distinct from those with the anti-Hu antibodies. In young men, it is almost exclusively associated with testicular germ-cell tumors, which can be microscopic and difficult to demonstrate [130]. In the older age group, the most common associated cancers are lung and breast cancers [133]. Anti-Ma2-associated encephalitis characteristically affects the limbic system, hypothalamus, and BS [130]. The presenting symptoms can result from the involvement of any of these regions and can progress to involve the others. BS encephalitis predominantly affects the midbrain and most commonly manifests as supranuclear vertical gaze palsy, followed by involvement of the oculomotor nuclei. Involvement of the other brain regions results in a variety of symptoms including excessive daytime sleepiness, narcolepsy, cataplexy, rapid eye movement (REM)-sleep abnormalities, hyperphagia, and memory impairment. Brain MRI may show T2-hyperintense lesions in the superior colliculi and periaqueductal region. Roughly one-third of patients are expected to respond to tumor resection and immunotherapy [133].

Anti-Ri antibodies also have a tropism for the BS [134]. These are the least common of the paraneoplastic auto-antibodies, mostly encountered in patients with breast and ovarian cancer. Patients typically present with signs of BS, cerebellar and spinal cord dysfunction. BS dysfunction often manifests as OpM, ophthalmoplegia, and facial sensory symptoms [134–136]. Treatment of the underlying cancer can lead to a decrease in the antibody titer and improvement of symptoms [134].

10.5 Conclusion

It is important to keep in mind that the differential diagnosis of a BS lesion is not limited to BS tumors, infections, and inflammatory/autoimmune disorders. Other disease states can also affect the BS such as hypertensive BS encephalopathy [137, 138], central pontine myelinolysis [139, 140], Wallerian degeneration [141], hepatic encephalopathy [97], and neurodegenerative diseases such as multiple system atrophy [142].

Non-neoplastic BS lesions span a wide range of pathologies, including infections, inflammatory, and autoimmune disorders. Broad and in-depth knowledge of the various disorders with possible BS manifestations is therefore essential to guide the diagnostic approach. The latter involves a detailed history, a thorough physical examination, and an array of ancillary tests such as brain imaging, and serum and CSF analysis. In more difficult cases where the etiology remains unknown, a BS biopsy may be indicated; the need for tissue diagnosis, however, has steadily dropped since the introduction and continuous optimization of imaging techniques and serum/CSF testing. This chapter addressed the various infectious and inflammatory disorders of the brainstem, with a particular emphasis on their clinical presentation, key radiological and laboratory findings, and general principles of management.

References

1. Hardy TA, Reddel SW, Barnett MH, Palace J, Lucchinetti CF, et al. Atypical inflammatory demyelinating syndromes of the CNS. *Lancet Neurol*. 2016;15(9):967–81.
2. Shams PN, Waldman A, Plant GT. B cell lymphoma of the brain stem masquerading as myasthenia. *J Neurol Neurosurg Psychiatry*. 2002;72(2):271–3.
3. Glaser CA, Honarmand S, Anderson LJ, Schnurr DP, Forghani B, Cossen CK, et al. Beyond viruses: clinical profiles and etiologies associated with encephalitis. *Clin Infect Dis*. 2006;43(12):1565–77.
4. Ahdab R, Thomas D. Palatal tremor, focal seizures, repeated miscarriages and elevated anti-thyroid antibodies. *Clin Neurol Neurosurg*. 2008;110(4):381–3.
5. Moragas M, Martínez-Yélamos S, Majós C, Fernández-Viladrich P, Rubio F, Arbizu T. Rhombencephalitis: a series of 97 patients. *Medicine (Baltimore)*. 2011;90(4):256–61.
6. Wong A. An update on opsoclonus. *Curr Opin Neurol*. 2007;20(1):25–31.
7. Louis ED, Lynch T, Kaufmann P, Fahn S, Odel J. Diagnostic guidelines in central nervous system Whipple's disease. *Ann Neurol*. 1996;40(4):561–8.
8. Koga M, Kusunoki S, Kaida K, Uehara R, Nakamura Y, Kohriyama T, et al. Nationwide survey of patients in Japan with Bickerstaff brainstem encephalitis: epidemiological and clinical characteristics. *J Neurol Neurosurg Psychiatry*. 2012;83(12):1210–5.
9. Pittock SJ, Debruyne J, Krecke KN, Giannini C, van den Aemele J, De Herdt V, et al. Chronic lymphocytic inflammation with pontine perivascular enhancement responsive to steroids (CLIPPERS). *J Clin Rheumatol*. 2015;21(3):144–8.
10. Giunta F, Grasso G, Marini G, Zorzi F. Brain stem expanding lesions: stereotactic diagnosis and therapeutical approach. *Acta Neurochir Suppl (Wien)*. 1989;46:86–99.
11. Omuro AM, Leite CC, Mokhtari K, Delattre JY. Pitfalls in the diagnosis of brain tumours. *Lancet Neurol*. 2006;5(11):937–48. Review.
12. Russell JA, Shaw MD. Chronic abscess of the brain stem. *J Neurol Neurosurg Psychiatry*. 1977;40(7):625–9.
13. Stein M, Schiroztek I, Preussa M, Scharbrodta W, Oertela M. Brainstem abscess caused by *Haemophilus influenzae* and *Peptostreptococcus* species. *J Clin Neurosci*. 2011;18(3):425–8.
14. Yuh WT, Nguyen HD, Gao F, Tali ET, Fisher DJ, Mayr NA, et al. Brain parenchymal infection in bone marrow transplantation patients: CT and MR findings. *AJR Am J Roentgenol*. 1994;162(2):425–30.
15. Mathisen GE, Johnson JP. Brain abscess. *Clin Infect Dis*. 1997;25(4):763–79.
16. Soares-Fernandes JP, Beleza P, Cerqueira JJ, Ribeiro M, Maré R, Lourenço E, et al. Simultaneous supratentorial and brainstem abscesses due to *Listeria monocytogenes*. *J Neuroradiol*. 2008;35(3):173–6.
17. Chow FC, Marson A, Liu C. Successful medical management of a *Nocardia farcinica* multiloculated pontine abscess. *BMJ Case Rep*. 2013;5:2013.
18. Rajshekhar V, Chandy MJ. Computerized tomography-guided stereotactic surgery for brainstem masses: a risk benefit analysis in 71 patients. *J Neurosurg*. 1995;82(6):976–81.
19. Ansari MK, Jha S. Tuberculous brain abscess in an immunocompetent adolescent. *J Nat Sci Biol Med*. 2014;5(1):170–2.
20. Kumar R, Jain R, Kaur A, Chhasbra DK. Brainstem tuberculosis in children. *Br J Neurosurg*. 2000;14(4):356–61.
21. Toorn R, Schoeman JF, Donald PR. Brainstem tuberculoma presenting as eight-and-a-half syndrome. *Eur J Paediatr Neurol*. 2006;10(1):41–4.
22. Eide F, Gean A, So Y. Clinical and radiographic findings in disseminated tuberculosis of the brain. *Neurology*. 1993;43(7):1427–9.
23. Talamás O, Del Brutto OH, García-Ramos G. Brain-stem tuberculoma. An analysis of 11 patients. *Arch Neurol*. 1989;46(5):529–35.
24. Garg RK. Tuberculous meningitis. *Acta Neurol Scand*. 2010;122(2):75–90.

25. Garcia HH, Gonzalez AE, Evans CA, Gilman RH. *Taenia solium* cysticercosis. *Lancet*. 2003;362(9383):547–56.
26. Del Brutto OH, Del Brutto VJ. Isolated brainstem cysticercosis: a review. *Clin Neurol Neurosurg*. 2013;115(5):507–11.
27. Porter SB, Sande MA. Toxoplasmosis of the central nervous system. *N Engl J Med*. 1992;327(23):1643–8.
28. Daras M, Koppel BS, Samkoff L, Joseph M. Brainstem toxoplasmosis in patients with acquired immunodeficiency syndrome. *J Neuroimaging*. 1994;4(2):85–90.
29. Gupta A, Raja A, Mahadevan A, Shankar SK. *Toxoplasma* granuloma of brainstem: a rare case. *Neurol India*. 2008;56(2):189–91.
30. Pezzini A, Zavarise P, Palvarini L, Viale P, Oladeji O, Padovani A. Holmes' tremor following midbrain *Toxoplasma* abscess: clinical features and treatment of a case. *Parkinsonism Relat Disord*. 2002;8(3):177–80.
31. Kure K, Harris C, Morrin LS, Dickson DW. Solitary midbrain toxoplasmosis & olivary hypertrophy in a patient with acquired immunodeficiency syndrome. *Clin Neuropathol*. 1989;8(1):35–40.
32. Adurthi S, Mahadevan A, Bantwal R, Satishchandra P, Ramprasad S, Sridhar H, et al. Diagnosis of cerebral toxoplasmosis. *Ann Indian Acad Neurol*. 2011;14(2):145–6.
33. Vidal JE, Colombo FA, Penalva de Oliveira AC, Focaccia R, Pereira-Chiocola VL. PCR assay using cerebrospinal fluid for diagnosis of cerebral toxoplasmosis in Brazilian AIDS patients. *J Clin Microbiol*. 2004;42(10):4765–8.
34. Sonnevile R, Schmidt M, Messika J, Ait Hssain A, da Silva D, Klein IF, et al. Neurologic outcomes and adjunctive steroids in HIV patients with severe cerebral toxoplasmosis. *Neurology*. 2012;79(17):1762–6.
35. Riestra-Castaneda JM, Riestra-Castaneda R, Gonzalez-Garrido AA, Pena Moreno P, Martinez AJ, Visvesvara GS, et al. Granulomatous amebic encephalitis due to *Balamuthia mandrillaris* (Leptomyxiidae): report of four cases from Mexico. *Am J Trop Med Hyg*. 1997;56(6):603–7.
36. Rommel D, Ragé M, Duprez T, Parent M, Sindic CJ. Paucisymptomatic brainstem lesions revealing CNS schistosomiasis. *Acta Neurol Belg*. 2005;105(2):89–93.
37. De Medeiros BC, de Medeiros CR, Werner B, Neto JZ, Loddo G, Pasquini R, et al. Central nervous system infections following bone marrow transplantation: an autopsy report of 27 cases. *J Hematother Stem Cell Res*. 2000;9(4):535–40.
38. Gottfredsson M, Perfect JR. Fungal meningitis. *Semin Neurol*. 2000;20(3):307–22.
39. Kume H, Yamazaki T, Abe M, Tanuma H, Okudaira M, Okayasu I. Increase in aspergillosis and severe mycotic infection in patients with leukemia and MDS: comparison of the data from the Annual of the Pathological Autopsy cases in Japan in 1989, 1993, 1997. *Pathol Int*. 2003;53(11):744–50.
40. Tunkel AR, Glaser CA, Bloch KC, Sejvar JJ, Marra CM, Roos KL, et al. Infectious Diseases Society of America. The management of encephalitis clinical practice guidelines by the Infectious Diseases Society of America. *Clin Infect Dis*. 2008;47(3):303–27.
41. Tyler KT. Acute viral encephalitis. *N Engl J Med*. 2018;379(6):557–66.
42. Alper G, Knepper L, Kanal E. MR findings in listerial rhombencephalitis. *AJNR Am J Neuroradiol*. 1996;17(3):593–6.
43. Miura S, Kurita T, Noda K, Ayabe M, Aizawa H, Taniwaki T. Symmetrical brainstem encephalitis caused by herpes simplex virus. *J Clin Neurosci*. 2009;16(4):589–90.
44. Petropoulou KA, Gordon SM, Prayson RA, Ruggieri PM. West Nile virus meningoencephalitis: MR imaging findings. *AJNR Am J Neuroradiol*. 2005;26(8):1986–95.
45. Zagardo MT, Shanholtz CB, Zoarski GH, Rothman MI. Rhombencephalitis caused by adenovirus: MR imaging appearance. *AJNR Am J Neuroradiol*. 1998;19(10):1901–3.
46. Angelini L, Bugiani M, Zibordi F, Cinque P, Bizzi A. Brainstem encephalitis resulting from Epstein-Barr virus mimicking an infiltrating tumor in a child. *Pediatr Neurol*. 2000;22(2):130–2.
47. Shen WC, Chiu HH, Chow KC, Tsai CH. MR imaging findings of enteroviral encephalomyelitis: an outbreak in Taiwan. *AJNR Am J Neuroradiol*. 1999;20(10):1889–95.

48. Tien RD, Felsberg GJ, Osumi AK. Herpesvirus infections of the CNS: MR findings. *AJR Am J Roentgenol.* 1993;161(1):167–76.
49. Handique SK, Das RR, Barman K, Medhi N, Saharia B, Saikia P, et al. Temporal lobe involvement in Japanese encephalitis: problems in differential diagnosis. *AJNR Am J Neuroradiol.* 2006;27(5):1027–31.
50. Wasay M, Mekan SF, Khelaeni B, Saeed Z, Hassan A, Cheema Z, et al. Extra temporal involvement in herpes simplex encephalitis. *Eur J Neurol.* 2005;12(6):475–9.
51. Rose JW, Stroop WG, Matsuo F, Henkel J. Atypical herpes simplex encephalitis: clinical, virological and neuropathologic evaluation. *Neurology.* 1992;42(9):1809–12.
52. Roman-Campos G, Toro G. Herpetic brainstem encephalitis. *Neurology.* 1980;30(9):981–5.
53. Dennett C, Cleator GM, Klapper PE. HSV-1 and HSV-2 in herpes simplex encephalitis: a study of sixty-four cases in the United Kingdom. *J Med Virol.* 1997;53(1):1–3.
54. Ballaekere JS, Chebbi PP, Sundarmurthy H, Parameshwarappa A. Weber syndrome: herpes simplex virus brainstem encephalitis as an etiology. *Am J Med.* 2014;127(12):e5–6.
55. Chen F, Li J, Liu T, Wang L, Li Y. MRI characteristics of brainstem encephalitis in hand-foot-mouth disease induced by enterovirus type 71--will different MRI manifestations be helpful for prognosis? *Eur J Paediatr Neurol.* 2013;17(5):486–91.
56. McMinn PC. An overview of the evolution of enterovirus 71 and its clinical and public health significance. *FEMS Microbiol Rev.* 2002;26(1):91–107.
57. Casas-Alba D, de Sevilla MF, Valero-Rello A, Fortuny C, García-García JJ, Ortez C, et al. Outbreak of brainstem encephalitis associated with enterovirus-A71 in Catalonia, Spain (2016): a clinical observational study in a children's reference centre in Catalonia. *Clin Microbiol Infect.* 2017;23(11):874–81.
58. Zeng H, Wen F, Gan Y, Huang W. MRI and associated clinical characteristics of EV71-induced brainstem encephalitis in children with hand-foot-mouth disease. *Neuroradiology.* 2012;54(6):623–30.
59. Chea S, Cheng YB, Chokephaibulkit K, Chotpitayasunondh T, Rogier van Doorn H, Hafy Z, et al. Workshop on use of intravenous immunoglobulin in hand, foot and mouth disease in 448 Southeast Asia. *Emerg Infect Dis.* 2015;21:1.
60. Tobin WO, Pittock SJ, Weinschenker BG. Teaching NeuroImages: primary Sjögren syndrome presenting as isolated lesion of medulla oblongata. *Neurology.* 2015;85(2):204–5.
61. Wasay M, Diaz-Arrastia R, Suss RA, Kojan S, Haq A, Burns D, et al. St. Louis encephalitis: a review of 11 cases in a 1995 Dallas, Tex, epidemic. *Arch Neurol.* 2000;57(1):114–8.
62. Kumar A. Isolated involvement of substantia nigra in Japanese encephalitis. *J Indian Med Assoc.* 2010;108(8):525–7.
63. Cerna F, Mehrad B, Luby JP, Burns D, Fleckenstein JL. St. Louis encephalitis and the substantia nigra: MR imaging evaluation. *AJNR Am J Neuroradiol.* 1999;20(7):1281–3.
64. Çelik T, Çelik Ü, Tolunay O, Kömür M, Başpınar H, Yılmaz C, et al. Epstein-Barr virus encephalitis with substantia nigra involvement. *J Pediatr Neurosci.* 2015;10(4):401–3.
65. Bosanko CM, Gilroy J, Wang AM, Sanders W, Dulai M, Wilson J, et al. West Nile virus encephalitis involving the substantia nigra: neuroimaging and pathologic findings with literature review. *Arch Neurol.* 2003;60(10):1448–52.
66. Goh KJ, Tan CT, Chew NK, Tan PS, Kamarulzaman A, Sarji SA, et al. Clinical features of Nipah virus encephalitis among pig farmers in Malaysia. *N Engl J Med.* 2000;342(17):1229–35.
67. Mihara M, Utsugisawa K, Konno S, Tohgi H. Isolated lesions limited to the bilateral substantia nigra on MRI associated with influenza A infection. *Eur Neurol.* 2001;45(4):290–1.
68. Hu S, Walker M, Czartoski T, Cheng A, Forghani B, Golden DH, et al. Acyclovir responsive brain stem disease after the Ramsay Hunt syndrome. *J Neurol Sci.* 2004;217(1):111–3.
69. Sauer R, Göllitz P, Jacobi J, Schwab S, Linker RA, Lee DH. Good outcome of brain stem progressive multifocal leukoencephalopathy in an immunosuppressed renal transplant patient: importance of early detection and rapid immune reconstitution. *J Neurol Sci.* 2017;375:76–9.
70. Kleinschmidt-DeMasters BK, Tyler KL. Progressive multifocal leukoencephalopathy complicating treatment with natalizumab and interferon beta-1a for multiple sclerosis. *N Engl J Med.* 2005;353(4):369–74.

71. Kastrup O, Göricke S, Kretzschmar H, Wauschkuhn B, Diener HC. Progressive multifocal leukoencephalopathy of the brainstem in an immunocompetent patient--JC and BK polyomavirus coinfection? A case report and review of the literature. *Clin Neurol Neurosurg*. 2013;115:2390–2.
72. Yousry T, Pelletier D, Cadavid D, Gass A, Richert ND, Radue EW, et al. Magnetic resonance imaging pattern in natalizumab-associated progressive multifocal leukoencephalopathy. *Ann Neurol*. 2012;72(5):779–87.
73. Reynaud L, Graf M, Gentile I, Cerini R, Ciampi R, Noce S, et al. A rare case of brainstem encephalitis with *Listeria monocytogenes* with isolated mesencephalic localization. Case report and review. *Diagn Microbiol Infect Dis*. 2007;58:121–3.
74. Armstrong RW, Fung PC. Brainstem encephalitis (rhombencephalitis) due to *Listeria monocytogenes*: case report and review. *Clin Infect Dis*. 1993;16(5):689–702.
75. Clauss HE, Lorber B. Central nervous system infection with *Listeria monocytogenes*. *Curr Infect Dis Rep*. 2008;10(4):300–6.
76. Ratnaik RN. Whipple's disease. *Postgrad Med J*. 2000;76(902):760–6.
77. Adams M, Rhyner PA, Day J, DeArmond S, Smuckler EA. Whipple's disease confined to the central nervous system. *Ann Neurol*. 1987;21(1):104–8.
78. Panegyres PK, Edis R, Beaman M, Fallon M. Primary Whipple's disease of brain: characterization of the clinical syndrome and molecular diagnosis. *QJM*. 2006;99(9):609–23.
79. Odaka M, Yuki N, Yamada M, Koga M, Takemi T, Hirata K, et al. Bickerstaff's brainstem encephalitis: clinical features of 62 cases and a subgroup associated with Guillain-Barré syndrome. *Brain*. 2003;126(Pt 10):2279–90.
80. Wakerley BR, Uncini A, Yuki N, for the GBS Classification Group, and the GBS Classification Group. Guillain-Barré and Miller Fisher syndromes—new diagnostic classification. *Nat Rev Neurol*. 2014;10(9):537–44.
81. Silvia MT, Licht DL. Pediatric central nervous system infections and inflammatory white matter disease. *Pediatr Clin N Am*. 2005;52(4):1107–26.
82. Menge T, Hemmer B, Nessler S, Wiendl H, Neuhaus O, Hartung HP, et al. Acute disseminated encephalo-myelitis: an update. *Arch Neurol*. 2005;62(11):1673–80.
83. Schwartz S, Mohr A, Knauth M, Wildemann B, Storch-Hagenlocher B. Acute disseminated encephalomyelitis: follow up study of 40 adult patients. *Neurology*. 2001;56(10):1313–8.
84. Baumann M, Sahin K, Lechner C, Hennes EM, Schanda K, Mader S, et al. Clinical and neuroradiological differences of paediatric acute disseminating encephalomyelitis with and without antibodies to the myelin oligodendrocyte glycoprotein. *J Neurol Neurosurg Psychiatry*. 2015;86(3):265–72.
85. Peng F, Hu X, Zhong X, Wei Q, Jiang Y, Bao J, et al. CT and MR findings in HIV-negative neurosyphilis. *Eur J Radiol*. 2008;66(1):1–6.
86. Holland BA, Perrett LV, Mills CM. Meningovascular syphilis: CT and MR findings. *Radiology*. 1986;158(2):439–42.
87. Garkowski A, Zajkowska J, Zajkowska A, Kułakowska A, Zajkowska O, Kubas B, et al. Cerebrovascular manifestations of Lyme Neuroborreliosis-A systematic review of published cases. *Front Neurol*. 2017;8:146.
88. Monteventi O, Steinlin M, Regényi M, Roulet-Perez E, Weber P, Fluss J. Pediatric stroke related to Lyme neuroborreliosis: data from the Swiss NeuroPaediatric stroke registry and literature review. *Eur J Paediatr Neurol*. 2018;22(1):113–21.
89. Lin HC, Chien CW, Ho JD. Herpes zoster ophthalmicus and the risk of stroke: a population-based follow-up study. *Neurology*. 2010;74(10):792–7.
90. Willeit J, Schmutzhard E. Cervical herpes zoster and delayed brainstem infarction. *Clin Neurol Neurosurg*. 1991;93(3):245–7.
91. Confavreux C, Vukusic S, Moreau T, Adeleine P. Relapses and progression of disability in multiple sclerosis. *N Engl J Med*. 2000;343(20):1430–8.
92. Lublin FD, Reingold SC. Defining the clinical course of multiple sclerosis: results of an international survey. National Multiple Sclerosis Society (USA) Advisory Committee on Clinical Trials of New Agents in Multiple Sclerosis. *Neurology*. 1996;46(4):907–11.

93. Sastre-Garriga J, Tintore M, Nos C, Tur C, R o J, T llez N, et al. Clinical features of CIS of the brainstem/cerebellum of the kind seen in MS. *J Neurol.* 2010;257(5):742–6.
94. Thompson AJ, Banwell BL, Barkhof F, Carroll WM, Coetzee T, Comi G, et al. Diagnosis of multiple sclerosis: 2017 revisions of the McDonald criteria. *Lancet Neurol.* 2018;17(2):162–73.
95. Sastre-Garriga J, Tintore M, Rovira A, Griv  E, Pericot I, Comabella M, et al. Conversion to multiple sclerosis after a clinically isolated syndrome of the brainstem: cranial magnetic resonance imaging, cerebrospinal fluid and neurophysiological findings. *Mult Scler.* 2003;9(1):39–43.
96. da Silva CJ, da Rocha AJ, Mendes MF, Maia AC Jr, Braga FT, Tilbery CP. Trigeminal involvement in multiple sclerosis: magnetic resonance imaging findings with clinical correlation in a series of patients. *Mult Scler.* 2005;11(3):282–5.
97. Rovira A, Alonso J, Cordoba J. MR imaging findings in hepatic encephalopathy. *AJNR Am J Neuroradiol.* 2008;29(9):1612–21.
98. Lucchinetti CF, Parisi J, Bruck W. The pathology of multiple sclerosis. *Neurol Clin.* 2005;23(1):77–105.
99. Lucchinetti CF, Gavrilova RH, Metz I, Parisi JE, Scheithauer BW, Weigand S, et al. Clinical and radiographic spectrum of pathologically confirmed tumefactive multiple sclerosis. *Brain.* 2008;131(Pt 70):1759–75.
100. Cerqueira JJ, Compston DAS, Geraldes R, Rosa MM, Schmierer K, Thompson A, et al. Time matters in multiple sclerosis: can early treatment and long-term follow-up ensure everyone benefits from the latest advances in multiple sclerosis? *J Neurol Neurosurg Psychiatry.* 2018;89(8):844–50.
101. Pittock SJ, Lennon VA, Krecke K, Wingerchuk DM, Lucchinetti CF, Weinshenker BG. Brain abnormalities in neuromyelitis optica. *Arch Neurol.* 2006;63(3):390–6.
102. Wingerchuk DM, Hogancamp WF, O’Brien PC, Weinshenker BG. The clinical course of neuromyelitis optica (Devic’s syndrome). *Neurology.* 1999;53(5):1107–14.
103. Marignier R, Bernard-Valnet R, Giraudon P, Collongues N, Papeix C, Zephir H, et al. NOMADMUS Study Group. Aquaporin-4 antibody-negative neuromyelitis optica: distinct assay sensitivity-dependent entity. *Neurology.* 2013;80(24):2194–200.
104. Hamid SHM, Whittam D, Mutch K, Linaker S, Solomon T, Das K, et al. What proportion of AQP4-IgG-negative NMO spectrum disorder patients are MOG-IgG positive? A cross sectional study of 132 patients. *J Neurol.* 2017;264(10):2088–94.
105. Kremer L, Mealy M, Jacob A, Nakashima I, Cabre P, Bigi S, et al. Brainstem manifestations in neuromyelitis optica: a multicenter study of 258 patients. *Mult Scler J.* 2014;20:843–7.
106. Cheng C, Jiang Y, Lu X, Gu F, Kang Z, Dai Y, et al. The role of anti-aquaporin 4 antibody in the conversion of acute brainstem syndrome to neuromyelitis optica. *BMC Neurol.* 2016;16(1):203.
107. Apiwattanakul M, Popescu BF, Matiello M, Weinshenker BG, Lucchinetti CF, Lennon VA, et al. Intractable vomiting as the initial presentation of neuromyelitis optica. *Ann Neurol.* 2010;68(5):757–61.
108. Misu T, Fujihara K, Nakashima I, Sato S, Itoyama Y. Intractable hiccup and nausea with periaqueductal lesions in neuromyelitis optica. *Neurology.* 2005;65(9):1479–82.
109. Kitley JL, Leite MI, George JS, Palace JA. The differential diagnosis of longitudinally extensive transverse myelitis. *Mult Scler.* 2012;18(3):271–85.
110. Hajj-Ali RA, Calabrese LH. Central nervous system vasculitis. *Curr Opin Rheumatol.* 2009;21(1):10–8.
111. Delalande S, De Seze J, Fauchais AL, Hachulla E, Stojkovic T, Ferriby D, et al. Neurologic manifestations in primary Sj gren syndrome: a study of 82 patients. *Medicine (Baltimore).* 2004;83(5):280–91.
112. Matsui Y, Takenouchi T, Narabayashi A, Ohara K, Nakahara T, Takahashi T. Childhood Sj gren syndrome presenting as acute brainstem encephalitis. *Brain and Development.* 2016;38(1):158–62.

113. Natsis KS, Boura E, Kyriazis O, Iliadis A, Syntila SA, Kostopoulos I, et al. Bilateral internuclear ophthalmoplegia as a presenting manifestation of primary Sjögren's syndrome. *Neuroophthalmology*. 2016;40(5):247–50.
114. Alexander EL, Makinow K, Lejewski JE, Jerdan MS, Provost TT, Alexander GE. Primary Sjögren's syndrome with central nervous system disease mimicking multiple sclerosis. *Ann Intern Med*. 1986;104(3):323–30.
115. Isshi K, Hirohata S, Hashimoto T, Miyashita H. Systemic lupus erythematosus presenting with diffuse low density lesions in the cerebral white matter on computed axial tomography scans: its implication in the pathogenesis of diffuse central nervous system lupus. *J Rheumatol*. 1994;21(9):1758–62.
116. Kumar S, Sharma N, Sharma A, Mahi S, Bhalla A, Varma S. A case of systemic lupus erythematosus with extensive brain stem involvement. *Clin Rheumatol*. 2009;28(Suppl 1):S69–71.
117. Mimenza-Alvarado AJ, Téllez-Zenteno JF, Cantú-Brito C, García-Ramos G. Systemic lupus erythematosus with affection to brainstem: report of three cases. *Rev Neurol*. 2002;35(2):128–31.
118. Pittock SJ, Lennon VA, de Seze J, Vermersch P, Homburger HA, Wingerchuk DM, et al. Neuromyelitis optica and non organ-specific autoimmunity. *Arch Neurol*. 2008;65(1):78–83.
119. Al-Araji A, Kidd DP. Neuro-Behçet's disease: epidemiology, clinical characteristics, and management. *Lancet Neurol*. 2009;8(2):192–204.
120. Akman-Demir G, Serdaroglu P, Tasci B. Clinical patterns of neurological involvement in Behçet's disease: evaluation of 200 patients. The Neuro-Behçet study Group. *Brain*. 1999;122(Pt 11):2171–82.
121. Kocer N, Islak C, Siva A, Saip S, Akman C, Kantarci O, et al. CNS involvement in neuro-Behçet syndrome: An MR study. *AJNR Am J Neuroradiol*. 1999;20(6):1015–24.
122. Kidd D, Steuer A, Denman AM, Rudge P. Neurological complications in Behçet's syndrome. *Brain*. 1999;122(Pt 11):2183–94.
123. Hajj-Ali RA, Calabrese LH. Diagnosis and classification of central nervous system vasculitis. *J Autoimmun*. 2014;48–49:149–52.
124. Nabika S, Kiya K, Satoh H, Mizoue T, Araki H, Oshita J, et al. Primary angiitis of the central nervous system mimicking dissemination from brainstem neoplasm: a case report. *Surg Neurol*. 2008;70(2):182–5.
125. Valavanis A, Friede R, Schubiger O, Hayek J. Cerebral granulomatous angiitis simulating brain tumor. *J Comput Assist Tomogr*. 1979;3(4):536–8.
126. Abdulrahman AA, William JP. Prognosis of patients with suspected primary CNS angiitis and negative brain biopsy. *Neurology*. 2003;61(6):831–3.
127. Jones JL, Dean AF, Antoun N, Scoffings DJ, Burnet NG, Coles AJ. 'Radiologically compatible CLIPPERS' may conceal a number of pathologies. *Brain*. 2011;134(Pt 8):e187.
128. Taieb G, Uro-Coste E, Clanet M, Lassmann H, Benouaich-Amiel A, Laurent C. A central nervous system B-cell lymphoma arising two years after initial diagnosis of CLIPPERS. *J Neurol Sci*. 2014;344(1–2):224–6.
129. Esmaeilzadeh M, Yildiz Ö, Lang JM, Wegner F, Haubitz B, Feuerhake F, et al. CLIPPERS syndrome: an entity to be faced in neurosurgery. *World Neurosurg*. 2015;84(6):2077.e1–3.
130. Dalmau J, Rosenfeld MR. Paraneoplastic syndromes of the CNS. *Lancet Neurol*. 2008;7(4):327–40.
131. Saiz A, Bruna J, Stourac P, Vigliani MC, Giometto B, Grisold W, et al. Anti-Hu-associated brainstem encephalitis. *J Neurol Neurosurg Psychiatry*. 2009;80(4):404–7.
132. Lee KS, Higgin MJ, Patel BM, Larson JS, Rady MY. Paraneoplastic coma and acquired central alveolar hypoventilation as a manifestation of brainstem encephalitis in a patient with ANNA-1 antibodies and small-cell lung cancer. *Neurocrit Care*. 2006;4(2):137–9.
133. Dalmau J, Graus F, Villarejo A, Posner JB, Blumenthal D, Thiessen B, et al. Clinical analysis of anti-Ma2-associated encephalitis. *Brain*. 2004;127(Pt 8):1831–44.
134. Pittock SJ, Lucchinetti CF, Lennon VA. Anti-neuronal nuclear autoantibody type 2: paraneoplastic accompaniments. *Ann Neurol*. 2003;53(5):580–7.

135. Kim H, Lim Y, Kim KK. Anti-ri-antibody-associated paraneoplastic syndrome in a man with breast cancer showing a reversible pontine lesion on MRI. *J Clin Neurol.* 2009;5(3):151–2.
136. Sutton IJ, Barnett MH, Watson JD, Ell JJ, Dalmau J. Paraneoplastic brainstem encephalitis and anti-Ri antibodies. *J Neurol.* 2002;249(11):1597–8.
137. Cruz-Flores S, de Assis A, Gondim F, Leira EC. Brainstem involvement in hypertensive encephalopathy: clinical and radiological findings. *Neurology.* 2004;62(8):1417–9.
138. de Seze J, Mastain B, Stojkovic T, Ferriby D, Pruvo JP, Destée A, et al. Unusual MR findings of the brain stem in arterial hypertension. *AJNR Am J Neuroradiol.* 2000;21(2):391–4.
139. Brown WD. Osmotic demyelination disorders: central pontine and extrapontine myelinolysis. *Curr Opin Neurol.* 2000;13(6):691–7.
140. Kiley MA, King M, Burns RJ. Central pontine myelinolysis. *J Clin Neurosci.* 1999;6(2):155–7.
141. Uchino A, Sawada A, Takase Y, Egashira R, Kudo S. Transient detection of early Wallerian degeneration on diffusion-weighted MRI after an acute cerebrovascular accident. *Neuroradiology.* 2004;46(3):183–8.
142. Shrivastava A. The hot cross bun sign. *Radiology.* 2007;245(2):606–7.

Chapter 11

Surgical Approaches to Mesencephalic (Midbrain) Tumors



Nir Shimony, David S. Hersh, and Frederick A. Boop

Abbreviations

CNS	Central nervous system
CSF	Cerebrospinal fluid
CST	Corticospinal tract
DTI	Diffusion tensor imaging
ETV	Endoscopic third ventriculostomy
LGGs	Low-grade gliomas
MR	Magnetic resonance
PCGP	Pediatric Cancer Genome Project
PPN	Pedunculopontine nucleus

11.1 Introduction: Anatomy and Embryology

The midbrain, which lies between the diencephalon and the pons, contains the motor fibers of the corticospinal tracts (CSTs), important connections for the visual and auditory systems, and the third and fourth cranial nerve nuclei. Embryologically,

N. Shimony (✉)

Johns Hopkins University, School of Medicine, Department of Neurosurgery, Baltimore, MD, USA

Geisinger Commonwealth School of Medicine, Department of Neurosurgery, Danville, PA, USA

e-mail: nshimony@geisinger.edu

D. S. Hersh

Pediatric Neurosurgery, Department of Neurosurgery, Le Bonheur Children's Hospital, Memphis, TN, USA

F. A. Boop

St. Jude Endowed Chair of Pediatric Neurosurgery, University of Tennessee Health Sciences Center, Memphis, TN, USA

Le Bonheur Neurosciences Institute, Memphis, TN, USA

Semmes Murphey Clinic, Memphis, TN, USA

the midbrain is of ectodermal origin. The anterior portion of the neural tube creates three primordial vesicles, which ultimately form the forebrain (prosencephalon), midbrain (mesencephalon), and hindbrain (rhombencephalon). Although the prosencephalon and rhombencephalon undergo further segmentation, the mesencephalon does not; it differentiates into the midbrain instead [1].

Anatomically, the midbrain consists of the tectum dorsally and the tegmentum ventrally. The midbrain harbors numerous nuclei and fibers, serving as a relay station via the superior cerebellar peduncles. The cerebral peduncles, cerebral aqueduct and periaqueductal gray, quadrigeminal plate and four colliculi (corpora quadrigemina), and the third and fourth cranial nerve nuclei are all located within the midbrain. The oculomotor nerve (third cranial nerve) can be identified along the ventral midbrain within the interpeduncular fossa, where small blood vessels penetrate the posterior perforated substance [1]. The trochlear nerve (fourth cranial nerve), on the other hand, emerges from the dorsal midbrain near the inferior colliculus [2].

The **tectum and the quadrigeminal plate** consist of the superior and inferior colliculi. The superior colliculus nuclei are complex-layered structures that play a role in ocular movements and visual reflexes through afferent connections with other regions of the central nervous system (CNS). The inferior colliculi consist of a triad of gray matter nuclei and play a significant role in the auditory pathway. This triad is composed of a central nucleus at the core (responsible for the tonotopic organization of auditory information), a pericentral nucleus, and a more lateral, external nucleus (which receives auditory and non-auditory inputs) [2].

The **tegmentum**, located at the ventral aspect of the midbrain, harbors white matter fibers en route to and from the cerebral cortex, cerebellum, and spinal cord. The brachium conjunctivum (a.k.a. superior cerebellar peduncle), a bundle of fibers arising from the cerebellum and connecting to the thalamus and red nucleus, traverses the tegmentum and plays an important role in fine motor coordination. The medial lemniscus, trigeminal lemniscus, and spinothalamic tracts also pass through the tegmentum; these are sensory tracts that typically course laterally within the tegmentum, whereas tracts that are responsible for coordinating eye movements, the medial longitudinal fasciculi, run centrally and paracentrally in the tegmentum.

Several groups of nuclei are also located within the tegmentum, particularly at the level of the inferior colliculus. The nucleus parabrachialis pigmentosus is a continuation of the tegmental area of Tsai and is located dorsal to the substantia nigra. The ventral tegmental nucleus is dorsal to the brachium conjunctivum and regulates behavior and emotions via connections with the mammillary bodies. The dorsal tegmental nucleus is located within the periaqueductal gray and sends projections to the reticular formation and autonomic nuclei of the brainstem. The dorsal raphe nucleus (nucleus supratrochlearis) is the largest serotonergic nucleus [2]. The lateral tegmentum harbors the pedunculopontine nucleus (PPN), lateral dorsal tegmental nucleus and parabigeminal areas, all of which are cholinergic nuclei.

The red nucleus resides medially within the rostral tegmentum at the level of the superior colliculus. The red nucleus acts as a relay point for projections from the cerebrum, cerebellum, reticular formation, and inferior olive. The oculomotor nucleus, which is responsible for eye movements, lies ventral to the periaqueductal gray matter within the medial tegmentum [2]; this nucleus is located at the levels of

the lower half of the superior colliculus and upper half of the inferior colliculus [3]. The trochlear nuclei are located at the level of the inferior colliculus and reside in the midline and ventral to the cerebral aqueduct. Its axons travel dorsal and lateral to the aqueduct and eventually pierce the dorsal surface of the midbrain, close to the midline. These nuclei are positioned adjacent to the midline and on average are 9.5 mm medial to the surface of the lateral mesencephalic sulcus [3].

The **cerebral peduncles** contain the corticocerebellar, corticobulbar and corticospinal fibers. The dominant component is the CST, which occupies the central three-fifths of the cerebral peduncle [2]. The tract's fibers are organized with the efferent cortical motor axons and are arranged somatotopically from medial to lateral: arm, face, then leg representations. The corticobulbar tract resides dorsomedial to the CST.

The midbrain is primarily vascularized via the posterior cerebral circulation, including the basilar, superior cerebellar and posterior cerebral arteries. In cross-section, the medial aspect of the midbrain is supplied by the basilar artery and its paramedian branches, while the lateral aspect is supplied by the superior cerebellar artery at the level of the inferior colliculus and the posterior cerebral artery branches at the level of the superior colliculus [2]. The superior colliculus and the adjacent tectum are vascularized by the superior cerebellar artery.

11.2 Midbrain Lesions

The midbrain is not specifically affected by unique lesions, and the same pathologies that are found in other regions of the brain and brainstem are also found in the midbrain, including but not limited to gliomas, germ cell tumors, cavernous malformations, and arteriovenous malformations. Although not unique regarding pathology, the anatomic location of the midbrain allows for unique patterns of tumor spread, with lesions tending to progress along white matter tracts, thus giving rise to thalamopeduncular tumors. Alternatively, lesions may localize to discrete locations within the midbrain, including the aqueduct, the periaqueductal area, and the quadrigeminal plate.

11.2.1 *Thalamopeduncular Tumors*

In 2007, Puget et al. presented a series of patients with thalamic tumors that included a newly defined subset of thalamopeduncular tumors [4]. In children, these tumors can present clinically with progressive spastic hemiparesis (secondary to mass effect on the CSTs) and are typically found to be low-grade tumors, such as pilocytic astrocytomas, at the interface of the thalamus and cerebral peduncle [5]. Other potential clinical signs include homonymous hemianopsia, ptosis and/or ophthalmoplegia secondary to mass effect on the optic tracts and oculomotor nerves, and obstructive hydrocephalus, which may arise if there is significant mass effect on the cerebral aqueduct.

Given the low incidence of thalamopeduncular tumors, treatment strategies are being developed while awaiting larger sample sizes and better sub-classification schemes [5]. The majority of these tumors are low-grade gliomas (LGGs), and as such, conventional

chemotherapy is associated with a cure rate of only 0–10% [5–8]. Radiation therapy can cause long-term sequelae, including neurocognitive deficits and endocrinopathies [9]. Therefore, surgical resection remains one of the primary treatment options for these tumors, despite the challenges of the surgery in this region. With careful planning, particularly with respect to the location of the CSTs, optimal surgical outcomes can be achieved, potentially sparing the patient from adjuvant therapy (Figs. 11.1 and 11.2).

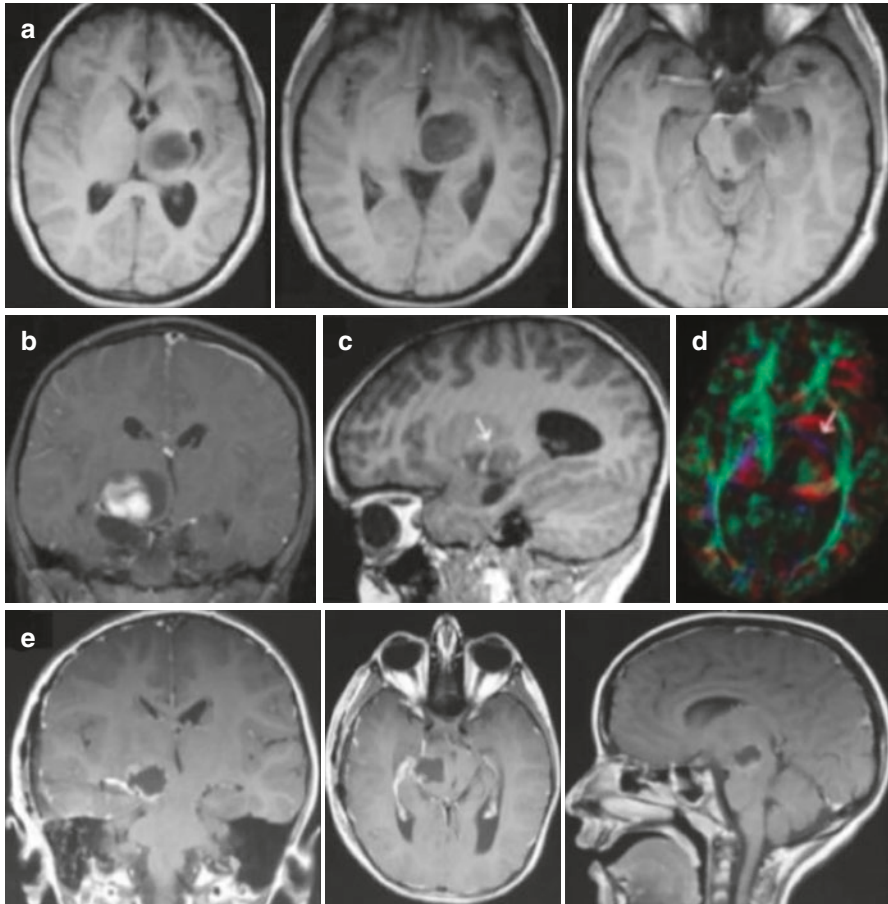


Fig. 11.1 Left thalamopeduncular pilocytic astrocytoma. **(a)** A composite of three axial T1-weighted Gadolinium-enhanced images demonstrates that the tumor arises from the lateral aspect of the peduncle underneath the thalamus, pushing the normal thalamus superiorly. The thalamic displacement made a transcallosal approach to the tumor a poor choice, because the surgeon could have violated the normal thalamus to reach the tumor. **(b, c)** The optic tract, a structure that must be carefully avoided while removing the tumor, is displaced superior and lateral to the tumor. The *arrow* designates the CST. **(d)** An axial DTI of the same tumor shows the CSTs deviated anteriorly and laterally (*arrow*; CSTs are in *blue*); this was the most common pattern of CST displacement in the series of patients described by Foley and Boop [52]. This pattern of tract displacement made a transsylvian approach unattractive; one would have to transect the tracts to reach the tumor. **(e)** An approach was chosen through the middle temporal gyrus by using frameless stereotactic navigation to approach the tumor just posterior to the CSTs. (Modified from Foley and Boop [52]. With permission from Springer Nature)

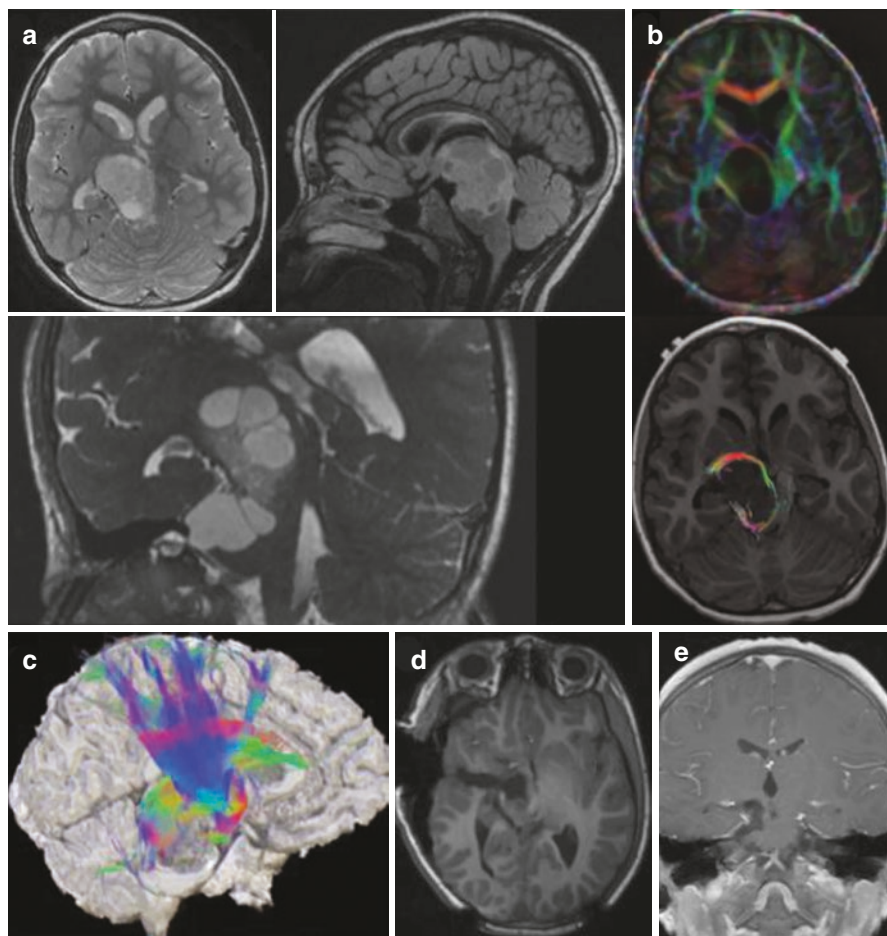


Fig. 11.2 A 5-year-old child presenting with a 3-week history of progressive hemiparesis – arm worse than leg, and a several-days history of headache, nausea, and vomiting. **(a)** Preoperative images. **(b)** Axial DTI. **(c)** Sagittal DTI. **(d)** Postoperative axial image following a transtemporal transchoroidal approach. **(e)** Coronal, post-contrast T1-weighted image at 1 year postop showing complete tumor resection. (Modified from Foley and Boop [52]. With permission from Springer Nature)

Molecular targeted therapies represent another opportunity as we learn more about the molecular drivers of pediatric LGGs. For instance, the *KIAA1549-BRAF* fusion has been found in pediatric pilocytic astrocytomas [10–12], where the Pediatric Cancer Genome Project (PCGP) identified the fusion in 75% of pilocytic astrocytomas, including 80% of brainstem tumors and 59% of diencephalic lesions [13]. Thalamopeduncular tumors, in particular, are also associated with a high frequency of the *KIAA1549-BRAF* fusion, suggesting that these tumors are more likely to originate from the midbrain rather than the thalamus [5]. This hypothesis is also supported by the anterolateral displacement of the CST in most patients with thalamopeduncular tumors. Regardless of the site of origin, the high

frequency of the *KIAA1549-BRAF* fusion in thalamopeduncular tumors implies that BRAF inhibitors may play a potential role in the treatment of these tumors.

11.2.2 Tectal Gliomas

Tectal gliomas are rare tumors with a predilection to occur in the pediatric population [14]. Tectal gliomas typically present with symptoms of raised intracranial pressure, and the diagnosis may be delayed, with most reports describing onset of symptoms at 3–6 months before the actual diagnosis [15]. Alternatively, tectal gliomas may be an incidental finding, as it was reported in up to 27% of patients in prior series; this percentage may rise with the increasingly widespread use of magnetic resonance (MR) imaging [16, 17].

Tectal gliomas are most commonly LGGs and are almost exclusively identified in children [15]. Tumor growth typically causes tectal expansion and, hence, compression of the aqueduct; it may also extend to the pulvinar region. Tectal tumors are usually isointense on T1- and hyperintense on T2-weighted imaging, and usually do not enhance after contrast administration [18]. Predictors of tumor progression include tumor size greater than 3 cm², contrast enhancement, and cystic changes at diagnosis [15, 19, 20].

Tectal gliomas have a similar morphology to other LGGs but demonstrate a unique molecular/biological profile: (1) only 25% of tectal gliomas harbor the *KIAA1549-BRAF* fusion, in contrast to LGGs of the cerebellum (92%) or the supratentorial compartment (59%); (2) the *BRAF V600E* mutation is uncommon in tectal gliomas, occurring in only around 7–8% of these tumors [21]; (3) although the *H3 K27M* mutation tends to be found in midline gliomas and portends a more aggressive disease, it is usually absent in tectal gliomas; (4) the methylation profile of tectal gliomas is unique compared to other LGGs [15]. These findings suggest that tectal gliomas are a unique entity and most often represent a chronic disease.

Given the usually indolent course and the risks associated with surgical resection in such an eloquent area, the general recommendation is cerebrospinal fluid (CSF) diversion in patients with hydrocephalus, followed by close observation [15]. The main options for CSF diversion include endoscopic third ventriculostomy (ETV) or a ventricular shunt. ETV has become more widely advocated due to the high rates of success in patients with obstructive hydrocephalus (particularly older children and adults) and the ability to avoid issues such as shunt malfunction, obstruction, and infection. Some authors suggested the use of Ommaya reservoirs, which allows for emergent access to CSF in the event of ETV failure [22]; the authors have also reported two cases in which the presumed tectal gliomas have spontaneously involuted and disappeared following ETV placement for hydrocephalus.

Approximately one-third of patients described in the literature have ultimately undergone surgical resection. Potential complications are significant and include

motor deficits, visual deficits, gaze palsies, and intracranial hemorrhage. As a result, biopsy or resection of tectal gliomas is typically reserved for tumors with an atypical radiographic appearance or to guide targeted treatment (such as BRAF and MEK inhibitors) at progression [15, 23–25]. Radiation therapy or chemotherapy may be considered in cases of progressive disease. Although tectal gliomas tend to progress in about 25% of children, long-term survival is typically achieved with salvage adjuvant treatment [15]. Tectal gliomas are rarely diagnosed in adults, but some authors hypothesize that these patients had undiagnosed indolent tumors in childhood [26]. As a result, the treatment strategy tends to be similar in adults.

11.2.3 Aqueductal and Periaqueductal Tumors

In most publications, tectal gliomas are grouped along with true aqueductal and periaqueductal tumors, without differentiating between the groups. In recent years, however, some authors described true aqueductal tumors, which is a rare entity [18]. True aqueductal tumors may include both LGGs and high-grade gliomas and are more likely to include enhancing tumors than other types of tectal tumors. It is important that the true aqueductal tumors are recognized as such. Given that the majority are benign and of soft consistency, those located at the rostral aqueduct can be resected from a third ventricular approach, whereas those located at the caudal aqueduct can be approached from a cerebellar fourth ventricular approach. As aqueductal tumors displace the normal tectum dorsally, these tumors should never be approached through the tectum, which is a risk associated with not recognizing aqueductal tumors as a separate entity. Nevertheless, data regarding true aqueductal tumors remain scarce [27].

11.3 Surgical Approaches to Midbrain Tumors

Surgical treatment of midbrain tumors should be guided by an understanding of the underlying anatomy as well as by advanced imaging, including diffusion tensor imaging (DTI), in order to define the location of critical white matter tracts, such as the CSTs, in relation to the tumor. Various safe entry zones have been described: periculomotor area for anterior lesions, supracollicular, infracollicular and intercollicular zones for posterior lesions, and lateral mesencephalic sulcus for anterolateral lesions [3]. More recently, additional surgical options included obtaining an endoscopic biopsy whenever the tumor extends into the third ventricle [28, 29] and the use of tubular retractors to facilitate resection [30, 31].

11.3.1 Anterior Midbrain

Tumors in the anterior portion of the midbrain usually tend to grow towards either the third ventricle or the interpeduncular cistern. In this setting, the key determinants for the surgical approach are the relation of the tumor to the third ventricle (i.e., how much of the tumor is in the ventricle versus how much is in the cistern) and the relation of the tumor to the oculomotor nerve. For tumors growing mainly into the third ventricle, an intraventricular approach may involve interforaminal, transcallosal, transchoroidal or transforaminal approaches. Transsphenoidal and transclival approaches have also been proposed, particularly for anterior pontine lesions but also for lesions of the anterior mesencephalon [32]. The use of an endoscope is usually reserved for biopsies or for resection of small lesions.

The unique location of the CST (intermediate three-fifths of the peduncle) allows for a possible surgical window from either pure anterior or anterolateral (pterional, orbito-zygomatic, supraorbital) or more lateral (transylvian, subtemporal or trans-temporal) approaches [33]. Combined approaches have also been popularized over the years. In 1911, Krause and colleagues described the subtemporal transtentorial approach, which allows for good visualization of the incisural space, the ambient cistern, and part of the quadrigeminal cistern [3]. In 1980, Sano and colleagues described the temporopolar approach, which allows for good visualization of the anterolateral interpeduncular fossa [34]. Each approach poses specific risks because of the potential neurovascular components that can be compromised. When the trajectory is more lateral, the approach usually includes some degree of tentorial resection and dissection. In particular, these lateral approaches are associated with a risk of injury to the vein of Labbe, as well as possible ophthalmoparesis due to third and fourth cranial nerve injury along the tentorial incisura.

11.3.1.1 Transchoroidal and Subchoroidal Approaches

These approaches will allow to expand the surgical window to the third ventricle, reaching the anterior and, in some cases, the central midbrain. Both approaches are based on safe anatomic passage through the choroidal fissure. The choroidal fissure is a cleft between the body of the fornix and the thalamus in the cavity of the lateral ventricle; it is situated below the choroid plexus, between the tenia fornices and tenia thalami. Anteriorly, it begins at the posterior edge of the foramen of Monro and runs posteriorly between fornix and thalamus. The thalamostriate, septal, caudate and superior choroidal veins run in close proximity to the choroidal fissure; some of these veins cross it as well. The choroidal fissure is the thinnest area in the wall of the lateral ventricle, bordering the basal cisterns and the roof of the third ventricle [35]. Upon entry to the lateral ventricle, either by parasagittal opening through an interhemispheric/corpus callosum dissection or by a transcortical corridor to the lateral ventricle, the choroid plexus and its anatomical complexity is appreciated. It is then coagulated laterally to expose the tenia fornix. The dissection proceeds through the tenia fornix to reach the velum interpositum, and then to the third ventricle. If necessary, the anterior septal vein is coagulated and transected at

the entry site to the foramen of Monro [36]. This opening allows for a wide view of the posterior and middle part of the third ventricle, hence to the anterior midbrain. Some surgeons advocate for a wider window, where the choroid plexus is coagulated and dissected laterally to use the tenia fornices as a route for expanding the foramen of Monro.

In the subchoroidal approach, the choroid fissure is opened lateral to the choroid plexus, between the choroid plexus and the thalamus [37]. After the choroid fissure is opened, there are two ways to enter the third ventricle: one route is between the internal cerebral veins, and another route is between the internal cerebral vein and the thalamus [37]. We recommend utilizing this approach in cases where the lesion invades and has a significant component inside the third ventricle. In case the surgeon chooses to further dissect through the velum interpositum along the medial wall of the ipsilateral internal cerebral vein, which allows to further expand the surgical window into the third ventricle, care should be taken to avoid injury to the thalamoperforator arteries running in close proximity to the internal cerebral vein [38]. As mentioned earlier, this approach is mostly useful whenever the midbrain tumor is superficial or exophytic and extending into the third ventricle. The surgical corridor through the third ventricle can provide access to anterior midbrain lesions, periaqueductal area, and some posterior lesions.

11.3.1.2 Peritemporal Approaches

We use this term for approaches that include the classic pterional and orbito-fronto-zygomatic craniotomies, allowing the surgeon to choose between several approaches: subtemporal with or without transtentorial, transtemporal, and transsylvian (pretemporal) [34]. The detailed description of these classic craniotomies is beyond the scope of this chapter. In general terms, we advocate a regular temporo-frontal or a small question mark skin opening with exposure of the zygomatic root. The temporalis muscle is elevated using interfacial dissection, allowing for more retraction of the muscle and further exposure of the zygomatic arch while protecting facial nerve branches. The temporal craniotomy should be low, just adjacent to the zygomatic root. There is no need to go above the superior temporal line, and the craniotomy flap is cut just above the zygomatic root in the coronal plan [39]. This craniotomy is a bit anterior to the traditional one and will sometimes lead to additional retraction on the temporal lobe, yet it lowers the risk of injuring the vein of Labbé and inducing a significant venous infarct. The dura is exposed, and the dural flap is usually retracted towards the zygomatic arch. Some surgeons advocate zygomatic arch drilling to decrease its prominence so that it does not interfere with the view towards the subtemporal area [39]. In some cases, CSF drainage is needed and can be done using a spinal drain that is placed before surgery or using an external ventricular catheter. In case the transsylvian approach is selected, CSF can be drained from the cisterns. Brain relaxation is necessary before attempting any temporal lobe retraction or manipulation. In the subtemporal approach, once the temporal lobe is retracted and the arachnoid layer of the mesiotemporal region is exposed, one can usually appreciate the pulsation of the P2 segment of the posterior cerebral artery running in the

ambient cistern. The arachnoid layer is widely excised using an arachnoid knife, allowing for more CSF drainage and evaluating the perimesencephalic area with a good view of the anterolateral midbrain. The subtemporal approach has several modifications that are basically different perspectives on the angle of attack (anterior, middle or posterior subtemporal), which allows for different views of the ambient cistern. The subtemporal approach does not usually allow for good visualization of the quadrigeminal cistern but provides adequate visualization of the interpeduncular cistern and the first half of the ambient cistern. The main obstacle for more posterior exposure is the presence of vein of Labbé and, in some cases, the parahippocampal gyrus [40]. The transsylvian, a.k.a. pretemporal, approach allows for a relatively quick drainage of CSF once the sylvian fissure is dissected, access to the sylvian cistern, and then to the cisterns around the carotid artery and the optic nerve. This approach usually demands relatively significant lateral and posterior retraction of the temporal lobe. It allows for fairly good control and view of the basilar area, hence the interpeduncular cistern, but lacks good visualization of the ambient cistern components, hence the perimesencephalic safe entry zone [40]. In both cases, the anterolateral midbrain can be exposed, and the perioculomotor safe entry zone can be utilized. At the level of the oculomotor nerve exit site from the midbrain, the CST occupies only the intermediate three-fifths of the cerebral peduncle, which permits only a small corridor between the oculomotor nerve exit site and the CSTs [3, 33]. This narrow window is delimited by the posterior cerebral artery above, the superior cerebellar artery below, the emergence of the third cranial nerve and the basilar artery medially, and the pyramidal tract laterally [3]. Since tumors in the anterior part of the midbrain are usually exophytic in nature, this safe entry zone is rarely used.

An approach that allows for some visualization of the perimesencephalic area, including the transition zone between the ambient and quadrigeminal cisterns, is the transtemporal-transchoroidal approach. In this approach, the surgeon can have a small corridor to attack lesions residing in the anterior and middle parts of the midbrain. The exposure is very similar to that of the subtemporal approach, with the understanding that the temporal horn is usually 2.5–3.5 cm posterior to the temporal tip and 2–2.5 cm deep to the surface [40]. The entry point is along the inferior temporal gyrus, aiming to access the temporal horn and identify the choroid plexus as well as the hippocampal head and body. The temporal choroidal fissure lies between the choroid plexus and the hippocampus. Crossing the fissure from the hippocampal side rather than from the thalamic side will help in avoiding the highly vascularized area just adjacent to the thalamus.

11.3.2 Central Midbrain

Tumors located in the central midbrain region tend to extend either towards the fourth ventricle inferiorly or towards the pineal region superiorly. The direction of extension may guide the surgical approach. If the major component of the tumor extends towards the fourth ventricle, a suboccipital craniotomy and telovelar

approach may be appropriate. When the major component of the tumor extends toward the pineal region, the various approaches to the pineal region itself may be utilized. In particular, the midline or paramedian supracerebellar infratentorial approach can open a relatively wide window to the midbrain and pericolicular area, as well as to the transition zone between the upper part of the midbrain and the pineal region [41–43]. Alternatively, the occipital transtentorial approach can be considered.

When approaching the pericolicular region, extra care should be taken to protect the fourth cranial nerve, which is situated directly below the inferior colliculus. Safe entry zones to the pericolicular region have been described. Supracolicular access can be obtained by performing a transverse incision above the superior colliculus; dissection continues until the periaqueductal gray is reached. Alternatively, infracolicular access can be obtained by entering between the trochlear nerve and the inferior colliculus [3].

Similar to anterior midbrain lesions, central midbrain tumors may extend into the third ventricle, in which case they may be accessed via interforaminal, transcallosal,

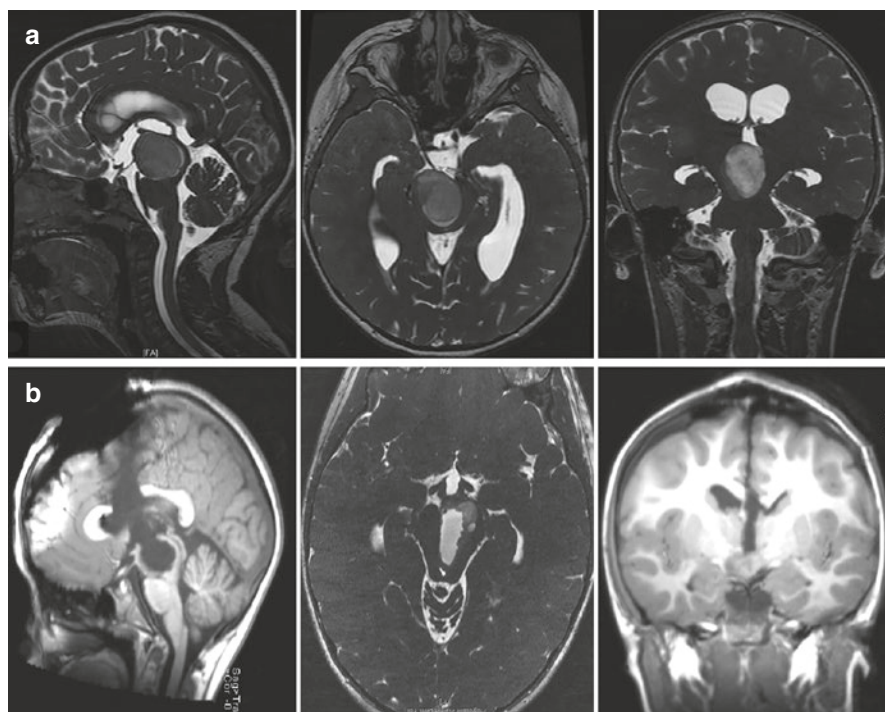


Fig. 11.3 A 6-year-old girl presented with headaches, right third nerve palsy, and left hemiparesis. (a) Preoperative MRI demonstrated a midbrain tumor with extension into the third ventricle. (b) Postoperative MRI following a transcallosal subchoroidal approach. The third nerve palsy did not improve but she is otherwise intact, and 5 years postop, the residual has not progressed. The patient did not require additional treatment to date

transchoroidal or transforaminal approaches (Fig. 11.3). Most of the approaches described in the Sect. 11.3.1 can be utilized for central midbrain lesions as well. The transchoroidal approach can be very helpful in achieving a good angle of attack to lesions that invade the third ventricle [38]. A similar view can be achieved using the interforaminal approach [36, 37, 44]; this approach works well for patients with a cavum septum pellucidum, but if the surgeon tries to separate the fornices after they have fused, the patients have a high likelihood of developing permanent memory deficits as a consequence of manipulating both fornices. Finally, the different peritemporal approaches are helpful in achieving a good angle of attack to lesions that either exophyte through the lateral midbrain or are fairly close to it.

11.3.3 Posterior (Dorsal) Midbrain

The posterior midbrain, or quadrigeminal plate, lies posterior to the cerebral aqueduct [3]. The unique proximity of the posterior part of the midbrain to the aqueduct of Sylvius makes tumors in this location more likely to cause obstructive hydrocephalus. As a result, endoscopic biopsy has become an attractive option, since it can be performed for diagnosis at the same time as an ETV for CSF diversion is performed (Fig. 11.4). The endoscopic procedure can be carried out using a flexible or rigid endoscope and, in some cases, the combination of the two [29]. The entry point is usually more anterior than the regular entry point used for ETV, which is just anterior to the coronal suture [29, 45]. Once inside the lateral ventricle, the endoscope is introduced through the foramen of Monro while aiming to reach the posterior part of the third ventricle. The resection of the tumor can be carried out using endoscopic instruments or the NICO Myriad® (NICO Corporation) in order to achieve meaningful resection.

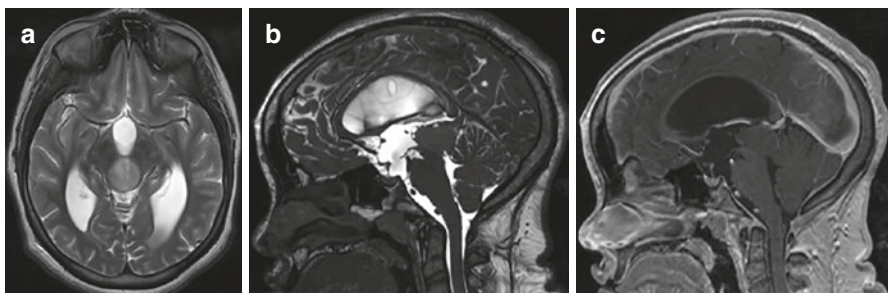


Fig. 11.4 A 14-year-old girl who presented to an outside facility with obstructive hydrocephalus and was diagnosed with a tectal plate mass. The patient underwent an endoscopic third ventriculostomy; given that the tumor was exophytic into the posterior aspect of the 3rd ventricle, an endoscopic biopsy was recommended. (a) Axial T2-weighted and (b) sagittal FIESTA images demonstrate an avoid, well-circumscribed mass centered on the tectum and extending into the posterior aspect of the third ventricle. (c) Sagittal, post-contrast T1-weighted image demonstrates that the mass was not contrast-enhancing

Some tumors ultimately require a more invasive approach for surgical resection. Most of these tumors are exophytic. Surgical corridors include many of those described previously, including the transchoroidal, interforaminal, supracerebellar infratentorial, and occipital transtentorial approaches. When the tumor is extending superiorly and laterally, the occipital transtentorial approach provides a very wide view that includes the pineal region, posterior part of the third ventricle, tectal plate and upper fourth ventricle, posterolateral surface of the mesencephalon, tentorial surface of the cerebellum, and splenium of the corpus callosum. The main pitfall, however, is that excessive retraction on the occipital lobe can injure the visual cortex [46]. The midline approaches for the posterior midbrain, as well as the posterior third ventricle, usually start as interhemispheric, either parietal or occipital. CSF diversion prior to manipulation can significantly reduce potential injury to the brain from manipulation and retraction. In the interhemispheric transcallosal approach, either intervenous or paravenous, the patient is positioned in a supine position with the head in a neutral angle of rotation and considerably flexed. It is advised to even consider a semi-sitting position. Once the interhemispheric approach is achieved, a minimal callosotomy is performed, utilizing the navigation system in order to minimize the opening at the posterior corpus callosum. A midline callosotomy will allow dissection through an avascular plane that runs between the two internal cerebral veins [47]. In order to approach the third ventricle, the surgeon needs to decide on either separating the internal cerebral veins or dissecting next to them; the approach is thus called intervenous or interforaminal, respectively. In the intervenous approach, it is best to aim close to the confluence of the internal cerebral veins and the vein of Galen. Just proximal to this point, there is a natural separation between the two internal cerebral veins [47]. The dissection can be elongated anteriorly as needed. Another important benefit of the intervenous approach is that at this posterior location, the foraminal crura are not fused and always lateral to the internal cerebral veins. After dissecting between the two veins, the surgeon should be cautious not to excessively compress or manipulate the veins to avoid venous injury or thrombosis. This approach allows for direct visualization of the posterior midbrain, periaqueductal area, tectal plate, and pineal region. The drawback of this approach is the potential injury to venous structures, starting with the cortical veins, which may be sacrificed in some cases during the interhemispheric approach (although every effort should be taken to preserve them in order to avoid venous congestion or infarcts), and ending with the internal cerebral veins, which may be attached to tumors originating from the midbrain or pineal region.

The occipital interhemispheric approach to midbrain tumors usually includes the addition of either tentorial transection, falcine transection, or both. The quoted name in the literature is the occipital interhemispheric transtentorial approach. The angle of attack can be a direct one, from ipsilateral to the center of the tumoral mass, or contralateral permitting a different trajectory. This approach, along with the supracerebellar infratentorial approach, allows for a good trajectory to the quadrigeminal plate and the pericollicular area. Some surgeons advocate the sitting position [48], while others prefer the prone position – in a way that the confluence of sinuses is the highest point, the concord position, or the three-quarters prone position [49]. The

tentorial opening is usually done at 1 cm lateral and parallel to the straight sinus. If an ipsilateral approach is chosen, usually only an ipsilateral view of the ambient and quadrigeminal plate can be achieved. Yet, the addition of falcine dural transection usually at around 1 cm above and parallel to the straight sinus allows for a much broader view of the quadrigeminal plate. In recent years, there is growing literature that supports the use of an endoscope to augment the occipital interhemispheric approach [50, 51].

The supracerebellar infratentorial is the most inferior approach to the midbrain. In this approach, the surgeon has a wide view of the quadrigeminal plate. The patient can be positioned in either the sitting or the three-quarters prone position. The opening can be midline or paramedian, preparing for a craniotomy that will be either on the edge of the sinus or crossing the sinus, so that the dural opening will have a horse-shoe pattern with the stalk against the sinus. In this way, the surgeon can elevate the dura upwards, helping to further open the junction between the cerebellum and the tentorium. The dissection is carried out by resecting the arachnoid adhesions at this junction, including the thick arachnoid matter covering the quadrigeminal plate. Care should be taken to avoid injury to the precerebellar veins or the vermian vein. The vascular structures exposed include the posterior cerebral artery, a tentorial branch of the superior cerebellar and medial posterior choroidal arteries, the vein of Galen, and the internal occipital and cerebral veins [49]. The endoscope can be an efficient and important tool in this approach as well.

In recent years, several publications suggested the use of tubular retractors to attack these deep-seated lesions, including midbrain tumors. The use of advanced imaging and understanding of the exact location of the CST is of paramount importance [52].

11.4 Surgical Decision-Making

The main surgical consideration is typically to achieve CSF diversion. ETV, with a possible endoscopic biopsy, is often preferred. In some cases, a ventricular shunt may be necessary (e.g., if the patient's anatomy is unfavorable to an ETV). In cases in which the initial diagnosis is questionable, or in cases where there is clear tumor progression, surgical biopsy or resection should be considered. Regardless of the surgical approach, DTI to detect the CSTs location is critical for planning the best approach [52] (Fig. 11.5). Most thalamopeduncular tumors, for example, displace the CST anterolaterally, and a transsylvian approach would violate the CST. In these cases, as well as in cases where the CST is displaced medially, a transtemporal transchoroidal approach is appropriate and facilitates complete removal of the tumor while protecting the CST. In cases where the CST is displaced laterally, however, a transcortical middle frontal gyrus approach is more appropriate. In addition to the CSTs, other critical structures that should be identified on preoperative imaging and protected intraoperatively include the optic tract, basal vein of Rosenthal, and the third cranial nerve [52].

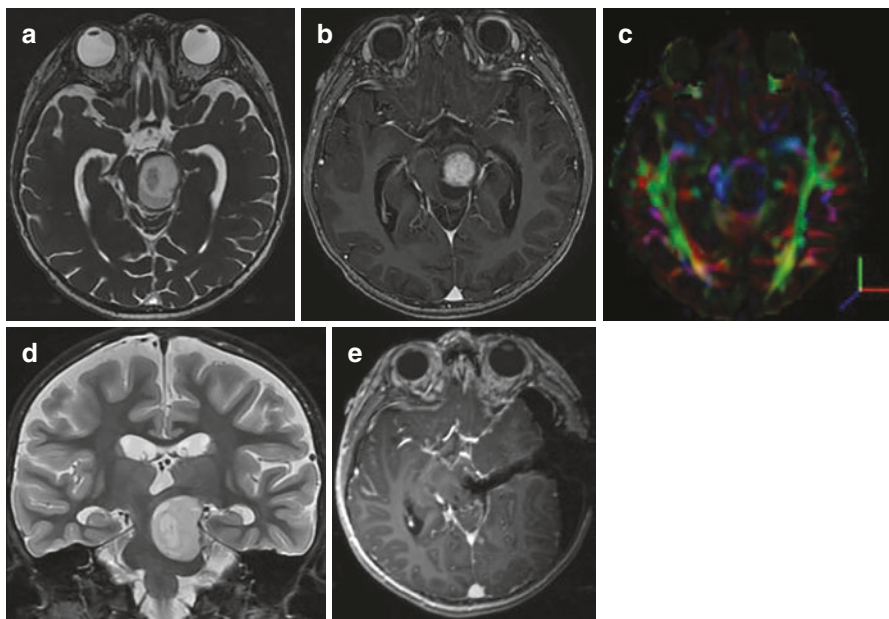


Fig. 11.5 A 4-year-old boy who presented with progressive right hemiparesis. **(a)** Preoperative axial FIESTA image demonstrates a mixed solid and cystic left pontomesencephalic lesion. **(b)** Axial, post-contrast T1-weighted image demonstrates diffuse enhancement of the center of the lesion. **(c)** Axial DTI demonstrating medial displacement of the corticospinal tract fibers, facilitating a transtemporal transchoroidal approach. **(d)** Coronal T2-weighted image. **(e)** Postoperative axial, post-contrast T1-weighted image

11.5 Prognosis

Prognosis depends on several parameters. Tumor histology (high-grade versus LGG), as well as specific molecular features such as the *H3K27 M* mutation, are known to significantly affect the prognosis. Although the classic tectal glioma is typically considered indolent with a good prognosis, up to 20% of cases are diagnosed as high-grade gliomas. Radiographic disease progression may occur, with an average duration from diagnosis to progression ranging from 3 months to 7.8 years. Patient outcomes were reported in 28 studies, with 495/508 patients (97.4%) surviving for an average duration that ranged between 2 and 10 years [15].

11.6 Conclusion

Midbrain tumors are complex lesions, and a stepwise approach regarding diagnosis and treatment is critical. Although most tectal gliomas will possibly require CSF diversion and have an otherwise indolent course, care should be taken to ensure that

the diagnosis is certain. Additionally, any evidence of tumor progression demands intervention. Most other midbrain tumors will mandate either surgical resection or biopsy and oncological treatment. There are several surgical approaches to the midbrain, which are divided into approaches targeting the anterior, middle and/or posterior areas of the midbrain. For the anterior midbrain, many of the approaches utilize either the transventricular or the peritemporal trajectories. For the central portion of the midbrain, many tumors will invade the third ventricle; hence, the surgeon uses various techniques to expand the view through the third ventricle. For the posterior part of the midbrain, some approaches utilize the interhemispheric corridor, either from the parietal or the occipital areas, whereas some tumors can be approached through the posterior fossa. In recent years, endoscopes and exoscopes have been used more often, the goal of which is to achieve better visualization of the deep areas of the brain, such as the midbrain. Meticulous planning before surgery will assist in choosing the best treatment strategy as well as the right surgical approach for this highly complex area.

References

1. Angeles Fernández-Gil M, Palacios-Bote R, Leo-Barahona M, Mora-Encinas JP. Anatomy of the brainstem: a gaze into the stem of life. *Semin Ultrasound CT MR*. 2010;31(3):196–219.
2. Ruchalski K, Hathout GM. A medley of midbrain maladies: a brief review of midbrain anatomy and syndromology for radiologists. *Radiol Res Pract*. 2012;2012:258524.
3. Cavalheiro S, Yagmurlu K, da Costa MD, Nicacio JM, Rodrigues TP, Chaddad-Neto F, et al. Surgical approaches for brainstem tumors in pediatric patients. *Childs Nerv Syst*. 2015;31(10):1815–40.
4. Puget S, Crimmins DW, Garnett MR, Grill J, Oliveira R, Boddaert N, et al. Thalamic tumors in children: a reappraisal. *J Neurosurg*. 2007;106(5 Suppl):354–62.
5. Lee RP, Foster KA, Lillard JC, Klimo P, Ellison DW, Orr B, et al. Surgical and molecular considerations in the treatment of pediatric thalamopeduncular tumors. *J Neurosurg Pediatr*. 2017;20(3):247–55.
6. Bouffet E, Jakacki R, Goldman S, Hargrave D, Hawkins C, Shroff M, et al. Phase II study of weekly vinblastine in recurrent or refractory pediatric low-grade glioma. *J Clin Oncol*. 2012;30(12):1358–63.
7. Grigsby PW, Thomas PR, Schwartz HG, Fineberg B. Irradiation of primary thalamic and brainstem tumors in a pediatric population. A 33-year experience. *Cancer*. 1987;60(12):2901–6.
8. Gnekow AK, Falkenstein F, von Hornstein S, Zwiener I, Berkefeld S, Bison B, et al. Long-term follow-up of the multicenter, multidisciplinary treatment study HIT-LGG-1996 for low-grade glioma in children and adolescents of the German Speaking Society of Pediatric Oncology and Hematology. *Neuro-Oncology*. 2012;14(10):1265–84.
9. Armstrong GT, Conklin HM, Huang S, Srivastava D, Sanford R, Ellison DW, et al. Survival and long-term health and cognitive outcomes after low-grade glioma. *Neuro-Oncology*. 2011;13(2):223–34.
10. Cin H, Meyer C, Herr R, Janzarik WG, Lambert S, Jones DT, et al. Oncogenic FAM131B-BRAF fusion resulting from 7q34 deletion comprises an alternative mechanism of MAPK pathway activation in pilocytic astrocytoma. *Acta Neuropathol*. 2011;121(6):763–74.
11. Lin A, Rodriguez FJ, Karajannis MA, Williams SC, Legault G, Zagzag D, et al. BRAF alterations in primary glial and glioneuronal neoplasms of the central nervous system with

- identification of 2 novel KIAA1549:BRAF fusion variants. *J Neuropathol Exp Neurol.* 2012;71(1):66–72.
12. Dougherty MJ, Santi M, Brose MS, Ma C, Resnick AC, Sievert AJ, et al. Activating mutations in BRAF characterize a spectrum of pediatric low-grade gliomas. *Neuro-Oncology.* 2010;12(7):621–30.
 13. Zhang J, Wu G, Miller CP, Tatevossian RG, Dalton JD, Tang B, et al. Whole-genome sequencing identifies genetic alterations in pediatric low-grade gliomas. *Nat Genet.* 2013;45(6):602–12.
 14. Guillamo JS, Doz F, Delattre JY. Brain stem gliomas. *Curr Opin Neurol.* 2001;14(6):711–5.
 15. Liu APY, Harreld JH, Jacola LM, Gero M, Acharya S, Ghazwani Y, et al. Tectal glioma as a distinct diagnostic entity: a comprehensive clinical, imaging, histologic and molecular analysis. *Acta Neuropathol Commun.* 2018;6(1):101.
 16. Gass D, Dewire M, Chow L, Rose SR, Lawson S, Stevenson C, et al. Pediatric tectal plate gliomas: a review of clinical outcomes, endocrinopathies, and neuropsychological sequelae. *J Neuro-Oncol.* 2015;122(1):169–77.
 17. Pollack IF, Shultz B, Mulvihill JJ. The management of brainstem gliomas in patients with neurofibromatosis 1. *Neurology.* 1996;46(6):1652–60.
 18. Roth J, Chaichana KL, Jallo G, Mirone G, Cinalli G, Constantini S. True aqueductal tumors: a unique entity. *Acta Neurochir.* 2015;157(2):169–77.
 19. Ternier J, Wray A, Puget S, Bodaert N, Zerah M, Sainte-Rose C. Tectal plate lesions in children. *J Neurosurg.* 2006;104(6 Suppl):369–76.
 20. Poussaint TY, Kowal JR, Barnes PD, Zurakowski D, Anthony DC, Goumnerova L, et al. Tectal tumors of childhood: clinical and imaging follow-up. *AJNR Am J Neuroradiol.* 1998;19(5):977–83.
 21. Berghthold G, Bandopadhyay P, Hoshida Y, Ramkissoon S, Ramkissoon L, Rich B, et al. Expression profiles of 151 pediatric low-grade gliomas reveal molecular differences associated with location and histological subtype. *Neuro-Oncology.* 2015;17(11):1486–96.
 22. Drake J, Chumas P, Kestle J, Pierre-Kahn A, Vinchon M, Brown J, et al. Late rapid deterioration after endoscopic third ventriculostomy: additional cases and review of the literature. *J Neurosurg.* 2006;105(2):118–26.
 23. Boydston WR, Sanford RA, Muhlbauer MS, Kun LE, Kirk E, Dohan FC, et al. Gliomas of the tectum and periaqueductal region of the mesencephalon. *Pediatr Neurosurg.* 1991;17(5):234–8.
 24. Robertson PL, Muraszko KM, Brunberg JA, Axtell RA, Dauser RC, Turrisi AT. Pediatric mid-brain tumors: a benign subgroup of brainstem gliomas. *Pediatr Neurosurg.* 1995;22(2):65–73.
 25. Stark AM, Fritsch MJ, Claviez A, Dörner L, Mehdorn HM. Management of tectal glioma in childhood. *Pediatr Neurol.* 2005;33(1):33–8.
 26. Yeh DD, Warnick RE, Ernst RJ. Management strategy for adult patients with dorsal midbrain gliomas. *Neurosurgery.* 2002;50(4):735–8; discussion 8–40.
 27. Bowers DC, Georgiades C, Aronson LJ, Carson BS, Weingart JD, Wharam MD, et al. Tectal gliomas: natural history of an indolent lesion in pediatric patients. *Pediatr Neurosurg.* 2000;32(1):24–9.
 28. Javadpour M, Mallucci C. The role of neuroendoscopy in the management of tectal gliomas. *Childs Nerv Syst.* 2004;20(11–12):852–7.
 29. Roth J, Constantini S. Combined rigid and flexible endoscopy for tumors in the posterior third ventricle. *J Neurosurg.* 2015;122(6):1341–6.
 30. Weiner HL, Placantonakis DG. Resection of a pediatric thalamic juvenile pilocytic astrocytoma with whole brain tractography. *Cureus.* 2017;9(10):e1768.
 31. Recinos PF, Raza SM, Jallo GI, Recinos VR. Use of a minimally invasive tubular retraction system for deep-seated tumors in pediatric patients. *J Neurosurg Pediatr.* 2011;7(5):516–21.
 32. Essayed WI, Singh H, Lapadula G, Almodovar-Mercado GJ, Anand VK, Schwartz TH. Endoscopic endonasal approach to the ventral brainstem: anatomical feasibility and surgical limitations. *J Neurosurg.* 2017;127(5):1139–46.
 33. Bricolo A, Turazzi S. Surgery for gliomas and other mass lesions of the brainstem. *Adv Tech Stand Neurosurg.* 1995;22:261–341.

34. Sano K. Temporo-polar approach to aneurysms of the basilar artery at and around the distal bifurcation: technical note. *Neurol Res.* 1980;2(3–4):361–7.
35. Fujii K, Lenkey C, Rhoton AL. Microsurgical anatomy of the choroidal arteries: lateral and third ventricles. *J Neurosurg.* 1980;52(2):165–88.
36. Wen HT, Rhoton AL, de Oliveira E. Transchoroidal approach to the third ventricle: an anatomic study of the choroidal fissure and its clinical application. *Neurosurgery.* 1998;42(6):1205–17; discussion 17–9.
37. Bozkurt B, Yağmurlu K, Belykh E, Tayebi Meybodi A, Staren MS, Aklinski JL, et al. Quantitative anatomic analysis of the transcallosal-transchoroidal approach and the transcallosal-subchoroidal approach to the floor of the third ventricle: an anatomic study. *World Neurosurg.* 2018;118:219–29.
38. Patel P, Cohen-Gadol AA, Boop F, Klimo P. Technical strategies for the transcallosal transforaminal approach to third ventricle tumors: expanding the operative corridor. *J Neurosurg Pediatr.* 2014;14(4):365–71.
39. Nakov VS, Spiriev TY, Todorov IT, Simeonov P. Technical nuances of subtemporal approach for the treatment of basilar tip aneurysm. *Surg Neurol Int.* 2017;8:15.
40. Ulm AJ, Tanriover N, Kawashima M, Campero A, Bova FJ, Rhoton A. Microsurgical approaches to the perimesencephalic cisterns and related segments of the posterior cerebral artery: comparison using a novel application of image guidance. *Neurosurgery.* 2004;54(6):1313–27; discussion 27–8.
41. Yamamoto I. Pineal region tumor: surgical anatomy and approach. *J Neuro-Oncol.* 2001;54(3):263–75.
42. Stein BM. The infratentorial supracerebellar approach to pineal lesions. *J Neurosurg.* 1971;35(2):197–202.
43. Stein BM. Supracerebellar-infratentorial approach to pineal tumors. *Surg Neurol.* 1979;11(5):331–7.
44. Figueiredo EG, Beer-Furlan A, Welling LC, Ribas EC, Schafranski M, Crawford N, et al. Microsurgical approaches to the ambient cistern region: an anatomic and qualitative study. *World Neurosurg.* 2016;87:584–90.
45. Kim IY, Jung S, Moon KS, Jung TY, Kang SS. Neuronavigation-guided endoscopic surgery for pineal tumors with hydrocephalus. *Minim Invasive Neurosurg.* 2004;47(6):365–8.
46. Ausman JI, Malik GM, Dujovny M, Mann R. Three-quarter prone approach to the pineal-tentorial region. *Surg Neurol.* 1988;29(4):298–306.
47. Patel PG, Cohen-Gadol AA, Mercier P, Boop FA, Klimo P. The posterior transcallosal approach to the pineal region and posterior third ventricle: intervenous and paravenous variants. *Oper Neurosurg (Hagerstown).* 2017;13(1):77–88.
48. Sun Q, Zhao X, Gandhi S, Tayebi Meybodi A, Belykh E, Valli D, et al. Quantitative analysis of ipsilateral and contralateral supracerebellar infratentorial and occipital transtentorial approaches to the cisternal pulvinar: laboratory anatomical investigation. *J Neurosurg.* 2019:1–10.
49. Akiyama O, Matsushima K, Gungor A, Matsuo S, Goodrich DJ, Tubbs RS, et al. Microsurgical and endoscopic approaches to the pulvinar. *J Neurosurg.* 2017;127(3):630–45.
50. Liu JK. Endoscopic-assisted interhemispheric parieto-occipital transtentorial approach for microsurgical resection of a pineal region tumor: operative video and technical nuances. *Neurosurg Focus.* 2016;40(Video Suppl 1):2016.1.FocusVid.15450.
51. Tanikawa M, Yamada H, Sakata T, Hayashi Y, Sasagawa Y, Watanabe T, et al. Exclusive endoscopic occipital transtentorial approach for pineal region tumors. *World Neurosurg.* 2019;131:167. [Epub ahead of print].
52. Foley R, Boop F. Tractography guides the approach for resection of thalamopeduncular tumors. *Acta Neurochir.* 2017;159(9):1597–601.

Chapter 12

Surgical Approaches to Pontine Tumors



Mohammad Hassan A. Noureldine, Nir Shimony, and George I. Jallo

Abbreviations

AICA	Anterior inferior cerebellar artery
BA	Basilar artery
CN	Cranial nerve
CSF	Cerebrospinal fluid
CT	Computed tomography
EEA	Endoscopic endonasal approach
ENT	Ear, Nose and Throat
ICA	Internal carotid artery
MCP	Middle cerebellar peduncle
MLF	Medial longitudinal fasciculus
MRI	Magnetic resonance imaging
PCA	Posterior cerebral artery
PICA	Posterior inferior cerebellar artery
SCA	Superior cerebellar artery
SCP	Superior cerebellar peduncle
VA	Vertebral artery

M. H. A. Noureldine · G. I. Jallo (✉)

Department of Neurosurgery, Institute for Brain Protection Sciences, Johns Hopkins University School of Medicine, Johns Hopkins All Children's Hospital, Saint Petersburg, FL, USA
e-mail: gjallo1@jhmi.edu

N. Shimony

Institute of Neuroscience, Geisinger Medical Center, Geisinger Commonwealth School of Medicine, Danville, PA, USA

12.1 Introduction

The current chapter discusses the entire current armamentarium of surgical approaches to lesions residing in different regions of the pons, from which a neurosurgeon can choose to perform the least invasive, maximally safe surgery. That said, the surgeon should implement a 360-degree evaluation of the lesion for the best approach based on the concept of adopting a surgical trajectory that avoids crossing of the important neurovascular elements. The pons is reported to harbor most of the cavernous malformations in the brainstem, with higher tendency to bleed, as well as most of the pediatric brainstem tumors [1–3]. In some publications reporting on the likelihood to find a vascular lesion or a tumor in the brainstem by location, 61% of symptomatic brainstem cavernous malformations and 35% of pediatric brainstem tumors were located in the pons [3–6]. While several of the discussed approaches and their variations can be utilized to tackle lesions in the midbrain and medulla oblongata, these are discussed in detail in other chapters of this book (see Chaps. 11 and 13). Indications and technical nuances for obtaining a biopsy are discussed in Chap. 8 as well. From the senior author's experience, it is important to emphasize the role of intraoperative neuromonitoring in brainstem surgery in order to obtain the best postoperative outcomes, a topic that is comprehensively discussed in Chap. 5 of this book.

Surgical resection of pontine lesions demands mastery of neurosurgical skills and thorough knowledge of anatomy as well as the various approaches and available technologies to achieve excellent surgical results. The hidden location of the pons in between the cerebellum, petrous bone, clivus and major blood vessels demands utilizing different approaches to reach specific locations inside the pons.

12.2 Surgical Anatomy of the Pons

The anterolateral surface of the pons has a protuberant, convex shape. Anteriorly, a shallow median groove (a.k.a. basilar sulcus) marks the track of the basilar artery (BA); the two pyramidal eminences running parallel along both sides of this groove contain corticospinal fibers crossing rostrocaudally through the substance of the pons. Another vertical shallow groove, the lateral pontine sulcus, smoothly separates the belly of the pons medially from the middle cerebellar peduncle (MCP) laterally, the latter of which seems to be in continuation with the belly. The pontomesencephalic and pontomedullary sulci run in the horizontal plane and mark the upper and lower limits of the pons with the midbrain and medulla, respectively (Fig. 12.1).

The anterior two-thirds of the pons contain corticospinal and corticobulbar fibers, which traverse vertically and more anteriorly than most of the horizontal transverse pontine fibers that course between the MCPs. However, a thin layer of superficial transverse fibers cross anterior to and cover the corticospinal/corticobulbar fibers superiorly and inferiorly. The pontine nuclei, a relay station for the corticopontocerebellar fibers, are interspersed between the transverse pontine fibers (Fig. 12.2). The

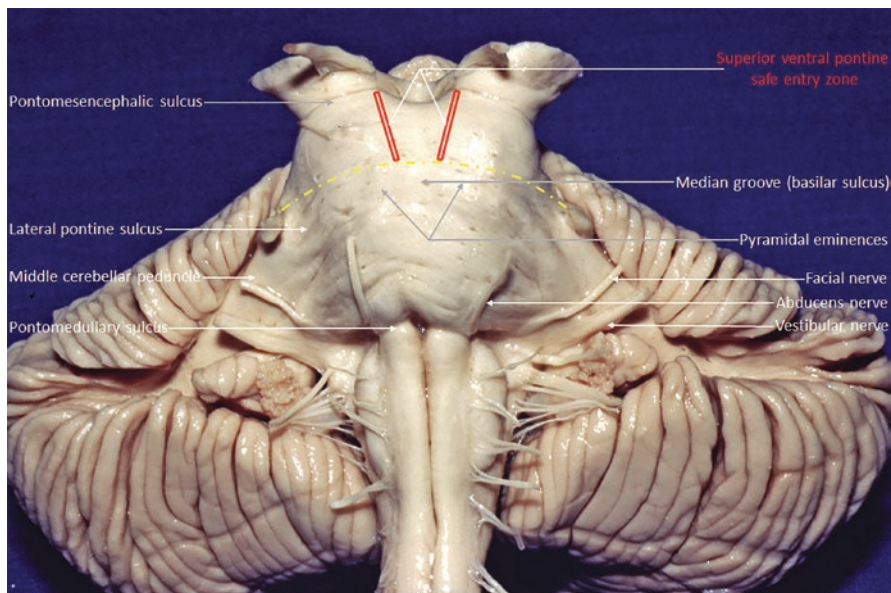


Fig. 12.1 Anterior surface of the pons. The superior ventral pontine safe entry zones are located paramedian, are limited by the pontomesencephalic sulcus superiorly, and a virtual horizontal line connecting the root entry zones of CNs V marks the lower limit as shown (see Sect. 12.3 of this chapter for full description of safe entry zones)

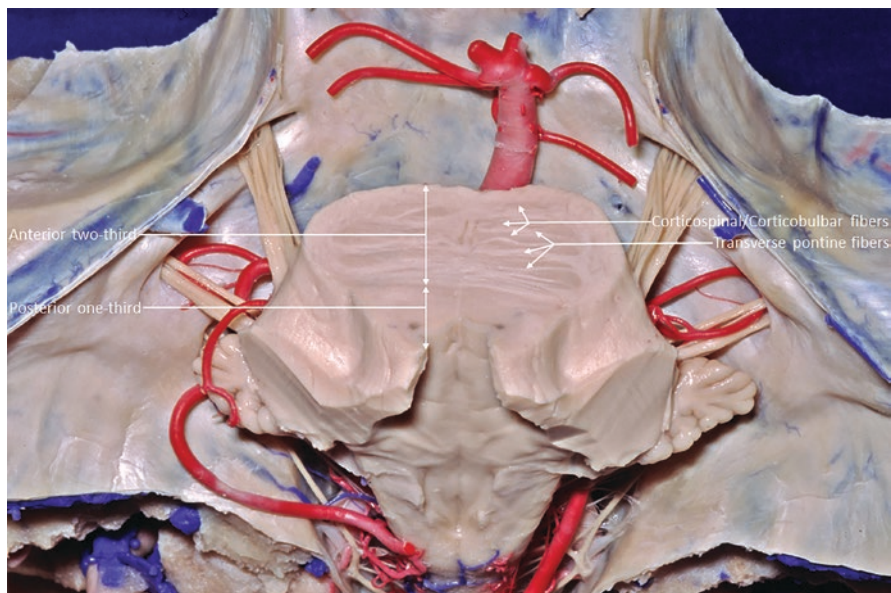


Fig. 12.2 Horizontal cut through the substance of the pons showing the corticospinal/corticobulbar and transverse pontine fibers

posterior one-third of the pons houses several cranial nerve (CN) nuclei, ascending tracts, and the upper portion of the floor of the fourth ventricle (see Fig. 12.2). The trigeminal nerve enters at the midlevel of the pons just lateral to the lateral pontine sulcus but medial to the MCP and can be considered as the limit between the MCP and the pons; its small motor root lies superomedially, and its large sensory root lies inferolaterally (Fig. 12.3). Understanding the anatomical organization of the trigeminal nerve is important to plan a safe entry point, which is discussed in detail later in this chapter. The trigeminal nerve courses obliquely in the substance of the pons to reach the motor and main sensory nuclei of the trigeminal nerve, located ventral to the superior cerebellar peduncle (SCP) in the posterior one-third of the pons; the mesencephalic nucleus lies dorsomedial to the motor(medial)/main sensory(lateral) nuclei complex, closer to the surface of the fourth ventricle, and medial to the SCP. The trigeminal mesencephalic and the trigeminal spinal tracts extend from the motor/main sensory nuclei rostrally and caudally, respectively. The central tegmental tract runs medial to the trigeminal mesencephalic tract to connect the red nucleus superiorly with the inferior olivary nucleus inferiorly, and the medial longitudinal fasciculus (MLF) runs just medial to it. From a microsurgical standpoint, these vertically-traversing structures can be projected onto the posterior surface of the fourth ventricle – above the level of the facial colliculus – and from medial to lateral as per the following: the median sulcus of the fourth ventricle runs at the center, followed by MLF (and facial colliculus inferiorly), sulcus limitans,



Fig. 12.3 Anterolateral surface of the pons

trigeminal nuclei/mesencephalic tract, and SCP (Fig. 12.4). Note that both nuclei (sensory and motor) can be projected onto the surface of the fourth ventricle just above the point of intersection of an imaginary axial line connecting the upper edges of the facial colliculi with the medial edge of the SCP (see Fig. 12.4). Medial to the trigeminal nerve lies the abducens and facial nerves and nuclei. The abducens nucleus lies very close to the surface of the fourth ventricle (see Fig. 12.4) and projects its intrapontine fibers anteriorly to emerge from the pontomedullary sulcus just lateral to the eminence formed by the corticospinal tract (see Fig. 12.1). The more anterior motor nucleus of the facial nerve projects its intrapontine fibers posteromedially to form an inferior-to-superior and medial-to-lateral loop (a.k.a. internal genu of the facial nerve) around the abducens nucleus (see Fig. 12.4), which then emerges from the most lateral edge of the pontomedullary sulcus (see Fig. 12.1). It is imperative to understand not only the location of the facial nucleus but also the projection of its fibers, since the mass effect from a tumor can displace the normal trajectory. It is also important to learn the anatomical organization of the facial colliculi in order to recognize the safe entry zones related to its location. On the surface of the

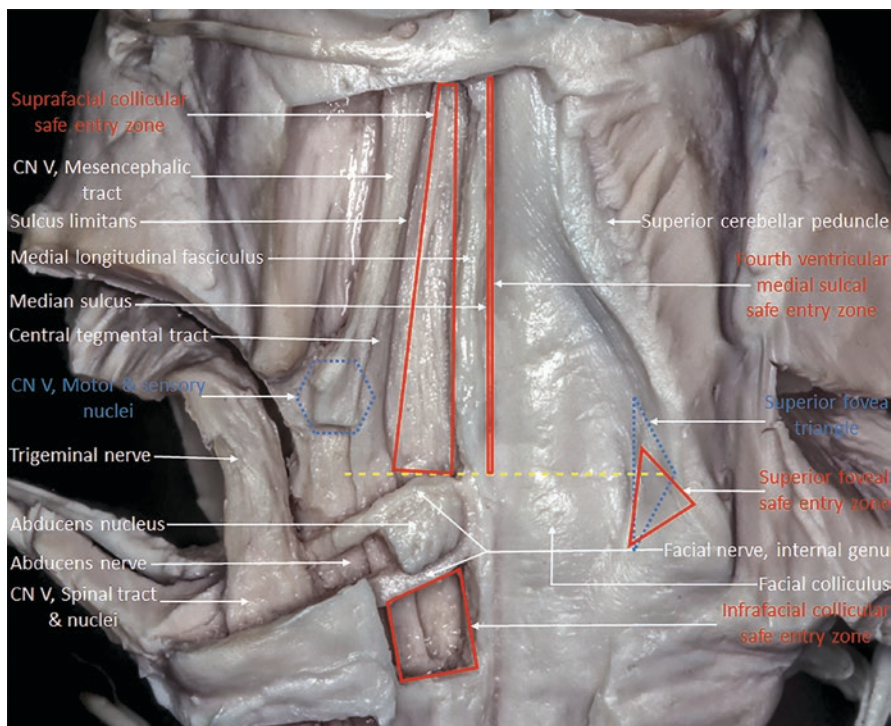


Fig. 12.4 Posterior surface of the pons. The approximate location of the superior fovea triangle and the motor/sensory nuclei of CN V are shown on the right (nondissected) and left (dissected) sides. The superior foveal (lateral sulcus limitans) safe entry zones coincides with the lower half of the superior fovea triangle. The fourth ventricular medial sulcal (interfacial), suprafacial collicular (suprafacial triangle), and infracollicular (infracollicular triangle) safe entry zones are also shown (see Sect. 12.3 of this chapter for full description of safe entry zones)

fourth ventricle, the facial colliculi reside in the median eminences that run vertically parallel to the median sulcus and are limited laterally by the sulcus limitans; the facial colliculi are formed by the abducens nuclei causing an impression on the surface of the fourth ventricle (see Fig. 12.4). The superior fovea is situated just lateral to the facial colliculus (see Fig. 12.4). At the level of pontomedullary junction, only the superior, medial and lateral vestibular nuclei can be noted, while the inferior vestibular nucleus is situated at the level of the upper medulla. The former three nuclei are located dorsal to the trigeminal spinal tract and superomedial to the upper part of the inferior cerebellar peduncle. Other nuclei and tracts residing in the posterior one-third of the pons and should be accounted for while planning for the surgical approach include the periaqueductal gray matter, dorsal and ventral trigeminothalamic tracts, rubrospinal tract, spinothalamic tract, medial lemniscus, raphe nuclei, tectospinal tract, reticular formation, lateral lemniscus and its nuclei, locus ceruleus, dorsal longitudinal fasciculus, ventral spinocerebellar tract, trapezoid body, superior olivary nucleus, among others.

The anterior prepontine and lateral cerebellopontine cisterns border the pons and house its associated neurovascular structures. The prepontine cistern is much smaller and bordered by the interpeduncular cistern superiorly, premedullary cistern inferiorly, and lateral cerebellopontine cisterns laterally. It contains the BA, lying on top of anteromedian pontomesencephalic vein, and the origins of the superior cerebellar arteries (SCAs), anterior inferior cerebellar arteries (AICAs), and the pontine perforating arteries (Fig. 12.5). The lateral cerebellopontine cisterns house most of the neurovascular structures related to the pons. The vein of pontomesencephalic sulcus runs in the pontomesencephalic sulcus and drains into the basal vein

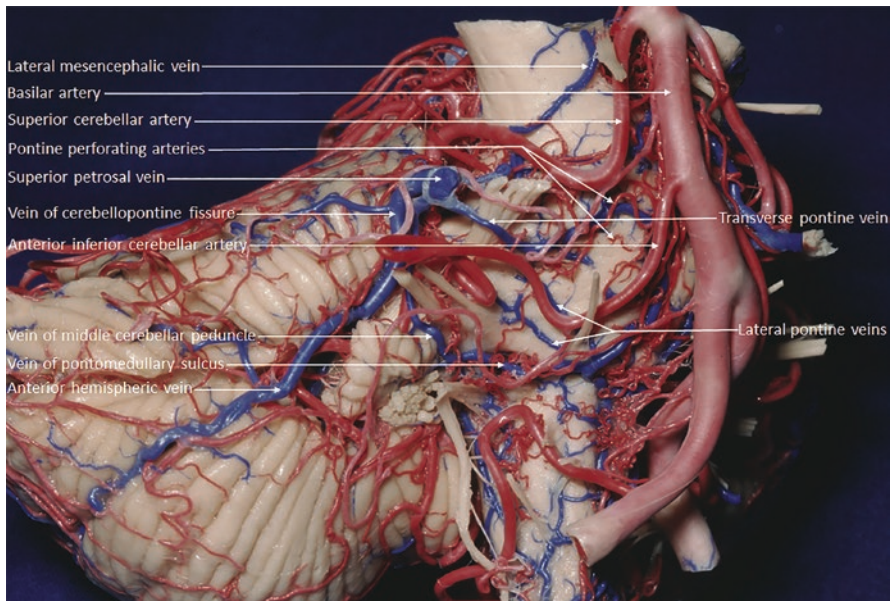


Fig. 12.5 Posterior fossa vessels and their relationship to the pons

of Rosenthal through the lateral mesencephalic vein, and the vein of pontomedullary sulcus runs in the pontomedullary sulcus and drains into the superior petrosal vein by means of the vein of the MCP (see Fig. 12.5). In between runs a complex and highly variable circuit of veins, the most prominent of which are the transverse pontine veins, anterolateral pontomesencephalic veins, lateral pontine veins, pontine trigeminal veins, and parts of the veins of cerebellopontine and cerebellomedullary fissures; all these veins eventually drain into either the superior petrosal vein or the basal vein of Rosenthal (see Fig. 12.5). The SCA originates from the BA at the level of the pontomesencephalic sulcus, and the AICA originates at variable levels of the lower half of the BA; in the lateral cerebellopontine cistern, s1 and s2 of SCA run close to the midbrain and SCP, whereas a1 and a2 of AICA are associated with the abducens, facial and vestibulocochlear nerves and the MCP. Finally, portions of CNs V-VIII initially run in the lateral cerebellopontine cistern (see Fig. 12.1) before entering/exiting through their corresponding foramina.

12.3 Safe Entry Zones

The entry zone for exophytic tumors is usually straightforward, where resection begins with a entry point and trajectory that trails the exophytic part, followed by debulking the tumor center, attempting to create a surgical plane, and ends with careful removal of the remaining tumor that is closest to the pontine tissue. Preoperative planning using advanced imaging techniques such as diffusion tensor imaging is imperative for success in this complex neurovascular anatomical region. If removing the rest of the tumor will create neurological deficits, surgical resection is halted, and postoperative adjuvant therapies are pursued as needed.

Pontine lesions that do not reach the surface present an additional challenge to the surgeon, who will have to plan not only the shortest and least invasive surgical corridor and approach, but also identify the safest entry into the pontine tissue and secure the lesion without postoperative sequelae. The following safe entry zones into the pons are discussed in the context of non-distorted anatomy, a rule that typically applies to small lesions exhibiting minimal mass effect and distortion of nearby structures. However, given that a large number of important tracts and nuclei swarm in the small volume of the pons, one should consider that the safe entry zones described in the literature may ‘no longer be safe’ secondary to distortion of the normal anatomy; preoperative vigilant analysis of the imaging studies is required to devise an alternative, safe plan, which is also significantly facilitated by detailed overview of the intraoperative anatomy and intraoperative monitoring and mapping.

12.3.1 *Peritrigeminal*

The peritrigeminal safe entry zone permits access to the anterolateral pons through a narrow surgical window, which is suitable for obtaining a biopsy or partial resection. It also can be used for resection of cavernous malformations in proximity [7].

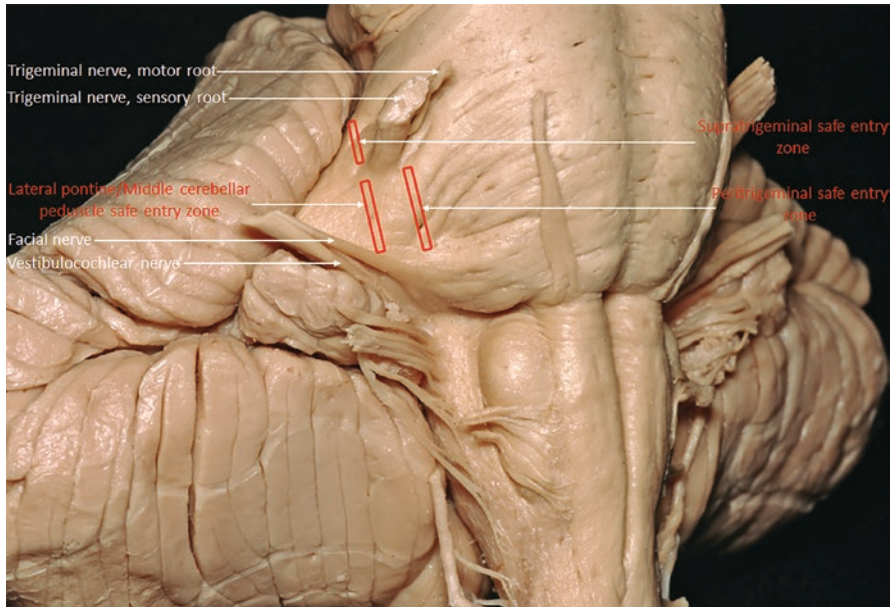


Fig. 12.6 Approximate locations of the peritrigeminal, supratrigeminal and lateral pontine (middle cerebellar peduncle) safe entry zones (see Sect. 12.3 of this chapter for full description of safe entry zones)

Recalde and colleagues [8] described the peritrigeminal entry zone as one that starts rostrally, just in front of the takeoff of the trigeminal nerve (Fig. 12.6). Inside the pontine tissue, the trajectory proceeds through the white matter in a vertical plane that is anterior and parallel to the plane formed by the motor/main sensory nuclei of trigeminal nerve and their laterally projecting fibers, and posterior to the lateral edge of the descending corticospinal tracts (Fig. 12.7). On the axial plane, the mean width of the corridor is around 4–5 mm [8], and the length is around 9–13 mm [8]. Staying within this plane and avoiding dissection above the trigeminal or below the facial/vestibulocochlear nerves should be safe if normal anatomy is not distorted.

12.3.2 *Supratrigeminal*

The supratrigeminal safe entry zone permits access to the anterolateral pons. On surface anatomy, it corresponds to a vertical line on the MCP, where the pontomesencephalic sulcus and superior edge of the origin of the trigeminal nerve mark its rostral and caudal limits, respectively (see Fig. 12.6). Inside the pontine tissue, the trajectory proceeds in a coronal plane that runs in the middle of and along the MCP and pontine transverse fibers (see Fig. 12.7). After entering through the described surface landmarks, extending the dissection within the middle one-third of the pons on axial cuts is allowed, but with extreme caution so as not to reach the posterior

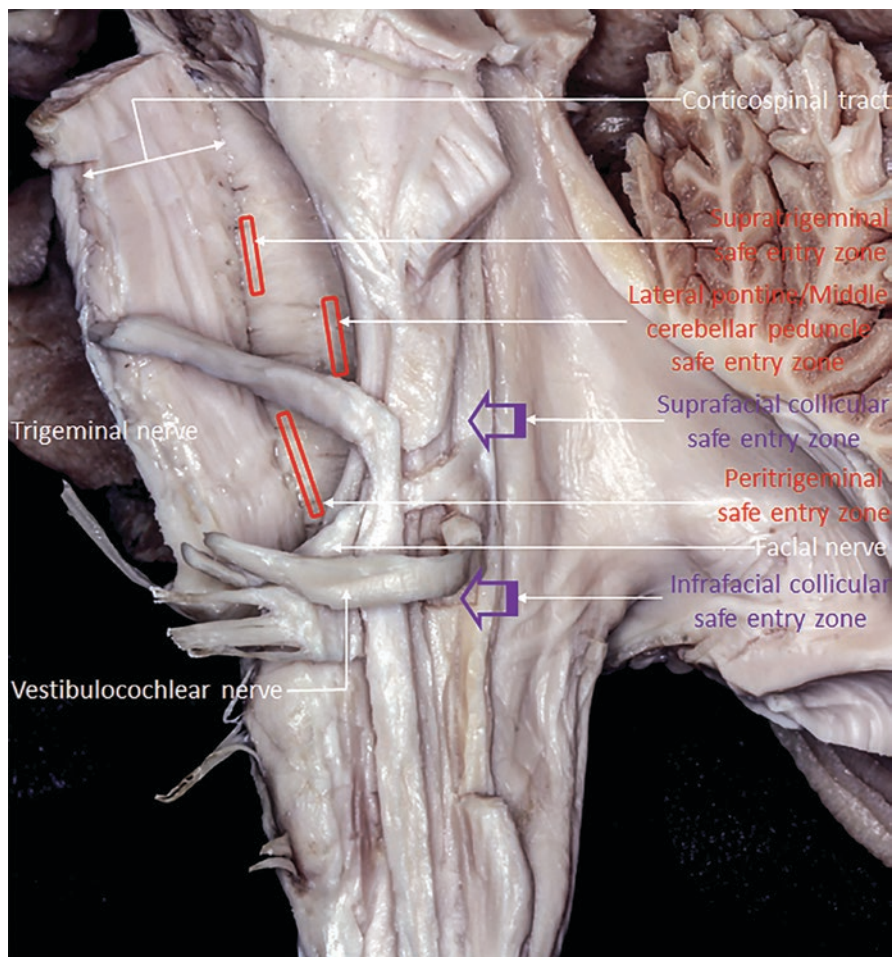


Fig. 12.7 Lateral dissection into the pontine substance, showing the approximate intrapontine trajectories of the peritrigeminal, supratrigeminal, lateral pontine (middle cerebellar peduncle), suprafacial collicular and infrafacial collicular safe entry zones (see Sect. 12.3 of this chapter for full description of safe entry zones)

edge of the descending corticospinal tracts (use of white matter dissection monitoring is important) or the anterior limit of the dorsal one-third of the pons.

12.3.3 *Lateral Pontine (Middle Cerebellar Peduncle)*

The lateral pontine (MCP) safe entry zone lies in the vicinity of the trigeminal root entry zone and allows for resection of anterolateral pontine lesions. Some experts consider this entry zone as a natural elongation of the supratrigeminal safe entry

zone; it lies on the same line of the supratrigeminal safe entry zone, separated only by the trigeminal nerve root. This safe corridor is situated on the junction between the MCP and the pons, with the trigeminal nerve and facial-vestibulocochlear complex as its rostral and caudal limits, respectively [9] (see Fig. 12.6). Inside the pontine tissue, the trajectory proceeds superior and almost perpendicular to the intrapontine segment of the trigeminal nerve (see Fig. 12.7). Similar to the peritrigeminal and supratrigeminal safe entry zones, the lateral pontine safe entry zone allows relatively safe dissection posterior and lateral to the corticospinal tracts. A combination of this entry zone and the supratrigeminal safe entry zone can potentially permit a wide safe corridor to the anterolateral pons. Alternatively, utilizing this corridor on its own gives a relatively narrow corridor that does not allow a lot of manipulation [2].

12.3.4 Suprafacial Collicular (Suprafacial Triangle)

The facial colliculus is a prominence visualized on the floor of the fourth ventricle, corresponding to the facial nerve looping around the nucleus of the abducens nerve in the posterior one-third of the lower pons. The suprafacial collicular safe entry zone permits access to the dorsal pons through the fourth ventricular floor. On surface anatomy, it corresponds to a quadrilateral (also referred to as a triangle), where the superior edge of the facial colliculus (base of quadrilateral lies on top of it) marks its caudal limit, the frenulum veli (through which the trochlear nerve crosses) marks its rostral limit, the MLF marks its medial limit, and the sulcus limitans marks its lateral limit (see Fig. 12.4). Inside the pontine tissue, the trajectory proceeds in a sagittal plane that is strictly parallel to the median sagittal plane (see Fig. 12.7). The longitudinal arm that is parallel to the MLF is around 13–14 mm in length (between facial colliculus and CN IV decussation); this line should stretch around 0.6 mm away from the midline in order to avoid MLF injury [10]. The main structure that limits the lateral dissection is the motor nucleus of the trigeminal nerve, which is located at 6–7 mm from midline [10]. Within this plane, the surgeon should avoid dissecting deeper than 4–5 mm (medial lemniscus depth [11]) on axial cuts.

12.3.5 Infracollicular (Infracollicular Triangle)

The infracollicular safe entry zone is another area that permits a relatively safe corridor to the dorsal pons through the floor of the fourth ventricle. Like its suprafacial collicular counterpart, it is shaped as quadrilateral, where the inferior edge of the facial colliculus (formed by the inferior intrapontine segment of the facial nerve) marks its rostral limit, the superior edge of the hypoglossal trigone, harboring the hypoglossal nerve and the dorsal nucleus of the vagal nerve, marks its caudal limit, the MLF marks its medial border, and the facial nerve (and the facial

nucleus and nucleus ambiguus just below the ventricular surface) marks its lateral limit (see Fig. 12.4). Inside the pontine tissue, the trajectory proceeds in the sagittal planes (within the limits of the quadrilateral) that are parallel to the median sagittal plane (see Fig. 12.7). As in the case of suprafacial collicular safe entry zone, the surgeon should avoid dissecting deeper than 4–5 mm on axial cuts. The maximum length of the quadrilateral from hypoglossal trigone to the facial colliculus was found to be around 9 mm [10].

12.3.6 Superior Foveal (Lateral Sulcus Limitans)

The superior foveal zone is another relatively safe entry zone that permits access to the dorsal pons through the fourth ventricular floor. On surface anatomy, it corresponds to the lower half of the superior fovea triangle, where the most lateral point of the upper fourth ventricle coincides with its apex, the SCP marks its superolateral edge, the vestibular area marks its inferolateral edge, and the sulcus limitans marks its base medially (see Fig. 12.4). Inside the pontine tissue, the trajectory proceeds in the lower half of the triangle in a plane parallel to the median sagittal plane, keeping in mind that the motor and sensory nuclei of the trigeminal nerve sit deep to the superolateral edge (medial edge of the SCP) of the triangle (see Fig. 12.7).

12.3.7 Fourth Ventricular Median Sulcal (Interfacial)

The median sulcal safe entry zone permits access to the dorsal pons through the floor of the fourth ventricle. The main limitation for this approach is the potential risk of injuring midline decussating fibers or the MLF due to excessive lateral retraction. On surface anatomy, it corresponds to the median sulcus, where the frenulum veli (through which the trochlear nerve crosses) marks its superior limit, and a transvers line connecting the lower edges of the facial colliculi marks its inferior limit [12] (see Fig. 12.4). Inside the pontine tissue, the trajectory proceeds strictly in the median sagittal plane, keeping in mind that both MLFs run immediately lateral to the median sulcus and close to the surface. Note that even mild lateral retraction can injure the MLFs and should be avoided as well.

12.3.8 Superior Ventral Pontine

Anterior pontine safe entry zones are not as feasible as their anterolateral and posterior counterparts due to the dense eloquence imposed by the median location of the BA and its pontine perforating branches, as well as the corticospinal tracts, which descend immediately lateral to the trajectory of the BA. One safe entry zone described by Cavalheiro and colleagues [13] permits access to the superior ventral

pons. Note that the authors labeled it as “supratrigeminal”; to avoid confusion with the supratrigeminal safe entry zone discussed in Sect. 12.3.2, we will refer to it as “superior ventral pontine” safe entry zone. On surface anatomy, it corresponds to a vertical line (around 4 mm), where the pontomesencephalic sulcus at the level of the origin of oculomotor nerve marks its rostral limit, a line connecting the pontine surface origins of the trigeminal nerves marks its caudal limit, the BA (and any of its pontine perforating branches originating close to this vertical line) marks its medial limit, and the corticospinal tract marks its lateral limit (see Fig. 12.1). Inside the pontine tissue, the trajectory proceeds in a plane that is strictly parallel to the median sagittal plane. Note that this entry zones takes advantage of the obliquely oriented (lateral to medial) descending tracts (medial frontopontine, middle corticospinal, and lateral temporopontine tracts); therefore, entry above the level of the line connecting the surface origins of the trigeminal nerves does not risk injuring the corticospinal tracts, although some frontopontine fibers may be disrupted by dissection in that plane.

12.4 Anterior (Ventral) Pons

12.4.1 *Orbito-Fronto-Zygomatic Approach*

The orbito-fronto-zygomatic approach, a modification of the extended pterional and supraorbital craniotomy, allows a relatively convenient angle to access the upper ventral pons through the superior ventral pontine safe entry zone discussed in Sect. 12.3.8. It is rarely utilized to tackle pontine lesions as it only exposes the upper pons; it is not practical to approach lesions localizing towards the middle and inferior pons.

12.4.1.1 Surgical Setup and Patient Positioning

The patient is placed in a supine position with his/her head turned slightly (15–30°) to the opposite side, along with slight hyperextension. This position allows for a convenient corridor from above the orbit to the upper brainstem and uses gravity to allow the brain to fall from the anterior skull base, decreasing the need for brain retraction.

12.4.1.2 Surgical Corridor(s) and Approach

A hemicoronal or fronto-temporal incision begins in the preauricular area, extending upwards towards the vertex in a straight line and then curves forward towards the midline. The skin flap is reflected anteriorly along with the temporal fascia. The next

step is to expose the zygomatic arch from its root at the temporal bone to its frontal process; an interfascial dissection is performed. A wide pterional craniotomy is performed, followed by an orbitozygomatic osteotomy. The dura is opened widely to allow full dissection of the sylvian fissure. The dissection is carried towards the carotico-oculomotor triangle, then to the interpeduncular cistern. This approach sufficiently exposes the midbrain, pontomesencephalic junction, and upper anterior pons.

12.4.2 Endoscopic Endonasal Transclival Approach (Fig. 12.8)

The endoscopic endonasal approach (EEA) has been proposed as a potential alternative for ventral brainstem lesions [14]. It is currently utilized for superficial or exophytic small lesions. The BA and its perforating branches as well as the cortico-spinal tracts are the most eloquent structures in the ventral brainstem and must be cautiously localized after dural opening [15]. The abducens nerves, which have an anterolateral course, are also at risk of injury during this approach.

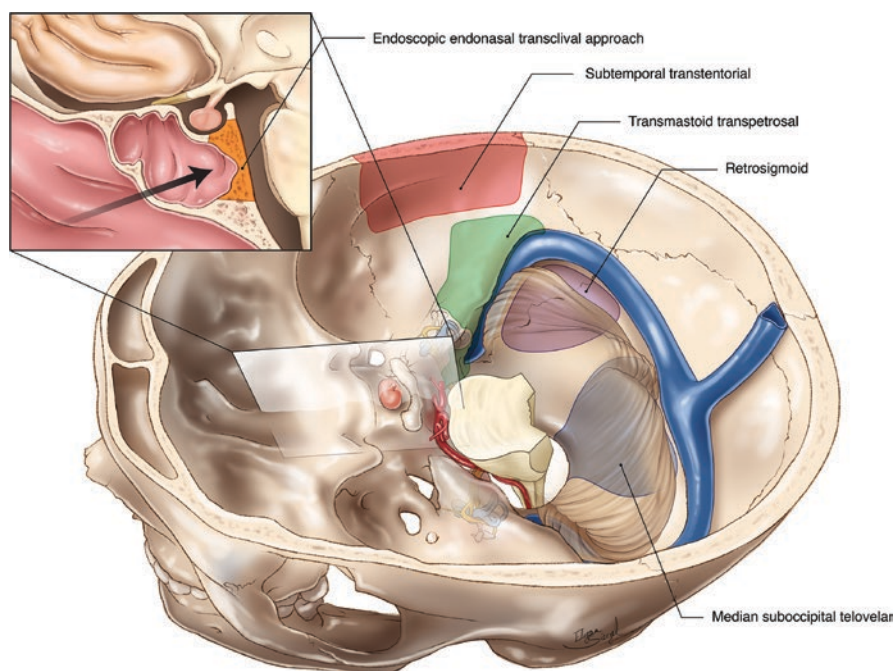


Fig. 12.8 Schematic illustration of various surgical approaches used to reach the anterior, anterolateral and posterior surfaces of the pons (printed with permission from Mohammad Hassan A. Noureldine, Nir Shimony, and George I. Jallo)

12.4.2.1 Surgical Setup and Patient Positioning

The distinct surgical trajectory of the EEA dictates a different surgical setup and patient positioning compared to other classic approaches to the pons. This is a relatively new approach and not very well reported in the literature. It demands high skills in the realm of endonasal endoscopic surgeries and, in many cases, a collaboration between the ear, nose and throat (ENT) and neurosurgery teams. The patient is positioned supine with a slight neck extension and a slight head rotation towards the surgeon's side; right-handed surgeons will find it easier to operate from the right side of the patient, and vice versa.

12.4.2.2 Surgical Corridor(s) and Approach

Inspection of the anterior compartment of the nasal cavity gives an idea about any variations (septal deviation; size of turbinates) that may alter normal anatomy. The use of preoperative computed tomography (CT) scan is recommended to evaluate the presence of such variations and help in identifying the optimal alternate trajectory; the same CT scan can also be used for stereotactic navigation. The initial approach is very much similar to any other trans-sphenoidal approach to reach the sellar region, yet in this case there is no need to dissect towards the ethmoid area since the surgical trajectory is directed to a lower level. The extent of bone exposure (e.g., need for wide trans-sphenoidal dissection) depends on the location and rostro-caudal extension of the pathology within the pons. For tumors extending towards the upper part of the pons and pontomesencephalic sulcus, sphenoidal dissection is required to achieve the correct trajectory.

Prior to surgery, the nasal cavity is infiltrated with lidocaine/epinephrine-soaked gauzes for 5–10 minutes to shrink the conchal mucosa and induce vasospasm for better hemostasis. Upon introducing the endoscope into the nostril, the nasal septum is seen medially and the middle and inferior turbinates laterally. The use of stereotactic navigation can be very helpful. The endoscope is then passed through the middle meatus, the passage between the middle and inferior nasal conchae, and the middle turbinate is lateralized or preferably resected for better exposure and identification of critical neurovascular structures, as well as to provide more space for the simultaneous use of the endoscope and several instruments later during the procedure. After removing the middle turbinate, the uncinate process may be seen just anterior to the ethmoid bulla on the lateral side of the surgical view. Note that the superior half of the uncinate process is part of the medial orbital wall, while the inferior half forms the medial maxillary wall. On the medial side of the surgical view, the choana and sphenoid rostrum can be noted. Before proceeding with any further dissection, the sphenopalatine artery should be identified at the sphenopalatine foramen of the palatine bone by following the posterior root extension of the resected middle turbinate; this artery should be preserved as it constitutes the main vascular supply of the nasal septal flap, which is being used in most of these cases. The immediate next step is to identify the Vidian nerve, a key landmark that will

help to locate and prevent injury to the internal carotid artery (ICA) while drilling the clivus. The location of the Vidian nerve can be approximated at around 5 mm lateral to the midline and 10 mm superior to the choana. To find the exact location, however, the palatovaginal bundle running under the mucosa of the choanal roof is followed to the sphenopalatine ganglion, pointing to the Vidian nerve as it passes through the pterygoid canal. Then, the posterior septum and posterior/inferior segments of the vomer are resected to allow for bilateral exposure of the sphenoid sinus (covering the upper one-third of the clivus) superiorly and the lower two-thirds of the clivus and odontoid/C1 through the choana inferiorly. Before proceeding with clival drilling and opening, the surgeon should develop an understanding of the complete relationship of the ICA anatomy to the planned opening.

A pontine pathology localized at or extending into the level of the upper one-third of the clivus necessitates the creation of a trans-sphenoidal corridor. The same steps of the trans-nasal corridor are repeated for the trans-sphenoid corridor. The sphenoid ostia, which may be hidden deep to and necessitating resection of the inferior one-third of the superior turbinate, are bilaterally enlarged inferiorly and medially, followed by removing the anterior wall of the sphenoid sinus bilaterally. Removing the intersinus septae can be tricky as the fractured segments may twist and injure the carotid arteries; therefore, drilling the intersinus septum until it flushes to the posterior wall of the sphenoid is preferred over fracturing it with a rongeur. The mucosa is then scraped off the inside walls of the sinus. Careful identification of the planum, tuberculum, sella, medial optico-carotid recess (at the inferomedial angle between ICA and optic nerve), carotid arteries, lateral optico-carotid recess (at the superolateral angle between ICA and optic nerve), cavernous sinuses, optic nerves, Vidian nerves/pterygoid canals, and clival process of the sphenoid bone is imperative before proceeding with the trans-clival approach.

The trans-clival approach begins with maximizing the approach exposure to its natural limits, i.e. pituitary gland superiorly, ICAs and eustachian tubes laterally, and soft palate floor inferiorly. In cases where tumor extension demands exposing the anterior arch of C1, soft tissue dissection should proceed by removing the nasopharyngeal mucosa and pharyngobasilar fascia, followed by sequential incision of the longus capitis, rectus capitis anterior, and atlanto-occipital ligaments; this will fully expose the clivus laterally and inferiorly as well as the anterior arch of the atlas, dens of the axis, and bilateral occipital condyles. The anterior arch of C1 and sometimes the upper part of the dens can be resected, which according to several publications does not cause occipitocervical instability unless the patient had stability and alignment issues before surgery [16]. Again, before drilling the clivus, meticulous overview of the planned opening should be undertaken by the surgical team; the lateral clival limits are identified by the location of the Vidian nerve, which points to the turning of the ICA at the foramen lacerum, and the location of the supracondylar groove, where CN XII crosses through the hypoglossal canal that is located just posterolateral to the groove [17]. The clivus is then cautiously micro-drilled in a way that allows sufficient exposure for tumor resection and can be extended from the dorsum sellae to the anterior arch of atlas; controlling bleeding from the basilar venous plexus while drilling is critical to maintain a clear surgical

view, keeping in mind the nonuniform rostro-caudal bony thickness of the clivus. Given that the most rostral edge of the clivus extends behind the posterior sellar wall, in some cases, the sella turcica may need to be opened, the posterior clinoid processes removed, and the pituitary gland lateralized or pushed superiorly to provide further rostral access to the clivus. The intercavernous sinus is cauterized, and the dura is opened in a trap-door shape and reflected towards the right or left side; care should be taken not to injure the transdural segment of the abducens nerve as it crosses towards Dorello's canal at around 5 mm medial to the lateral edge of the exposure, just above a horizontal line connecting the foramina lacerum [18]. Opening the dura exposes segment 4 of the vertebral arteries (VA), with the proximal anterior spinal artery and proximal posterior inferior cerebellar arteries (PICAs) (p1 segment) arising from VA medially and laterally, respectively; CN XII (in close association with PICAs) and the medullary pyramids at the preolivary sulcus; entire BA, with AICAs originating anywhere from its caudal half and associated with the cisternal segment of CN VI; many pontine perforators of different sizes arising from the lateral/posterior surfaces of the BA, which proceed to supply the ventrolateral pontine tissue; SCAs originating from the BA superiorly at the level of the pontomesencephalic sulcus; posterior cerebral arteries (PCAs) at the superior bifurcation of the BA (a.k.a. basilar apex); CN III crossing between the proximal segments of the PCAs and SCAs; thalamostriate perforating arteries that arise from the posterior/superior surfaces of the basilar apex and P1 PCAs; the ventral surface of the pontine belly; and a circuit of pontine veins. The far-medial (trans-condylar and trans-jugular tubercle) trans-clival approach is a coronal expansion of the dissection at the level of the lower one-third of the clivus, which provides further access to the ventrolateral surface of the pontomedullary junction. Specifically, the cisternal segments of the CN IX-XII and the inferior petrosal sinus as it enters the jugular foramen can be visible with the far-medial approach.

Note that different variations of the above steps could be implemented depending on the location and extension of the pathology within the prepontine cistern/pontine tissue as well as variant normal anatomy of the nasal cavity and skull base structures.

One of the drawbacks of the endoscopic endonasal trans-clival approach is the limited safe access it provides to tackle intraaxial pontine lesions. Lesions with exophytic components extending to the ventral pontine surface tend to create a safe passage by expanding and pushing viable brainstem tissue away from the trajectory. Hence, exophytic tumors can be tackled by debulking and piecemeal removal of the lesions with minimal risk of injury to critical nearby structures. Alternatively, ventral intraaxial lesions without an exophytic component demand utilizing ventral safe entry zones, which are currently limited to the superior ventral pontine safe entry zone (Sect. 12.3.8) (Fig. 12.9). To our knowledge, there is no reported ventral pontine safe entry zone to the inferior pons; intraaxial lesions located in this area are better tackled through anterolateral surgical approaches (Sect. 12.5) and safe entry zones (Sect. 12.3). When comparing the endoscopic approach to the microscopic anterolateral approaches, the endoscope can provide direct and clear view to the center of the pons and less so to the peritrigeminal area, which is more reachable with the classic microscopic approaches. Various cadaveric publications showed that one of the main obstacles is the BA and its perforators. The BA does not always

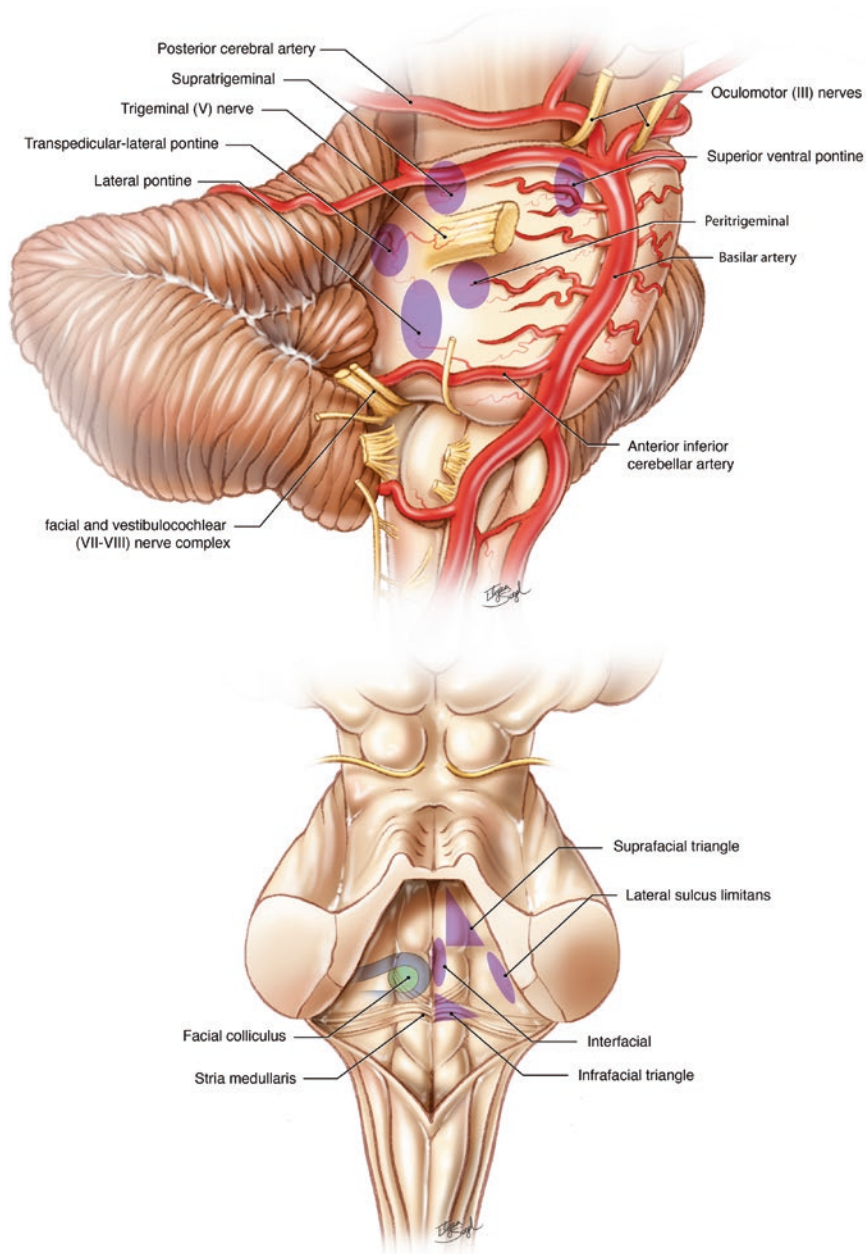


Fig. 12.9 Schematic illustration of the approximate locations of the pontine safe entry zones as reported in the literature (see Sect. 12.3 of this chapter for full description of safe entry zones) (printed with permission from Mohammad Hassan A. Noureldine, Nir Shimony, and George I. Jallo)

reside and course along the pontine midline [19]. Covering most of the anterior surface of the pons, the basilar perforators traverse and supply the superficial corticospinal tracts, medial lemniscus, MLF, CN VI nuclei, and other deep pontine structures. Injury to one of the perforators can lead to the devastating locked-in syndrome; therefore, unnecessary and excessive manipulation should be avoided [8, 19]. Locked-in syndrome is classically associated with a mid-basilar occlusion, which leads to infarction in the basis pontis [20]. The complex inner architecture of the pons, including the anteriorly located corticospinal tracts, mandates that the anterior approach should be advocated for those lesions that come to the surface.

Closure and skull base reconstruction following an endoscopic endonasal transclival approach are challenging due to the risk of developing high-flow cerebrospinal fluid (CSF) leak, intracranial infections, and pneumocephalus. Water-tight and air-tight closure should follow thorough hemostasis and can be accomplished by performing a multilayered reconstruction composed of returning the dural flap in place, followed by applying a synthetic/heterologous material (collagen matrix or acellular dermal matrix from cadaveric skin), free autograft (fascia lata, free cartilage/bone, or mucoperiosteal/mucoperichondrial autograft), fat graft of sufficient volume to fill up the clival defect, and the previously prepared nasal septal flap (other intranasal options include the inferior turbinate flap and the posterior, lateral nasal wall flap). It is prudent to securely cover all exposed intracranial vessels, CNs and brain tissue with the innermost layer to prevent desiccation, totally separate the cranial cavity from the sinonasal cavities, and leave no dead space behind the reconstructed area. Sneezing and cough suppressants are added to the medication list, and 2–3 days of lumbar CSF drainage is highly recommended in many cases in order to divert the burden of CSF flow from the surgical bed and potential skull base defect.

12.5 Anterolateral Pons

For pathologies residing in the anterolateral pons, the workhorse approach is mostly the retrosigmoid. Yet, the surgeon should keep in mind the exact lesion location in the anterolateral pons, since a higher location might require or suggest the addition of a petrosectomy, whereas in some cases, the more orthogonal trajectory to the lateral pons may necessitate a presigmoid approach.

12.5.1 *Transpetrosal (See Fig. 12.8)*

A large portion of the anterolateral pons is hindered by the petrous bone. An anterior petrosectomy to reach the upper pons and a posterior petrosectomy (described in this section) help to significantly increase the exposure.

Three transmastoid transpetrosal approaches exist: retrolabyrinthine, translabyrinthine, and transcochlear. All three essentially fall into a spectrum of graded dissection through the posterior petrous ridge, where surgical exposure is balanced by

surgical morbidity (i.e., higher chance for hearing loss with/without facial nerve palsy). Yet, the transmastoid transpetrosal approaches, specifically the transcochlear, provide wide access to the anterolateral pons. When patients present with irreversible hearing loss and/or facial nerve palsy secondary to pontine lesions damaging the facial/vestibulocochlear nuclei/nerves, surgeons are more confident to utilize the advantages of surgical access offered by the transcochlear approach, which is the most invasive among the three, but provides maximal access to lesions residing in the anterolateral pons.

12.5.1.1 Surgical Setup and Patient Positioning

Proper patient positioning for the transpetrosal presigmoid approach is of utmost importance to allow easier maneuvering and efficient drilling as well as prevent early fatigue of the surgeon's hands by bringing the surface mastoid part of the temporal bone into a position that is perpendicular to the sight of the surgeon (who is sitting in a neutral position). All three presigmoid approaches can be positioned in a similar manner. Some surgeons advocate a simple supine positioning with a shoulder roll under the ipsilateral shoulder and the head turned to the opposite side. Yet, most surgeons prefer the lateral positioning, where the patient is placed in a lateral decubitus position (resting on the side contralateral to the lesion), the head is fixed with pins and flexed, the neck is set in slight lateral flexion (head tilted towards the ground) and ipsilateral rotation, and the operative table is tilted in reverse Trendelenburg position. Additionally, changing the angles of the operative table and microscope allows for direct visualization of various parts of the surgical field at different steps of the approach and, most importantly, the prepontine cistern and anterolateral pons after total petrosectomy.

12.5.1.2 Surgical Corridor(s) and Approach

The transpetrosal approach should be performed with neuromonitoring, focusing on hearing preservation whenever possible and facial nerve function, in addition to CNs and corticospinal tracts monitoring for lesion resection within the pons. As a general rule, transmastoid approaches has a C-shaped postauricular suboccipital incision that starts at around 1 cm above the vertex of the pinna, loops around the helix with a width of around 5 cm from the retroauricular fold and ends on the sternocleidomastoid muscle at approximately 1 cm below the lobule of the pinna. The incision will expose the posterior one-third of the temporalis muscle, the posterior auricular muscle, and the insertion and superior part of the belly of the sternocleidomastoid muscle; it is preferable to recognize and dislodge these muscle attachments from the underlying bone without separating them from the overlying skin, reflect the whole musculocutaneous flap anteriorly over the ear, and, if necessary, secure it using fish hook retractors. This exposes the attachments of the longissimus capitis (anterior) and splenius capitis (posterior) muscles as well as the occipital artery (coursing in the deep layer of the splenius capitis muscle and piercing the superficial

fascia between the sternocleidomastoid and trapezius muscles near the superior nuchal line), which are reflected inferiorly without sacrificing or injuring the occipital artery. The posterior belly of the digastric muscle is visible at this stage, and the mastoid process of the temporal bone is clear for craniectomy. This opening exposes the Asterion, i.e., the intersection of the lambdoid, squamosal and occipitomastoid sutures, which is the point of possible junction between the transverse and sigmoid sinus. Navigation is not necessary to locate the sinuses but can help in orientation. The location of several other critical structures can also be inferred from surface landmarks with an acceptable level of certainty: the base of the transverse sinus is usually located at the same level of the superior nuchal line; the point of intersection of the squamosal and parietomastoid sutures predicts the location of the sinodural angle (at the junction of sigmoid sinus and superior petrosal sinus along the temporal lobe dura; a.k.a. Citelli's angle); the anterior aspect of the posterior belly of the digastric muscle helps to delineate the intra-mastoid course of the sigmoid sinus; the temporal line (posterior extension of the upper edge of the zygomatic process root, which becomes the supramastoid crest further posteriorly) defines the levels of the tentorium and the tegmen tympani, i.e. roof of the temporal bone separating the tympanic and cranial cavities; the suprameatal triangle (supero-posterior to the external acoustic meatus and spine of Henle and inferior to the temporal line; a.k.a. MacEwen's triangle) sits on top of the mastoid antrum (at around 1.5–2 cm in depth), and helps to locate the mastoid segment of the facial nerve (slightly anterior and inferior to the mastoid antrum) and the lateral semicircular canal (deep and posterior to the spine of Henle).

The least invasive of the three transmastoid approaches is the *retrolabyrinthine*, which is limited to drilling the mastoid process down until, but without violating, the wall of the lateral semicircular canal. The first step is to remove the mastoid cortical layer (may be preserved for later use in reconstruction), followed by careful and even drilling of the cancellous bone of mastoid process. The sigmoid sinus is initially encountered as the bone turns bluish and denser towards the digastric muscle anteriorly. In the depth of MacEwen's triangle, the change in bone consistency from cancellous to dense should alert the surgeon about the proximity of the lateral semicircular canal, which may be the next critical structure to be encountered. Nonetheless, a dense bony plate (inferior extension of the petrosquamosal suture into the mastoid air cells; a.k.a. Koerner's septum) may be encountered before reaching, and should not be mistaken for, the wall of the lateral semicircular canal (identified as a faint blue line corresponding to the canal lumen appearing through the thin bony wall). The next step is to further expose Trautmann's triangle, which is bordered by the sinodural angle superiorly (base), posterior semicircular canal anteriorly, sigmoid sinus posteriorly, and jugular bulb inferiorly (vertex). The facial nerve runs perpendicular and inferior to the lateral semicircular canal, and vigilant drilling in that area exposes the trajectory of the facial nerve as it enters the facial (fallopian) canal. The retrofacial recess is entered with posterior expansion of the exposure until the sigmoid sinus is reached; the endolymphatic sac is noted in close relationship to the posterior semicircular canal, both of which should be preserved to prevent hearing loss. The superior exposure limit is the sinodural angle, where the tegmen tympani is drilled superior to, and without damaging, the superior semicir-

cular canal (again, the lumen of which is identified as a faint blue line) until the superior petrosal sinus is seen running parallel to the temporal lobe dura. Dural opening will follow, with the presigmoid dura freed until just behind the posterior semicircular canal [21]. The dura is usually opened in a T-shape while the tentorium is split until the incisura, which allows for better manipulation of the dura and better control over and view of the trigeminal area. The T-shaped opening is created along the lines forming the sinodural angle, i.e., infero-superior line parallel to the sigmoid sinus and antero-posterior line parallel to the temporal lobe dura; the last dural cut is placed across the superior petrosal sinus, which is ligated on both ends and transposed with the dural flap anteriorly. As mentioned earlier, the retrolabyrinthine approach provide a small working window (posterior to the vestibular complex) into the lateral aspect of the pons; the working window can be expanded as will be shown below in the translabyrinthine and transcochlear approaches, however, at the expense of hearing loss and facial nerve palsy.

The translabyrinthine approach is less utilized as the risk of perioperative morbidity is much higher. It proceeds with drilling through and exposing the lumen of the semicircular canals, the goal of which is to identify the borders of the internal acoustic meatus. The roof of the internal acoustic meatus is located deep to a line connecting the sinodural angle with the (anterior) ampulla of the superior semicircular canal, or it can be identified by exposing the subarcuate artery, located deep inside the semicircle of the superior semicircular canal and sitting on top of the roof. The floor of the internal acoustic meatus can be anticipated by drilling through the semicircular canals to reach the ampulla of the posterior semicircular canal, sitting on top of the floor. The posterior wall of the internal acoustic meatus is exposed by direct drilling into the vestibule, which is drilled down to reveal the dura covering the neurovascular structures within the internal acoustic meatus. At this posterior location, the dura covers the superior and inferior vestibular nerves, separated by the transverse (falciiform) crest. Note that a vertical bony crest (a.k.a. Bill's bar) divides the superior half of the meatus, where the translabyrinthine segment of the facial nerve runs supero-anteriorly and the superior vestibular nerve runs supero-posteriorly. In the inferior half of the meatus, the cochlear nerve runs infero-anteriorly, and the inferior vestibular nerve runs infero-posteriorly; the singular foramen, through which the singular (posterior) ampullary nerve runs, is located in the infero-posterior wall of the meatus, medial to the inferior vestibular nerve. It is also important to note that the labyrinthine artery and its branches run intradurally along with the vestibulocochlear nerve at variable locations and may inadvertently be injured while opening the dura posteriorly. The next step is to expose the different segments of the facial nerve. The translabyrinthine segment is first exposed by pulling out the superior vestibular nerve from the drilled internal acoustic meatus and transposing it posteriorly, followed by removing the vertical crest. The tympanic segment and the chorda tympani are skeletonized inside the middle ear, which is reached by drilling through the posterior wall of the external acoustic meatus. Opening the external acoustic meatus posteriorly exposes the incus and stapes as well as the chorda tympani as it extends from its anterior canaliculus, crosses through the tympanic cavity, and enters its posterior canaliculus just below the footplate of the stapes to join the facial nerve. Using fine drilling movements, the lateral

side (facing the surgeon sight) of the chorda tympani is initially exposed, followed by the posterior then anterior sides. To safely reroute the facial nerve, it is skeletonized from the internal acoustic meatus to the stylomastoid foramen. The facial canal is drilled open, and the greater superficial petrosal nerve is transected at the geniculate ganglion. At this point, the facial nerve can be freely, yet cautiously, transposed posteriorly to allow for proceeding with the transcochlear approach. Care should be taken not to apply traction or kinking to any segment of the facial nerve, especially near the geniculate ganglion, mastoid genu, and stylomastoid foramen where the nerve is most susceptible to injury, and it should be covered with wet patties at all times.

Once the malleus is removed, the cochlear promontory becomes almost completely visible. The promontory is then drilled to reach the cochlea, which is subsequently drilled starting with the basal turn; this exposes the petrous segment of the ICA. Further drilling medial to the ICA completes the anterior petrosectomy by reaching the petrous tip and clivus; the bone is also drilled inferiorly to reach the inferior petrosal sinus and jugular bulb, and the superior petrosal sinus is followed to Meckel's cave superiorly. This exposure grants maximal access to the dura covering the anterolateral pons and related structures, where its boundaries are: ICA anteriorly; lateral clivus medially; superior petrosal sinus superiorly; and below and medial to the inferior petrosal sinus into the clivus inferiorly.

Reflecting on what was discussed earlier in this section, the choice of the transmastoid transpetrosal approach depends on the type, location, and extent of involvement of the lesion in the pontine tissue. The extent of exposure, however, significantly differs between the three approaches, where the retrolabyrinthine grants a small working corridor and potentially limited access to the pons through one safe entry zone (peritrigeminal); the translabyrinthine increases the width of the corridor, allowing for better maneuverability and exposing more safe entry zones; and finally the transcochlear allows for the largest surgical corridor and grants access to potentially all safe entry zones through the anterolateral pons (peritrigeminal, lateral pontine (MCP), supratrigeminal) (see Fig. 12.9).

Closure proceeds with reapproximating the dural flap after hemostasis is secured. The facial nerve, which was transposed posteriorly earlier during the procedure, is returned to its anterior position, and the drilled cavity is filled with abdominal fat. If the cortical bone layer was preserved at the beginning of the surgery, cranioplasty proceeds with fixing the bone using screws and plates; otherwise, a titanium mesh cranioplasty reconstructs the mastoid bone defect. A lumbar drain may be placed for 2–3 days as prophylaxis against CSF leak.

12.5.2 Retrosigmoid

The retrosigmoid approach, as the name implies and in contrast to the transmastoid transpetrosal presigmoid approaches, dictates a surgical trajectory that starts posterior to the sigmoid sinus. It is considered the workhorse for posterior fossa pathologies, including brainstem pathologies, along with the telovelar and subtemporal

approaches. This approach permits a wide corridor to the ponto-cerebellar angle and the lateral pontine surface as well as to the MCP area [22]. This approach allows for a favorable angle of attack to enter the pons through the supratrigeminal and lateral pontine (MCP) safe entry zones, and a relatively good angle to the peritrigeminal safe entry zone, which is better exposed by the retrolabyrinthine approach [2]. Although the presigmoid approaches provide a more straightforward angle to the lateral pons and safe entry zones as mentioned above, they mandate more bone exposure and drilling that is time-consuming, and the risk for morbidity is higher [2]. The retrosigmoid approach is mostly composed of a lateral suboccipital craniotomy, with bony exposure almost all the way to the sigmoid sinus and above or at the same level of the transverse sinus. It exposes the posterolateral aspect of the cerebellopontine cistern and angle, reaching up to the tentorium and down to the lower cranial nerves, and permitting optimal access to the posterolateral pons and minimal access to the anterolateral pons and prepontine cistern.

12.5.2.1 Surgical Setup and Patient Positioning

The sitting, supine, oblique, and park-bench (or its variations) positions have been used for the retrosigmoid approach; the latter, however, is associated with less cerebellar retraction and lower risk of air embolism. In the sitting position, the head is turned to the ipsilateral shoulder in a sniffing position. In the lateral decubitus or park-bench position, the head may stay parallel to the floor or is slightly turned (usually contralateral but can be turned slightly ipsilateral as needed). When a more supine position is chosen, the degree of head rotation as well as lateral bending depends on the angle of attack and the way in which the surgeon would like the cerebellar hemisphere to fall away from the trajectory. Accordingly, it is imperative to thoroughly study the preoperative magnetic resonance imaging (MRI) scan and choose the best trajectory (between the petrous bone and cerebellar hemisphere) that intersects with the epicenter of the pontine lesion.

12.5.2.2 Surgical Corridor(s) and Approach

The classical skin incision for a retrosigmoid approach is a curvilinear postauricular/lateral suboccipital incision that starts at around 2 cm above the vertex of the pinna, loops around the helix with a width of around 6–8 cm from the retroauricular fold and ends at/beyond the posterior edge of the sternocleidomastoid muscle at approximately 1 cm below the tip of the mastoid process. Rough estimation of the Asterion location prior to opening the skin is highly recommended, given that the Asterion is thought to lie on top of the posterior edge of the sigmoid sinus, immediately after the sigmoid-transverse sinuses junction. However, variations do exist, and some surgeons advocate the use of navigation systems in planning for the approach and opening. On the skin, the location of the Asterion is estimated at the intersection between a line connecting the external occipital protuberance (a.k.a.inion) and the temporal/supramastoid line and a vertical line rising from the poste-

rior edge of the mastoid process. Posterior to the Asterion, the inferior margin of the transverse sinus coincides with the supramastoid line posteriorly, and the posterior edge of the sigmoid sinus is approximated to be deep to the vertical line at the posterior edge of the mastoid.

The skin is incised down to the superficial muscular fascia and periosteum. The posterior one-third of the temporalis, the posterior auricular, and the insertion of the sternocleidomastoid muscles are exposed. Care should be taken so that the great auricular and lesser occipital nerves are not transected as they cross over the upper segment of the sternocleidomastoid muscle. Contrary to the transmastoid transpetrosal approach, the temporalis is preserved in place. Access to the suboccipital triangle requires careful peeling of the muscular layers. The posterior auricular muscle, part of the sternocleidomastoid muscle, and the overlying skin (no need to fully separate the skin from these muscles) form the superficial musculocutaneous flap, which is reflected anteriorly over the ear, and if necessary, secured with fish hook retractors. At this stage, the longissimus capitis, splenius capitis, and occipital artery (should be preserved) are exposed. The longissimus capitis and nuchal muscles are transected at 1–2 cm below their attachments to the nuchal lines and reflected infero-medially. Careful dissection and hemostasis using a bipolar (rather than cautery) cannot be overemphasized while approaching the suboccipital triangle to avoid damage to the VA and branches of the occipital artery, as well as the occipital nerves.

The craniotomy begins with placing a burr hole over the transverse-sigmoid sinuses junction, which is usually adjacent to the Asterion; thorough review of the preoperative images, especially CT scans, will help to identify the relation between the Asterion and the sinuses junction. Using a footplate high-speed drill, a 4-cm circular bone flap is created without trespassing the inferior and posterior borders of the transverse and sigmoid sinuses, respectively. In order to get a better window on the vertical plane, some surgeons advocate for extending the craniotomy above the transverse sinus in a way that allows to pull the dura upwards with the sinus. Note that the mastoid emissary vein drains anywhere along the posterolateral border of the sigmoid sinus; if injured, bleeding from this vein may be profuse and should be differentiated from injury to the sigmoid sinus. Some surgeons also advocate further drilling over and up to the anterior border of the sigmoid, exposing it from the transverse-sigmoid junction to the jugular bulb, with/without inferior craniectomy to expose the foramen magnum and jugular foramen; this extension, for example, is indicated for large tumors spanning multiple levels of the brainstem and adjacent structures. Any exposed air cells should be closed with bone wax to prevent CSF leak postoperatively.

The dura is inspected for meningeal branches of the occipital and ascending pharyngeal arteries, which are coagulated *in situ* using a bipolar at a low voltage level. There are several acceptable ways to open the dura, such as a trapdoor and C-shaped (with base of the dural flap reflected anteriorly towards the ear), or the cruciate opening, where two incisions, spanning the craniotomy borders diagonally and intersecting in the middle, cut the dura into four triangular pieces, of which the bases of the superior and anterior pieces are parallel and closely related to the trans-

verse and sigmoid sinuses, respectively. Acting as a protective layer and to further pull the sinuses away from the craniotomy field, the latter two pieces are then reflected onto their respective sinuses (superiorly over the transverse and anteriorly over the sigmoid) and fixed with sutures. A variation of the cruciate is the T-shaped incision, again with two superior and anterior dural flaps reflected over the transverse and sigmoid sinuses, respectively. The immediate next step is to drain as much CSF as possible from the cisterna magna, cerebellopontine cistern, and/or superior cerebellar cistern to relieve intracranial pressure and allow for better inspection of the cerebellopontine angle contents. Some authors recommend the use of a lumbar drain immediately before surgery to achieve cerebellar relaxation [23].

The cerebellar hemisphere regresses after sufficient CSF drainage and is gently retracted to explore the cerebellopontine cistern; arachnoid dissection is started in the lateral portion of the cistern. It is important to recognize the borders of the cerebellopontine cistern, including the ambient cistern superiorly, the prepontine cistern antero-medially, and the cerebellomedullary cistern inferiorly, where the lateral pontomedullary membrane separates the two cisterns. Further postero-medial retraction of the cerebellar hemisphere exposes the facial-vestibulocochlear nerves bundle on its trajectory towards the internal acoustic meatus. Supero-medial to the facial-vestibulocochlear bundle are the large sensory and small motor segments of the trigeminal nerve. The next step is to identify the AICA and track it as much as possible proximally to its origin from the inferior half of the BA and distally towards the petrosal surface of the cerebellum. In the lateral portion of the cerebellopontine cistern, the AICA segment around the internal acoustic meatus is divided into premeatal, meatal and postmeatal parts. Important branches of the AICA that should be preserved are the labyrinthine artery, which supplies the facial and vestibulocochlear nerves, accompanies these nerves into the internal acoustic meatus, and, if damaged, can lead to hearing loss; the recurrent perforating arteries, which loop back and supply the brainstem tissue and, if damaged, can lead to ischemic strokes in various parts of the brainstem. Another structure that should be protected is the superior petrosal vein, which is an important vein that drains the lateral pontine surface and cerebellopontine fissure into the superior petrosal sinus and must be freed to avoid injuring it during dissection of the petrosal fissure.

Wide dissection of the cerebellopontine angle and petrosal fissure exposes the lateral pontine surface, allowing the surgeon to tackle pontine lesions through the lateral pontine (MCP) (most accessible), supratrigeminal and peritrigeminal (least accessible) safe entry zones (see Fig. 12.9). The lateral pontine (MCP) safe entry zone, located on the MCP, is of special interest, since it can be fully exposed without retraction or transgression of the cerebellar hemisphere if the petrosal fissure is split open between the superior and inferior semilunar lobules of the cerebellum. To enter the pons, a sharp neurotomy dissects the pia over the MCP, which is expanded rostro-caudally, then antero-posteriorly along the MCP fibers to reach the lesion in the anterior two-thirds of the pons. That said, preoperative planning and choice of the safe entry zone is an essential step for the retrosigmoid approach, which will guide the arachnoid dissection and creation of a surgical corridor towards that entry point, avoiding the risks of surgical exploration and retraction in this eloquent area.

Before closure, thorough hemostasis must be performed, especially on the lateral cerebellar surface, followed by removing blood products from the intracranial space by irrigation. Closure then proceeds with re-approximation and water-tight suturing of the dura and, if necessary, duraplasty using a synthetic dural substitute. Bone wax is re-applied to close air cells, and the bone flap is secured using titanium plates and screws. Finally, the myocutaneous flap is closed layer by layer in a water-tight fashion.

12.6 Posterior (Dorsal) Pons

12.6.1 Median Suboccipital Telovelar/Subvermian; Transvermian

Access to the posterior surface of the pons is achieved through the floor of the fourth ventricle. Safe entry zones through the floor of the fourth ventricle have long been discussed in the literature. The general approach is best performed through a classical median suboccipital craniotomy. The anatomical and technical pearls of the different suboccipital approaches utilized to reach the posterior pontine surface are discussed in this section.

12.6.1.1 Surgical Setup and Patient Positioning

The classic positioning is prone with the head in a concord position, where a high gel roll positioned across the table, just underneath the shoulder girdle, allows for more flexion of the neck without compromising the airway. The operative table is tilted around 30° in anti-Trendelenburg position, allowing for efficient venous drainage. The head and neck are then flexed up to 45° anteriorly, with or without lateral head rotation (depending on the location and extent of lateralization of the pontine lesion) to provide an optimal surgical view of the caudal cerebellar surface. The head is then rotated so that the chin approaches the neck while the occipital protuberance moves away from the neck; this maneuver opens the cervicomedullary junction and allows for a better angle of attack to the floor of the fourth ventricle.

Another option is the modified park-bench position with the head flexed and turned toward the floor. Similar to the concord position, this neck posture opens the space along the craniocervical junction and gives a better view of the floor of the fourth ventricle. In this positioning, the upper patient's shoulder is mobilized inferiorly and anteriorly, opening the craniocervical junction and allowing for more freedom for the surgeon.

Some surgeons advocate utilizing the sitting position, although it is less popular for pure fourth ventricle related tumors. A common benefit of both the modified park-bench and the sitting position is the fact that the gravity retracts the cerebellum away from the field as well as drain the blood out of the field. The sitting position, however, is inherently associated with potentially severe complications,

which include but are not limited to air embolism, CSF over-drainage and ventricular collapse, cardiopulmonary instability secondary to anesthesia, severe postoperative pneumocephalus, and cerebellar contusion due to retraction against gravity.

12.6.1.2 Surgical Corridor(s) and Approach

External anatomical landmarks are used to roughly estimate the location and course of critical structures such as the transverse sinus and torcula, of which the relationship to theinion can be estimated on preoperative imaging. The skin incision is a vertical midline extending from theinion to the spinous process of C2. To more accurately define the location of the torcula and the paramedian transverse sinus, it is important to note that the medial muscle insertion line crosses the lower margin of the torcula, whereas it lies lower than the inferior edge of the transverse sinus laterally in most cases [24]; specifically, the insertion of semispinalis capitis muscle does not cross the inferior edge of the transverse sinus by more than 5 mm, according to an anatomical study [25]. To avoid bleeding and excessive postoperative pain from the suboccipital paramedian muscles, the dissection is carried out in the midline nuchal ligament until the suboccipital bone is reached, and the caudal insertions of the rectus capitis posterior minor are disconnected from the posterior tubercle of C1, exposing the opisthion and posterior arch of C1. The myocutaneous flap is held open using a self-retaining retractor, where the median nuchal line (a.k.a. median occipital crest) is at the center of the field. The craniotomy of the occipital bone can be carried out in various ways. Some surgeons advocate performing two burr holes on both upper edges of the median nuchal line, exposing the cerebellar dura, followed by using either the craniotome or Kerrison punches of the internal occipital crest to connect the burr holes. Note that damaging the median dura might cause profuse bleeding from the occipital sinus, which may be relatively large in some patients. The footplate high-speed drill is then used to create two curved craniotomy lines starting from the burr holes, extending laterally to include all of the exposed bone, and ending on the posterolateral margins of the foramen magnum, as close as possible to the occipital condyles. Others advocate the use of a twist drill with the matchstick or cutting round-head drill bits to create the craniotomy path by gradually thinning the bone till the dura is exposed, and then complete the craniotomy using Kerrison punches. Care should be taken not to injure the VAs at this level. The bone flap is elevated using a blunt dissector and disconnected from the atlantooccipital ligament, exposing the underlying dura mater.

Variations in the size of the craniotomy and the need to resect the posterior arch of C1 are quite wide. The surgeon should plan the preferred angle of work that he would like to achieve. Resecting the posterior arch of C1, with or without the spinous process of C2 (we advocate not removing the posterior arch of C2 but only undercut it if needed to get more release; in most cases, no manipulation of C2 is required), allows for visualizing the fourth ventricle at a steeper angle, with the advantage of minimizing the need for retraction and avoiding splitting of the inferior vermis.

Dural opening usually follows the craniotomy and release of C1 with a Y-shaped dural incision. Dural channels and lakes maybe present at this level, and profuse bleeding may necessitate the use of hemoclips or sutures for rapid hemostasis. Again, care should be taken when approaching the occipital sinus, which may still be patent, especially in children. Then, the arachnoid membranes of the cerebellomedullary cistern are sharply dissected, allowing for CSF drainage and relaxation of the cerebellar hemispheres. The caudal components of the cerebellum, cerebellomedullary junction, first denticulate ligament, cervical root of CN XI, and VAs with/without the caudal loop of PICA, which proceeds into the cerebellomedullary fissure, are identified before entering the fourth ventricle. Lateral inspection after retraction of the brainstem reveals CN XII as it exits through the hypoglossal canal, whereas retraction of the cerebellum exposes CN X and the fourth ventricular choroid plexus. The telovelar approach is the classic trajectory for accessing the fourth ventricle. The cerebellar tonsils are carefully mobilized so as not to injure the PICAs as they enter the vallecula, exposing the foramen of Magendie. Enlarging the foramen of Magendie is performed by dissecting the tela choroidea away from the taenia of the medulla, and the caudal half of the fourth ventricular floor is exposed after gentle retraction of the vermis and medullary velum. At this point, the area postrema, hypoglossal and vagal trigones, and medullary striae are identified. Although splitting of the caudal vermis (a.k.a. transvermian approach) allows for direct access to the cranial half of the fourth ventricular floor, this maneuver is strongly discouraged as it may lead to postoperative truncal ataxia. A better alternative is to further dissect the tela choroidea and change the angle of the microscope; this will significantly expose the cranial half of the fourth ventricular floor, superior medullary velum, and cerebral aqueduct, albeit at the expense of working at an angle $<90^\circ$. The facial colliculi, median eminences, median sulcus, and sulci limitans can be seen at this point. Further lateral dissection and inspection within the fourth ventricle reveals, from caudal to cranial, the lateral recess, vestibular area, and locus coeruleus area.

At this point, all important anatomical landmarks are identified to enter the dorsal pons through safe entry zones and tackle intraaxial pontine lesions. The suprafacial collicular (suprafacial triangle), infrafacial collicular (infrafacial triangle), superior foveal (lateral sulcus limitans) and median sulcal (interfacial) safe entry zones (Sects. 12.3.4, 12.3.5, 12.3.6, and 12.3.7; see Fig. 12.9) are all viable options, and the best choice depends on the 2-point rule, i.e. shortest distance and least disturbance of the pontine tissue. As mentioned earlier, the safest entry to remove lesions with exophytic components is to debulk the lesion and follow its planes within the pons.

Meticulous irrigation with warmed isotonic fluids to remove blood products and replace CSF is done before dural closure. This is followed by water-tight dural closure using interrupted sutures, with or without a dural graft or a fascial layer to cover dural defects. Bio-adhesive glue may be used or a piece of gelfoam is placed on top of the dura, the occipital bone is fixed using titanium plates, the muscles are reapproximated after adequate hemostasis and sutured according to anatomical layers, and the subcutaneous and skin layers are closed using interrupted and running sutures, respectively. Postoperative lumbar drainage for 2–3 days is optional in some cases.

12.7 Conclusion

The current armamentarium of surgical approaches to pontine lesions allows for almost a 360-degree angle of attack. The surgeon's comprehensive anatomical knowledge is the most important variable to achieve a maximally safe surgery. Preoperative surgical planning and choice of the least invasive trajectory and safest entry zone dictates the surgical approach. Mastering endoscopic intranasal procedures is highly recommended as more ventral approaches will be used to tackle anteriorly located pontine lesions. The significance of intraoperative neuromonitoring cannot be overemphasized. More research evaluating and fine-tuning the current surgical approaches, as well as discovering new variations and safe entry zones into the pons, is very much needed, especially that the existing technology (microscope, endoscope, navigation systems, neuromonitoring and mapping, etc.) permits safe entry to deep skull base locations, which were deemed inaccessible few decades ago.

Acknowledgments Figures 12.1–12.7 are courtesy of the Rhoton Collection (<http://rhoton.ineurodb.org>). Dissections were carried out by Hiroshi Abe, Antonio Mussi, Hung Wen, and Kaan Yağmurlu.

References

1. Abila AA, Lekovic GP, Turner JD, de Oliveira JG, Porter R, Spetzler RF. Advances in the treatment and outcome of brainstem cavernous malformation surgery: a single-center case series of 300 surgically treated patients. *Neurosurgery*. 2011;68(2):403–14; discussion 14–5.
2. Cavalcanti DD, Preul MC, Kalani MY, Spetzler RF. Microsurgical anatomy of safe entry zones to the brainstem. *J Neurosurg*. 2016;124(5):1359–76.
3. Cavalheiro S, Yagmurlu K, da Costa MD, Nicacio JM, Rodrigues TP, Chaddad-Neto F, et al. Surgical approaches for brainstem tumors in pediatric patients. *Childs Nerv Syst*. 2015;31(10):1815–40.
4. Wang CC, Liu A, Zhang JT, Sun B, Zhao YL. Surgical management of brain-stem cavernous malformations: report of 137 cases. *Surg Neurol*. 2003;59(6):444–54; discussion 54.
5. Zaidi HA, Mooney MA, Levitt MR, Dru AB, Abila AA, Spetzler RF. Impact of timing of intervention among 397 consecutively treated brainstem cavernous malformations. *Neurosurgery*. 2017;81(4):620–6.
6. Cavalcanti DD, Figueiredo EG, Preul MC, Spetzler RF. Anatomical and objective evaluation of the main surgical approaches to pontine intra-axial lesions. *World Neurosurg*. 2019;121:e207–e14.
7. Yang Y, van Niftrik B, Ma X, Velz J, Wang S, Regli L, et al. Analysis of safe entry zones into the brainstem. *Neurosurg Rev*. 2019;42:721.
8. Recalde RJ, Figueiredo EG, de Oliveira E. Microsurgical anatomy of the safe entry zones on the anterolateral brainstem related to surgical approaches to cavernous malformations. *Neurosurgery*. 2008;62(3 Suppl 1):9–15; discussion -7.
9. Baghai P, Vries JK, Bechtel PC. Retromastoid approach for biopsy of brain stem tumors. *Neurosurgery*. 1982;10(5):574–9.
10. Strauss C, Lütjen-Drecoll E, Fahlbusch R. Pericollicular surgical approaches to the rhomboid fossa. Part I. Anatomical basis. *J Neurosurg*. 1997;87(6):893–9.
11. Yagmurlu K, Rhoton JA, Tanriover N, Bennett J. Three-dimensional microsurgical anatomy and the safe entry zones of the brainstem. *Neurosurgery*. 2014;10:602–19; discussion 19–20.

12. Bricolo A, Turazzi S. Surgery for gliomas and other mass lesions of the brainstem. *Adv Tech Stand Neurosurg.* 1995;22:261–341.
13. Cavalheiro S, Yagmurlu K, Nicácio J, Rodrigues T, Chaddad-Neto F, Rhoton A. Surgical approaches for brainstem tumors in pediatric patients. *Childs Nerv Syst.* 2015;31(10):1815–40.
14. Fomichev D, Kalinin P, Gavrushin A. Endoscopic transnasal transclival resection of endodermal cyst on ventral surface of brainstem. *World Neurosurg.* 2017;97:756.e7–e11.
15. Fernandes Cabral DT, Zenonos GA, Nuñez M, Celtikci P, Snyderman C, Wang E, et al. Endoscopic endonasal transclival approach for resection of a pontine glioma: surgical planning, surgical anatomy, and technique. *Oper Neurosurg (Hagerstown).* 2018;15(5):589–99.
16. Gladi M, Iacoangeli M, Specchia N, Re M, Dobran M, Alvaro L, et al. Endoscopic transnasal odontoid resection to decompress the bulbo-medullary junction: a reliable anterior minimally invasive technique without posterior fusion. *Eur. Spine J.* 2012;21(Suppl 1):S55–60.
17. Morera V, Fernandez-Miranda J, Prevedello D, Madhok R, Barges-Coll J, Gardner P, et al. “Far-medial” expanded endonasal approach to the inferior third of the clivus: the transcondylar and transjugular tubercle approaches. *Neurosurgery.* 2010;66(6 Suppl Operative):211–9; discussion 9–20.
18. Barges-Coll J, Fernandez-Miranda JC, Prevedello DM, Gardner P, Morera V, Madhok R, et al. Avoiding injury to the abducens nerve during expanded endonasal endoscopic surgery: anatomic and clinical case studies. *Neurosurgery.* 2010;67(1):144–54.
19. Essayed WI, Singh H, Lapadula G, Almodovar-Mercado GJ, Anand VK, Schwartz TH. Endoscopic endonasal approach to the ventral brainstem: anatomical feasibility and surgical limitations. *J Neurosurg.* 2017;127(5):1139–46.
20. Raibagkar P, Chavali RV, Kaplan TB, Kim JA, Nitka MV, Chou SH, et al. Reverse locked-in syndrome. *Neurocrit Care.* 2017;27(1):108–14.
21. Hauck EF, Barnett SL, White JA, Samson D. The presigmoid approach to anterolateral pontine cavernomas. *Clinical article. J Neurosurg.* 2010;113(4):701–8.
22. Kalani MY, Yagmurlu K, Martirosyan NL, Spetzler RF. The Retrosigmoid petrosal fissure transpeduncular approach to central pontine lesions. *World Neurosurg.* 2016;87:235–41.
23. Cohen-Gadol AA. Microvascular decompression surgery for trigeminal neuralgia and hemifacial spasm: nuances of the technique based on experiences with 100 patients and review of the literature. *Clin Neurol Neurosurg.* 2011;113(10):844–53.
24. Kivelev J, Kivisaari R, Niemelä M, Hernesniemi J. Muscle insertion line as a simple landmark to identify the transverse sinus when neuronavigation is unavailable. *World Neurosurg.* 2016;94:394–7.
25. Tubbs R, Salter G, Oakes W. Superficial surgical landmarks for the transverse sinus and torcular herophili. *J Neurosurg.* 2000;93(2):279–81.

Chapter 13

Surgical Approaches to Medullary Tumors



Helmut Bertalanffy, Souvik Kar, and Christian Hartmann

Abbreviations

cIMPACT-NOW	Consortium to Inform Molecular and Practical Approaches to CNS Tumor Taxonomy
CSF	Cerebrospinal fluid
CT	Computed tomography
DIPG	Diffuse intrinsic pontine glioma
DMG	Diffuse midline glioma WHO grade IV H3 K27M-mutant
GG	Ganglioglioma
GTR	Gross total resection
IDH	Isocitrate dehydrogenase
MAPK	Mitogen-activated protein kinase
MRI	Magnetic resonance imaging
NTR	Near total resection
PA	Pilocytic astrocytoma
PET	Positron emission tomography
PICA	Posterior inferior cerebellar artery
WHO	World Health Organization

H. Bertalanffy (✉)

Vascular Neurosurgery, International Neuroscience Institute, Hannover, Germany

e-mail: bertalanffy@ini-hannover.de

S. Kar

International Neuroscience Institute, Hannover, Germany

C. Hartmann

Department of Neuropathology, Institute of Pathology, Hannover Medical School – MHH, Hannover, Germany

13.1 Introduction

Gliomas of the medulla oblongata (bulbar gliomas) belong to a heterogeneous group of brainstem gliomas. These tumors arise within the medulla and may extend into adjacent structures such as the pons, inferior cerebellar peduncle, cerebellum, and upper spinal cord. Bulbar gliomas occur in children as well as in adult patients. However, their biology differ between pediatric and adult individuals [11]. While brainstem gliomas account for almost one-fifth of all pediatric brain tumors, they account for only less than 2% of all adult gliomas [26]. Among all brainstem gliomas, approximately one-fourth originate within the medulla oblongata [2]. Considered together, medullary gliomas form a heterogeneous group of several tumor entities, rendering it difficult to predict the overall prognosis. Exophytic bulbar gliomas seem to occur more frequently in children and are generally considered more favorable in terms of operability and postsurgical outcomes [22].

This chapter intends to demonstrate that microsurgical resection of medullary gliomas is possible in a well-selected patient population with a low complication rate and a favorable clinical outcome.

13.2 Clinical Presentation

The clinical features of bulbar gliomas reflect their location within the medulla oblongata. Frequent symptoms are lower cranial nerve dysfunction (dysphagia, dysphonia, tongue deviation), cerebellar dysfunction (ataxia, gait disturbance, tremor), and long-tract signs with sensory and motor deficits. Occasionally, tracheostomy and nasogastric tube feeding become necessary in an advanced stage of the disease. Symptoms may develop insidiously and can fluctuate, but they generally tend to deteriorate without appropriate treatment.

13.3 Neuroradiological Evaluation

The primary and most important diagnostic tool is the magnetic resonance imaging (MRI) with various sequences, including T1-weighted contrast-enhanced images. In rare instances, computed tomography (CT) scans may show evidence of intratumoral calcifications. On MRI, the most important morphological aspects of the underlying tumor become evident: focal or diffuse parenchymal infiltration, cystic and exophytic components, size, and degree of extension into adjacent structures. The majority of focal bulbar gliomas are low-grade tumors; they are generally more suitable for surgical resection than diffusely infiltrating tumors, which occur mostly in the pons and less frequently within the medulla.

In addition to MRI, spectroscopy and positron emission tomography (PET) may help in excluding other pathological entities within the medulla such as an abscess,

inflammation, demyelination, vascular malformation, metastatic tumor, ependymoma, or focal ischemia.

13.4 Management Strategies

In contrast to many gliomas located in other parts of the brain, bulbar gliomas and brainstem gliomas are generally not regarded as good candidates for surgical resection. Frequently, the term ‘brainstem glioma’ is associated with inoperability without further specification. On one hand, this may be understandable since a significant number of brainstem gliomas, particularly in children, are diffuse intrinsic pontine gliomas (DIPGs), which certainly cannot be treated reasonably with surgery. On the other hand, many neurosurgeons are reluctant to attempt extensive microsurgical resection even in focal bulbar (and pontine and mesencephalic) gliomas because of the anticipated postoperative disabling symptoms [11]. Therefore, tumor debulking or only a limited biopsy is preferred in many instances, followed by radio-chemotherapy.

In recent years, however, several reports describing successful surgical resection of brainstem gliomas, including bulbar tumors, were published. Individuals harboring dorsally exophytic or cervicomedullary tumors were carefully selected for surgery, which resulted in better prognosis for patients suffering from such focal gliomas [1, 4, 12, 13, 25, 30]. Surgery was complemented by standard radiotherapy combined with chemotherapy using various agents to achieve a satisfactory long-term result [25].

13.5 Our Patient Series

For more than two decades, the senior author (HB) has focused on brainstem surgery and has microsurgically treated almost 500 patients suffering from various intrinsic brainstem lesions, including gliomas, ependymomas, and cavernous malformations [2]. This large patient series also comprises 43 adult and pediatric patients who harbored a bulbar glioma and underwent microsurgical tumor removal by the senior author in the period of 1996–2019; this group constitutes the patient population discussed in this chapter.

13.5.1 Patient Selection

No precise and widely accepted selection criteria are available in the pertinent literature for bulbar gliomas. Generally, focal, dorsally exophytic and cervicomedullary gliomas have been treated surgically so far; however, the number of published reports on this subject is rather limited [13].

The senior author has applied a differentiated view on every single tumor of this series and selected the patients in a highly individualized fashion based on his previous experience with brainstem surgery and his personal assessment of reasonable operability in each case. A reasonable operability was considered mainly in focal bulbar tumors either confined to the medulla or extending extra-axially in an exophytic manner, in which a significant amount of the lesion (generally, at least half of tumor volume) was expected to be removed without causing additional permanent neurological morbidity. In very few cases, only partial tumor removal (extended biopsy) appeared to be indicated, mainly in order to establish a precise histopathological diagnosis based on the latest tumor classification system. The senior author selected 43 individuals who fulfilled these criteria and treated them microsurgically. Table 13.1 summarizes the characteristics of this subpopulation of brainstem glioma cases.

13.5.2 Tumor Characteristics

This patient series comprises exclusively astrocytic, oligodendroglial, neuronal and mixed-neuronal-glia tumors found in children as well as in adults. Ependymal or other tumor entities affecting the brainstem were not considered here because of their different characteristics and behavior.

Table 13.1 Patient characteristics and tumor entities

Patients	<i>n</i> = 43
Females/Males	20/23
Mean age (years)	26.65 (STD ± 18.37)
Median age (years)	27
Age range (years)	1–67
Pediatric group	<i>n</i> = 16
Females/Males	10/6
Mean age (years)	8.37 (STD ± 5)
Median age (years)	7
Age range (years)	1–17
Adult group	<i>n</i> = 27
Females/Males	10/17
Mean age (years)	38.83 (STD ± 12.98)
Median age (years)	35
Age range (years)	21–67
Tumor entities	
Pilocytic astrocytoma	16 (9) ^a
Anaplastic astrocytoma	14 (2) ^a
Ganglioglioma	8 (5) ^a
Glioblastoma	5 (0) ^a

Abbreviations: *n* number, *STD* standard deviation

^a(in parenthesis), number of pediatric cases

13.5.2.1 Tumor Location and Extent

As exemplified in Fig. 13.1, the bulbar gliomas encountered in this patient series varied in their morphological aspect. We distinguished 4 different types, resulting in a sub-classification that appeared helpful in choosing the appropriate surgical exposure; thirteen tumors were confined to the lower brainstem (medullary intrinsic type); other lesions grew exophytically, mainly in lateral (9 tumors) or mainly in posterior direction (13 tumors), while the remaining 8 gliomas extended inferiorly from the medulla into the spinal cord (Table 13.2).

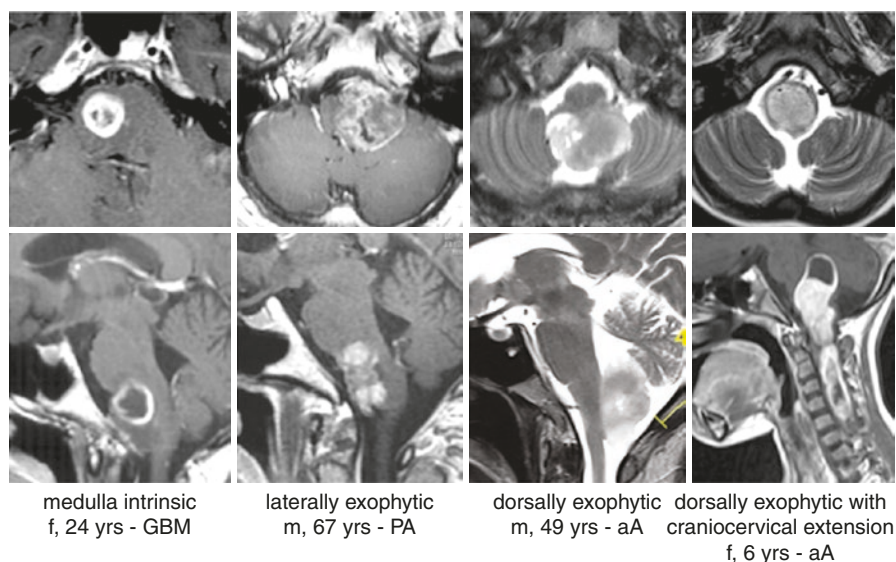


Fig. 13.1 Axial and sagittal MRI scans show representative examples of bulbar tumor location and extent. Each of the 4 columns corresponds to a different patient from this series. Abbreviations: aA anaplastic astrocytoma, f female, *GBM* glioblastoma, m male, PA pilocytic astrocytoma, yrs years

Table 13.2 Tumor location and extent

Pathology/Location and Extent	Intrinsic	Laterally Exophytic	Dorsally Exophytic	Dorsally Exophytic with Cervical Extension	<i>n</i>
Pilocytic astrocytoma	5	5	2	4	16
Anaplastic astrocytoma	5	2	4	3	14
Ganglioglioma	0	2	5	1	8
Glioblastoma	3	0	2	0	5
Total	13 (30.2%)	9 (21%)	13 (30.2%)	8 (18.6%)	43

Abbreviation: *n* number

13.5.2.2 Tumor Entities

Four different histopathological tumor entities were encountered in the medulla: pilocytic astrocytoma (PA), anaplastic astrocytoma, ganglioglioma (GG), and glioblastoma (see Table 13.1). While the majority of these lesions emerged as well-circumscribed tumors (see Fig. 13.1), others diffusely infiltrated the lower brainstem and adjacent structures.

Interestingly, no additional tumor entities that we found in the pons or in the midbrain of other patients, such as fibrillary astrocytoma, rosette-forming glioneuronal tumor, anaplastic GG, papillary glioneuronal tumor, pleomorphic xanthoastrocytoma, and anaplastic oligodendroglioma [2], were encountered in this patient series of medullary gliomas.

13.5.2.3 Molecular Signature

Up until the revised fourth edition of the 2016 World Health Organization (WHO) Brain Tumor Classification [19], brainstem gliomas were classified and graded in the same fashion as supratentorial lesions. However, the significant amount of new scientific evidence, particularly those on the molecular signature, mandated an updated classification of these tumors.

High-Grade Brainstem Gliomas

A new entity, the diffuse midline glioma WHO grade IV H3 K27M-mutant (DMG) was introduced into the WHO classification in 2016 [19]. DMG is defined as a glial tumor with an H3 K27M mutation, which occurs in the midline region of the brain, i.e., from the diencephalon to the spinal cord, thus also encompassing the medulla oblongata. Histopathological grading criteria of diffuse (supratentorial) gliomas were regarded as irrelevant for this lesion, so that a WHO grade IV was inevitably assigned to corresponding tumors upon detection of an H3 K27M mutation. In the meantime, however, other tumors have been reported to also emerge in the midline region with histopathological resemblance to ependymomas [8], GGs [16, 17], and PAs [20], as well as exhibiting an H3 K27M mutation. Therefore, in the Consortium to Inform Molecular and Practical Approaches to CNS Tumor Taxonomy (cIMPACT-NOW) Update 3, the DMG definition was complemented by the criterion of diffuse infiltration to avoid the necessity of diagnosing the other entities as WHO grade IV lesions [3]. A systematic analysis regarding the frequency of diffuse gliomas with an H3 K27M mutation in the medulla oblongata is currently not available; consequently, data on this question have to be extrapolated from information on all DMGs. Furthermore, the situation is complicated by the fact that significantly more scientific findings have been published in pediatric than in adult patients regarding the proportion of diffuse gliomas with an H3 K27M mutation, and it remains unclear whether the distribu-

tion pattern remains stable throughout different life decades. Currently, it is assumed that up to 80% of all diffuse gliomas of the brainstem have an H3 K27M mutation and can be classified as DMG [28, 29, 31]. The remaining diffuse gliomas of the brainstem show the molecular signature of supratentorial lesions such as an isocitrate dehydrogenase (IDH) mutation, *EGFR* amplification and/or *CDKN2A* deletions [32]. Interestingly, however, infratentorial gliomas show significantly fewer *IDH1* and *IDH2* mutations than supratentorial gliomas [7, 14, 26], where the R132H variant is found predominantly in about 90% of cases [10]. It is unclear whether, and to what extent, the grading criteria of supratentorial gliomas also have infratentorial validity in the absence of an H3 K27M mutation. However, according to the current WHO classification, only a histopathological grading (diffuse astrocytoma WHO grade II, anaplastic astrocytoma WHO grade III, glioblastoma WHO grade IV) of infratentorial diffuse gliomas with a negative H3 K27M status is recommended [19].

Fourteen patients of the present series were diagnosed as harboring an anaplastic astrocytoma of the medulla (Fig. 13.2), while 5 other individuals suffered from a bulbar glioblastoma. The MRI scans of 1 glioblastoma patient are shown in Fig. 13.1 (leftmost column), while those of 3 other patients can be seen in Fig. 13.3.

Pilocytic Astrocytoma

PAs are tumors that usually exhibit a clearly demarcated border to the adjacent brain parenchyma; they continue to be assigned to a WHO grade I by the WHO classification [19]. Extensive molecular analyses have shown that all PAs usually have a mutation in 1 gene of the mitogen-activated protein kinase (MAPK) pathway, indicating that these lesions are single pathway tumors [15]. While cerebellar PAs show *BRAF:KIAA1549* duplication and fusion in almost all cases, a corresponding genetic alteration is found in only about 60% of extracerebellar tumors of this type. Extracerebellar PA alternately shows *BRAF V600E*, *FGFR1*, *NF1* and *NTRK2* mutations [15]. The molecular profile of PA of the medulla has not been systematically investigated yet. It is assumed that bulbar PAs show genetic alterations comparable to all other extracerebellar tumors of this type. While the current WHO classification only discusses the possibility of anaplastic PA [19], a corresponding entity could perhaps be defined molecularly. The most common single genetic change in these anaplastic PAs is the homozygous *CDKN2A* deletion [24].

Presently, brainstem gliomas with typical histopathological characteristics of PAs, as well as those with diffuse parenchymal infiltration and concomitant H3 K27M mutation, constitute an unsolved problem. Several publications imply that patients harboring such tumors have a significantly worse prognosis. Indeed, we also could observe an unexpectedly unfavorable clinical course in 2 patients of this series who harbored a bulbar glioma that was histopathologically classified as

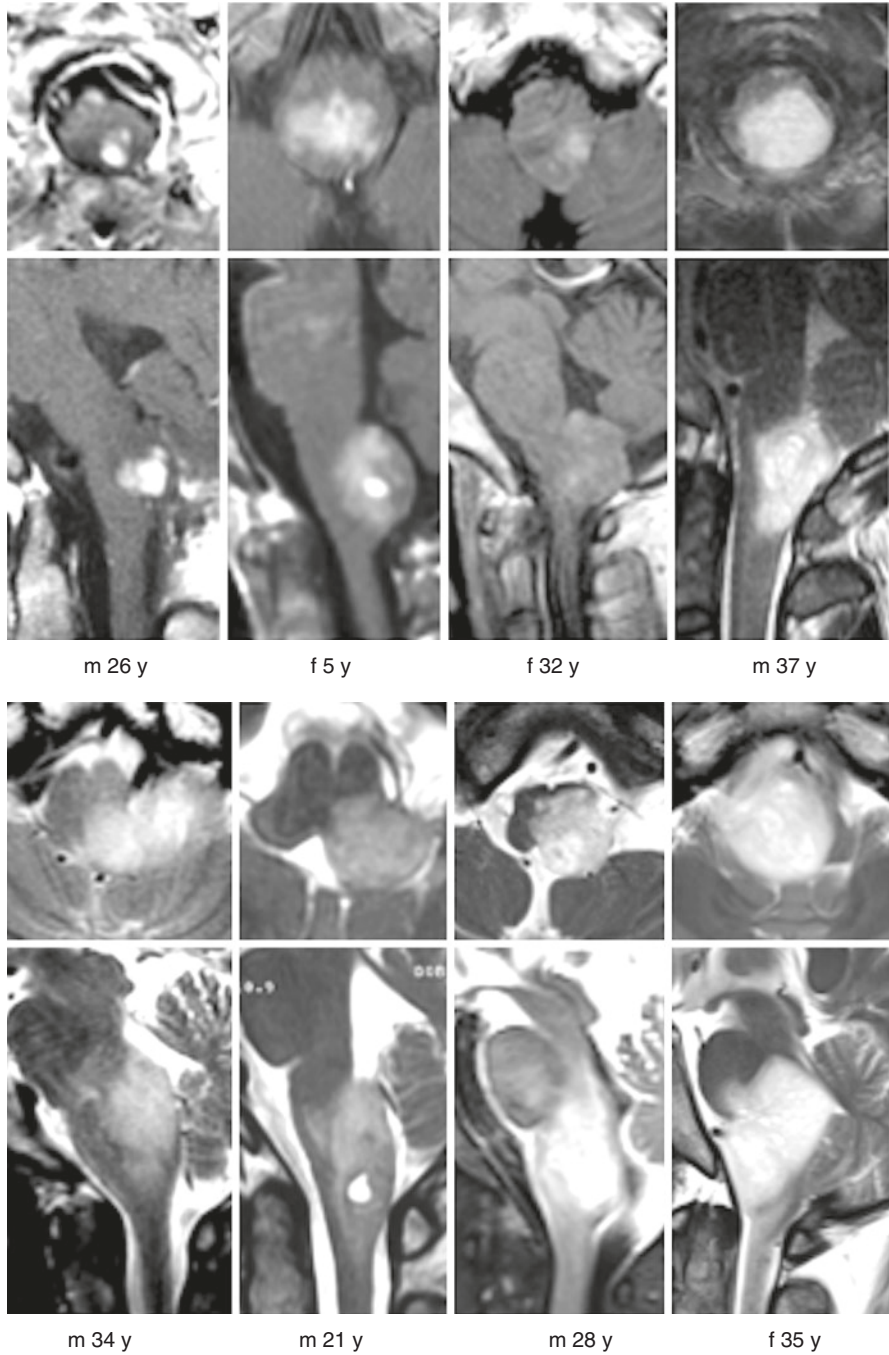


Fig. 13.2 Axial and sagittal MRI scans show typical anaplastic astrocytomas arising from the medulla oblongata. Each column with axial and sagittal MRI, respectively, corresponds to one of 8 illustrative cases from the present surgical series. Abbreviations: f female, m male, y years

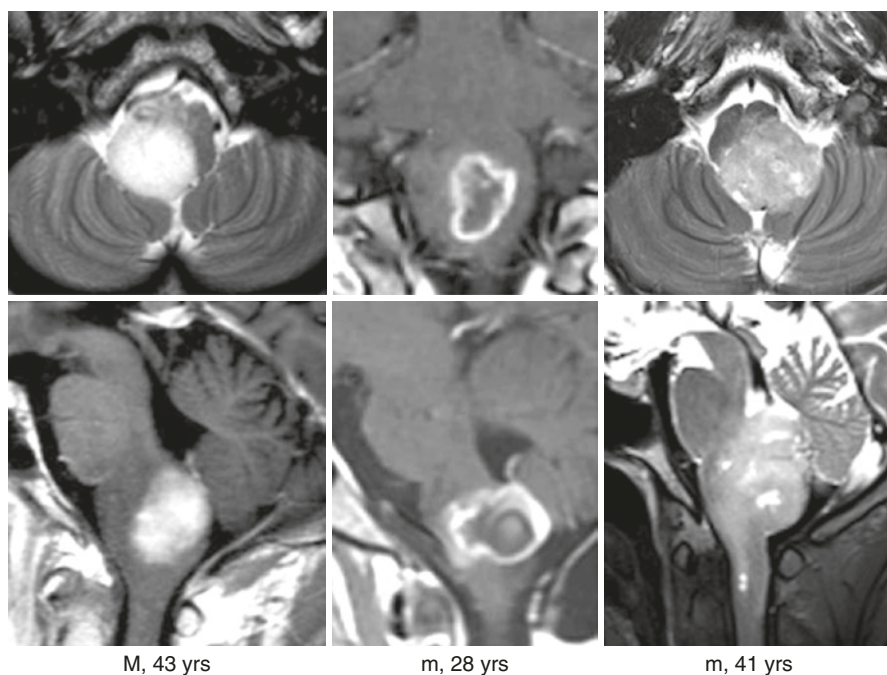


Fig. 13.3 Axial and sagittal MRI scans of 3 patients from this series who harbored a glioblastoma. Abbreviations: m male, yrs years

PA. One of them is exemplified in Figs. 13.4 and 13.5. In this context, some authors have characterized such tumors as anaplastic PAs [6, 23]. However, it appears worthwhile to attempt clarifying in the future whether a tumor with morphological features of a PA and concomitant H3 K27M mutation actually corresponds to a DMG WHO grade IV when epigenetic analyses, early tumor recurrence, and patient's overall reduced survival are taken into account.

The present patient series comprises 16 individuals who harbored a bulbar PA (Fig. 13.6).

Ganglioglioma

GG WHO grade I, and the very rare anaplastic GG WHO grade III, typically show a *BRAF* V600E mutation [19]. However, the reported mutation frequency of *BRAF* V600E varies between 20% and 60% [18, 27]. The histopathological architecture of GG is thought to explain these significant differences: the tumors show much smaller ganglion cell and glial components. If the *BRAF* V600E status is determined using a mutation-specific antibody rather than genetically, it can sometimes be demonstrated that only the ganglion cell component expresses the mutated protein. It is assumed that the number of tumor DNA with a *BRAF* V600E mutation is partially below the detection limit. Consequently, these tumors are then identified as *BRAF* wild-type in the genetic analysis, although

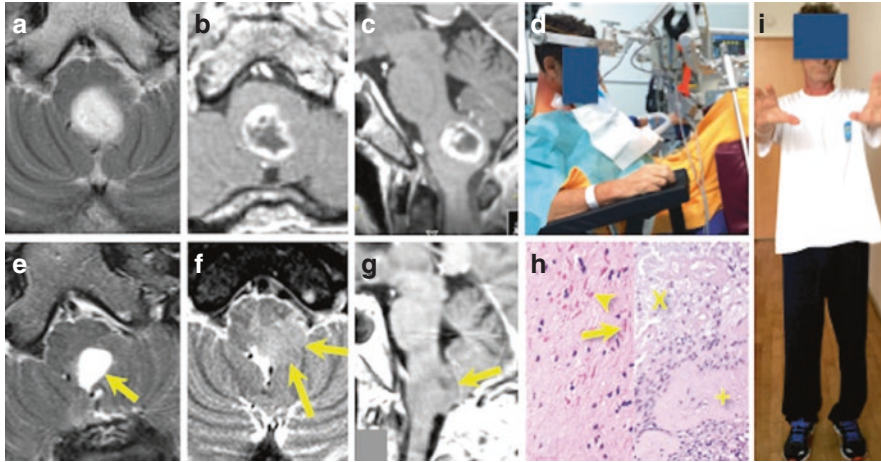


Fig. 13.4 Ten months prior to surgery, this 56-year-old man developed progressive dysphagia, imbalance, slight right-sided hemiparesis, and left-sided hemihyperesthesia. Preoperative T2-weighted axial (a) and contrast-enhanced T1-weighted axial and sagittal MRI (b, c) show evidence of an intrinsic tumor of the medulla. The patient underwent surgery in the semi-sitting position (d) via midline suboccipital craniotomy, including the posterior rim of the foramen magnum and combined with C1 laminectomy. Postoperative MRI documented gross total tumor resection (e, arrow). Only 3 months later, however, the patient developed new symptoms, and a local tumor recurrence was detected on a follow-up MRI (f and g, arrows). Histopathological examination (h) showed a predominantly biphasic, astrocytic tumor with low cellularity, which contained Rosenthal fibers (arrow), protein droplets (arrowhead), and, in various locations, hyalinized blood vessels (+) and small areas of necrosis (X). The final diagnosis was pilocytic astrocytoma (PA) WHO grade I without any signs of anaplasia. As the patient did very well immediately after the surgical intervention, and since there were no additional neurological deficits by that time (i), the diagnosis of PA was not questioned initially. Following the early local tumor recurrence, however, we suspected the presence of a diffuse midline glioma (DMG) despite the former histopathological diagnosis. Subsequently, the patient underwent combined radio-chemotherapy

the small ganglion cell component actually has the mutation [18]. The processing of the *BRAF* wild-type GG revealed that these tumors, similar to PAs, also show mutations in genes of the MAPK pathway [21]. GGs of the posterior fossa and spinal cord, as well as bulbar GGs with *BRAF* V600E mutations, were divided into two groups: (a) classical GGs with *BRAF* V600E mutation and (b) PAs with gangliocytoma differentiation, which typically exhibited *BRAF:KIAA1549* duplication and fusion [9]. In summary, it can be concluded that there are frequent morphological overlaps in the group of glial/glioneuronal tumors [19], and that these tumors are also epigenetically related to each other [5].

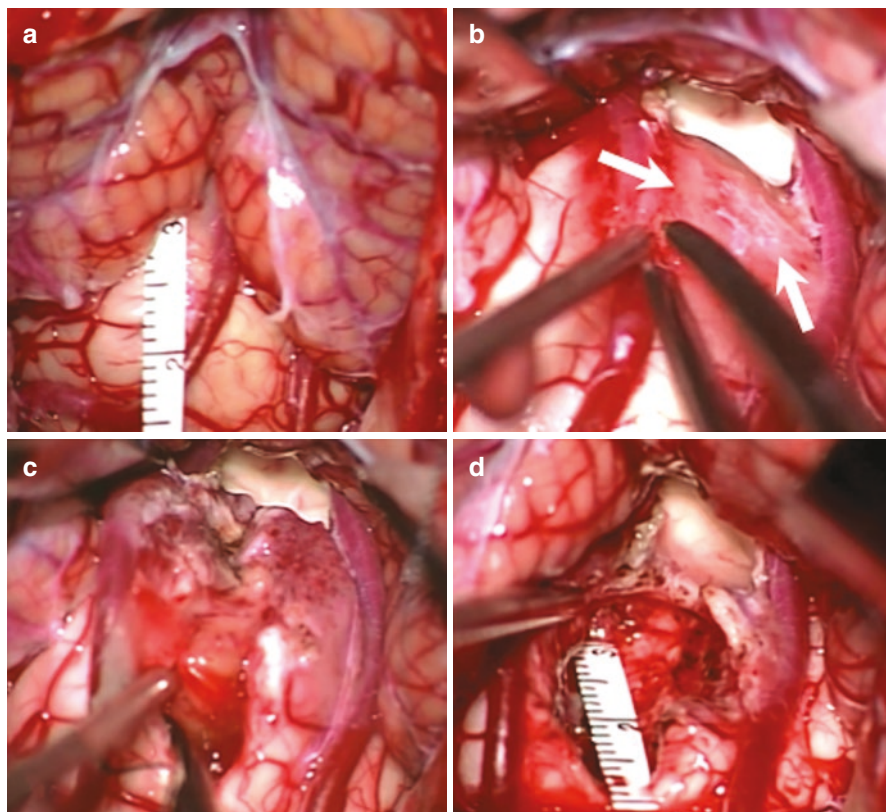


Fig. 13.5 Intraoperative photographs of the patient shown in Fig. 13.4. After opening the dura mater, the surface of the medulla appeared bulging posteriorly between the cerebellar tonsils due to the underlying tumor. A millimeter scale demonstrates the local dimensions (a). Adhesions (arrows) between the reddish tumor surface and cerebellum were present. After detaching the tumorous medulla from the cerebellum, the rhomboid fossa became visible above the lesion (b). Enough tumor tissue was harvested for histopathological examination (revealing a pilocytic astrocytoma), and the tumor was gradually diminished in volume with the aid of an ultrasonic aspirator. Obviously, there was no clear dissection plane between lesion and brainstem parenchyma (c). Eventually, gross total tumor resection was achieved as could be estimated macroscopically. The millimeter scale placed into the tumor resection cavity helped in determining the extent of safe tumor removal (d)

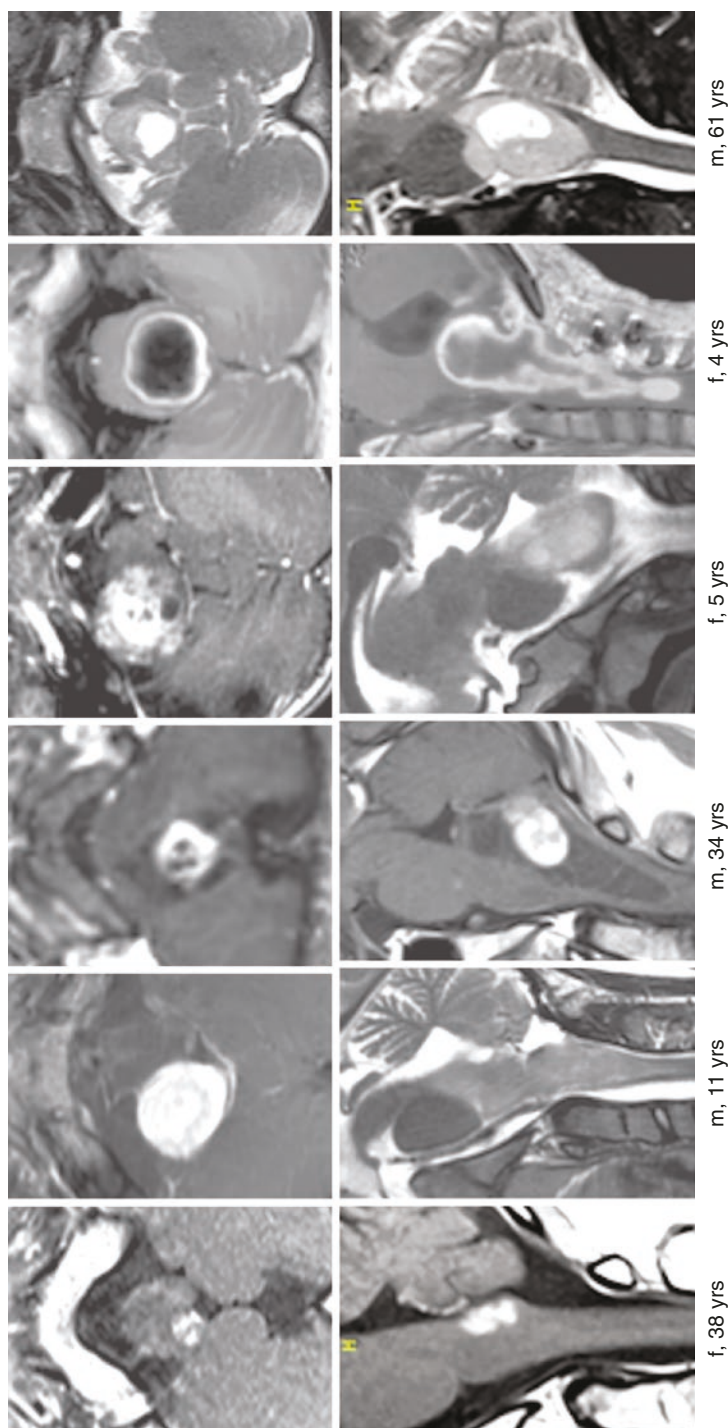


Fig. 13.6 Axial and sagittal MRI scans show typical pilocytic astrocytomas of the medulla oblongata. The images belong to 6 illustrative cases from the present surgical series, with each column representing a different individual. Patients shown here were aged 4–61 years. Abbreviations: f female, m male, yrs years

In the present series we have selected 8 individuals harboring a bulbar GG for microsurgical treatment (Fig. 13.7).

13.5.3 Surgical Strategies

Surgery, the mainstay of therapy for low-grade gliomas in other intracranial locations, was also considered in low-grade gliomas of the medulla. The role of surgery in high-grade bulbar gliomas has not yet been established. Despite the poor prognosis, we have attempted surgery in these malignant tumors as well, hoping to achieve a comprehensible benefit for the patient in these cases.

Once the indication for surgery has been established in a patient, we proceed with defining the goals of surgery and precisely planning the procedure.

13.5.3.1 Goals of Surgery

In principle, the surgery is aimed primarily at removing as much of the pathological tissue as possible without damaging the underlying central nervous system paren-

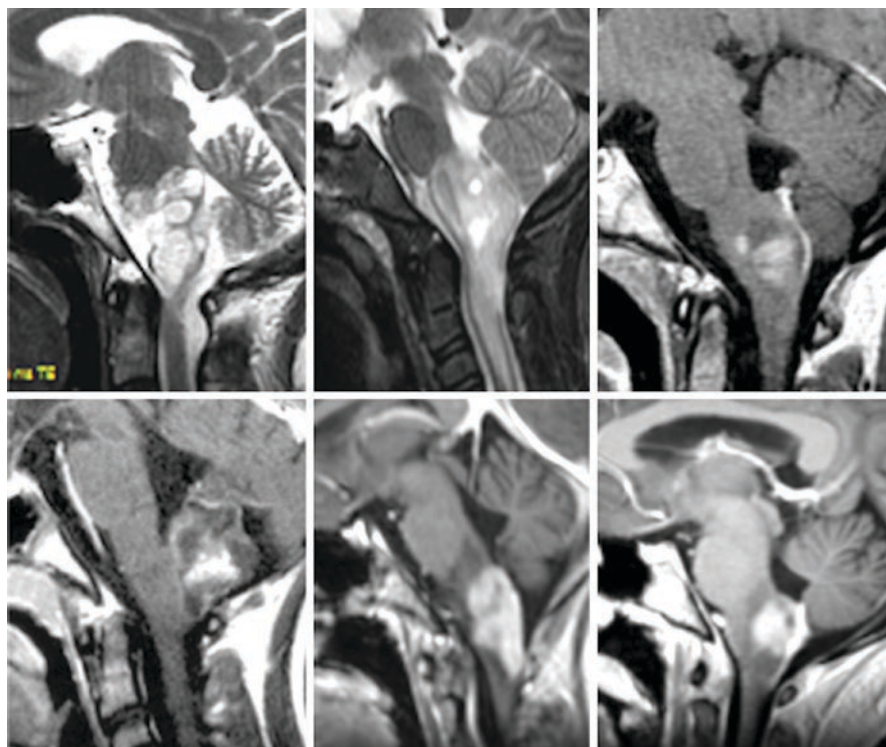


Fig. 13.7 Sagittal MRI scans demonstrate typical bulbar gangliogliomas. Each image belongs to one of 6 illustrative cases from the present surgical series. The patients were aged 8–53 years

chyma. The main goal was to decompress the brainstem and interrupt the pathological mechanism of long tracts and bulbar nuclei damage caused by the tumor. In high-grade gliomas, we attempted to achieve at least a better result than just good palliative care in terms of prolonging the patient's survival with an acceptable quality of life. In well-circumscribed lesions, we attempted to achieve a total or near-total tumor removal, while tumor volume reduction without an attempt of radical resection appeared as a reasonable alternative in less well-delineated low-grade tumors, or in high-grade tumors that usually lacked a clear demarcation toward the brainstem or spinal cord parenchyma. Deliberate partial tumor volume reduction was the goal in rather very voluminous symptomatic tumors, in which radical resection would have been possible only at the price of significant clinical deterioration.

13.5.3.2 Timing of Surgery

In patients in whom a bulbar glioma was suspected and the lesion appeared operable, we recommended surgery in the near future to avoid further tumor progression and possible clinical deterioration. Rapidly progressing symptoms, however, required surgery without further delay. Observation and repeat MRI were generally indicated only in individuals presenting with mild symptoms and in a stable clinical condition, in whom the diagnosis remained unclear after an initial MRI examination.

13.5.3.3 Preoperative Planning and Tumor Exposure

In each case, we tailored the surgical approach according to the morphological features of the underlying bulbar glioma. For preoperative planning, we used a high-quality MRI, and in cervicomedullary tumors, we also utilized CT scans of the upper cervical spine with a bone window technique to assess the exact shape of the vertebrae. We informed the patients and their families about the goals of surgery in detail, the specific possibilities of tumor resection, and the risks associated with the planned procedure. To be prepared for adequate therapeutic measures, we preoperatively discussed with our anesthetists the possible occurrence of intraoperative vagal reaction with sudden bradycardia or a sudden rise in blood pressure due to manipulation within the medulla oblongata.

While intraoperative neuronavigation played almost no role in the surgery of bulbar gliomas, continuous electrophysiological monitoring was a mandatory tool that was applied in all surgical procedures. Somatosensory and motor evoked potentials were routinely used throughout the intervention. In some instances, we also used intraoperative electromyography of the vagal and hypoglossal nuclei.

Surgical access to the medulla was usually less demanding than exposing the pons or the midbrain. Basically, we used only two access routes to resect tumors confined to the medulla: a standard midline suboccipital exposure with opening of the foramen magnum posteriorly (*see* Sect. 12.6.1 of Chap. 12 for detailed description of the medial suboccipital approach and surgical technique), and a lateral suboccipital exposure that was sometimes extended laterally and inferiorly (paracondylar

or transcondylar exposure) for laterally exophytic tumors (see the section below for detailed description of the far-lateral approach and surgical technique). We always expose the floor of the fourth ventricle (rhomboid fossa) by dissecting between the cerebellar tonsils and uvula, and by transecting the posterior medullary velum and tela choroidea (telovelar exposure). In a few instances, particularly for dorsally exophytic tumors with significant lateral extension, we applied a combined lateral and midline exposure that was necessary to sufficiently expose the entire lesion (Fig. 13.8).

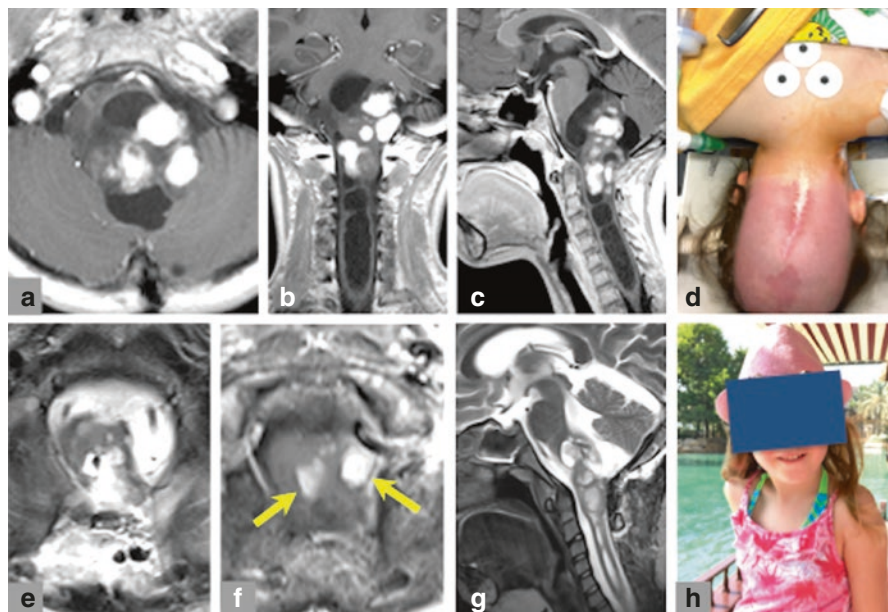


Fig. 13.8 This 8-year-old girl became symptomatic at the age of 1.5 years when her parents observed a slight limping in her left leg. Years later, following detection of a large craniovertebral junction tumor, the girl underwent suboccipital craniotomy at another institution. By that time, the surgical procedure consisted of local tumor biopsy and enlargement of the dura mater (duraplasty). Histopathological examination revealed the presence of a pilocytic astrocytoma, and chemotherapy with Vincristine and steroid medications were initiated. Subsequently, however, there was no detectable change of the lesion size on MRI. The tumor originated from the posterior medulla and consisted of large contrast-enhancing portions in addition to non-enhancing areas combined with adjacent cysts. The tumor mass had invaded the upper cervical cord reaching the C3 level and caused a space-occupying intramedullary syrinx extending inferiorly to the T1 level (a–c). Clinically, slight left-sided hemiparesis was noted. Tumor volume reduction became necessary at this stage because of repeated matutinal nausea and vomiting despite steroid medications. Surgery was undertaken with the child in the prone position and the head placed in the headrest coil unit for intraoperative MRI scanning (d). Tumor exposure was carried out again via a suboccipital craniotomy and an additional C1 laminectomy and C2 and C3 laminoplasty. Postoperative MRIs documented a significant tumor volume reduction of approximately 80–90% and small contrast-enhancing residual tumor portions (e–g, arrows). There were no perioperative complications, and no additional neurological deficits occurred. The child tolerated the surgical intervention without problems and was mobilized from the second postoperative day. Two years after surgery (h), the girl is neurologically intact with stable tumor remnants on control MRI

Although not described in this series, tumors confined to the pontomedullary junction and upper medulla or exophyting into the cerebellomedullary cistern can be tackled with a retrosigmoid approach (see Sect. 12.5.2 of Chap. 12 for detailed description of the retrosigmoid approach and surgical technique). Cervicomedullary tumors always required an additional exposure of the upper spinal cord, achieved by C1 laminectomy and C2 laminotomy down to the caudal tumor extension (Fig. 13.8), sometimes down to the level of C7 or T1 in very extensive lesions. At the end of the intradural procedure, we usually replaced the blocks of spinous processes and vertebral laminae and fixed them *in situ* with osteosynthetic titanium microplates and screws (cervical laminoplasty).

Far-Lateral Approach

The far-lateral approach permits access to the cisterna magna, cerebellomedullary and premedullary cisterns, exposing the antero-lateral and posterior surfaces of the medulla oblongata. Compared to a suboccipital craniotomy that only exposes the posterior surface of the medulla, the far-lateral approach is most suitable to resect medullary tumors through the antero-lateral safe entry zones, namely the pre-olivary sulcus (limited by the pyramidal tract anteriorly and the olive posteriorly) and the retro-olivary sulcus (limited by the olive anteriorly and the inferior cerebellar peduncle and cranial nerves IX/X posteriorly). The transcondylar, supracondylar and paracondylar variants of the far-lateral approach are extensions of a basic lateral suboccipital craniotomy. Although the paracondylar variant is mostly used to expose lesions involving the lateral aspect of the clivus and jugular process as opposed to the transcondylar and supracondylar variants that provide access to the antero-lateral surface of the medulla oblongata, all three variants are described below for the sake of completion. The far-lateral approach maybe combined with transmastoid and/or supratentorial approaches to access higher levels of lateral and antero-lateral aspects of the brainstem.

The patient is usually positioned in the three-quarter prone (a.k.a. park bench) position, where the patient side that is ipsilateral to the lesion is elevated at 45° from a prone position, and the head is rotated 45° to the contralateral side of the lesion with lateral flexion to the floor. The skin can be incised in two ways: the lazy S incision is relatively smaller than the inverted hockey stick incision, starting around the Asterion level, passing through the foramen magnum level, and ending with a medial curvature towards the C2 spinous process; whereas the inverted hockey stick incision follows a much longer trajectory, starting at 2 cm below the mastoid tip, proceeds vertically above the level of the superior nuchal line, turns medially towards the inion, then turns again to proceed inferiorly to the C2/C3 level. The wide exposure of the inverted hockey stick incision allows for utilizing the benefits of exposing the C1 transverse process during the paracondylar variant of the far-lateral approach, while the lazy S generally provides exposure for the transcondylar and supracondylar variants only.

The dissection starts by cutting the nuchal muscles (sternocleidomastoid, trapezius, longissimus capitis, splenius capitis, and semispinalis capitis) in a single bundle just below the superior nuchal line, which exposes the suboccipital triangle

(formed by the superior oblique, inferior oblique and rectus capitis posterior major muscles). Within the suboccipital triangle, the vertebral artery (third segment), posterior arch of atlas, and C1 nerve dorsal ramus are then identified after meticulous dissection of the vertebral venous plexus. Care should be taken not injure a posterior inferior cerebellar artery or posterior spinal artery of extradural origin in this region. After reflecting the muscles of the suboccipital triangle, three additional muscles are exposed: rectus capitis posterior minor (medial to the rectus capitis major muscle), rectus capitis lateralis (connects the transverse process of atlas to the inferior surface of the jugular process, just lateral to the occipital condyle; an important landmark for the paracondylar variant of the far-lateral approach), and levator scapulae (originates at the postero-inferior border of the transverse process of the atlas; extends lateral to the second segment of the vertebral artery and medial to the carotid compartment).

Bone window opening proceeds with a lateral suboccipital craniotomy. Important landmarks include the Asterion (just posterior to the sigmoid and inferior to the transverse sinuses), superior nuchal line (approximates the level of the transverse sinus and torcula), and the external occipital crest (medial limit of craniotomy). Part or all of the condylar fossa may be included in the initial craniotomy, where the posterior condylar emissary vein is identified and cauterized. The C2 spinal nerve root courses medial to the atlantoaxial joint and should be protected before the next step. The vertebral artery is then dissected away from the posterior arch of the atlas, the ipsilateral half of which is cut (medially in the midline and laterally close to the lateral mass of atlas) and elevated in one piece after unroofing the foramen transversarium and freeing the vertebral artery; the vertebral artery should now be easily displaced laterally and away from the subsequent craniectomy and dissection field.

The transcondylar variant follows a trajectory to the mid-to-lower antero-lateral medulla and lower clivus and exposes the intracranial segment of the vertebral artery. It starts with drilling the posterior third of the condyle until the posterior wall of the hypoglossal canal (dark blue color due to presence of venous plexus; cortical bone as opposed to the cancellous bone of the condyle) is encountered, then proceeds medial and inferior to the hypoglossal canal to reach the anterior medullary region and clivus.

The supracondylar variant provides access to the upper antero-lateral medulla and foramen magnum, as well as the petroclival junction and mid-clivus. Using a diamond bur, the posterior portion of the jugular tubercle is drilled above the hypoglossal canal and below the sigmoid sinus sitting in the sigmoid compartment of the jugular foramen; the lateral limit is the jugular bulb. Knowing that the glossopharyngeal, vagus and accessory nerves run in the neural compartment (which lies between the sigmoid compartment posteriorly and petrous compartment anteriorly of the jugular foramen), these nerves are exposed medially and are at risk of injury, especially the spinal rootlets of the accessory nerve running along the dura in this area.

The paracondylar has the most lateral trajectory of the three variants and is utilized for lesions involving the jugular process and posterior aspect of the mastoid. Intraoperative neurophysiologic monitoring of cranial nerves IX, X and XI is man-

datory throughout the procedure. It requires raising the posterior belly of the digastric muscle to expose the digastric groove, which will help to locate the exit of the facial nerve through the stylomastoid foramen. Fine drilling using a diamond bur proceeds supero-lateral to the condyle, around the exocranial aspect of the jugular foramen, and is directed towards the jugular process, onto which the rectus capitis lateralis is inserted posterior to the jugular foramen. Optimally, the neural compartment of the jugular foramen, lower and distal sigmoid sinus, jugular bulb, internal jugular vein, and internal carotid artery (pharyngeal segment) are seen in the final exposure.

A wide dural flap is incised, and cerebrospinal fluid (CSF) is drained by opening the cisterna magna; the posterior spinal artery should be identified and protected from this step onwards. The vertebral artery pierces the dura at the infero-medial corner of the occipital condyle, after which it is attached to the atlanto-occipital junction by the intracranial denticulate (dentate) ligament. Along its anteromedial trajectory to join the contralateral vertebral artery, the posterior inferior cerebellar artery (PICA) branches off in the premedullary cistern before the vertebrobasilar junction. Access to the antero-medial compartment of the posterior fossa is granted through the vagoaccessory triangle, bordered by the medulla medially, the vagus and medullary rootlets superiorly, and the body of the accessory nerve laterally. This triangle is also divided into a superior window and an inferior window by the hypoglossal nerve, the latter of which is maximally exposed during the trancondylar variant. The accessory nerve runs posterior to the dentate ligament at the spinal level but crosses the ligament as it runs antero-superiorly to exit through the neural compartment of the jugular foramen. The vertebral artery, however, remains anterior to the accessory nerve, thus facilitating dissection towards the lateral medullary surface. By combining the trancondylar and supracondylar variants, angulating the microscope towards the brainstem (as opposed to the petrous bone) allows for maximal access to the upper and lower antero-lateral medullary surface as well as the neurovascular structures in the cerebellomedullary and premedullary cisterns. Visualizing the antero-medial medullary surface, however, is facilitated by the help of angled endoscopes passed through the vagoaccessory triangle.

13.5.3.4 Microsurgical Dissection Technique

We have encountered both gliomas that were easily discernable from the normal brain parenchyma as well as tumors that tended to diffusely infiltrate the brainstem and lacked a plane of dissection, some of which were PAs. In contrast to other tumor entities, GGs showed a tendency toward firm adhesion to adjacent cranial nerve rootlets or blood vessels, thus usually preventing a 100% tumor removal. Generally, many tumors encountered in this series were well-vascularized, gray-reddish in color, soft, and easily aspirated using the suction tube or the ultrasonic aspirator (Fig. 13.9).

With few exceptions, most of the PAs were well-demarcated, and the surrounding brainstem parenchyma was not edematous. GGs were of higher consistency than PAs and appeared as a rather compact tumor tissue. In high-grade gliomas,

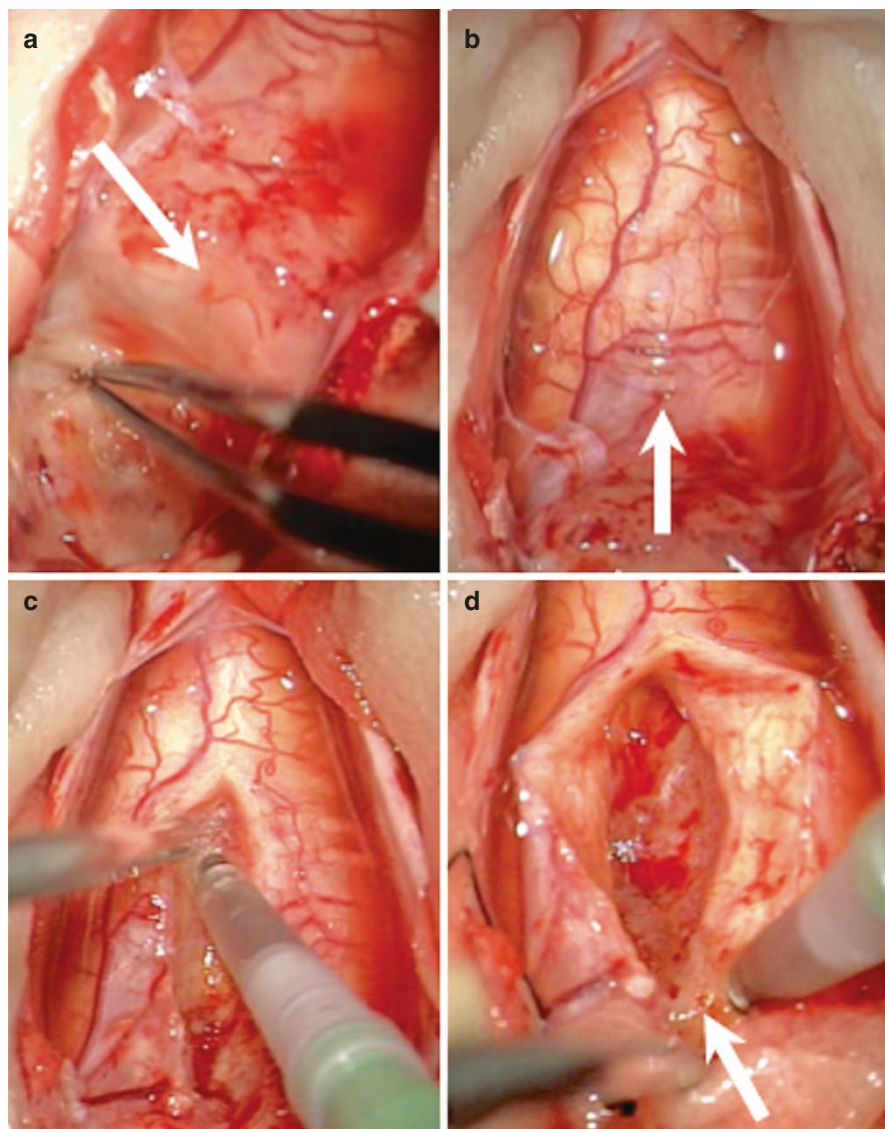


Fig. 13.9 Intraoperative photograph of the patient shown in Fig. 13.8. Due to the initial surgical intervention with tumor biopsy and duraplasty performed at another hospital, severe scar formation and adhesions between the dorsal tumor surface and surrounding structures were encountered, particularly at the level of the transition between the medulla and spinal cord (a, arrow). In this area, the tumor had invaded the upper cervical cord in an infiltrative manner (b, arrow). Tumor resection was started in the cervical area and was carried out via a midline myelotomy at C1 and C2 levels using the ultrasonic aspirator (c). Particularly on the left side, the tumor had diffusely invaded the spinal cord and medulla (d, arrow). Consequently, no clearly demarcated dissection plane could be found in this area between the tumor and CNS parenchyma. For safety reasons, small residual tumor portions were therefore deliberately left behind

only rarely did we find a well-defined tumor border. These tumors usually grew in a diffusely infiltrative manner, and the adjacent parenchyma was edematous and contained fragile blood vessels, sometimes rendering local hemostasis quite difficult.

Initially, we started with microsurgical tumor volume reduction in a safe remote region and then gradually worked toward the tumor-parenchyma transition area.

In the 13 intrinsic gliomas of this series, the tumors were not readily visible on the surface of the brainstem. In these cases, we had to choose an optimal entry zone into the medulla. Depending on tumor location, this was either the posterior midline of the medulla (posterior median sulcus, above and/or below the obex) and, in many instances, combined with a midline myelotomy of the upper spinal cord, or the lateral or even anterolateral aspect of the medulla, such as the pre-olivary and retro-olivary sulci. Alternate safe entry zones through the dorsal surface of the medulla also include the posterior intermediate and posterior lateral sulci. Occasionally, during microsurgical tumor dissection within the medulla, sudden bradycardia and/or a significant rise in blood pressure occurred. In such instances, microsurgical manipulation was immediately interrupted for several minutes to allow for the cardiovascular situation to normalize again.

13.5.3.5 Extent of Tumor Resection

In principle, we always attempted removing as much of the tumor mass as deemed safely possible. Not surprisingly, the medulla did not tolerate excessive surgical manipulation because long-tract pathways and cranial nerve nuclei are concentrated here in a tight fashion. In the case of focal tumors in which the pathological tissue was clearly distinguishable from the medullary parenchyma, we were able to remove a larger amount of the tumor without affecting the brainstem parenchyma. Somewhat differently, we resected diffusely infiltrating bulbar tumors only to a certain degree, while correlating the tumor size known from preoperative MRIs with local measurements using a millimeter scale (see Fig. 13.5), and guided by the stability of intraoperative evoked potentials, heart rate, and blood pressure. In every case, we also concentrated on distinguishing tumor feeders from perforating pial arteries supplying the medulla to avoid local ischemic damage.

Table 13.3 gives an overview of the extent of tumor resection according to the underlying tumor entity. In half of our cases (approximately 51%), we achieved

Table 13.3 Extent of tumor resection

Tumor Entity/Extent of Resection	GTR	NTR	STR	Biopsy or Debulking
Pilocytic astrocytoma	8	3	4	1
Anaplastic astrocytoma	3	3	6	2
Ganglioglioma	1	3	3	1
Glioblastoma	0	1	2	2
Total	12 (27.9%)	10 (23.2%)	15 (34.9%)	6 (14%)

Abbreviations: *GTR* gross-total resection (99–100% of tumor volume removed), *NTR* near-total resection (90–98%), *STR* subtotal resection (50–89%), Biopsy/debulking, (<50%)

Table 13.4 Outcome and surgical characteristics

	Pilocytic Astrocytoma	Anaplastic Astrocytoma	Ganglioglioma	Glioblastoma
Lost to follow-up	1	3	1	0
No new neurologic deficits	12	11	6	1
Additional morbidity	4	3	2	4
Surgical complications	1	0	0	0
Postoperative tracheostomy required	2	1	0	2
Tumor progression/recurrence	4	5	2	5
Repeat tumor surgery	2	0	1	1
Disease-related death	2	3	0	5

gross-total resection (GTR) or near-total resection (NTR), which is a quite satisfactory rate for bulbar gliomas. Expectedly, the resection rate was somewhat higher in PAs, even in patients suffering from large tumors. Tumor volume reduction of less than 50% (tumor debulking) was carried out in only 14% of cases, as expected in high-grade tumors.

13.5.4 Clinical Outcome

Fortunately, there was no direct surgical mortality, and no patient suffered from permanently or severely disabling neurological deficits attributable to the surgical intervention. All patients who did not ultimately survive died later on from their primary disease, the bulbar glioma.

Remarkably, no additional neurological deficits occurred in 30 of 43 individuals (approximately 70%) as shown in Table 13.4. Moreover, there was no patient of this series in whom, retrospectively, management of the bulbar glioma would have appeared more favorable without surgical intervention, which also supports our method of patient selection.

13.5.4.1 Pilocytic Astrocytoma

In 12 of 16 individuals suffering from a PA, there were no additional neurological deficits after surgery. Four patients experienced temporary neurological deterioration such as the patient shown in Fig. 13.10, who was the only individual suffering from a postoperative complication, namely CSF leak that required re-operation. Two male patients (56 and 61 years old) passed away due to progression of the tumor at 3 years and 8 months after surgery, respectively. They had experienced no or only mild additional symptoms immediately after surgery, but an early local tumor recurrence occurred in both; one of them is shown in Fig. 13.4. We suspect

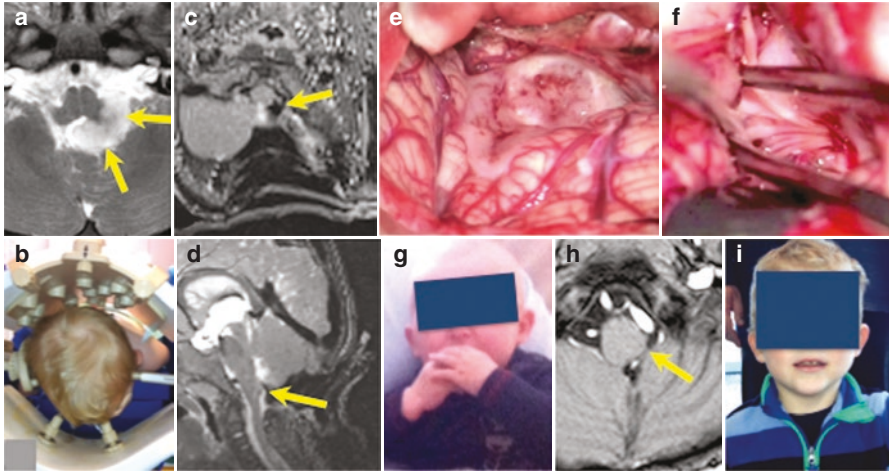


Fig. 13.10 The parents of this 15-month-old boy noticed an abnormal head tilt to the left side in their child since he was 10 months old. Obviously, these symptoms were caused by left-sided partial sixth nerve palsy. Moreover, the child developed recurrent laryngitis. Preoperative MRI revealed a homogeneous tumor originating from the left lateral medulla, which extended posteriorly and laterally (a, arrows). The boy underwent surgery in the prone position with the head fixed in a special headrest coil unit (b) for intraoperative magnetic resonance imaging (BrainLAB, 1.5-T MR imager Magnetom Espree, Siemens). Intraoperative T1- and T2-weighted images were obtained during surgery to rule out any tumor remnants (c and d, arrows). The tumor (a pilocytic astrocytoma) was exposed via combined posterior median and left lateral suboccipital craniotomy with wide opening of the foramen magnum. The tumor tissue was homogeneous, of soft consistency, and well distinguishable from the normal brainstem parenchyma (e). Tumor volume reduction was carried out with an ultrasonic aspirator. In the left lateral recess, the tumor was adherent to the rootlets of the caudal cranial nerves; nevertheless, it was successfully separated from these structures while preserving their integrity. Gross-total tumor removal was achieved (f). Postoperatively, dysphagia precluded oral nutrition for 9–10 days; due to subcutaneous collection of cerebrospinal fluid, the boy underwent a second surgical intervention after 4 days for dural repair. Subsequently, the child's deglutition gradually normalized again, and the boy was symptom-free at 2 weeks after surgery (g). Three years after surgery, T1-weighted contrast-enhanced MRIs documented complete tumor removal (h), and the boy is in excellent clinical condition without neurological deficits (i)

that the diagnosis of PA might not have been accurate in either case. Circumstantial evidence suggests that these individuals may rather have suffered from an anaplastic PA or DMG. Tumor progression was documented in two additional patients during the long-term follow-up, while repeat surgery was carried out in only two of the four individuals at 2 years and 3 years after the first intervention.

13.5.4.2 Ganglioglioma

There were no surgical complications in this subgroup of patients. Only two females, 17 and 53 years old, suffered from postoperative augmentation of preoperative symptoms (facial palsy in one and ataxia in the other), but these symptoms gradually faded away thereafter. Due to local tumor recurrence, one 10-year-old boy

underwent a second surgical intervention at 4 years after the first operation and remained symptom- and tumor progression-free until now, 15 years following the second surgery. A 27-year-old female also with local tumor recurrence is scheduled to undergo a repeat surgery in the near future. All remaining patients repeatedly showed stable serial MRIs and remained in excellent condition after surgery.

13.5.4.3 Anaplastic Astrocytoma

Despite harboring a high-grade tumor, the vast majority of patients with anaplastic astrocytoma (11/14) also did not experience new neurological deterioration after surgery. There were only mild additional symptoms, such as sensory deficits or a deteriorating facial palsy in three other individuals. Fortunately, no surgical complications were observed in the 14 patients suffering from anaplastic astrocytoma. To prevent aspiration pneumonia due to exacerbation of pre-existing dysphagia, one male individual required tracheostomy at 8 days after surgery. While three individuals were lost to follow-up, we know from three others that they have died from their bulbar glioma between 10 months and 3 years postoperatively. Clear tumor progression was documented in 5 of 14 patients during the follow-up period. Repeat surgery might be considered in these patients.

13.5.4.4 Glioblastoma

Gratifyingly, there was also no surgical complication in any patient harboring a glioblastoma. While one female aged 24 years did not deteriorate neurologically after surgery, augmentation of pre-existing symptoms was observed in the remaining four individuals. Two of them required postoperative tracheostomy for 3 and 4 months, respectively. In all patients, the tumor eventually progressed despite combined radio-chemotherapy after surgery. One male aged 43 years with hypermethylated MGMT promoter underwent a second surgical intervention at 2 years after the initial operation and survived in an excellent clinical condition for additional 2 years until he died from diffuse local tumor recurrence. The remaining four patients died between 8 months and 2.5 years after surgery. Postoperatively, all patients did well according to the circumstances, and in all patients, surgery did favorably modify the course of the disease, at least for a certain time period. According to the preoperative clinical condition with rapid neurological deterioration, as well as taking into account the preoperative MRIs, none of the five glioblastoma patients would have survived more than a few months at most without surgical intervention.

13.6 Conclusion

From reviewing the pertinent literature, it is known that many physicians regard bulbar gliomas at first glance as inoperable lesions. However, with a reasonable patient selection policy, microsurgical tumor removal is feasible even in complex

lesions as demonstrated in this chapter, with an acceptable resection rate, good to excellent outcome, and a very low complication rate. The authors are convinced that surgery plays an important role in the overall management of medullary gliomas. In the context of modern molecular diagnosis, tumor sampling may gain even more importance in the near future. Continuous electrophysiological monitoring during surgery is helpful in guiding tumor resection and in avoiding surgical complications. A flexible attitude of the surgeon during the microsurgical intervention, for instance by not attempting an ideally high tumor resection rate in diffuse lesions that lack clear demarcation from the bulbar parenchyma, may help in avoiding irreversible damage to the medulla. On the other hand, radical tumor resection should be attempted in at least all focal low-grade tumors that are well-discernable from the brainstem parenchyma, since the tumor resection rate may favorably influence the patient's long-term outcome and survival. The final decision regarding the degree of tumor volume reduction, however, should always be taken during surgery, based on the local circumstances and specific tumor tissue properties. While a desirable resection rate, as well as a good-to-excellent outcome can be achieved also in grade III bulbar gliomas, surgery may influence the natural history of bulbar glioblastomas in a positive manner.

References

1. Babu R, Kranz PG, Agarwal V, McLendon RE, Thomas S, Friedman AH, et al. Malignant brainstem gliomas in adults: clinicopathological characteristics and prognostic factors. *J Neuro-Oncol.* 2014;119(1):177–85.
2. Bertalanffy H, Tsuji Y, Banan R, Kar S. Adult brainstem gliomas. In: Spetzler RF, Kalani MYS, Lawton MT, editors. *Surgery of the brainstem.* New York: Thieme; 2019.
3. Brat DJ, Aldape K, Colman H, Holland EC, Louis DN, Jenkins RB, et al. cIMPACT-NOW update 3: recommended diagnostic criteria for diffuse astrocytic glioma, IDH-wildtype, with molecular features of glioblastoma, WHO grade IV. *Acta Neuropathol.* 2018;136(5):805–10.
4. Bricolo A. Surgical management of intrinsic brain stem gliomas. *Oper Tech Neurosurg.* 2000;3(2):137–54.
5. Capper D, Jones DTW, Sill M, Hovestadt V, Schrimpf D, Sturm D, et al. DNA methylation-based classification of central nervous system tumours. *Nature.* 2018;555(7697):469–74.
6. El Ahmadieh TY, Plitt A, Kafka B, Aoun SG, Raisanen JM, Orr B, et al. H3 K27M mutations in thalamic pilocytic astrocytomas with anaplasia. *World Neurosurg.* 2019;124:87–92.
7. Ellezam B, Theeler BJ, Walbert T, Mammoser AG, Horbinski C, Kleinschmidt-DeMasters BK, et al. Low rate of R132H IDH1 mutation in infratentorial and spinal cord grade II and III diffuse gliomas. *Acta Neuropathol.* 2012;124(3):449–51.
8. Gessi M, Capper D, Sahm F, Huang K, von Deimling A, Tippelt S, et al. Evidence of H3 K27M mutations in posterior fossa ependymomas. *Acta Neuropathol.* 2016;132(4):635–7.
9. Gupta K, Orisme W, Harreld JH, Qaddoumi I, Dalton JD, Punchihewa C, et al. Posterior fossa and spinal gangliogliomas form two distinct clinicopathologic and molecular subgroups. *Acta Neuropathol Commun.* 2014;2:18.
10. Hartmann C, Meyer J, Balsas J, Capper D, Mueller W, Christians A, et al. Type and frequency of IDH1 and IDH2 mutations are related to astrocytic and oligodendroglial differentiation and age: a study of 1,010 diffuse gliomas. *Acta Neuropathol.* 2009;118(4):469–74.

11. Hu J, Western S, Kesari S. Brainstem Glioma in Adults. *Front Oncol.* 2016;6:180.
12. Hundsberger T, Tonder M, Hottinger A, Brugge D, Roelcke U, Putora PM, et al. Clinical management and outcome of histologically verified adult brainstem gliomas in Switzerland: a retrospective analysis of 21 patients. *J Neuro-Oncol.* 2014;118(2):321–8.
13. Jallo GIFTD, Roonprapunt C, Epstein F. Current management of brainstem gliomas. *Ann Neurosurg.* 2003;3(1):1–17.
14. Javadi SA, Hartmann C, Walter GF, Banan R, Samii A. IDH1 mutation in brain stem glioma: case report and review of literature. *Asian J Neurosurg.* 2018;13(2):414–7.
15. Jones DT, Hutter B, Jager N, Korshunov A, Kool M, Warnatz HJ, et al. Recurrent somatic alterations of FGFR1 and NTRK2 in pilocytic astrocytoma. *Nat Genet.* 2013;45(8):927–32.
16. Joyon N, Tauziède-Espariat A, Alentorn A, Giry M, Castel D, Capelle L, et al. K27M mutation in H3F3A in ganglioglioma grade I with spontaneous malignant transformation extends the histopathological spectrum of the histone H3 oncogenic pathway. *Neuropathol Appl Neurobiol.* 2017;43(3):271–6.
17. Kleinschmidt-DeMasters BK, Donson A, Foreman NK, Dorris K. H3 K27M mutation in gangliogliomas can be associated with poor prognosis. *Brain Pathol.* 2017;27(6):846–50.
18. Koelsche C, Wohrer A, Jeibmann A, Schittenhelm J, Schindler G, Preusser M, et al. Mutant BRAF V600E protein in ganglioglioma is predominantly expressed by neuronal tumor cells. *Acta Neuropathol.* 2013;125(6):891–900.
19. Louis DN, et al. WHO classification and grading of tumours of the central nervous system. Revised 4th ed. World Health Organization classification of tumours. Lyon: IARC Press; International Agency for Research on Cancer; 2016.
20. Orillac C, Thomas C, Dastagirzada Y, Hidalgo ET, Golfinos JG, Zagzag D, et al. Pilocytic astrocytoma and glioneuronal tumor with histone H3 K27M mutation. *Acta Neuropathol Commun.* 2016;4(1):84.
21. Pekmezci M, Villanueva-Meyer JE, Goode B, Van Ziffle J, Onodera C, Grener JP, et al. The genetic landscape of ganglioglioma. *Acta Neuropathol Commun.* 2018;6(1):47.
22. Purohit B, Kamli AA, Kollias SS. Imaging of adult brainstem gliomas. *Eur J Radiol.* 2015;84(4):709–20.
23. Reers S, Krug D, Stummer W, Hasselblatt M. Malignant progression of a histone H3.3 K27M-mutated spinal pilocytic astrocytoma in an adult. *Clin Neuropathol.* 2017;36(2):83–5.
24. Reinhardt A, Stichel D, Schrimpf D, Sahm F, Korshunov A, Reuss DE, et al. Anaplastic astrocytoma with piloid features, a novel molecular class of IDH wildtype glioma with recurrent MAPK pathway, CDKN2A/B and ATRX alterations. *Acta Neuropathol.* 2018;136(2):273–91.
25. Reithmeier T, Kuzeawu A, Hentschel B, Loeffler M, Trippel M, Nikkhah G. Retrospective analysis of 104 histologically proven adult brainstem gliomas: clinical symptoms, therapeutic approaches and prognostic factors. *BMC Cancer.* 2014;14:115.
26. Reyes-Botero G, Giry M, Mokhtari K, Labussière M, Idbaih A, Delattre JY, et al. Molecular analysis of diffuse intrinsic brainstem gliomas in adults. *J Neuro-Oncol.* 2014;116(2):405–11.
27. Schindler G, Capper D, Meyer J, Janzarik W, Omran H, Herold-Mende C, et al. Analysis of BRAF V600E mutation in 1,320 nervous system tumors reveals high mutation frequencies in pleomorphic xanthoastrocytoma, ganglioglioma and extra-cerebellar pilocytic astrocytoma. *Acta Neuropathol.* 2011;121(3):397–405.
28. Schwartzentruber J, Korshunov A, Liu XY, Jones DT, Pfaff E, Jacob K, et al. Driver mutations in histone H3.3 and chromatin remodelling genes in paediatric glioblastoma. *Nature.* 2012;482(7384):226–31.
29. Sturm D, Witt H, Hovestadt V, Khuong-Quang DA, Jones DT, Konermann C, et al. Hotspot mutations in H3F3A and IDH1 define distinct epigenetic and biological subgroups of glioblastoma. *Cancer Cell.* 2012;22(4):425–37.
30. Theeler BJ, Ellezam B, Melguizo-Gavilanes I, de Groot JF, Mahajan A, Aldape KD, et al. Adult brainstem gliomas: correlation of clinical and molecular features. *J Neurol Sci.* 2015;353(1–2):92–7.

31. Wu G, Broniscer A, McEachron TA, Lu C, Paugh BS, Becksfors J, et al. Somatic histone H3 alterations in pediatric diffuse intrinsic pontine gliomas and non-brainstem glioblastomas. *Nat Genet.* 2012;44(3):251–3.
32. Wu G, Diaz AK, Paugh BS, Rankin SL, Ju B, Li Y, et al. The genomic landscape of diffuse intrinsic pontine glioma and pediatric non-brainstem high-grade glioma. *Nat Genet.* 2014;46(5):444–50.

Chapter 14

Radiation and Chemotherapy for Brainstem Tumors



Katherine E. Warren

Abbreviations

[¹²⁴ I]-8H9	Radioisotope iodine 124 conjugated to antiglioma monoclonal anti-body 8H9
BBB	Blood-brain barrier
BMP	Bone morphogenetic protein
BRD4	Bromodomain containing protein 4
CDK7	Cyclin dependent kinase 7
CED	Convection enhanced delivery
CNS	Central nervous system
CSF	Cerebrospinal fluid
DIPG	Diffuse intrinsic pontine glioma
EFS	Event-free survival
EGFR	Epidermal growth factor receptor
FLAIR	Fluid attenuated inversion recovery
HDAC	Histone deacetylase
HR	Hazard ratio
IgG1	Immunoglobulin G-1
IL13-PE	Interleukin-13-pseudomonas exotoxin
MRI	Magnetic resonance imaging
N	Number
NF-I	Neurofibromatosis type I
OS	Overall survival
PCV	Procarbazine, lomustine and vincristine
PEG-Intron	Pegylated interferon alpha-2b
PFS	Progression-free survival
TPCV	6-thioguanine, procarbazine, lomustine and vincristine

K. E. Warren (✉)

Pediatric Neuro-Oncology, Dana Farber Cancer Institute, Boston, MA, USA

e-mail: KatherineE_Warren@dfci.harvard.edu

TTP	Time to progression
WHO	World Health Organization
WT	Wild type

14.1 Introduction

Brainstem gliomas are a heterogeneous group of tumors. Because clinical presentation and prognosis can differ significantly, treatment options vary, and a risk-to-benefit analysis is employed [1, 2]. In children, brainstem gliomas are often distinguished as diffuse intrinsic pontine glioma (DIPG) or non-DIPG. The biology and prognosis of adult “DIPG” differ from pediatric DIPG; unlike non-DIPG brainstem gliomas in children that are frequently low-grade, adult non-DIPG brainstem gliomas are frequently malignant and portend a poor prognosis. Therefore, differences in prognosis between adult DIPG and non-DIPG are not as evident as in the pediatric population. Treatment recommendations consider surgical resectability, clinical presentation, radiographic appearance, and tumor grade. Other factors such as length of time of symptoms, rapidity of symptom progression, present or impending cerebrospinal fluid (CSF) obstruction, patient age, and other prognostic factors may play a role in treatment decisions.

DIPG are diffuse, infiltrative lesions with tumor cells intertwined amongst critical neural structures in the brainstem and, therefore, lack a realistic surgical option. Histologically, these lesions are World Health Organization (WHO) Grades II-IV gliomas. Pediatric patients with typical DIPG tend to have similar outcomes regardless of tumor grade [3], while glioma grading in adults does appear to impact outcome [4]. Additionally, H3K27M mutations are found in up to 80% of children with DIPG [5], yet this mutation does not appear to be as common in the adult disease. The presence of this mutation is *prognostic*, with patients having lower overall survival (OS) compared to those children with wild type (WT) H3 [6, 7]. Despite this, standard treatment regimens remain the same for children with and without these mutations, as no clinically effective therapy has yet been identified; i.e., H3K27M mutations are not yet *predictive* of response. As will be discussed in the chemotherapy section, biopsy with identification of specific mutations, including H3K27M, has led to clinical trials involving molecularly targeted agents with the hope that therapy aimed at specific mutations will be more effective than empiric therapies.

In contrast to the malignant biology observed in DIPG, pediatric non-DIPG brainstem gliomas frequently display a more benign nature and clinical course. Non-DIPG brainstem gliomas are further categorized as focal, dorsal exophytic, or cervicomedullary gliomas [8]. Whereas diffuse brainstem gliomas most frequently occur in the pons, low-grade, well-circumscribed gliomas typically involve mid-brain and medulla locations [9], suggesting oncogenic contributions from the microenvironment and different cells of origin. Notably, the survival rates of patients with focal and exophytic brainstem gliomas, which are typically discrete masses, and even cervicomedullary gliomas, which are frequently pilocytic astrocytomas,

are significantly higher than those with diffuse lesions involving the pons, as these tend to be amenable to surgical resection (complete or partial resection or debulking) [1, 10–12].

Adult brainstem gliomas account for <2% of all adult gliomas [4, 13, 14], and approximately 60% have their epicenter in the pons [15]. Although the data is limited, adults with diffuse pontine gliomas tend to have modestly better outcomes than children with DIPG [13]. In contrast to typical pediatric DIPG in which median survival is less than 1 year from diagnosis, median survival for adults with brainstem glioma is 30–49 months [4, 16], although the number of patients included in adult studies are small, and it is unclear how many patients display the characteristic clinical and radiographic findings of typical pediatric DIPG. In adult brainstem glioma, there is an association between the presence of contrast enhancement with survival (worse outcomes with increasing grade and contrast-enhancement) [4, 16], although this correlation is not clear in pediatric DIPG [17]. However, differences in outcome between adult and pediatric DIPG do not appear solely related to differences in histologic grade [18].

For clarity, this chapter will be organized to discuss the treatment of (a) pediatric DIPG, (b) pediatric non-DIPG brainstem gliomas, and (c) adult brainstem gliomas.

14.2 Treatment of Pediatric Diffuse Intrinsic Pontine Glioma (DIPG)

There are limited therapeutic options for patients with DIPG. The *only* therapy that has demonstrated significant, albeit temporary, clinical benefit to children with DIPG is radiation therapy, which remains the standard of care [17, 19]. Patients often present with rapid onset (days-to-weeks) and progressively worsening symptoms. Glucocorticoids are typically initiated at diagnosis or early in the radiation course to alleviate symptoms attributed to peritumoral edema. While radiation therapy is frequently instituted as soon as possible in efforts to relieve or reduce symptoms, a retrospective study demonstrated that the time from diagnosis to the start of radiation therapy did not affect event-free survival (EFS) or OS [20].

14.2.1 Radiation Therapy

The standard therapeutic approach for patients diagnosed with DIPG is external beam radiation therapy, administering 54–60 Gy via focal photon radiation therapy in 180–200 cGy fractions, 5 days per week, over approximately 6 weeks [17, 21–25]. This schedule, applicable to patients with any malignant glioma, has not changed over the past 5 decades and was originally established based upon the convenience of the 5-day schedule and experience of radiotherapists regarding acute tolerability of patients [26]. The total dose of radiation administered is critical for

malignant glioma. In a retrospective study evaluating a dose-effect of 50, 55 or 60 Gy for malignant glioma, there was a direct relationship between increasing dose and increased survival [26]. For children with DIPG, it is generally agreed that doses less than 50 Gy are inadequate, and doses higher than 60 Gy may introduce additional toxicities without added benefit [27]. The gross tumor volume is defined based on T2-weighted, fluid attenuated inversion recovery (FLAIR), and T1-weighted post-contrast sequences, with the clinical target volume including the gross tumor volume and a 1–2 cm margin [20]. Conformal radiation therapy approaches may be used to decrease the volume irradiated and protect critical structures. In a study utilizing fractionated stereotactic radiation therapy, 41 patients ($n = 26$ adults; $n = 15$ children) with brainstem gliomas, including DIPG, received fractionated, high precision radiation therapy to a total dose of 54 Gy [27]. The pattern of failure was local in the majority of patients. Despite the heterogeneous group of patients, this study demonstrated the feasibility of fractionated stereotactic radiation therapy to improve target point precision and decrease exposure to critical structures. However, DIPG commonly extends beyond the pons, and some authors advocate more extended, rather than more precise, radiation fields [3, 28]. In this same context, most experts agree that there is no role for proton radiation therapy approaches in typical DIPG patients.

Radiation therapy improves neurological symptoms in approximately 75% of patients with DIPG and increases OS from a median of 4.7 months [29] to 8–11 months [17, 21]. Unfortunately, any beneficial anti-tumor effects of radiation therapy are short-lived, with tumor growth or clinical progression generally noted within 3–6 months of completion [17, 19, 30–32]. The pattern of failure is usually local [30], although the tumor is frequently also found outside the radiation field, with leptomeningeal and/or subventricular zone disease detected in most patients at autopsy [28]. Despite these findings at autopsy, craniospinal radiation at diagnosis is not typically performed unless indicated by clinical symptoms.

14.2.1.1 Hyperfractionated Radiotherapy

While there are some variations to the standard dose and schedule for DIPG [33], including higher total doses or alternate schedules, a limited number of studies have been performed to determine the optimal schedule providing the best therapeutic index and clinical benefit [34]. Because there is a known dose-response relationship for radiation in malignant gliomas [26], higher doses have been investigated in children with brainstem tumors. In reviewing the impact of these trials, it is important to note that many initial clinical trials did not distinguish DIPG from other brainstem gliomas. In a study comparing a total dose of 70.2 Gy administered in 117 cGy twice daily fractions over 6 weeks with conventional radiation therapy (total dose was 54 Gy administered in 180 cGy fractions over 6 weeks), OS, EFS and toxicities of the $n = 130$ patients did not significantly differ (OS 8 months versus 8.5 months,

respectively) [31]. A Phase I/II clinical trial of escalating doses of hyperfractionated radiation therapy initially suggested a trend toward clinical benefit, with increased OS and time to progression (TTP) with increasing total radiation doses of 66–72 Gy; subsequently, the dose was increased to 75.6 Gy [35]. However, while neurological improvement was still noted in about 75% of patients, higher doses of radiation therapy again did not improve the median TTP or OS (7 months versus 10 months, respectively) [35]. The pattern of failure again was local progression, although 6 of 39 patients also had leptomeningeal disease. Notably, more than 60% of patients required steroids for at least 3 months, and 45% had evidence of intratumoral necrosis on imaging. Another study evaluated hyperfractionated radiotherapy doses of 78 Gy in children with brainstem gliomas [36]. Although this dose was relatively well-tolerated, results were similar, with no improvement in patient outcomes, evidence of prolonged steroid-dependency, and apparent radiation necrosis on imaging. In a follow-up study comparing conventional versus hyperfractionated radiation therapy and incorporating cisplatin as a radiation sensitizer in both arms in children with newly diagnosed brainstem gliomas, there was no significant difference in EFS or OS [31]. Thus, given the evidence to date, there is no role for hyperfractionated radiation therapy in this population.

14.2.1.2 Hypofractionated Radiation Therapy

In an effort to shorten the 6-week radiation timeline and reduce the treatment burden, hypofractionated radiotherapy delivered over shorter time periods, usually 3–4 weeks, has been investigated in several studies of children with newly diagnosed DIPG [30, 37]. In a single institution study of 22 children with newly diagnosed DIPG [37], 14 patients received the prescribed dose of 45 Gy in 15 fractions of 3 Gy, while 5 patients required a reduced daily dose due to toxicities, and 1 patient died due to severe intracranial hypertension after two fractions. Median TTP and OS were 5.7 and 7.6 months, respectively. In a second study that was a multi-center retrospective analysis, $n = 27$ children with newly diagnosed DIPG treated with one of two hypofractionated regimens administered over 3–4 weeks (39 Gy in 3 Gy fractions or 44.8 Gy in 2.8 Gy fractions) were compared to a randomly selected matched cohort receiving conventional radiation therapy [30]; TTP and OS were reported as not significantly different between the two groups (TTP 5.0 vs. 7.6 months [$p = 0.24$], and OS 9 vs. 9.4 months, respectively), although the number of patients was small [30]. In a randomized control study of $n = 71$ patients comparing hypofractionated therapy (total dose was 39 Gy administered in 3 Gy fractions; 13 fractions over 2.6 weeks) versus conventional radiation therapy (54 Gy in 180 cGy fractions over 6 weeks), median OS for the hypofractionated group was 7.8 months versus 9.5 months in the conventional radiation therapy group [38]. No significant difference in OS (hazard ratio [HR] 1.03) or toxicities were noted between the two groups [34]. Taken together, these studies suggest that shorter radi-

ation treatment periods may be appropriate for some patients, e.g., those needing daily anesthesia; however, although statistically significant differences have not been observed in each study, patient numbers are small, there appears to be a trend toward shorter TTP, and larger, randomized trials are needed.

14.2.1.3 Radiosensitizing Agents

Agents that increase a cancer cell's vulnerability to radiation have been investigated in further attempts to optimize the anti-tumor effects of radiation therapy for DIPG. However, no radiosensitizing agent to date has significantly improved outcomes for this patient population. Cisplatin was one of the earliest agents to be clinically investigated as a radiosensitizer given its ability to potentiate radiation effects preclinically *in vitro* and *in vivo* [39, 40]. In a clinical trial comparing hyperfractionated radiation therapy with and without cisplatin as a radiosensitizer in children with diffuse intrinsic brainstem gliomas, patients receiving cisplatin had a worse outcome compared to those receiving radiation therapy only, suggesting increased toxicity in those receiving combination therapy [41]. Motexafin-gadolinium is another radiosensitizing agent evaluated in children with DIPG [42, 43]. Its metalloporphyrin localizes in tumors and inhibits oxidative stress-related proteins, resulting in a decreased ability to repair radiation-induced damage [44]. Despite its ability to penetrate into the tumor as assessed on magnetic resonance imaging (MRI) scans, addition of Motexafin-gadolinium to conventional radiation therapy did not improve OS in a clinical trial for children with DIPG [43]. Additional chemotherapeutic agents, such as gemcitabine [45] and capecitabine [46] have been evaluated as radiosensitizers and/or given in the adjuvant setting as "chemoradiation" therapy. As with other chemotherapeutic agents, no improvement in outcomes has been demonstrated; furthermore, there is some concern for additional toxicities and potential delays in radiation therapy [41].

14.2.2 Chemotherapy

As stated above, DIPG tumor cells are infiltrative, intertwined with normal cells in the brainstem. They may extend contiguously into the midbrain and medulla, locally into the cerebellar peduncles, and involve the subventricular space and leptomeninges, suggesting that non-focal adjuvant treatment is needed. Despite a number of investigational trials, no therapy except radiation therapy has ever demonstrated any significant anti-tumor effect, clinical benefit, or significant improvement in outcomes in a clinical trial for children with DIPG. Consequently, the standard treatment for children with DIPG has not changed in decades. Many children with DIPG are enrolled in clinical trials; these have investigated various chemotherapeutic

agents and strategies, including conventional cytotoxic agents, high-dose chemotherapy strategies, chemo-radiotherapy, and molecularly targeted agents. Attempts to address the lack of chemotherapy efficacy by varying the timing of chemotherapy administration have been explored, including pre-radiation chemotherapy, chemotherapy concurrently with radiation therapy, and post-radiation chemotherapy. A number of obstacles have been identified as a result of these approaches; despite wide-ranging approaches, DIPG has remained elusive. While subsequent clinical trials have been designed to overcome specific obstacles, the typical drug development and standard clinical trial paradigm has not significantly changed to *collectively* address these obstacles.

14.2.2.1 Empiric Therapies

For years, we had been hampered by the assumption that the biology of DIPG was similar to adult supratentorial malignant glioma as they appear histologically similar. Consequently, chemotherapeutic agents evaluated in clinical trials for children with DIPG have been selected based upon adult malignant glioma data or empirically, as disease-specific pre-clinical tools, such as DIPG cell lines and animal models, were non-existent until relatively recently. The combination of procarbazine, lomustine and vincristine (PCV), a regimen that is modestly active in adult malignant glioma, was one of the earliest therapies explored in children with high-grade glioma, including diffuse intrinsic brainstem glioma [47]. However, the outcome for these patients was not improved. As the PCV regimen was replaced by radiation therapy with concomitant, followed by adjuvant, temozolomide as the standard therapy for adults with glioblastoma multiforme [48], interest in evaluating temozolomide for children with DIPG peaked. Despite its activity in adult glioblastoma, its good central nervous system (CNS) tissue penetration [49], easy accessibility, tolerability, and numerous clinical trials in children with DIPG, *no* clinical trial has demonstrated significant activity of temozolomide in children with DIPG [6, 50–59] (Table 14.1). Accordingly, the multiple trials demonstrating the lack of temozolomide efficacy in DIPG generated suspicion that DIPG may biologically differ from adult glioblastoma and heralded further exploration into DIPG biology.

Administering chemotherapy at different timepoints in the disease course has been evaluated in children with DIPG. In a study evaluating pre-radiation chemotherapy followed by hyperfractionated radiation therapy (total dose was 66 Gy), children with newly diagnosed high risk brainstem tumors were treated with four cycles of cisplatin and cyclophosphamide [61]. Notably, approximately two-thirds of eligible patients (n = 32) clinically improved with steroids and chemotherapy, and radiographic responses were observed with three partial responses. However, the median survival of 9 months was similar to historical controls, and significant chemotherapy-related toxicities were observed.

Table 14.1 Temozolomide studies in diffuse intrinsic pontine glioma (or brainstem glioma, where indicated)

Study Treatment Regimen	Population	Results	Reference
XRT + concurrent TMZ [75 mg/m ² /d] then TMZ [75–100 mg/m ² daily × 21/28 × 12 courses]	Newly diagnosed DIPG [n = 43]	Median TTP 5.6 mo Median OS 9.5 mo	[59]
XRT + concurrent TMZ [75 mg/m ² /d] then TMZ [200 mg/m ² /d Days 1–5 q 28 d]	Newly diagnosed DIPG [n = 20]	Median PFS 6.9 mo Median OS 9.15 mo	[53]
XRT + concurrent TMZ [75 mg/m ² /d] then TMZ [200 mg/m ² /d Days 1–5 q 28 d × 6 cycles]	Newly diagnosed DIPG [histologically confirmed] [n = 21]	Median TTP 7.5 mo Median OS 11.7 mo	[54]
XRT + TMZ [90 mg/m ² /d] then TMZ [200 mg/m ² /d Days 1–5 q 28 d × 10 cycles]	Newly diagnosed DIPG [n = 63]	Median TTP 6.1 mo Median OS 9.6 mo	[52]
XRT then TMZ [150 mg/m ² /d Days 1–5/28] Or XRT + TMZ [75 mg/m ² /d] then TMZ [150 mg/m ² /d Days 1–5/28]	Newly diagnosed DIPG [n = 18]	Median PFS 7.4 mo [n = 10] Median PFS 6.4 mo [n = 8] Median OS 12.3 mo [all]	[60]
XRT + TMZ [85 mg/m ² /d] × 6 weeks, followed by TMZ [85 mg/m ² /d]	Newly diagnosed diffuse BSG [n = 15]	Median TTP 5.13 mo Median OS 9.8 mo	[57]
XRT + concurrent TMZ [75 mg/m ² /d] then TMZ [200 mg/m ² /d Days 1–5 q 28 d]	Newly diagnosed DIPG [n = 15]	Median PFS 7.15 mo Median OS 15.6 mo	[58]
XRT + TMZ [75 mg/m ² /d] then [200 mg/m ² /d] × 5 with cis-retinoic acid [100 mg/m ² /d] × 21 d/28-d cycle.	Newly diagnosed DIPG [n = 12]	Median TTP 10.2 Median OS 13.5	[50]
TMZ [200 mg/m ² /d × 5 q 28 d]	Progressive diffuse BSG [n = 21]	Median OS 6.2 mo	[55]
XRT [pre-XRT irinotecan, optional] then TMZ [200 mg/m ² /d × 5 d q 28 d × 6 cycles]	Newly diagnosed diffuse BSG [n = 33]	Median PFS ~ 8.5 mo Median OS 12 mo	[56]
TMZ [75 mg/m ² /d × 5 d q 28 d cycle] + O ⁶ -BG	Recurrent, progressive BSG [n = 16]	6-mo PFS = 0% Median OS = 60 days	[51]

Abbreviations: *BSG* brainstem glioma, *d* day(s), *DIPG* diffuse intrinsic pontine glioma, *mo* months, *n* number, *OS* overall survival, *O⁶-BG* O⁶-Benzylguanine, *PFS* progression-free survival, *q* every, *TMZ* temozolomide, *TTP* time to progression, *XRT* radiation therapy

Pre-radiation chemotherapy with BCNU, tamoxifen, cisplatin and methotrexate was explored in $n = 23$ children with diffuse brainstem glioma on the BSG 98 trial [62, 63]. Patients on this study had a reported OS of 17 months compared to 9 months in historical controls. While this difference appears significant, the two groups were not prospectively matched. Additionally, children treated with pre-radiation chemotherapy had significantly longer hospital stays compared to the control group. A follow up retrospective review of patients ($n = 16$) treated as per BSG 98 from 2004–2014 at a single institution was performed and compared these patients to children ($n = 9$) who underwent stereotactic biopsy for treatment on targeted therapy protocols at the same institution [63]. Median OS was 16.1 versus 8.8 months, respectively. However, again, the groups were not matched by prognostic factors such as length of symptoms, age at diagnosis, biopsy or debulking, or shunt placement. The clinical benefit of this approach, therefore, should be interpreted with caution, and further randomized trials are needed.

14.2.2.2 Disease-Specific Targeted Therapy

The early 2000's ushered molecularly targeted agents into the clinic, and, as with temozolomide, a number of targeted agents were evaluated in clinical trials for children with DIPG (Table 14.2). These trials were frequently performed without knowledge of the target being present or if the "target" was a factor in driving tumorigenesis, as our understanding of DIPG was limited given that biopsy was not routinely performed in the United States, even for research purposes, until later. Targeted agents selected for clinical trials in children with DIPG were primarily those being evaluated in adult glioblastoma patients. While targets, such as epidermal growth factor receptor (EGFR), had been identified in some DIPG cells using tissue obtained at surgical biopsy or autopsy [64], targeted therapies have not improved the outcomes to date. In an initial study of nimotuzumab, a humanized immunoglobulin G-1 (IgG1) monoclonal antibody targeting ERBB1/EGFR, administered with radiation therapy in children with DIPG, median progression-free survival (PFS) and OS were 5.8 months and 9.4 months, respectively [65]. In a follow-up study, Massimino et al. [66] evaluated the efficacy of nimotuzumab with vinorelbine and radiation therapy in children with newly diagnosed DIPG. Unfortunately, median PFS of the 25 eligible patients was 8.5 months. Of note, biopsy to confirm the presence of EGFR expression in the clinical trials was not routinely performed; the authors report one of four biopsied patients demonstrating cytoplasmic membrane expression of EGFR [66]. Additional clinical trials incorporating molecularly targeted agents for children with DIPG are listed, along with outcomes, in Table 14.2. While studies from autopsies of children with DIPG suggest the possible presence of these targets in some patients with DIPG, confirmation of the presence of the target was not performed prospectively for eligibility

Table 14.2 Diffuse intrinsic pontine glioma clinical trials involving molecularly targeted agents

Target(s)	Phase	Study Drug(s)	Confirmation of target present in DIPG required for eligibility? Y/N	Outcomes	Reference
PDGFR	I	Imatinib	N	Median EFS ~7.2 mo Median OS ~11 mo	[67]
VEGFR-2 EGFR	I	Vandetanib + XRT	N	Median PFS ~8 mo Median OS ~11.5 mo	[68]
VEGFR-2 PDGFR	I	Vandetanib + Dasatinib	N	Median OS ~ 12 mo	[69]
EGFR	I	Erlotinib + XRT	Y for newly diagnosed BSG	PFS 8 mo OS 12 mo No correlation of EGFR and OS	[70]
EGFR	I	Gefitinib + XRT	N for BSG	1-year PFS 16.1% 1-year OS 48%	[71]
EGFR	II	Gefitinib + XRT	N	Median PFS 7.4 mo Median OS ~12 mo	[72]
Farnesyl transferase	I	Tipifarnib + XRT	N	Median PFS ~ <6 mo Median OS ~8.5 mo	[73]
Farnesyl transferase	II	Tipifarnib + XRT	N	Median PFS 6.8 mo Median OS 8.3 mo	[74]
Farnesyl transferase	II	Tipifarnib	N	For recurrent, progressive BSG 6-mo PFS 3% +/- 3%	[75]
Gamma secretase	I	MK-0752	N	Refractory BSG [n = 6]: no responses, no long-term stable disease	[76]
Protein kinase C PI3K/Akt pathways	I	Enzastaurin	N	BSG [n = 5]: no objective responses but 2/5 BSG had stable disease >3 cycles	[77]

Abbreviations: *BSG* brainstem glioma, *EFS* event-free survival, *EGFR* epidermal growth factor receptor, *mo* months, *n* number, *N* no, *OS* overall survival, *PDGFR* platelet derived growth factor receptor, *PFS* progression-free survival, *PI3K* phosphatidylinositol-3-kinase, *VEGFR* vascular endothelial growth factor receptor, *XRT* radiation therapy, *Y* yes

in the majority of these studies. Additionally, most targets, including EGFR, identified in DIPG are not found in *all* tumor cells [64], suggesting that additional/combinatorial therapies may be necessary.

Over the past decade, we have learned that there are significant biological differences between adult glioblastoma and DIPG, and even between pediatric supratentorial malignant glioma and DIPG [78]. Subsequently, there has been a rapid expansion in our understanding of the biology of DIPG due to increasingly available autopsy/biopsy tissue and development of DIPG cell lines and animal models.

The availability of this material, paired with the advent of next generation sequencing tools, has enabled groundbreaking research, revealing a complex genomic and epigenetic landscape that characterizes DIPG as a unique disease entity. The recurrent failures of prior clinical trials in DIPG, the identification of potential therapeutic targets from autopsies of children with DIPG, and the safety of routine biopsy of children with DIPG as demonstrated in Europe [79] support performance of biopsy within the context of clinical trials, particularly for confirmation of targets of molecularly targeted agents for children with DIPG [79–84]. However, while clinical trials incorporating biopsy to identify potential targets in individual patients with DIPG have been performed and are ongoing, no improvement in patient outcomes has been reported yet. The lack of efficacy of molecularly targeted agents, as with other chemotherapeutic agents, is likely multifactorial (Table 14.3).

Unfortunately, routine assessment of tumors before and after treatment to confirm target presence and effects of therapy or development of resistance are not routinely or easily performed, especially for DIPG, where repeat patient tumor sampling raises ethical issues, and animal models do not faithfully represent the patient condition. However, continued development and utilization of DIPG disease-specific pre-clinical tools, including cell lines and xenograft models, have allowed the performance of high throughput drug screens and validation of drug activity in animal models. The initial in-depth DIPG-specific drug-screen utilized a panel of sixteen cell lines derived from children with DIPG to evaluate the activity of eighty-three drugs [85]. The histone deacetylase (HDAC) inhibitor, panobinostat, demonstrated significant activity in 12 of 16 cell lines; this activity was validated in an orthotopic xenograft model of DIPG [85]. The demonstration of HDAC activity in DIPG coincided with the identification of histone mutations in up to 80% of children with DIPG [5, 86, 87], providing a rationale for clinical trials of panobinostat in children with progressive [88] and newly diagnosed post-radiation therapy DIPG (NCT02717455).

Table 14.3 Requirements for efficacious molecularly targeted agents for central nervous system tumors

Requirement	Means of Assessment
Active agent(s)	Identify and validate pre-clinically in DIPG cell lines; tumor models
Presence of target	Patient biopsy prior to treatment
Agent delivered to tumor cells	Determine CNS penetration pre-clinically; patient biopsy after drug administration; imaging of drug/metabolites
Effective exposure [adequate concentration over the necessary period of time] at the tumor site	Determine CNS penetration pre-clinically; imaging of drug/metabolites
Patient able to tolerate doses needed to achieve effective exposure	Phase I clinical trial with pharmacokinetic analysis
Lack of resistance mechanisms	Evaluate patient tumor at time of progression/treatment failure

Abbreviations: *CNS* central nervous system, *DIPG* diffuse intrinsic pontine glioma

Most DIPGs harboring histone H3 mutations have distinct genetic partner mutations that may drive tumorigenesis and may be targetable [85, 89, 90]. This is important as resistance to HDAC inhibition develops in DIPG tumor cells [85], suggesting that combinatorial therapy is necessary. Several pre-clinical studies have demonstrated synergistic activity of agents with HDAC inhibitors [91]. For example, combinatorial therapy of HDAC inhibitors with bromodomain containing protein 4 (BRD4) or cyclin dependent kinase 7 (CDK7) inhibition is synergistic against DIPG cells [91]. Other partner mutations, such as *ACVRI*, typically associated with the H3.1K27M mutation, lead to activation of bone morphogenetic protein (BMP) signaling and, ultimately, increases the transcription of tumor growth promoting genes [92–94], suggesting that targeting *ACVRI* concurrently may have an anti-tumor effect. Pre-clinical studies evaluating combinations of agents are currently underway to validate *in vivo* efficacy to strengthen the rationale for clinical trials in children with DIPG.

14.2.2.3 Biologic Agents

In addition to traditional chemotherapeutic agents, alternate therapeutic approaches, including biologic agents, have been explored. Agents with multiple potential anti-tumor mechanisms, such as thalidomide and its derivatives, and a variety of interferons have been clinically evaluated for the treatment of malignant gliomas with mixed results [95–101]. Several clinical trials utilizing interferons, a family of glycoproteins with antiproliferative and immunomodulatory effects, have been studied for the treatment of malignant gliomas, but the optimal type of interferon, schedule and dosing remains unclear. Based on a pre-clinical study demonstrating that continuous low-dose interferon alfa may be more efficacious than intermittent high doses [102], Warren et al. performed a Phase II study in children with DIPG, initiating weekly low-dose pegylated interferon alpha-2b (PEG-Intron®) after completion of radiation therapy [101]. Although well-tolerated, median TTP was 7.8 months and OS was 11.7 months, which was not significantly different from historical controls.

Given that malignant gliomas are recognized as vascular tumors with overexpression of basic fibroblast growth factor, vascular endothelial growth factor, and platelet derived growth factor, agents such as thalidomide and its subsequent derivatives, including lenalidomide, have been evaluated in clinical trials for children with brainstem gliomas [100, 103]. In a study of thalidomide with radiation therapy, followed by thalidomide, median TTP was 5 months and median survival was 9 months [100]. In a study evaluating thalidomide and temozolomide with and following radiation therapy in children with diffuse pontine glioma, median PFS was 7.2 months and OS was 12.7 months [103], again, not significantly different from historical controls. Most recently, the thalidomide derivative and immunomodulatory agent, lenalidomide, has been evaluated concurrently and following radiation therapy in a Phase I trial in children with newly diagnosed DIPG [104]. This study

has demonstrated tolerability of lenalidomide in this population and long-term (3+ years) survival of a child with H3.3K27M DIPG; additional outcome results have not been reported to date.

14.2.2.4 Different Modes of Delivery

A major obstacle to optimal anti-tumor effect of chemotherapeutic agents is the blood-brain barrier (BBB), which prevents delivery to, and achievement of, effective exposure to the majority of therapeutics at the tumor site. Because potentially druggable targets have been identified in children with DIPG, and agents designed to target them are available clinically, alternate modes of drug delivery are being explored. These alternative modes of delivery include intrathecal delivery, which is limited by diffusion across the brain parenchyma; intranasal delivery, which continues to be preclinically investigated for optimal drug formulations and validation; and direct intratumoral delivery using techniques such as convection enhanced delivery (CED).

In CED, a therapeutic agent is administered through a catheter, attached to a pump, and infused with low, slow continuous pressure [105]. This technique is being evaluated as a means to improve outcomes for DIPG patients by bypassing the BBB and directly infusing a therapeutic agent into the tumor. The first CED case in a child with DIPG involved the administration of interleukin-13-pseudomonas exotoxin (IL13-PE) directed at the IL13 receptor, which had been shown to be present in a subset of patients with DIPG [106]. While this demonstrated safety and feasibility, this case and the subsequent clinical trial identified, and have sought to rectify, technical issues to optimize delivery to the tumor [107, 108].

Additional studies incorporating different agents have confirmed the relative safety and feasibility of this technique for children with DIPG [109]. Souweidane et al. recently published results of a CED Phase I study in children with DIPG in which the radiolabeled antibody, radioisotope iodine 124 conjugated to antiglioma monoclonal antibody 8H9 (^{124}I]-8H9), which targets the glioma-associated B7-H3 antigen, was infused [109]. This study again confirmed the safety and feasibility of this technique, and elegantly assessed the volume of distribution of the agent. Development of multiple-catheter, implanted CED devices that allow repeat drug administration to the tumor have also been investigated and shown to be safe and feasible [110, 111]. With each of the direct delivery techniques, drug selection is key; as with all tumors, tumor cells need to be sensitive, and effective exposure at the tumor site needs to be maintained. One of the limitations of CED is complete coverage of the tumor. While CED studies to date have targeted the MRI-defined tumor volume, DIPG tumor cells frequently reside outside the pons [28], likely necessitating the combination of CED and systemic drug administration.

Regardless of type of chemotherapy and route of administration, for chemotherapy to be effective, it has to meet the following minimum criteria: tumor cells must be sensitive to the agent(s); the drug must be delivered to its site of action (i.e. tumor

cells in pons as well as the invasive edge, subventricular zone, etc.); effective exposure (concentration over time) of the active drug or metabolite must be achieved at the tumor site; and patients need to tolerate the doses necessary to achieve these criteria. Unfortunately, pre-clinical studies addressing each of these criteria specifically for DIPG are not routinely performed. Drug penetration into the CNS after systemic delivery is limited for most (>95%) compounds; only small, lipophilic compounds are able to cross the BBB and then must traverse the brain parenchyma to reach the tumor cells [112]. Until each and all of these requirements are addressed, the likelihood of identifying effective chemotherapeutic agents for DIPG remains minute.

14.3 Treatment of Pediatric Non-DIPG Brainstem Gliomas

Questions that commonly arise for benign or low-grade appearing lesions on MRI, particularly in patients who are asymptomatic, minimally symptomatic, or have associated neurofibromatosis type I (NF-I) are: (1) is there a need for biopsy, (2) when to institute treatment, and (3) what treatment is recommended. Focal and dorsal exophytic brainstem gliomas and cervicomedullary gliomas are most commonly low-grade lesions. These patients may have a surgical option depending on tumor size and tumor location [10, 12]; safe, maximal surgical resection is the initial treatment of choice [113]. For most cases, obtaining tumor tissue for histologic diagnosis is optimal if the lesion is accessible, particularly if the lesion is rapidly increasing in size. Enhancement patterns alone in pediatric brainstem gliomas are not used as diagnostic criteria or a rationale for biopsy. In adults, malignant gliomas typically enhance, while low-grade gliomas are less likely to enhance, therefore in adults, enhancement on MRI may be an indication for biopsy. In contrast, in pediatric brainstem gliomas, diffuse malignant lesions such as DIPG may not enhance or have minimal enhancement, while non-DIPG tumors, which are frequently pilocytic astrocytomas, often do enhance [17, 114].

For asymptomatic patients and patients who undergo subtotal/incomplete resection, conservative management with a period of watchful waiting and close monitoring may be appropriate [113, 115].

In patients with NF-I, non-enhancing enlarging lesions in the brainstem are sometimes presumed to be low-grade gliomas and treated as such. In a retrospective study of brainstem tumors in children with NF-1 and brainstem tumors, 12 of 21 patients had progression of the lesion in a 3.75 year follow-up, and in 7 patients, the lesion stabilized or regressed without intervention [116], suggesting that a conservative approach of watchful waiting/observation is appropriate.

The optimal timing for initiating non-surgical treatment for non-DIPG brainstem gliomas in children is not clear. In general, if a lesion is causing symptoms and/or there is evidence of progression, treatment is instituted. Surgical resection may be performed at diagnosis in lesions that are readily accessible surgically. If debulking or partial resection is performed and the lesion is found to be a pilocytic astrocytoma, sometimes watchful waiting is done as the residual lesion may spontaneously

regress [117]. If there is evidence of tumor growth or worsening tumor-associated symptoms, the recommended treatment takes into consideration the patient age, evidence of malignancy, rapidity of growth, risk of loss of function, and presence of targetable mutations.

14.3.1 Radiation Therapy

Radiation therapy can be utilized for unresectable or incompletely resected lesions, rapidly progressing lesions, or disease progression after chemotherapy [1, 118, 119]. In a retrospective analysis of children with focal brainstem lesions, tumor control after surgery or radiation therapy were comparable [10]. However, the risk of radiation-induced toxicities, including long-term toxicities such as secondary malignancy, must be taken into consideration given that the vast majority of children with non-DIPG brainstem tumors will survive and effective chemotherapeutic regimens exist [120, 121]. When radiation therapy is indicated, focal tumor volumes are generally used to decrease the potential for acute and long-term toxicities [113].

Cervicomedullary tumors are also frequently low-grade gliomas including pilocytic astrocytomas, fibrillary astrocytomas, and gangliogliomas [11, 114, 122]. Despite their diffuse appearance, safe surgical resection is generally the treatment of choice. However, this is not possible in a number of cases; subtotal resection may be feasible and is frequently followed by radiation therapy [11]. Robertson et al. reported a 70% PFS rate in 17 children with histologically low-grade cervicomedullary tumors (n = 15) or anaplastic gangliogliomas (n = 2) that were treated with surgical resection alone. Again, watchful waiting/close observation may be appropriate. If tumor size or symptoms are rapidly progressive or there is impending loss of function, radiation therapy may be indicated. If there is slow progression, chemotherapy may be an option, particularly if BRAF V600E mutations are present [123, 124]. OS is significantly better than diffuse tumors involving the pons, with over 80% 5-year survival [11].

14.3.2 Chemotherapy

There is no standard of care for the use of chemotherapy in the treatment of pediatric non-DIPG brainstem gliomas. Rather, standard chemotherapeutic regimens utilized for children with low-grade gliomas in other locations are frequently employed. Chemotherapy is often recommended for patients with unresectable tumors, those with residual tumor following surgical resection, and those with progressive or symptomatic lesions. One report advocated pre-surgery chemotherapy as a means to improve the brainstem/tumor interface of cervicomedullary gliomas to allow for more successful resection [122]. However, specific chemotherapy regimens have not been prospectively evaluated in clinical trials in this population.

Historically, several cytotoxic chemotherapy regimens, such as vincristine and carboplatin [125], 6-thioguanine, procarbazine, lomustine and vincristine (TPCV) regimen [126], and vinblastine [127], have been used with some success in the management of children with low-grade gliomas, including those involving the brainstem [128]. Recent advances in our understanding of glioma biology and identification of potential targets, such as BRAF in low-grade gliomas and gangliogliomas, have led to more directed treatment. For example, the BRAF-KIAA1549 fusion is found in approximately two-thirds of brainstem pilocytic astrocytomas [129, 130] and BRAF V600E is frequent in gangliogliomas, found in more than 50% of pediatric patients [131, 132].

14.4 Treatment of Adult Brainstem Gliomas

As discussed, the incidence of adult brainstem gliomas is relatively low as the vast majority of malignant gliomas in adults are supratentorial. As a result, treatment for adult brainstem glioma is not standardized but rather based upon provider/institution experience and individual patient factors. Over the past decade, a limited number of retrospective studies have been performed to assess and characterize the clinical management of this patient population. These studies involve heterogeneous populations, relatively small patient numbers, and varied treatment approaches, including radiation therapy, chemoradiation therapy, chemotherapy alone, surgery only, or watchful waiting [133–136]. While pediatric brainstem tumors are typically characterized as DIPG versus non-DIPG, a functional approach for the classification of adult brainstem gliomas appears to more commonly be high-grade (WHO III/IV) versus low-grade (WHO I/II) gliomas, as this seems to have the strongest prognostic implications [133]. Therefore, stereotactic biopsy has been suggested as the standard of care in adult brainstem gliomas [13, 133, 137], particularly given the fact that, unlike in pediatrics, a considerable proportion of adult brainstem lesions are not gliomas [4, 137]. Additionally, some adult brainstem gliomas may be described as focal, dorsally exophytic or cervicomedullary lesions [12] as in the pediatric population, and these may be amenable to surgical resection as discussed above.

14.4.1 Radiation Therapy

Radiation therapy is commonly employed for adults with brainstem glioma [4, 134], particularly those that are high-grade or unresectable, progressive lesions [136], although the indication for radiation therapy is not defined in many cases. Most patients do have improvement in clinical symptoms after radiation therapy,

although the impact on survival is not clear [138]. As with other malignant gliomas, radiation doses of 50–60 Gy administered via focal fractionated external beam irradiation is commonly utilized [133, 139].

14.4.2 Chemotherapy

The role of chemotherapy in the treatment of adult brainstem gliomas has not been established [135], and only few studies have evaluated chemotherapy specifically in this population. A retrospective analysis of 28 patients that compared OS for adults with brainstem glioma treated with radiation and concurrent temozolomide, followed by temozolomide, versus those receiving radiation alone did demonstrate a survival advantage (23.1 vs. 4.0 months) [16], and several retrospective analyses indicate that temozolomide, alone or concurrently with radiation therapy, is frequently employed for adults with brainstem glioma [135]. However, the clinical benefit from chemotherapy, including temozolomide, is unclear as randomized prospective trials comparing similar populations have not been performed.

Other chemotherapeutic agents commonly used in adult supratentorial malignant glioma have been employed at the time of recurrence/progression of brainstem glioma. These therapies include bevacizumab, nitrosoureas, PCV regimen, and platinum compounds, among others [135]. As with upfront chemotherapy, their role is unclear as patient numbers are small, tumors are heterogeneous, and these have not been evaluated in clinical trials [135].

14.5 Treatment at Relapse

Unfortunately, the vast majority of patients with malignant glioma involving the brainstem will progress after upfront therapy. Treatment options at this time are limited, and many patients opt for clinical trials or palliative care. Frequently, patients are ineligible for clinical trials given their poor performance status, short life expectancy [140], or exclusion of patients with tumors located in the brainstem. A number of institutions are revisiting the idea of re-irradiation in this patient population. With advanced radiation therapy and imaging techniques, re-irradiation in patients with progressive malignant brainstem glioma has been shown to be feasible and relatively safe, with possible modest efficacy; however, re-irradiation is not standardized, the optimal dose, technique, fraction and volume are unknown, ideal patient selection is unclear, and management of toxicities is necessary. Re-irradiation has resulted in mixed results including improved symptoms and modest survival improvements (median survival 2–9 months) [66, 141–144].

14.6 Conclusion

Brainstem gliomas are a heterogeneous group of tumors that span histologic grades and age groups. The treatment of adults and children with brainstem glioma varies, depending on the radiographic appearance, patient age, tumor type, and tumor biology. Tumor biology is age- and location-dependent. While low-grade gliomas in the brainstem may have surgical and chemotherapeutic options, the treatment of malignant brainstem gliomas is limited to radiation therapy and investigational chemotherapeutic regimens. Unfortunately, the outcome for patients with diffuse brainstem glioma remains poor. Our understanding of DIPG in particular has advanced dramatically over the past decade, yet clinical advances to improve outcomes have been stalled due to obstacles with identifying and delivering effective agents to the tumor site. As we identify tumor targets and molecularly targeted agents and validate these in pre-clinical disease-specific models, we must now focus on overcoming the obstacles of drug delivery and drug resistance. Despite all the limitations, the hope is that a deeper understanding of the microenvironment, tumor biology and brainstem development will soon lead to effective treatments that will improve outcomes for our patients.

References

1. Schild S, Stafford S, Brown P, Wood C, Scheithauer B, Schomberg P, et al. The results of radiotherapy for brainstem tumors. *J Neuro-Oncol.* 1998;40(2):171–7.
2. Mehta V, Chandra P, Singh P, Garg A, Rath G. Surgical considerations for ‘intrinsic’ brainstem gliomas: proposal of a modification in classification. *Neurol India.* 2009;57(3):274–81.
3. Buczkowicz O, Bartels U, Bouffet E, Becher O, Hawkins C. Histopathological spectrum of paediatric diffuse intrinsic pontine glioma: diagnostic and therapeutic implications. *Acta Neuropathol.* 2014;128(4):573–81.
4. Reyes-Botero G, Giry M, Mokhtari K, Labussiere M, Idbaih A, Delattre J-Y, et al. Molecular analysis of diffuse intrinsic brainstem gliomas in adults. *J Neuro-Oncol.* 2014;116:405–11.
5. Wu G, Broniscer A, McEachron T, Lu C, Paugh B, Becksfort J, et al. Somatic histone H3 alterations in pediatric diffuse intrinsic pontine gliomas and non-brainstem glioblastomas. *Nat Genet.* 2012;44(3):251–3.
6. Hassan H, Pinches A, Picton S, Phillips R. Survival rates and prognostic predictors of high grade brain stem gliomas in childhood: a systematic review and meta-analysis. *J Neuro-Oncol.* 2017;135(1):13–20.
7. Huang T, Garcia R, Qui J, Lulla R, Horbinski C, Behdad A, et al. Detection of histone H3 K27M mutation and post-translational modifications in pediatric diffuse midline glioma via tissue immunohistochemistry informs diagnosis and clinical outcomes. *Oncotarget.* 2018;9(98):37112–24.
8. Freeman C, Farmer J. Pediatric brain stem gliomas. *Int J Radiat Oncol Biol Phys.* 1998;40(2):265–71.
9. Baker S, Ellison D, Gutmann D. Pediatric gliomas as neurodevelopmental disorders. *Glia.* 2016;64:879–95.
10. Klimo PJ, Pai Panandiker A, Thompson C, Boop F, Qaddoumi I, Gajjar A, et al. Management and outcome of focal low-grade brainstem tumors in pediatric patients: the St. Jude experience. *J Neurosurg Pediatr.* 2013;11(3):274–81.

11. McAbee J, Modica J, Thompson C, Broniscer A, Orr B, Choudri A, et al. Cervicomedullary tumors in children. *J Neurosurg Pediatr.* 2015;16(4):357–66.
12. Epstein F, McCleary E. Intrinsic brain-stem tumors of childhood: surgical indications. *J Neurosurg.* 1986;64:11–5.
13. Reyes-Butero G, Mokhtari K, Martin-Duverneuil N, Delattre J, Laigle-Donadey F. Adult brainstem gliomas. *Oncologist.* 2012;17(3):388–97.
14. Ostrom Q, Gittleman H, Liao P, et al. CBTRUS statistical report: primary brain and other central nervous system tumors diagnosed in the United States in 2010-2014. *Neuro-Oncology.* 2017;19(suppl_5):v1–v-88.
15. Kesari S, Kim R, Markos V, Drappatz J, Wen P, Pruitt A. Prognostic factors in adult brainstem gliomas: a multicenter, retrospective analysis of 101 cases. *J Neuro-Oncol.* 2008;88(2):175–83.
16. Theeler B, Ellezam B, Melguizo-Gavilanes I, de Groot J, Mahajan A, Aldape K, et al. Adult brainstem gliomas: correlation of clinical and molecular features. *J Neurol Sci.* 2015;353(1–2):92–7.
17. Warren K. Diffuse intrinsic pontine glioma: poised for progress. *Front Oncol.* 2012;2:205.
18. Selvapandian S, Rajshekhar V, Chandy M. Brainstem glioma: comparative study of clinico-radiological presentation, pathology and outcome in children and adults. *Acta Neurochir.* 1999;141(7):721–6.
19. Kaye E, Baker J, Broniscer A. Management of diffuse intrinsic pontine glioma in children: current and future strategies for improving prognosis. *CNS Oncol.* 2014;3(6):421–31.
20. Pai Panandiker A, Wong J, Nedelka M, Wu S, Gajjar A, Broniscer A. Effect of time from diagnosis to start of radiotherapy on children with diffuse intrinsic pontine glioma. *Pediatr Blood Cancer.* 2014;61(7):1180–3.
21. Hargrave D, Bartels U, Bouffet E. Diffuse brainstem glioma in children: critical review of clinical trials. *Lancet Oncol.* 2006;7:241–8.
22. Lee F. Radiation of infratentorial and supratentorial brainstem tumors. *J Neurosurg.* 1975;43:65–8.
23. Littman P, Jarrett P, Bilaniuk L, Rorke L, Zimmerman R, Bruce D, et al. Pediatric brain stem gliomas. *Cancer.* 1980;45(11):2787–92.
24. Freeman C, Suissa S. Brainstem tumors in children: results of a survey of 62 patients treated with radiotherapy. *Int J Radiat Oncol Biol Phys.* 1986;12:1823–8.
25. Cohen K, Broniscer A, Glod J. Pediatric glial tumors. *Curr Treat Options in Oncol.* 2001;2(6):529–36.
26. Walker M, Strike T, Sheline G. An analysis of dose-effect relationship in the radiotherapy of malignant gliomas. *Int J Radiat Oncol Biol Phys.* 1979;5:1725–31.
27. Schulz-Ertner D, Debus J, Lohr F, Frank C, Hoss A, Wannemacher M. Fractionated stereotactic conformal radiation therapy of brain stem gliomas: outcome and prognostic factors. *Radiother Oncol.* 2000;57:215–23.
28. Caretti V, Bugiani M, Freret M, Schellen P, Jansen M, van Vuurden D, et al. Subventricular spread of diffuse intrinsic pontine glioma. *Acta Neuropathol.* 2014;128(4):605–7.
29. Langmoen I, Lundar T, Storm-Mathisen I, Lie S, Hovind K. Management of pediatric pontine gliomas. *Childs Nerv Syst.* 1991;7:13–5.
30. Janssens G, Jansen M, Lauwers S, Nowak P, Oldenburger F, Bouffet E, et al. Hypofractionated vs conventional radiation therapy for newly diagnosed diffuse intrinsic pontine glioma: a matched cohort analysis. *Int J Radiat Oncol Biol Phys.* 2013;85(2):315–20.
31. Mandell L, Kadota R, Freeman C, Douglass E, Fontanesi J, Cohen M, et al. There is no role for hyperfractionated radiotherapy in the management of children with newly diagnosed diffuse intrinsic brainstem tumors: results of a Pediatric Oncology Group phase III trial comparing conventional vs hyperfractionated radiotherapy. *Int J Radiat Oncol Biol Phys.* 1999;43(5):959–64.
32. Donaldson S, Laningham F, Fisher P. Advances toward an understanding of brainstem gliomas. *J Clin Oncol.* 2006;24:1266–72.

33. Halperin E. Pediatric brain stem tumors: patterns of treatment failure and their implications for radiotherapy. *Int J Radiat Oncol Biol Phys.* 1985;11:1293–8.
34. Hu X, Fang Y, Hui X, Jv Y, You C. Radiotherapy for diffuse brainstem glioma in children and young adults. *Cochrane Database Syst Rev.* 2016;6:CD010439.
35. Freeman C, Krischer J, Sanford R, Cohen M, Burger P, del Carpio R, et al. Final results of a study of escalating doses of hyperfractionated radiotherapy in brain stem tumors in children: a Pediatric Oncology Group study. *Int J Radiat Oncol Biol Phys.* 1993;27(2):197–206.
36. Packer R, Boyett J, Zimmerman R, Albright A, Kaplan A, Rorke L, et al. Outcome of children with brain stem gliomas after treatment with 7800 cGy of hyperfractionated radiotherapy. A Childrens Cancer Group Phase I/II Trial. *Cancer.* 1994;74(6):1827–34.
37. Negretti L, Bouchireb K, Levy-Piedbois C, Habrand J, Dhermain F, Kalifa C, et al. Hypofractionated radiotherapy in the treatment of diffuse intrinsic pontine glioma in children: a single institution's experience. *J Neuro-Oncol.* 2011;104:773–7.
38. Zaghoul M, Eldebawy E, Ahmed S, Mousa A, Amin A, Refaat A, et al. Hypofractionated conformal radiotherapy for pediatric diffuse intrinsic pontine glioma (DIPG): a randomized controlled trial. *Radiother Oncol.* 2014;111(1):35–40.
39. Coughlin C, Richmond R. Biologic and clinical developments of cisplatin combined with radiation. *Semin Oncol.* 1989;16:31–43.
40. Dewit L. Combined treatment of radiation and cisdiamminedichloroplatinum (II): a review of experimental and clinical data. *Int J Radiat Oncol Biol Phys.* 1987;13(3):403–26.
41. Freeman C, Kepner J, Kun L, Sanford R, Kadota R, Mandell L, et al. A detrimental effect of a combined chemotherapy-radiotherapy approach in children with diffuse intrinsic brain stem gliomas? *Int J Radiat Oncol Biol Phys.* 2000;47(3):561–4.
42. Bradley K, Pollack I, Reid J, Adamson P, Ames M, Vezina G, et al. Motexafin gadolinium and involved field radiation therapy for intrinsic pontine glioma of childhood: a Children's Oncology Group phase I study. *Neuro-Oncology.* 2008;10:752–8.
43. Bradley K, Zhou T, McNall-Knapp R, Jakacki R, Levy A, Vezina G, et al. Motexafin-gadolinium and involved field radiation therapy for intrinsic pontine glioma of childhood: a children's oncology group phase 2 study. *Int J Radiat Oncol Biol Phys.* 2013;85(1):e55–60.
44. Hashemy S, Ungerstedt J, Zahedi Avval F, Holmgren A. Motexafin gadolinium, a tumor-selective drug targeting thioredoxin reductase and ribonucleotide reductase. *J Biol Chem.* 2006;281(16):10691–7.
45. Veldhuijzen van Zanten S, El-Khouly F, Jansen M, Bakker D, Sanchez Aliaga E, Haasbeek C, et al. A phase I/II study of gemcitabine during radiotherapy in children with newly diagnosed diffuse intrinsic pontine glioma. *J Neuro-Oncol.* 2017;135(2):307–15.
46. Kilburn L, Kocak M, Baxter P, Poussaint T, Paulino A, McIntyre C, et al. A pediatric brain tumor consortium phase II trial of capecitabine rapidly disintegrating tablets with concomitant radiation therapy in children with newly diagnosed diffuse intrinsic pontine gliomas. *Pediatr Blood Cancer.* 2018;65(2).
47. Jakacki R, Siffert J, Jamison C, Velasquez L, Allen J. Dose-intensive, time compressed procarbazine, CCNU, vincristine (PCV) with peripheral blood stem cell support and concurrent radiation in patients with newly diagnosed high-grade gliomas. *J Neuro-Oncol.* 1999;44(1):77–83.
48. Stupp R, Mason W, van den Bent M, Weller M, Fisher B, Taphoorn M, et al. Radiotherapy plus concomitant and adjuvant temozolomide for glioblastoma. *N Engl J Med.* 2005;352(10):987–96.
49. Patel M, McCully C, Godwin K, Balis F. Plasma and cerebrospinal fluid pharmacokinetics of intravenous temozolomide in non-human primates. *J Neuro-Oncol.* 2003;61(3):203–7.
50. Sirachainan N, Pakakasama S, Visudithbhan A, Chiamchanya S, Tuntiyatorn L, Dhanachai M, et al. Concurrent radiotherapy with temozolomide followed by adjuvant temozolomide and cis-retinoic acid in children with diffuse intrinsic pontine glioma. *Neuro-Oncology.* 2008;10(4):577–82.
51. Warren K, Gururangan S, Geyer J, McLendon R, Poussaint T, Wallace D, et al. A phase II study of O6-benzylguanine and temozolomide in pediatric patients with recurrent or progressive high-grade gliomas and brainstem gliomas: a Pediatric Brain Tumor Consortium study. *J Neuro-Oncol.* 2012;106(3):643–9.

52. Cohen K, Heideman R, Zhou T, Holmes E, Lavey R, Bouffet E, et al. Temozolomide in the treatment of children with newly diagnosed diffuse intrinsic pontine gliomas: a report from the Children's Oncology Group. *Neuro-Oncology*. 2011;13(4):410–6.
53. Jalali R, Raut N, Arora B, Gupta T, Dutta D, Munshi A, et al. Prospective evaluation of radiotherapy with concurrent and adjuvant temozolomide in children with newly diagnosed diffuse intrinsic pontine glioma. *Int J Radiat Oncol Biol Phys*. 2010;77(1):113–8.
54. Chassot A, Canale S, Varlet P, Puget S, Roujeau T, Negretti L, et al. Radiotherapy with concurrent and adjuvant temozolomide in children with newly diagnosed diffuse intrinsic pontine glioma. *J Neuro-Oncol*. 2012;106(2):399–407.
55. Lashford L, Thiesse P, Jouvett A, Jaspan T, Couanet D, Griffiths P, et al. Temozolomide in malignant gliomas of childhood: a United Kingdom Children's Cancer Study Group and French Society for Pediatric Oncology Intergroup Study. *J Clin Oncol*. 2002;20(24):4684–91.
56. Broniscer A, Iacono L, Chintagumpala M, Fouladi M, Wallace D, Bowers D, et al. Role of temozolomide after radiotherapy for newly diagnosed diffuse brainstem glioma in children: results of a multiinstitutional study (SJHG-98). *Cancer*. 2005;103(1):133–9.
57. Sharp J, Bouffet E, Stempak D, Gammon J, Stephens D, Johnston D, et al. A multi-centre Canadian pilot study of metronomic temozolomide combined with radiotherapy for newly diagnosed paediatric brainstem glioma. *Eur J Cancer*. 2010;46(18):3271–9.
58. Rizzo D, Scalzone M, Ruggiero A, Maurizi P, Attinà G, Mastrangelo S, et al. Temozolomide in the treatment of newly diagnosed diffuse brainstem glioma in children: a broken promise? *J Chemother*. 2015;27(2):106–10.
59. Bailey S, Howman A, Wheatley K, Wherton D, Boota N, Pizer B, et al. Diffuse intrinsic pontine glioma treated with prolonged temozolomide and radiotherapy—results of a United Kingdom phase II trial (CNS 2007 04). *Eur J Cancer*. 2013;49(18):3856–62.
60. Chiang K, Chang K, Lee Y, Huang P, Hsu T, Chen Y, et al. Role of temozolomide in the treatment of newly diagnosed diffuse brainstem glioma in children: experience at a single institution. *Childs Nerv Syst*. 2010;26(8):1035–41.
61. Kretschmar C, Tarbell N, Barnes P, Krischer J, Burger P, Kun L. Pre-irradiation chemotherapy and hyperfractionated radiation therapy 66 Gy for children with brain stem tumors. A phase II study of the Pediatric Oncology Group, Protocol 8833. *Cancer*. 1993;72:4.
62. Frappaz D, Schell M, Thiesse P, Marec-Berard P, Mottolese C, Perol D, et al. Preradiation chemotherapy may improve survival in pediatric diffuse intrinsic brainstem gliomas: final results of BSG 98 prospective trial. *Neuro-Oncology*. 2008;10(4):599–607.
63. Gokce-Samar Z, Beuriat P, Faure-Contier C, Carrie C, Chabaud S, Claude L, et al. Pre-radiation chemotherapy improves survival in pediatric diffuse intrinsic pontine gliomas. *Childs Nerv Syst*. 2016;32(8):1415–23.
64. Gilbertson R, Hill D, Hernan R, Kocak M, Geyer R, Olson J, et al. ERBB1 is amplified and overexpressed in high-grade diffusely infiltrative pediatric brain stem glioma. *Clin Cancer Res*. 2003;9:3620–4.
65. Bode U, Massimino M, Bach F, Zimmermann M, Khuhlaeva E, Westphal M, et al. Nimotuzumab treatment of malignant gliomas. *Expert Opin Biol Ther*. 2012;12(12):1649–59.
66. Massimino M, Biassoni V, Miceli R, Schiavello E, Warmuth-Metz M, Modena P, et al. Results of nimotuzumab and vinorelbine, radiation and re-irradiation for diffuse pontine glioma in childhood. *J Neuro-Oncol*. 2014;118:305–12.
67. Pollack I, Jakacki R, Blaney S, Hancock M, Kieran M, Phillips P, et al. Phase I trial of imatinib in children with newly diagnosed brainstem and recurrent malignant gliomas: a Pediatric Brain Tumor Consortium report. *Neuro-Oncology*. 2007;9(2):145–60.
68. Broniscer A, Baker J, Tagen M, Onar-Thomas A, Gilbertson R, Davidoff A, et al. Phase I study of vandetanib during and after radiotherapy in children with diffuse intrinsic pontine glioma. *J Clin Oncol*. 2010;28(31):4762–8.
69. Broniscer A, Baker S, Wetmore C, Pai Panandiker A, Huang J, Davidoff A, et al. Phase I trial, pharmacokinetics, and pharmacodynamics of vandetanib and dasatinib in children with newly diagnosed diffuse intrinsic pontine glioma. *Clin Cancer Res*. 2013;19(11):3050–8.

70. Georger B, Hargrave D, Thomas F, Ndiaye A, Frappaz D, Andreiuolo F, et al. Innovative therapies for children with cancer pediatric phase I study of erlotinib in brainstem glioma and relapsing/refractory brain tumors. *Neuro-Oncology*. 2011;13(1):109–18.
71. Geyer J, Stewart C, Kocak M, Broniscer A, Phillips P, Douglas J, et al. A phase I and biology study of gefitinib and radiation in children with newly diagnosed brain stem gliomas or supratentorial malignant gliomas. *Eur J Cancer*. 2010;46(18):3287–93.
72. Pollack I, Stewart C, Kocak M, Poussaint T, Broniscer A, Banerjee A, et al. A phase II study of gefitinib and irradiation in children with newly diagnosed brainstem gliomas: a report from the Pediatric Brain Tumor Consortium. *Neuro-Oncology*. 2011;13(3):290–7.
73. Haas-Kogan D, Banerjee A, Kocak M, Prados M, Geyer JR, Fouladi M, et al. Phase I trial of tipifarnib in children with newly diagnosed intrinsic diffuse brainstem glioma. *Neuro-Oncology*. 2008;10(3):341–7.
74. Haas-Kogan D, Banerjee A, Poussaint T, Kocak M, Prados M, Geyer J, et al. Phase II trial of tipifarnib and radiation in children with newly diagnosed diffuse intrinsic pontine gliomas. *Neuro-Oncology*. 2011;13:298–306.
75. Fouladi M, Nicholson H, Zhou T, Laningham F, Helton K, Holmes E, et al. A phase II study of the farnesyl transferase inhibitor, tipifarnib, in children with recurrent or progressive high-grade glioma, medulloblastoma/primitive neuroectodermal tumor, or brainstem glioma. *Cancer*. 2007;110:2535–41.
76. Fouladi M, Stewart C, Olson J, Wagner L, Onar-Thomas A, Kocak M, et al. Phase I trial of MK-0752 in children with refractory CNS malignancies: a Pediatric Brain Tumor Consortium study. *J Clin Oncol*. 2011;29:3529–34.
77. Kilburn L, Kocak M, Decker R, Wetmore C, Chintagumpala M, Su J, et al. A phase I and pharmacokinetic study of enzastaurin in pediatric patients with refractory primary central nervous system tumors: a pediatric brain tumor consortium study. *Neuro-Oncology*. 2015;17(2):303–11.
78. Paugh B, Qu C, Jones C, Liu Z, Adamowicz-Brice M, Zhang J, et al. Integrated molecular genetic profiling of pediatric high-grade gliomas reveals key differences with the adult disease. *J Clin Oncol*. 2010;28(18):3061–8.
79. Puget S, Beccaria K, Blauwblomme T, Roujeau T, James S, Grill J, et al. Biopsy in a series of 130 pediatric diffuse intrinsic Pontine gliomas. *Childs Nerv Syst*. 2015;31(10):1773–80.
80. Grill J, Puget S, Andreiuolo F, Philippe C, MacConaill L, Kieran M. Critical oncogenic mutations in newly diagnosed pediatric diffuse intrinsic pontine glioma. *Pediatr Blood Cancer*. 2012;58(4):489–91.
81. Warren K, Killian K, Suuriniemi M, Wang Y, Quezado M, Meltzer P. Genomic aberrations in pediatric diffuse intrinsic pontine gliomas. *Neuro-Oncology*. 2012;14(3):326–32.
82. Zarghooni M, Bartels U, Lee E, Buczkowicz P, Morrison A, Huang A, et al. Whole-genome profiling of pediatric diffuse intrinsic pontine gliomas highlights platelet-derived growth factor receptor alpha and poly (ADP-ribose) polymerase as potential therapeutic targets. *J Clin Oncol*. 2010;28(8):1337–44.
83. Puget S, Philippe C, Bax D, Job B, Varlet P, Junier M, et al. Mesenchymal transition and PDGFRA amplification/mutation are key distinct oncogenic events in pediatric diffuse intrinsic pontine gliomas. *PLoS One*. 2012;7(2):e30313.
84. Gupta N, Goummerova L, Manley P, Chi S, Neuberger D, Puligandla M, et al. Prospective feasibility and safety assessment of surgical biopsy for patients with newly diagnosed diffuse intrinsic pontine glioma. *Neuro-Oncology*. 2018;20(11):1547–55.
85. Grasso C, Yang Y, Truffaux N, Berlow N, Liu L, Diebly M-A, et al. Functionally defined therapeutic targets in diffuse intrinsic pontine glioma. *Nat Med*. 2015;21(6):555–9.
86. Schwartztruber J, Korshunov A, Liu X, Jones D, Pfaff E, Jacob K, et al. Driver mutations in histone H3.3 and chromatin remodelling genes in paediatric glioblastoma. *Nature*. 2012;482(7384):226–31.
87. Khuong-Quang D, Buczkowicz P, Rakopoulos P, Liu X, Fontebasso A, Bouffet E, et al. K27M mutation in histone H3.3 defines clinically and biologically distinct subgroups of pediatric diffuse intrinsic pontine gliomas. *Acta Neuropathol*. 2012;124(3):439–47.

88. Cooney T, Onar-Thomas A, Huang J, Lulla R, Fangusaro J, Kramer K, et al. A phase I trial of the histone deacetylase inhibitor panobinostat in pediatric patients with recurrent or refractory diffuse intrinsic pontine glioma: a Pediatric Brain Tumor Consortium (PBTC) study. *Neuro-Oncology*. 2018;20(suppl 2):i53.
89. Jones C, Baker S. Unique genetic and epigenetic mechanisms driving paediatric diffuse high-grade glioma. *Nat Rev Cancer*. 2014;14(10).
90. Panditharatna E, Yaeger K, Kilburn L, Packer R, Nazarian J. Clinicopathology of diffuse intrinsic pontine glioma and its redefined genomic and epigenomic landscape. *Cancer Genet*. 2015;208(7–8):367–73.
91. Nagaraja S, Vitanza N, Woo P, Taylor KR, Liu F, Zhang L, et al. Transcriptional dependencies in diffuse intrinsic pontine glioma. *Cancer Cell*. 2017;31:635–52.
92. Taylor K, Mackay A, Truffaux N, Butterfield Y, Morozovo O, Philippe C, et al. Recurrent activating ACVR1 mutations in diffuse intrinsic pontine glioma. *Nat Genet*. 2014;46(5):457–61.
93. Buczkowicz P, Hoeman C, Rakopoulos P, Pajovic S, Letourneau L, Dzamba M, et al. Genomic analysis of diffuse intrinsic pontine gliomas identifies three molecular subgroups and recurrent activating ACVR1 mutations. *Nat Genet*. 2014;46(5):451–6.
94. Fontebasso A, Papillon-Cavanagh S, Schwartzentruber J, Nikbakht H, Gerges N, Fiset P-O, et al. Recurrent somatic mutations in ACVR1 in pediatric midline high-grade astrocytoma. *Nat Genet*. 2014;46(5):462–6.
95. Fine H, Figg W, Jaeckle K, Wen P, Kyritsis A, Loeffler J, et al. Phase II trial of the anti-angiogenic agent thalidomide in patients with recurrent high-grade gliomas. *J Clin Oncol*. 2000;18(4):708–15.
96. Groves M, Puduvali V, Gilbert M, Levin V, Conrad C, Liu V, et al. Two phase II trials of temozolomide with interferon-alpha2b (pegylated and non-pegylated) in patients with recurrent glioblastoma multiforme. *Br J Cancer*. 2009;101(4):615–20.
97. Allen J, Packer R, Bleyer A, Zeltzer P, Prados M, Nirenberg A. Recombinant interferon beta: a phase I-II trial in children with recurrent brain tumors. *J Clin Oncol*. 1991;9(5):783–8.
98. Mahaley M, Urso M, Whaley R, Williams T, Guaspari A. Interferon as adjuvant therapy with initial radiotherapy of patients with anaplastic gliomas. *J Neurosurg*. 1984;61(6):1069–71.
99. Nagai M, Arai T. Clinical effect of interferon in malignant brain tumours. *Neurosurg Rev*. 1984;7(1):55–64.
100. Turner C, Chi S, Marcus K, MacDonald T, Packer R, Poussaint T, et al. Phase II study of thalidomide and radiation in children with newly diagnosed brain stem gliomas and glioblastoma multiforme. *J Neuro-Oncol*. 2007;82(1):95–101.
101. Warren K, Bent R, Wolters P, Prager A, Hanson R, Packer R, et al. A phase 2 study of pegylated interferon α -2b (PEG-Intron®) in children with diffuse intrinsic pontine glioma. *Cancer*. 2012;118(14):3607–13.
102. Slaton J, Perrotte P, Inoue K, Dinney C, Fidler I. Interferon-alpha-mediated down-regulation of angiogenesis-related genes and therapy of bladder cancer are dependent on optimization of biological dose and schedule. *Clin Cancer Res*. 1999;5(10):2726–34.
103. Kim C-Y, Kim S-K, Phi J, Lee M, Kim I, Kim I, et al. A prospective study of temozolomide plus thalidomide during and after radiation therapy for pediatric diffuse pontine gliomas: preliminary results of the Korean Society for Pediatric Neuro-Oncology study. *J Neuro-Oncol*. 2010;100:193–8.
104. Hipp S, Goldman S, Kaushal A, Glod J, Shih J, Garvin J, et al. A phase I trial of lenalidomide plus radiotherapy in children with newly diagnosed diffuse intrinsic pontine gliomas or high-grade gliomas. *Neuro-Oncology*. 2016;18(suppl_3):iii27.
105. Bobo R, Laske D, Akbasak A, Morrison P, Dedrick R, Oldfield E. Convection-enhanced delivery of macromolecules in the brain. *Proc Natl Acad Sci U S A*. 1994;91(6):2076–80.
106. Lonser R, Warren K, Butman J, Quezado Z, Robison R, Wallbridge S, et al. Real-time image-guided direct convective perfusion of intrinsic brainstem lesions. Technical note. *J Neuro-Oncol*. 2007;107(1):190–7.
107. Heiss J, Jamshidi A, Shah S, Martin S, Wolters P, Argersinger D, et al. Phase I trial of convection-enhanced delivery of IL13-Pseudomonas toxin in children with diffuse intrinsic pontine glioma. *J Neurosurg Pediatr*. 2018:1–10.

108. Chittiboina P, Heiss J, Warren K, Lonser R. Magnetic resonance imaging properties of convective delivery in diffuse intrinsic pontine gliomas. *J Neurosurg Pediatr.* 2014;13(3):276–82.
109. Souweidane M, Kramer K, Pandit-Taskar N, Zhou Z, Haque S, Zanzonico P, et al. Convection-enhanced delivery for diffuse intrinsic pontine glioma: a single-centre, dose-escalation, phase I trial. *Lancet Oncol.* 2018;19(8):1040–50.
110. Lewis O, Woolley M, Johnson D, Rosser A, Barua N, Bienemann A, et al. Chronic, intermittent convection-enhanced delivery devices. *J Neurosci Methods.* 2016;259:47–56.
111. Barua N, Lowis S, Woolley M, O'Sullivan S, Harrison R, Gill S. Robot-guided convection-enhanced delivery of carboplatin for advanced brainstem glioma. *Acta Neurochir.* 2013;155(8):1459–65.
112. Warren K. Beyond the blood:brain barrier: the importance of Central Nervous System (CNS) pharmacokinetics for the treatment of CNS tumors, including diffuse intrinsic pontine glioma. *Front Oncol.* 2018;8:239.
113. Upadhyaya S, Koschmann C, Murasko K, Venneti S, Garton H, Hamstra D, et al. Brainstem low-grade gliomas in children- excellent outcomes with multimodality therapy. *J Child Neurol.* 2017;32(2):194–203.
114. Lesniak M, Klem J, Weingart J, Carson B. Surgical outcome following resection of contrast-enhanced pediatric brainstem gliomas. *Pediatr Neurosurg.* 2003;39:314–22.
115. Fried I, Hawkins C, Scheinemann K, Tsangaris E, Hesselson L, Bartels U, et al. Favorable outcome with conservative treatment for children with low grade brainstem tumors. *Pediatr Blood Cancer.* 2012;58:556–60.
116. Pollack I, Shultz B, Mulvihill J. The management of brainstem gliomas in patients with neurofibromatosis 1. *Neurology.* 1996;46(6):1652–60.
117. Gaudino S, Quaglio F, Schiarella C, Martucci M, Tartaglione T, Gualano M, et al. Spontaneous modifications of contrast enhancement in childhood non-cerebellar pilocytic astrocytomas. *Neuroradiology.* 2012;54(9):989–95.
118. Farmer J, Montes J, Freeman C, Meagher-Villemure K, Bond M, O'Gorman A. Brainstem gliomas. A 10-year institutional review. *Pediatr Neurosurg.* 2001;34:206–14.
119. Kortmann R, Timmerman B, Taylor R, Scarzello G, Plasswilm L, Paulsen F, et al. Current and future strategies in radiotherapy of childhood low-grade glioma of the brain. Part I: treatment modalities of radiation therapy. *Strahlenther Onkol.* 2003;179(8):509–20.
120. Pierre-Kahn A, Hirsch J, Vinchon M, Payan C, Sainte-Rose C, Renier D, et al. Surgical management of brain-stem tumors in children: results and statistical analysis of 75 cases. *J Neurosurg.* 1993;79(6):845–52.
121. Robertson P, Murasko K, Brunberg J, Axtell R, Dauser R, Turrisi A. Pediatric midbrain tumors: a benign subgroup of brainstem gliomas. *Pediatr Neurosurg.* 1995;22(2):65–73.
122. Di Maio S, Gul S, Cochrane D, Henderson G, Sargent M, Steinbok P. Clinical, radiologic and pathologic features and outcome following surgery for cervicomedullary gliomas in children. *Childs Nerv Syst.* 2009;25:1401–10.
123. del Bufalo F, Carai A, Figà-Talamanca L, Pettorini B, Mallucci C, Giangaspero F, et al. Response of recurrent BRAFV600E mutated ganglioglioma to Vemurafenib as single agent. *J Transl Med.* 2014;12:356.
124. Aguilera D, Janss A, Mazewski C, Castellino R, Schniederjan M, Hayes L, et al. Successful retreatment of a child with a refractory brainstem Ganglioglioma with Vemurafenib. *Pediatr Blood Cancer.* 2016;63(3):541–3.
125. Packer R, Ater J, Allen J, Phillips P, Geyer R, Nicholson H, et al. Carboplatin and vincristine chemotherapy for children with newly diagnosed progressive low-grade gliomas. *J Neurosurg.* 1997;86(5):747–54.
126. Ater J, Zhou T, Holmes E, Mazewski C, Booth T, Freyer D, et al. Randomized study of two chemotherapy regimens for treatment of low-grade glioma in young children: a report from the Children's Oncology Group. *J Clin Oncol.* 2012;30(21):2641–7.
127. Bouffett E, Jakacki R, Goldman S, Hargrave D, Hawkins C, Shroff M, et al. Phase II study of weekly vinblastine in recurrent or refractory pediatric low-grade glioma. *J Clin Oncol.* 2012;30(12):1358–63.

128. Ronghe M, Hargrave D, Bartels U, Tabori U, Vaidya S, Chandler C, et al. Vincristine and carboplatin chemotherapy for unresectable and/or recurrent low-grade astrocytoma of the brainstem. *Pediatr Blood Cancer*. 2010;55(3):471–7.
129. Jeuken J, Wesseling P. MAPK pathway activation through BRAF gene fusion in pilocytic astrocytomas; a novel oncogenic fusion gene with diagnostic, prognostic, and therapeutic potential. *J Pathol*. 2010;222(4):324–8.
130. Jacob K, Albrecht S, Sollier C, Faury D, Sader E, Montpetit A. Duplication of 7q34 is specific to juvenile pilocytic astrocytomas and a hallmark of cerebellar and optic pathway tumours. *Br J Cancer*. 2009;101(4):722–33.
131. Janjua M, Ivasyk I, Pisapia D, Souweidane M. Ganglioglioma of brain stem and cervicomedullary junction: a 50years review of literature. *J Clin Neurosci*. 2017;44:34–46.
132. Donson A, Kleinschmidt-DeMasters B, Aisner D, Bemis L, Birks D, Levy J, et al. Pediatric brainstem gangliogliomas show BRAF(V600E) mutation in a high percentage of cases. *Brain Pathol*. 2014;24(2):173–83.
133. Hundsberger T, Tonder M, Hottinger A, Brugge D, Roelcke U, Putora P, et al. Clinical management and outcome of histologically verified adult brainstem gliomas in Switzerland: a retrospective analysis of 21 patients. *J Neuro-Oncol*. 2014;118:321–8.
134. Ueoka D, Nogueira J, Campos J, Maranhao F, Ferman S, Lima M. Brainstem gliomas: retrospective analysis of 86 patients. *J Neurol Sci*. 2009;281:20–3.
135. Salmaggi A, Fariselli L, Milanese I, Lamperti E, Silvani A, Bizzi A, et al. Natural history and management of brainstem gliomas in adults. A retrospective Italian study. *J Neurol*. 2008;255:171–7.
136. Guillamo J-S, Monjour A, Taillandier L, Devaux B, Varlet P, Haie-Meder C, et al. Brainstem gliomas in adults: prognostic factors and classification. *Brain*. 2001;124:2528–39.
137. Dellaretti M, Touzet G, Reyns N, Dubois F, Gusmao S, Pereira J, et al. Correlation between magnetic resonance imaging findings and histological diagnosis of intrinsic brainstem lesions in adults. *Neuro-Oncology*. 2012;14:381–5.
138. Eisele S, Reardon D. Adult brainstem gliomas. *Cancer*. 2016;122(18):2799–809.
139. Babu R, Kranz P, Karikari I, Friedman A, Adamson C. Clinical characteristics and treatment of malignant brainstem gliomas in elderly patients. *J Clin Neurosci*. 2013;20:1382–6.
140. Cooney T, Lane A, Bartels U, Bouffet E, Goldman S, Leary S, et al. Contemporary survival endpoints: an international diffuse intrinsic pontine glioma registry study. *Neuro-Oncology*. 2017;19(9):1279–80.
141. Freese C, Takiar V, Fouladi M, DeWire M, Breneman J, Peter L. Radiation and subsequent reirradiation outcomes in the treatment of diffuse intrinsic pontine gliomas and a systematic review of the reirradiation literature. *Pract Radiat Oncol*. 2017;7:86–92.
142. Fontanilla H, Pinnix C, Ketonen K, Woo S, Vats T, Rytting M, et al. Palliative reirradiation for progressive diffuse intrinsic pontine glioma. *Am J Clin Oncol*. 2012;35(1):51–7.
143. Lassaletta A, Strother D, Laperriere N, Hukin J, Vanan M, Goddard K, et al. Reirradiation in patients with diffuse intrinsic pontine gliomas:the Canadian experience. *Pediatr Blood Cancer*. 2017;65(6):e26988.
144. Wolff J, Rytting M, Vats T, Zage P, Ater J, Woo S, et al. Treatment of recurrent diffuse intrinsic pontine glioma: the MD Anderson Cancer Center experience. *Neuro-Oncology*. 2012;106:391–7.

Chapter 15

Future Therapies for Malignant Brainstem Tumors



Zhiping Zhou and Mark M. Souweidane

Abbreviations

AA	Anaplastic astrocytoma
ABC	ATP-binding cassette
ABCG	ATP-binding cassette, subfamily G
ACVR1	Activin A receptor, type I
Ad5	Adenovirus serotype 5
ADC	Antibody-drug conjugate
ADCC	Antibody-dependent cell-mediated cytotoxicity
ALA	5-aminolevulinic acid
AlPcS _{2a}	Aluminum phthalocyanine disulfonate
AML	Acute myeloid leukemia
ATRT	Atypical teratoid rhabdoid tumor
ATRX	Alpha thalassemia/mental retardation syndrome X-linked
BBB	Blood-brain barrier
BMPs	Bone morphogenic proteins
CARs	Chimeric antigen receptors
CAR-T	Chimeric antigen receptor T-cell
CBTRUS	Central Brain Tumor Registry of the United States
CDC	Complement-dependent cytotoxicity
CED	Convection-enhanced delivery
CMV	Cytomegalovirus
CNS	Central nervous system
CPT-11	Camptothecin-11

Z. Zhou (✉)

Department of Pediatrics, Memorial Sloan Kettering Cancer Center, New York, NY, USA

M. M. Souweidane

Department of Neurological Surgery, Weill Medical College of Cornell University, New York, NY, USA

Department of Pediatrics, Weill Medical College of Cornell University, New York, NY, USA

Department of Neurosurgery, Memorial Sloan Kettering Cancer Center, New York, NY, USA

CSF	Cerebrospinal fluid
CTLA-4	Cytotoxic T-lymphocyte-associated protein 4
CYP450s	Cytochromes P450
DIPG	Diffuse intrinsic pontine glioma
DNA	Deoxyribonucleic acid
DT	Diphtheria toxin
EGFR	Epidermal growth factor receptors
EGFRvIII	EGFR variant III
ETANTR	Embryonal tumor with abundant neuropil and true rosettes
ETX	Epsilon toxin, active form
ETXp	Epsilon prototoxin
EZH2	Enhancer of zeste homolog 2
FUS	Focused ultrasound
G34R	Glycine-to-arginine missense at position 34
GBM	Glioblastoma multiforme
Gd-DTPA	Gadolinium-diethylenetriamine penta-acetic acid
HDACi	Histone deacetylase inhibitor
HER2	Human epidermal growth factor receptor 2
HGG	High-grade glioma
HLA	Human leukocyte antigen
HSV	Herpes simplex virus
ICOS	Inducible costimulator
IDH	Isocitrate dehydrogenase
IDO1	Indoleamine 2,3-dioxygenase 1
IFN	Interferon
K27M	Lysine-to-methionine missense at position 27
LAG-3	Lymphocyte activation gene 3
LDLR	Low-density lipoproteins receptor
LRPs	LDLR-related proteins
MDR	Multidrug resistance
MHC	Major histocompatibility complex
MRI	Magnetic resonance imaging
MRP	Multidrug-resistance-associated protein
NK	Natural killer
PCI	Photochemical internalization
PD-1	Programmed death-1
PDGFR	Platelet-derived growth factor receptors
PDT	Photodynamic therapy
PE	Pseudomonas exotoxin
PET	Positron emission tomography
P-gp	P-glycoprotein
PNET	Primitive neuroectodermal tumor
PRC2	Polycomb repressive complex 2
PTEN	Phosphatase and tensin homolog
RNA	Ribonucleic acid

RTKs	Receptor tyrosine kinases
scFv	Single-chain variable fragment
SPECT	Single photon emission computed tomography
TCRs	T-cell receptors
Tf	Transferrin
TGF- β 1	Transforming growth factor β 1
TIL	Tumor-infiltrating lymphocyte
TIM-3	T-cell immunoglobulin and mucin domain-containing 3
TK	Thymidine kinase
Treg	Regulatory T cell
TTRNA-DC	Total tumor mRNA-pulsed autologous dendritic cell
VEGF	Vascular endothelial growth factors
WHO	World Health Organization
α	Alpha
β	Beta

15.1 Introduction

Malignant brainstem tumors are a heterogeneous group of tumors occurring in the brainstem and cervicomedullary junction. According to the Central Brain Tumor Registry of the United States (CBTRUS), in all age groups, there were about 1200 primary brainstem tumors per year between 2010 and 2014 in the United States, among which 900 cases were malignant [1]. These numbers account for 1.6% of all primary central nervous system (CNS) tumors and 3.8% of all malignant primary CNS tumors. Brainstem tumors occur more often in children than in adults. Among 0–14 year-olds, about 450 cases of primary brainstem tumors occurred during the same period in the United States, accounting for 13.4% of all primary CNS tumors in this age group [1].

Approximately 90% of brainstem tumors are gliomas in origin [2]. In children, most of these are diffuse intrinsic pontine gliomas (DIPGs), accounting for at least 80% of brainstem gliomas [3, 4]. They have a dismal prognosis with a median survival of only 1 year [4]. Other malignant brainstem tumors in children include embryonal tumors such as atypical teratoid rhabdoid tumors (ATRTs), embryonal tumors with abundant neuropil and true rosettes (ETANTR) and primitive neuroectodermal tumors (PNETs) (the latter two disease entities were folded into embryonal tumors with multilayered rosettes [ETMR] in the WHO 2016 classification), and high-grade glial tumors that are not classified as DIPG [5]. These tumors are rarer than DIPG. Even rarer are high-grade mixed neuronal-glial tumors (anaplastic ganglioglioma) in the brainstem. Primary malignant tumors in the brainstem in adults are less common than in children and are mainly anaplastic astrocytoma (AA) and glioblastoma multiforme (GBM) [6]. Malignant tumors from nearby structures, such as choroid plexus carcinoma of the fourth ventricle, can also invade the brainstem.

The discussion in this chapter will focus on investigational therapeutic options for DIPG, sometimes with references to related diseases such as glioma in general.

15.2 Obstacles in the Treatment of Malignant Brainstem Tumors

15.2.1 Maximal Safe Cytoreduction Surgery

The brainstem is a compact structure and plays pivotal roles in cardiovascular and respiratory control, alertness, awareness, and consciousness, as well as serving as the passageway for motor and sensory tracts and housing the cranial nerve nuclei. DIPG, the most common malignant primary brainstem tumor, infiltrates the brainstem extensively, precluding meaningful cytoreduction surgery. As a result, in the clinical management of DIPG, surgery is typically only used for relieving hydrocephalus or for biopsy. The diffuse growth pattern of DIPG is demonstrated in Fig. 15.1.

15.2.2 Blood-Brain Barrier

An important limitation of systemic chemotherapy in primary brain tumor treatment is the existence of the blood-brain barrier (BBB). The BBB is a barrier that isolates the circulating blood from the cerebrospinal fluid (CSF) and the interstitial fluid in the CNS. It occurs along the cerebral capillaries and consists of tight junctions (zona occludens) that do not exist in vasculatures in other organs. Endothelial cells restrict the diffusion of microscopic objects (e.g., bacteria) and large or hydrophilic molecules from the brain vasculature, while allowing the diffusion of small hydrophobic molecules (e.g., O₂, CO₂, and certain hormones). Typically, molecules larger than ~40 kD are unlikely to penetrate the intact barrier. For the brain's supply of nutrients and removal of metabolites, cells of the brain vasculature actively transport glucose and metabolic products across the barrier using transporters.

The BBB acts effectively to protect the brain from many common bacterial infections and some toxic substances. Yet, it presents a major challenge in delivering therapeutic agents to specific regions of the brain for the treatment of brain tumors and certain other disorders. Most cancer drugs are not able to permeate the BBB because they are polar in structure or too large in molecular weight. Even for drugs that are able to cross the cerebral capillary bed, it is difficult to achieve optimal concentrations in the brain due to the limitations posed by systemic toxicity.

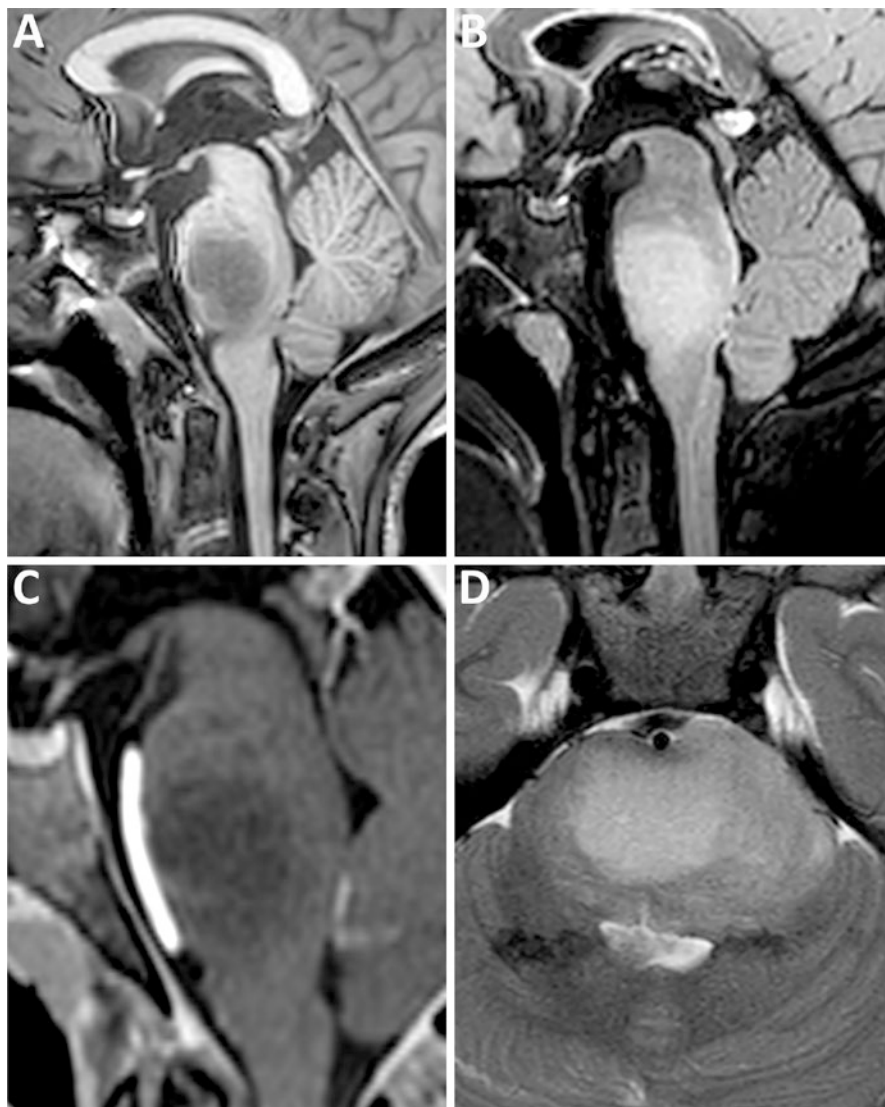


Fig. 15.1 Imaging presentation of a DIPG. These representative images were acquired from the same patient in one study. (a) The tumor is hypointense on T1-weighted images (sagittal view). (b) The tumor is hyperintense on FLAIR images (sagittal view). (c) The tumor lacks enhancement on post-contrast T1-weighted images (sagittal view). (d) The tumor is hyperintense on T2-weighted images (axial view). Note the diffuse growth pattern of the tumor and the ventral expansion of the pons caused by the tumor growth, partially engulfing the basilar artery

Another related challenge in the delivery of drugs for the treatment of primary brain tumors and certain other CNS diseases is how to direct drugs to the lesion while sparing healthy neural tissues from disturbance of normal neurological functions.

Clinically, gadolinium contrast enhancement on magnetic resonance imaging (MRI) serves as an indicator of the integrity of the BBB. DIPGs either do not show contrast enhancement or have only a small volume of contrast enhancement [7], suggesting that the BBB is largely intact in this tumor. Another piece of indirect evidence of the relatively intact BBB is that in a clinical study of tyrosine kinase inhibitors dasatinib and vandetanib in DIPG patients, the CSF to plasma exposure of the two drugs was only approximately 2% [8]. An animal study suggests that tumor location, instead of histone mutation status, may be the main reason for this relatively intact BBB in brainstem infiltrative gliomas [9]. While a more permeable BBB, as indicated by contrast enhancement, may allow chemotherapeutic drugs to reach the tumor more easily, it is also associated with shorter survival in DIPG patients [7].

15.2.3 ATP-Binding Cassette Transporters

ATP-binding cassette (ABC) transporters are a family of transporter proteins that contribute to drug resistance by functioning as ATP-dependent drug efflux pumps. At least four dozens of human ABC genes have been identified [10]. The best-known ABC transporter that is involved in multidrug resistance is P-glycoprotein (P-gp), an organic cation pump. P-gp is encoded by the MDR1 gene. The physiological function of P-gp is the excretion of toxins from cells, and it contributes to drug resistance in a pharmacological context. P-gp is overexpressed in chemotherapy-resistant tumors, conferring resistance to certain chemotherapeutic agents, and is upregulated after disease progression following chemotherapy in cancers. Other transporter proteins mediating drug resistance include those in the multidrug-resistance-associated protein (MRP) family and ABC, subfamily G (ABCG). Among members of the MRP family, only MRP1 has shown convincing evidence to be associated with clinical resistance. ABCG2, a half transporter in the ABCG subfamily, confers resistance to topotecan, camptothecin-11 (CPT-11), and mitoxantrone [11]. The expression and regulation of the MRP family and ABCG2 have not been extensively studied in cancers.

In the normal brain, ABC transporters are predominantly expressed on endothelial cells of micro blood vessels, but can also be found in astrocytes, microglia, and neurons [12, 13]. In brain capillary endothelial cells, P-gp is primarily found in the luminal (blood-facing) membrane [14, 15]. However, it is also expressed on the abluminal (brain-facing) membranes of capillary endothelial cells as well as adjacent pericytes and astrocytes [16].

A recent study demonstrated the expression of P-gp, MRP1, and ABCG2 in tumor vasculature, and the expression of MRP1 in glioma cells themselves in DIPG

as well as in pediatric supratentorial high-grade glioma (HGG) samples [17], suggesting that these drug efflux transporters may be a major factor in the failure of systemic chemotherapy in treating DIPG.

15.2.4 Intratumoral Heterogeneity

Intratumoral heterogeneity has been recognized as a common phenomenon in malignant solid tumors for several decades [18, 19]. Heterogeneity can be appreciated both histologically and molecularly. Intratumoral genetic heterogeneity has been documented in a large number of tumors recently [20–23]. Tumors are dynamically evolving genetically and epigenetically, both spatially within the local tumor and across metastatic sites, and temporally throughout the disease course. As a result of intratumoral heterogeneity, sampling different parts of the same tumor may produce different results for pathology studies and genetic and epigenetic profiling [24–29]. In glioblastoma, a single tumor consisted of a heterogeneous mixture of cells harboring diverse types of mutations, both by copy number analysis and transcription analysis [29, 30].

Intratumoral heterogeneity plays an important role in therapeutic resistance. Clonal variations in response to chemotherapeutic agents, hyperthermia or ionizing radiation have been well documented [31]. Most cancer therapies present selection pressure on the numerous and diverse clones of tumor cells [32, 33]. Clones that survive the therapy will dominate in the post-treatment or recurrent tumor. The impact of clonal variation on therapeutic resistance may be more pronounced for the contemporary signal transduction pathway-targeted therapies than the conventional cytotoxic chemotherapy. Targeting of receptor tyrosine kinases (RTKs), such as epidermal growth factor receptors (EGFR), platelet-derived growth factor receptors (PDGFR) and vascular endothelial growth factors (VEGF), has been a focus of some recent clinical trials for GBM. Therapy with single agents leads to clonal selection, enriching therapy-resistant clones that give rise to recurrent GBM [34]. Possibly a result of this phenomenon in part, clinical trials with signal transduction pathway-targeted therapies failed to show significant improvement in survival in GBM, as well as in DIPG patients [8, 35].

DIPGs show intratumoral T2-weighted signal heterogeneity [36, 37] as well as diffusivity heterogeneity [36, 38, 39]. Histologically, DIPGs show considerable intratumoral heterogeneity, with over 50% even showing focal areas resembling World Health Organization (WHO) grade I morphology [40]. Intratumoral molecular heterogeneity has also been demonstrated recently [40–42], with PDGFRA amplification and mutation as well as BCOR, ATRX, MYC and TP53 mutations [42], and H3-K27me3 mark [40] showing marked spatial heterogeneity. One of the studies also demonstrated that the histone 3 (H3) lysine-to-methionine missense at position 27 (K27M) mutation is spatially conserved [42], arguing that molecular intratumoral heterogeneity in DIPG is less significant than in adult GBM.

15.2.5 Immune Privilege and Specialization of the Central Nervous System

Immune privilege of the CNS refers to the experimental phenomenon where tissues grafted into the CNS survive for extended periods of time without rejection. Immune privilege of the CNS was thought as the result of CNS isolation from the immune system by the BBB, the lack of draining lymphatics, and the less immunocompetent microglia instead of regular macrophages. However, recent evidence shows that the CNS is neither isolated nor passive in its interactions with the immune system; rather, the CNS is immune-competent in that peripheral immune cells can cross the intact BBB. CNS neurons and glia actively interact with the peripheral immune system to regulate macrophage and lymphocyte responses. Microglia are immunocompetent but function differently from regular macrophage and dendritic cells. Thus, it may be more accurate to describe the CNS as a site of immune specialization.

Immune privilege or specialization of the CNS reflects the difference of initiating adaptive immune responses in the CNS compared to the process in the peripheral immune system, as a result of the composition of the immune system in the CNS, which is different from that of the peripheral system. The CNS can mount a robust immune response that can be used for immunotherapy. But the relative lack of understanding of the immune system in the CNS presents a bigger challenge in designing immunotherapy for brain tumors than for other tumors.

Parallel to evidence of immune competence of the CNS is the existence of immunosuppressive mechanisms in the CNS. One of the immunosuppressive pathways that are the focus of research is the programmed death-1 (PD-1) pathway. PD-1 is a member of the B7 family. Upon binding of programmed death-ligand 1 (PD-L1), the activated pathway leads to loss of the T-cell effector function. Both human GBM [43] and tumor-infiltrating macrophages [44] express high levels of PD-L1, and cytotoxic T-cells infiltrating GBM express high levels of PD-1 [45].

The expression and functions of PD-1 and other B7 family members have not been extensively studied in brainstem tumors. Recently, we found that in a small group of samples, all DIPGs expressed B7-H3 at various levels [46].

Another immunosuppressive pathway involved in the immune response to brain tumors is the cytotoxic T-lymphocyte-associated protein 4 (CTLA-4) pathway. CTLA-4 is upregulated during CD8(+) T-cell activation and is a negative regulator of this process [47]. CTLA-4 is also expressed on CD4(+) T-cells, including CD4(+) CD25(+) [48] and CD4(+)Foxp3(+) [49] regulatory T-cells (Tregs), and enhances Treg-mediated immunosuppression [48, 49]. CTLA-4 inhibits the activation and proliferation of effector T-cells in GBM [50]. The interaction of CTLA-4 with B7 on dendritic cells induces expression of indoleamine 2,3-dioxygenase 1 (IDO1) [51], another major immunosuppressive pathway involved in the immune response to brain tumors.

IDO1 is a tryptophan catabolic enzyme that converts tryptophan into kynurenines, a catabolite mediating the inhibition of effector T-cells and the induction of apoptosis in these cells [52]. It may also amplify immunosuppression by CD4(+)CD25(+)FoxP3(+) Tregs. IDO1 is expressed in over 90% of resected glioblastoma, with the upregulation correlating with a worse prognosis [53, 54]. In xenograft studies, malignant brain tumors deficient for IDO1 result in spontaneous rejection mediated by a T-cell-dependent mechanism [54], which implies that tumor-derived IDO1 is essential for Treg accumulation and immunosuppression.

A recent study characterized the immune microenvironment of DIPG [55] and found that these tumors do not have increased macrophage or T-cell infiltration compared to nontumor controls, nor do they overexpress immunosuppressive factors such as PD-L1 and/or transforming growth factor β 1 (TGF- β 1). H3.3-K27M DIPG cells do not repolarize macrophages but are ineffectively targeted by activated allogeneic T-cells. All DIPG cell cultures in the study could be lysed by natural killer (NK) cells. The results provide insights for the development of immunotherapy in the recruitment, activation and retention of tumor-specific effector cells.

15.3 Molecular Characteristics of Malignant Brainstem Tumors

DIPGs are genetically complex and distinct from both adult and childhood supratentorial HGGs. Recent evidence points to PDGF and its receptor PDGFR as among the major driving forces of tumorigenesis in the majority of cases [56–60]. Another growth factor receptor, EGFR, shows strong immunohistochemistry staining in about 27% of cases [57] and amplification of the gene at a rate of 7–9% [57, 59]. Approximately 50% of DIPGs have *TP53* mutations [61, 62], and three groups report loss of a region of 17p containing the *TP53* gene in 31%, 57% and 64% of cases, respectively [57, 63, 64]. In approximately 50% of DIPG patients, allelic loss of a region of 10q, where the phosphatase and tensin homolog (*PTEN*) gene is located, is observed [63, 65, 66].

Another commonly mutated gene in DIPG is the gene for activin A receptor, type I (ACVR1), which transduces signals of the bone morphogenic proteins (BMPs). The mutation occurs in approximately 20–32% of DIPGs [67–69]. ACVR1 mutations result in ligand-independent constitutive activation of the BMP signaling pathway [70–72]. Seven different ACVR1 mutations have been reported in DIPG, and they have been shown to increase the levels of phosphorylated SMAD1/5 [67–69, 73] as well as increased gene expression of the downstream BMP signaling targets, ID1 and ID2 [67].

Alpha thalassemia/mental retardation syndrome X-linked (ATRX) gene was found to be mutated in ~ 9% of DIPGs and predominantly in older children [74]. ATRX encodes a subunit of a chromatin remodeling complex required for histone H3.3 incorporation at telomeric regions.

Unlike the case in childhood supratentorial HGG, *CDKN2A* deletion is non-existent [59, 64] or only occurs at a low rate (3%) [58] in DIPG. Amplification of *CDK4* and *CDK6* in DIPG occurs at a rate of 7% and 11.6%, respectively [59].

Histone H3, which forms part of the nucleosome core, plays an essential role in the epigenetic regulation of deoxyribonucleic acid (DNA) replication and gene transcription. Recent studies of histone mutations indicate that DIPGs are also epigenetically distinct from pediatric supratentorial HGGs. Recurrent adenine-to-thymine transversions in the *H3F3A* gene, encoding a K27M mutation of histone H3.3, is seen in 60–75% of DIPGs [74, 75], significantly higher than that in pediatric supratentorial GBM (14–19%) [75, 76]. The *H3F3A* mutation is not present in the matching germline DNA samples [75], suggesting its somatic nature. The K27M mutation is found in 66–77% of pretreatment DIPG samples [74, 75], indicating that it is not the result of a selection or mutation process secondary to therapies.

In contrast to the H3.3-K27M mutation profiles, a guanine-to-adenine transition in *H3F3A*, resulting in a glycine-to-arginine missense at position 34 (G34R) of H3.3, is identified in 10–14% of pediatric supratentorial GBM [75, 76] but not in any of the 90 DIPG samples analyzed by two groups [74, 75].

The presence of mutations in the *HIST1H3B* gene, which encodes histone H3.1, is less conclusive. One study found that the adenine-to-thymine transversion that encodes the K27M mutation was present in 18% (9/50) of DIPGs [75], whereas another group did not detect the mutation in any of their DIPG samples (0/27) [74].

The H3.3-K27M mutation is associated with poorer prognosis in DIPG patients [74, 77]. The significance of this mutation has led to the new category (diffuse midline glioma, H3 K27M-mutant) in the 2016 version of the WHO classification of CNS tumors [78].

Some of the described mutations of DIPG are demonstrated in Fig. 15.2.

15.4 Drug Delivery

A number of strategies have been explored to address the BBB as a major obstacle in brainstem tumor treatment. In general, these strategies can be summarized into three categories: (1) bypassing the BBB via local delivery such as convection-enhanced delivery (CED); (2) opening the BBB using physical or chemical methods (paracellular approaches); and (3) delivery across the BBB (transcellular approaches).

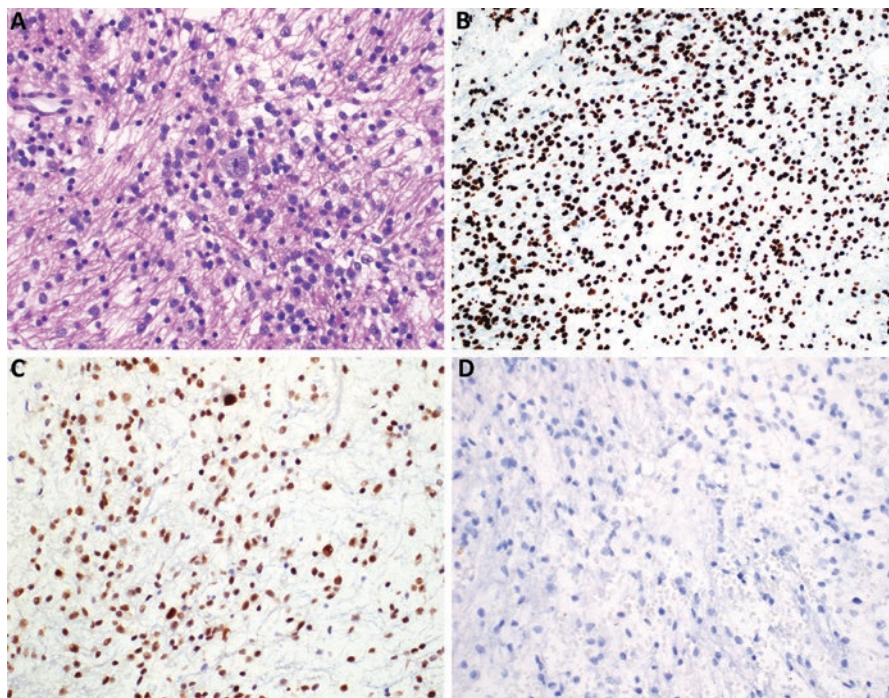


Fig. 15.2 Histology and immunohistochemistry staining of a DIPG sample. (a) H&E stain demonstrating a hypercellular, infiltrating astrocytoma with a non-neoplastic entrapped pontine neuron at center. (b) Immunohistochemical staining for H3 K27M showing positive labeling in neoplastic nuclei, confirming K27M mutation. (c) Immunohistochemical staining for ATRX demonstrating preserved expression, correlating with an absence of mutation. (d) Immunohistochemical staining for p53 demonstrating a complete absence of staining, correlating with a truncating mutation

15.4.1 Convection-Enhanced Delivery

CED is a drug delivery method first developed in the early 1990s [79]. In this method, a drug-containing solution is distributed into the interstitial space driven by a small, persistent hydraulic pressure (i.e., forced convection). In contrast to diffusion that depends on a concentration gradient to distribute the molecules, the use of hydraulic pressure in CED allows for a homogeneous distribution of small and large molecules over large distances by displacing the interstitial fluid with the infusate. In practice, the agent is delivered into the parenchyma or tumor driven by a pump through a microcatheter, or multiple microcatheters, inserted into the tissue. Infusion rates typically range from 0.1 to 10 $\mu\text{l}/\text{min}$ for application in the brainstem, and higher infusion rates are being explored (Fig. 15.3).

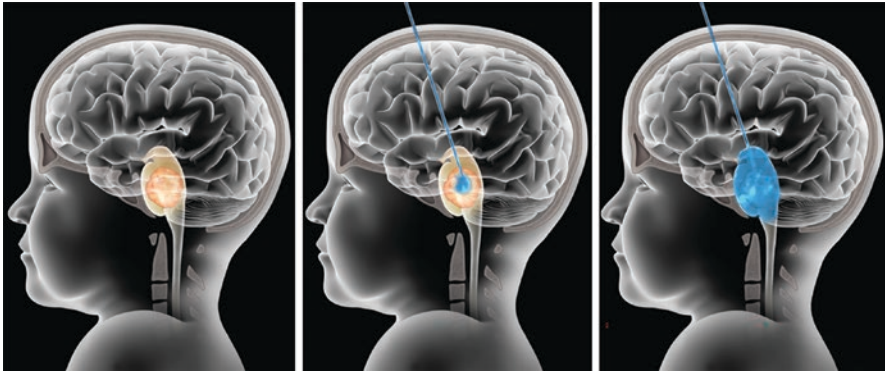


Fig. 15.3 Convection-enhanced delivery into a diffuse pontine lesion

In CED, the distribution from a single point source results in an elliptical to spherical distribution, and spatial distribution is to some degree dependent on the tissue type (i.e., gray versus white matter). In a given tissue type, the distribution volume is roughly linear to the infusion volume.

CED into brain parenchyma, both white and gray matters, has shown reproducible large volumes of distribution with homogeneous drug concentration. Early work showed that the concentration fall-off at the border is steep [79], resulting in a potentially large benefit in cancer drug delivery whenever reducing toxicity to surrounding normal brain tissue is desired.

The volume of distribution can be affected by the retrograde movement of fluid along the outside of the catheter (backflow or reflux). Reflux is determined by catheter material, catheter diameter, infusion rate, and tissue density, among other factors. The larger the catheter diameter, the greater is the chance of backflow along its outer wall. If reflux reaches a low-pressure zone (necrosis or CSF space), the fluid will inadvertently be lost into these spaces; this leads to the accumulation of drug in these regions, which may cause toxicity. Increasing the infusion rate can increase the overall volume of distribution; however, this will also increase the chance of reflux, potentially shunting fluid away from the target region.

Ideally, agents delivered via CED should be contained within the target region of brain parenchyma or tumor mass. However, there are low-pressure regions in some tumors along which the infusate will flow, sometimes into the ventricles or subarachnoid space. This phenomenon is usually referred to as leakage and has often been observed in both humans and experimental animals. One study indicates that this can happen in 20% of CED procedures [80]. This obvious waste of therapeutic agent will consequently reduce the volume of distribution and drug concentration in the planned target region. It may also cause untoward effects on normal brain tissue. It is, therefore, critical to follow the flow of infused agents. When leakage happens, it might be helpful to adjust the catheter placement to move the opening away from the low-pressure region. It is unknown yet whether this leakage is reversible. If reversible, pausing the infusion for a period of time and subsequently restarting the infusion could eliminate the leakage.

Monitoring the distribution and concentration of an infused drug is critical for numerous reasons. In addition to its biological effectiveness, a drug would need to be distributed within the tumor in therapeutic concentrations to be effective. Exposure of normal tissue to the drug should be controlled to reduce the probability of toxicity. It is also highly desirable to monitor for possible reflux and leakage so that the cannula placement can be adjusted to correct any problems that may arise. In the brainstem, the transverse and longitudinal fiber bundles may direct the infusate flow, which also needs to be monitored. The importance of monitoring *in vivo* distribution and concentration is highlighted by the difficulty in achieving optimal therapeutic efficacy in recent clinical trials. In the recent TGF α -PE38 study and the phase III PRECISE trial for glioblastoma, poor drug distribution was cited as one of the reasons for the unsatisfactory efficacy results [81, 82].

Monitoring the distribution and concentration of the CED infusate in humans is difficult due to the fact that the majority of therapeutic agents cannot be seen on any of the clinical imaging methods. Nevertheless, the distribution can be visualized under certain circumstances. T2-weighted MR images are helpful in identifying the infusate distribution in regions of relatively normal intensity, but identifying the distribution is more difficult when infused into already hyperintense regions, such as in DIPG [83]. Another choice is to use surrogate tracers. Gadolinium-diethylenetriamine penta-acetic acid (Gd-DTPA) and ^{123}I -albumin have been co-infused as surrogate tracers, viewable on T1-weighted and single photon emission computed tomography (SPECT) images, respectively, in clinical studies [81, 83–86]. The shortcomings of surrogate markers are that they are only able to accurately estimate the initial distribution. Differences in biological activities and clearance confound their ability to follow the distribution of the therapeutic agent over time. Moreover, neither T2-weighted signals nor surrogate tracers are able to provide information on the concentration of the infused therapeutic agent. The ideal scenario would be to directly image the therapeutic compound. With calibration, the concentration as well as the distribution of the drug can be determined.

The concept of using CED for DIPG treatment is appealing given that this particular tumor is relatively compact, has growth patterns simulating white matter tracts, seldom metastasizes before local relapse occurs, and no surgical resection is performed. Our group first established the feasibility of this delivery route in the brainstem in small animals for potential clinical application in 2002 [87]. Subsequently, the safety of inert agents, characteristics of distribution, and toxicity of potential therapeutic agents in the brainstem of small animals and non-human primates have been studied [88–93]. These studies showed that CED does not cause clinically relevant mechanical injury to the brainstem, and this approach has a promising therapeutic application in humans. In clinical practice, image-guided frameless stereotaxy can be utilized to target the brainstem in children for biopsy or cannula insertion with high accuracy and low risks of temporary or permanent morbidity [94–96], providing supportive evidence of the safety of applying CED in the brainstem.

A few groups in the United States and Europe are pursuing clinical studies of brainstem CED to treat DIPG [86, 97–99]. These small series reported reasonably good safety and tolerance. In a clinical trial to treat DIPG patients with IL13-PE38QQR CED in the brainstem (NCT00880061), all five patients tolerated the therapy well, and two patients showed temporary signs of anti-tumor effects on MRI [100]. The most comprehensive results of brainstem CED in DIPG patients have been reported by our group [101]. In this interim report of results of the phase I clinical trial (NCT01502917), 28 patients had been treated without any dose-limiting toxicities. Utilizing a theranostic agent (^{124}I -labelled 8H9 a.k.a. omburtamab), this study also reported that the radiation absorbed dose to the lesion was 1200-fold that of the systemic exposure. These results directly demonstrated the safety of CED in the human brainstem, as well as validated the principle that CED efficiently delivers therapeutics to the target with minimal systemic exposure.

Other ongoing CED clinical trials recruiting exclusively DIPG patients include NCT03086616 (CED of an irinotecan liposome formulation) and NCT03566199 (CED of a panobinostat nanoparticle formulation).

Future advances in CED for DIPG treatment will occur on a few fronts: (1) the selection or development of therapeutic agents for DIPG; this will depend on the better understanding of the disease biology and development of novel therapeutic strategies. (2) The improvement of the technique of CED; this includes a new design of the devices to facilitate easier and accurate deployment of the cannula, implementation of prolonged and repeated infusions lasting up to weeks for optimal time sequence of therapy, and better understanding of the infusate distribution and its influencing factors so that catheters can be placed to achieve optimal tumor coverage. It is also desirable to have devices that can be embedded to allow patients to remain ambulatory while undergoing continuous or multiple sessions of CED.

Perhaps more important is the need to evaluate the pharmacokinetics and regional therapeutic response in CED. Results from systemic pharmacokinetic and pharmacodynamic studies cannot be directly applied to CED applications of the same therapeutic agents. To evaluate pharmacokinetics and pharmacodynamics, imaging should accompany the therapy to ensure effective drug distribution and concentration as well as to determine the retention and clearance of therapeutic agents in the tumor and tumor-infiltrated brain tissue in individual patients whenever possible. This would require the improvement of current imaging techniques or the development of new imaging agents and methods, such as contrast agents that respond to effector molecules or end products of apoptosis. Such techniques as microdialysis may also have a place in the pharmacokinetic evaluations of CED. For evaluating the regional therapeutic response, an innovative noninvasive method is in desperate need, as the current methods of radiological evaluation are not sufficient. At this stage where CED is used as an investigational therapeutic platform, the pharmacokinetic and pharmacodynamic evaluation would allow for determination of the effectiveness of CED-based therapies. In the future, treatment strategies would be able to be dynamically adjusted based on the regional response, incorporating multiple modalities of therapeutic options.

15.4.2 Intraarterial Delivery

Intraarterial chemotherapy is now widely used for the treatment of retinoblastoma and advanced liver cancer, improving the quality of life and extending overall survival. In the case of retinoblastoma, super-selective intraarterial chemotherapy can produce high cure rates. Beyond these two well-established applications, intraarterial chemotherapy has been also used, with variable success, in the treatment of other cancers such as breast cancer, head and neck cancer, colorectal cancer, penile cancer, and pancreatic cancer.

Intraarterial therapy for malignant brain tumors, especially HGGs, has been administered since 1950s. Most of these attempts rely on the general belief that transiently generating high arterial blood concentrations would lead to the desired pharmacodynamic effects. However, in these early attempts, no objective comparisons with intravenous administration were performed. The advantages of intraarterial delivery were first demonstrated when intraarterial infusion led to a higher tissue concentration compared to non-targeted tissue [102]. In the 1970s, osmotic BBB disruption was studied to improve intraarterial delivery [103, 104]. With the miniaturization of catheters and other endovascular devices, selective and super-selective intraarterial delivery was developed and studied in the treatment of brain tumors since 1990s. They allow for accurate and super-selective targeting of the tumor's supplying vessels, compared to early intraarterial attempts of carotid or vertebral artery infusion.

A critical factor in intraarterial delivery is the BBB. Studies have shown that the BBB can be reversibly modified to be more permeable by hyperosmotic solutions such as mannitol [103]. Other methods of BBB disruption include vasoactive agents, such as bradykinin analogs, and focused ultrasound (FUS). Concurrent flow arrest appears to enhance the regional effectiveness of intraarterial delivery by achieving higher arterial concentrations, as well as more consistent concentrations in the arterial distribution, and increased transit time. Without flow arrest, for effective intraarterial delivery, drugs must be rapidly taken up during their first pass through the tissue circulation, lasting between 1 and 10 seconds in the brain. As another way of improving BBB penetration, intraarterial delivery can be combined with the transcellular approach of delivery using BBB-penetrating delivery vehicles such as cell-penetrating peptides. There is some evidence that intraarterial delivery of cell-penetrating peptides can penetrate the BBB, and preliminary results suggest that they can lead to tumor-specific drug uptake [105].

There are a number of clinical trials of intraarterial therapy for DIPG patients (NCT01688401) or for pediatric brain tumor patients, including DIPG (NCT01884740). Results have not been reported yet.

15.4.3 *Manipulating the Blood-Brain Barrier*

The BBB can be opened by hyperosmolar solutions (e.g., mannitol) or vasoactive drugs (e.g., bradykinin and adenosine) for drug delivery. The BBB, when opened this way, remains open for only a short period of time, and the procedure may need to be repeated in drug delivery sessions lasting longer than several minutes. Non-selective opening of the BBB exposes large volumes of normal brain to undesirable substances that may be toxic.

Site-specific disruption of the BBB represents an improvement to non-selective BBB disruption for drug delivery into the brain. This has been accomplished using either FUS [106] or laser-based approaches such as photodynamic therapy (PDT) [107] and photochemical internalization (PCI) [108]. These techniques have a number of advantages over non-selective BBB disruption. The site of BBB disruption is the only site receiving sufficient ultrasound or laser intensity. With imaging guidance, and through careful placement of the probes and adjustment of parameters, the site of BBB disruption can match the lesion with maximum coverage while the normal brain is minimally affected. In addition, these highly focused approaches do not cause permanent damage to the BBB, as long as the ultrasound or laser intensity remain below threshold levels. With these site-specific approaches, the BBB may remain open for relatively long periods of time, thus facilitating longer drug delivery.

15.4.3.1 **Focused Ultrasound**

FUS, which can be aimed at a spot of just a few mm in diameter, is capable of achieving selective disruption of the BBB. In this direct approach, it is difficult to identify parameters producing reliable opening of the BBB without damage to normal brain. Albumin-coated microbubbles were introduced to address this concern [109]. The microbubbles, when injected intravenously, confine the ultrasound effects to the walls of blood vessels resulting in BBB disruption with minimal damage to the surrounding brain tissue [110]. This has allowed for selective disruption of the BBB at much lower acoustic power levels than previously employed [111].

The exact mechanisms of BBB disruption by microbubble-enhanced FUS remain to be elucidated. The effect is likely due to a combination of cavitation and acoustic radiation forces [106]. Cavitation is the acoustically-induced activities of microscopic bubbles within the medium. The generation of microbubbles requires high acoustic power densities, which may result in tissue damage [112]. With the introduction of albumin-coated microbubbles, high powers are no longer required and, therefore, the risk of tissue damage has significantly decreased (Fig. 15.4).

The BBB opening by FUS is relatively short, ranging from 10 minutes to 5 hours following the sonication [106]. This may be sufficient for a single dose administration of drugs, but for prolonged drug administration, repeated sonication may be required, which can limit its feasibility.

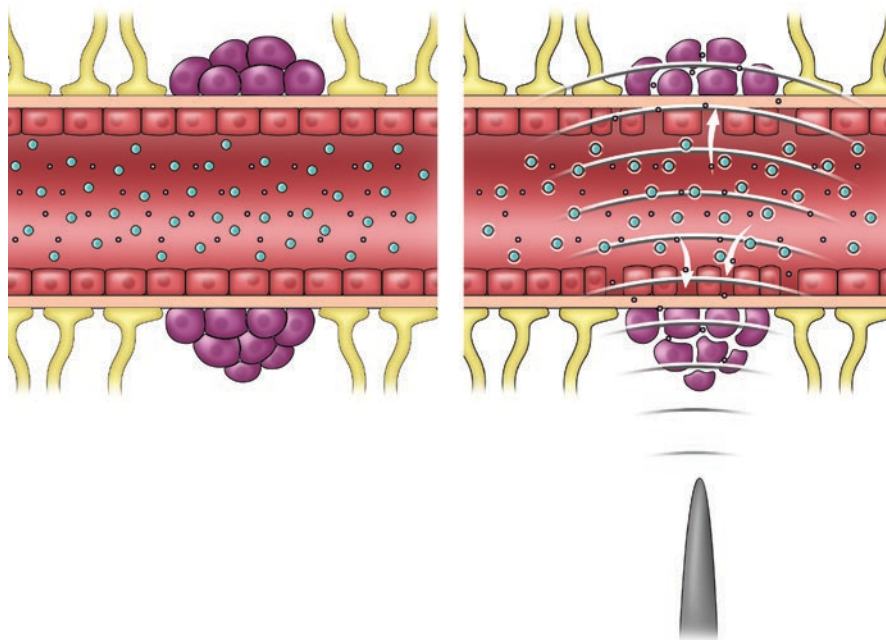


Fig. 15.4 Focused ultrasound for opening the BBB. (Left) Albumin-coated microbubbles are injected into the blood stream before focused ultrasound is applied. (Right) Upon application of focused ultrasound, the oscillation of the microbubbles helps open the BBB

Animal studies suggest that FUS-induced BBB disruption does not result in permanent damage to the brain as evidenced by the lack of ischemic or apoptotic changes [111]. The minor effects observed, such as small extravasations and mild inflammatory reactions, do not appear to affect the neurons up to four weeks following the sonication [111].

A major limitation of transcranial FUS is that the skull is highly absorbing of ultrasound. This causes strong attenuation and phase distortion [113]. At high powers, FUS also causes heating during the sonication.

The safety of FUS in opening the BBB is being investigated in a clinical trial (NCT02343991) in brain tumor patients.

15.4.3.2 Photodynamic Therapy

PDT is the use of a tumor-localizing photosensitizer that is subsequently activated by an excitation light [114]. The photochemical and photobiological events would induce therapeutic effects.

PDT using either hematoporphyrin derivatives or 5-aminolevulinic acid (ALA) has been reported to induce brain edema surrounding the site of phototherapy [115–117], suggesting a local breakdown of the BBB.

ALA-PDT-mediated disruption of the BBB was found to be apparent as early as 2 hours following PDT, and the BBB was approximately 90% restored within 72 hours [107]. This is longer than the FUS-induced BBB opening.

The mechanisms of PDT-mediated BBB opening likely include rounding and contraction of endothelial cells mediated by PDT-induced microtubule depolarization [118]. The formation and enlargement of endothelial gaps have been observed in PDT [119]. Electron microscopy studies demonstrated that the treatment had minimal impact on the normal subcellular structures of endothelial cells [120], suggesting there were no permanent damages.

15.4.3.3 Photochemical Internalization

PCI is the use of specially designed photosensitizers that localize preferentially in the membranes of endocytic vesicles. Upon light activation, the photosensitizer disrupts the vesicular membrane, releasing encapsulated macromolecules into the cell cytosol. This can be used to enhance the delivery of macromolecules in a site-specific manner [121].

PCI-delivered *Clostridium perfringens* epsilon prototoxin (ETXp) was used for localized BBB opening [108], because the active toxin (ETX) can cause widespread but reversible opening of the BBB [122–124]. Following administration, ETXp is converted to ETX by proteolytic cleavage. Disruption of the BBB was accomplished by combining sub-threshold doses of ETXp with sub-threshold light fluences. The membrane-localizing photosensitizer used was aluminum phthalocyanine disulfonate (AlPcS_{2a}). The results show that ETXp-PCI is capable of causing localized BBB disruption at very low light fluences, and no significant damage was noted in rat brains at these conditions. In comparison, the BBB remained relatively intact when exposed to AlPcS_{2a} without ETXp at these light levels. At higher fluences, the PDT effect was so pronounced that without ETXp, necrosis and inflammation were already evident, and the addition of ETXp had no apparent effect on BBB disruption.

15.4.4 Inhibition of ATP-Binding Cassette Transporters

One mechanism that is responsible for multidrug resistance (MDR) is the active efflux of drugs by ABC transporters. Several agents have been developed to block ABC transporter-mediated drug efflux, and some have entered phase II/III clinical trials.

The first-generation inhibitors included drugs developed for other conditions such as verapamil, quinine, and cyclosporine A. Despite their efficacy in inhibiting P-gp1-dependent drug efflux *in vitro* [125], these inhibitors lack specificity and cause significant toxicity when used as ABC transporter inhibitors [126].

The second-generation P-gp1 inhibitors were designed to improve specificity. Valspodar is a derivative of cyclosporine A, with higher specificity and potency and no immunosuppressive effects [127]. However, it inhibits cytochromes P450 (CYP450s) [128] and causes pharmacokinetic effects. As a result, it failed to improve outcomes; it even produced worse outcomes in phase III clinical trials with the anticancer drugs vincristine and doxorubicin [129], or daunorubicin and etoposide [130] in patients with acute myeloid leukemia (AML).

The third-generation inhibitors were developed focusing on not to inhibit liver enzymes such as CYP450s. P-gp1 specificity was another focus. Tariquidar (an anthranilamide), elacridar (an acridone caroxamide), zosuquidar (quinolone derivative), CBT-1 (quinolone derivative) and laniquidar (a piperidine) are at various stages of clinical trials. Tariquidar and zosuquidar entered Phase II/III trials in combination with vinorelbine and doxorubicin, respectively, for a variety of advanced solid tumors or AML. Phase III trials of tariquidar in non-small cell lung cancer produced high rates of side effects without improving the patient response. Zosuquidar has also shown neurotoxicity [131] and drug-drug interactions with doxorubicin and vinorelbine [132].

These examples show that the strategies of inhibiting ABC transporters need further improvements. The way to these inhibitors' application to brainstem tumor therapies may take even longer than their use in non-CNS tumors. However, optimism is warranted with further improvement of such agents' specificity, strategies of more specific targeting of drugs beyond the drug's structure, and better selection of patients with improved diagnostic techniques.

15.4.5 Carriers and Packaging Vehicles

Several approaches for drug delivery across the BBB have been attempted, including encapsulation into liposomes and nanoparticles. By incorporation into liposomes or nanoparticles, the drugs are stabilized for more efficient direct delivery or paracellular delivery. The incorporation can also include targeting moieties, such as proteins (e.g., insulin, Apolipoprotein E, and transferrin) that are known to traverse the BBB by receptor-mediated endocytosis, making the formulation suitable for transcellular delivery. This molecular Trojan horse approach has been successful in delivering a number of therapeutic proteins. However, limitations still exist, including rapid removal from the circulation, low delivery yields, and the need for repeated injections.

15.4.5.1 Liposomes

Liposomes are small vesicles consisting of one or more lipid bilayers surrounding an aqueous compartment. They are nanometers-to-micrometers in diameter. They were discovered in early 1960s; the exploration of their potential use as a carrier

system for therapeutically active compounds began soon after that. In recent years, their application has been explored for the diagnosis and/or treatment of neurological diseases in particular. Due to the unique physicochemical characteristics of lipid bilayers, liposomes are able to incorporate hydrophilic, lipophilic, and hydrophobic therapeutic agents. Hydrophilic compounds may either be entrapped into the aqueous core of the liposomes or be located at the interface between the lipid bilayer and the external water phase. Lipophilic or hydrophobic drugs are generally entrapped almost completely in the hydrophobic core of the lipid bilayers. The use of cationic lipids further allows the adsorption of polyanions, such as DNA and ribonucleic acid (RNA). The surface of liposomes can be modified by the inclusion of other macromolecules, such as polysaccharides, peptides, antibodies, or aptamers, to improve its stability in blood circulation and brain-specific delivery. Several liposomal drugs are either approved for clinical use or in clinical trial studies [133, 134], but efficient brain-specific drug delivery by liposomes is not at the clinical stage yet.

Liposomes can be conjugated with specific antibodies or ligands to enhance their ability to cross the BBB through receptor-mediated endocytosis by the BBB cells. Several studies using transferrin (Tf), lactoferrin, insulin, glutathione, apolipoproteins and peptides reported successful delivery of liposomes to the brain parenchyma or tumor [135–137]. In one of the studies, it was also shown that Tf-conjugated liposomes were taken up by BBB cells more than unconjugated liposomes and were subjected to transcytosis [137].

Recently, magnetic liposomes have emerged as an interesting targeting moiety for delivery of therapeutic molecules across the BBB. In one study, one or more drug molecules could be reversibly bound to the surface of iron oxide nanoparticles and encapsulated within the core of liposomes [138]. When an external magnetic field was applied, the liposomes bypassed an *in vitro* model of the BBB. It has further been shown that magnetic liposomes can also be taken up into human monocytes, followed by the entry of nonmagnetic monocytes into the brain [138].

Various routes of administration have been tested for delivery using liposomes to the brain. Intravenous injection seems to be the preferred route in practice. Alternative routes of administration (oral, ocular, or mucosal) have also been explored. For example, intranasal administration is a noninvasive approach to deliver drugs to the brain. It was shown that a liposomal formulation of rivastigmine was able to prevent degradation of the drug in the nasal cavity and to carry it through the mucosal barriers [139]. The ability of cationic liposomes to deliver proteins to the brain via the intranasal route has also been demonstrated [140].

15.4.5.2 Nanoparticles

Nanoparticles commonly refer to carriers with a size between 10 and 1000 nm. They can be made with a broad range of materials such as sugar derivatives, fatty acids, peptides and proteins.

Experimental evidence shows that nanoparticles enhance delivery across the BBB through mechanisms of passive (nonspecific endocytosis) or active targeting

(receptor-mediated endocytosis). In one study, the nanoparticles were mainly taken up via nonspecific endocytosis [141]. The size, chemical structure, and surface properties of nanoparticles are critical factors influencing their uptake by cells of the BBB. Nanoparticles smaller than 20 nm can pass through the BBB endothelial cells by transcytosis [142].

Surface features of nanoparticles, such as charge and coating, may be more important than their core structure in determining their ability to cross the BBB. Surface charge may determine the pathway through which nanoparticles are taken up. In one study [143], at 4 °C, when active endocytosis was stopped and only passive diffusion was present, cationic nanoparticles remained outside the BBB cells, neutral nanoparticles were associated with cell surface, and anionic nanoparticles were detected on cell surface and in paracellular space; at 37 °C, only neutral and anionic nanoparticles had undergone endocytosis and transcytosis. This study further showed that neutral and anionic nanoparticles followed the caveolae-mediated endocytotic pathway, whereas cationic nanoparticles did not.

The presence of noncovalently- or covalently-bound ligands on the surface of nanoparticles can further improve delivery across the BBB by receptor-mediated endocytosis [142, 144]. The most common receptors utilized for this purpose are the insulin receptor, the Tf receptor, the low-density lipoproteins receptor (LDLR), the LDLR-related proteins (LRPs), the folic acid receptor, and the diphtheria toxin receptor. The delivery of Tf-conjugated nanoparticles was more efficient than unconjugated ones within the CNS [145, 146] due to the abundance of Tf receptor in the BBB [142]. LDLR and LRPs trigger efficient receptor-driven endocytosis followed by transcytosis [147]. The major drawback of using Tf, folic acid or apolipoproteins as targeting ligands on nanoparticles is that their receptors are widespread; therefore, there is a risk of nanoparticle uptake by other tissues.

Current ongoing clinical trials of liposomes and nanoparticles recruiting exclusively DIPG patients include NCT03086616 (CED of an irinotecan liposome formulation) and NCT03566199 (CED of a panobinostat nanoparticle formulation).

15.5 Signal Transduction Pathway Targeted Therapy

As discussed in Sect. 15.3, a number of mutations have been discovered in DIPG. Some of the mutations observed in DIPG are targetable, such as the PDGFR pathway, while many others are not currently targetable yet. Targeting the RTK signal transduction pathways such as the PDGFR pathway has been a focus of some recent research. In GBM, therapy with single agents leads to clonal selection, enriching therapy-resistant clones that give rise to recurrent tumors [34]. Possibly and partially a result of this phenomenon, clinical trials with signal transduction pathway-targeted therapies failed to show significant improvement in survival in GBM, as well as in DIPG [8, 35]. In addition, RTKs downstream and parallel signal transduction pathways may be regulated in a compensatory fashion with redundancy that contributes to drug resistance, especially in single target therapies.

Therefore, it is not surprising that drug resistance has been inevitable in almost all single-drug targeted therapies. How to target multiple points in signal transduction pathways without causing much toxicity is the subject of active studies.

Ongoing clinical trials of signal transduction pathway targeted therapies recruiting DIPG patients include NCT03352427 (combination of dasatinib and everolimus), NCT01644773 (combination of crizotinib and dasatinib), NCT02420613 (combination of vorinostat and temsirolimus) and NCT03632317 (combination of panobinostat and everolimus).

As long as a molecule is differentially expressed between tumor cells and normal tissue, it does not need to be growth-promoting to be considered a therapeutic target. One example is IL-13R α 2, whose functions are not well understood in brain tumors. Like in adult malignant gliomas, IL-13R α 2 is highly expressed in DIPG [148, 149]; therefore, recombinant toxins using IL-13 as a targeting moiety are also potentially effective therapeutic agents for DIPG. CED of IL13-PE38QQR in the brainstem has shown a good safety profile in both a preclinical study [88] and a clinical trial in DIPG patients (NCT00880061) [100].

15.6 Modulating Gene Expression Status: Epigenetic Modulators

The importance of epigenetic changes in pediatric brainstem gliomas has recently been recognized. Most notable is the histone methylation status associated with the H3K27M mutation. It is thought that inhibition of the histone methyltransferase Polycomb repressive complex 2 (PRC2) and hypomethylation of H3K27 play an important role in the effects of H3.3K27M mutation on the tumorigenesis of DIPG [150].

One approach of investigational therapy used GSKJ4, an H3K27 demethylase inhibitor, to counter the effects of hypomethylation of H3K27 caused by H3.3K27M mutation. GSKJ4 increased cellular H3K27 methylation in K27M tumor cells, reduced tumor size of K27M xenografts, and prolonged survival of mice bearing these xenografts [151].

Another approach focuses on enhancer of zeste homolog 2 (EZH2). EZH2 is part of PRC2 and, hence, has been considered as a potential therapeutic target. However, preclinical studies of inhibiting EZH2 using tazemetostat showed different results from two research groups. In one study, tazemetostat did not show activity in pediatric glioma cells *in vitro* with or without H3.3 mutations [152]. In another, results showed that tazemetostat may affect growth of primary H3K27M-positive glioma cells in the presence of a functional p16INK4A [153]. Genetic studies showed that short-term EZH2 depletion in glioblastoma cells without H3 or isocitrate dehydrogenase (IDH) mutations has been associated with reduced proliferation [154], but prolonged EZH2 depletion caused a switch in cell fate, enhancing proliferation and DNA damage repair and resulting in tumor progression [155].

Other studies show that activation of PRC2 and hypermethylation of H3K27 may be driving the initiation of medulloblastoma [156], ependymoma [157], and lymphoma [158]. These pieces of evidence suggest that rebalancing the H3K27 methylation pathway for therapeutic purposes may not be an easy task.

Histone acetylation is another epigenetic target in cancer therapy. The rationale of using histone deacetylase inhibitors (HDACi) in cancer therapy is to reverse dysregulated gene expression by modulating histone acetylation. Acetylation of lysine residue on histones is a mark of active enhancers that control the expression of associated distal genes. HDAC inhibition causes hyperacetylation of histones and affects the expression of a large number of genes.

Vorinostat has been tested in clinical trials of recurrent glioblastoma. As a single agent, it showed good tolerability in glioblastoma patients and induced increased histone acetylation in the tumors [159]. However, when tested in combination with the protease inhibitor bortezomib, vorinostat did not show efficacy [160]. In newly diagnosed glioblastoma, the addition of vorinostat to the standard regimen of temozolomide and radiation therapy did not meet the primary endpoint of efficacy in a phase I/II trial [161]. An ongoing study is evaluating the safety of vorinostat in combination with temsirolimus in DIPG patients (NCT02420613).

Panobinostat, another HDAC inhibitor, reduced the viability of cultured DIPG cells, reduced tumor size of DIPG orthotopic xenografts, and prolonged the survival of mice bearing these xenografts [162]. Combination testing with GSKJ4 showed that they had synergistic effects [162]. Clinically, two patients with progressive DIPG tolerated concomitant panobinostat and reirradiation well [163]. An ongoing phase I clinical study is more systematically evaluating the safety and pharmacokinetics of panobinostat in both recurrent/progressive and non-progressed DIPG patients (NCT02717455). Other clinical trials of panobinostat with DIPG as an eligible disease include NCT03632317 (panobinostat in combination with everolimus). MTX110, a nanoparticle formulation of panobinostat, is being tested in treating DIPG patients via brainstem CED (NCT03566199).

15.7 Immunotherapy

15.7.1 *Therapeutic Antibodies, Radiolabeled Antibodies, and Immunotoxins*

To some degree, the main underlying assumption of using antibodies to treat malignant tumors is the specific recognition and elimination of malignant cells by antibodies. Several types of therapeutic antibodies have been developed to treat malignant tumors, including HGGs, where antibodies targeting growth factor receptors were among the most actively investigated recently.

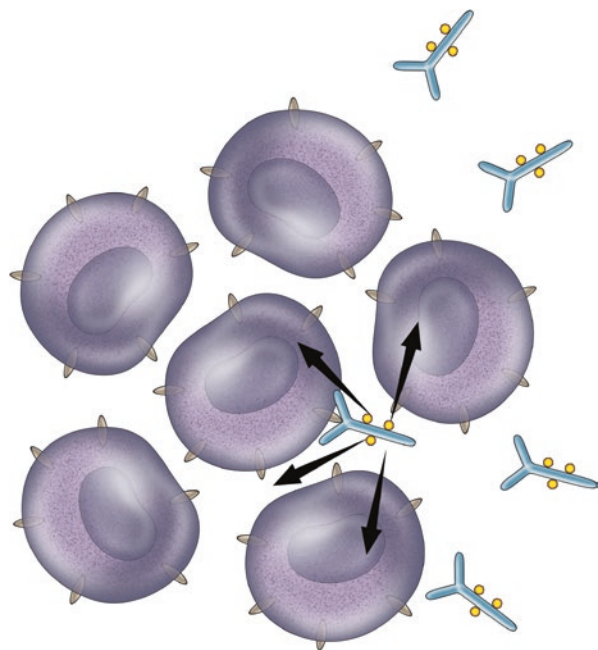
Growth factors have been shown to support tumor initiation and progression in malignant gliomas, including DIPG. Recent evidence showed that PDGF, along

with its receptor, PDGFR, is one of the most commonly involved oncogenic signal transduction pathways in the majority of DIPG cases [56–60]. Another growth factor receptor, EGFR, is also involved in a significant numbers of cases [57, 59].

Therapeutic antibodies against these growth factor receptors block activation of the receptor and have the potential to cause cell death. Additionally, binding of antibodies to cell surface antigens can induce antibody-dependent cell-mediated cytotoxicity (ADCC) and complement-dependent cytotoxicity (CDC), even though effector cells of ADCC and CDC are not abundant in the CNS. Antibodies against PDGFRs, such as olaratumab (IMC-3G3) and MEDI-575, have been proposed to treat DIPG. Currently, there are a few clinical trials of olaratumab (e.g., NCT02677116) on treating pediatric solid tumors via intravenous administration, with DIPG as an eligible disease. No results have been published from these trials yet. Due to the large molecular weight of the antibodies, we believe that CED would be an ideal delivery option of therapeutic antibodies in treating DIPG.

Therapeutic antibodies can be labeled with radionuclides to strengthen their therapeutic capability. In addition to the effects of the antibody itself, the therapeutic effects of radiolabeled antibodies are achieved by the energy deposited into the tissue by the radiation from the radionuclide that is tagged to the antibody (Fig. 15.5). The choice of a radionuclide for a specific application depends on the disease to be treated, physical characteristics of the nuclide, its commercial availability, and the labeling chemistry. Radionuclides used in oncologic therapy are typically Beta (β)- and alpha (α)-emitters. β emissions from radionuclides such as ^{131}I , ^{90}Y , and ^{186}Re have a particle range of 2–12 mm in soft tissue; therefore, nearby tissue is impacted

Fig. 15.5 Radiolabeled antibodies. In addition to the therapeutic effects of antibodies, emissions from radioisotopes on radiolabeled antibodies also have therapeutic effects. In the case of α and β emissions, their ranges reach neighboring cells (“shoot the neighbor” effects)



along with the cells that the radiolabeled antibody binds to, which is suitable for the treatment of bulky tumors. α emissions from radionuclides such as ^{212}Bi and ^{225}Ac have a particle range of tens of microns in soft tissue and can reach a few layers of cells surrounding the cells to which the radiolabeled antibodies are bound. The Auger and conversion electron emitters are also used for therapeutic purposes. Their particle range in soft tissue is approximately 1 micron, resulting in highly localized targeting without impacting adjacent cells, which is suitable for single cell situations as in certain micrometastatic diseases, minimal residual diseases, and blood malignancies.

The use of radiolabeled antibodies in the treatment of DIPG has been explored. Currently, there is a clinical trial (NCT01502917) of delivering ^{124}I -labeled 8H9 (omburtamab) via CED to treat children with DIPG. ^{124}I allows for the quantification of radiation dose by positron emission tomography (PET) imaging. The results showed that the drug as well as the delivery are safe. Uniquely, the quantification allowed for validating the principle that CED efficiently delivers therapeutics to the target with minimal systemic exposure by showing that the radiation absorbed dose to the lesion was 1200-fold that of the systemic exposure [101].

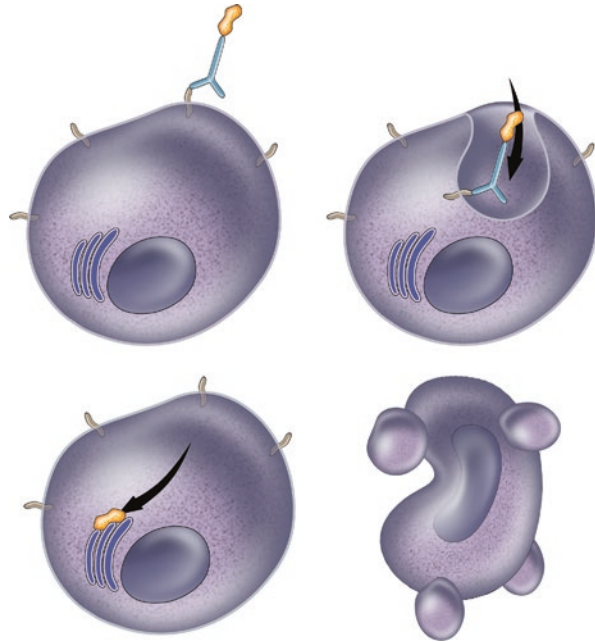
Immunotoxins are chimeric or recombinant molecules that contain a toxin linked to an antibody that binds specifically to its targets. Sometimes, growth factor or cytokine toxin fusions or conjugates are also considered immunotoxins, as they bind to target cells and contain a toxin that kills cells similar to classical immunotoxins [164].

In the early history of immunotoxin development, full-length antibodies were coupled with plant toxins like ricin or gelonin without the toxin's binding domain. Subsequently, bacterial protein toxins such as the *Pseudomonas* exotoxin (PE) and diphtheria toxin (DT) were used. The first-generation immunotoxins were made of full-length PE attached to whole monoclonal antibodies. These immunotoxins could bind to normal cells due to the existence of the toxin's binding domain. In second-generation immunotoxins, regions of the toxin that were not essential for cytotoxicity were removed to produce a truncated toxin that could not bind to normal cells, then the toxin was linked to an antibody. Second-generation immunotoxins such as PE38-based immunotoxins are more specific than first-generation immunotoxins.

Similarly, chemical drugs can be conjugated to antibodies forming antibody-drug conjugates (ADC). ADCs, like immunotoxins, take advantage of the antibody's specificity to improve targeting cells and reduce the drug's toxicity. While each specific immunotoxin or ADC has its specific mechanism of action, the general pathway is that upon binding to the antigens on the cell membrane, the immunotoxin or ADC molecules undergo internalization via receptor-mediated endocytosis and are then released into the cytosol to exert their toxicity on target organelles (Fig. 15.6). Some immunotoxins and ADCs may also undergo enzymatic conversion during the internalization and release process.

The potential clinical application of immunotoxins 8H9scFv-PE38 and IL13-PE38QQR in the treatment of DIPG has been investigated. In an animal study, 8H9scFv-PE38 was well tolerated and significantly shrank the tumor xenograft when delivered via CED [91]. Similarly, IL13-PE38QQR showed good safety and

Fig. 15.6 Immunotoxins and antibody-drug conjugates (ADCs). Binding of immunotoxins and ADCs onto membrane receptors triggers receptor-mediated endocytosis. Internalized immunotoxins and ADCs reach end organelles (such as the rough endoplasmic reticulum) to exert their cytotoxic effects



efficacy in a xenograft DIPG model [88] and clinical safety in a phase I clinical trial (NCT00880061) [100], using CED to deliver the immunotoxin into the brainstem lesions in DIPG patients. IL-13 is an immune molecule normally present in the body. About 90% of malignant gliomas have high levels of IL-13 receptors while the normal brain tissue has only a low level of these receptors.

Current and future efforts in the development of antibody-based immunotherapies (including therapeutic antibodies, radiolabeled antibodies, immunotoxins, and ADCs) include the identification of therapeutic targets, development of antibodies against these targets, identification and/or development of radionuclides, drug conjugates and toxins with improved specificity and efficacy, and optimization of delivery methods.

15.7.2 Therapeutic Vaccines

Malignant tumors evade the host's immune surveillance. Therapeutic cancer vaccines induce immune responses against antigens specifically or highly selectively expressed by tumor cells or tumor-associated cells, such as stromal cells, while the host would not be able to mount such effective immune responses without assistance [165]. Such tumor antigens can be mutated peptides [166] or altered post-translational modifications [167]. Tumor antigen(s) are administered with immuno-stimulatory adjuvant(s) to enhance antigen presentation and subsequently

activate and expand tumor-reactive T-cells. The biggest challenge in designing such vaccines is the selection of optimal antigen(s) and adjuvant(s), because many tumor-associated antigens are not identified as foreign by the host's immune system [168]. Another reason for this challenge is that some antigens are not exclusively expressed by tumor cells, which can result in immunization against normal cells.

Results from clinical studies involving adult GBM patients suggest that immunization against a single tumor-associated peptide is not sufficient to control the progression of the tumor. In one study, where patients were immunized with dendritic cells loaded with glioma-associated peptides combined with adjuvant poly-ICLC, approximately 60% of patients demonstrated glioma-associated immune responses (vaccine immunogenicity), but only <10% of recurrent glioma patients demonstrated stable tumor regression [169].

Tumor neoantigens, generated by mutations occurring during tumor initiation and progression, are considered to have a higher potential for therapeutic vaccination. These neoantigens are often unique in individual patients [168, 170]. Some neoantigens, such as EGFR variant III (EGFRvIII), are present in a higher percentage of tumors and are rational targets for vaccination that would not be cost- and time-prohibitive. EGFRvIII is present in approximately 20–30% of newly diagnosed GBM [171] and is associated with worse prognosis for patients who survive more than 1 year [172]. EGFRvIII is capable of inducing both cellular and humoral immunity [173]. The clinical study results of an EGFRvIII peptide vaccine (rindopepimut) demonstrated vaccine immunogenicity and increased overall survival, with median survival of approximately 24 months [173–175], while the standard of care produces a median survival of approximately 15 months; the survival advantage also correlated with the induced tumor immunity. However, tumor relapse occurred with loss of EGFRvIII expression based on immunohistochemical detection [173–175]. The loss of antigen detection could be a result of clonal selection or the generation of antibodies by the hosts, which may have masked the antigens. A multicenter study confirmed that immune-mediated eradication of tumor cells bearing EGFRvIII contributed to prolonged progression-free survival and overall survival in patients having received the vaccine, as well as increased host-produced antibodies against EGFRvIII in some patients [174].

There are various recent efforts to address the immune evasion in vaccination by targeting a broad range of antigens simultaneously. One example is to utilize autologous dendritic cells that are pulsed with the tumor lysate. A vaccine using this approach (DCVax@-L) recently completed a phase III trial for patients with newly diagnosed GBM (NCT00045968). Results showed that the addition of DCVax-L to standard therapy is safe in glioblastoma patients and may extend survival [176].

There are several therapeutic vaccines in clinical trials for the treatment of DIPG. One peptide vaccine trial aims to vaccinate patients with HLA-A2-restricted glioma-associated antigen peptides with poly-ICLC in newly diagnosed DIPG and some other glioma patients (NCT01130077). Interim results showed that no dose-limiting non-CNS toxicity was encountered. In about 80% of the patients, immune responses were detected against glioma-associated antigens (IL-13R α 2, EphA2 and survivin). About 20% of patients had symptomatic pseudoprogression, which

responded to dexamethasone and was associated with prolonged survival [177]. Dexamethasone reduced the pseudoprogression, a presentation of inflammation, as well as immune responses to glioma-associated antigens. Another peptide vaccine trial aims to vaccinate patients with H3.3-K27M-specific peptides with poly-ICLC in patients with HLA-A2(+) H3.3-K27M(+) DIPG or other gliomas (NCT02960230).

One of the dendritic cell vaccines trials for DIPG patients is the NCT02840123, in which patients are vaccinated with autologous dendritic cells that are pulsed with allogenic tumor line lysate. Another dendritic cell vaccine, total tumor mRNA-pulsed autologous dendritic cell (TTRNA-DC) vaccine, is being tested as part of NCT03396575.

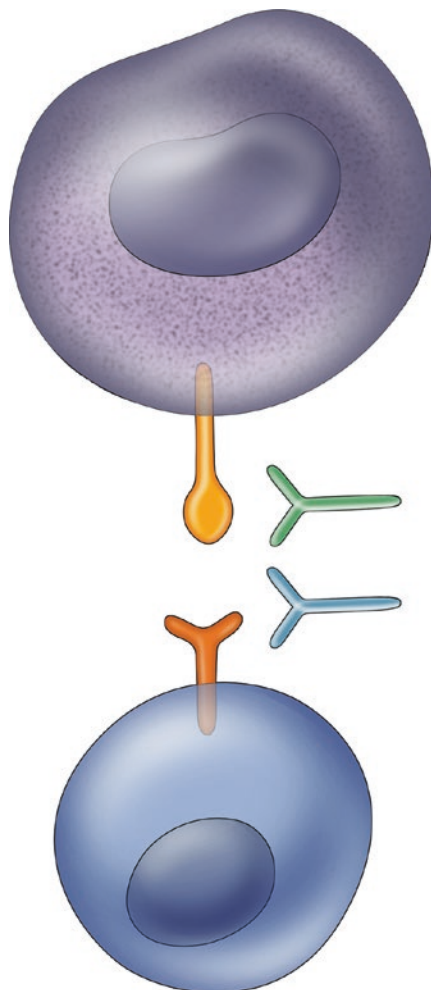
Recent advances in technology of genome-wide sequencing and peptide affinity algorithms can expedite the identification of mutations and related neoantigens, and the screening of peptides with high affinity to the major histocompatibility complex (MHC) for antigen presentation. The high efficiency of these new technologies may improve the feasibility of personalized vaccines.

15.7.3 Immune Checkpoint Inhibitors

Immune checkpoints are inhibitory receptors on T-cells that play an important role in suppressing T-cell-mediated antitumor responses [178]. Under physiological conditions, they prevent inappropriate activation and regulate the intensity and duration of activation. The most studied checkpoints for therapeutic purposes are CTLA-4 and PD-1. CTLA-4 plays a role of negative feedback during CD8(+) T-cell activation [47]. CTLA-4 expressed on CD4(+) T-cells enhances Treg-mediated immunosuppression [49]. In mice bearing intracranial gliomas, CTLA-4 monoclonal antibody (9H10) treatment induced robust antitumor immunity without affecting Treg function [50]. The humanized CTLA-4 antibody ipilimumab is the first Food and Drug Administration (FDA)-approved immune checkpoint inhibitor. Ipilimumab has only been used in a small number of GBM patients in the recurrent setting. On the other hand, it has been used in treating metastatic melanoma, with approximately 2% durable complete response rate [179]. Responses have been observed against both non-CNS and CNS-infiltrated melanoma metastases [180]. Based on the common neuroectodermal origin of gliomas and melanomas, the results from the melanoma studies may provide some insights into its application to glioma treatment.

Recent efforts at inhibiting the PD-1/PD-L1 pathway (Fig. 15.7) have produced robust clinical results. Tumor-infiltrating lymphocytes in GBM [45], among numerous cancers, express high levels of PD-1. The high expression levels of PD-1 is thought to be a result of chronic stimulation by the tumor antigen. When the T-cells with high PD-1 levels interact with PD-L1, their effector functions are inhibited [181]. A number of mechanisms, such as loss of PTEN, paracrine IL-10 signaling [44], and interferon (IFN)- γ paracrine signaling [182], may contribute to the upregulation of PD-L1 in GBM. Clinical trials studying PD-1 and PD-L1 blockade in GBM patients (NCT02337491 and NCT02336165) recently completed patient recruitment, and their results may be reported soon.

Fig. 15.7 PD-1/PD-L1 pathway and its blocking. PD-1/PD-L1 pathway can be blocked at either or both sides of the PD-1 – PD-L1 interaction. Blue: T-cell. Purple: tumor cell



Immune checkpoint inhibition has produced the most significant results with the combination of CTLA-4 and PD-1 blockade [183–185]. In a randomized trial of untreated advanced melanoma, which shares neuroectodermal origin with gliomas, dual CTLA-4 and PD-1 blockade produced an improved objective response rate (58%) compared to CTLA-4 only (19%) and PD-1 only (44%) [185]. For GBM, a preclinical study using an animal model showed high rates of survival with IDO, PD-L1 and CTLA-4 triple blockade, as compared to the respective monotherapies [186]. Few clinical trials of treating GBM patients with a combination of CTLA-4 and PD-1 inhibition have completed recruiting patients recently (NCT02311920 and NCT02017717), and the results may be reported soon. There are also clinical trials evaluating the combination of CTLA-4 and PD-1 inhibition in patients with brain melanoma metastasis (NCT02374242 and NCT02320058), which will conclude and report results soon.

A retrospective study showed that 12 patients with recurrent DIPG tolerated nivolumab (an anti-PD-1 monoclonal antibody) well [187]. However, recruitment of DIPG patients in clinical trials of nivolumab have all been discontinued in North America due to unexpected serious adverse events as of 2017. A phase I consortium clinical trial of pembrolizumab (another anti-PD-1 monoclonal antibody) treating brain tumors, including DIPG, is ongoing (NCT02359565).

Other immune pathways being investigated for therapeutic purposes include the inhibitory lymphocyte activation gene 3 (LAG-3) [188] and T-cell immunoglobulin and mucin domain-containing 3 (TIM-3) [189] pathways and the stimulatory inducible costimulator (ICOS) [190] and 4-1BB [191] pathways. LAG-3 and PD-1 dual blockade therapy has progressed to a clinical study in non-CNS solid tumors (NCT01968109).

15.7.4 Adoptive Cell Therapies

Adoptive cell therapies are the transfer of cells into a patient for therapeutic purposes. The two most investigated adoptive cell therapies for cancer treatment are tumor-infiltrating lymphocyte (TIL) therapy and chimeric antigen receptor T-cell (CAR-T) therapy.

In the TIL therapy, lymphocytes are isolated from resected tumor tissue and cultured with a high-dose cytokine (typically IL-2) in single cell suspensions. The cultures are expanded and tested for antigen specificity against the patient's tumor. Cultures with evidence of specific reactivity to the tumor are selected for rapid expansion before being infused into the patient.

Chimeric antigen receptors (CARs) in CAR-T therapy are receptors engineered to activate T-cells by binding to a specific antigen. They have both antigen-binding and T-cell activating functions by including an extracellular single-chain variable fragment (scFv) and a T-cell activating domain (typically the zeta chain of the CD3 complex) into a single receptor. Therefore, they redirect the specificity and functions of T-cells. The CARs with the minimal antigen-binding and T-cell activating domains are termed first-generation CARs. They recognize antigens without the human leukocyte antigen (HLA), but do not lead to sustained T-cell responses [192] because sustained activation of T-cells requires the engagement of both T-cell receptors (TCRs) and co-stimulatory molecules. Second-generation CARs also include a costimulatory domain (CD28 or 4-1BB), directing sustained T-cell responses upon activation [193] and generating persistent "living drugs," which showed great clinical success recently.

In CAR-T therapy, T-cells are harvested from the patient, then in a laboratory, the cells are purified, cultured and transfected with DNA for the chimeric antigen receptor. The cells with successful transfection (CAR-T cells) are expanded before being infused into the patient. The CAR-T cells continue to multiply after infusion and attack tumor cells expressing the targeted antigen (Fig. 15.8).

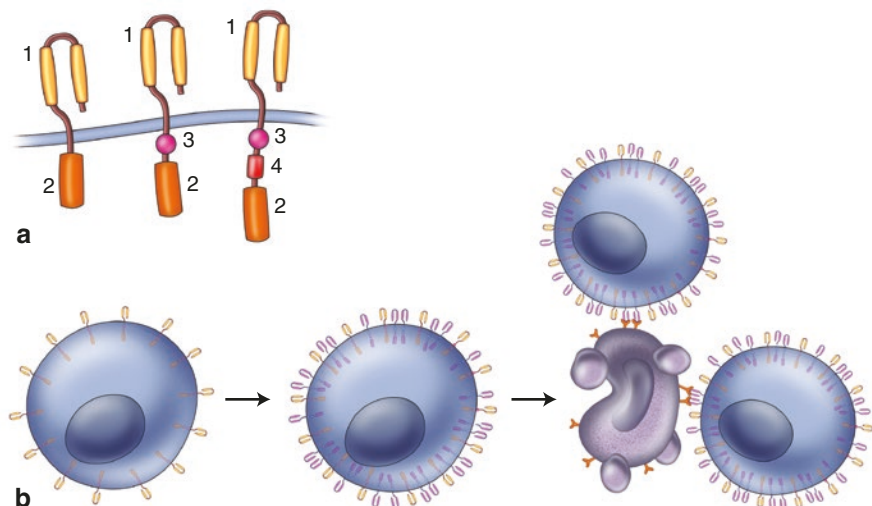


Fig. 15.8 CAR-T therapy. **(a)** From left to right, first-generation CARs consist of a minimal design. Second-generation CARs contain a costimulatory domain to enable sustained T cell activation. Third-generation CARs contain at least two co-stimulatory domains. (1) scFv (2) T-cell activating domain (CD3 ζ) (3) co-stimulatory domain (e.g., 4-1BB or CD28) (4) second co-stimulatory domain (e.g., CD28, ICOS or OX40). **(b)** General procedures of CAR-T therapy. T cells are collected, cultured and purified in a laboratory before being transfected with DNA constructs encoding the CAR. Successfully transfected T cells become CAR-T cells. These cells are cultured and purified before being infused into the blood stream of patients. CAR-T cells bind to tumor cells to exert their cytotoxic effects. In **(b)**, yellow color denotes native T-cell receptors and purple represents CARs

As a clinical success, both the TIL therapy and the CAR-T therapy demonstrated their capability in eradicating a large amount of tumor burden. The TIL therapy achieved a durable complete response in treating metastatic melanoma [194], and the CAR-T therapy was successful in treating CD19(+) B-cell leukemia [195].

TIL therapy targeting human cytomegalovirus (CMV) antigens expressed by tumor cells has been investigated for treating GBM. A clinical study treating recurrent GBM patients with autologous infusion of tumor-infiltrating T lymphocytes recognizing CMV antigens led to a median overall survival of over 57 weeks, with four patients remaining progression-free throughout the study period [196].

CAR-T therapies targeting human epidermal growth factor receptor 2 (HER2) and EGFRvIII produced impressive results in animal models of glioma [197, 198]. Clinical trials of CAR-T therapies targeting EGFRvIII (NCT02209376 and NCT01454596) and bispecific HER2/CMV (NCT01109095) in GBM patients have recently completed recruiting patients and may report detailed results soon. Preliminary results of the HER2/CMV bispecific CAR-T trial reported on the 30th Annual Meeting of the Society for Immunotherapy of Cancer (SITC, 2015, National Harbor, MD) showed that the therapy was well tolerated, and a durable clinical

benefit was observed in ~ 38 patients. A trial of CAR-T therapy targeting IL13Ra2 (NCT02208362) in malignant glioma patients is ongoing.

CAR-T therapy for DIPG is still at the preclinical stage. A recent preclinical CAR-T study targeting GD2, a disialoganglioside expressed on tumors of neuroectodermal origin, for DIPG was able to clear most of the tumor cells, but it produced dangerous levels of brain swelling in some animals [199]. Because of the essential anatomical and functional features of the brainstem, as well as its proximity to the thalamus, the safety issue of CAR-T therapy may be more difficult to solve in DIPG than in supratentorial gliomas.

15.8 Oncolytic Viruses

Oncolytic viruses are viruses that can infect and replicate in tumor cells in a tumor-selective conditional fashion, resulting in lytic destruction of tumor cells. The cell lysis results in the release of a large number of viral progenies, which go on to infect neighboring tumor cells.

A successful oncolytic virus requires a conditional, tumor-restricted viral replication with subsequent lysis of tumor cells. Certain tumor cell mutations would allow selective viral replication based on either inherent or engineered viral mechanisms. Such mechanisms can include any stage of the viral life cycle such as receptor-mediated viral attachment for infection initiation, DNA replication and protein synthesis, as well as the host's cytosolic antiviral mechanisms and innate and adaptive immune responses.

The most widely studied viruses for cancer treatment are herpes simplex virus (HSV) and adenovirus. The first experimental application of a genetically modified, replication-competent oncolytic virus for glioblastoma was reported in 1991 using a thymidine kinase (TK)-deficient HSV mutant, HSV-*dl*sptk, which was shown to be highly attenuated in non-dividing cells such as neurons but effective in infecting, replicating inside and lysing U87 cells *in vitro* and xenografts *in vivo* [200]. A number of oncolytic HSV mutants have been isolated or engineered since then, with R3616, HSV-1716, hrR3, G207, and G47 Δ being the most studied examples for targeting glioblastoma. After preclinical studies showed anti-glioma activity and good safety in rodents and non-human primates, G207 was tested in a clinical trial for glioblastoma that commenced in February 1998 [201]. HSV-1716 was tested in a clinical study in Europe at approximately the same time [202]. M032, an oncolytic HSV carrying human IL-12 gene, has shown enhanced glioma cell cytotoxicity in animal models [203], and a clinical trial of M032 in treating recurrent malignant gliomas is ongoing (NCT02062827).

Genetically engineered recombinants of adenovirus serotype 5 (Ad5) that show conditional replication are among the most studied oncolytic viruses. Early gene products of the adenovirus interact with Rb and p53. Adenoviruses with E1A or E1B deficiencies are replication-incompetent in normal cells and, therefore, tumor-selective. ONYX-015, a conditionally replicating adenovirus mutant with the

E1B-55 kD gene deletion was effective in killing p53-mutant U373 glioma cells but not p53-normal U87 cells [204]. However, a later study in glioma xenografts derived from primary human tumors reported increased oncolytic activity of ONYX-015 in p53 wild-type glioma xenografts compared to p53 mutants [205]. ONYX-015 was studied in a glioblastoma clinical trial [206]. DNX-2401, a newer adenovirus construct that combined Ad-delta-24 with Arg-Gly-Asp (RGD)-containing peptide modifications, has shown increased oncolytic activity against glioblastoma [207]. It was studied in a clinical trial showing dramatic responses with long-term survival in recurrent HGGs, which are probably due to direct oncolytic effects of the virus followed by elicitation of an immune-mediated anti-glioma response [208].

DNX-2401 is currently studied in DIPG patients in a phase I clinical trial (NCT03178032). Preliminary results reported at the 18th Biennial International Symposium for Pediatric Neuro-Oncology (ISPNO, 2018, Denver, Colorado, USA) showed that six DIPG patients were treated with DNX-2401 with no grade 3 or 4 adverse events, indicating that it may be a safe therapy for DIPG patients.

15.9 Conclusion

The most prominent example of malignant brainstem tumors is DIPG, which is considered one of the most difficult to treat in pediatric oncology. The standard of care for this tumor has not seen major changes in decades despite the disease's dismal outcome. A number of therapeutic options, many of which have shown dramatic therapeutic effects in other tumors, are being investigated for the treatment of DIPG. Despite the challenges presented by the critical anatomical and functional properties of the brainstem and its proximity to the thalamus and the unique biology of the tumor, it is hopeful that the outcome of this disease will improve with further refinement of these investigational therapies as well as development of new therapies.

Acknowledgments The authors would like to thank David J. Pisapia, MD, for providing histology and immunohistochemistry photographs of DIPG.

References

1. Ostrom QT, Gittleman H, Liao P, Vecchione-Koval T, Wolinsky Y, Kruchko C, et al. CBTRUS statistical report: primary brain and other central nervous system tumors diagnosed in the United States in 2010-2014. *Neuro-Oncology*. 2017;19(suppl_5):v1–v88. <https://doi.org/10.1093/neuonc/nox158>.
2. Pierre-Kahn A, Hirsch JF, Vinchon M, Payan C, Sainte-Rose C, Renier D, et al. Surgical management of brain-stem tumors in children: results and statistical analysis of 75 cases. *J Neurosurg*. 1993;79(6):845–52. <https://doi.org/10.3171/jns.1993.79.6.0845>.
3. Freeman CR, Farmer JP. Pediatric brain stem gliomas: a review. *Int J Radiat Oncol Biol Phys*. 1998;40(2):265–71.

4. Hargrave D, Bartels U, Bouffet E. Diffuse brainstem glioma in children: critical review of clinical trials. *Lancet Oncol.* 2006;7(3):241–8. S1470-2045(06)70615-5 [pii]. [https://doi.org/10.1016/S1470-2045\(06\)70615-5](https://doi.org/10.1016/S1470-2045(06)70615-5).
5. Klimo P Jr, Nesvick CL, Broniscer A, Orr BA, Choudhri AF. Malignant brainstem tumors in children, excluding diffuse intrinsic pontine gliomas. *J Neurosurg Pediatr.* 2016;17(1):57–65. <https://doi.org/10.3171/2015.6.PEDS15166>.
6. Babu R, Kranz PG, Agarwal V, McLendon RE, Thomas S, Friedman AH, et al. Malignant brainstem gliomas in adults: clinicopathological characteristics and prognostic factors. *J Neuro-Oncol.* 2014;119(1):177–85. <https://doi.org/10.1007/s11060-014-1471-9>.
7. Poussaint TY, Kocak M, Vajapeyam S, Packer RI, Robertson RL, Geyer R, et al. MRI as a central component of clinical trials analysis in brainstem glioma: a report from the Pediatric Brain Tumor Consortium (PBTC). *Neuro-Oncology.* 2011;13(4):417–27. <https://doi.org/10.1093/neuonc/noq200>.
8. Broniscer A, Baker SD, Wetmore C, Pai Panandiker AS, Huang J, Davidoff AM, et al. Phase I trial, pharmacokinetics, and pharmacodynamics of vandetanib and dasatinib in children with newly diagnosed diffuse intrinsic pontine glioma. *Clin Cancer Res.* 2013;19(11):3050–8. <https://doi.org/10.1158/1078-0432.CCR-13-0306>.
9. Subashi E, Cordero FJ, Halvorson KG, Qi Y, Nouls JC, Becher OJ, et al. Tumor location, but not H3.3K27M, significantly influences the blood-brain-barrier permeability in a genetic mouse model of pediatric high-grade glioma. *J Neuro-Oncol.* 2016;126(2):243–51. <https://doi.org/10.1007/s11060-015-1969-9>.
10. Dean M, Rzhetsky A, Allikmets R. The human ATP-binding cassette (ABC) transporter superfamily. *Genome Res.* 2001;11(7):1156–66. <https://doi.org/10.1101/gr.184901>.
11. Brangi M, Litman T, Ciotti M, Nishiyama K, Kohlhagen G, Takimoto C, et al. Camptothecin resistance: role of the ATP-binding cassette (ABC), mitoxantrone-resistance half-transporter (MXR), and potential for glucuronidation in MXR-expressing cells. *Cancer Res.* 1999;59(23):5938–46.
12. Ashraf T, Kao A, Bendayan R. Functional expression of drug transporters in glial cells: potential role on drug delivery to the CNS. *Adv Pharmacol.* 2014;71:45–111. <https://doi.org/10.1016/bs.apha.2014.06.010>.
13. Chen J, Zhang X, Kusumo H, Costa LG, Guizzetti M. Cholesterol efflux is differentially regulated in neurons and astrocytes: implications for brain cholesterol homeostasis. *Biochim Biophys Acta.* 2013;1831(2):263–75. <https://doi.org/10.1016/j.bbali.2012.09.007>.
14. Miller DS, Graeff C, Droulle L, Fricker S, Fricker G. Xenobiotic efflux pumps in isolated fish brain capillaries. *Am J Physiol Regul Integr Comp Physiol.* 2002;282(1):R191–8. <https://doi.org/10.1152/ajpregu.00305.2001>.
15. Bauer B, Hartz AM, Fricker G, Miller DS. Modulation of p-glycoprotein transport function at the blood-brain barrier. *Exp Biol Med (Maywood).* 2005;230(2):118–27.
16. Bendayan R, Ronaldson PT, Gingras D, Bendayan M. In situ localization of P-glycoprotein (ABCB1) in human and rat brain. *J Histochem Cytochem.* 2006;54(10):1159–67. <https://doi.org/10.1369/jhc.5A6870.2006>.
17. Veringa SJ, Biesmans D, van Vuurden DG, Jansen MH, Wedekind LE, Horsman I, et al. In vitro drug response and efflux transporters associated with drug resistance in pediatric high grade glioma and diffuse intrinsic pontine glioma. *PLoS One.* 2013;8(4):e61512. <https://doi.org/10.1371/journal.pone.0061512>.
18. Heppner GH. Tumor heterogeneity. *Cancer Res.* 1984;44(6):2259–65.
19. Spremulli EN, Dexter DL. Human tumor cell heterogeneity and metastasis. *J Clin Oncol.* 1983;1(8):496–509. <https://doi.org/10.1200/JCO.1983.1.8.496>.
20. Burrell RA, McGranahan N, Bartek J, Swanton C. The causes and consequences of genetic heterogeneity in cancer evolution. *Nature.* 2013;501(7467):338–45. <https://doi.org/10.1038/nature12625>.
21. Kreso A, Dick JE. Evolution of the cancer stem cell model. *Cell Stem Cell.* 2014;14(3):275–91. <https://doi.org/10.1016/j.stem.2014.02.006>.

22. Swanton C. Intratumor heterogeneity: evolution through space and time. *Cancer Res.* 2012;72(19):4875–82. <https://doi.org/10.1158/0008-5472.CAN-12-2217>.
23. Yates LR, Campbell PJ. Evolution of the cancer genome. *Nat Rev Genet.* 2012;13(11):795–806. <https://doi.org/10.1038/nrg3317>.
24. Bashashati A, Ha G, Tone A, Ding J, Prentice LM, Roth A, et al. Distinct evolutionary trajectories of primary high-grade serous ovarian cancers revealed through spatial mutational profiling. *J Pathol.* 2013;231(1):21–34. <https://doi.org/10.1002/path.4230>.
25. Campbell PJ, Yachida S, Mudie LJ, Stephens PJ, Pleasance ED, Stebbings LA, et al. The patterns and dynamics of genomic instability in metastatic pancreatic cancer. *Nature.* 2010;467(7319):1109–13. <https://doi.org/10.1038/nature09460>.
26. Gerlinger M, Horswell S, Larkin J, Rowan AJ, Salm MP, Varela I, et al. Genomic architecture and evolution of clear cell renal cell carcinomas defined by multiregion sequencing. *Nat Genet.* 2014;46(3):225–33. <https://doi.org/10.1038/ng.2891>.
27. Gerlinger M, Rowan AJ, Horswell S, Math M, Larkin J, Endesfelder D, et al. Intratumor heterogeneity and branched evolution revealed by multiregion sequencing. *N Engl J Med.* 2012;366(10):883–92. <https://doi.org/10.1056/NEJMoa1113205>.
28. Haffner MC, Mosbrugger T, Esopi DM, Fedor H, Heaphy CM, Walker DA, et al. Tracking the clonal origin of lethal prostate cancer. *J Clin Invest.* 2013;123(11):4918–22. <https://doi.org/10.1172/JCI70354>.
29. Sottoriva A, Spiteri I, Piccirillo SG, Touloumis A, Collins VP, Marioni JC, et al. Intratumor heterogeneity in human glioblastoma reflects cancer evolutionary dynamics. *Proc Natl Acad Sci U S A.* 2013;110(10):4009–14. <https://doi.org/10.1073/pnas.1219747110>.
30. Patel AP, Tirosh I, Trombetta JJ, Shalek AK, Gillespie SM, Wakimoto H, et al. Single-cell RNA-seq highlights intratumoral heterogeneity in primary glioblastoma. *Science.* 2014;344(6190):1396–401. <https://doi.org/10.1126/science.1254257>.
31. Dexter DL, Leith JT. Tumor heterogeneity and drug resistance. *J Clin Oncol.* 1986;4(2):244–57. <https://doi.org/10.1200/JCO.1986.4.2.244>.
32. Almendro V, Cheng YK, Randles A, Itzkovitz S, Marusyk A, Ametller E, et al. Inference of tumor evolution during chemotherapy by computational modeling and in situ analysis of genetic and phenotypic cellular diversity. *Cell Rep.* 2014;6(3):514–27. <https://doi.org/10.1016/j.celrep.2013.12.041>.
33. Merlo LM, Pepper JW, Reid BJ, Maley CC. Cancer as an evolutionary and ecological process. *Nat Rev Cancer.* 2006;6(12):924–35. <https://doi.org/10.1038/nrc2013>.
34. Wei W, Shin YS, Xue M, Matsutani T, Masui K, Yang H, et al. Single-cell phosphoproteomics resolves adaptive signaling dynamics and informs targeted combination therapy in glioblastoma. *Cancer Cell.* 2016;29(4):563–73. <https://doi.org/10.1016/j.ccell.2016.03.012>.
35. Pollack IF, Jakacki RI, Blaney SM, Hancock ML, Kieran MW, Phillips P, et al. Phase I trial of imatinib in children with newly diagnosed brainstem and recurrent malignant gliomas: a Pediatric Brain Tumor Consortium report. *Neuro-Oncology.* 2007;9(2):145–60. <https://doi.org/10.1215/15228517-2006-031>.
36. Clerk-Lamallice O, Reddick WE, Li X, Li Y, Edwards A, Glass JO, et al. MRI evaluation of non-necrotic T2-Hyperintense foci in pediatric diffuse intrinsic Pontine glioma. *AJNR Am J Neuroradiol.* 2016;37(10):1930–7. <https://doi.org/10.3174/ajnr.A4814>.
37. Harward S, Harrison Farber S, Malinzak M, Becher O, Thompson EM. T2-weighted images are superior to other MR image types for the determination of diffuse intrinsic pontine glioma intratumoral heterogeneity. *Childs Nerv Syst.* 2018;34(3):449–55. <https://doi.org/10.1007/s00381-017-3659-8>.
38. Steffen-Smith EA, Sarlls JE, Pierpaoli C, Shih JH, Bent RS, Walker L, et al. Diffusion tensor histogram analysis of pediatric diffuse intrinsic pontine glioma. *Biomed Res Int.* 2014;2014:647356. <https://doi.org/10.1155/2014/647356>.
39. Poussaint TY, Vajapeyam S, Ricci KI, Panigrahy A, Kocak M, Kun LE, et al. Apparent diffusion coefficient histogram metrics correlate with survival in diffuse intrinsic pontine glioma:

- a report from the Pediatric Brain Tumor Consortium. *Neuro-Oncology*. 2016;18(5):725–34. <https://doi.org/10.1093/neuonc/nov256>.
40. Bugiani M, Veldhuijzen van Zanten SEM, Caretti V, Schellen P, Aronica E, Noske DP, et al. Deceptive morphologic and epigenetic heterogeneity in diffuse intrinsic pontine glioma. *Oncotarget*. 2017;8(36):60447–52. <https://doi.org/10.18632/oncotarget.19726>.
 41. Mackay A, Burford A, Carvalho D, Izquierdo E, Fazal-Salom J, Taylor KR, et al. Integrated molecular meta-analysis of 1,000 pediatric high-grade and diffuse intrinsic Pontine glioma. *Cancer Cell*. 2017;32(4):520-37 e5. <https://doi.org/10.1016/j.ccell.2017.08.017>.
 42. Hoffman LM, DeWire M, Ryall S, Buczkowicz P, Leach J, Miles L, et al. Spatial genomic heterogeneity in diffuse intrinsic pontine and midline high-grade glioma: implications for diagnostic biopsy and targeted therapeutics. *Acta Neuropathol Commun*. 2016;4:1. <https://doi.org/10.1186/s40478-015-0269-0>.
 43. Parsa AT, Waldron JS, Panner A, Crane CA, Parney IF, Barry JJ, et al. Loss of tumor suppressor PTEN function increases B7-H1 expression and immunoresistance in glioma. *Nat Med*. 2007;13(1):84–8. <https://doi.org/10.1038/nm1517>.
 44. Bloch O, Crane CA, Kaur R, Safaee M, Rutkowski MJ, Parsa AT. Gliomas promote immunosuppression through induction of B7-H1 expression in tumor-associated macrophages. *Clin Cancer Res*. 2013;19(12):3165–75. <https://doi.org/10.1158/1078-0432.CCR-12-3314>.
 45. Berghoff AS, Kiesel B, Widhalm G, Rajky O, Ricken G, Wohrer A, et al. Programmed death ligand 1 expression and tumor-infiltrating lymphocytes in glioblastoma. *Neuro-Oncology*. 2015;17(8):1064–75. <https://doi.org/10.1093/neuonc/nou307>.
 46. Zhou Z, Luther N, Ibrahim GM, Hawkins C, Vibhakar R, Handler MH, et al. B7-H3, a potential therapeutic target, is expressed in diffuse intrinsic pontine glioma. *J Neuro-Oncol*. 2013;111(3):257–64. <https://doi.org/10.1007/s11060-012-1021-2>.
 47. Krummel MF, Allison JP. CD28 and CTLA-4 have opposing effects on the response of T cells to stimulation. *J Exp Med*. 1995;182(2):459–65.
 48. Takahashi T, Tagami T, Yamazaki S, Uede T, Shimizu J, Sakaguchi N, et al. Immunologic self-tolerance maintained by CD25(+)CD4(+) regulatory T cells constitutively expressing cytotoxic T lymphocyte-associated antigen 4. *J Exp Med*. 2000;192(2):303–10.
 49. Wing K, Onishi Y, Prieto-Martin P, Yamaguchi T, Miyara M, Fehervari Z, et al. CTLA-4 control over Foxp3+ regulatory T cell function. *Science*. 2008;322(5899):271–5. <https://doi.org/10.1126/science.1160062>.
 50. Fecci PE, Ochiai H, Mitchell DA, Grossi PM, Sweeney AE, Archer GE, et al. Systemic CTLA-4 blockade ameliorates glioma-induced changes to the CD4+ T cell compartment without affecting regulatory T-cell function. *Clin Cancer Res*. 2007;13(7):2158–67. <https://doi.org/10.1158/1078-0432.CCR-06-2070>.
 51. Grohmann U, Orabona C, Fallarino F, Vacca C, Calcinaro F, Falorni A, et al. CTLA-4-Ig regulates tryptophan catabolism in vivo. *Nat Immunol*. 2002;3(11):1097–101. <https://doi.org/10.1038/ni846>.
 52. Zhai L, Lauing KL, Chang AL, Dey M, Qian J, Cheng Y, et al. The role of IDO in brain tumor immunotherapy. *J Neuro-Oncol*. 2015;123(3):395–403. <https://doi.org/10.1007/s11060-014-1687-8>.
 53. Mitsuka K, Kawataki T, Satoh E, Asahara T, Horikoshi T, Kinouchi H. Expression of indoleamine 2,3-dioxygenase and correlation with pathological malignancy in gliomas. *Neurosurgery*. 2013;72(6):1031–8; discussion 8-9. <https://doi.org/10.1227/NEU.0b013e31828cf945>.
 54. Wainwright DA, Balyasnikova IV, Chang AL, Ahmed AU, Moon KS, Auffinger B, et al. IDO expression in brain tumors increases the recruitment of regulatory T cells and negatively impacts survival. *Clin Cancer Res*. 2012;18(22):6110–21. <https://doi.org/10.1158/1078-0432.CCR-12-2130>.
 55. Lieberman NAP, DeGolier K, Kovar HM, Davis A, Høglund V, Stevens J, et al. Characterization of the immune microenvironment of diffuse intrinsic pontine glioma: implications for development of immunotherapy. *Neuro-Oncology*. 2019;21(1):83–94. <https://doi.org/10.1093/neuonc/noy145>.

56. Becher OJ, Hambardzumyan D, Walker TR, Helmy K, Nazarian J, Albrecht S, et al. Preclinical evaluation of radiation and perifosine in a genetically and histologically accurate model of brainstem glioma. *Cancer Res.* 2010;70(6):2548–57. 0008-5472.CAN-09-2503 [pii]. <https://doi.org/10.1158/0008-5472.CAN-09-2503>.
57. Zarghooni M, Bartels U, Lee E, Buczkowicz P, Morrison A, Huang A, et al. Whole-genome profiling of pediatric diffuse intrinsic pontine gliomas highlights platelet-derived growth factor receptor alpha and poly (ADP-ribose) polymerase as potential therapeutic targets. *J Clin Oncol.* 2010;28(8):1337–44. *JCO.*2009.25.5463 [pii]. <https://doi.org/10.1200/JCO.2009.25.5463>.
58. Puget S, Philippe C, Bax DA, Job B, Varlet P, Junier MP, et al. Mesenchymal transition and PDGFRA amplification/mutation are key distinct oncogenic events in pediatric diffuse intrinsic pontine gliomas. *PLoS One.* 2012;7(2):e30313. <https://doi.org/10.1371/journal.pone.0030313>.
59. Paugh BS, Broniscer A, Qu C, Miller CP, Zhang J, Tatevossian RG, et al. Genome-wide analyses identify recurrent amplifications of receptor tyrosine kinases and cell-cycle regulatory genes in diffuse intrinsic pontine glioma. *J Clin Oncol.* 2011;29(30):3999–4006. <https://doi.org/10.1200/JCO.2011.35.5677>.
60. Paugh BS, Qu C, Jones C, Liu Z, Adamowicz-Brice M, Zhang J, et al. Integrated molecular genetic profiling of pediatric high-grade gliomas reveals key differences with the adult disease. *J Clin Oncol.* 2010;28(18):3061–8. *JCO.*2009.26.7252 [pii]. <https://doi.org/10.1200/JCO.2009.26.7252>.
61. Badhe PB, Chauhan PP, Mehta NK. Brainstem gliomas—a clinicopathological study of 45 cases with p53 immunohistochemistry. *Indian J Cancer.* 2004;41(4):170–4.
62. Zhang S, Feng X, Koga H, Ichikawa T, Abe S, Kumanishi T. p53 gene mutations in pontine gliomas of juvenile onset. *Biochem Biophys Res Commun.* 1993;196(2):851–7. S0006291X83723272 [pii]. <https://doi.org/10.1006/bbrc.1993.2327>.
63. Louis DN, Rubio MP, Correa KM, Gusella JF, von Deimling A. Molecular genetics of pediatric brain stem gliomas. Application of PCR techniques to small and archival brain tumor specimens. *J Neuropathol Exp Neurol.* 1993;52(5):507–15.
64. Barrow J, Adamowicz-Brice M, Cartmill M, MacArthur D, Lowe J, Robson K, et al. Homozygous loss of ADAM3A revealed by genome-wide analysis of pediatric high-grade glioma and diffuse intrinsic pontine gliomas. *Neuro-Oncology.* 2011;13(2):212–22. <https://doi.org/10.1093/neuonc/1158>.
65. Cheng Y, Wu H. Recent advances on molecular biology of diffuse astrocytoma. *Zhonghua Bing Li Xue Za Zhi.* 1999;28(3):165–8.
66. Cheng Y, Ng HK, Zhang SF, Ding M, Pang JC, Zheng J, et al. Genetic alterations in pediatric high-grade astrocytomas. *Hum Pathol.* 1999;30(11):1284–90.
67. Buczkowicz P, Hoeman C, Rakopoulos P, Pajovic S, Letourneau L, Dzamba M, et al. Genomic analysis of diffuse intrinsic pontine gliomas identifies three molecular subgroups and recurrent activating ACVR1 mutations. *Nat Genet.* 2014;46(5):451–6. <https://doi.org/10.1038/ng.2936>.
68. Taylor KR, Mackay A, Truffaux N, Butterfield Y, Morozova O, Philippe C, et al. Recurrent activating ACVR1 mutations in diffuse intrinsic pontine glioma. *Nat Genet.* 2014;46(5):457–61. <https://doi.org/10.1038/ng.2925>.
69. Wu G, Diaz AK, Paugh BS, Rankin SL, Ju B, Li Y, et al. The genomic landscape of diffuse intrinsic pontine glioma and pediatric non-brainstem high-grade glioma. *Nat Genet.* 2014;46(5):444–50. <https://doi.org/10.1038/ng.2938>.
70. Kaplan FS, Xu M, Seemann P, Connor JM, Glaser DL, Carroll L, et al. Classic and atypical fibrodysplasia ossificans progressiva (FOP) phenotypes are caused by mutations in the bone morphogenetic protein (BMP) type I receptor ACVR1. *Hum Mutat.* 2009;30(3):379–90. <https://doi.org/10.1002/humu.20868>.
71. Petrie KA, Lee WH, Bullock AN, Pointon JJ, Smith R, Russell RG, et al. Novel mutations in ACVR1 result in atypical features in two fibrodysplasia ossificans progressiva patients. *PLoS One.* 2009;4(3):e5005. <https://doi.org/10.1371/journal.pone.0005005>.

72. Song GA, Kim HJ, Woo KM, Baek JH, Kim GS, Choi JY, et al. Molecular consequences of the ACVR1(R206H) mutation of fibrodysplasia ossificans progressiva. *J Biol Chem*. 2010;285(29):22542–53. <https://doi.org/10.1074/jbc.M109.094557>.
73. Fontebasso AM, Papillon-Cavanagh S, Schwartzentruber J, Nikbakht H, Gerges N, Fiset PO, et al. Recurrent somatic mutations in ACVR1 in pediatric midline high-grade astrocytoma. *Nat Genet*. 2014;46(5):462–6. <https://doi.org/10.1038/ng.2950>.
74. Khuong-Quang DA, Buczkowicz P, Rakopoulos P, Liu XY, Fontebasso AM, Bouffet E, et al. K27M mutation in histone H3.3 defines clinically and biologically distinct subgroups of pediatric diffuse intrinsic pontine gliomas. *Acta Neuropathol*. 2012;124(3):439–47. <https://doi.org/10.1007/s00401-012-0998-0>.
75. Wu G, Broniscer A, McEachron TA, Lu C, Paugh BS, Becksfors J, et al. Somatic histone H3 alterations in pediatric diffuse intrinsic pontine gliomas and non-brainstem glioblastomas. *Nat Genet*. 2012;44(3):251–3. <https://doi.org/10.1038/ng.1102>.
76. Schwartzentruber J, Korshunov A, Liu XY, Jones DT, Pfaff E, Jacob K, et al. Driver mutations in histone H3.3 and chromatin remodelling genes in paediatric glioblastoma. *Nature*. 2012;482(7384):226–31. <https://doi.org/10.1038/nature10833>.
77. Castel D, Philippe C, Calmon R, Le Dret L, Truffaux N, Boddaert N, et al. Histone H3F3A and HIST1H3B K27M mutations define two subgroups of diffuse intrinsic pontine gliomas with different prognosis and phenotypes. *Acta Neuropathol*. 2015;130(6):815–27. <https://doi.org/10.1007/s00401-015-1478-0>.
78. Hawkins CE, Ellison DW, Sturm D. Diffuse midline glioma, H3 K27M-mutant. WHO classification of tumors of the central nervous system. 2016:57–59.
79. Bobo RH, Laske DW, Akbasak A, Morrison PF, Dedrick RL, Oldfield EH. Convection-enhanced delivery of macromolecules in the brain. *Proc Natl Acad Sci U S A*. 1994;91(6):2076–80.
80. Varenika V, Dickinson P, Bringas J, LeCouteur R, Higgins R, Park J, et al. Detection of infusate leakage in the brain using real-time imaging of convection-enhanced delivery. *J Neurosurg*. 2008;109(5):874–80. <https://doi.org/10.3171/JNS/2008/109/11/0874>.
81. Sampson JH, Akabani G, Archer GE, Berger MS, Coleman RE, Friedman AH, et al. Intracerebral infusion of an EGFR-targeted toxin in recurrent malignant brain tumors. *Neuro-Oncology*. 2008;10(3):320–9. 15228517-2008-012 [pii]. <https://doi.org/10.1215/15228517-2008-012>.
82. Sampson JH, Archer G, Pedain C, Wembacher-Schroder E, Westphal M, Kunwar S, et al. Poor drug distribution as a possible explanation for the results of the PRECISE trial. *J Neurosurg*. 2010;113(2):301–9. <https://doi.org/10.3171/2009.11.JNS091052>.
83. Sampson JH, Raghavan R, Provenzale JM, Croteau D, Reardon DA, Coleman RE, et al. Induction of hyperintense signal on T2-weighted MR images correlates with infusion distribution from intracerebral convection-enhanced delivery of a tumor-targeted cytotoxin. *AJR Am J Roentgenol*. 2007;188(3):703–9. 188/3/703 [pii]. <https://doi.org/10.2214/AJR.06.0428>.
84. Sampson JH, Akabani G, Friedman AH, Bigner D, Kunwar S, Berger MS, et al. Comparison of intratumoral bolus injection and convection-enhanced delivery of radiolabeled anti-tenascin monoclonal antibodies. *Neurosurg Focus*. 2006;20(4):E14. 200414 [pii]. <https://doi.org/10.3171/foc.2006.20.4.9>.
85. Sampson JH, Brady ML, Petry NA, Croteau D, Friedman AH, Friedman HS et al. Intracerebral infusate distribution by convection-enhanced delivery in humans with malignant gliomas: descriptive effects of target anatomy and catheter positioning. *Neurosurgery*. 2007;60(2 Suppl 1):ONS89–98; discussion ONS-9. 00006123–200702001-00013 [pii]. <https://doi.org/10.1227/01.NEU.0000249256.09289.5F>.
86. Lonser RR, Warren KE, Butman JA, Quezado Z, Robison RA, Walbridge S, et al. Real-time image-guided direct convective perfusion of intrinsic brainstem lesions. *Technical note. J Neurosurg*. 2007;107(1):190–7. <https://doi.org/10.3171/JNS-07/07/0190>.
87. Sandberg DI, Edgar MA, Souweidane MM. Convection-enhanced delivery into the rat brainstem. *J Neurosurg*. 2002;96(5):885–91.

88. Souweidane MM, Occhiogrosso G, Mark EB, Edgar MA. Interstitial infusion of IL13-PE38QQR in the rat brain stem. *J Neuro-Oncol.* 2004;67(3):287–93.
89. Souweidane MM, Occhiogrosso G, Mark EB, Edgar MA, Dunkel IJ. Interstitial infusion of carmustine in the rat brain stem with systemic administration of O6-benzylguanine. *J Neuro-Oncol.* 2004;67(3):319–26.
90. Luther N, Cheung NK, Dunkel IJ, Fraser JF, Edgar MA, Gutin PH, et al. Intraparenchymal and intratumoral interstitial infusion of anti-glioma monoclonal antibody 8H9. *Neurosurgery.* 2008;63(6):1166–74; discussion 74. 00006123-200812000-00030 [pii]. <https://doi.org/10.1227/01.NEU.0000334052.60634.84>.
91. Luther N, Cheung NK, Souliopoulos EP, Karempelas I, Bassiri D, Edgar MA, et al. Interstitial infusion of glioma-targeted recombinant immunotoxin 8H9scFv-PE38. *Mol Cancer Ther.* 2010;9(4):1039–46. 1535-7163.MCT-09-0996 [pii]. <https://doi.org/10.1158/1535-7163.MCT-09-0996>.
92. Luther N, Zhou Z, Zanzonico P, Cheung NK, Humm J, Edgar MA, et al. The potential of theraagnostic (1)(2)(4)I-8H9 convection-enhanced delivery in diffuse intrinsic pontine glioma. *Neuro-Oncology.* 2014;16(6):800–6. <https://doi.org/10.1093/neuonc/not298>.
93. Ho SL, Singh R, Zhou Z, Lavi E, Souweidane MM. Toxicity evaluation of prolonged convection-enhanced delivery of small-molecule kinase inhibitors in naive rat brainstem. *Childs Nerv Syst.* 2014; <https://doi.org/10.1007/s00381-014-2568-3>.
94. Giese H, Hoffmann KT, Winkelmann A, Stockhammer F, Jallo GI, Thomale UW. Precision of navigated stereotactic probe implantation into the brainstem. *J Neurosurg Pediatr.* 2010;5(4):350–9. <https://doi.org/10.3171/2009.10.PEDS09292>.
95. Pincus DW, Richter EO, Yachnis AT, Bennett J, Bhatti MT, Smith A. Brainstem stereotactic biopsy sampling in children. *J Neurosurg.* 2006;104(2 Suppl):108–14. <https://doi.org/10.3171/ped.2006.104.2.108>.
96. Roujeau T, Machado G, Garnett MR, Miquel C, Puget S, Georger B, et al. Stereotactic biopsy of diffuse pontine lesions in children. *J Neurosurg.* 2007;107(1 Suppl):1–4. <https://doi.org/10.3171/PED-07/07/001>.
97. Barua NU, Lowis SP, Woolley M, O'Sullivan S, Harrison R, Gill SS. Robot-guided convection-enhanced delivery of carboplatin for advanced brainstem glioma. *Acta Neurochir.* 2013;155(8):1459–65. <https://doi.org/10.1007/s00701-013-1700-6>.
98. Chittiboina P, Heiss JD, Warren KE, Lonser RR. Magnetic resonance imaging properties of convective delivery in diffuse intrinsic pontine gliomas. *J Neurosurg Pediatr.* 2014;13(3):276–82. <https://doi.org/10.3171/2013.11.PEDS136>.
99. Anderson RC, Kennedy B, Yanes CL, Garvin J, Needle M, Canoll P, et al. Convection-enhanced delivery of topotecan into diffuse intrinsic brainstem tumors in children. *J Neurosurg Pediatr.* 2013;11(3):289–95. <https://doi.org/10.3171/2012.10.PEDS12142>.
100. Heiss JD, Jamshidi A, Shah S, Martin S, Wolters PL, Argersinger DP, et al. Phase I trial of convection-enhanced delivery of IL13-Pseudomonas toxin in children with diffuse intrinsic pontine glioma. *J Neurosurg Pediatr.* 2018;23(3):333–42. <https://doi.org/10.3171/2018.9.PEDS17225>.
101. Souweidane MM, Kramer K, Pandit-Taskar N, Zhou Z, Haque S, Zanzonico P, et al. Convection-enhanced delivery for diffuse intrinsic pontine glioma: a single-centre, dose-escalation, phase 1 trial. *Lancet Oncol.* 2018;19(8):1040–50. [https://doi.org/10.1016/S1470-2045\(18\)30322-X](https://doi.org/10.1016/S1470-2045(18)30322-X).
102. Eckman WW, Patlak CS, Fenstermacher JD. A critical evaluation of the principles governing the advantages of intra-arterial infusions. *J Pharmacokinet Biopharm.* 1974;2(3):257–85.
103. Rapoport SI, Hori M, Klatzo I. Testing of a hypothesis for osmotic opening of the blood-brain barrier. *Am J Phys.* 1972;223(2):323–31. <https://doi.org/10.1152/ajplegacy.1972.223.2.323>.
104. Neuwelt EA, Maravilla KR, Frenkel EP, Rapoport SI, Hill SA, Barnett PA. Osmotic blood-brain barrier disruption. Computerized tomographic monitoring of chemotherapeutic agent delivery. *J Clin Invest.* 1979;64(2):684–8. <https://doi.org/10.1172/JCI109509>.

105. Joshi S, Cooke JRN, Ellis JA, Emala CW, Bruce JN. Targeting brain tumors by intra-arterial delivery of cell-penetrating peptides: a novel approach for primary and metastatic brain malignancy. *J Neuro-Oncol.* 2017;135(3):497–506. <https://doi.org/10.1007/s11060-017-2615-5>.
106. Vykhodtseva N, McDannold N, Hynynen K. Progress and problems in the application of focused ultrasound for blood-brain barrier disruption. *Ultrasonics.* 2008;48(4):279–96. <https://doi.org/10.1016/j.ultras.2008.04.004>.
107. Hirschberg H, Uzal FA, Chighvinadze D, Zhang MJ, Peng Q, Madsen SJ. Disruption of the blood-brain barrier following ALA-mediated photodynamic therapy. *Lasers Surg Med.* 2008;40(8):535–42. <https://doi.org/10.1002/lsm.20670>.
108. Hirschberg H, Zhang MJ, Gach HM, Uzal FA, Peng Q, Sun CH, et al. Targeted delivery of bleomycin to the brain using photo-chemical internalization of *Clostridium perfringens* epsilon prototoxin. *J Neuro-Oncol.* 2009;95(3):317–29. <https://doi.org/10.1007/s11060-009-9930-4>.
109. Hynynen K, McDannold N, Vykhodtseva N, Jolesz FA. Noninvasive MR imaging-guided focal opening of the blood-brain barrier in rabbits. *Radiology.* 2001;220(3):640–6. <https://doi.org/10.1148/radiol.2202001804>.
110. Hynynen K, McDannold N, Sheikov NA, Jolesz FA, Vykhodtseva N. Local and reversible blood-brain barrier disruption by noninvasive focused ultrasound at frequencies suitable for trans-skull sonications. *NeuroImage.* 2005;24(1):12–20. <https://doi.org/10.1016/j.neuroimage.2004.06.046>.
111. McDannold N, Vykhodtseva N, Raymond S, Jolesz FA, Hynynen K. MRI-guided targeted blood-brain barrier disruption with focused ultrasound: histological findings in rabbits. *Ultrasound Med Biol.* 2005;31(11):1527–37. <https://doi.org/10.1016/j.ultrasmedbio.2005.07.010>.
112. Vykhodtseva NI, Hynynen K, Damianou C. Histologic effects of high intensity pulsed ultrasound exposure with subharmonic emission in rabbit brain in vivo. *Ultrasound Med Biol.* 1995;21(7):969–79.
113. Choi JJ, Pernot M, Small SA, Konofagou EE. Noninvasive, transcranial and localized opening of the blood-brain barrier using focused ultrasound in mice. *Ultrasound Med Biol.* 2007;33(1):95–104. <https://doi.org/10.1016/j.ultrasmedbio.2006.07.018>.
114. Dougherty TJ, Gomer CJ, Henderson BW, Jori G, Kessel D, Korbek M, et al. Photodynamic therapy. *J Natl Cancer Inst.* 1998;90(12):889–905.
115. Stummer W, Gotz C, Hassan A, Heimann A, Kempski O. Kinetics of Photofrin II in perifocal brain edema. *Neurosurgery.* 1993;33(6):1075–81; discussion 81–2.
116. Hebeda KM, Saarnak AE, Olivo M, Sterenborg HJ, Wolbers JG. 5-Aminolevulinic acid induced endogenous porphyrin fluorescence in 9L and C6 brain tumours and in the normal rat brain. *Acta Neurochir.* 1998;140(5):503–12; discussion 12–3.
117. Ito S, Rachinger W, Stepp H, Reulen HJ, Stummer W. Oedema formation in experimental photo-irradiation therapy of brain tumours using 5-ALA. *Acta Neurochir.* 2005;147(1):57–65; discussion. <https://doi.org/10.1007/s00701-004-0422-1>.
118. Sporn LA, Foster TH. Photofrin and light induces microtubule depolymerization in cultured human endothelial cells. *Cancer Res.* 1992;52(12):3443–8.
119. Fingar VH. Vascular effects of photodynamic therapy. *J Clin Laser Med Surg.* 1996;14(5):323–8. <https://doi.org/10.1089/clm.1996.14.323>.
120. Hu SS, Cheng HB, Zheng YR, Zhang RY, Yue W, Zhang H. Effects of photodynamic therapy on the ultrastructure of glioma cells. *Biomed Environ Sci.* 2007;20(4):269–73.
121. Berg K, Selbo PK, Prasmickaite L, Tjelle TE, Sandvig K, Moan J, et al. Photochemical internalization: a novel technology for delivery of macromolecules into cytosol. *Cancer Res.* 1999;59(6):1180–3.
122. Worthington RW, Mulders MS. Effect of *Clostridium perfringens* epsilon toxin on the blood brain barrier of mice. *Onderstepoort J Vet Res.* 1975;42(1):25–7.
123. Nagahama M, Sakurai J. Distribution of labeled *Clostridium perfringens* epsilon toxin in mice. *Toxicol.* 1991;29(2):211–7.

124. Dorca-Arevalo J, Soler-Jover A, Gibert M, Popoff MR, Martin-Satue M, Blasi J. Binding of epsilon-toxin from *Clostridium perfringens* in the nervous system. *Vet Microbiol.* 2008;131(1–2):14–25. <https://doi.org/10.1016/j.vetmic.2008.02.015>.
125. Tsuruo T, Iida H, Tsukagoshi S, Sakurai Y. Overcoming of vincristine resistance in P388 leukemia in vivo and in vitro through enhanced cytotoxicity of vincristine and vinblastine by verapamil. *Cancer Res.* 1981;41(5):1967–72.
126. Ozols RF, Cunnion RE, Klecker RW Jr, Hamilton TC, Ostchega Y, Parrillo JE, et al. Verapamil and adriamycin in the treatment of drug-resistant ovarian cancer patients. *J Clin Oncol.* 1987;5(4):641–7. <https://doi.org/10.1200/JCO.1987.5.4.641>.
127. Boesch D, Gaveriaux C, Jachez B, Pourtier-Manzanedo A, Bollinger P, Loor F. In vivo circumvention of P-glycoprotein-mediated multidrug resistance of tumor cells with SDZ PSC 833. *Cancer Res.* 1991;51(16):4226–33.
128. Wandel C, Kim RB, Kajiji S, Guengerich P, Wilkinson GR, Wood AJ. P-glycoprotein and cytochrome P-450 3A inhibition: dissociation of inhibitory potencies. *Cancer Res.* 1999;59(16):3944–8.
129. Friedenbergr WR, Rue M, Blood EA, Dalton WS, Shustik C, Larson RA, et al. Phase III study of PSC-833 (valsopodar) in combination with vincristine, doxorubicin, and dexamethasone (valsopodar/VAD) versus VAD alone in patients with recurring or refractory multiple myeloma (E1A95): a trial of the Eastern Cooperative Oncology Group. *Cancer.* 2006;106(4):830–8. <https://doi.org/10.1002/encr.21666>.
130. Baer MR, George SL, Dodge RK, O'Loughlin KL, Minderman H, Caligiuri MA, et al. Phase 3 study of the multidrug resistance modulator PSC-833 in previously untreated patients 60 years of age and older with acute myeloid leukemia: Cancer and Leukemia Group B Study 9720. *Blood.* 2002;100(4):1224–32.
131. Rubin EH, de Alwis DP, Pouliquen I, Green L, Marder P, Lin Y, et al. A phase I trial of a potent P-glycoprotein inhibitor, Zosuquidar.3HCl trihydrochloride (LY335979), administered orally in combination with doxorubicin in patients with advanced malignancies. *Clin Cancer Res.* 2002;8(12):3710–7.
132. Sandler A, Gordon M, De Alwis DP, Pouliquen I, Green L, Marder P, et al. A phase I trial of a potent P-glycoprotein inhibitor, zosuquidar trihydrochloride (LY335979), administered intravenously in combination with doxorubicin in patients with advanced malignancy. *Clin Cancer Res.* 2004;10(10):3265–72. <https://doi.org/10.1158/1078-0432.CCR-03-0644>.
133. Vieira DB, Gamarra LF. Getting into the brain: liposome-based strategies for effective drug delivery across the blood-brain barrier. *Int J Nanomedicine.* 2016;11:5381–414. <https://doi.org/10.2147/IJN.S117210>.
134. Vieira DB, Gamarra LF. Advances in the use of nanocarriers for cancer diagnosis and treatment. *Einstein (Sao Paulo).* 2016;14(1):99–103. <https://doi.org/10.1590/S1679-45082016RB3475>.
135. Chen H, Tang L, Qin Y, Yin Y, Tang J, Tang W, et al. Lactoferrin-modified procationic liposomes as a novel drug carrier for brain delivery. *Eur J Pharm Sci.* 2010;40(2):94–102. <https://doi.org/10.1016/j.ejps.2010.03.007>.
136. Sun X, Pang Z, Ye H, Qiu B, Guo L, Li J, et al. Co-delivery of pEGFP-hTRAIL and paclitaxel to brain glioma mediated by an angiopep-conjugated liposome. *Biomaterials.* 2012;33(3):916–24. <https://doi.org/10.1016/j.biomaterials.2011.10.035>.
137. Doi A, Kawabata S, Iida K, Yokoyama K, Kajimoto Y, Kuroiwa T, et al. Tumor-specific targeting of sodium borocaptate (BSH) to malignant glioma by transferrin-PEG liposomes: a modality for boron neutron capture therapy. *J Neuro-Oncol.* 2008;87(3):287–94. <https://doi.org/10.1007/s11060-008-9522-8>.
138. Nair Madhavan PN, Saiyed Zainulabedin M, inventors; FLORIDA INTERNAT UNIVERSITY BOARD OF TRUSTEES, assignee. Magnetic Nanodelivery of Therapeutic Agents Across the Blood Brain Barrier 2009/08/28/Application date.
139. Arumugam K, Subramanian GS, Mallayasamy SR, Averineni RK, Reddy MS, Udupa N. A study of rivastigmine liposomes for delivery into the brain through intranasal route. *Acta Pharma.* 2008;58(3):287–97. <https://doi.org/10.2478/v10007-008-0014-3>.

140. Migliore MM, Vyas TK, Campbell RB, Amiji MM, Waszczak BL. Brain delivery of proteins by the intranasal route of administration: a comparison of cationic liposomes versus aqueous solution formulations. *J Pharm Sci.* 2010;99(4):1745–61. <https://doi.org/10.1002/jps.21939>.
141. Garcia-Garcia E, Andrieux K, Gil S, Kim HR, Le Doan T, Desmaele D, et al. A methodology to study intracellular distribution of nanoparticles in brain endothelial cells. *Int J Pharm.* 2005;298(2):310–4. <https://doi.org/10.1016/j.ijpharm.2005.03.030>.
142. Smith MW, Gumbleton M. Endocytosis at the blood-brain barrier: from basic understanding to drug delivery strategies. *J Drug Target.* 2006;14(4):191–214. <https://doi.org/10.1080/10611860600650086>.
143. Jallouli Y, Paillard A, Chang J, Sevin E, Betbeder D. Influence of surface charge and inner composition of porous nanoparticles to cross blood-brain barrier in vitro. *Int J Pharm.* 2007;344(1–2):103–9. <https://doi.org/10.1016/j.ijpharm.2007.06.023>.
144. Jones AR, Shusta EV. Blood-brain barrier transport of therapeutics via receptor-mediation. *Pharm Res.* 2007;24(9):1759–71. <https://doi.org/10.1007/s11095-007-9379-0>.
145. Mishra V, Mahor S, Rawat A, Gupta PN, Dubey P, Khatri K, et al. Targeted brain delivery of AZT via transferrin anchored pegylated albumin nanoparticles. *J Drug Target.* 2006;14(1):45–53. <https://doi.org/10.1080/10611860600612953>.
146. Pang Z, Gao H, Yu Y, Chen J, Guo L, Ren J, et al. Brain delivery and cellular internalization mechanisms for transferrin conjugated biodegradable polymersomes. *Int J Pharm.* 2011;415(1–2):284–92. <https://doi.org/10.1016/j.ijpharm.2011.05.063>.
147. Zensi A, Begley D, Pontikis C, Legros C, Mihoreanu L, Wagner S, et al. Albumin nanoparticles targeted with Apo E enter the CNS by transcytosis and are delivered to neurones. *J Control Release.* 2009;137(1):78–86. <https://doi.org/10.1016/j.jconrel.2009.03.002>.
148. Joshi BH, Puri RA, Leland P, Varricchio F, Gupta G, Kocak M, et al. Identification of interleukin-13 receptor alpha2 chain overexpression in situ in high-grade diffusely infiltrative pediatric brainstem glioma. *Neuro-Oncology.* 2008;10(3):265–74. 15228517-2007-066 [pii]. <https://doi.org/10.1215/15228517-2007-066>.
149. Okada H, Low KL, Kohanbash G, McDonald HA, Hamilton RL, Pollack IF. Expression of glioma-associated antigens in pediatric brain stem and non-brain stem gliomas. *J Neuro-Oncol.* 2008;88(3):245–50. <https://doi.org/10.1007/s11060-008-9566-9>.
150. Lewis PW, Muller MM, Koletsy MS, Cordero F, Lin S, Banaszynski LA, et al. Inhibition of PRC2 activity by a gain-of-function H3 mutation found in pediatric glioblastoma. *Science.* 2013;340(6134):857–61. <https://doi.org/10.1126/science.1232245>.
151. Hashizume R, Andor N, Ihara Y, Lerner R, Gan H, Chen X, et al. Pharmacologic inhibition of histone demethylation as a therapy for pediatric brainstem glioma. *Nat Med.* 2014;20(12):1394–6. <https://doi.org/10.1038/nm.3716>.
152. Wiese M, Schill F, Sturm D, Pfister S, Hulleman E, Johnsen SA, et al. No significant cytotoxic effect of the EZH2 inhibitor Tazemetostat (EPZ-6438) on pediatric glioma cells with wildtype Histone 3 or mutated histone 3.3. *Klin Padiatr.* 2016;228(3):113–7. <https://doi.org/10.1055/s-0042-105292>.
153. Mohammad F, Weissmann S, Leblanc B, Pandey DP, Hojfeldt JW, Comet I, et al. EZH2 is a potential therapeutic target for H3K27M-mutant pediatric gliomas. *Nat Med.* 2017;23(4):483–92. <https://doi.org/10.1038/nm.4293>.
154. Orzan F, Pellegatta S, Poliani PL, Pisati F, Caldera V, Menghi F, et al. Enhancer of Zeste 2 (EZH2) is up-regulated in malignant gliomas and in glioma stem-like cells. *Neuropathol Appl Neurobiol.* 2011;37(4):381–94. <https://doi.org/10.1111/j.1365-2990.2010.01132.x>.
155. de Vries NA, Hulsman D, Akhtar W, de Jong J, Miles DC, Blom M, et al. Prolonged Ezh2 depletion in glioblastoma causes a robust switch in cell fate resulting in tumor progression. *Cell Rep.* 2015; <https://doi.org/10.1016/j.celrep.2014.12.028>.
156. Northcott PA, Jones DT, Kool M, Robinson GW, Gilbertson RJ, Cho YJ, et al. Medulloblastomics: the end of the beginning. *Nat Rev Cancer.* 2012;12(12):818–34. <https://doi.org/10.1038/nrc3410>.

157. Mack SC, Witt H, Piro RM, Gu L, Zuyderduyn S, Stutz AM, et al. Epigenomic alterations define lethal CIMP-positive ependymomas of infancy. *Nature*. 2014;506(7489):445–50. <https://doi.org/10.1038/nature13108>.
158. Morin RD, Johnson NA, Severson TM, Mungall AJ, An J, Goya R, et al. Somatic mutations altering EZH2 (Tyr641) in follicular and diffuse large B-cell lymphomas of germinal-center origin. *Nat Genet*. 2010;42(2):181–5. <https://doi.org/10.1038/ng.518>.
159. Galanis E, Jaeckle KA, Maurer MJ, Reid JM, Ames MM, Hardwick JS, et al. Phase II trial of vorinostat in recurrent glioblastoma multiforme: a north central cancer treatment group study. *J Clin Oncol*. 2009;27(12):2052–8. <https://doi.org/10.1200/JCO.2008.19.0694>.
160. Friday BB, Anderson SK, Buckner J, Yu C, Giannini C, Geoffroy F, et al. Phase II trial of vorinostat in combination with bortezomib in recurrent glioblastoma: a north central cancer treatment group study. *Neuro-Oncology*. 2012;14(2):215–21. <https://doi.org/10.1093/neuonc/nor198>.
161. Galanis E, Anderson SK, Miller CR, Sarkaria JN, Jaeckle K, Buckner JC, et al. Phase I/II trial of vorinostat combined with temozolomide and radiation therapy for newly diagnosed glioblastoma: results of Alliance N0874/ABTC 02. *Neuro-Oncology*. 2018;20(4):546–56. <https://doi.org/10.1093/neuonc/nox161>.
162. Grasso CS, Tang Y, Truffaux N, Berlow NE, Liu L, Debily MA, et al. Functionally defined therapeutic targets in diffuse intrinsic pontine glioma. *Nat Med*. 2015;21(6):555–9. <https://doi.org/10.1038/nm.3855>.
163. Wang ZJ, Ge Y, Altinok D, Poulik J, Sood S, Taub JW, et al. Concomitant use of panobinostat and reirradiation in progressive DIPG: report of 2 cases. *J Pediatr Hematol Oncol*. 2017;39(6):e332–e5. <https://doi.org/10.1097/MPH.0000000000000806>.
164. Kreitman RJ. Immunotoxins for targeted cancer therapy. *AAPS J*. 2006;8(3):E532–51. <https://doi.org/10.1208/aapsj080363>.
165. Thomas DL, Kim M, Bowerman NA, Narayanan S, Kranz DM, Schreiber H, et al. Recurrence of intracranial tumors following adoptive T cell therapy can be prevented by direct and indirect killing aided by high levels of tumor antigen cross-presented on stromal cells. *J Immunol*. 2009;183(3):1828–37. <https://doi.org/10.4049/jimmunol.0802322>.
166. Binder DC, Engels B, Arina A, Yu P, Schlauch JM, Fu YX, et al. Antigen-specific bacterial vaccine combined with anti-PD-L1 rescues dysfunctional endogenous T cells to reject long-established cancer. *Cancer Immunol Res*. 2013;1(2):123–33. <https://doi.org/10.1158/2326-6066.CIR-13-0058>.
167. Brooks CL, Schietinger A, Borisova SN, Kufer P, Okon M, Hirama T, et al. Antibody recognition of a unique tumor-specific glycopeptide antigen. *Proc Natl Acad Sci U S A*. 2010;107(22):10056–61. <https://doi.org/10.1073/pnas.0915176107>.
168. Schietinger A, Philip M, Schreiber H. Specificity in cancer immunotherapy. *Semin Immunol*. 2008;20(5):276–85. <https://doi.org/10.1016/j.smim.2008.07.001>.
169. Okada H, Kalinski P, Ueda R, Hoji A, Kohanbash G, Donegan TE, et al. Induction of CD8+ T-cell responses against novel glioma-associated antigen peptides and clinical activity by vaccinations with α -type I polarized dendritic cells and polyinosinic-polycytidylic acid stabilized by lysine and carboxymethylcellulose in patients with recurrent malignant glioma. *J Clin Oncol*. 2011;29(3):330–6. <https://doi.org/10.1200/JCO.2010.30.7744>.
170. Monach PA, Meredith SC, Siegel CT, Schreiber H. A unique tumor antigen produced by a single amino acid substitution. *Immunity*. 1995;2(1):45–59.
171. Pelloski CE, Ballman KV, Furth AF, Zhang L, Lin E, Sulman EP, et al. Epidermal growth factor receptor variant III status defines clinically distinct subtypes of glioblastoma. *J Clin Oncol*. 2007;25(16):2288–94. <https://doi.org/10.1200/JCO.2006.08.0705>.
172. Heimberger AB, Hlatky R, Suki D, Yang D, Weinberg J, Gilbert M, et al. Prognostic effect of epidermal growth factor receptor and EGFRvIII in glioblastoma multiforme patients. *Clin Cancer Res*. 2005;11(4):1462–6. <https://doi.org/10.1158/1078-0432.CCR-04-1737>.
173. Sampson JH, Heimberger AB, Archer GE, Aldape KD, Friedman AH, Friedman HS, et al. Immunologic escape after prolonged progression-free survival with epidermal growth factor

- receptor variant III peptide vaccination in patients with newly diagnosed glioblastoma. *J Clin Oncol.* 2010;28(31):4722–9. <https://doi.org/10.1200/JCO.2010.28.6963>.
174. Schuster J, Lai RK, Recht LD, Reardon DA, Paleologos NA, Groves MD, et al. A phase II, multicenter trial of rindopepimut (CDX-110) in newly diagnosed glioblastoma: the ACT III study. *Neuro-Oncology.* 2015;17(6):854–61. <https://doi.org/10.1093/neuonc/nou348>.
175. Sampson JH, Aldape KD, Archer GE, Coan A, Desjardins A, Friedman AH, et al. Greater chemotherapy-induced lymphopenia enhances tumor-specific immune responses that eliminate EGFRvIII-expressing tumor cells in patients with glioblastoma. *Neuro-Oncology.* 2011;13(3):324–33. <https://doi.org/10.1093/neuonc/noq157>.
176. Liao LM, Ashkan K, Tran DD, Campian JL, Trusheim JE, Cobbs CS, et al. First results on survival from a large phase 3 clinical trial of an autologous dendritic cell vaccine in newly diagnosed glioblastoma. *J Transl Med.* 2018;16(1):142. <https://doi.org/10.1186/s12967-018-1507-6>.
177. Pollack IF, Jakacki RI, Butterfield LH, Hamilton RL, Panigrahy A, Potter DM, et al. Antigen-specific immune responses and clinical outcome after vaccination with glioma-associated antigen peptides and polyinosinic-polycytidylic acid stabilized by lysine and carboxymethylcellulose in children with newly diagnosed malignant brainstem and nonbrainstem gliomas. *J Clin Oncol.* 2014;32(19):2050–8. <https://doi.org/10.1200/JCO.2013.54.0526>.
178. Leach DR, Krummel MF, Allison JP. Enhancement of antitumor immunity by CTLA-4 blockade. *Science.* 1996;271(5256):1734–6.
179. Hodi FS, O'Day SJ, McDermott DF, Weber RW, Sosman JA, Haanen JB, et al. Improved survival with ipilimumab in patients with metastatic melanoma. *N Engl J Med.* 2010;363(8):711–23. <https://doi.org/10.1056/NEJMoa1003466>.
180. Margolin K, Ernstoff MS, Hamid O, Lawrence D, McDermott D, Puzanov I, et al. Ipilimumab in patients with melanoma and brain metastases: an open-label, phase 2 trial. *Lancet Oncol.* 2012;13(5):459–65. [https://doi.org/10.1016/S1470-2045\(12\)70090-6](https://doi.org/10.1016/S1470-2045(12)70090-6).
181. Barber DL, Wherry EJ, Masopust D, Zhu B, Allison JP, Sharpe AH, et al. Restoring function in exhausted CD8 T cells during chronic viral infection. *Nature.* 2006;439(7077):682–7. <https://doi.org/10.1038/nature04444>.
182. Taube JM, Anders RA, Young GD, Xu H, Sharma R, McMiller TL, et al. Colocalization of inflammatory response with B7-h1 expression in human melanocytic lesions supports an adaptive resistance mechanism of immune escape. *Sci Transl Med.* 2012;4(127):127ra37. <https://doi.org/10.1126/scitranslmed.3003689>.
183. Curran MA, Montalvo W, Yagita H, Allison JP. PD-1 and CTLA-4 combination blockade expands infiltrating T cells and reduces regulatory T and myeloid cells within B16 melanoma tumors. *Proc Natl Acad Sci U S A.* 2010;107(9):4275–80. <https://doi.org/10.1073/pnas.0915174107>.
184. Postow MA, Chesney J, Pavlick AC, Robert C, Grossmann K, McDermott D, et al. Nivolumab and ipilimumab versus ipilimumab in untreated melanoma. *N Engl J Med.* 2015;372(21):2006–17. <https://doi.org/10.1056/NEJMoa1414428>.
185. Larkin J, Hodi FS, Wolchok JD. Combined Nivolumab and Ipilimumab or monotherapy in untreated melanoma. *N Engl J Med.* 2015;373(13):1270–1. <https://doi.org/10.1056/NEJMc1509660>.
186. Wainwright DA, Chang AL, Dey M, Balyasnikova IV, Kim CK, Tobias A, et al. Durable therapeutic efficacy utilizing combinatorial blockade against IDO, CTLA-4, and PD-L1 in mice with brain tumors. *Clin Cancer Res.* 2014;20(20):5290–301. <https://doi.org/10.1158/1078-0432.CCR-14-0514>.
187. Kline C, Liu SJ, Duriseti S, Banerjee A, Nicolaides T, Raber S, et al. Reirradiation and PD-1 inhibition with nivolumab for the treatment of recurrent diffuse intrinsic pontine glioma: a single-institution experience. *J Neuro-Oncol.* 2018;140(3):629–38. <https://doi.org/10.1007/s11060-018-2991-5>.
188. Woo SR, Turnis ME, Goldberg MV, Bankoti J, Selby M, Nirschl CJ, et al. Immune inhibitory molecules LAG-3 and PD-1 synergistically regulate T-cell function to promote tumoral

- immune escape. *Cancer Res.* 2012;72(4):917–27. <https://doi.org/10.1158/0008-5472.CAN-11-1620>.
189. Sakuishi K, Apetoh L, Sullivan JM, Blazar BR, Kuchroo VK, Anderson AC. Targeting Tim-3 and PD-1 pathways to reverse T cell exhaustion and restore anti-tumor immunity. *J Exp Med.* 2010;207(10):2187–94. <https://doi.org/10.1084/jem.20100643>.
190. Fan X, Quezada SA, Sepulveda MA, Sharma P, Allison JP. Engagement of the ICOS pathway markedly enhances efficacy of CTLA-4 blockade in cancer immunotherapy. *J Exp Med.* 2014;211(4):715–25. <https://doi.org/10.1084/jem.20130590>.
191. Belcaid Z, Phallen JA, Zeng J, See AP, Mathios D, Gottschalk C, et al. Focal radiation therapy combined with 4-1BB activation and CTLA-4 blockade yields long-term survival and a protective antigen-specific memory response in a murine glioma model. *PLoS One.* 2014;9(7):e101764. <https://doi.org/10.1371/journal.pone.0101764>.
192. Brocker T, Karjalainen K. Signals through T cell receptor-zeta chain alone are insufficient to prime resting T lymphocytes. *J Exp Med.* 1995;181(5):1653–9.
193. Maher J, Brentjens RJ, Gunset G, Riviere I, Sadelain M. Human T-lymphocyte cytotoxicity and proliferation directed by a single chimeric TCRzeta /CD28 receptor. *Nat Biotechnol.* 2002;20(1):70–5. <https://doi.org/10.1038/nbt0102-70>.
194. Rosenberg SA, Yang JC, Sherry RM, Kammula US, Hughes MS, Phan GQ, et al. Durable complete responses in heavily pretreated patients with metastatic melanoma using T-cell transfer immunotherapy. *Clin Cancer Res.* 2011;17(13):4550–7. <https://doi.org/10.1158/1078-0432.CCR-11-0116>.
195. Maude SL, Frey N, Shaw PA, Aplenc R, Barrett DM, Bunin NJ, et al. Chimeric antigen receptor T cells for sustained remissions in leukemia. *N Engl J Med.* 2014;371(16):1507–17. <https://doi.org/10.1056/NEJMoa1407222>.
196. Schuessler A, Smith C, Beagley L, Boyle GM, Rehan S, Matthews K, et al. Autologous T-cell therapy for cytomegalovirus as a consolidative treatment for recurrent glioblastoma. *Cancer Res.* 2014;74(13):3466–76. <https://doi.org/10.1158/0008-5472.CAN-14-0296>.
197. Ahmed N, Salsman VS, Kew Y, Shaffer D, Powell S, Zhang YJ, et al. HER2-specific T cells target primary glioblastoma stem cells and induce regression of autologous experimental tumors. *Clin Cancer Res.* 2010;16(2):474–85. <https://doi.org/10.1158/1078-0432.CCR-09-1322>.
198. Johnson LA, Scholler J, Ohkuri T, Kosaka A, Patel PR, McGettigan SE, et al. Rational development and characterization of humanized anti-EGFR variant III chimeric antigen receptor T cells for glioblastoma. *Sci Transl Med.* 2015;7(275):275ra22. <https://doi.org/10.1126/scitranslmed.aaa4963>.
199. Mount CW, Majzner RG, Sundaresh S, Arnold EP, Kadapakkam M, Haile S, et al. Potent antitumor efficacy of anti-GD2 CAR T cells in H3-K27M(+) diffuse midline gliomas. *Nat Med.* 2018;24(5):572–9. <https://doi.org/10.1038/s41591-018-0006-x>.
200. Martuza RL, Malick A, Markert JM, Ruffner KL, Coen DM. Experimental therapy of human glioma by means of a genetically engineered virus mutant. *Science.* 1991;252(5007):854–6.
201. Markert JM, Medlock MD, Rabkin SD, Gillespie GY, Todo T, Hunter WD, et al. Conditionally replicating herpes simplex virus mutant, G207 for the treatment of malignant glioma: results of a phase I trial. *Gene Ther.* 2000;7(10):867–74. <https://doi.org/10.1038/sj.gt.3301205>.
202. Rampling R, Cruickshank G, Papanastassiou V, Nicoll J, Hadley D, Brennan D, et al. Toxicity evaluation of replication-competent herpes simplex virus (ICP 34.5 null mutant 1716) in patients with recurrent malignant glioma. *Gene Ther.* 2000;7(10):859–66.
203. Parker JN, Gillespie GY, Love CE, Randall S, Whitley RJ, Markert JM. Engineered herpes simplex virus expressing IL-12 in the treatment of experimental murine brain tumors. *Proc Natl Acad Sci U S A.* 2000;97(5):2208–13. <https://doi.org/10.1073/pnas.040557897>.
204. Heise C, Sampson-Johannes A, Williams A, McCormick F, Von Hoff DD, Kirn DH. ONYX-015, an E1B gene-attenuated adenovirus, causes tumor-specific cytolysis and antitumoral efficacy that can be augmented by standard chemotherapeutic agents. *Nat Med.* 1997;3(6):639–45.

205. Georger B, Grill J, Opolon P, Morizet J, Aubert G, Terrier-Lacombe MJ, et al. Oncolytic activity of the E1B-55 kDa-deleted adenovirus ONYX-015 is independent of cellular p53 status in human malignant glioma xenografts. *Cancer Res.* 2002;62(3):764–72.
206. Chiocca EA, Abbed KM, Tatter S, Louis DN, Hochberg FH, Barker F, et al. A phase I open-label, dose-escalation, multi-institutional trial of injection with an E1B-attenuated adenovirus, ONYX-015, into the peritumoral region of recurrent malignant gliomas, in the adjuvant setting. *Mol Ther.* 2004;10(5):958–66. <https://doi.org/10.1016/j.ymthe.2004.07.021>.
207. Fueyo J, Alemany R, Gomez-Manzano C, Fuller GN, Khan A, Conrad CA, et al. Preclinical characterization of the antiglioma activity of a tropism-enhanced adenovirus targeted to the retinoblastoma pathway. *J Natl Cancer Inst.* 2003;95(9):652–60.
208. Lang FF, Conrad C, Gomez-Manzano C, Yung WKA, Sawaya R, Weinberg JS, et al. Phase I study of DNX-2401 (Delta-24-RGD) oncolytic adenovirus: replication and immunotherapeutic effects in recurrent malignant glioma. *J Clin Oncol.* 2018;36(14):1419–27. <https://doi.org/10.1200/JCO.2017.75.8219>.

Index

A

- Abducens nucleus palsy, 98, 99
- Abductor pollicis brevis (APB), 116
- Acute disseminated encephalomyelitis (ADEM), 229, 230
- Acute hemorrhage, 77–79
- Acute ischemic stroke, 79–81
- Adenovirus, 378
- Adoptive cell therapies, 376–378
- Adult malignant tumor
 - chemotherapy, 148, 149
 - clinical presentation, 146
 - focal malignant brainstem gliomas, 146–148
 - focal tectal gliomas, 148
 - genetic complexity, 149
 - neurofibromatosis type 1, 148
 - tectal/cervicomedullary tumors, 149
- Alexander disease, 84
- Alpha thalassemia/mental retardation syndrome X-linked (ATRX) gene, 356
- Anaplastic astrocytoma, 315, 317
- Aneurysms
 - clinical presentation, 197, 198
 - imaging, 198–200
 - medulla
 - anatomic variants, 210
 - arteriovenous malformations, 212
 - CMs, 213
 - deployment, 211
 - intracranial dissection, 211
 - locations, 210
 - re-rupture after placement, 212
 - unclippable aneurysm, 210, 211
 - midbrain
 - arteriovenous malformations, 203, 204
 - CMs, 204–206
 - ISAT, 202, 203
 - OZ osteotomy, 201
 - posterior circulation, 201
 - posterior communicating artery, 201, 202
 - recurrence, 201
 - SCIT approach, 202
 - vascular microneurosurgeons, 201
 - natural history, 197
 - pons
 - arteriovenous malformations, 207, 209
 - CMs, 209, 210
 - critical pontine perforating arteries, 206
 - dolichoectatic basilar aneurysms, 207, 208
 - endovascular techniques, 206
 - morbid transpetrous approaches, 206
 - open procedures, 206
 - stent-assisted coiling, 206
- Antibody-drug conjugates (ADC), 371, 372
- Aquaporin 4 (AQ4), 221
- Aqueductal tumors, 253
- Arterial spin labeling (ASL), 65
- Arteriovenous malformations (AVMs), 75
 - medulla, 212
 - midbrain, 203, 204
 - pons, 207, 209
- ATP-binding cassette (ABC) transporters, 352, 353
- Atypical teratoid rhabdoid tumor (ATRT), 151–155
- Autoimmune diseases, 220

B

- Babinski-Nageotte syndrome, 104
- Behçet disease, 220
- Blood-brain barrier (BBB), 350, 352
 - ABC transporters, 364, 365
 - FUS, 362, 363
 - PCI, 364
 - PDT, 363, 364
 - site-specific disruption, 362
- Brainstem
 - ambient cisterns, 54
 - anatomy
 - arterial supply, 46–49
 - brainstem and cerebellum, 50
 - lower neurovascular complex, 51
 - medulla oblongata, 45, 46
 - mesencephalon (midbrain), 43–45
 - middle neurovascular complex, 50, 51
 - pons (bridge), 45
 - posterior fossa, 50
 - sensations, 42
 - sulcus limitans, 42, 43
 - tegmentum, 43
 - upper neurovascular complex, 50
 - venous drainage, 49, 50
 - vertebrates, 42
 - vessels, 43, 44
 - cerebellopontine angle, 56–58
 - cerebral peduncle, 48, 51
 - computed tomography, 66
 - example, 110
 - extra-axial lesions
 - epidermoid cyst, 89–91
 - meningioma, 89, 90
 - parenchymal edema, 87, 88
 - schwannoma, 88, 89
 - ¹⁸F-FDG PET, 66, 67
 - fourth ventricle, 54–56
 - interpeduncular fossa, 51
 - mapping techniques, 110
 - medullary syndrome, 104, 105
 - midbrain syndrome, 103, 104
 - MRI
 - b-SSFP, 64
 - DTI, 65
 - ¹H-MRSI, 65
 - patient compliance, 63
 - pediatric imaging, 65, 66
 - PWI, 65
 - structural characterization, 63, 64
 - superior tissue contrast, 63
 - SWI, 64
 - T2-FLAIR images, 64
 - T2-weighted imaging, 64
 - neoplastic lesions
 - BSGs (*see* Brainstem gliomas)
 - metastatic disease, 73, 74
 - PCNSL (*see* Primary CNS lymphoma)
 - neurological examination, 96
 - abducens nucleus palsy, 98, 99
 - clinical signs, 96
 - facial nerve palsy, 98–100
 - fundoscopic changes, 102, 103
 - LCN, 100–102
 - nystagmus, 103
 - pyramidal cells, 100–102
 - trigeminal nerve, 97, 98
 - trochlear nerve nucleus, 96, 97
 - truncal ataxia, 102
 - non-neoplastic lesions
 - acute hemorrhage, 77–79
 - acute ischemic stroke, 79–81
 - capillary telangiectasia, 76, 77
 - cavernous malformation, 75, 76
 - demyelination, 83–86
 - HOD, 81–83
 - infection, 86, 87
 - patient history, 95, 96
 - pontine syndrome, 104
 - quadrigeminal cistern, 52–54
 - safe entry zones, 51, 52
 - structures, 110–112
 - T-SSEPs, 125, 126
 - ultrasound, 67
- Brainstem (BS)
 - clinical presentation, 219, 220
 - diagnostic approach, 220, 221
 - infectious lesions
 - bacterial encephalitis, 228, 229
 - clinical manifestations, 225
 - fungus infections, 225
 - hematogenous route, 222
 - increased intracranial pressure, 223
 - infectious vasculitis, 230
 - outcome, 225
 - parasitic infections, 224, 225
 - perilesional edema, 222, 223
 - physical examination, 225
 - postinfectious encephalitis, 222, 228–230
 - pyogenic brain abscesses, 223, 224
 - sensitivity and specificity, 225
 - severe immunosuppression, 223
 - sinusitis, otitis media, and mastoiditis, 222
 - TB brain abscess, 224
 - viral encephalitis, 226–228
 - inflammatory lesions

- CLIPPERS, 236, 237
- CTDs, 234, 235
 - in isolation, 231
 - manifestations, 231
 - multiple sclerosis, 231–233
 - NMO, 232–234
 - PACNS, 236
 - paraneoplastic diseases, 236–238
 - systemic vasculitis, 235, 236
 - variants, 231
- Brainstem auditory evoked potentials (BAEPs), 117–119
- Brainstem cavernous malformations (BSCMs), 75, 76
- Brainstem gliomas (BGs)
 - anatomic dissections, 2, 3
 - cerebellum and brainstem, 4
 - Cerebri Anatome*, 5–8
 - classical period, 2
 - cranial nerves, 4–6
 - early twentieth century
 - brainstem lesions, 29
 - clinical diagnosis, 32, 33
 - conservative approach, 28
 - contralateral paresis, 27, 28
 - mortality rate, 29
 - neurological localization, 26
 - neurosurgical procedures, 25, 26
 - posterior fossa decompression, 25
 - posterior fossa surgery, 29–32
 - surgical outcomes, 27
 - surgical procedures, 28, 29
 - surgical resection, 27
 - tentorium, 26
 - ventriculography, 31, 32
 - in 18th century, 7, 9, 13
 - Gautier D’Agoty’s seminal work, 13–15
 - illustration by Vicq D’Azyr, 11, 12
 - Portrait of Morgagni, 9, 10
 - Soemmering’s overview, 10, 11
 - Greco-Roman teachings, 3
 - imaging, 68–71
 - low-grade type, 68
 - mid-to-late twentieth century
 - chemotherapy, 35
 - clinical correlation, 34
 - cystic, infectious, and inflammatory collections, 33
 - epidemiological evidence, 33
 - epidemiological factors, 35
 - focal lesions, 33, 34
 - heterogeneous lesions, 34
 - homogeneous lesions, 34
 - long-term survival for, 36, 37
 - multicenter clinical trials, 35
 - novel therapeutics, 35
 - outcomes, 34
 - patient presentations, 34
 - patient’s papilledema and ataxia, 34
 - radiographic classification systems, 34
 - resections of brainstem lesions, 33
 - suboccipital craniectomy, 33
 - surface discoloration/abnormalities, 35
 - surgical management of, 36
 - ventricular catheter, 33
 - in 19th century, 13, 15–18, 21, 23–25
 - Bell’s description, 18, 19
 - Bright’s seminal work, 22, 23
 - Cruveilhier’s *Anatomie Pathologique de Corpus Humain*, 19, 20
 - epidermoid tumor, 21
 - Gigli saw, 25
 - Lister’s monograph, 16, 17
 - pons lesion, 24
 - pontine glioma, 22
 - past and reconciled inaccuracies, 6
 - pathophysiological descriptions, 6
 - in pediatric population, 67
 - posterior fossa and brainstem, 3, 4
- Brainstem tumors
 - adult brainstem gliomas, 323
 - non-DIPG, 322
 - pediatric DIPG
 - biology and prognosis, 322
 - definition, 322
 - glucocorticoids, 323
 - overall survival, 322
 - radiation therapy (*see* Diffuse intrinsic pontine glioma (DIPG))
- C**
- Capillary telangiectasia, 76, 77
- Cavernous malformations (CMs)
 - medulla, 213
 - midbrain, 204–206
 - pons, 209, 210
- Central Brain Tumor Registry of the United States (CBTRUS), 349
- Central Nervous System Primitive Neuroectodermal Tumor (CNS-PNET), 155
- Cervicomedullary tumors, 310
- Cestan-Chenais syndrome, 104
- Choreoathetosis, 220
- Choroid fissure, 255
- Choroidal fissure, 254

- CLIPPERS, 236, 237
 Computed tomography (CT), 66
 Connective tissue diseases (CTDs), 234, 235
 Convection-enhanced delivery (CED), 185
 clinical imaging methods, 359
 clinical trial, 360
 DIPG treatment, 359, 360
 infusion rates, 357
 in vivo distribution and concentration, 359
 microdialysis, 360
 pharmacokinetics, 360
 reflux, 358
 spherical distribution and spatial distribution, 358
 Corticospinal tracts (CSTs), 113, 115, 116, 247
 Cytochromes P450 (CYP450s), 365
 Cytotoxic T-lymphocyte-associated protein 4 (CTLA-4) pathway, 354
- D**
De Humani Corporis Fabrica, 4
 Demyelination, 83–86
 Developmental venous anomaly (DVA), 75
 Diffuse intrinsic pontine glioma (DIPG), 149, 297
 adult malignant type, 163
 chemotherapy
 clinical trials, 326
 disease-specific targeted therapy, 329–332
 empiric therapies, 327, 329
 clinical presentation, 163–165
 genetic and epigenetic peculiarities, 163
 glucocorticoids, 323
 imaging characteristics, 165–170
 pathology, 173–175
 pediatric brainstem tumors, 161
 pontine glioma, 161
 prognosis, 163
 radiation therapy
 acute tolerability, 323–324
 gross tumor volume, 324
 hyperfraction, 324, 325
 hypofraction, 325, 326
 neurological symptoms, 324
 radiosensitizing agents, 326
 radio-chemotherapy studies, 176–183
 school-aged children, 163
 surgical options, 171
 safety, 171, 172
 trans-cerebellar approach, 172, 173
 survival rates, 163
 targeted therapy, 184, 185
- Diffuse midline glioma (DMG), 69–71, 300, 301
 Diffusion tensor imaging (DTI), 65, 139
 Dorsal medullary zone, 58
 Dorsal tegmental nucleus, 248
 Drug delivery method
 blood-brain barrier
 ABC transporters, 364, 365
 FUS, 362, 363
 PCI, 364
 PDT, 363, 364
 site-specific disruption, 362
 carriers and packaging vehicles
 liposomes, 365, 366
 nanoparticles, 366, 367
 CED
 clinical imaging methods, 359
 clinical trial, 360
 DIPG treatment, 359, 360
 in vivo distribution and concentration, 359
 infusion rates, 357
 microdialysis, 360
 pharmacokinetics, 360
 reflux, 358
 spherical distribution and spatial distribution, 358
 intraarterial therapy, 361
 Dynamic contrast enhancement (DCE), 65
 Dynamic susceptibility contrast (DSC), 65
- E**
 Endoscopic third ventriculostomy (ETV), 252
 EGFR variant III (EGFRvIII), 373
 Embryonal tumor with multilayered rosettes (ETMR), 153–155
 Endoscopic endonasal approach (EEA)
 dural opening, 277
 patient position, 278
 surgical corridor, 278–282
 surgical setup, 278
 Enhancer of zeste homolog 2 (EZH2), 175, 368
 Epigenetic modulators, 368, 369
- F**
 Facial nerve palsy, 98–100
¹⁸F-2-fluoro-2-deoxy-D-glucose positron emission tomography (¹⁸F-FDG PET), 66, 67
 Fluorescence in situ hybridization (FISH), 152
 Focal gliomas, 68
 Focal low-grade glioma, 69
 “4D imaging” techniques, 198

G

Ganglioglioma (GG), 303, 304, 307, 316, 317
Germinoma, 88
Glioblastoma, 317

H

Herpes simplex virus (HSV), 378
High-grade gliomas (HGG), 150, 151, 156
High-resolution 3D balanced steady-state free precession (b-SSFP), 64
Histone deacetylase inhibitors (HDACi), 369
¹H-magnetic resonance spectroscopic imaging (¹H-MRSI), 65
Horner's syndrome, 104
Hydrocephalus, 252
Hypertrophic olivary degeneration (HOD), 81–83

I

Immune checkpoints, 374–376
Immune privilege, 354, 355
Immunoglobulin G (IgG), 221
Immunotherapy
 adoptive cell therapies, 376–378
 immune checkpoints, 374–376
 immunotoxins, 371, 372
 radiolabeled antibodies, 370, 371
 therapeutic antibodies, 369–371
 vaccination, 372–374
Indoleamine 2,3-dioxygenase 1 (IDO1), 354, 355
Infiltrating glioma, 31
International Subarachnoid Aneurysm Trial (ISAT), 202, 203
Internuclear ophthalmoplegia (INO), 219
Intraarterial therapy, 361
Intraoperative neurophysiology (ION), 110
Intratumoral heterogeneity, 353

K

***KIAA1549-BRAF* fusion**, 251

L

Lateral medullary (Wallenberg) syndrome, 104, 105
Lateral pontine (MCP), 273, 274, 289, 290
Liposomes, 365, 366
Lower cranial nerves (LCN), 100–102
Low-grade brainstem gliomas (LGBSG), 249
 biopsy, 137, 138

 classification, 132–134
 diagnosis, 135
 differential diagnosis, 137
 follow-up method, 141
 imaging, 136
 low-grade tumor, 141, 142
 outcomes, 140, 141
 pathology, 136, 137
 symptoms, 134, 135
 treatment
 adjuvant treatment, 140
 hydrocephalus, 138
 postoperative complications, 140
 rationale for, 137
 tumor resection, 139

M

Magnetic resonance imaging (MRI)
 b-SSFP, 64
 DTI, 65
 ¹H-MRSI, 65
 patient compliance, 63
 pediatric imaging, 65, 66
 PWI, 65
 structural characterization, 63, 64
 superior tissue contrast, 63
 SWI, 64
 T2-FLAIR images, 64
 T2-weighted imaging, 64
Mapping techniques, 110
Maximal safe cytoreduction surgery, 350
Medial longitudinal fasciculus (MLF), 268
Medial medullary (Dejerine) syndrome, 104
Medulla oblongata, surgery of
 calamus scriptorius, 122
 lower cranial nerve monitoring, 124, 125
 IX/X and XII cranial nerves, 123, 124
 nucleus ambiguus, 122
Medullary gliomas
 anaplastic astrocytoma, 315, 317
 brainstem gliomas, 296
 clinical outcome, 315
 clinical presentation, 296
 extent of tumor resection, 314, 315
 far-lateral approach
 bone window opening, 311
 hockey stick incision, 310
 lazy S incision, 310
 nuchal muscles, 310
 paracondylar variant, 310, 311
 suboccipital craniotomy, 310
 supracondylar variant, 311
 transcondylar variant, 311

- Medullary gliomas (cont.)
 vertebral artery, 311
 wide dural flap, 312
 glioblastoma, 317
 goals of surgery, 307, 308
 management strategies, 297
 microsurgical dissection
 technique, 312–314
molecular signature
 ganglioglioma, 303, 304, 307, 316, 317
 high-grade brainstem gliomas, 300–303
 pilocytic astrocytoma, 301, 303–306,
 315, 316
 neuroradiological evaluation, 296, 297
 patient selection, 297, 298
 preoperative planning, 308–310
 timing of surgery, 308
 tumor entities, 299, 300
 tumor exposure, 308–310
 tumor location and extent, 299
 Medullary syndromes, 104, 105
 Meningioma, 90
 Mesencephalic (midbrain) tumors
 anterior midbrain
 peritemporal approach, 255, 256
 setting, 254
 subchoroidal approach, 254, 255
 temporopolar approach, 254
 transchoroidal approach, 254, 255
 aqueductal tumors, 253
 BAEPs, 117–119
 central midbrain, 256–258
 cerebral peduncles, 249
 mMEP monitoring, 116, 117
 oculomotor nerve, 248
 periaqueductal tumors, 253
 posterior (dorsal) midbrain
 ETV, 258
 interhemispheric approach, 259, 260
 intervenous approach, 259
 occipital transtentorial approach, 259
 supracerebellar infratentorial, 260
 primordial vesicles, 248
 prognosis, 261
 surgical approach, 260, 261
 tectal gliomas, 252, 253
 tectum and quadrigeminal plate, 248
 tegmentum, 248, 249
 thalamopeduncular tumors, 249–252
 Midbrain surgery
 CSTs, 113, 115, 116
 oculomotor nerve nuclei, 112–114
 Molecular characteristics, 355, 356
 Motor deficits, 219
 Motor evoked potentials (MEPs), 121, 122
 Multidrug resistance (MDR), 364
 Multiple sclerosis (MS), 83–85, 231–233
 Muscle motor evoked potential (mMEP)
 monitoring, 116, 117
N
 Nanoparticles, 366, 367
 NMO spectrum disorder (NMOSD), 232–234
O
 Oculomasticatory myorhythmia (OMM), 220
 Oculomotor nucleus, 248
 Oncolytic viruses, 378, 379
 Opsoclonus-myoclonus (OpM), 220
 Orbitozygomatic (OZ) osteotomy, 201
 Osmotic demyelination syndrome
 (ODS), 83, 85
P
 Panobinostat, 369
 Paraneoplastic diseases, 220
 Pediatric malignant tumor
 ATRT, 151–155
 clinical presentation, 150
 CNS-PNET, 155
 DIPG, 149
 ETMR, 153–155
 HGG, 150, 151, 156
 histologic entity, 150
 initial management plan, 154
 non-DIPG, 149
 outcomes, 154
 WHO classification, 150
 Perfusion-weighted imaging (PWI), 65
 Periaqueductal tumors, 253
 Photochemical internalization (PCI), 364
 Photodynamic therapy (PDT), 363, 364
 Pilocytic astrocytoma (PA), 301, 303–306,
 315, 316
 Pons surgery
 facial colliculus, 119, 120
 facial MEPs, 121, 122
 free-running EMG, 120, 121
 Pontine syndrome, 104
 Pontine tumors
 corticospinal and corticobulbar fibers, 266

- EEA
 dural opening, 277
 patient position, 278
 surgical corridor, 278–282
 surgical setup, 278
- facial colliculi, 269, 270
- lateral cerebellopontine cisterns, 270, 271
- median suboccipital craniotomy, 290
 dural opening, 292
 external anatomical landmarks, 291
 meticulous irrigation, 292
 patient positioning, 290, 291
 safe entry zones, 292
 variations, 291
- mesencephalic tract, 269
- MLF, 268
- orbito-fronto-zygomatic approach
 modification of, 276
 patient position, 276
 surgical corridor, 276, 277
 surgical setup, 276
- pontomesencephalic and pontomedullary sulci, 266, 267
- prepontine cistern, 270, 271
- retrosigmoid approach
 cerebellopontine cistern, 289
 craniotomy, 288
 MCP, 289, 290
 occipital and ascending pharyngeal arteries, 288, 289
 patient positioning, 287
 periosteum, 288
 postauricular/lateral suboccipital incision, 287, 288
 posterolateral aspect, 287
 presigmoid approaches, 287
 superficial muscular fascia, 288
 surgical trajectory, 286
- safe entry zones
 fourth ventricular median sulcal, 275
 infrafacial collicular, 274, 275
 MCP, 273, 274
 neurological deficits, 271
 peritrigeminal, 271–273
 preoperative planning, 271
 superior foveal zone, 275
 superior ventral pontine, 275, 276
 suprafacial collicular, 274
 supratrigeminal, 272, 273
- shallow median groove, 266
- transpetrosal approach
 anterior petrosectomy, 277, 282
 dural flap, 286
 neuromonitoring, 283
 patient positioning, 273
 pontine tissue, 286
 posterior petrosectomy, 277, 282
 retrolabyrinthine, 284
 sigmoid sinus, 284
 sternocleidomastoid muscle, 283, 284
 translabyrinthine approach, 285, 286
 transmastoid, 282, 283
 Trautmann's triangle, 284, 285
 transverse pontine fibers, 266, 267
 trigeminal nerve, 268, 269
- Primary angiitis of the CNS (PACNS), 236
- Primary CNS lymphoma (PCNSL)
 imaging, 72, 73
 primary lymphomas, 71
- Primary pontine hemorrhage (PPH), 78
- Procarbazine, lomustine and vincristine (PCV), 327
- Proton magnetic resonance spectroscopy (MRS) findings, 170
- R**
- Receptor tyrosine kinases (RTKs), 353
- Reinhold syndrome, 104
- Relapsing–remitting course (RRMS), 231
- Relative cerebral blood volume (rCBV), 65
- S**
- Schwannoma, 89
- Signal transduction pathway targeted therapies, 367, 368
- Sjögren's syndrome (SS), 234
- Supracerebellar infratentorial (SCIT) approaches, 202
- Surgery of the Brain and Spinal Cord*, 26
- Susceptibility-weighted imaging (SWI), 64
- T**
- Tectal gliomas, 68, 252, 253
- Tegmentum, 248, 249
- T2 fluid-attenuated inversion recovery (FLAIR) images, 64
- Thalamopeduncular tumors, 249–252
- Tibialis anterior (TA), 116
- Total intravenous anesthesia (TIVA), 139
- Transylvian approach, 255

Trigeminal nerve palsy, 97, 98
Trigeminal SSEPs (T-SSEPs), 125, 126
Trochlear nerve nucleus, 96, 97
Trochlear nuclei, 249
Tuberculoma, 87
Tuberculous (TB) brain abscess, 224

V

Vorinostat, 369

W

Whipple's disease (WD), 220

Z

Zygomatic arch, 255

Zygomatic root, 255